

Development of a New Generation of Metal-Based Anticancer Drugs

Dissertation

In partial fulfilment for the degree of
Doctor of natural sciences
(Dr. rer. nat.)

Presented to the Department of Chemistry
of the Philipps-Universität Marburg
by

Elisabeth Katharina Martin, M.Sc.

Gießen, Germany

Marburg/Lahn 2017

The experimental work presented in this thesis was prepared from April 2012 to December 2015 under the supervision of Prof. Dr. Eric Meggers at the Department of Chemistry of the Philipps-Universität Marburg.

Submission date: 29.05.2017

Accepted by the Department of Chemistry of the Philipps-Universität Marburg (University ID: 1180) as dissertation: 23.06.2017

Date of oral examination: 29.06.2017

Supervisor: Prof. Dr. Eric Meggers

Second reviser: Prof. Dr. Armin Geyer

Acknowledgement

I would like to thank first and foremost Prof. Dr. Eric Meggers for giving me the opportunity to work on this great topic for the last couple of years, and for giving me the support and freedom, whatever needed at the moment, to fully drive my project and as well as my personal development forward.

I also need to thank Prof. Dr. Armin Geyer for kindly taking over the role as second referee as well as teaching me many basics in organic chemistry during my studies.

Thank you Prof. Dr. Ulrich Tallarek for taking part in the examination board and teaching me that mass spectrometry is the universal weapon in analytical chemistry.

Thank you to Angela for giving me the great opportunity to spend some months in your former lab in Groningen and for giving me the chance to gain a deeper understanding of all that *in vitro/ex vivo* stuff. Thank you as well to everybody welcoming me in the lab and helping me out with everything Natalia, Sophie, Sarah, Andreia, Viktoriia, Suresh, Mirja, Gerian, Margot, Bernard, Ming, Vivianna and Sylvia. Thanks for the great time!

A big thank you goes to Dr. Stefan Peukert for not only being a great collaborator, but also for giving me the chance to come to Cambridge (MA, USA) and get to know all the basic assays for ADME prediction at NIBR and to learn soooo many things during my stay there. A big thank you also goes to everyone involved in the project who helped me so much in learning the basics for interpretation and understanding of the data (Doug, Bing, Sandrine, Suzanne, Dallas, Carrie, Gina, Phong and Brad and everybody else).

I also need to thank all the department staff, be it from the MS, NMR or X-ray department, for all the help and support with the measurements. A special thanks goes to Dr. Uwe Linne and Jan Bamberger from the MS department for the ICP-MS measurements and all the work I was loading on them besides all the trouble the MS department was running through anyways. Thank you to Dr. Klaus Harms for X-ray structure determination and to Michael Hellwig for SEM measurements.

A huge thank you to each and every member and former member of our group for all the help, support and fun times! Katja, Ina and Andrea I am forever grateful for all the support with everything organisational! A special thanks goes to my lab husbands and wife Manu, Flo and Conní for keeping motivation up and for day to day support! Cheers to everybody else from “der harte Kern” Katja, Sandra, Kathrin, Anja, Janne, Melanie, Jens, Netti, Sabine and Henne. I will never forget the great time we had together! Thank you guys from the big lab, especially Raji, Markus and

die Thomase, and of course to Sabrina and Olalla for all the support you gave me. Also a big thanks to all my Schäfchen and Bääättchis (Johanna, Henne times two, Matthias, Bene, Felix, Sebweb and Maddie) for their support in my various projects. Thanks to everybody from my semester: Even “Versuchskaninchen” can survive, and: We did it!

I can't forget my non-chemist friends at that point (Mella, der Alex, Anika, Martin and everybody else)! Thank you for keeping me in “the real life” and sorry for always being the smart-arse. But I am sure you can cope with that, you had enough practice over the last couple of years.

Thanks to all my besties who supported me with proofreading of the thesis, you will of course not stay unmentioned! Conni, Manu, Martin, Raji, Nina, Jens, Netti, Sabine, Sabrina, Thomas C., Thomas M., Sabrina, Olalla. Thank you very much indeed.

Last but not least: A huge thanks goes to each and every member my family! I would never ever have been able to do all this without you guys!!! Thanks for the support, however little time there was left for you!

The same holds true for Sam. Thank you for being there and accepting me the way I am. I know it hasn't been always easy, so thank you so much for your support and love!

Publication list

Abstracts of this work have previously been published as peer-review articles or in conferences.

Peer-Review Articles

1. R. Rajaratnam, E. K. Martin, M. Dörr, K. Harms, A. Casini, E. Meggers, *Nonracemic Octahedral Rhodium-Prolinato Complexes as Protein Kinase Inhibitors*, *Inorg. Chem.*, **2015**, *54*(16), 8111-8120.
2. E. K. Martin, N. Pagano, M. E. Sherlock, K. Harms, E. Meggers, *Synthesis and anticancer activity of ruthenium half-sandwich complexes comprising combined metal centrochirality and planar chirality*, *Inorg. Chim. Acta*, **2014**, *423*, 530-539.

Conference Activities

1. E. K. Martin, E. Meggers *Drug-like properties of inert metal-based kinase inhibitors*. Poster Presentation. Frontiers in Medicinal Chemistry. (Marburg, Germany, 15.03.2015 - 18.03.2015).
2. E. K. Martin, E. Meggers *Development of inert rhodium complexes as potential drug candidates*. Poster Presentation. MCB Symposium: Joining forces in pharmaceutical analysis and medicinal chemistry. Awarded the RSC books poster price (Groningen, The Netherlands, 25.08.2014 - 26.08.2014).
3. S. Peukert*, E. Martin, D. Chin, F. Lombardo, E. Meggers. *Expanding the druggable chemical space with inert metal-organic complexes*. Poster. Gordon Research Conference: Metals in Medicine: Defining the Future of Medicinal Inorganic Chemistry. (Andover, MA, USA, 22.06.2014 - 27.06.2014) * presenting author
4. E. K. Martin, E. Meggers *Development of inert rhodium complexes as potential drug candidates*. Poster Presentation. Protein Kinases in Drug Discovery - Europe. (Berlin, Germany, 08.05.2014 - 09.05.2014).
5. E. K. Martin *Development of a new generation of metal-based anticancer drugs*. Oral presentation during the 2nd Whole Action Meeting of the COST Action CM1105 at the 1st International Symposium on Functional Metal Complexes that Bind to Biomolecules. (Barcelona, Spain, 09.09.2013 - 10.09.2013).
6. E. K. Martin, K. Harms, E. Meggers *Development of a new generation of metal-based anticancer drugs*. Poster presentation. Selected for oral poster presentation. 20th EuCheMS Conference on Organometallic Chemistry. (St. Andrews, Scotland, 30.06.2014 - 04.07.2014).

Zusammenfassung

Seit der Entdeckung der zentralen Rolle von Kinasen in der intrazellulären Signaltransduktion und der Entdeckung von Naturstoffen wie Staurosporin, die als unselektive Inhibitoren für Kinasen fungieren können, hat sich die Entwicklung von potenten Kinaseinhibitoren zu einem elementaren Teil der biologischen und medizinischen Forschung entwickelt. Während der letzten zwei Jahrzehnte hat die MEGGERS-Gruppe eine große Auswahl an selektiven und hoch-spezifischen ATP-kompetitiven Kinaseinhibitoren entwickelt, die auf inerten Koordinationskomplexen mit Metallzentren basieren, welche als strukturelles Templat zur Nachahmung des zuvor erwähnten Staurosporins dienen. Die generelle Struktur dieser Metallo-Pyridocarbazole ist in Abbildung 1 dargestellt. Es konnte gezeigt werden, dass diese Verbindungen sehr potent sind und oft selektiv Kinasen in Enzymassays, in Krebszelllinien *in vitro* und einfachen eukaryotischen Systemen *in vivo* inhibieren können. Dabei hat die Gruppe neue und innovative Chemotypen entwickelt, welche einen weitgehend unerforschten Bereich des chemischen Raums einnehmen, und kann damit die stark besiedelten urheberrechtlich geschützten Gebiete umgehen. Basierenden auf dieser Grundlage werden diese Verbindungen als potentielle Krebstherapeutika angesehen.

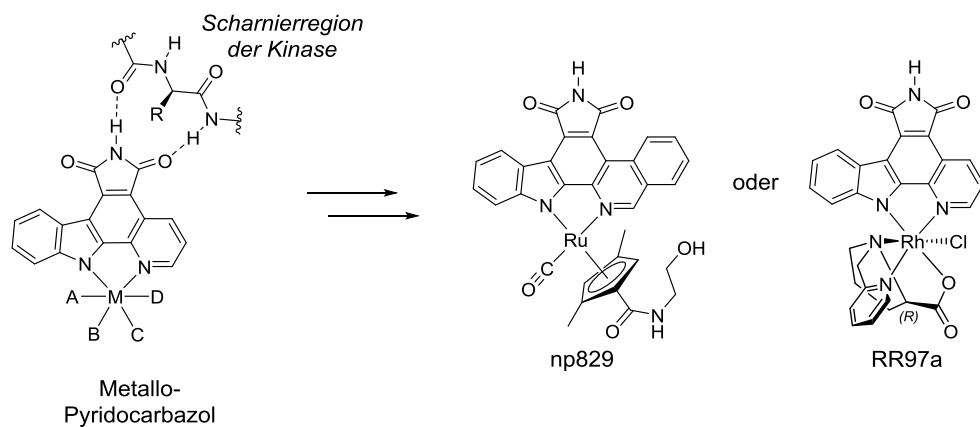


Abbildung 1: Strukturelles Templat der ATP-kompetitiven Kinaseinhibitoren, welche in der Meggers-Gruppe entwickelt wurden. Zusätzlich sind die zwei entwickelten Beispielkomplexe np829 und RR97a dargestellt.

Weiterführende Untersuchungen ihrer Eignung als potentielle Therapeutika, basierenden auf u.a. ihren pharmakokinetischen und pharmakodynamischen Eigenschaften, wurden dabei in der Vergangenheit nicht verwirklicht. Daher beschäftigt sich diese Arbeit mit der Eignung dieser Verbindungsklasse als potentielle Krebstherapeutika. Dabei sollte die beste Verbindung identifiziert und als Leitstruktur zur Optimierung der benötigten Eigenschaften verwendet werden.

Im ersten Ansatz wurden dabei, basierend auf der bereits bekannten Funktion als Kinase- bzw. ATPase-Inhibitoren und der damit inhärenten Eigenschaft als zielgerichtete molekulare Agenzien, die Verbindungen in einer Substanzbibliothek von 441 Verbindungen zusammengefasst und in einem klassischen empirischen Screening bezüglich ihrer Wirkung gegen Krebszellen in einem MTT-basierten Zytotoxizitätsassay in HT-29 Zellen getestet. Die dabei erfolgversprechendste Verbindung np829 (Abbildung 1), sowie attraktive synthetisierte Derivate, zeigten aber Toxizität, die vermutlich nicht alleine durch die Inhibition von Kinasen zu begründen ist. Daher wurden in einem zweiten Ansatz selektierte Verbindungen auf ihre Wirkstoffartigkeit in Bezug auf Löslichkeit, Permeabilität und metabolische Stabilität in Kollaboration mit den Novartis Institutes of BioMedical Research *in vitro* getestet. Zwei interessante stereoisomere Verbindungen wurden dabei selektiert und nach Bestätigung ihrer allgemeinen Stabilität, ihr pharmakokinetisches Verhalten über 7 bzw. 24 h *in vivo* in rodentia untersucht. Für den attraktivsten Kinaseinhibitor (RR97a (Abbildung 1) u.a. Inhibition der Kinase Pim1 im niedrigen nanomolaren Bereich) wurde zusätzlich die Organverteilung 7 h und 24 h nach intravenöser Gabe untersucht, und die Lunge als primäres Ziel der Verbindung identifiziert. Eine Ausscheidung des Zentralmetalls, vermutlich in Form des ursprünglichen Komplexes, über Urin und Kot wurde ebenfalls gezeigt, wobei diese über die betrachteten 24 h unvollständig war. Weiterhin wurden die Verbindungen in verschiedenen Krebszelllinien *in vitro* und in einem Hepatotoxizitätsassay *ex vivo* untersucht. Um diese Tests durchführen zu können, wurde zusätzlich der synthetische Zugang, sowie die Möglichkeit einer Hochskalierung des Syntheseansatzes untersucht. Abschließend wurden Derivate der interessanteren Verbindung dargestellt, um die Wirkstoffartigkeit weiter zu verbessern. Dabei konnte insbesondere die Löslichkeit erhöht werden, teilweise unter Erhalt oder Verbesserung der ursprünglichen Eigenschaften als Pim1 Kinaseinhibitor. Die Kombination der gewonnenen Erkenntnisse könnte dabei zukünftig genutzt werden, um die ADME-Eigenschaften der Leitstruktur oder anderer Pyridocarbazol-basierter Komplexe weiter zu optimieren. ADME ist dabei der Überbegriff für die Parameter Absorption, Distribution, Metabolismus und Eliminierung welche den Wirkstoff-Spiegel und die pharmakologische Aktivität einer Verbindung im Körper beeinflussen.

Als Nebenprojekt dieser Arbeit wurden in Prof. Angela Casinis Labor an der Rijksuniversiteit Groningen bekannte dinukleare Gold(III)-Komplexe als potentielle Histondeacetylaseinhibitoren untersucht. Histondeacetylasen (HDACs) sind dabei ein weiteres potentielles Ziel für die Behandlung von Krebs. Ein spezifischer Gold-Komplex (Abbildung 2), dessen antiproliferative Wirkung bereits zuvor gezeigt werden konnte, ist dabei der zytotoxischste Komplex aus einer Serie von Verbindungen in verschiedenen Krebszelllinien und zeigte dabei geringe Toxizität in einem Hepatotoxizitätsassay.

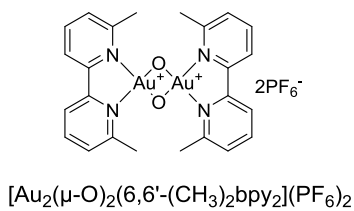


Abbildung 2: Struktur des zytotoxischsten Gold-Komplexes aus einer Serie von potentiellen Histondeacetylase-Inhibitoren.

In der Arbeit konnte in einem enzymbasierten Assay gezeigt werden, dass die Inhibition von Histondeacetylasen ein möglicher Grund der gezeigten Toxizität gegenüber Krebszellen ist. Der Effekt konnte dabei in Zellextrakt aus vorbehandelten Zellen nicht bestätigt werden, vermutlich aufgrund unterschiedlicher Zellzahlen der Kontrolle im Vergleich zu den behandelten Proben und damit verbundener unterschiedlicher Ausprägung der HDAC Expression basierenden auf Differenzen in der Zellzyklus-Verteilung. Weitere Untersuchungen sind dabei nötig um die Assay-Bedingungen besser zu verstehen und zu optimieren, um anschließende Experimente zur Untersuchung des zugrundeliegenden Mechanismus der Verbindung durchführen zu können.

Table of content

1. Introduction	1
1.1. A brief history of cancer and its treatment strategies	1
1.2. Kinases	3
1.2.1. Kinases and their medical relevance.....	7
1.2.2. Inhibition of kinases	7
1.2.3. The kinase Pim1 and its family members as cancer target.....	12
1.3. Histone deacetylases.....	16
1.3.1. HDACs and their medical relevance.....	18
1.3.2. Inhibitors of the zinc-dependant HDAC isoforms	19
1.4. Metals in medicine	22
1.4.1. Metal templates as structural feature for enzyme inhibitors.....	23
1.4.2. Metal-based kinase inhibitors and their <i>in vitro</i> and <i>in vivo</i> properties.....	25
1.4.3. Metal-based HDAC inhibitors	34
2. Concrete task.....	37
3. Results and discussion.....	39
3.1. Classical cytotoxicity-based approach.....	39
3.1.1. Database development.....	40
3.1.2. Library-based cytotoxicity screening.....	41
3.1.2.1. Development of a simplified structural derivative of the hit 80b	48
3.1.2.2. Further structural analogues of 119	50
3.1.3. Synthesis and upscaling of the hits 80b and 93b	52
3.1.3.1. Synthesis of further derivatives of 80b and 93b for the determination of structure activity relationship (SAR)	56
3.1.4. Determination of stereoinformation in 80a	58
3.1.5. Integrity and purity of 80a and 80b	59
3.1.6. Cytotoxicity determination of 80b and 93b	60
3.1.6.1. Solubility studies in cell medium of 80a and 80b	62
3.2. Drug-like properties of metal-based kinase inhibitors.....	65
3.2.1. Analysis and quantification of compounds in drug-like property assays.....	68
3.2.2. <i>In vitro</i> solubility, metabolic stability and permeability determination.....	70

3.2.2.1. Thermodynamic solubility assessment	70
3.2.2.2. Determination of metabolic stability in microsomes.....	72
3.2.2.3. Membrane and cell permeability assessment.....	75
3.2.2.4. Drug-like properties of further complexes.....	77
3.2.2.4.1. Metal-based MTH1 inhibitor.....	77
3.2.2.4.2. Drug-like properties investigations on stereoisomers of 201b	78
3.2.2.4.3. Stability of 201a , 201b , 204a and 204b against light, solvents and physiological conditions	82
3.2.3. Toxicity evaluation of 201a , 201b , 204a and 204b	86
3.2.3.1. <i>In vitro</i> cytotoxicity in cancer cells	86
3.2.3.2. <i>Ex vivo</i> hepatotoxicity of 201a and 201b in precision cut liver slices	88
3.2.3.2.1. Metal uptake of PCLS after treatment with RR97a and RR97b	90
3.2.3.2.2. Morphology of PCLS after treatment	91
3.2.4. <i>In vivo</i> studies of RR97a and RR97b	93
3.2.4.1. <i>In vivo</i> pharmacokinetic-studies of RR97b in C57BL/6 mice	93
3.2.4.2. <i>In vivo</i> pharmacokinetic-studies of RR97a in Sprague Dawley rats.....	96
3.2.4.3. Metabolisation of RR97a <i>in vitro</i> and <i>in vivo</i>	98
3.2.4.4. Excretion of RR97a <i>in vivo</i>	98
3.2.4.5. Tissue distribution of rhodium after 7 h and 24 h post IV injection of RR97a.....	99
3.3. Upscaling possibilities of RR97a and derivatives.....	102
3.3.1. Upscaling of the amount of starting material	102
3.3.2. Optimisation of reaction conditions	103
3.4. Solubility and permeability optimisation.....	107
3.4.1. Structural optimisation – <i>in silico</i> studies.....	109
3.4.2. Derivatisation of the proline derived ligand 206 – theoretical considerations	113
3.4.2.1. <i>In silico</i> investigation of possible solubility and permeability improvement	115
3.4.3. Modifications of the pyridocarbazole ligand – theoretical considerations	116
3.4.3.1. <i>In silico</i> investigation of possible solubility and permeability improvements.....	119
3.4.4. Synthetic realisation of structural modifications of 201a and 201b	120
3.4.4.1. Modifications of (pyridine-2-ylmethyl)-D-proline in the 4-pyridine position	120
3.4.4.1.1. Synthesis of ((4-chloropyridine-2-yl)methyl)-D-proline.....	121
3.4.4.1.2. Synthesis of ((4-(3-morpholinopropoxy)pyridine-2-yl)methyl)-D-proline and ((4-((3-morpholinopropyl)amino)pyridine-2-yl)- D-proline.....	122
3.4.4.1.3. Synthesis of ((4-(3-morpholinopropoxy)pyridine-2-yl)methyl)-D-proline.....	124
3.4.4.1.4. Synthesis of ((4-((dimethylamino)methyl)pyridine-2-yl)methyl)-D-proline	124
3.4.4.1.5. Synthesis of methyl ((4-hexylpyridine-2-yl) methyl)-D-proline	126
3.4.4.2. Complex synthesis with modified (pyridine-2-ylmethyl)-D-proline ligands	128

3.4.4.2.1. Synthesis of the 4-chloro pyridine modified complexes	128
3.4.4.2.2. Synthesis of 4-(3-morpholinopropan-1-ol) pyridine derivatised complexes.....	129
3.4.4.2.3. Synthesis of the 4-((dimethylamino)methyl) pyridine derivatised complexes.....	129
3.4.4.2.4. Synthesis of the 4-hexyl pyridine derivatised complexes	130
3.4.4.3. Complex synthesis with modified pyridocarbazole ligands	130
3.4.4.3.1. Synthesis of 5-methylpyridine derivatised complexes.....	130
3.4.4.3.2. Synthesis of 5-methoxypyridine derivatised complex.....	131
3.4.4.3.3. Synthesis of indole-5-ol derivatised complex.....	132
3.4.4.3.4. Synthesis of pyridine-6-yl methanol derivatised complex	133
3.4.5. Drug-like properties of (4-pyridine-2-ylmethyl)-D-proline derivatives	134
3.4.5.1. Drug-like properties of <i>trans</i> -isomers (a isomers).....	134
3.4.5.2. Drug-like properties of <i>cis</i> -isomers (b isomers)	135
3.4.6. Drug-like properties of pyridocarbazole derivatives.....	136
3.4.6.1. Drug-like properties of <i>trans</i> -isomers (a isomers).....	136
3.4.6.2. Drug-like properties of <i>cis</i> -isomers (b isomers)	137
3.4.7. Kinase inhibition properties of derivatives	138
3.5. Gold-based HDAC inhibitors as potential anticancer drugs	140
3.5.1. Toxicity evaluation.....	140
3.5.1.1. <i>In vitro</i> cytotoxicity in cancer cell lines	140
3.5.1.2. <i>Ex vivo</i> hepatotoxicity of 262	142
3.5.2. HDAC inhibitory properties	144
4. Summary and outlook.....	148
4.1. Summary and outlook metal-based kinase inhibitors	148
4.2. Summary and outlook gold-based HDIs	155
5. Experimental part	156
5.1. General methods	156
5.1.1. Chromatography methods.....	156
5.1.2. Analytical methods.....	157
5.1.2.1. Nuclear magnetic resonance spectroscopy.....	157
5.1.2.2. Infrared spectroscopy	157
5.1.2.3. Mass spectrometry	158
5.2. Compound preparation for toxicity approach	159
5.2.1. Synthesis of structural derivatives of np829 (80b) and np830 (80a).....	159

5.2.1.1. Synthesis of (η^6 -benzene)(η^5 -N-(2-methoxyethyl)cyclopentadienyl carboxamide) ruthenium hexafluorophosphate	159
5.2.1.2. Synthesis of η^5 -N-(2-methoxyethyl)cyclopentadienyl carboxamide precursor 123	159
5.2.1.3. Synthesis of TBS-protected η^5 -N-(2-methoxyethyl)cyclopentadienyl carboxamide complex 125	160
5.2.1.4. Synthesis of η^5 -N-(2-methoxyethyl)cyclopentadienyl carboxamide complex 119	161
5.2.2. Preparation of 80b	162
5.2.2.1. Synthesis of <i>E/Z</i> -ethyl 4-bromo-3-methylbut-2-enoate	162
5.2.2.2. Synthesis of ethyl-2,4-dimethylcyclopenta-1,2-diencarboxylate.....	163
5.2.2.3. Synthesis of (η^6 -benzene)(η^5 -ethyl 2,4-dimethylcyclopentadienylcarboxylate) ruthenium hexafluorophosphate	164
5.2.2.4. Synthesis of (η^6 -benzene)(η^5 -2,4-dimethylcyclopentadienylcarboxylic acid) ruthenium hexafluorophosphate	165
5.2.2.5. Synthesis of (η^6 -benzene)(η^5 -2-(trimethylsilyl)ethyl-2,4-dimethylcyclopenta-dienylcarboxylat) ruthenium hexafluorophosphate.....	165
5.2.2.6. Synthesis of η^5 -2-(trimethylsilyl)ethyl-2,4-dimethylcyclopentadienyl carboxylate) ruthenium hexafluorophosphate	166
5.2.2.7. Synthesis of η^5 -2-(trimethylsilyl)ethyl-2,4-dimethylcyclopentadienyl carboxylate) diastereomeric complexes 182a and 182b	167
5.2.2.8. Synthesis of η^5 -2,4-dimethylcyclopentadienylcarboxylic acid complex 183a	169
5.2.2.9. Synthesis of η^5 -2,4-dimethylcyclopentadienylcarboxylic acid complex 183b	170
5.2.2.10. Synthesis of NHS-ester complex 184a	171
5.2.2.11. Synthesis of NHS-ester complex 184b	172
5.2.2.12. Synthesis of np830 (80a)	173
5.2.2.13. Synthesis of np829 (80b)	174
5.2.3. Synthesis of structural derivatives of 80a and 80b	175
5.2.3.1. Synthesis of picolylamine derivative (93a).....	175
5.2.3.2. Synthesis of picolylamine derivative (93b)	176
5.2.3.3. Libraries of derivatives of np829 (80b).....	177
5.3. Compound preparation for the drug-like abilities approach.....	178
5.3.1. General working procedures for complex synthesis.....	178
5.3.1.1. Standard working procedure I	178
5.3.1.2. Standard working procedure II	178
5.4. Compound preparation drug-like abilities approach	179
5.4.1. Modification of the (pyridine-2-ylmethyl)-D-proline in the 4-pyridine position	179
5.4.1.1. 4-chloropyridine modification	179
5.4.1.1.1. Synthesis of methyl 4-chloropicolinate	179
5.4.1.1.2. Synthesis of (4-chloropyridine-2-yl)methanol.....	180

5.4.1.1.3. Synthesis of methyl ((4-chloropyridine-2-yl)methyl)-D-proline	181
5.4.1.1.4. Synthesis of ((4-chloropyridine-2-yl)methyl)-D-proline.....	182
5.4.1.1.5. Synthesis of the 4-chloro-pyridine modified complexes 258a and 258b	183
5.4.1.2. 4-(3-(pyridine-4-yloxy)propyl)morpholine modification	185
5.4.1.2.1. Synthesis of (4-(3-morpholinopropoxy)pyridine-2-yl)methanol.....	185
5.4.1.2.2. Synthesis of methyl ((4-(3-morpholinopropoxy)pyridine-2-yl)methyl)-D-proline	186
5.4.1.2.3. Synthesis of ((4-(3-morpholinopropoxy)pyridine-2-yl)methyl)-D-proline.....	187
5.4.1.2.4. Synthesis of 3-morpholinopropan-1-ol derivatised complexes 210a and 210b	188
5.4.1.3. ((4-((dimethylamino)methyl)pyridine-2-yl)methyl) modification	190
5.4.1.3.1. Synthesis of 2-hydroxymethyl-4-cyanopyridine.....	190
5.4.1.3.2. Synthesis of 2-hydroxymethyl-4-(dimethylamino)pyridine	191
5.4.1.3.3. Synthesis of methyl((4-((dimethylamino)methyl)pyridine-2-yl)methyl)-D-proline.....	192
5.4.1.3.4. Synthesis of ((4-((dimethylamino)methyl)pyridine-2-yl)methyl)-D-proline	193
5.4.1.3.5. Synthesis of the 4-((dimethylamino)methyl) pyridine complexes 212a and 212b	194
5.4.1.4. 4-hexylpyridine modification	196
5.4.1.4.1. Synthesis of 4-hexylpyridine	196
5.4.1.4.2. Synthesis of (4-hexylpyridine-2yl)-methanol.....	197
5.4.1.4.3. Synthesis of methyl ((4-hexylpyridine-2-yl)methyl)-D-proline	198
5.4.1.4.4. Synthesis of ((4-hexylpyridine-2-yl)methyl)-D-proline.....	199
5.4.1.4.5. Synthesis of the hexyl derivatised complexes 213a and 213b	200
5.4.2. Modification of the pyridocarbazole ligand	202
5.4.2.1. Synthesis of 5-methylpyridine derivatised complexes 223a and 223b	202
5.4.2.2. Synthesis of 5-methoxypyridine derivatised complexes 225a and 225b	204
5.4.2.3. Synthesis of indole-5-ol derivatised complexes 226a and 226b	206
5.4.2.4. Synthesis of pyridine-6-yl methanol derivatised complexes 209a and 209b	208
5.5. Preparation of single crystals for X-ray analysis.....	210
5.5.1. Preparation of single crystals of 80a	210
5.5.2. Preparation of single crystals of 225a	210
5.6. Cell experiments.....	211
5.6.1. Cell cultures.....	211
5.6.2. Determination of cell viability.....	212
5.6.3. Scanning electron microscopy	213
5.6.3.1. Chemical fixation	213
5.6.3.2. Freeze drying of cells	213
5.7. Enzyme inhibition assays	214
5.7.1. Pim1 inhibition assay.....	214

5.7.2. HDAC inhibition assay	215
5.7.2.1. Preparation of A549 nuclear extracts	215
5.7.2.2. HDAC activity assay	216
5.7.2.3. Quantification of HDAC 4 expression in treated cells.....	217
5.7.2.3.1. Cell treatment and protein extracts for Western Blot.....	217
5.7.2.3.2. SDS-PAGE and Western Blot	218
5.8. Assays for drug-like abilities determination	219
5.8.1. Stability studies	219
5.8.1.1. Ligand exchange and racemisation studies of 204b	219
5.8.1.2. Stability of 201a and 201b at physiological conditions	219
5.8.2. Equilibrium solubility assay (miniaturised shake-flask method)	220
5.8.3. Metabolic stability in rat liver microsomes (<i>in vitro</i> half-life approach).....	220
5.8.4. Metabolic stability in hepatocytes	223
5.8.5. Permeability assessment via hexadecane membrane (HDM)-PAMPA	224
5.8.6. Permeability assessment in Caco-2 cells	225
5.8.7. Permeability assessment in MDCK cells	226
5.8.8. Determination of MDR1 impact on efflux	227
5.8.9. Determination of <i>ex vivo</i> hepatotoxicity in PCLS	228
5.8.10. Determination of metal uptake of PCLS after treatment with 201a and 201b	230
5.8.11. Preparation of PCLS for morphology studies	230
5.9. <i>In vivo</i> studies	231
5.9.1. <i>In vivo</i> pharmacokinetics of 201b in mice	231
5.9.2. <i>In vivo</i> pharmacokinetics of 201a in rats.....	233
5.9.3. Metabolic stability of 201a <i>in vivo</i>	234
5.9.4. <i>In vivo</i> distribution of 201a in rats	234
5.9.4.1. Sample preparation for ICP-MS quantification.....	234
5.9.4.2. ICP-MS based determination of Rh content.....	235
6. Appendix	236
6.1. List of abbreviations.....	236
6.1.1. Amino Acids	236
6.1.2. Nucleobases	236
6.1.3. General abbreviations.....	237

6.2. Bibliography.....	247
6.3. List of newly developed compounds	268
6.3.1. List of synthesised compounds from chapter 3.1	268
6.3.2. List of synthesised compounds from chapter 3.4	268
6.4. Crystal structure data	270
6.4.1. Crystallographic data of complex 80a	270
6.4.2. Crystallographic data of complex 225a	271
6.5. NMR-spectra of selected compounds	272
6.5.1. ^1H - and ^{13}C -NMR-spectra of 119	272
6.5.2. ^1H - and ^{13}C -NMR-spectra of 209a	273
6.5.3. ^1H - and ^{13}C -NMR-spectra of 209b	274
6.5.4. ^1H - and ^{13}C -NMR-spectra of 210a	275
6.5.5. ^1H - and ^{13}C -NMR-spectra of 210b	276
6.5.6. ^1H - and ^{13}C -NMR-spectra of 212a	277
6.5.7. ^1H - and ^{13}C -NMR-spectra of 212b	278
6.5.8. ^1H -NMR-spectrum of 213a	279
6.5.9. ^1H - and ^{13}C -NMR-spectra of 213b	280
6.5.10. ^1H - and ^{13}C -NMR-spectra of 223a	281
6.5.11. ^1H - and ^{13}C -NMR-spectra of 223b	282
6.5.12. ^1H - and ^{13}C -NMR-spectra of 225a	283
6.5.13. ^1H - and ^{13}C -NMR-spectra of 225b	284
6.5.14. ^1H - and ^{13}C -NMR-spectra of 226a	285
6.5.15. ^1H - and ^{13}C -NMR-spectra of 226b	286
6.5.16. ^1H -NMR-spectrum of 258a	287
6.5.17. ^1H - and ^{13}C -NMR-spectra of 258b	288
6.6. Content of the electronic supporting information.....	289
7. Statement.....	291
8. Biographical Sketch	293

1. Introduction

1.1. A brief history of cancer and its treatment strategies

Today the second leading cause of disease related death in the world just after cardiovascular conditions is still cancer. In all its infinite variety, there is one common aspect in all cancer forms: It is always based on certain DNA-mutations that trigger cells to behave out of control in a way that they continue to grow and divide instead of dying. Some cancer cells are thereby able to travel to other parts of the body through blood circulation or lymph vessels, where they settle and form metastases.^[1] It is important to acknowledge that tumours *in vivo* are not just a collection of cancer cells with one defined genome, but organ-like structures, that consist of different cancer as well as host stromal cells embedded in an extracellular matrix and nourished by a vascular network.^[2] Tumours thereby have a high diversity of blood supply in individual areas, and even worse, inherit a certain genetic instability.^[2,3] This makes “cancer” an umbrella term for very heterogeneous conditions, which, under the selective pressure of drug treatment, might develop resistance to certain drugs, if it was not already inherited in their original genome. In many cases, drug treatment of cancer, especially based on single agent therapy, therefore leads to a remission rather than a cure.^[4]

A brief glance into the history of cancer and treatment strategies shows us that the disease was already acknowledged in written form 5000 years ago by Egyptian physicians. Treatment options for cancer and other conditions during that time were based on a very elementary form of “chemotherapy”, using drugs derived from minerals, plant material or animal sources. The Greek physician Hippocrates (ca. 460–370 BC) later coined the term cancer, after noting crab leg like extensions emanating from certain tumours and calling them carcinos (Greek for crab), which was later translated to the Latin word cancer. From these early times on, through the medieval period and the Dark and Middle Ages, the practice of medicine and the understanding of cancer changed very little. The use of surgery, cautery, herbal medications, caustic pastes, and blood-letting persisted with little to no innovation, and represented almost 2000 years of relative medical stagnation, which was only supplemented around 1900 by the use of radiation therapy after the discovery of its beneficial effect against cancer.^[5]

The first development of new chemotherapeutic treatment methods in the 20th century was based on empirical, clinical observations, starting with nitrogen mustard. This substance was investigated after it was noted that upon exposure to mustard gas, which was used in WWI as a chemical weapon, severe lymphoid depletion, bone marrow aplasia, and neutropenia takes place in the human body. In 1935 it was discovered that nitrogen mustard however also had antitumor activity against murine lymphoma. This was followed by first trials of therapeutic use, in which several

A brief history of cancer and its treatment strategies

lymphoma patients showed marked, but temporary, regression after treatment with nitrogen mustard.^[5] Parallel developments during WWII led to the discovery or creation of various other compounds with clinical value. Thus, by the end of the “empirical” phase, drugs like nitrogen mustards, mechlorethamine, cyclophosphamide and the folic acid antagonists amethopterin and aminopterin were all used successfully to treat certain types of cancer.^[2] All these drugs could produce impressive cancer remissions, however often being short or incomplete,^[5] so that surgery and radiotherapy still dominated the field of cancer treatment.^[6]

Based on those remarkable first results, the research towards more and better drugs continued during the post-war years.^[5] Different research centres started to use easily transplantable mouse models to screen compounds for their antitumor activity, narrowing down the universe of potential drugs.^[5,6] These studies led to the discovery of various agents like the cytostatic (inhibition of cell growth and multiplication) taxanes and the cytotoxic (toxic towards cells) vinca alkaloids. In the late 1960s the first combinational therapies followed those single agent treatments, increasing the remission rates to such an extent, that people started to think about the possibility to one day be able to cure cancer. Overall, the higher confidence in chemotherapy led to a more routine use of it in earlier stages of the disease and in combination with surgery, radiation therapy, or both.^[5]

Starting in 1984, the signalling pathways that regulate normal cellular activities, such as proliferation and survival, were subsequently uncovered and many of these were found to be radically altered in cancer cells.^[5] With the consecutive discovery of different oncogenes, tumour suppressor genes, and signalling pathways that are related to the carcinogenic process and angiogenesis, the idea of identifying new drug targets and matching drugs encouraged research activities even further.^[2]

Finally, in 1990, the mortality of cancer began to decline. As random screening was replaced by screening against specific critical molecular targets, the era of targeted therapy had begun.^[6] Targeted therapy might include both small molecules (SM) and monoclonal antibodies (mAb)^[5] as signal transduction inhibitors, gene expression modulators, apoptosis inducers or angiogenesis inhibitors, but also hormone- and immunotherapy. The first achievement in this area was the discovery of tamoxifen as an inhibitor for the estrogen receptor, which is an important target in certain breast cancer types. Subsequently, a number of drugs have been approved that e.g. block oncogene induced signal transduction such as imatinib (**1**, Chapter 1.2.2, Fig. 4) and others that affect proteins that regulate gene function, exemplified by vorinostat (**32**, Chapter 1.3.2, Fig. 9). Clearly, drugs designed to inhibit precise molecular targets or specific signalling pathways represent a valid approach for cancer therapeutics.^[7] Two established target families, kinases and histone deacetylases, together with their FDA approved treatment options, will be discussed in more depth in the following chapters.

1.2. Kinases

Kinases are proteins which belong to the transferase enzyme class and catalyse the transfer of the γ -phosphate group of ATP onto a specific side chain of their substrate, mainly serine, threonine and tyrosine, but also histidine.^[8] In doing so, they mediate most signal transductions^[9] and regulate various critical cellular activities, including proliferation, survival, apoptosis, metabolism, transcription, differentiation, and a wide array of other cellular processes.^[10] Phosphorylation, and thereby regulation of signal transduction, is a reversible process which is not only governed by kinases but also counteracting phosphatases.^[8]

Protein kinases represent one of the largest gene families in eukaryotic genomes, which accounts for a percentage of 2-4% of all genes. In humans, at least 538 different members of the protein kinase family have been identified.^[11] As every kinase thereby mediates a similar phosphoryl transfer process, it is unsurprising that a degree of sequence and structural homology exists, particularly in the active site regions, across all family members. This is further exaggerated within subclasses, where the catalytic activity is identical to a certain degree.^[12] Human kinases can be divided into 9 defined families, plus one catch-all category (“Other-Orphan”),^[11] which are summarised in Table 1. However, around 50% of the identified kinases are thought to be still largely uncharacterised, so that their function and structure is still unknown or speculated at the most.^[13]

Table 1: Kinase group classification based on phylogeny.^[11,14]

Kinase group	Details
AGC	Protein kinases A, G and C-like
CaMK	Calcium-calmodulin-regulated kinases
CMGC	Cyclin-dependant, mitogen-activated, glycogen synthase, and DDK-like kinases
TK	Tyrosine kinases (including both receptor and non-receptor kinases)
STE	Homologues of the yeast sterile kinases
CK1	Casein kinase 1 group
TKL	Tyrosine kinase like (similar but distant to TK)
RGC	Receptor guanylate cyclase related
Atypical	Diverse group with no structural similarity to eukaryotic protein kinases
Others/Orphan	Kinases that are not members of a larger family

An example for the highly conserved overall structure of kinases is given in Fig. 1. Generally, the N-terminal domain consists of 5 β -sheets and some α -helices, including the so-called c-helix. The C-terminal domain on the other hand consist mainly of α -helices and contains the so-called activation loop, which is activated by phosphorylation, leading to structural reorganisation. Both domains are connected via a hinge-region, where, upon activation, the catalytically active centre is located.^[3]

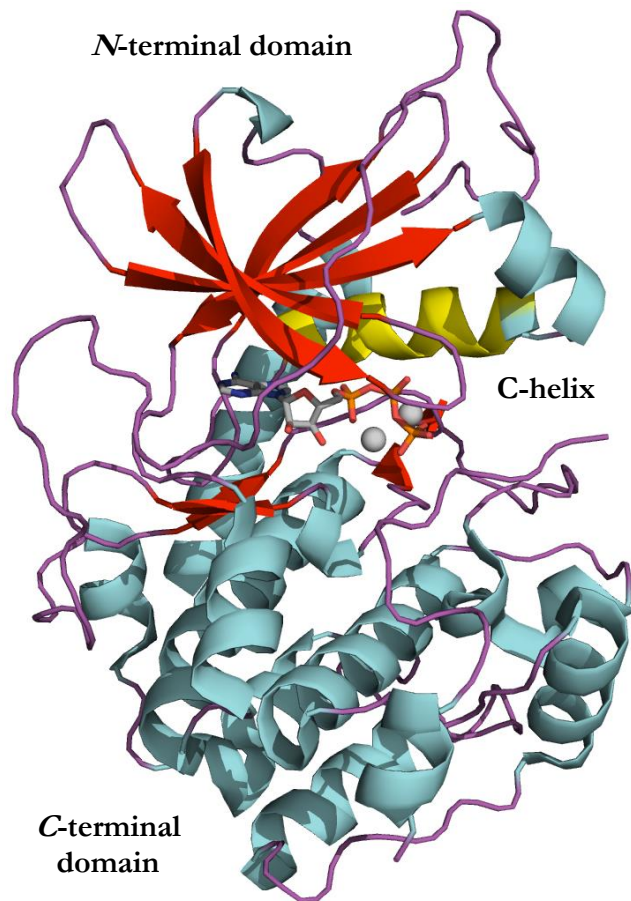


Fig. 1: ATP bound to the cAMP-dependant protein kinase A (catalytic alpha subunit, pdb 4WB5)^[15] as an example for the general structure of kinases. The N-terminal domain (residues 5-120, upper part) consists of 5 β -sheets (red) and some α -helices (cyan) including the C-helix (residues 85-97, yellow), the C-terminal domain (residues 128-350, lower part) consist mainly of α -helices (cyan). This domain interacts with a bound phosphoracceptor substrate and contains the so called activation loop (residues 184-208), which is activated by phosphorylation at Thr197 in PKA, following structural reorganisation. Both domains are connected via a hinge-region (residues 121-127 please refer to Fig. 2) which is the active site of the kinase. ^[3]

A closer look into the active site upon binding of ATP is given in Fig. 2. The recognition of ATP takes place in the hinge region, where typically two parallel H-bonds are formed between the co-substrate and the enzyme. The adenine part is thereby located in the adenine pocket, ribose in the sugar pocket and the triphosphate group in the phosphate pocket.^[14] The α - and β - phosphates of ATP interact with the ammonium group of a conserved K-residue, and are covered by the

phosphate binding loop (P-loop), which is a glycine rich loop in the N-terminal domain that is not involved in the phosphate transfer.^[16] All three phosphates are further chelated to two Mg²⁺ ions.^[14] An additional back pocket (selectivity pocket) might be accessible based on the size of the so called gatekeeper residue, and the outer lipophilic pocket or front pocket is generally solvent exposed.^[14] An additional pocket might be formed by the so called DFG-motif, which is a highly conserved region on the activation loop.

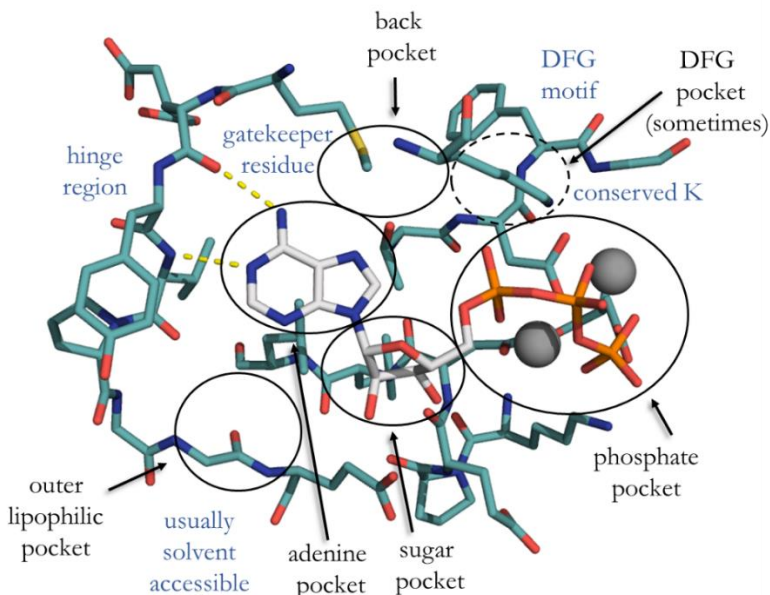


Fig. 2: ATP bound to the cAMP-dependant protein kinase A (catalytic alpha subunit; pdb 4WB5).^[15] Schematic illustration of key interactions and pockets in the ATP-binding region, which might be used to modulate potency, selectivity and inhibitor properties. Adenine is recognised by two parallel H-bonds from the hinge regions (residues 121-127) protein backbone. The α - and β - phosphates of ATP interact with the ammonium group of the conserved K-residue, and all phosphates are further chelated to two Mg²⁺ ions (grey spheres). The outer lipophilic pocket or front pocket is solvent exposed. The entrance to the allosteric back pocket or selectivity pocket is limited by the gatekeeper residue.

As indicated by the term activation loop, kinases normally exist in an activated and an inactivated state, which differ in the structural organisation of the enzymes shape. The active state of kinases is characterised by the presence of the conserved lysine – glutamate salt bridge (e.g. K67 and G89 in the kinase Pim1), a closed lobe conformation and a well-structured activation segment, which is often unorganised in kinases that require phosphorylation for catalytic activity. Upon phosphorylation, the activation segment folds onto the lower lobe and structures the peptide-binding site leading to enzymatic activation.^[17] Thereby both the affinity for ATP and phosphoracceptor substrates, as well as the catalytic activity are increased.^[3]

In a subset of kinases, the equilibrium between the active and inactive conformation is based on the orientation of the highly conserved DFG-motif. Phosphorylation of the activation loop thereby triggers activation by shifting the equilibrium to the active form (DFG-in, meaning the aspartate of the sequence faces into the ATP binding pocket Fig. 3 B).

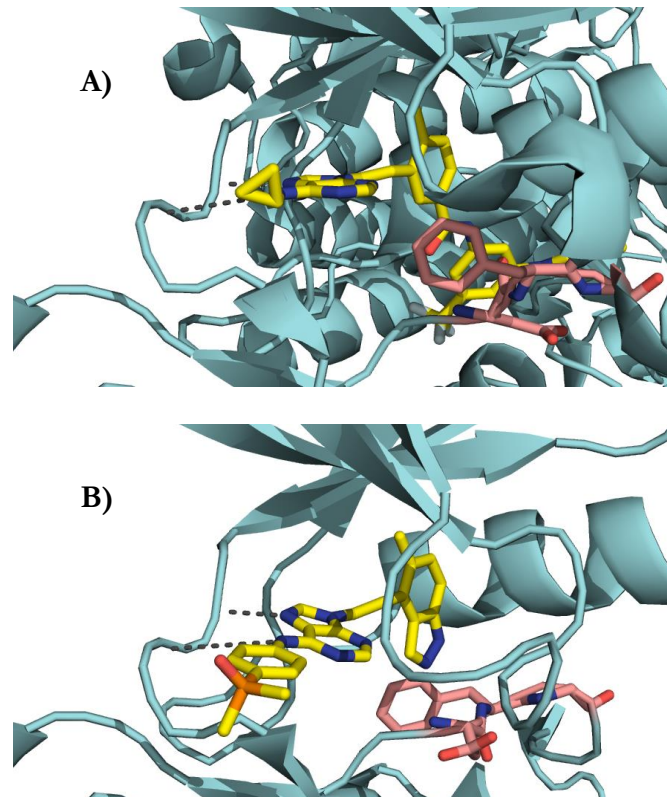


Fig. 3: A) DFG-out conformation of the protein kinase BCR-Abl (pdb 3KFA) with the bound inhibitor AP24283. B) AP24163 bound to the DFG-in conformation of BCR-Abl (3KF4).^[18] The DFG motif is shown in pink, the respective inhibitor in yellow and the hinge binding is depicted as dotted lines.

The c-helix-in form is the active form of a further subset of kinases including EGFR, where activation and formation of the c-helix-in form is often driven by dimerisation. Based on the rotation of the DFG motif or c-helix, specific allosteric pockets become accessible in regions adjacent as well as remote to the ATP-binding site.^[12,19] In inactive conformations on the other hand, special regions like the so called switch pocket (a pocket which is created when a kinase converts between its active and inactive form), or special hydrophobic motifs (e.g. in the autoinhibited inactive form of cMET) can be found.^[20]

1.2.1. Kinases and their medical relevance

Given the importance of phosphoryl transfer processes in cellular signalling, it is no surprise that the kinome has been extensively investigated as a family of potential drug targets.^[12] After the identification of the first kinase oncogene in 1978,^[21] the continuing development has led to a point where kinases are the second most pursued drug target family after G-protein coupled receptors,^[12] mainly because of the presence of an ATP binding pocket, which makes them easily amenable to medicinal chemistry efforts.^[7] Their signalling cascades regulate diverse cellular activities related to various diseases and indications including inflammation, pain, CNS disorders, autoimmune disorders, respiratory conditions, ophthalmology, cardiovascular disease and diabetes.^[19,22] The most important indication for kinase inhibition however is cancer, which is based on the deregulation of kinase function as one of the major mechanisms by which cancer cells avoid normal constraints on growth and proliferation.^[7] There is a vast amount of dysregulated kinase signalling known which influences the formation, growth and metastasis of cancer, however a summary of this data is beyond the scope of this introduction. One example, the kinase Pim1, will be covered at a later point.

1.2.2. Inhibition of kinases

A large number of small molecule kinase inhibitors (SMKIs) have been studied in the context of human diseases including cardiovascular diseases,^[23] autoimmune disorders such as rheumatoid arthritis,^[24] neurodegenerative conditions like Alzheimer's disease, diabetes or liver disorders.^[25] An overwhelming focus however lies, as previously mentioned, in the oncology field, where several protein kinase inhibitors have progressed through development and onto the market as approved therapeutic agents.^[12] Imatinib (**1**) was thereby the first small molecule, which has been FDA approved against cancer in 2001.^[21,26] This approval was a breakthrough, not only because kinases were considered an undruggable class of targets by some in the early days of kinase drug discovery, mainly because of the challenge to achieve selectivity and to avoid side effects related to their close structural similarities,^[12] but more importantly because it represented additional years of life span and a progress to cure for patients with several types of leukemia.^[27]

This milestone was thus followed by a slow yet steady approval of kinase inhibitors in the first 10 years of this century (see Fig. 4 for structures and binding modes). Concurrently, our understanding of kinase signalling networks and disease pathology steadily grew, culminating in the approval of yet another set of new small-molecule kinase inhibitors until 2016 (Fig. 5),^[19] giving a total of 28 SMKIs by the middle of 2016,^[26] along with a large number of other compounds

currently being evaluated in clinical and preclinical trials.^[19] All inhibitors, apart from nintedanib (**24**, indication: idiopathic pulmonary fibrosis) and tofacitinib (**16**, indication: arthritis), are thereby approved for different cancer indications.^[26] A regularly updated list of all FDA approved SMKIs and indications can be found on the internet.^[28]

In addition to the ever growing field of SMKIs, three macrolides including sirolimus (**29**, also known as rapamycin), temsirolimus (**30**), and everolimus (**31**), which are mammalian target of rapamycin (mTOR) inhibitors, have been approved by the FDA as immunosuppressants and anticancer agents.^[26] To cap it all, yet another significant amount of other pharmacological agents, which show their therapeutic effect by interacting with targets related to protein kinase signalling, have been FDA approved over the last 20 years or so, some even prior to imatinib (**1**). These include monoclonal antibodies like trastuzumab, cetuximab, bevacizumab and panitumumab, antibody fragments like ranibizumab, antibody-drug conjugates like trastuzumab emtansine, fusion proteins like afibercept, recombinant growth factors like becaplermin, palifermin and mecasermin, aptamers like pegaptanib, as well as recombinant insulin.^[29] However, when discussing kinase inhibitors in this work, macrolides and biologically designed pharmacological agents will not be further analysed, since their development and interaction modes differ highly from that of small molecules.

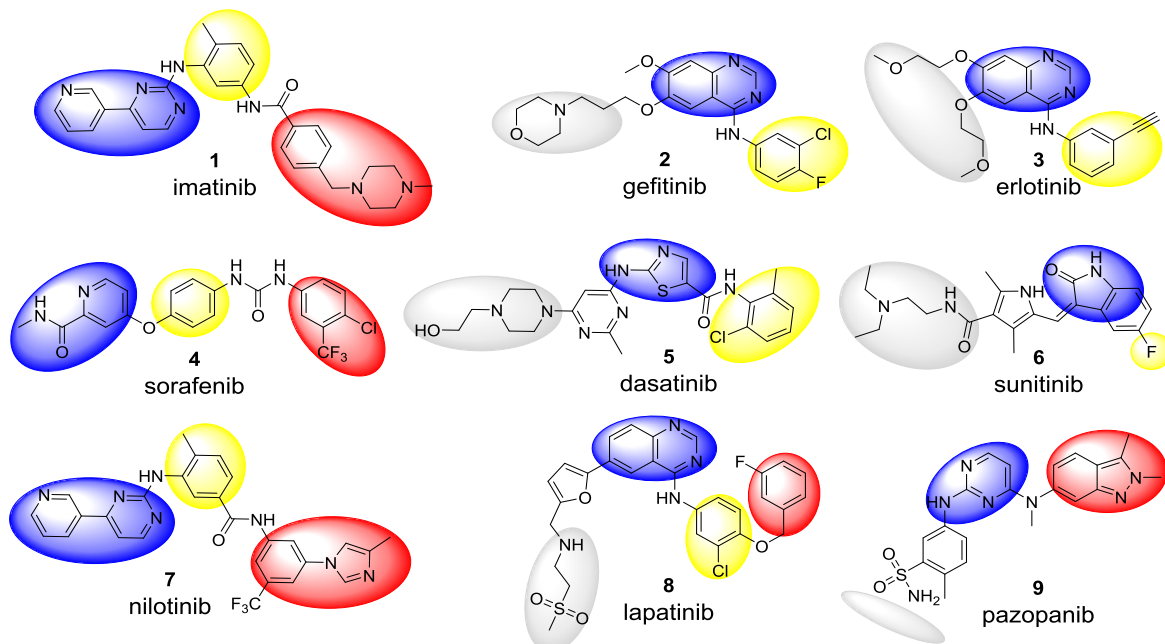


Fig. 4: First nine approved small molecule kinase inhibitors (2001-2009). Structural features are marked according to their binding sites to the kinases BCR-Abl (**1, 5, 7**), EGFR (**2, 3, 8**), VEGFR2 (**4, 6, 9**) which might not be their major targets: blue = adenine pocket, yellow = hydrophobic pocket, red = allosteric pocket, grey = solvent exposed region.^[19]

SMKIs are categorised according to their binding modes, and are grouped into the two classes reversible and irreversible. The former tend to covalently bind with a reactive nucleophilic cysteine residue proximal to the ATP-binding site, resulting in the irreversible blockage of the ATP site.^[19] The most prominent examples are the only two FDA approved irreversible kinase inhibitors ibrutinib (**20**) and afatinib (**21**), which use a chemically-active Michael acceptor electrophile that reacts with a cysteine nucleophile adjacent to the hinge region of the ATP-binding pocket to form a covalent adduct.^[19,26] Reversible inhibitors on the other hand, can be further classified into four main types based on the conformation of the binding pocket and the DFG motif.^[19] Many of them are ATP-competitive, typically displaying a H-bond donor-acceptor motif which interacts with key amino acid residues in the adenine binding pocket. The majority thereby binds in the active DFG-in state (type I inhibitors), mimicking the interaction of the adenine ring in ATP with the hinge region, thus often inhibiting multiple kinases.^[12] These type I inhibitors include gefitinib (**2**), erlotinib (**3**), dasatinib (**5**), sunitinib (**6**) and vandetanib (**13**).^[12] The selectivity of these inhibitors is thought to be triggered by interactions with the hydrophobic back cavity (selectivity pocket) based on structural differences between kinases found in this region. The size of that pocket, as well as the access to it, is controlled by the first residue of the hinge region (gatekeeper residue, Fig. 2). Targeting this pocket offers the potential of achieving good levels of selectivity, if the gatekeeper residue is appropriately small.^[12] Thereby, if mutations occur in the gatekeeper region, resistance may develop, meaning that inhibitors which do not use this allosteric pocket might be less sensitive to resistance mutations.^[3]

Type II inhibitors on the other hand, interact with the kinase in its inactive state e.g. DFG-out or c-helix out state, where an additional allosteric hydrophobic pocket is formed adjacent to the ATP-binding site, which the inhibitors might exploit. By binding to that state in a non ATP-competitive manner, they stabilise the inactive conformation.^[19,26] Leading examples include imatinib (**1**), sorafenib (**4**), nilotinib (**7**) and lapatinib (**8**). It was originally thought that these inhibitors are more selective by binding to these unique allosteric sites,^[12] however recent analysis showed, that this lead is unreliable.^[26] Still they often benefit from slower enzyme off-rates compared to type I inhibitors.^[20]

Both type III and IV inhibitors achieve certain levels of selectivity by using unique structural features of allosteric pockets of the targeted kinase. In the type III binding mode, inhibitors like trametinib (**23**)^[26] bind exclusively in an allosteric pocket adjacent to ATP without assuming any interaction with the ATP-binding pocket.^[19] Type IV inhibitors bind to an allosteric site remote from the ATP-binding pocket, but no inhibitor of this type has been FDA approved yet. Some kinase inhibitors, such as bisubstrate and bivalent inhibitors (type V), exhibit more than one of

these binding modes.^[19] The leading example is lenvatinib (**27**), which shows binding features of both type I and type II inhibition.^[26]

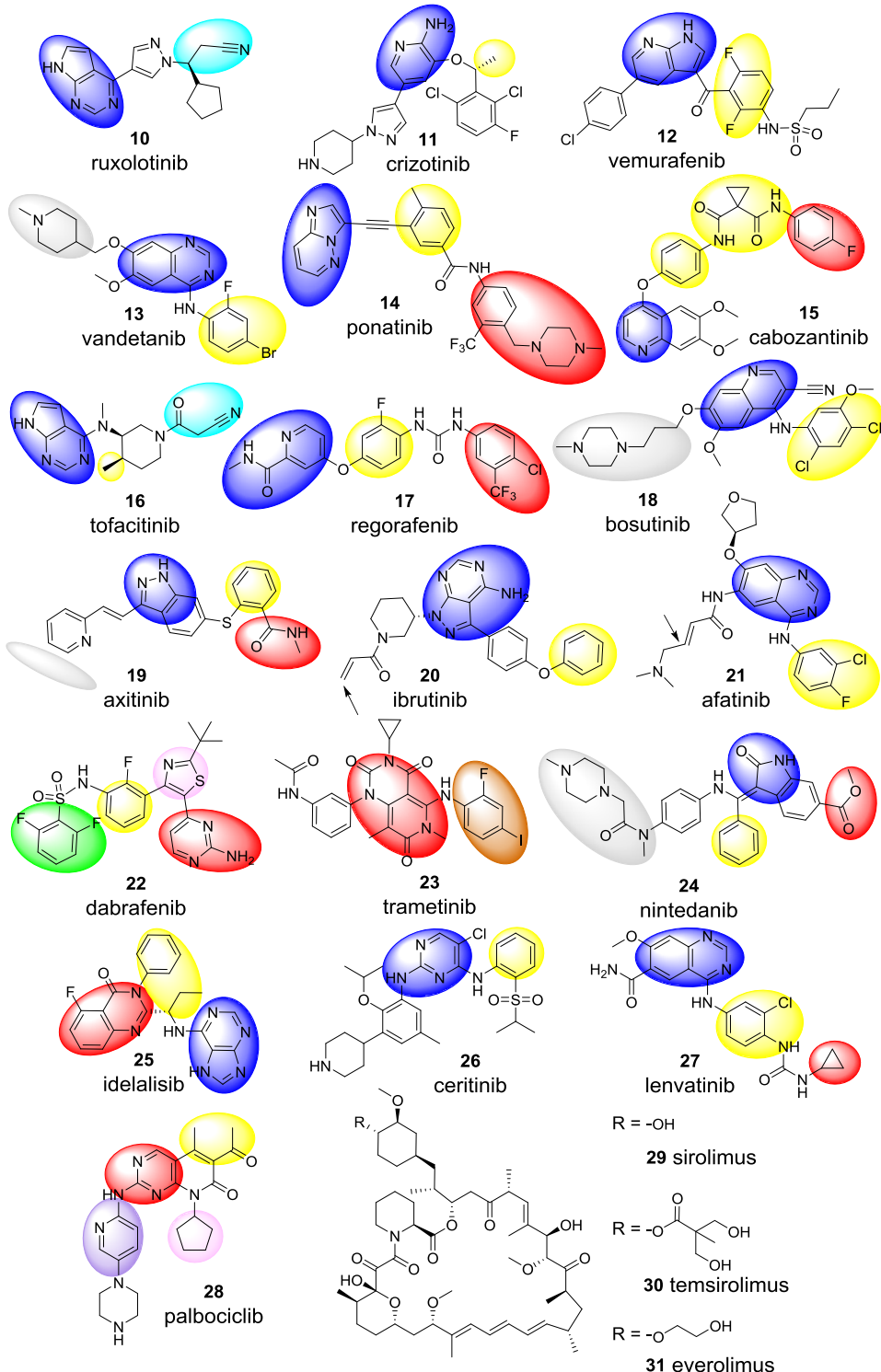


Fig. 5: FDA approved small molecule (2011-2016) and macrocyclic (1999-2007) kinase inhibitors. Structural features are marked according to their binding sites to JAK 2/3 (10*, 16), ALK (11, 26), B-Raf (12, 22*), RET (13), BCR-Abl (14, 18), MET (15*), VEGFR2 (17*, 19, 24, 27), BTK (20*), EGFR (21), PI3K δ (25) and CDK (28) (*based on homology to other inhibitors available in co-crystal structures^[19]): blue = adenine pocket, yellow = hydrophobic pocket, red = allosteric pocket, grey = solvent exposed region, cyan = P-loop cleft, pink = ribose pocket, purple = specificity pocket, green = RAS pocket, brown = MEK selective hydrophobic pocket, an arrow indicates the reactive group of irreversible inhibitors.^[19]

Introduction

As can be taken from the amount of FDA approved inhibitors, pharmaceutical companies have committed a major focus on kinase drug discovery over the last 20 years or so, producing a vast amount of compound collections well populated with agents able to provide hits within certain areas of this target class.^[20] In the development of SMKIs, as with most other drug targets, screening strategies frequently served as a starting point to find hits against a certain indication or target. Afterwards, medicinal chemistry approaches were used for further development, including additional screenings, computational chemistry methods and x-ray crystallography.^[14] This fact, in addition to the complexity of cancer signalling,^[13] is surely the reason that in the beginning of kinase inhibitor development, only a small subset of the human kinome has been studied, and that most kinase inhibition efforts are still limited to a select group of kinases.^[19] Among the 28 clinically approved kinase inhibitors, most are tyrosine kinase inhibitors, a few are serine/threonine kinase inhibitors, and only one, idelalisib (**25**), is a lipid kinase inhibitor that was approved in 2014.^[19] That being said, it is also important to mention, that various SMKIs are generally less selective, than originally suggested, ranging from highly selective inhibitors like lapatinib (**8**) which targets EGFR and ErbB2, to fairly promiscuous ones like sunitinib (**6**), which binds to multiple kinases.^[30] This demonstrates that probably more kinases are targeted than initially anticipated, probably as a result of their closely related binding sites. These non-selective kinase inhibitors (also called pankinase or multikinase inhibitors), which include approved drugs like dasatinib (**5**) and sorafenib (**4**), can be clinically useful, because simultaneous suppression of multiple kinases and thereby biological processes of the disease often seem to be required for a beneficial therapeutic effect.^[3,7] This is probably based on the possibility of homeostasis of kinase signalling networks. By recruitment of alternative kinases, signalling may be restored, which leads to an offset of inhibition. It is therefore also possible that inhibition of multiple kinases not severely comprise clinically tolerability.^[3] Therefore, although many of the initial SMKIs were not deliberately created for their multitargeting profile, a more rational design of molecules with multiple predefined targets has emerged, also embracing the concept of traditional combination chemotherapy and converting it to single molecules with multiple functions.^[7] Still the extent of selectivity required in order to deliver clinical efficacy against the intended disease together with imparting a favourable therapeutic window is a well debated subject.^[22] Though it is possible that homeostasis compensates for some unwanted effects, SMKIs are generally known to suffer from on-target, as well as unexpected off-target side effects (including inhibition of other enzymes binding ATP or adenine containing biomolecules) and cross-activity,^[3,14] still leaving a broad field concerning kinase signalling and inhibition for research to exploit.

1.2.3. The kinase Pim1 and its family members as cancer target

The proto-oncogene Pim1 (provirus integration site for Moloney murine leukemia virus)^[17] is a serine-threonine kinase belonging to the calcium/calmodulin-regulated kinases (CAMK) group,^[31] and the eponymous enzyme of the three members in the Pim family.^[32] It was originally identified from mouse lymphoma samples as a frequently activated gene resulting from the preferential integration of Moloney leukemia virus into the 3'-untranslated region of the *Pim1* gene.^[33] This integration created a premature stop codon in front of the AUUU(A) sequence at the 3' region in the *Pim1* transcript. The consequence is an unusually long-lived transcript (*Pim1* mRNA has generally a short half-life), which allows an increased level of translation and hence higher levels of Pim1 in the affected cells.^[34,35]

Rather than having to be activated by phosphorylation, the level of Pim enzymatic activity is dependent on the absolute amount of protein present,^[36] making the stability of the transcript the key regulator of Pim activity.^[37] This permanent catalytic activity is based on the large number of polar interactions from the activation segment with the lower kinase lobe, leading to a certain structural organisation. Generally Pim1 is an enzyme with a short half-life,^[32] which is protected from proteasomal degradation by HSP90 (heat shock protein 90), but marked by HSP70 for ubiquitylation and proteasomal degradation.^[38]

The *Pim1* gene encodes for two isoforms of 34 kD (Pim1S) and 44 kD (Pim1L) through the use of alternative initiation sites. Both isoforms contain the kinase domain and exhibit comparable *in vitro* kinase activity,^[32] but show distinct cellular functions, with Pim1S predominately localising to the nucleus and Pim1L localising to plasma membrane.^[39] Pim1 expression thereby is not only regulated at the transcriptional, but also at the posttranscriptional, translational and posttranslational levels^[32]. Transcription of Pim1 can be activated by several cytokines, such as IL-2 (interleukin-2), IL-3 and IL-6,^[39] followed by signalling transduction to the nucleus through two families of proteins, Janus kinase (JAK) or signal transducers and activators of transcription (STAT) (Fig. 6). Pim1 may thereby form a feedback loop with the JAK/STAT pathway via SOCS1 or 3 for tight regulation of its own expression and function.^[39]

Pim1 is a critical enzyme which is involved in multiple cellular functions such as cell cycle, cell growth, cell survival, differentiation, apoptosis, senescence and drug resistance.^[32,39] It is ubiquitously expressed throughout the body,^[32] and shows a high and specific expression in liver, spleen and bone marrow in typical hematopoietic progenitors during embryonic development.^[40,41] In the adult stage it is only slightly expressed in circulating granulocytes^[40] and shows nearly undetectable expression in healthy tissue in general.^[17,36] The expression of Pim1 during development and its subsequent shut off in adult tissues suggests that its untimely overexpression

may contribute to malignant transformation.^[41] And indeed, its activity and especially overexpression supports *in vitro* and *in vivo* tumour cell growth and survival through modification of a number of common as well as isoform-specific substrates, including several cell cycle regulators and apoptosis mediators.^[17,36,39] In hematopoietic malignancies and in a variety of solid tumours it is known to be overexpressed, with a higher expression level in hematologic than solid organ malignancies. The degree of expression has been shown to correlate with the stage of disease and a poor prognosis.^[17,36]

Pim1 overexpression appears to contribute to cancer development and survival in three major ways; by inhibiting apoptosis, by promoting cell proliferation and by promoting genomic instability,^[17,36] thereby making the cells prone to multiple drug resistance.^[42] However there are numerous mechanisms which involve Pims leading to oncogenic effects, too many to be covered here, which have recently been reviewed in literature.^[37] A brief overview over selected interaction partners is given in Fig. 6.

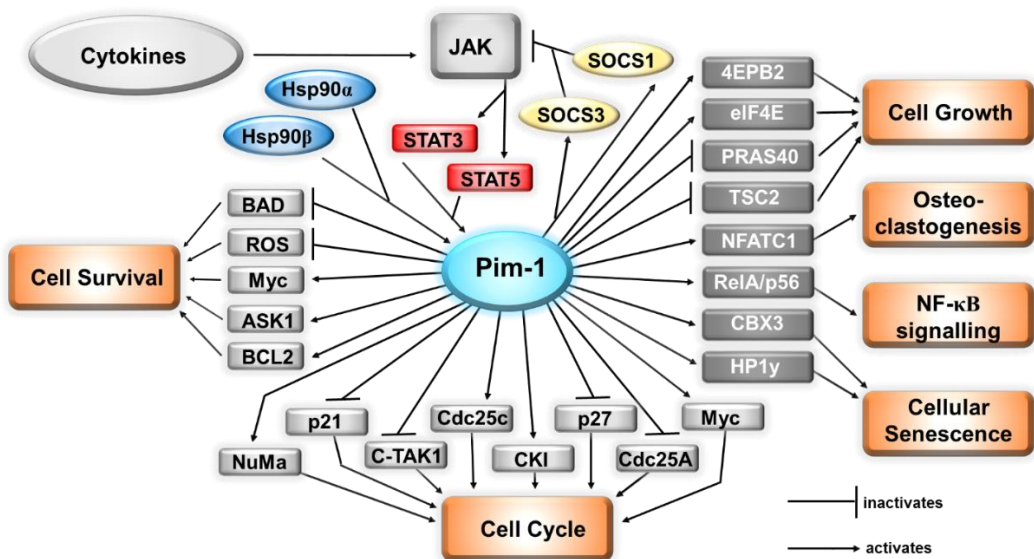


Fig. 6: Proviral integration site for Moloney murine leukemia virus-1 (Pim1) is regulated through the Janus kinase (JAK)/signal transducers and activators of transcription (STAT) pathway and regulates multiple signalling pathways, such as cell survival, cell cycle and cell growth.^[39]

One of the features, making Pim1 an attractive drug target, is that the knockout of *Pim1* in mice is not lethal nor does its absence induce any immediately obvious phenotype.^[36,43] Yet, elimination of Pim1 activity is lethal to overexpressing cancer cells, leading to the conclusion that targeting Pim1 would avoid detrimental side effects that occur with most conventional treatments.^[36]

Inhibition of Pim1 has shown to lead to effects like induction of apoptotic cancer cell death or sensitisation to chemotherapy.^[36] E.g. inhibition of Pim1 in the cytosol, nucleus and surface of

cancer cells by a monoclonal antibody was able to disrupt Pim1/Hsp90 complexes, inhibit the phosphorylation of BAD and induce the mitochondrial apoptotic pathway in cancer cells, while overcoming the Pim1 related drug resistance.^[17,41,44] That, in combination with its interaction with different proteins and association with various signalling pathways, some of them presented in Fig. 6, makes it an important therapeutic antitumor target.^[39] In fact several recent studies demonstrated that functional interference with Pim kinases impaired growth and survival of cancer cells.^[17] Studies with murine models of AML have demonstrated however, that a high tumour burden persists despite of improved survival with Pim inhibition,^[45] suggesting that disease control, rather than significant tumour killing, is the realistic effect of Pims as single target.^[37] By itself, Pim1 seems not to be a strong oncprotein, but when expressed with other proteins such as Myc, it exerts a potent synergistic transforming effect on cells, particularly when the functions of those proteins are involved in proliferation and cell survival.^[46]

Pim1 features a classic protein kinase domain architecture with all conserved structural elements, except from a unique beta hairpin insert located N-terminal to helix α C. The ATP-binding in this kinase however differs from usual kinases insofar, that a proline residue in the hinge region (P123 Fig. 7) prevents the formation of the second hydrogen bond from the hinge backbone to the adenine (c.f. Fig. 2). The hinge region additionally differs from other kinases, due to an additional residue in this region, resulting in the hinge sequence ERPXPX.^[17]

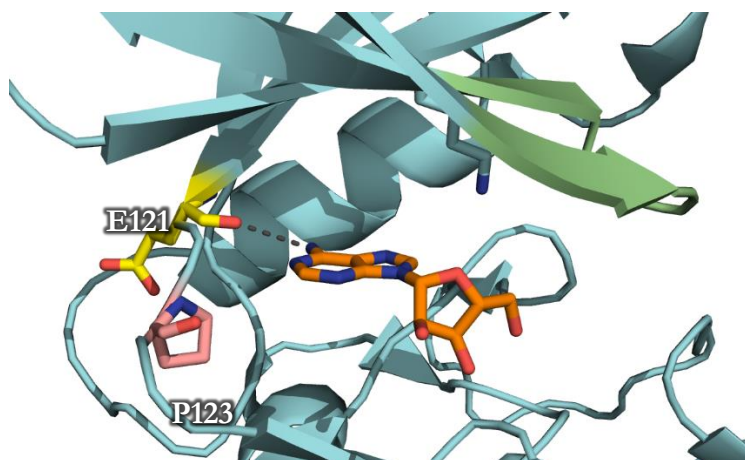


Fig. 7: Adenine (orange) bound to the active site of the kinase Pim1 (pdb 1YI4).^[47] Adenine binds to Pim1 via a hydrogen bond to E121 (yellow). The unique P123, which prevents adenine from forming a second hydrogen bond is shown in pink. K67, which is known to interact with many Pim1 inhibitors is indicated in stick format and the glycine rich loop is shown in green.

Based on this unique hinge architecture very selective inhibitors for the Pim kinases can be identified, and various inhibitors have been reported.^[17] A considerable amount of these inhibitors display different classes of highly potent Pim1 inhibitors, including ruthenium-containing

Introduction

organometallic complexes,^[48,49] bisindolylmaleimides,^[50] imidazo[1,2-*b*]pyridazines,^[51] pyridones,^[52] flavonoids,^[53,54] benzoisoxazoles,^[55] isoxazoloquinoline-3,4(1*H*,9*H*)-diones,^[56] 5-arylidene-2,4-thiazolidinediones,^[57] cinnamic acids,^[58] 3*H*-benzo[4,5]thieno[3,2-*d*]pyrimidin-4-ones,^[59] but also P9 monoclonal antibodies.^[39] Most Pim1 SM inhibitors work either as ATP competitors or ATP mimetic compounds.^[17,36] These compounds interact via polar interactions with the active site K67 and a conserved water molecule, anchoring the inhibitors to the back of the ATP binding pocket. The binding is additionally stabilised by a number of hydrophobic interactions,^[17] and several inhibitors use halogen atoms to interact with the hinge region.^[36]

A drawback in Pim1 inhibition can however be found in the fact that there exists a certain potential compensatory mechanism between the Pim family members, which suggests that inhibitors should block all Pim kinases for efficient cancer therapy, even if only Pim1 is thought to have a significant impact on tumour formation.^[7,17] Despite the high homology (>60% in amino acids) in the ATP binding pocket, several proposed small molecule Pim inhibitors preferentially inhibit the activity of Pim1 and Pim3 rather than Pim2,^[17] which might be related to the fact that the K_M (MICHAELIS-MENTEN constant, the concentration of substrate that leads to half maximal velocity) of Pim2 for ATP is up to 100-fold lower than that of Pim1 and Pim3.^[60] This fact makes the design of a pan-inhibitor more challenging in comparison to the development of specific inhibitors.^[37,60,61]

The development of pan-Pim inhibitors is still very successful. The first SM pan-inhibitor to enter the clinic was SGI-1776,^[7,31] which induces apoptosis in Pim1 overexpressing cells. In a preceding study using K562 and HEL92.1.7 cells with either an Hsp90 inhibitor or with the pan-histone deacetylase inhibitor panobinostat (**36**), it was shown that the Pim1–Hsp90 association was disrupted and, at the same time, Pim1 binding to Hsp70 was increased, which led to proteasomal degradation of Pim1.^[36] The clinical trials for this compound however were terminated early because of cardiac toxicity.^[31] A second generation inhibitor AZD1208 followed,^[39] but was discontinued due to lacking evidence of anti-tumour activity from monotherapy treatment.^[62] There are still two pan Pim inhibitors in clinical trials, one of them LGH447 (respectively PIM447) a specific pan-Pim kinase inhibitor, which is tested as single agent (e.g. NCT02078609) and in combination with midazolam (NCT01456689), a PIK3 α inhibitor (NCT02144038) and a JAK1/JAK2 or CDK4/6 inhibitor (NCT02370706). The second one is INC053914, a novel ATP-competitive SM pan-inhibitor of Pim kinases^[63,64] which is recruiting as of September 2016 (NCT02587598).^[65] All these efforts, not only basic research but also development for the clinic, suggest that the Pim family is a master drug target in numerous types of cancer.^[39]

1.3. Histone deacetylases

Due to their key role in the epigenetic gene expression by controlling the grade of acetylation of positively charged lysine residues located at the N-terminus of histones, which are the main protein component of chromatin, around which DNA coils, histone deacetylases (HDACs) are another oncologically interesting group of enzymes. If these N-terminal lysines are positively charged, they may interact with the negatively charged DNA phosphate backbone, leading to a very condensed chromatin structure, allowing little access for transcription proteins.^[66,67] Hyperacetylation of these N-termini on the other hand, by inducing a loss of positive charges, has the opposite effect and leads to an open chromatin structure and an increase in the expression of particular genes.^[66,68] The acetylation status thereby is not only governed by HDACs but also the counteracting histone acetyltransferases (HATs).^[66,69]

Apart from histone deacetylation, a function that the name “histone deacetylases” implies, HDACs also act as general lysine deacetylases, being responsible for the removal of acetyl groups on a vast array of nuclear and cytoplasmic proteins.^[70,71] A high-resolution mass spectrometry study for example identified 3600 lysine acetylation sites on 1750 mammalian proteins.^[69,72] However, research is just starting to grasp the role of acetylation of non-histone target proteins.^[71]

Overall 18 distinct human HDACs have been identified to date, which can be categorised into four classes based on the sequence homology to their *Saccharomyces cerevisiae* analogues. Class I (HDAC1, 2, 3 and 8), class IIa (HDAC4, 5, 7 and 9), class IIb (HDAC6 and 10), and class IV (HDAC11) are zinc(II)-dependant metalloproteins, while the class III proteins (also known as sirtuins (Sirt1–Sirt7)) are structurally distinct and characterised by their nicotinamide adenine dinucleotide (NAD⁺) dependency.^[69,71,73,74] In this thesis, when talking about HDACs, only the zinc-dependant isoforms are considered, hence the term HDAC is always used with respect to class I, II and IV.

Class I HDACs are homologous to yeast RPD3, share a compact structure (350-500 amino acids), and are ubiquitously expressed proteins, which are located almost exclusively in the cell nucleus.^[71,75,76] They show the strongest enzymatic activity amongst the HDAC classes and their function, with the exception of HDAC8, is dependent on the formation of large multiprotein complexes, which often involve more than one HDAC subunit and are frequently in association with corepressor proteins.^[68,69,75,77] HDAC8 is an atypical HDAC family member, which is expressed tissue specific and shows deacetylase activity as a single polypeptide.^[69] The main structural difference to the other class I HDACs is an abbreviated C-terminal domain.^[78]

Class II HDACs are homologous to yeast HDA1 protein and can be further subdivided into two subclasses, IIa (HDAC4, 5, 7 and 9) and IIb (HDAC6 and HDAC10), based on their protein sequence homology and domain organisation. Class IIa HDACs have one catalytic domain and a

Introduction

long N-terminal adaptor domain, while class IIb HDACs 6 and 10 contain a duplicated catalytic domain, although this duplication is partial and catalytically inactive, in the case of HDAC10.^[69,71,79] Compared to class I, class II HDAC expression pattern is more restricted and their function is more tissue specific. Class IIa HDACs seem to have weak deacetylase activity and they may therefore more likely function as histone readers or as scaffold proteins, incorporating enzymatically active HDACs into multiprotein complexes.^[80,81] They can shuttle between the nucleus and the cytosol in response to different stimuli, whereas HDAC6 and HDAC10 mainly localize in the cytoplasm.^[69,75,79]

HDAC11 is the only known member of class IV HDACs, but very little information is available about its expression and function.^[75] Size, cellular locations, expression patterns and physiological functions of the Zn-dependant HDAC-isoforms vary widely and were summarised in various publications.^[70,75,76,82]

The active site of the zinc-dependant HDAC isoforms is structurally highly conserved^[69] and comprises an 11 Å deep hydrophobic pocket which allows access to the catalytic centre in which the Zn(II)-ion can be found (Fig. 8). The residue composition of this tubular access is almost conserved in all HDACs and an alanine residue scan mutagenesis revealed the importance of all the residues found in the channel.^[76] The zinc ion in the active site of HDAC class I/II is coordinated to two aspartic acids and one histidine, and the environment around it is generally considered common to all zinc dependant HDACs, with some possible residue changes (Fig. 8 B).^[76] A systematic comparison of the crystal structures of HDAC1, 2, 3, 4, 7, and 8 however revealed the differences between the enzymes, which can be found at the surface close to the entrance of the active site, at the enzymatic site as well as at the acetate release channel placed at the bottom of the active site channel (foot pocket). One example is found in HDAC8, which, when co-crystallised with different inhibitors, may or may not possesses a deep hydrophobic pocket adjacent to the active site channel, indicating a highly dynamic region next to the opening of the active site.^[69] Another example is the replacement of a tyrosine residue by a histidine in class IIa HDACs, leading to the afore mentioned decreased catalytic activity towards acetyl-lysine substrates, as well as an enlarged cavity.^[69,81]

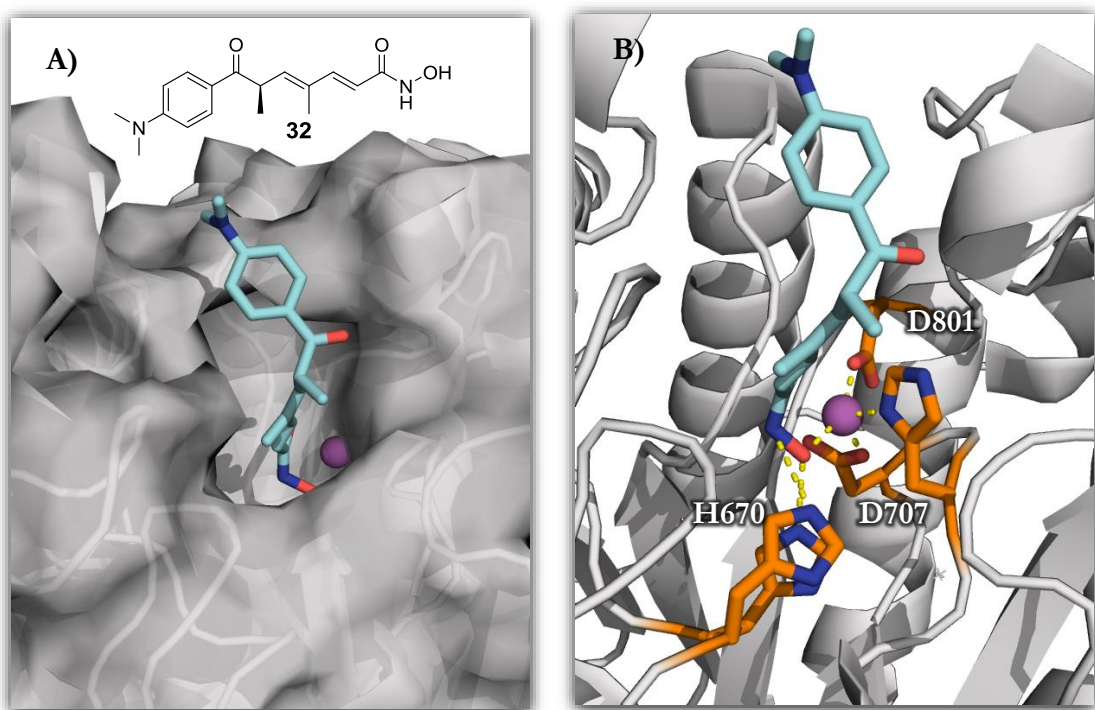


Fig. 8: The active site of human HDAC7 (grey) with the natural product trichostatin A (**32** TSA, cyan) bound to it (pdb entry 3C10).^[83] A) The hydroxamate of TSA lies deep in the hydrophobic pocket coordinating to the catalytically important zinc-ion (magenta), while the dimethylaminophenyl-group is pointing outwards. B) Key interactions of zinc-coordination: While the zinc-ion is directly coordinated by H709, D707 and D801, the two residues H669 and H670 form hydrogen bonds with the hydroxamate moiety of TSA, which itself forms a monodentate complex with the catalytic zinc ion. This is an atypical behaviour, which is triggered by a somewhat different topology of the active site related to the lack of a tyrosine residue in class IIa HDACs. This leads to a different orientation of the hydroxamate and a coordination of the carbonyl oxygen to a water molecule in the HDAC7 active site. Normally hydroxamates form a bidentate complex with the zinc-ion.^[69,83]

1.3.1. HDACs and their medical relevance

HDACs have shown to be involved in different pathologies such as diseases of the central nervous system, inflammation, infection^[69,70] and cardiac disease.^[71] The main focus on HDACs in a medical context is drawn towards their involvement in cancer. HDACs are known to be often over- or under-expressed in cancer cells and their inhibition may lead to variable cellular responses. According to different reviews these include, but are not limited to, cell cycle arrest, suppression of cell proliferation, inhibition of angiogenesis, reversal of differentiation, enhanced immunogenicity and antigen-presenting capacity, enhanced reactive oxygen species (ROS) production and decreased free radical scavenger production, accumulation of DNA damage through transcriptional downregulated and impaired DNA repair proteins, inhibition of DNA replication, immunogenic cell death, senescence, intrinsic and extrinsic apoptotic mechanisms, induction of differentiation and mitotic or autophagic cell death.^[66,70,73,75,80] The molecular mechanisms underlying these effects of inhibition however remain to be fully elucidated^[75] and it

is assumed that more than one mechanism of action is responsible for the antitumour effects across different tumour types mediated by inhibitors with diverse specificity profiles.^[75,80] The predominant mode of action is thought to be the induction of apoptosis,^[84] which occurs through altered expression of genes encoding proteins in both intrinsic and extrinsic apoptotic pathways; through effects on the proteasome/aggresome systems; through the production of reactive oxygen species and through alterations in the tumour microenvironment.^[85] Generally spoken, it is assumed that the overall modulation in gene expression is not solely based on an altered histone acetylation degree.^[71] This assumption is supported by diverse studies, one of them showing that, although inhibition of HDACs induces global protein acetylation, probably only 2–10% of genes' expression is significantly changed, with almost similar numbers of genes upregulated and downregulated.^[86] Additionally, analysis of two promoter regions from genes differently affected by HDAC inhibition showed that promoters of both, downregulated and upregulated genes, displayed increased acetylation.^[87]

1.3.2. Inhibitors of the zinc-dependant HDAC isoforms

HDAC inhibitors (HDIs) as potential anticancer agents, like various other drugs, were originally discovered through empirical screening for substances that induced tumour cell differentiation, without the initial knowledge of their molecular targets.^[70] Nowadays HDACs are attractive targets for drug discovery programs, with a significant number of inhibitors identified and over 400 PCT (Patent Cooperation Treaty) patent applications submitted over the last two decades.^[88] More than 350 clinical trials have been completed or are underway using HDAC inhibitors for the treatment of various human malignancies with a focus on haematological tumours, both as single agents and in combination with chemotherapies and other targeted therapeutics.^[70,75,80,82] To date, the FDA has approved three HDAC inhibitors for cutaneous or peripheral T-cell lymphoma (CTCL/PTCL): The suberanilohydroxamic acid SAHA **33** (vorinostat, approval for CTCL 2006), the cyclic peptide FK228 **34** isolated from *Chromobacterium violaceum* (romidepsin, approval for CTCL 2009, PTCL 2011) and the hydroxamic acid belinostat **35** (approval for PTCL 2014) (Fig. 9).^[69,80,82,89] Currently all three drugs are being further studied for other diseases as well as other haematological malignancies and solid tumours, either as a single agent or in combination with other drugs.^[82] More recently, in addition to that, the hydroxamic acid panobinostat **36** (approval 2015) (Fig. 9) has been FDA-approved as combination therapy with bortezomib (proteasome inhibitor) and dexamethasone (steroid medication) in patients with recurrent multiple myeloma, who have received at least two prior treatment regimens, including bortezomib and an immunomodulatory agent.^[90]

In general, HDIs are classified into distinct structural groups, including the previously mentioned hydroxamic acids and cyclic peptides, as well as carboxylic acids (valproate, butyrate), aminobenzamides (entinostat, mocetinostat), epoxyketones (trapoxins), and hybrid molecules.^[80] The most widely explored class of HDAC inhibitors, as evident from the FDA approvals, are hydroxamic acid-derived compounds.^[82] Based on the highly conserved active site of zinc-dependant HDACs, the pharmacophore for these inhibitors mostly includes three regions: a zinc-binding group, such as a hydroxamic acid, carboxylic acid or benzamide, which chelates the zinc-ion inside the active site, a solvent exposed cap-region which interacts with the protein-residues at the entrance of the active site pocket, and a linker which connects the other two regions and accommodates the hydrophobic tubular access of the active site (Fig. 9).^[70,76,82]

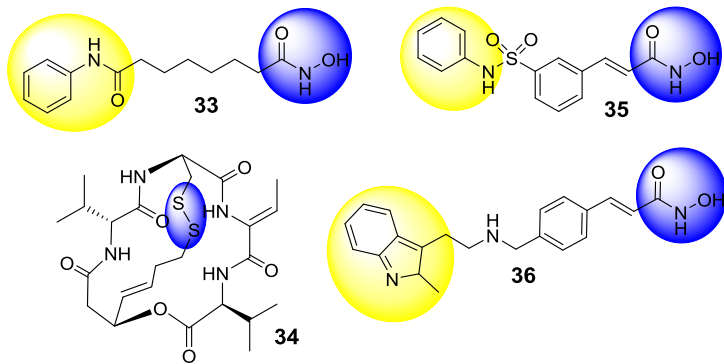


Fig. 9: The FDA approved HDAC inhibitors SAHA (33), FK228 (34), belinostat (35) and panobinostat (36). The regions which are thought to be the pharmacophore are highlighted: the zinc-binding groups are marked in blue, while for SAHA, belinostat and panobinostat the capping group (see below) is marked in yellow. In the three hydroxamic acid structures these two regions are connected by an organic linker which fills the hydrophobic pocket. For FK228 most of the peptide is seen as the capping group.

The first generation of HDIs, including the approved compounds SAHA **33** and panobinostat **36**, as well as the reference natural product TSA (**32** Fig. 8), did not show any particular selectivity towards specific isozymes, and are classified as pan-HDAC inhibitors.^[75,80] Other HDI derivatives are class I selective (e.g. the carboxylic acids like valproic acid (VPA) or sodium butyrate) or prefer class I over class II, like the depsipeptide FK228 **34**.^[69,75] The development of such class- or isoform-specific inhibitors for the treatment of different cancer forms seems highly desirable to avoid off-target effects, since for example knockdown of HDAC1 or 2 is sufficient to reduce tumour growth *in vivo* and knockdown of class IIb HDACs induced the growth arrest of a variety of human solid tumour cell lines.^[80] For achieving selectivity and specificity, variations in the zinc-binding groups have shown to be promising, including chelating groups like benzamide derivatives, thiols, sulphamides, ketones and trithiocarbonates.^[91] Additionally, variations in the cap region, which is considered predominantly responsible for selectivity, are being used to design inhibitors

Introduction

that target different HDAC isoforms by using the variation in amino acids at the entrance to the active site.^[67] Besides, HDACs involved in specific complexes may be targeted, as the cap region cannot only bind to the HDAC itself but also to other complex components near the active site.^[76,92] Finally, linker modifications may also serve to direct specificity, such as the addition of an aromatic ring that can fit into the enlarged catalytic pocket of HDAC7 that is not present in class I or class IIb HDACs.^[70,93] The target specificity of HDIs and the requirement for specific and selective inhibition of HDACs to achieve therapeutic efficacy still remain topics of debate.^[80] One reason for that might be, that no major differences concerning the toxicity profile were observed between pan-HDAC inhibitors, class I selective inhibitors or FK228.^[69]

Despite positive responses in patients with hematologic malignancies, existing HDIs have only proven effective for the treatment of a relatively small population of patients and their effect on most other tumours is marginal at best.^[80] Therefore, it has been speculated that HDIs, despite of the potency and reasonable toxicity profile of newer agents (second generation inhibitors), are unlikely to make a substantial impact in the clinic when used alone, and that the future of this very promising class of agents lies in rational combination therapy,^[80,84] where a growing number of preclinical and clinical studies have demonstrated synergistic effects and more efficient and tumour specific anticancer activities.^[75,82] A large number of rational HDI-based combinations is indeed possible, and new ones continue to emerge.^[94] For a deeper insight into this topic, diverse reviews are recommended.^[95–98] Briefly, combinations including cytotoxic chemotherapy, hypomethylating agents and proteasome inhibitors have advanced the farthest,^[94] but also UV rays,^[82] ionising radiation^[75,82,98,99] and dual inhibitors combining HDAC inhibition e.g. with targeted therapy against PI3K, tyrosine kinases, topoisomerase II or nuclear receptors,^[100] may be of interest for distinct cancer subtypes.^[80]

One particular example for the combination of HDIs and cytotoxic chemotherapy includes well established platinum drugs as promising treatment strategy. HDIs thereby act as chemosensitizers, since the chromatin relaxation, which is accompanied by histone hyperacetylation, allows easier access to the DNA and therefore more platinum-DNA adduct formation occurs. This concept has been proven successful *in vitro* and *in vivo* in various studies for many cancer types and stages and has also been reviewed recently.^[95]

1.4. Metals in medicine

Having mentioned platinum drugs in the previous chapter, it becomes clear that metal-based compounds might serve as promising drugs. Metal-based therapeutic or diagnostic agents have various applications today, with structurally most simple and probably best known examples being lithium carbonate (Li_2CO_3) for the treatment of bipolar disorder, or barium sulphate (BaSO_4) as X-ray contrast agent in the gastrointestinal tract.^[101] Interestingly the first accounts of pure inorganic compounds are as old as 3500 years, where a suspension of rust was administered as a cure of impotence, and iron compounds have often been used since for the treatment of anaemia.^[102] In addition to that, the earliest reports on therapeutic use of metals or metal based compounds in cancer and leukaemia date from the sixteenth century.^[103]

The first metal containing compound which was used in the clinic against cancer worldwide, and which is still probably one of the most successful anticancer drugs, is one of the afore mentioned platinum drugs, cisplatin [$\text{Pt}(\text{NH}_3)_2\text{Cl}_2$], which has been discovered by serendipity in the 1960s, and was FDA approved in 1978. Cisplatin is a prodrug, which, after entering a cell, undergoes aquation in a way that one chlorido ligand of the active metal centre is displaced by an aqua ligand due to the lower chloride concentration inside the cell. The new complex might then enter the cell nucleus and react with the DNA, by forming intrastrand, interstrand or DNA-protein cross-links. If the resulting lesions are not repaired, the cell undergoes apoptosis. The side effects associated with cisplatin treatment can be severe and may include renal and nervous toxicity, hearing difficulties, nausea, vomiting, and several others.^[104] Still, the clinical success of this anticancer compound has inspired extensive investigation into the utility of transition-metal complexes as diagnostic or therapeutic agents. Based on their wide spectrum of coordination numbers and geometries as well as kinetic properties, metal compounds offer mechanisms of drug action, that cannot be realised by organic agents, which still represent almost all drugs placed on the market nowadays.^[105,106]

Various newer generations of platinum-based drugs like carboplatin and oxaliplatin are available today,^[104] as well as other FDA approved metal-based compounds like auranofin for the treatment of rheumatoid arthritis or arsenic trioxide against acute promyelocytic leukemia, to just give some examples.^[102] In fact, to date practically all transition and main group metals have been tested for antitumour properties and other indications, with diverse outcomes.^[107] The platinum based compounds however remain the only approved precious metal-based anticancer drugs.^[108]

1.4.1. Metal templates as structural feature for enzyme inhibitors

Most metal-based compounds like cisplatin use active metal centres as source of bioactivity and, in one way or another, interact with DNA as the primary target. However, metals can also be used as inert anchors to shape the overall structure of a compound and to synthesise small and medium-sized globular molecules in a very economical fashion.^[109] Taking into account Emil Fischer's "Lock and Key Model" from 1894, where the lock is the specific structure of the enzyme in the active site and the key is the inhibitor,^[8] using a metal as the centre of the molecule, the key can be designed in a much tighter-fitting way due to the expanded structural complexity possible (Fig. 10, e.g. octahedral complexes may form up to 30 stereoisomers when using six different monodentate ligands). This enzyme-inhibitor concept was expanded in the 1950s by Daniel E. Koshland's "Induced Fit" theory, which gives a more accurate picture of the interactions, since an enzyme is not a static but flexible structure, which might undergo structural rearrangement when the substrate or inhibitor binds.^[8]

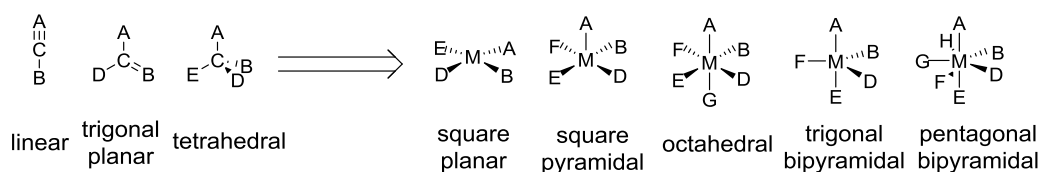


Fig. 10: Extension of coordination geometry from linear, trigonal planar and tetrahedral as it is formed by carbon, to square planar, square pyramidal, octahedral, trigonal and pentagonal bipyramidal possible around a metal centre (M). A-H are residues or ligands around the respective central atom.

Over the last decades, various groups have demonstrated the high versatility of inert metal complexes as powerful structural templates for the creation of such "key" structures for targeting proteins, with a large variety of reactive and inert protein-binding metal-containing compounds being available today as tools for chemical biology or as drug candidates.^[110–120] The unique possibility of fine tuning the shape of inert sophisticated structures, by projecting the coordinated ligands into three-dimensional space, which fit tightly into an enzymes active site, thereby improving affinity and selectivity, may be one reason for the increasing use of this type of compounds. While Dwyer pioneered the field, using polypyridyl complexes as biologically active compounds with inhibitory properties against acetylcholinesterase over 60 years ago,^[112,114] there is of course a much broader range of inert metal complexes as well as applications available today, still leaving polypyridyl complexes as one of the most important areas of research with their DNA-binding, cytotoxic and enzyme inhibiting properties.^[111,113,115–118]

A broad and important field of metal-based compounds are sandwich and half-sandwich complexes as scaffolds for metal complexes, which target biomolecules. Whereas octahedral coordination geometries offer a large structural complexity,^[120] half-sandwich complexes offer the advantage that they are typically much easier to synthesise.^[48,49,121,122] There are three main reasons to use sandwich complexes shown in the literature: The use as isosteres for purely organic groups, the improved uptake of cells and the occupation of unexplored chemical space.

Some recent studies confirm the efficiency of replacing organic moieties by ferrocene in different types of bioactive compounds, structural examples can be found in 1.4.2 and 1.4.3.^[118] Beyond ferrocene (**37**), ruthenocene (**38**) and ruthenium(II) pentamethylcyclopentadienyl benzene sandwich complexes have been reported as potent carbonic anhydrase inhibitors (Fig. 11),^[123–125] revealing that not only the structure, but also the metal itself has an impact on the inhibition potency. Complex **38** is thereby almost an order of magnitude more potent ($K_i = 9.7 \text{ nM}$) than the analogous ferrocene derivative **37** ($K_i = 80 \text{ nM}$) for human carbonic anhydrase II (hCA II).^[126]

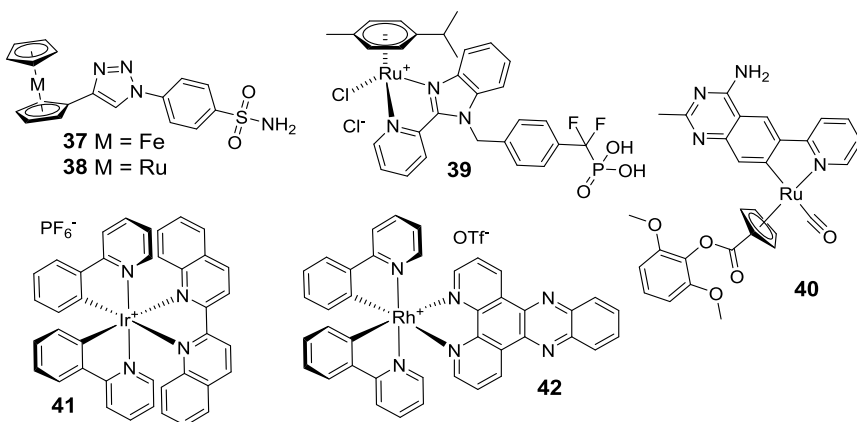


Fig. 11: Selected examples for metal-based compounds with enzyme inhibition properties, based on metallocenes, Ru half-sandwich complexes and Ir and Rh polypyridyl complexes.

Though, not every incorporation of a metal-containing moiety leads to an improvement in affinity or activity. This might be related to an increased space demand.^[127,128] An example for modulated cellular uptake was given using a ferrocene-containing bioorganometallic inspired by the antibiotic platensimycin, which, according to modelling, fits nicely into the targets (FabF) active site, but shows no antibacterial activity up to 200 mg/mL.^[129] Besides sandwich-compounds, half-sandwich complexes are popular metal-containing scaffolds for the design of protein binders, including recent reports of arene-Cr(CO)₃-containing analogues of the antibiotic platensimycin,^[130] Cr(CO)₃ coordination to anti-inflammatory diterpenes,^[131] Re(CO)₃- and ^{99m}Tc(CO)₃-cyclopentadienyl complexes for targeting of human carbonic anhydrase IX^[132] or amino acid transporters.^[133] In recent reports, η^6 -arene ruthenium half-sandwich complexes were used as templates for a broad

range of metal-based bioactive compounds, such as piano-stool complexes inhibiting carbonic anhydrase II,^[134] selective organoruthenium inhibitors of protein tyrosine phosphates 1B (**39**),^[135] as well as for the development of organoruthenium antagonists of human A3 adenosine receptor.^[136] A ⁵ η -cyclopentadienyl ruthenium half-sandwich complex (**40**) was recently reported as a single digit nanomolar inhibitor for the human repair enzyme 8-oxo-dGTPase.^[137] Octahedral complexes often cover the afore mentioned polypyridyl complexes, and recent examples are given with cyclometalated iridium(III) and rhodium(III) complexes **41** and **42** as tumour necrosis factor- α (TNF- α) and NEDD8-activating enzyme (NAE) inhibitors.^[138] For more examples of metal-based compounds as inhibitors for kinases and HDACs please refer to the following two chapters.

1.4.2. Metal-based kinase inhibitors and their *in vitro* and *in vivo* properties

The use of metals to design kinase inhibitors is an ever-growing field, still being in its infancy. However, a range of structures and purposes for the choice of using a metal can be found in literature. Apparently, these include hybrid molecules which incorporate platinum to enhance structural complexity and/or functionality such as drugs with dual mechanism of action. Structurally simple planar Pt(II) complexes, like the 1,10-phenanthroline derived **43** (Fig. 12) serve as micromolar MAPK and CDK2 inhibitor, with much higher potency of the complex compared for the ligand.^[139] Other examples for Pt-hybrids include Pt coordination compounds to organic TK like imatinib (**1**) or CDK inhibitors.^[140,141] An oxaliplatin based imatinib analogue was thereby shown to circumvent TKI resistance, predominately mediated by the emergence of secondary mutations on oncogenic kinases, probably based on their dual mechanism of acting both as KI for the same oncogenic kinases and as DNA damaging agents, as well as a slightly different binding to the ATP binding pocket of BCR-Abl E255K.^[140] CDK inhibitor-cisplatin hybrids like the 6-benzylamino-9-isopropylpurine derived dimer **45** have shown anticancer activity in the micromolar region in different human cancer cell lines, including K-562, MCF7, G-361 and HOS *in vitro*, being up to five times more effective compared for the free ligand and roughly as effective as cisplatin.^[141]

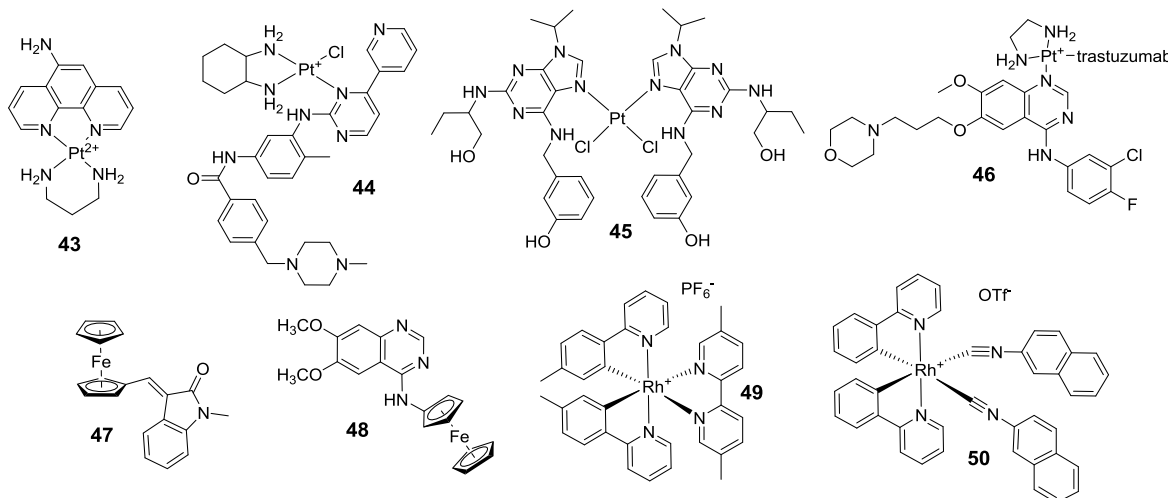


Fig. 12: Examples for metal-based kinase inhibitors based on platinum drug-conjugates (43–45), the universal linker system (46), ferrocenes (47–48) and inert rhodium complexes (49–50).

The feature of platinum and other metals to be coordinated by ligands, as exemplified by the previous represented compounds, or in biological systems as DNA strand or protein cross-links, can also be used to create compounds in which the coordination chemistry is applied for the development of metal-based linkers to connect inhibitors with bioconjugates, which might facilitate transport or cellular uptake and cell selectivity. This so called universal linker system (ULS) has for example been applied to create linker of oxindole-based multikinase inhibitors with bioconjugates such as lysozyme. The obtained conjugates showed enhanced cell specificity and intracellular retention, thereby prolonging its pharmacological activity while avoiding uptake in healthy tissue and unwanted side effects. Inside cells, the platinum ligands are dissociated by competitive displacement with endogenous thiols such as glutathione (GSH), leaving a metal-based kinase inhibitor binding to the active site.^[142] Another example is the conjugation of the approved kinase inhibitor gefitinib (2) with the approved mAb trastuzumab, which functions as anticancer drug by binding to HER2. The platinum centre is thereby coordinated by the gefitinib quinazoline nitrogen N1 and a methionine residue in trastuzumab (46). The linker is very stable in various media like PBS or serum but again cleaved by intracellular sulphur donors, probably by competing for the platinum binding.^[143]

Another example for metal-based kinase inhibitors are the previously mentioned ferrocene compounds. These include oxindole containing ferrocenes (e.g. 47), which inhibit DYRK3-4 and VEGFR2 at submicromolar to low micromolar levels, associated with antiangiogenic properties in *Xenopus* embryos^[144]. Other examples confirm the efficiency of replacing organic moieties by ferrocene in different types of bioactive compounds, such as derivatives of the anticancer drugs

Introduction

erlotinib (**3**) and gefitinib (**2**), the ferrocenyl quinazoline compound **48** thereby inhibits the epidermal growth factor receptor (EGFR) kinase with low micromolar IC₅₀ values.^[145]

Metal-based kinase inhibitors of course also include classical inert polypyridine complexes like the Rh-based mTOR inhibitor **49** or JAK2 inhibitor **50**.^[106,146] In molecules like this, the coordinative bonds are designed to be kinetically inert and thus stable in biological environments. Hence, such metal complexes should behave like purely organic compounds without displaying any metal related cytotoxicities.^[48] Complex **49** shows a similar mechanism of action to rapamycin (**29**), by first binding to FKBP12 to create a protein–protein interface that is subsequently recognised by the mTOR FKBP12-rapamycin-binding domain, thereby presumably functioning as protein–protein interaction stabiliser and antagonist of mTOR activity with an IC₅₀ of 0.01 μM in a cell-free system.^[106] The structurally related rhodium complex **50** on the other hand is a JAK2 inhibitor (IC₅₀ = 3.5 μM), which has been shown to inhibit JAK2 autophosphorylation and cancer cell growth in human erythroleukemia (HEL) cells.^[146] The field of inert metal-based inhibitors was pioneered by the MEGGERS group,^[109,119] who used inert metal complexes as structural scaffolds for the design of highly potent and selective inhibitors of various protein and some lipid kinases.^[48,49,109,120–122,147–161] The original template for these kinase inhibitors was the natural product and non-selective ATP-competitive kinase inhibitor staurosporine (**51**), which was structurally modified by using inert metal centres as “hypervalent carbon” with extended structural opportunities (Fig. 13).^[48]

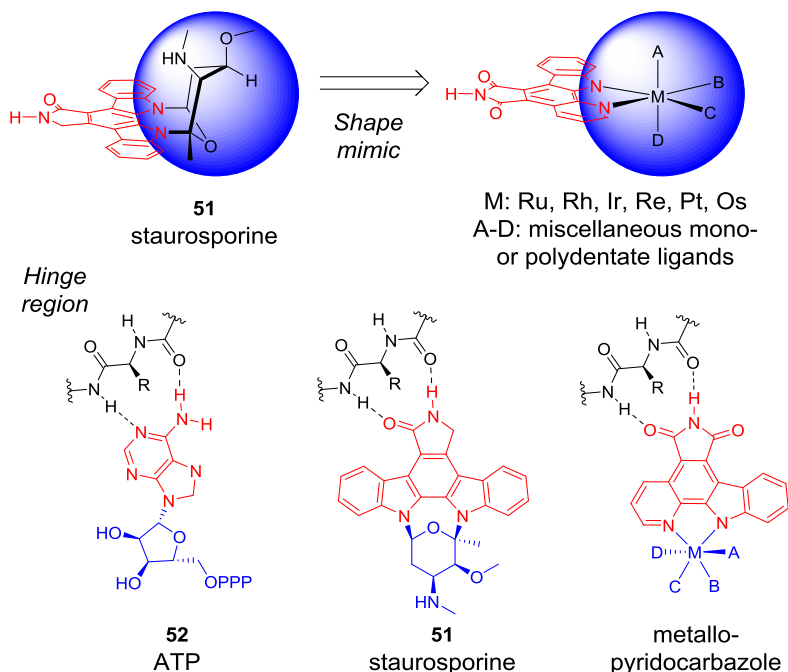


Fig. 13: The natural product staurosporine served as structural template for the development of various inert metal-based kinase inhibitors. The indolo[2,3-a]carbazole of **51** is thereby displaced by pyrido[2,3-a]carbazole which serves as bidentate ligand for easy metal-coordination, and both groups occupy the hydrophobic adenine-binding cleft with their lactam or maleimide functional group respectively, mimicking the hydrogen-bonding pattern of the adenine base in ATP (**52**), indicated by the dotted lines shown. The globular shape of the perpendicular orientated carbohydrate moiety (blue) on the other hand is mimicked and structurally enhanced using different inert metal centres and various mono- or polydentate ligands, both groups forming hydrophobic contacts and hydrogen bonds within the globular ribose-binding site. [48,109,119,120]

The close resemblance in globular shape and binding modes to kinases for staurosporine and the metallo-pyridocarbazole-based complexes has been confirmed in various crystal structures including PAK1,^[153] BRAF,^[156] Pim1,^[48,122,152] Pim2,^[155] GSK3 β ^[120,154,157] and DAPK1.^[120] One example for the alignment of Pim1 crystal structures of staurosporine (pdb 1YHS) and the pseudo-octahedral cyclopentadienyl complex (*S*)-**53** (pdb 2BZI) is given in Fig. 14.

The type of pseudo-octahedral or rather pseudo-tetrahedral complexes, such as ruthenium half-sandwich complex **53**, have been in the early research focus of the MEGGERS group,^[48,147,148,155,157,159,161] probably because of only 2 stereoisomers possible and their typically easy synthesis. It has repeatedly been proven that these complexes, containing modified or unmodified cyclopentadienyl-ligands, are promising scaffolds for ATP competitive protein kinase inhibitors, which can possess biological activities, such as anticancer properties, *in vitro* and *in vivo*,^[48,121,149,162–166] as discussed for certain highlights below.

This approach of using unique structural templates to populate previously inaccessible regions of chemical space with metal complexes has been proven to be very successful in regard to potency and affinity of the resulting complexes towards certain kinases, and the concept was soon expanded to true octahedral coordination geometries, which provide novel interactions with the glycine-rich loop, thus contributing significantly to binding potencies and selectivities.^[120] Some of these so called octasporines, in combination with their IC₅₀ values towards certain kinases are highlighted in Fig. 15.^[120,150,158]

In the years after the initial kinase inhibitor development, rapid access to compound libraries was explored using ligand scanning approaches e.g. based on a common precursor complexes^[150] or side chain active half-sandwich complexes.^[49,163] These and other structural modifications, driven by structure based design, combinatorial chemistry, library screening and other medicinal chemistry methods, finally lead to inhibitors which display nanomolar, and in some cases picomolar, kinase inhibitory properties with high selectivities, which is considered a core competency in kinase inhibitor design due to the highly conserved ATP binding sites.^[115,150] It could be shown that even slight modifications in the ligand sphere, like replacing a single monodentate ligand, lead to substantial differences in selectivity and potency towards different members of the kinase family. These changes are based on the interactions of the ligand spheres with different parts of the ATP-binding site other than the hinge-region.^[149] In addition to that, inhibition profiles and selectivity shifts were also envisioned by structural modifications of the indole and pyridine heterocycles of the pyridocarbazole ligand,^[122] as well as the use or design of single isomers, since stereochemistry obviously influences the interaction and binding affinities with biological targets. This has not only been shown by different kinase inhibition properties of single isomers,^[48,49,121,151,153,154,157] but also much earlier for example in case of induced fit DNA recognition with ruthenium η⁶-arene complexes by the Sadler group, in which the metal is described as dynamic stereogenic centre since it is prone to epimerisation allowing DNA-recognition by an induced fit mechanism.^[167]

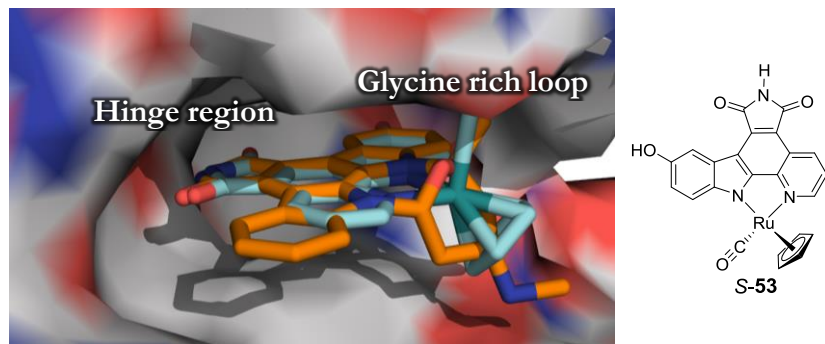


Fig. 14: Example for the close similarity in binding of a metallo-pyridocarbazole and staurosporine (**51**) to kinase active site. In this example, *S*-**53** (cyan) and **51** (orange) are bound to the kinase Pim1 (PDB 1YHS and 2BZI aligned to each other using PyMOL 1.5.0.4). The lactam and maleimide moieties are pointing towards the hinge region, where they bind according to **Fig. 13**, the cyclopentadienyl ring and monodentate CO ligand mimic the carbohydrate moiety and the CO points towards the glycine rich loop.

A vast amount of ligands, as well as various metals, have been used to sysnthesis a broad amount of metal-based kinase and ATPase inhibitors, often with a strong focus on pyridocarbazol compounds like **53-60** in Fig. 15. Apart from the ligand systems as discussed above, the choice of the metal centre plays a crucial role, since the complexes have to be easily designed and be inert in biological environment. Most of the developed complexes inherit ruthenium as the central metal (Fig. 15). This choice is based on some simple facts like its inexpensiveness. Ruthenium shows a preference for octahedral and pseudo-octahedral coordination spheres, in contrast to e.g. platinum, which prefers a square-planar coordination, with a predictable synthetic chemistry. Second, in its relevant oxidation states II and III it inherits a low toxicity, albeit due to the formation of inert bonds, the metall is by any means not considered free in biological systems.^[109] Classic complexes like *S*-**53** have been shown to be air- and water-stable, and can even withstand millimolar concentrations of thiols.^[109]

Rhodium, a d9 nobel metal, is also able to form very kinetically stable octahedral complexes. Its advantage over Ru(II) is that it can be coordinated to hard ligands like amines, with which Ru(II) would become prone to oxidation to the paramagnetic Ru(III). It has been shown that certain complexes like the highly selective picomolar Pim1 inhibitor **59** can also withstand millimolar concentrations of thiols. The downsides of using rhodium are its extremely high price and the not too well understood coordination chemistry, which is often reflected by overall modest yields.^[168]

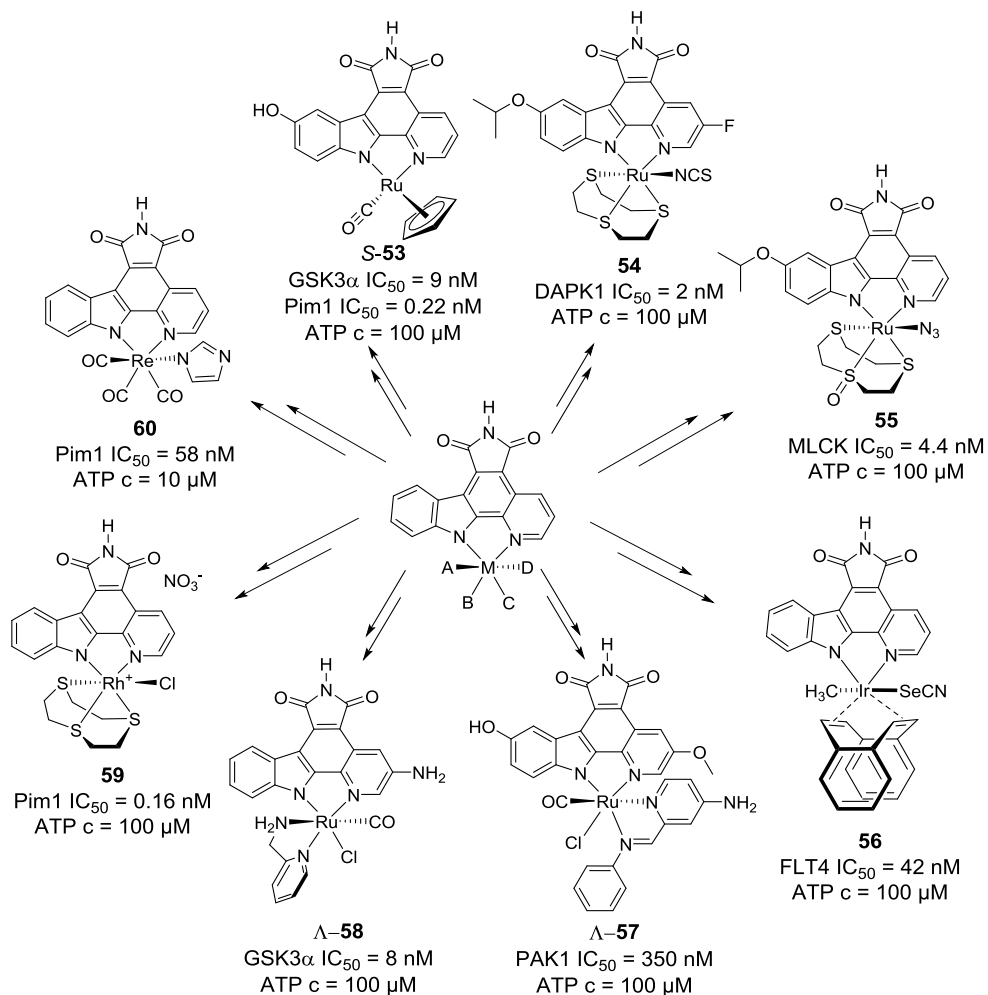


Fig. 15: Various kinase inhibitors based on the metallo-pyridocarbazole with their respective IC $_{50}$ values towards their targeted kinases and the ATP concentration used in the assay. If not otherwise indicated, the compounds are mixtures of their respective enantiomers. [120,150,168,169]

Iridium, the heavier d9 homologue metal scaffold used e.g. for the design of **56**, on the other hand is also fairly inert and octahedral complexes are easily accessible from square-planar complexes by stereoselective oxidative addition.^[164] Ir(III) has the great advantage to not only serve as a structural scaffold for kinase inhibitors, which show kinase inhibition related effects like antiangiogenetic properties based on FLT4 inhibitor like **56** does in 2D and 3D cell-based models, but might also be activated by visible-light to enhance cytotoxicity. With the given complex upon irradiation with visible light ($\lambda \geq 450$ nm for 60 min) the cellular survival in HeLa cells droped by a factor of 34. This photoinduced cytotoxicity is thought to be the result of apoptotic cell death based on elevated activity of the executioner caspases 3 and 7. The effect is thereby known to be unrelated to the kinase inhibitory properties, since an inactive form, containing methylated maleimide, shows a similar cytotoxicity effect upon irradiation which might be related to ligand exchange reactions, since the selenocyanate tends to be replaced by chloride in the presence of these ions under irradiation.^[165]

Another metal used in these scaffolds to combine kinase inhibitory properties and photoinduced cytotoxicity is rhenium. It was suggested that kinase inhibitors like the nanomolar Pim1 inhibitor **60** might serve as templates for photodynamic therapy, based on their singlet oxygen generation upon irradiation with red light and resulting photoinduced up to three fold increased antiproliferative activity.^[169]

Besides these more heavily studied metals, also proof of concept scaffolds like osmium have been tested for their ability to form inert kinase inhibitors. For example osmium has been used to synthesise a lighter homologue of **53** that remarkably displayed almost indistinguishable biological activities to the original ruthenium complex, which can be explained by their nearly identical three-dimensional structures and their identical mode of action as protein kinase inhibitors.^[152] A less obvious choice for inert metal-based compounds is platinum, which also has served as anchor for pyridocarbazole-based nanomolar inhibitors of the kinase GSK3 α . Although a good potency has been achieved, it has been suggested that this type of complexes is most likely not suitable for cellular application because of their respective charge and lower robustness in comparison to ruthenium complexes. Still the metal centre allows a differing coordination geometry and therefore might cover different parts of chemical space, suitable for exploring the kinase active sites.^[170]

As previously mentioned the first steps towards *in vivo* investigations concerning the suitability of these potent complexes as molecular probes in chemical biology or potential drugs have been done. The most interesting results will be briefly covered here. The previously introduced **53** for example was used to explore its GSK3 inhibitory properties in *Xenopus laevis* development. It is well understood that GSK3 is a negative regulator of the wnt signal transduction pathway that phosphorylates beta catenin, which itself is required for the dorsal axis formation in *Xenopus* embryos. Ectopic activation of the wnt pathway (e.g. with lithium), induces an ectopic dorsal axis. In the study, *Xenopus* embryos were exposed to 5-10 μM **53** from the 32-cell stage until the midblastula stage, and all embryos demonstrated a hyperdorsalised phenotype, with expansion of dorsal and anterior structures and loss of posterior tissues (Fig. 16 1.) similar to embryos exposed to lithium or other GSK3 inhibitors, showing the applicability of **53** and its GSK3 inhibitory properties, linked to activation of wnt signalling, in simple *in vivo* systems.^[149] A similarly positive outcome was concluded for the second generation picomolar GSK3 inhibitor R-**61** in *Danio rerio*. Again, the wnt signal transduction pathway is correlated with proper development of the species, here especially in the development of the metazoan. By inhibiting GSK3 e.g. with lithium, a perturbed development of the head structure with a no-eye phenotype, among others, is promoted. When the zebrafish embryos were treated with 1 μM of R-**61** at 4 h post fertilisation (hpf), at 25 h hpf a decrease of head structure without eyes and a stunted and crooked tail were observed (Fig. 16 2.), again showing the effect of successful GSK3 treatment *in vivo*.^[121]

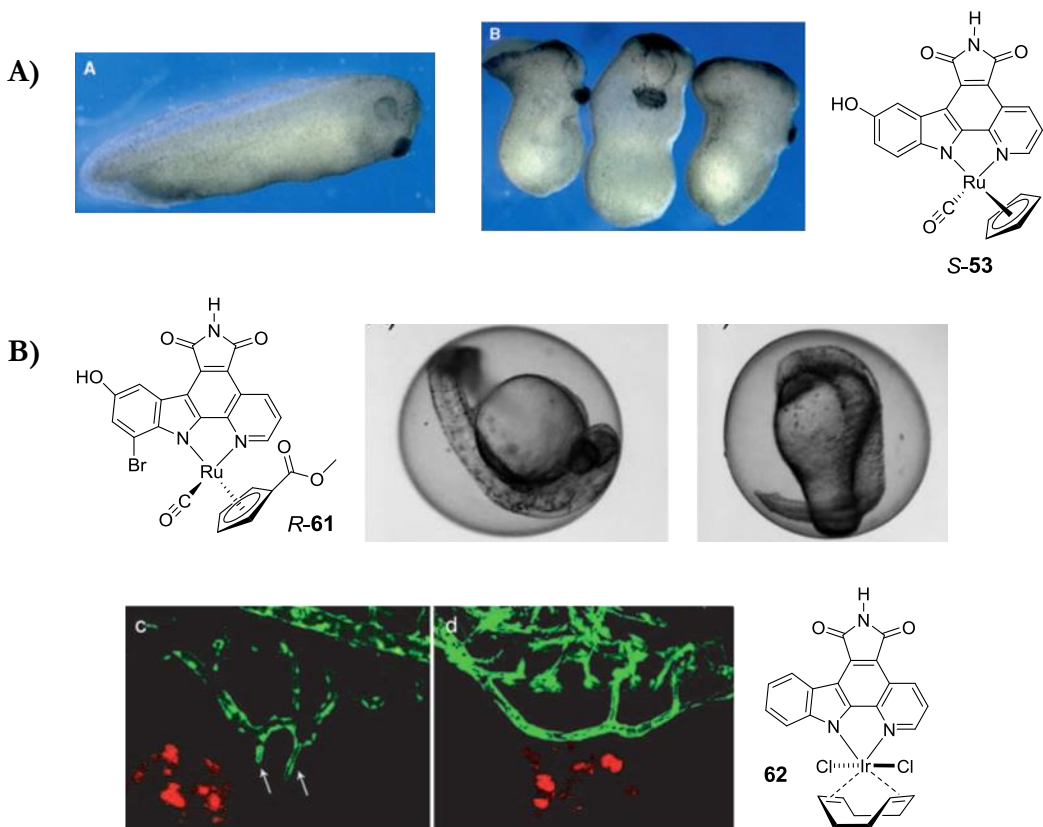


Fig. 16: Most successful *in vivo* results with metallo-pyridocarbazoles. A) Effect of GSK3 inhibition in *Xenopus laevis* embryos with (*S*)-53. Left: control. Right: after treatment with 10 μM of the complex *Xenopus* embryos show a hyperdorsalised phenotype.^[149] B) Effect of GSK3 inhibition in *Danio rerio* embryos. Left: control. Right: after treatment with 1 μM of (*R*)-61 show a phenotype with a decreased head structure without eyes and a stunted and crooked tail.^[121] C) FLT4-based antiangiogenic effect of 62 in a xenotransplanted proangiogenic human cancer cell model in GFP-labelled *Danio rerio*. Left: control, right: after treatment with 5 μM of 62 the vascular growth to the cancer cells is fully suppressed.^[164] All figures are reproduced from the indicated publications under permission from John Wiley and Sons.

The third important example includes the nanomolar FLT4 (VEGFR3) inhibitor **62**. FLT4 is known to play an important role in angiogenesis, therefore its inhibition should reduce vascular growth. And indeed, using a transgenic *Danio rerio* model, where the vascular system inherits a GFP-based green fluorescence, after treatment with 5 μM **62** all embryos showed significant damage in the development of their vascular system 72 hpf. Not only does this confirm the complex as a potential chemical probe for FLT4 and angiogenesis, but additional experiments using a xenotransplanted proangiogenic human cancer cell model in zebrafish embryos, in which full suppression of blood vessel development was observed after treatment with 5 μM of **62**, confirm the compound as potential anticancer drug.^[164,171]

1.4.3. Metal-based HDAC inhibitors

Different HDIs which incorporate a metal are known in literature, amongst others modifications of the FDA approved HDI SAHA. Some of them, especially platinum-based drugs, try to combine the previously mentioned approach behind combinational therapy of platinum drugs and HDIs into one drug molecule.^[172] These conjugates act by two independent mechanisms and are thought to have a greater capacity to circumvent resistance as compared to cisplatin.^[173] One example includes the addition of a malonate substituent to the phenyl ring of SAHA, allowing Pt to bind in an O,O'-bidentate mode on the coordination functionality, yielding in the associated cisplatin adduct *cis*-[Pt(NH₃)₂(malSAHA)] (**63** Fig. 17).^[174] This compound shows a dual mechanism of action by binding to DNA and inhibiting HDACs,^[172] e.g. HDAC1 in the single digit micromolar region.^[174] However **63** was also shown to increase HDAC activity in CH1 cells after 24 h treatment, indicating no inhibition, while showing lower cytotoxicity as compared to cisplatin or SAHA if applied alone or in a 1:1 mixture.^[172] Another HDI which is used heavily in conjugation with platinum is valproic acid. Early compounds like the Pt(II) complexes (*trans*-[Pt(VPA)₂(NH₃)(py)]) (**64**) and *trans*-[Pt(VPA)₂(py)₂] show IC₅₀ values in the range of 100 μM.^[175] A conjugate of the acid to a Pt(IV) prodrug, [*cis*Pt(NH₃)₂(Cl)₂(VPA)₂] (**65**), has been shown to induce cell cycle arrest and cell apoptosis in a time dependant manner after reductive activation to Pt(II) in the cytosol and release of VPA with a cytotoxicity in the sub-micromolar range. It showed a much better effect, when compared with the combination of VPA and the platinum prodrug. The compound also showed an inhibitory effect on tumour growth on A549-xenograft model with low systemic toxicity.^[176] Following the first publication, questions were raised whether the amount of VPA released is indeed sufficient to show HDAC inhibitory activity and whether a synergism is possible.^[177] However newer studies showed that treatment of cells resulted in enhanced histone H3 acetylation and more effective decondensation of heterochromatin than free VPA, and that a considerably higher fraction of Pt is bound to DNA compared to conjugates with biologically inactive ligands. Most recent studies with acetyl ligands instead of VPA showed that the HDAC inhibition effect is not based on the direct inhibition of catalytic activity of HDACs, but is rather associated with additional mechanisms involving downregulation of HDACs, resulting in a marked reduction of the level of HDACs in cells.^[178]

Another ligand used for platinum-based HDIs is derived from a malonate derivate of the HDI belinostat giving *cis*-[Pt(NH₃)₂(mal-*p*-Bel)] (**66**), which shows an enhanced cytotoxicity over the malSAHA conjugate, as well as better cytoselectivity than cisplatin and belinostat.^[173]

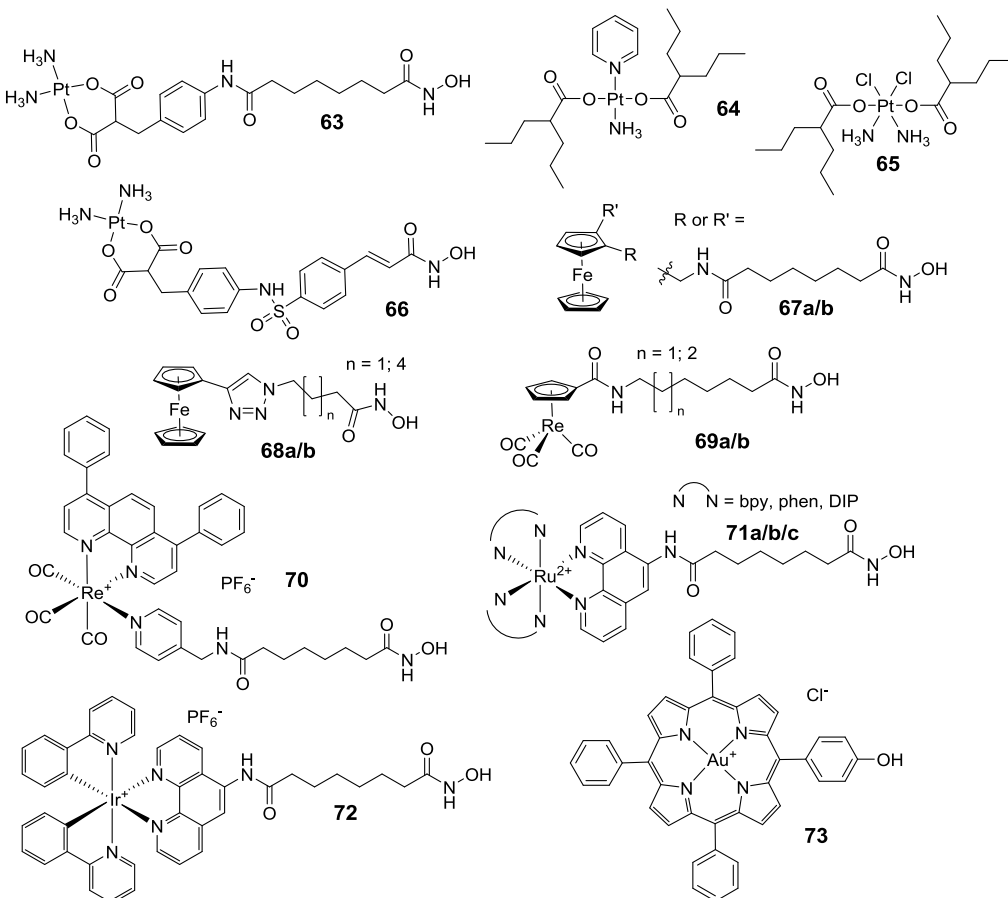


Fig. 17: Examples for metal-containing HDIs including SAHA-analogues and conjugates (**63**, **67 a/b**, **68 a/b**, **69 a/b**, **70**, **71 a/b/c**, **72**), VPA-conjugates (**64**, **65**) belinostat-malonate-conjugate (**66**), a gold-porphyrin (**73**).

As previously mentioned the HDI SAHA has been the inspiration for different metal containing compounds. These not only include platinum but also other metals like iron in ferrocene-based compounds called JAHAAs (Jay Amin hydroxamic acid), where a ferrocenyl group serves as bioisostere of the SAHA-phenyl (e.g. **67a/b**). Their IC₅₀ values against single isoforms of class I HDACs are in the nano-, their cytotoxicity in the micromolar region.^[179] This concept has been expanded to triazole-based analogues, namely click JAHAAs (e.g. **68a/b**) which showed IC₅₀ values for individual HDAC isoforms of down to single digit nanomolar values. However, these compounds tend to show poor cellular penetration.^[180] Another bioisostere of the SAHA-phenyl, which has been shown to have comparable antiproliferative activity (low micromolar IC₅₀ values) as the original organic inhibitor and other organic congeners in five different cancer cell lines, is a rhenium tricarbonyl cyclopentadiene half-sandwich complex (e.g. **69a/b**). The shown slight decrease of antiproliferative capacity c.f. SAHA indicates that the bulkier [Re(CO)₃(Cp)] moiety is disfavoured over a simple planar phenyl ring and might be the cause of a reduced ability of cellular penetration.^[132] A second rhenium compound, which contains a SAHA analogue is ReLMito ([Re(DIP)(CO)₃(L)](PF₆) (**70**) with L=(N¹-hydroxy-N⁸-(pyridine-4-ylmethyl)octanediamide and DIP=4,7-diphenyl-1,10-phenanthroline). The multifunctional Re(I)-HDI conjugate showed

similar cytotoxic properties to SAHA in five cancer cell lines and HDAC activity that is only slightly less potent than that of SAHA. In addition to that, the phosphorescent compound locates in mitochondria and induces caspase-independent paraptosis, which may provide a strategy to overcome acquired and innate chemotherapy resistance.^[181] Other metal-containing SAHA derivative complexes use ruthenium as central metal-ion. $[\text{Ru}(\text{N}^{\text{c}}\text{N})_2\text{L}](\text{PF}_6)_2$ (**71a/b/c**) with L: N1-hydroxy-N8-(1,10-phenanthrolin-5-yl)octanediamide, and $\text{N}^{\text{c}}\text{N}$ = 2,2'-bipyridine (bpy), 1,10-phenanthroline (phen) or DIP might function as dual imaging and therapeutic agents. These complexes show inhibitory effects in the micromolar region on HDACs *in vitro*. In addition to that, the DIP compound shows a cytotoxic potency that is higher than those of cisplatin and SAHA against five cancer cell lines examined and has been shown to significantly increase the acetylation of histone H3 in a dose- and time-dependant manner similar to that of SAHA.^[182] Recent literature also describes Ir(III) complexes of the type $[\text{Ir}(\text{N}^{\text{c}}\text{C})_2\text{L}](\text{PF}_6)$, where L is a phenanthroline derivative modelled after SAHA and $\text{N}^{\text{c}}\text{C}$ is phenylpyridine (ppy) (**72**), 3-(2-pyridinyl)-coumarin, 2-(2-thienyl)pyridine (thpy) or 2-(2,4-difluorophenyl)pyridine (dfppy), which may combine HDAC inhibition and photodynamic therapy and serve as a starting point for novel tumour-oriented multifunctional metallo-anticancer therapeutics. The compounds show nanomolar inhibition of HDACs in HeLa nuclear extract and micromolar cytotoxicity in HeLa cells with a phototoxicity index of 3-19, meaning 3-19 times more cytotoxic if irradiated with 365 nm or 425 nm when compared with a non-irradiated sample.^[183]

In addition to these Pt, Fe, Ru, Ir an and Re containing HDIs, also Au compounds with HDAC inhibitory activity have been described previously in literature. One example is the gold(III)porphyrin compound [5-hydroxyphenyl-10,15,20-triphenylporphyrinato Au(III) chloride] which showed a 100-fold to 3,000-fold higher cytotoxicity compared to cisplatin and IC₅₀ values in the nanomolar range in a panel of human breast cancer cell lines. The compound has been shown to selectively inhibit Wnt/β-catenin signalling through modulating histone deacetylase activities. Treatment with the complex resulted in a rapid decrease of the HDAC activities in MDA-MB-231 cells, cell extracts and immunoprecipitated class I HDACs, with HDAC 1,2,3 and 8 inhibited in the nanomolar region.^[184] The compound and derivatives have been patented amongst others in the USA.^[185] Recently, gold nanoparticles precipitated with quercetin, and loaded into poly(DL-lactide-co-glycolide) nanoparticles have been shown to reduce HDAC activity and the expression levels of HDAC1 and 2 in hepatocarcinoma cells.^[186] Other gold (III) compounds like bis(thiosemicarbazone) gold(III), which has been studied for *in vitro* reactivation of latent HIV-1, showed no inhibition of HDACs at 0.5 or 0.2 μM,^[187] indicating that gold-ions do not unselectively inhibit HDAC enzymes and showing the great potential for this type of HDIs.

2. Concrete task

Since the discovery of the pivotal role of kinases in intracellular signal transduction and their natural product inhibitors such as staurosporine (**51**), the development of potent kinase inhibitors has evolved to be an elemental part of biological and medical research. During the last two decades, the MEGGERS group has established a broad variety of selective and highly specific ATP-mimetic kinase inhibitors using metal centres for inert coordination compounds based on the aforementioned multiple kinase inhibitor staurosporine. Thereby, they created new and innovative chemotypes which occupy a rather unexplored part of the chemical space, avoiding the crowded intellectual property landscape in that field.^[12,19] As indicated in the introductory section these compounds have been shown to be very potent and often selective with purified kinases as well as in cancer cell lines *in vitro*, and to show positive results in basic eukaryotic organisms *in vivo*. However, their suitability towards a therapeutic use e.g. in cancer treatment, which is also based on their pharmacokinetic (PK) and pharmacodynamic (PD) properties, has not been explored to a further extent.

Therefore, the task of this work was the development of a lead compound based on these kinase inhibitors for a possible future metal-based anticancer drug by identifying the most suitable compounds and to further improve their properties, as well as to determine and enhance their overall synthetic access. This includes the evaluation and improvement of preclinical parameters like their overall anticancer and ADMET (absorption distribution metabolism excretion and toxicity) properties and determination of the possibility of upscaling of the compounds.

The quest for new drug molecules in oncology is most often based on two different main approaches, namely the more classical empiric screening for cytotoxic agents against cancer cell and tumour models and the more up-to-date investigation of molecularly targeted agents along with the appreciation of their pharmacokinetic (PK) and pharmacodynamic (PD) properties.^[188] Pharmacokinetics thereby studies the fate of a compound after administration, pharmacodynamics the effect of the drug on the body. Since these compounds comprise proven kinase inhibitory activity thereby being molecularly targeting agents, this knowledge was to be combined with a classical cytotoxicity screening against cancer cell lines, since toxicity and tumour regression most often are based on similar mechanisms and correlate to the dose.^[189] The identification of their distinct target, if it was not identified already, was not the focus of this work. As a first step, all compounds previously synthesised and still available, were to be collected in a compound library and tested as single dose in a simple cancer cell model to identify suitable anticancer compounds (Fig. 18).

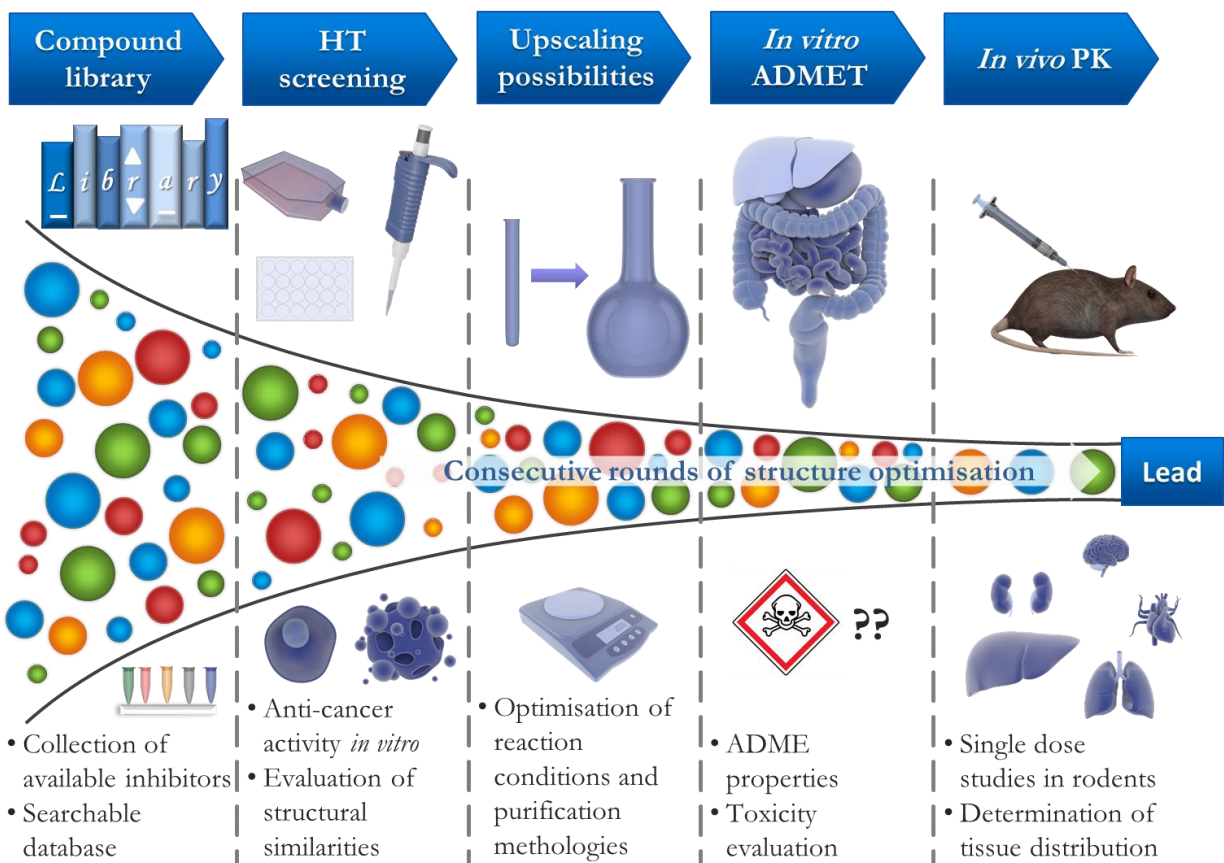


Fig. 18: Overview over the scope of this project. The goal was to find a lead structure for a potential clinical development of a metal-based anticancer drug. Starting with the composition of a compound library of available kinase and ATPase inhibitors developed in the MEGGERS group, a first high-throughput (HT) cytotoxicity screening in a cancer cell line was supposed to combine the molecularly targeting inhibitors with a basic screening for anticancer drugs. Selected molecules and structure derivatives were used to study possible upscaling to perform *in vitro* absorption, distribution, metabolism, excretion and toxicology (ADMET) studies for further selections. Finally, *in vivo* pharmacokinetic (PK) studies were to be performed parallel to further structural optimisation to improve relevant parameters, to give a final lead for a possible preclinical or clinical candidate.

In a second step, their synthesis was supposed to be evaluated and improved and upscaling studies were pursued to obtain compound quantities to be able to investigate their ADMET properties and PK parameters *in vivo* (Fig. 18). In the final step the compounds were to be evaluated as lead structures for the development of compounds with improved properties concerning ADMET and PK, while maintaining their original kinase or ATPase activities. Structure activity relationships of new derivatives concerning both kinase inhibitions as well as ADME properties were to be performed, to learn more about the relationship of optimising these parameters in metal-based compounds in comparison to pure organic compounds.

3. Results and discussion

3.1. Classical cytotoxicity-based approach

Cytotoxicity and structure-activity relationships of metal-containing compounds have been studied and reviewed extensively in recent years,^[117,190–198] revealing that many anticancer compounds under evaluation were either discovered through cytotoxicity screening or showed cytotoxicity against cancer cells in later stages of their investigation. In the MEGGERS group, numerous metal-based compounds, which possess demonstrated kinase inhibitory activities to different extents, were developed and synthesised over the last two decades as explained in more detail in the introductory section. Based on these inhibitory profiles, which are either very selective, or very broad (possible multi-kinase inhibitors), the question emerged, whether potential anticancer drugs based on these inhibitors might be identified by a classical *in vitro* cell-culture-based cytotoxicity pre-screening. Their properties should be investigated further as indicated in the concrete task section, after selecting the most promising candidates in this cell-based assay. These cell-culture screens are not only cost-effective for a first pre-selection, they might also be done in a relatively short time and avoid the use of animal models.^[189] In addition to that, a drop-off in potency, compared to assays with isolated enzymes, based on high intracellular ATP-concentrations, low membrane permeability, interactions with other enzymes like phosphatases, or the relative concentration of the target kinase and their substrates, can be discovered in this more native situation.^[12] On the other hand one must be aware, that testing in one cell line as the first instance means that the compounds are screened against only one single cancer type. In addition to that, cancer cell lines in general include inherent biases towards specific cell signalling and growth pathways that favour growth in cell culture, and therefore some pathway mutations are not well represented and drug molecules that target these pathways cannot be identified in such a simplified model.^[4] For that reason, and because such models often solely lead to successes in the field of rapidly growing malignancies like lymphomas, childhood leukaemia and germline tumours, while relatively fewer success is seen for slow-growing solid-tumours of adults like lung, breast and colorectal cancer,^[188,189] usually a variety of cell lines and tumour types are used in the pre-screening stage.^[189] Due to cost and time reason, further tests and other cell lines in this study were only done at a later stage for compounds which showed good results in the initial screening.

3.1.1. Database development

For the matter of screening compounds for their cytotoxicity, at first a database containing all previously synthesised eligible compounds in the group had to be developed, which in the best case also allows a structure and substructure search, to be able to compare the compounds structure-activity relationship. In this database, not only kinase inhibitors, but also potential inhibitors of other purine-based nucleoside or nucleotide using enzymes like ATPase inhibitors were included, since their discovery was another focus in the group in the last couple of years.

The LICCS system^[199] (Excel-CDK) is a freeware Microsoft (MS) Excel application which combines all the afore mentioned properties by using the open-source CDK (Chemistry Development Kit), which is a Java-based library for bio- and cheminformatics. Using SMILES (Simplified Molecular Input Line Entry Specification) strings, LICCS features structure display (using JChemPaint), substructure and similarity searching, R group table creation, clustering, diverse compound picking, sammon projections, molecular property calculations, name to SMILES conversion and so on, which makes it easy to link compound property with activity data. Considering the application is MS Excel-based, the developed database can be shared by different users, since once the worksheet is enabled, it is usable with all its features by anybody with a running installation of MS Excel. However, SMILES strings are limited as they do not support multi-centre coordinations like the η^5 -coordination of cyclopentadienyls. Therefore, for compounds falling in this category, the database includes chemaxon extended SMILES, which do include this additional information, but are not searchable via the CDK-tools. In addition to the LICCs features, the structures of all compounds are displayable using JChem for Excel, which allows a more accurate view on the coordination and structure of the complexes, which get lost to a certain degree using SMILES strings, and includes additional features like structure and substructure searches, compound profiling etc. including multi-centre coordination compounds. JChem for Excel however needs to be installed to use its features and is a commercial software for which free academic licenses can be obtained^[200] (valid as of December 2016). SMILES and extended SMILES were created using Marvin Sketch 15.2.16 from the same software package.

The database was prepared using inhibitors of former group members including LI FENG, NICHOLAS PAGANO, SEBASTIAN BLANCK, STEFAN MOLLIN, SANDRA DIECKMANN, ALEXANDER WILBUER, KATHRIN WÄHLER and MANUEL STREIB, and includes 270 initial compounds tested in the later described setting. Additionally, 33 compounds which were previously tested in HeLa cells by ANJA LUDEWIG were included. Most of these 33 compounds showed no major limitation in cell viability in HeLa cells at 1 μM compound concentration and 24 h incubation time and were therefore defined as unattractive for this study. All compounds (3) with cell survival below 80%

were tested again in HT-29 cells in this study. In the database, also compounds including negative controls (like methyl, ethyl or benzyl-protected maleimids, where the protection group prevents binding in the hinge region), potentially metabolic labile compounds (e.g. including free hydroxyl groups at the 5-indole position of the pyridocarbazole or reactive functional groups) and compounds which potentially do not cross cell membranes (e.g. cationic complexes) were included, to get a full picture of the cytotoxic properties of all compounds. In addition to that, compounds were sometimes included twice intentionally (e.g. due to different batches or owners), since the integrity and purity of the stock solutions was not examined in advance, which might lead to inaccurate results due to improper concentrations or toxicity of degradation products, making it able to compare the results of different batches.

The final updated library, as it can be found in the digital supplementary attachment, is based on MS Excel 2016 using LICSS V3.2., and includes a total of 440 compounds (some of them added at a later point, please refer to the digital supplementary information for the full list), of which 33 were solely tested in HeLa cells by ANJA LUDEWIG and 407 compounds were tested in HT-29 cells for this study at least as single determination in quadruplicates.

3.1.2. Library-based cytotoxicity screening

After getting an overview over the available compounds and establishing the library-database, all compounds were screened for their cytotoxic properties, and therefore potential anticancer activity, which was expected to be based on their kinase and ATPase inhibitory properties. For this screening the human colon adenocarcinoma cell line HT-29 was used, which is a cancer cell line derived from a primary tumour in 1964, and which showed generally lower sensitivity towards cytotoxicity against our compounds compared to the classical human cervical cancer cell line HeLa, which was established through practical experience by ANJA LUDEWIG in our group. The cytotoxicity in this assay was based on the cell viability compared to an untreated standard, as determined by the MTT-method,^[201] where light yellow water-soluble MTT (3-(4,5-dimethylthiazol-2-yl)-2,5-diphenyltetrazolium bromide) is reacted to insoluble purple formazan precipitate by healthy cells as direct function of redox potential (NADH and NADPH based). The amount of formazan formed is directly correlated to the vitality of the cells, which can further be correlated to the cytotoxic or cytostatic properties of the compound. The formazan is further dissolved in DMSO and its concentration measured via absorption spectroscopy. To keep the number of hits down to a manageable level, the compounds were screened using standard method I (see experimental section) at a single low concentration of 1 µM (using 1-1.5% DMSO) for 24 h,

and the limit for hits was set at a cell survival rate of <80%, which respects the fact, that the MTT-method has quite high deviations due to different problems like inexact cell number per well, inaccurate pipetting of compound (variation of concentrations) or removal of formazan during aspiration of cell medium. Additional problems might include incomplete dissolution of formazan precipitate, possible interference of the assay mechanism with compounds (e.g. interference in the redox reaction), additional absorption or light scattering from compound or protein precipitates, higher toxicity of MTT in wells with lower cell numbers or damaged cells due to cytotoxic or cytostatic effects of the compound tested and higher MTT dose per cell. The cell survival rates of these 303 initial compounds under the given assay conditions are summarised in Fig. 19.

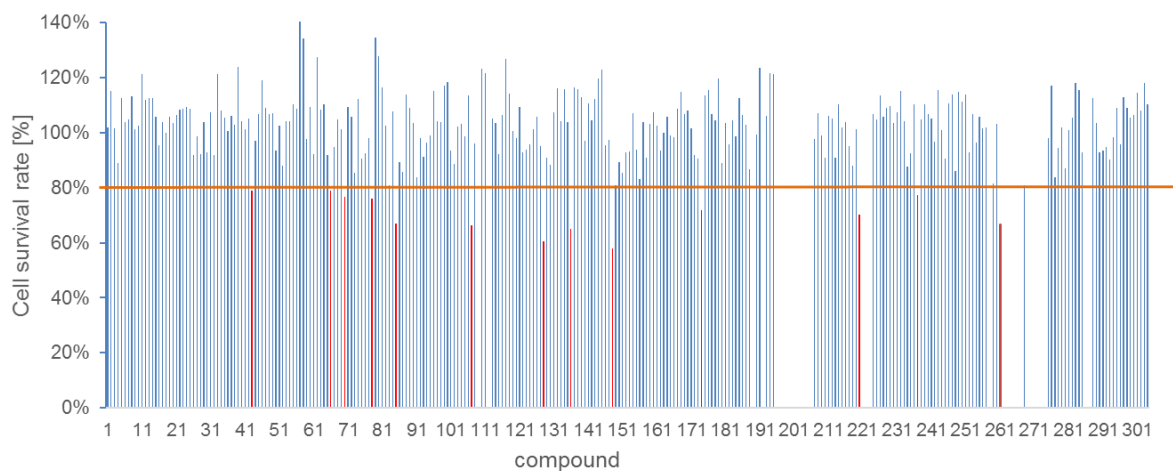


Fig. 19: Overview of cell survival rates of human colon adenocarcinoma cells HT-29 after 24 h incubation with 1 μM of the according compound, as determined by the MTT method. Missing values stand for compounds which were not tested due to insufficient toxicity, as determined by ANJA LUDEWIG in HeLa cells. All hits (in total 13), namely compounds inducing a cell survival rate below 80% under the given concentration are marked in red and will be discussed below.

Taken from Fig. 19 from the initial 303 compounds, of which 270 were tested in HT-29 cells, 13 compounds showed a cell survival rate of <80% under the given assay conditions. The corresponding structures are summarised in Fig. 20. Additionally, two compounds (**87** and **88**) are listed, which had cell survival rates in HeLa cells <80% as determined by ANJA LUDEWIG under the same assay conditions. However, both compounds showed higher values in HT-29, therefore not being hits under the set limits. In addition to that, the more attractive compound **88**, based on the MTT result in HT-29, is a reactive precursor molecule and does not fulfil the requirements for further studies of being an inert metal-based kinase inhibitor.

Results and discussion

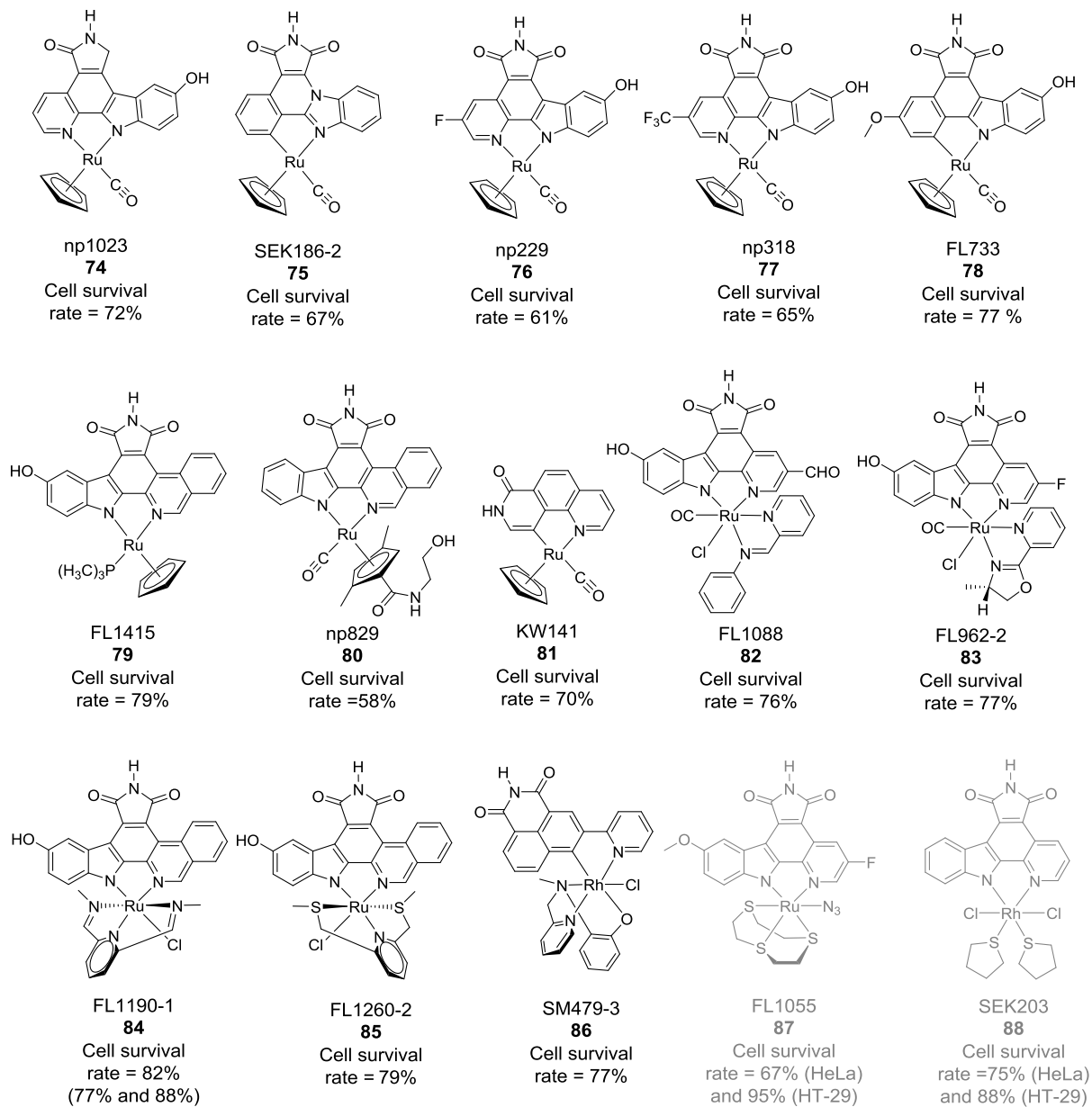


Fig. 20: Structures of the initial hits from **Fig. 19** sorted by common structural features and their respective cell survival rates under the given concentrations. If not indicated otherwise, the compounds are racemic mixtures. Some compounds were tested in duplicate or triplicate, given numbers are the average rates. Compounds **87** and **88** were hits from the initial screenings in HeLa cells by ANJA LUDEWIG and were not confirmed in the HT-29 cell-based screening.

Fig. 20 shows that the hits found cover a quite broad selection of compounds with a strong focus on classical pyridocarbazole-based ruthenium CpCO complexes (**74-78**), one non ATP-mimetic phenanthroline-based CpCO kinase inhibitor (**81**), octahedral pyridocarbazole-based ruthenium complexes with an additional bidentate ligand (**82** and **83**), octahedral isoquinolinocarbazole-based complexes (**79-80**, **84-85**) and one pyridylnaphthalimide-based octahedral rhodium complex (**86**).

After analysing the structures of these compounds, some of them were excluded directly from the study due to a very complicated synthesis with low yields (**74** and **86**) or too labile or even reactive groups (e.g. trimethylphosphane ligand in **79**). Others did not show the expected results in follow up concentration dependant MTT-tests (**75**, **78**, **81**, **82** and **85** Fig. 21) where the IC₅₀, the compound concentration which results in 50% cell survival rate, was either not within the tested concentration limits (**82** and **85**), was just reached at the highest concentration of 30 µM (**75** and **81**) or was reached at about 3 µM but the toxicity would not further increase with rising compound concentration, indicating a complicated mechanism or compound precipitation (**78**). Complex **84** was excluded, since it did not confirm in a second test under the same conditions.

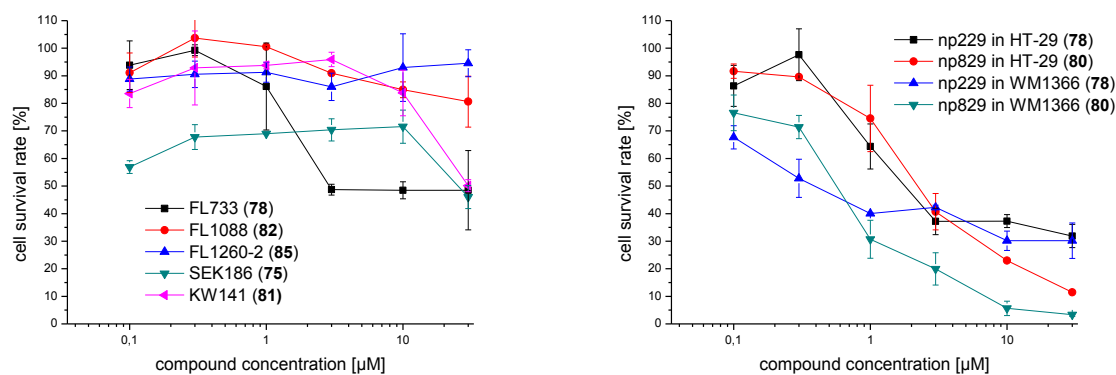


Fig. 21: Results of concentration dependant MTT assays in HT-29 cells of some of the hits from **Fig. 20**. Compounds were tested at a concentration of 30-0.1 µM in HT-29 as indicated in the experimental section. On the right side, results for the melanoma cell line WM1366 for compounds **78** and **80** are displayed.

What emerges from Fig. 21 is that the two compounds np229 (**78**) np829 (**80**) are very promising concerning their cytotoxicities for both HT-29 cells (IC₅₀ of 1.0 ± 0.2 µM and 2.9 ± 0.5 µM respectively using a sigmoidal fit in Origin Pro 8) and the NRAS mutated melanoma cell line WM1366 (IC₅₀ of 0.3 µM and 0.8 ± 0.3 µM respectively). However, **78** has previously been studied in a xenotransplanted tumour model in nude mice for its GSK3 inhibitory based anticancer activity and all mice either died or had to be sacrificed before the tumours in the control group went into an exponential growth phase (unpublished data). This acute toxicity meant an exclusion of this compound for our studies. It was also previously suggested, based on unpublished data, that this toxicity might be related to the 5-hydroxy group in the indole of the pyridocarbazole, which also poses a potential risk of enzymatic or chemical oxidation.^[122] Therefore, compounds **77** and **83** were also excluded from follow up studies for now. After these considerations np829 (**80**) was the obvious choice for pursuing in this project, which was supported by the fact that it was the

compound with the lowest cell survival rate in the initial screening and showed good results in the first concentration dependant assays.

It originally developed by NICHOLAS PAGANO together with a series of derivatives, which contain 31 different cyclopentadienyl side chains (Fig. 23), to determine their TrkA activity and selectivity over Pim1,^[202] using a rapid derivatisation methodology developed by HOWARD BREGMAN,^[49] in which the Cp side chains can be easily introduced using a reactive *N*-hydroxy succinimide (NHS) ester.

Based on the pseudo-tetrahedral ruthenium centre, in addition to two possibilities of the asymmetrical cyclopentadienyl moiety, a total of 4 stereoisomers are possible for this compound class, as indicated in Fig. 22.^[203] Therefore, the library contained a total of 62 compounds, since the diastereomers, as their racemic mixtures, were separated from each other, as explained later in chapter 3.1.3.

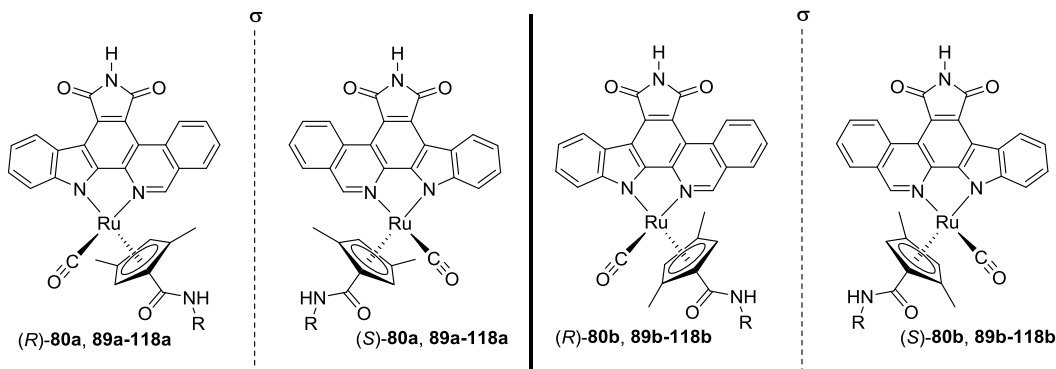


Fig. 22: Complex np829 ((*R*)- and (*S*)-88b) is actually a mixture of enantiomers, while 88a are their diastereomeric counterparts. For the validation of stereochemistry in this compound class see chapter 3.1.4.

The complete library synthesised by NICHOLAS PAGANO is shown in Fig. 23. The side chain selection was thereby based on an observation by HOWARD BREGMAN, which concluded, that with an unmethylated Cp moiety, a gain in selectivity towards GSK3 is achieved using amino acid side chains, but derivatives with an additional amine (which becomes an ammonium salt in assay buffer) and hydroxy functionalities display potency towards Pim1.^[204] In addition to that, based on previous observations, all derivatives (alcohol and ester amino acid derivative derived side chains) were supposed to provide potency towards the kinases TrkA and Pim1 for both derivatives. Complexes including the structurally simpler ethyl ester derivative of the ethyl 2,4-dimethylcyclopenta-1,3-diene for example, have been shown to have binding affinity towards Pim1 and TrkA but much less for GSK-3.

Both libraries were tested for their inhibitory potency towards Pim1 and TrkA at an ATP concentration of 100 μM by NICHOLAS PAGANO, with the b-series measured at a concentration of 30 nM, and the a-series at 100 nM. As a trend the Pim1 rest activity was most often lower compared for the TrkA activity. With restactivities towards TrkA and Pim1 under the given ATP concentrations of **80b** (<5% and <5%) and **80a** (6% and ~25%), these two compounds are by far not the most potent or selective compounds in the series. The diastereomers however follow the established design strategy towards metal-based protein kinase inhibitors,^[109] and might inhibit other kinases as well. It is therefore possible that their different cytotoxicities are due, at least in part, to distinct protein kinase inhibition properties.

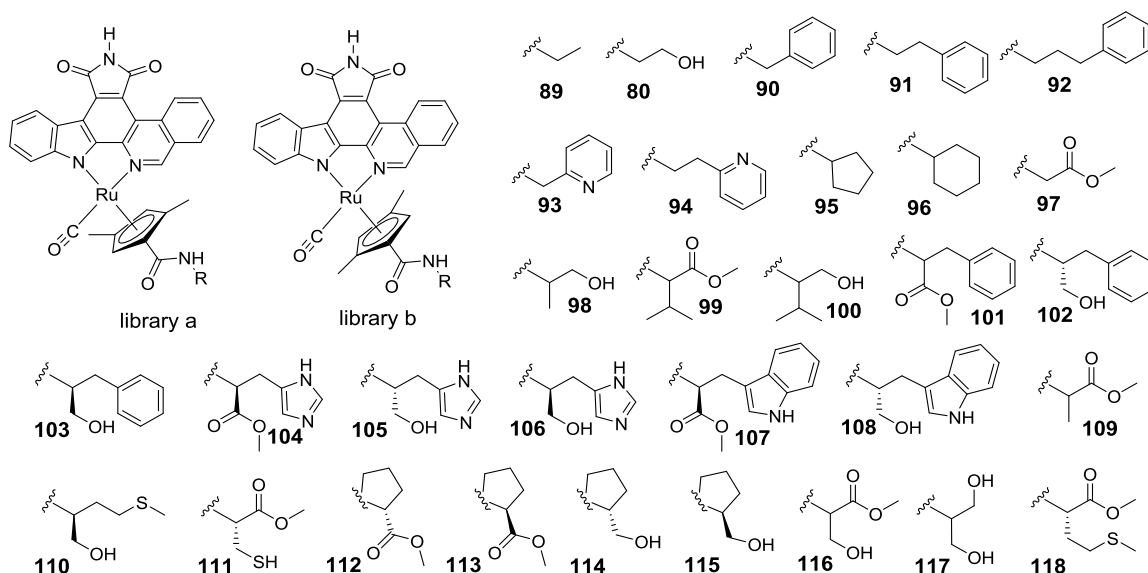


Fig. 23: Full list of compounds of the asymmetric library synthesised by NICHOLAS PAGANO, originally to identify TrkA inhibitors. For **112-115** the amine is part of the five membered pyrrolidine ring.

In order to evaluate the differences in cytotoxicity of the half-sandwich complex library, including different diastereomers based on the opposite planar chirality, all compounds were screened for their cytotoxicity against HT-29 cells at a single concentration of 1 μM . The results are summarised in Fig. 24 and were included into the initial database.

Results and discussion

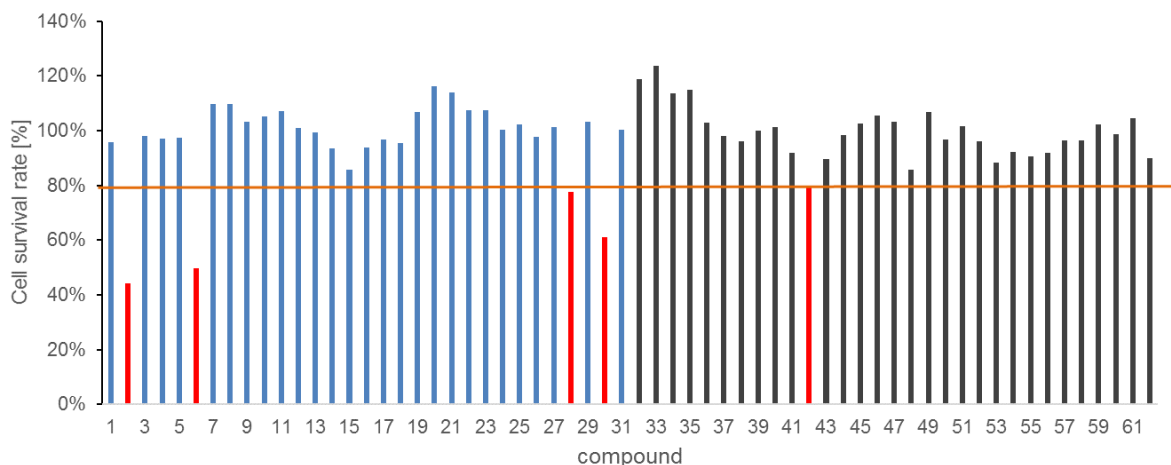


Fig. 24: MTT results of NICHOLAS PAGANOS library, which includes the initial screening hit np829 (**80b**). Compounds 1-31 represent the compounds **89b**, **80b** and **90-118b**, compounds 32-62 the analogue compounds of the a series. All compounds with cell survival rates below 80% at 1 μ M compound concentration for 24 h are indicated in red.

Based on the results four compounds from the b series (**80b**, **93b**, **115b**, **117b**) and one compound from the a series (**98a**) were identified as hits based on the previously set limits, while their diastereomers displayed no cytotoxicity under the same conditions. The results also confirmed **80b** again as a very potent compound. Based on the kinase inhibitory assay against Pim1 and TrkA, these kinases however are not the primary reason for its cytotoxicity, since other compounds showed much better values in the original assay but lower cytotoxicity in the MTT screening.

3.1.2.1. Development of a simplified structural derivative of the hit **80b**

The synthesis of the ethyl 2,4-dimethylcyclopenta-1,3-dienyl-based complexes as **80b** is quite time and resource extensive as shown in detail in chapter 3.1.3. Therefore, a simplified structural analogue was considered to avoid this problem. The easy access to varied side chain modifications using an active NHS ester functionality at an otherwise unmodified cyclopentadienyl ring has been described by the MEGGERS group.^[49,163] Since the elimination of the two Cp-methyl groups are thought to have an effect on both the biological and physical properties of the complex, based primarily on possible nonpolar interactions, it was hoped to be able to compensate that by modifying the free terminal hydroxy group of the coupled amide to a methyl ether (Fig. 25).

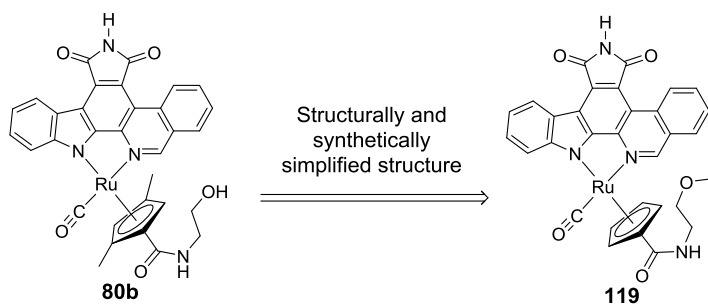
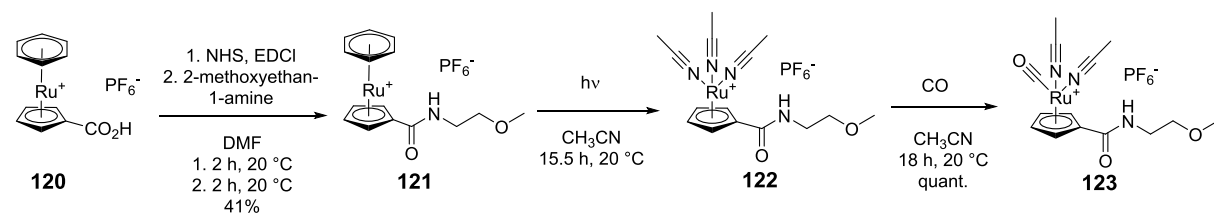


Fig. 25: Simplified structural analogue of **80b** in which the terminal hydroxy group is modified towards a methyl ether to compensate for the missing methyl effect of the elimination of two Cp-based methyl-groups.

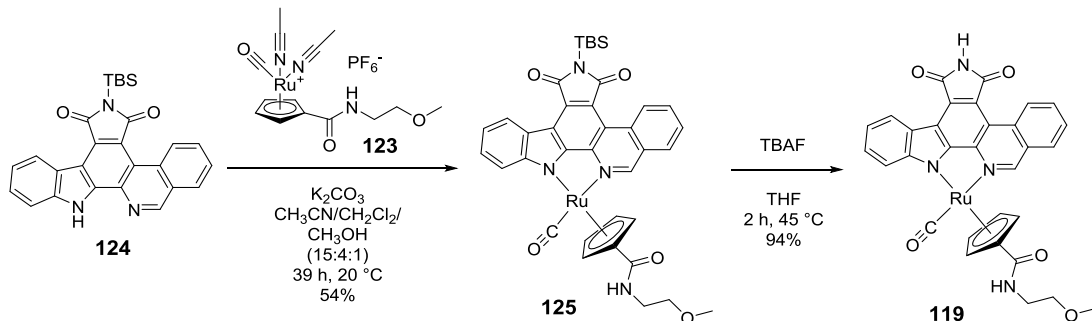
The complex was easily prepared based on the literature known isoquinolinocarbazole^[148] and some variations of the previously described NHS-ester approach (Scheme 1).^[49] Starting with sandwich complex **120** the hexafluorophosphate salt of (η^6 -benzene)(η^5 -N-(2-methoxyethyl)cyclopentadienyl carboxamide) ruthenium (**121**) was prepared by amine coupling using *N*-(3-dimethylaminopropyl)-*N'*-ethylcarbodiimide hydrochloride (EDCI) to form the according activated NHS-ester, which was further reacted with 2-methoxyethan-1-amine *in situ*. Following photochemical replacement of the benzene by three acetonitrile ligands and CO conversion (quantitative over 2 steps) led to the desired precursor complex **123**.



Scheme 1: Synthesis of metal precursor **123** based on a modified literature known synthesis.^[49,163] The carboxylic acid is reacted to the carboxamide by EDCI coupling of NHS and subsequent reaction of the active ester with the amine. This is followed by photochemical replacement of the benzene and CO conversion.

Results and discussion

The reaction of **123** with TBS-protected isoquinolinocarbazole **124**^[148] at 45 °C in the presence of K₂CO₃ provided the half-sandwich complex **125** in 69% yield, which was subsequently deprotected using TBAF to yield in **119** as racemic mixture in 94% yield.



Scheme 2: Reaction condition towards the desired complex **119**. The pharmacophore ligand and metal precursor are reacted in the presence of K₂CO₃ to yield in **125** which is subsequently deprotected using TBAF to yield in **119**.

The complex was further tested in the MTT setting in HT-29 cells in a concentration dependant assay and showed only marginal cytotoxicity up to 30 μM, indicating that either the methyl groups at the Cp ring are mandatory or the free terminal hydroxy group.

3.1.2.2. Further structural analogues of 119

Based on the previously mentioned NHS active ester approach NICHOLAS has not only created a library of structural analogues of **80b** but also of **119**, using 44 different amide side chains,^[202] to screen for a lead structure of improved MST-1 inhibitors. The respective structures are shown in Fig. 26.

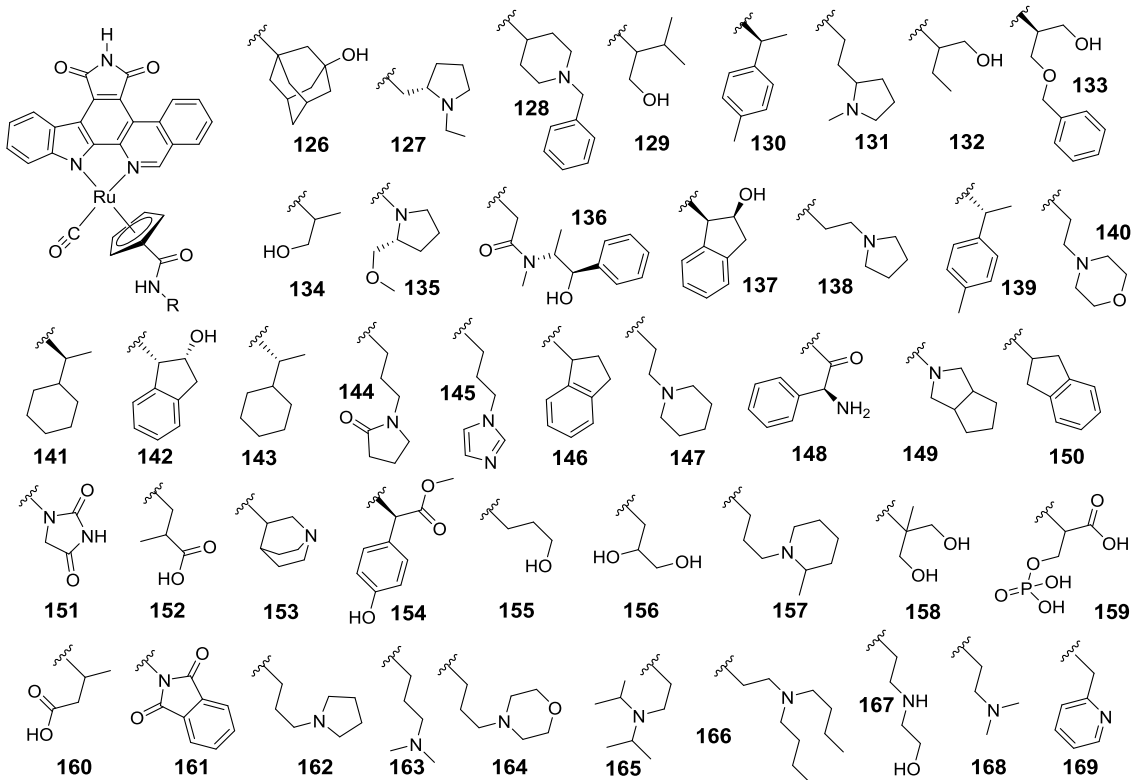


Fig. 26: Full list of structural analogues of **119** synthesised by NICHOLAS PAGANO for the identification of MST1 inhibitors.

Some of the compounds in this library respectively showed remaining MST-1 kinase activity of down to <10% under the screening conditions (615 nM inhibitor, 100 μM ATP) in a kinase assay.^[163] However, no compound showed significant cytotoxicity properties (<80%) in the subsequent cell-based MTT assay (Fig. 27), thereby indicating the importance of the methyl groups on the cyclopentadienyl moiety, especially when comparing the structurally very similar compounds **80b** to **134** (however **98b** represents no hit), **93b** to **169** and **117b** to **158**, where the first given structure each represents a hit in the 2,4-dimethylcyclopenta-1,3-diene-based library.

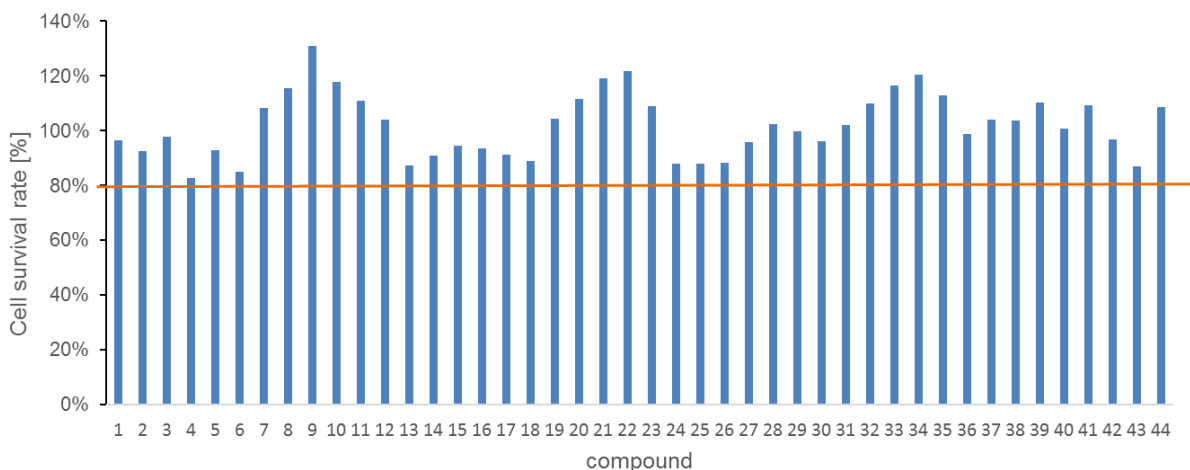
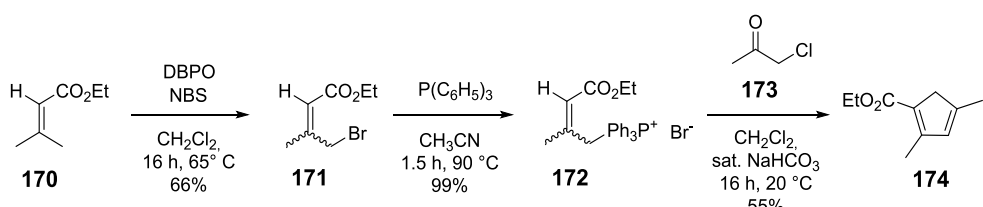


Fig. 27: MTT results of NICHOLAS PAGANOS second library (derivatives of **119**), which contains no hits for the set limits. This highlights the importance of the dimethylation of the Cp-ring in the former library. Please refer to Fig. 26 for the full list of structures, compound 1-44 equals **126-169**.

Based on all accumulated results it was decided to take the two most promising compounds concerning cytotoxicity in HT-29 cells ahead for further investigations, namely **80b** and **93b**, which showed the lowest cell survival rates in the initial screening.

3.1.3. Synthesis and upscaling of the hits 80b and 93b

As previously mentioned, the synthesis of ethyl 2,4-dimethylcyclopenta-1,3-dieyl-based complexes is quite complex. First, the ligand ethyl-2,4-dimethylcyclopenta-1,2-diencarboxylate had to be synthesised. Starting with ethyl-3-methylbut-2-enoate (**170**) *E/Z*-ethyl 4-bromo-3-methylbut-2-enoate (**171**) can be easily synthesised using a literature known method.^[205–207] All three publications however use carbon tetrachloride (CCl₄) as solvent for the classical WOHL-ZIEGLER bromination using *N*-bromosuccinimide (NBS) and a radical starter like dibenzoyl peroxide (DBPO)^[205,207] or azobis(isobutyronitrile) (AIBN)^[206] at reflux conditions. To avoid the use of CCl₄, the reaction conditions were optimised for the use of dichloromethane (CH₂Cl₂) using DBPO as radical starter and an increased reaction time, related to the reduced reaction temperature based on the lower boiling temperature of CH₂Cl₂. Please refer to the experimental section for reaction details of the most successful reaction conditions. Purified enoate **171** (Scheme 3) was further converted to its according phosphonium salt (**172**) using S_N2 conditions following a literature procedure.^[208] The phosphoniumbromide was directly converted further to the cyclopentadiene according to a modified literature procedure,^[209,210] using NaHCO₃ aq. as base and chloroacetone as reaction partner. In this reaction **172** is deprotonated in the allylic position, forming a Wittig ylide, which attacks the chloroacetone in an S_N2 reaction. After a second deprotonation, the cyclopentadiene is formed via a [2+2] cycloaddition (intramolecular WITTIG reaction) where triphenylphosphine oxide is eliminated. For obvious reasons of hindered rotation around the double bond, only the (*Z*)-isomer **172** can undergo the cyclisation to the five membered ring in **174**, which also explains the low yield in the reaction.

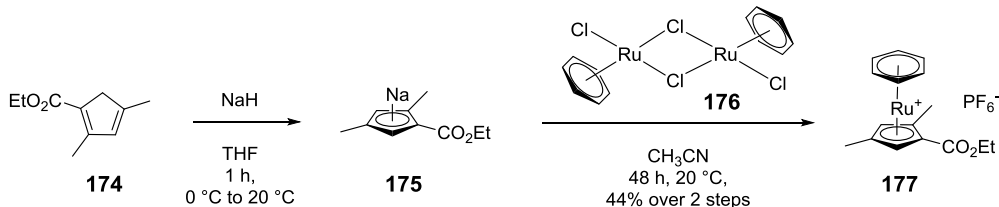


Scheme 3: Reaction conditions for the synthesise of ethyl-2,4-dimethylcyclopenta-1,2-diencarboxylate (**174**) based on variations of literature known methods. The enoate **170** was first brominated under WOHL-ZIEGLER bromination reaction conditions and further converted in an S_N2 reaction to the according triphenylphosphoniumbromide which was reacted with chloroacetone (**173**) to yield the final ligand. The final reaction step includes the formation of a WITTIG ylide and intramolecular WITTIG reaction.

Following the synthesis of the ligand **174**, a metal precursor for the complex synthesis had to be prepared. Literature describes the preparation of **177** using sodium hydride to form intermediate **175** from **174** and further conversion using thallium(I) (Tl₂SO₄) to form a cyclopentadienylation reagent before conversion to **177** using a metal source like **176**,^[203] which can be easily prepared

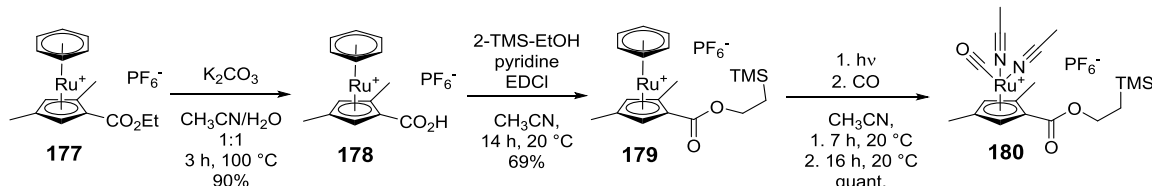
Results and discussion

using a well-established literature method.^[211] This reaction however also works, although in slightly lower yields, without the preparation of the Tl species, avoiding the use of the extremely toxic metal. While literature reports 67% yield over all steps,^[203] the avoidance of Tl(I) still gives 44% yield (Scheme 4) using **175** as Cp transfer reagent.



Scheme 4: Synthesis of metal precursor **177**. The cyclopentadiene **174** is reacted with NaH and further converted with μ -chloro ruthenium dimer **176** to yield in the racemic sandwich complex **177**. Only one isomer for **177** is shown for clarity.

Starting with sandwich complex **177**^[209,210] the racemic metal precursor **180** can be obtained over four additional steps (Scheme 5), based on a procedure that is analogous to a recent report from our group.^[49] Accordingly, the ethyl ester **177** was hydrolysed with K₂CO₃ to the analogous carboxylic acid **178** (90%) and subsequently protected with 2-(trimethylsilyl)ethanol by EDCl coupling (69%) to yield the ester **179**. Following photochemical replacement of the benzene by three acetonitrile ligands^[212] and CO conversion (quantitative over 2 steps) led to the desired metal precursor **180** in good yields.



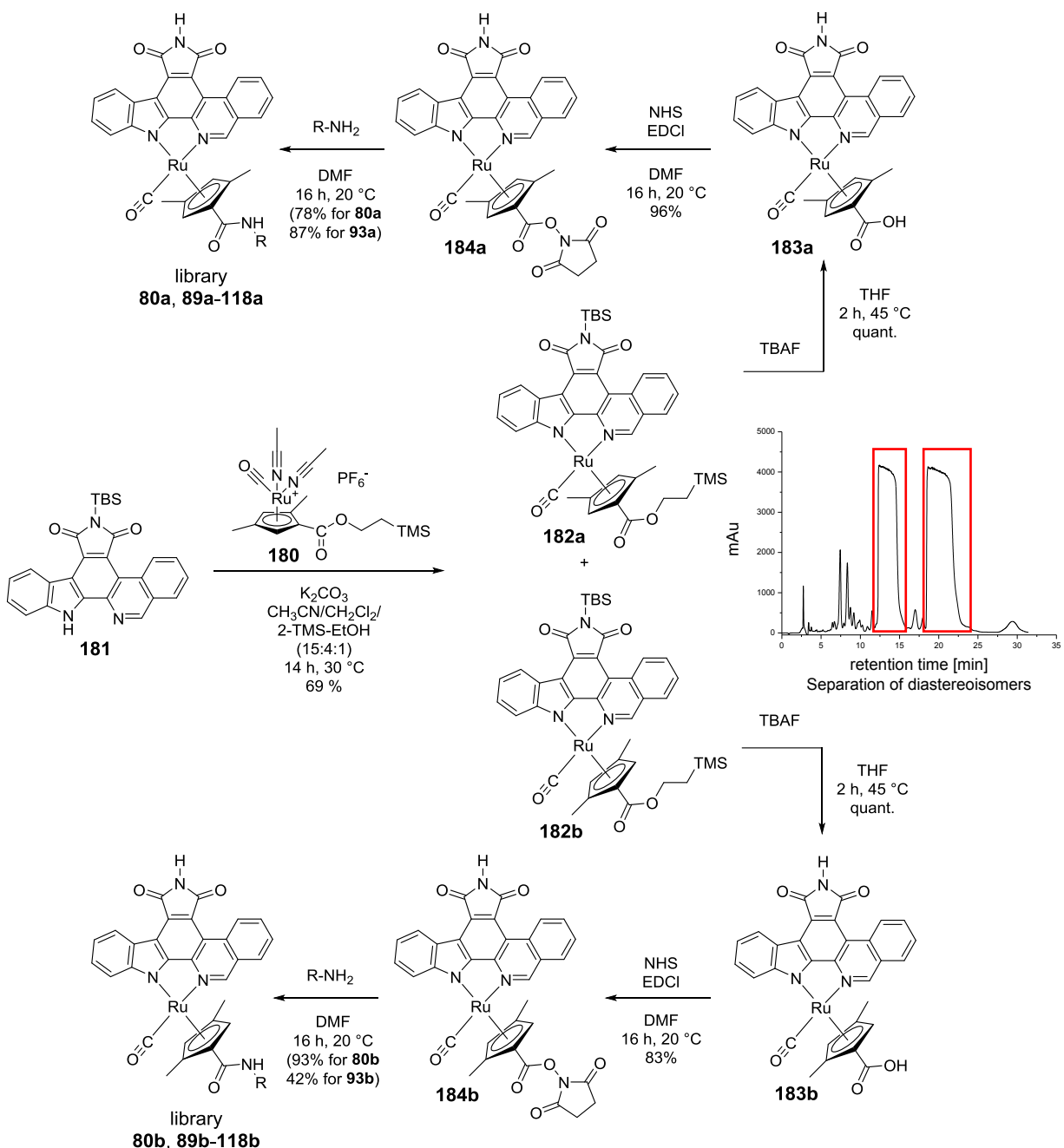
Scheme 5: Synthesis of racemic metal complex precursor **180**. Only one enantiomer each is shown. After the ester hydrolysis, the resulting carboxylic acid is protected using 2-TMS-EtOH in an EDCl coupling. Photochemical replacement of the benzene and subsequent CO conversion yields the final metal precursor **180**.

The reaction of **180** with TBS-protected isoquinolinocarbazole **181**^[148] in the presence of K₂CO₃ and 2-(trimethylsilyl)ethanol provided the two diastereomeric half-sandwich complexes **182a** and **182b** in 69% yield as nearly equal mixtures of diastereomers (Scheme 6), which were separated via preparative HPLC on a silica gel stationary phase using hexane/ethyl acetate (93:7) as eluting solvent. It has been previously shown, that the separation of diastereoisomers or enantiomers at this point is much more successful compared to the final complexes, as it is true for the analogue complexes using an unmethylated cyclopentadiene derivative.^[202] In smaller scales (0.39 mmol

based on the ligand) the separation can easily be done with standard silica flash chromatography using toluene as eluting solvent,^[202] however using larger scales (1.00 mmol) the insolubility of the compound leads to a strong smearing of the diastereomers based on low solubility and therefore a more complicated separation process. A dry load of the compound, which is stable enough to be heated on silica at 40 °C to remove the solvent, using CH₂Cl₂/acetone for loading improves the situation, but still leads to an unclear separation using either toluene or hexane/ethyl acetate in comparison to the HPLC approach using hexane/ethyl acetate (93:7) as confirmed by both TLC and NMR analysis. The same holds true using toluene as eluting solvent for HPLC or adding acids like acetic acid in the flash column chromatography approach, which seems to improve the overall solubility and therefore separation.

Deprotection of the maleimide and the carboxylic acid of the complexes **182a** and **182b** was subsequently achieved with TBAF treatment, providing **183a** and **183b** in quantitative yields (Scheme 6). In this step, some aliphatic impurities from the deprotection could not be removed, however those did not affect the following steps and could be eliminated after the conversion to the final product. The modification of the carboxylic acid attached to the cyclopentadienyl moiety was achieved most rapidly by conversion to activated NHS esters **184a** (96%) and **185b** (83%), followed by the conversion with ethanolamine to yield the diastereomeric complexes **80a** (78%) and **80b** (93%) which were purified via silica gel flash chromatography. Analogue reaction to **93a/b** by MADDIE SHERLOCK, using 2-picolyamine as reagent yielded in 87% and 42% respectively. The NHS esters can also be used to react with amides or esters simply by addition of the corresponding amine or alcohol, which may be used for the synthesise of the previously shown amide libraries.^[49,163]

Results and discussion



Scheme 6: Synthesis of **80b** and **80a**. Starting with TBS-protected isoquinolinocarbazole **181**, the diastereoisomers **182a** and **182b** were obtained by reaction with the metal precursor **180** in nearly equal amounts. Retention times during separation of diastereomers is shown on the used semi-preparative scale using an unmodified silica column with isocratic mixture of hexane/EtOAc 9:1 as indicated in the experimental section. The complexes were deprotected using TBAF in THF and further converted to the active ester with NHS using an EDCl coupling. The obtained active ester **184a/b** can be used for a library synthesis, as in **89a/b-118a/b** using the respective amine. Compounds **80a** and **80b** were prepared accordingly using ethanolamine.^[213]

Since for this work mainly the *N*-(2-hydroxyethyl) amide side chain was required, a much cleaner approach to the complexes **80a/b**, which also would limit the overall consumption of the ligand **181**, is the use of a precursor which inherits the final side chain, meaning less reaction steps of the

isoquinolinocarbazole complexes. For that matter it seemed simple to deprotect **179** and convert it via EDCl coupling to the active ester and to the side chain modified sandwich complex. After photolysis and CO conversion the metal precursor could just be reacted with **181** and the final complex only required TBAF deprotection. However, this “simple” approach was misguiding, since the sandwich complex seems to be far too water soluble to work up easily or it might have formed some kind of polymer in the subsequent photolysis. After flash column chromatography of the sandwich complex using CH₃CN/H₂O/KNO₃ _{aq.} 50:3:1 the precipitation with NH₄PF₆ yielded in almost no compound. After removal of the solvent and a second flash column, precipitation seemed to work with sodium tetraphenylborate. The complex could be extracted with CH₂Cl₂, in a way that no more complex was found in the aqueous layer according to TLC analysis. The ¹H-NMR spectrum of the complex was not clean but looked promising, so that the subsequent photolysis and CO conversion was followed up. However, after the standard reaction and work up, the benzene signal in the ¹H-NMR spectrum disappeared as expected, but no acetonitrile signals were found either. The Cp-signal did broaden as well in the spectra and no matching MS signal was found. The compound was not reactive when trying to react it with **181** and K₂CO₃ in CH₃CN/CH₂Cl₂/CH₃OH. Therefore, the approach was not followed up, since the original reaction conditions leaded to sufficient compound for further experiments.

3.1.3.1. Synthesis of further derivatives of **80b** and **93b** for the determination of structure activity relationship (SAR)

Based on the hits from NICHOLAS PAGANOS library, structural similarities of all interesting compounds could be identified, including a free hydroxy group (**80b**, **98a**, **115b**, **117b**) or the pyridine nitrogen in γ -position of the amide, indicating a probable trend for the importance of H-bond donor or acceptors in this position for either binding to a target which is responsible for the cytotoxicity or for physicochemical properties which might allow the compound to be transported or be uptaken. To also allow studying the effect of this position, 15 complexes of the a and b series (including **93a/b** for comparison) were synthesised by MADDIE SHERLOCK in a small library (Fig. 28) according to the experimental section.

Results and discussion

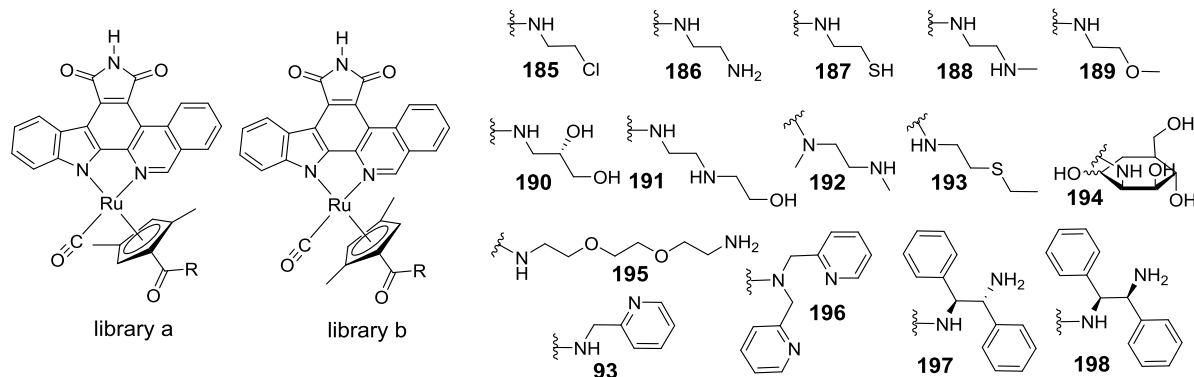


Fig. 28: Structural derivatives synthesised for SAR by MADDIE SHERLOCK.

The synthesised library was further tested in HT-29 cells at the same conditions as the previous compounds. The results are shown in Fig. 29.

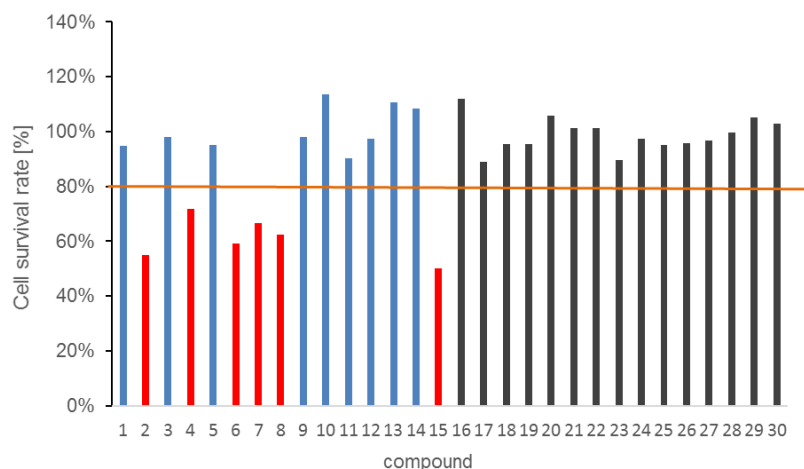


Fig. 29: MIT results of MADDIE SHERLOCKS library, which includes the initial screening hit **93b**. Compounds 1-15 represent the compounds **185b-198b** and **93b**, compounds 16-30 the analogue compounds of the **a** series.

The results confirm the initial assumption that compounds with an H-bond donor (based on OH and NH) in the γ -position indeed have generally a higher cytotoxicity (**186b**, **188b**, **190b-192b**) if the other substituents are not too bulky (**197b** and **198b** are no hits). γ -Cl (**185b**), SH (**187b**), OCH₃ (**189b**) residues and other compounds which miss a H-bond donor at this position (**193b-196b**) do not show any significant cytotoxicity. Still **93b** is a hit in this assay, even if only a very small portion to none of the pyridine should be protonated at the assay pH of around >7-8, why remains unclear. All compounds from the a-series show no significant cytotoxicity as expected, indicating, that **98a** might have been a wrong hit in the initial series with its cell survival rate of just below 80%.

3.1.4. Determination of stereoinformation in **80a**

The assignment of the relative configurations of the coordinated modified η^5 -N-(2-hydroxyethyl)-2,4-dimethylcyclopenta-1,3-dienylcarboxamide-ring in relation to the metal centre in **80a** and **80b** was achieved unambiguously with an X-ray crystal structure of the non-cytotoxic isomer **80a**. For that matter, single crystals were obtained upon slow diffusion of dichloromethane at 22 °C from a 10 mM DMSO solution of **80a** which was diluted with dichloromethane in a ratio of about 1:10. The other isomer formed only amorphous precipitate under the same conditions. The intensity data of the single crystals were collected at 100 K using a Bruker D8 Quest system. The data were corrected for absorption effects using multi-scanned reflections.^[214] The structure was solved using direct methods (SHELXS-97)^[215] and refined using full matrix least squares procedure (SHELXL-2013). Hydrogen atoms were included at calculated positions. Please be aware that only one enantiomer is shown. All previous drawings are based on the assigned stereochemistry of this crystal structure.

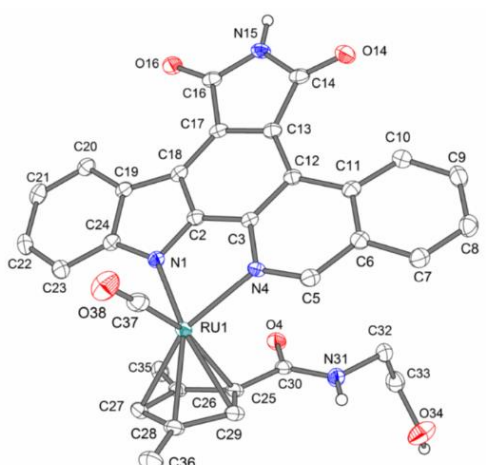


Fig. 30: Crystal structure of the diastereomer **80a** revealing the relationship between the facial π -coordination of the cyclopentadienyl moiety and the metal-centred chirality. ORTEP drawing with 50% probability thermal ellipsoids. Only one enantiomer is shown. Solvent is omitted for clarity.^[213]

3.1.5. Integrity and purity of **80a** and **80b**

To verify purity and integrity of the complexes **80a** and **80b**, also in regards to the possible interactions of impurities in biological assays, HPLC-chromatography was performed on an Agilent 1200 Series HPLC System. Therefore, the 10 mM DMSO stock solutions of **80a** and **80b** used in the biological experiments were diluted 1:99 with CH₃CN and 25 µL of the obtained (100 µM) solution was injected into the HPLC-system. The runs were performed with a LiChroCART® Purospher® STAR RP-8e (particle size 5 µM) column (250 x 4.6 mm): solvent A, CH₃CN; solvent B, 0.1% TFA in H₂O; 80-0% B in 20 min, flow rate 1.0 mL/min at a column temperature of 40 °C. UV absorption was detected at 254 nm. In those HPLC traces (Fig. 31) only minor impurities, as seen in the according NMR-spectra, can be detected.

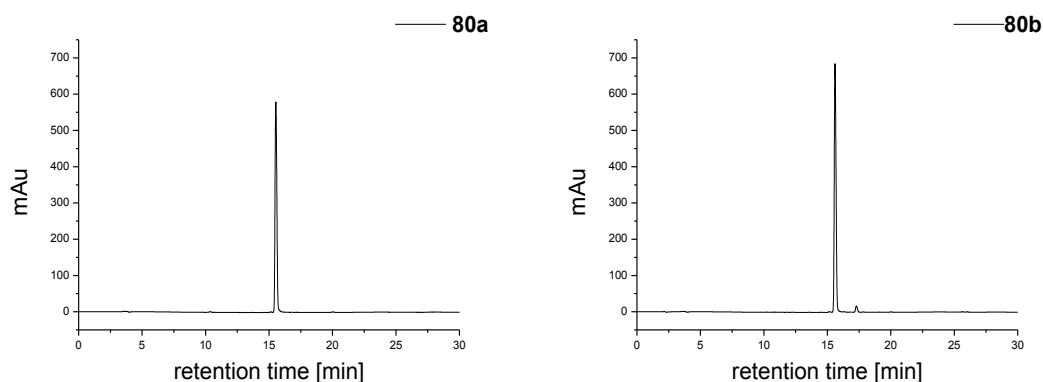


Fig. 31: HPLC traces of the complexes **80a** and **80b**, with retention times of 15.5 and 15.6 min respectively. HPLC conditions: LiChroCART® Purospher® STAR RP-8e (particle size 5 µM) column (250 x 4.6 mm); solvent A, CH₃CN; solvent B, 0.1% TFA in H₂O; 80-0% B in 20 min; flow rate 1.0 mL/min; column temperature, 40 °C; absorption detected at 254 nm. Only minor impurities can be detected in the HPLC-traces.^[213]

3.1.6. Cytotoxicity determination of **80b** and **93b**

To confirm and investigate the different effects of the diastereomers **80a** and **80b** on the viability of cancer cells, different cancer cell lines were exposed to various concentrations of the two diastereomers (racemic) for 24 h followed by cell viability determination via the MTT method. These cell lines include the afore used HT29 cells, the classical cervical cancer cell line HeLa, and two melanoma cell lines, the metastatic WM983B which inherits a natural BRAF mutation (V600E) and p53 wild-type (wt), and WM1366 with a NRAS mutation (61L).

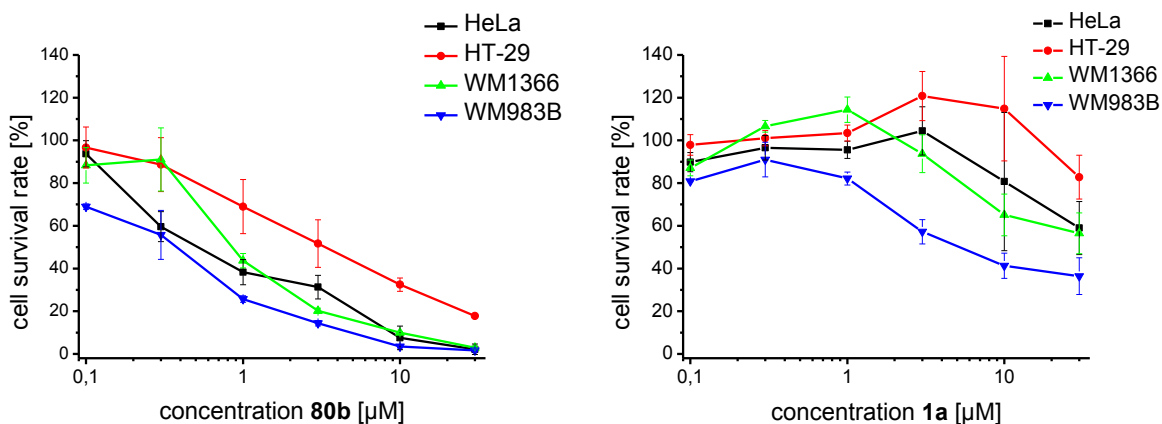


Fig. 32: Cell survival rates of cancer cells after treatment with racemic **80b** or racemic **80a** for 24 h. The cell viability was determined via the MTT method and calculated as percentage of surviving cells compared to untreated controls.^[213]

Indeed, Fig. 32 reveals again a different behaviour in terms of cytotoxicity for the different diastereomers. Whereas **80b** displays quite high cytotoxicities with estimated LD₅₀- or IC₅₀-values in the range of 2.9 μM (HT-29) to 0.4 μM (WM983B), **80a** is much less cytotoxic with cell survival rates of 82.8% (HT-29) to 36.4% (WM983B) at a concentration of 30 μM. Generally highest cytotoxicity was seen for both compounds in the p53 wt cell-line WM983B, lowest toxicity in HT-29 cells, confirming the previous mentioned trend of low sensitivity of these cells for our kinase inhibitors.

In addition to these in-depth cytotoxicity studies of **80b** and **80a**, also **93b** and **93a** were tested in a concentration dependant MTT assay in HT-29 cells. The results are shown in Fig. 33.

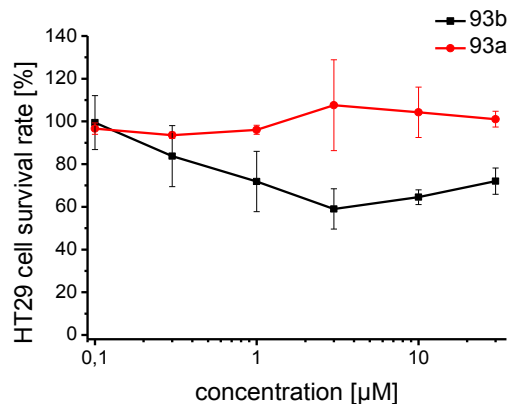


Fig. 33: Cell survival rates of HT-29 cells after 24 h treatment with **93a** and **93b**. The overall cytotoxicity is quiet low in comparison to **80b** and the **a** isomer again shows no significant cytotoxicity.

It becomes clear, that **93b** is much less cytotoxic than **80b**, and its diastereoisomer **93a** again shows no cytotoxicity at all. One should notice however, that during the experiments for both compounds large red crystals were observed in the cell medium, indicating solubility issues for both diastereoisomers as a new parameter which might influence cytotoxicity. This leads to further studies on **80a** and **80b**, to see whether differences in solubility might be one reason for their different cytotoxic behaviour, since we already experienced different crystallisation behaviour during crystal growth for X-ray determination of the stereochemistry.

3.1.6.1. Solubility studies in cell medium of **80a** and **80b**

To investigate possible solubility issues of **80a** and **80b**, both compounds were tested again for a cell-based cytotoxicity in HeLa cells, since these cells seem to detach later from the solid support in comparison to HT-29 cells when undergoing apoptosis. Throughout the incubation time with a compound concentration of 30 μM -0.1 μM , a crystallisation of **80a** and **80b** was monitored. Whereas **80a** obviously crystallises in the cell medium like **93a** and **93b**, **80b** seems to mainly enter the cells and to visibly crystallise inside or attached to the cells at concentrations of 30, 10, 7.5 and 5 μM (Fig. 34). Interestingly, in the higher concentration range this crystallisation effect, as well as first signs of apoptosis, could already be observed only 5-6 h after compound addition.

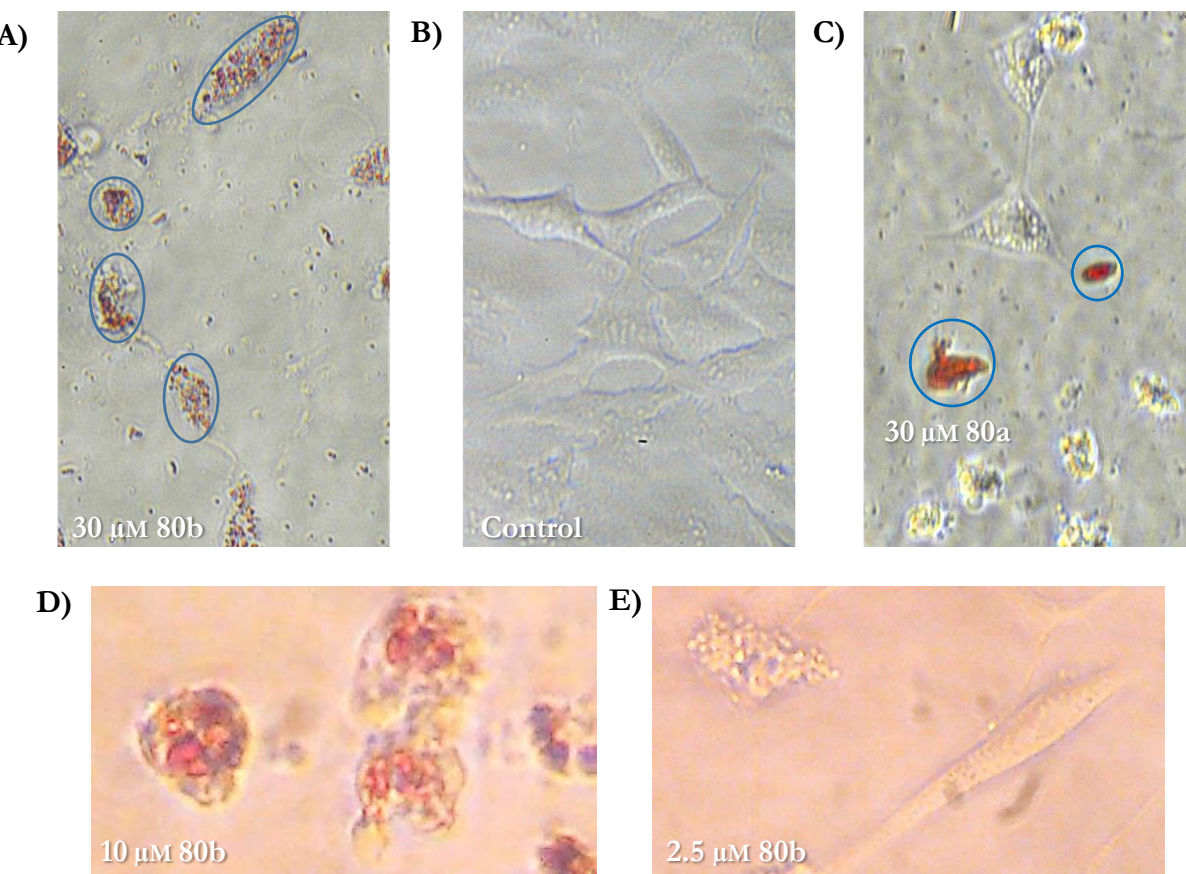


Fig. 34: HeLa cells 24 h after substance addition. A) 30 μM of **80b**: the compound seems to mainly enter the cells and crystallises until the cells die. A smaller amount forms crystals in the medium. Most of the cells died and only cell fragments remain. B) Reference: cells were incubated with 1% DMSO and the cells are healthy. C) 30 μM of **80a**: the compound forms large and small crystals in the cell medium which seems to have minor effect on the cells. Only a few cells have died, the others look healthy. D) 10 μM of **80b**: the cells show signs of apoptosis (rounding, detachment from the ground, blebbing) and obvious red spots inside or on top of the cells. E) With the lower concentration (2.5 μM of **80b**) some cells look apoptotic as well, most look healthy and no obvious localisation of compound can be seen. Samples A)-C) are prepared in medium without phenolred, while D) and E) are prepared in phenolred containing medium.

Results and discussion

To verify our assumption that the crystal formation of **80b** occurs inside cells and not on their surface, scanning electron microscopy (SEM) experiments were performed by Michael Hellwig at the centre for material sciences at the Philipps-Universität Marburg. Accordingly, HeLa cells were grown on small cover glasses without surface treatment in 6-well plates, incubated for 14-16 h with 5-10 μM of **80b** and were afterwards either chemically fixed or freeze dried. When simply washing and then freezing the cells in liquid nitrogen, they almost completely detach instantly. The shortened incubation time was chosen based on the fact, that detachment of the cells is much easier on simple glass in comparison to the treated surface of the well plates used previously. For freeze dried samples, the cells were first washed with PBS and afterwards quickly with $d\text{dH}_2\text{O}$ to avoid the formation of salt crystals on the surface. This however leads to a swelling of the cells due to osmotic effects, and following SEM experiments showed large holes in the cell membrane, as well as partially broken cells, indicating this method of fixation not suitable for our purposes.

Using chemical fixation on the other hand, by protein and lipid cross-linking with glutaraldehyde and osmium tetroxide followed by dehydration with ethanol,^[216] gave good results in cell surface and shape, as can be seen by the SEM images shown in Fig. 35. In both samples, freeze dried cells and chemically fixed cells, no sign of crystals on the cell surface could be found at compound concentrations of 5 μM or 10 μM , which strengthened our assumption that the compound crystallises after entering the cell. However, for chemically fixed cells the compound might have been dissolved during the washing steps with ethanol and for freeze dried cells disturbance in the cell membrane might have released the compound, indicating no final prove for **80b** to enter the cells before crystallisation. In addition to that, affected cells might have undergone apoptosis and thereby been detached from the glass surface before or during treatment.

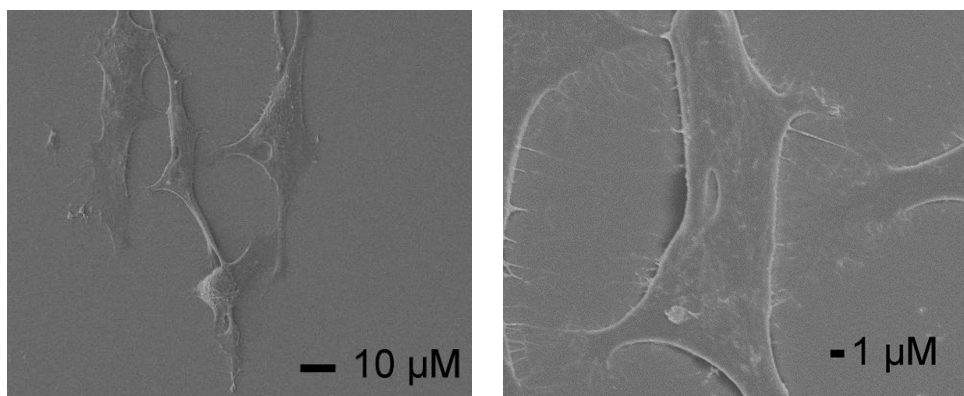


Fig. 35: HeLa cells which were chemically fixed 16 h after addition of 10 μM of **80b**. No signs of crystals on the cell surface were found in two independent samples.

Classical cytotoxicity-based approach

Assuming that **80b** indeed enters the cells, a similar crystallisation effect, called crystal-like drug inclusions (CLDIs), is known for the approved leprosy drug clofazimine (trade-name: Lamprene). The active ingredient accumulates to very high levels in tissue, forming intracellular liquid crystal-like supramolecular organisations, probably membrane-bound, multi-layered, liquid crystal-like, semi-synthetic cytoplasmic structures.^[217] Possible ways of crystal-formation discussed for clofazimine, including pH-dependant solubility through protonation state, protein-binding and associated complex formation with membranes, or precipitation as aggregates/crystals, which may be actively phagocytosed,^[217,218] are possible explanations for the crystal formation of **80b**.

Whether or not **80b** crystallises inside or on top of the cells, this effect is a deal-breaker for finding a suitable anticancer drug. Therefore, the classical cytotoxicity-based approach was dropped in favour for an approach investigating the drug like abilities of this compound class.

3.2. Drug-like properties of metal-based kinase inhibitors

The afore discussed cytotoxic approach led to a dead end with np829 (**80b**) and its derivatives. Therefore, an up-to-date approach to improve the chance of finding a suitable lead structure for a potential cancer drug was required. Since most of the MEGGERS group compounds possess kinase inhibitory properties, a screening of a selected range of compounds towards their so-called drug-like properties seemed to be the right choice. The profiling for these properties was done in collaboration with the Novartis Institutes for BioMedical Research (NIBR) in Cambridge, MA, USA.

Early *in vitro* profiling of drug-like properties has become an essential part of the drug discovery process. The term drug-like properties is thereby linked with all properties that affect ADMET (absorption, distribution, metabolism, excretion and toxicity) characteristics of the molecule.^[219] One of the first, and probably most known studies towards physicochemical properties and oral absorption has been published by LIPINSKI in 1997, pioneering the field.^[220] He defined drug-like compounds as those, that have sufficiently acceptable ADME and toxicity properties to survive through the completion of human phase I clinical trials.^[221] From his original study, LIPINSKI's rule of five were phrased, which describe the molecular properties important for a drug's pharmacokinetics in the human body after oral exposure. Accordingly, an orally active drug should have no more than two violations of the following criteria: 1) No more than five hydrogen bond donors, 2) No more than ten hydrogen bond acceptors, 3) A molecular mass less than 500 Da and 4) an octanol-water partition coefficient (logP) not greater than five.^[222,223] These properties however apply to purely organic molecules and can be considered as a rule of thumb and not absolute cut-off values. Organic KIs for example tend to have high molecular weight because of the need for special structural features to gain kinase selectivity.^[14] A recent study showed that more than 30% of FDA approved SMKI actually have a molecular weight exceeding 500 Da, and 50% have one greater than 480 Da, while the numbers of H-bond donors and acceptors are well within the set range.^[26] However metal-based KIs cannot be simply classified by the LIPINSKI rules, as the rule of five is empirically determined for approved small molecule drugs, and may not necessarily apply for metal-based drugs in the same way.^[224] Especially the molecular weight of these compounds often is much higher than 500 Da, due to the heavy metal centre, which does not affect the overall size as much as an organic fragment of pure organic origin would do. A simple estimation of drug-like properties based on these basic rules would therefore be insufficient.

Drug-like abilities nowadays however cover more than the criteria stated by LIPINSKI. They incorporate suitable biopharmaceutical properties such as solubility, stability, permeability, and first-pass effect, as well as pharmacokinetic (PK) properties like clearance rates, biological half-life,

Drug-like properties of metal-based kinase inhibitors

extent of protein binding and volume of distribution, which are responsible for the entry of a drug into the body and across various cellular barriers.^[222] The common strategy for the pharmaceutical industry today includes the evaluation of a holistic picture with the parallel assessment of efficacy, drug-like properties and safety with simple *in vitro* assays predictive for toxicology and pharmacological promiscuity of drug candidates, in order to assist efficient lead optimisation and reduce a high attrition rate of drug candidates in development and during early clinical trials due to ADME issues.^[225] In general achieving a good balance between all these parameters is important, since a drug must reach its target in the body and have a reasonable potency to elicit an *in vivo* response.^[219] Organic kinase inhibitors tend to have a high MW and during optimisation stages often highly hydrophobic and conformationally constrained drugs are derived, which have limited drug-like properties and a thermodynamic signature that is characterised by an entropically driven binding affinity. These compounds might show poor human pharmacological properties and limited *in vivo* target inhibition and efficacy, which continue to be a major source of clinical attrition in the oncology field with 53% from phase I to registration for KIs.^[226] These facts highlight the importance of monitoring drug-like abilities for KIs.

Drug-like abilities for metal-based drugs can also be described as metallomics, which characterise the entirety of metal and metalloid species present in a cell or tissue type, as well as their interactions with the genome, transcriptome, proteome, and metabolome.^[227] Metallomics also stands for the metabolism of these drugs, transport and interactions with biologically relevant molecules,^[228] and attempts to understand metal uptake, trafficking, function, and excretion in biological systems.^[228] In this study however, only very basic concepts of metallomics will be studied and discussed, since in depth interaction studies with biological molecules were not intended, but instead a basic understanding if the compound might reach its kinase target within a living individual, by studying basic PK parameters.

To get a first impression, the initial focus was set on the drug-like properties of metal-containing kinase inhibitors which are part of the composite parameter bioavailability, that is influenced by solubility, absorption and clearance as well as permeability.^[222,229] Solubility and absorption are thereby known to be some of the major issues concerned in the design of new ruthenium containing complexes,^[191] and may also apply to other metals. For the study an initial set of nine different literature known inhibitors, as racemic mixtures, racemic mixtures of single diastereoisomers or single enantiomer, have been selected, based on various criteria like positive results in the initial cytotoxicity screening, previous results including specifically attractive kinase inhibitory properties, special functionalities or additional possible medical or biological applications (Fig. 36).

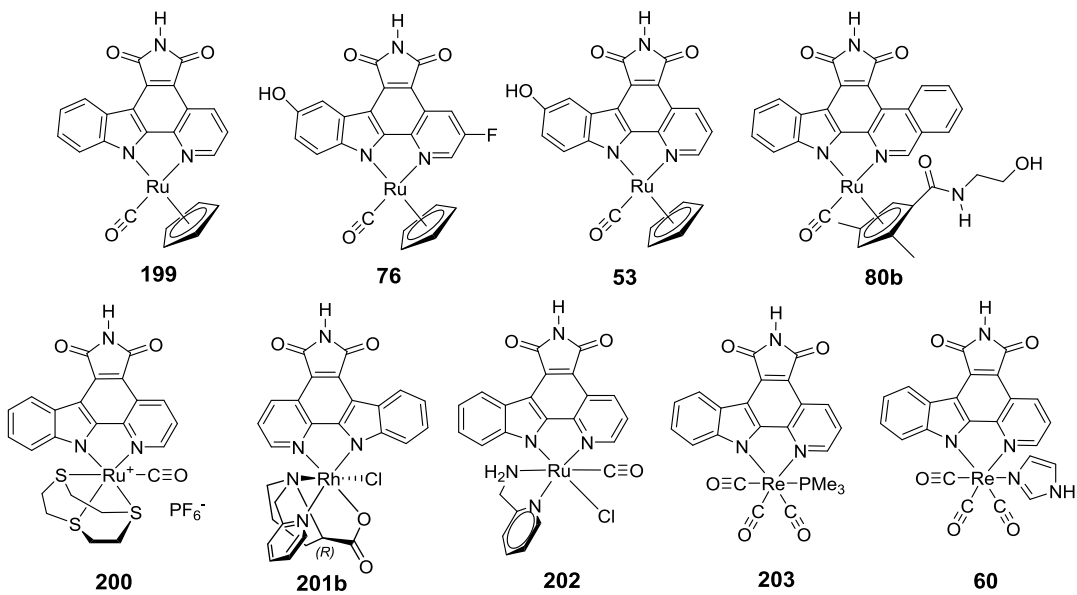


Fig. 36: Initial set of inhibitors intended to be tested for their drug-like properties in collaboration with NIBR Cambridge, USA. Complexes **199**, **76**, **53**, **80b**, **200**, **202**, **203**, and **60** are racemic mixtures. **80b** and **202** are thereby a racemic mixture of one of two diastereoisomers formed during their synthesis. **202** is a single enantiomer.

In detail, the RuCpCO-complexes **199**^[147], **76**^[122], **53**^[149] (resynthesised by FELIX KLEIN and SEBASTIAN WEBER)^[230,231] were previously reported as extremely potent inhibitors towards the kinases GSK3^[121,122,147,154] and Pim1^[48,121,122] and showed appealing properties in the original cytotoxicity screening as well as in previous *in vitro* anticancer studies.^[162] In addition to that the GSK3 inhibitory properties of **76** have been proven to activate p53 and induce apoptosis in melanoma cells *in vitro* and to disturb the embryonic development of *Xenopus laevis* *in vivo*, as it is expected for a GSK inhibitor and further elucidated in the introductory section.^[149] Ru complex **80b**^[213] was the most attractive compound from the original cytotoxicity screening in cancer cell lines. The compound **200**^[109,150] (resynthesised by MADDIE SHERLOCK) was included to evaluate the solubility and permeability of a charged compound, which should differ from uncharged compounds insofar as that the solubility should be improved and the permeability reduced in comparison to an uncharged compound.^[232] With the inherited CO-ligand it also belongs to the class of potent Pim1 and GSK3 inhibitors.^[109] Rh-complex **201b** (RR97b)^[233] (synthesised by RAJATHEES RAJARATNAM) belongs to a, at that point, newly developed class of stereoisomerically pure Rh-based compounds, which were thought to be good kinase inhibitors. This compound was especially alluring due to being isomerically pure, which should affect the results of the assays, e.g. solubility. The WALLACH rule states that racemic crystals are more stable and dense than their chiral counterparts, indicating, that **201b** might show an enhanced thermodynamic solubility c.f. the racemic mixtures.^[232] The compound **202**^[109,150] (resynthesised by SEBASTIAN WEBER),^[231] is another

potent GSK3 and less potent Pim1 inhibitor, which structurally differs from the CpCO-complexes, where the Cp ligand binds via a η^5 -mode, insofar that the bidentate ligand picolyamine and a monodentate chloride replace the Cp, whilst the important pharmacophore CO ligand in the plane perpendicular to the pyridocarbazole chelate stays in place.^[109] The final Re-compounds **60**^[169] and **203**^[169] (synthesised by KATHRIN WÄHLER) were originally developed as bifunctional compounds, with potential for photodynamic therapy as photosensitisers, and kinase inhibition. They produce ${}^1\text{O}_2$ upon light exposure, and are therefore photocytotoxic, as it has been shown in cancer cell experiments.^[169] Especially the imidazole derivative **60** shows good stability in the presence of β -mercaptoethanol and has an IC₅₀ against the kinase Pim1 of 58 nm,^[169] even if a kinome scan against 456 protein kinases showed that the compound is a selective but not very potent kinase inhibitor.^[234]

3.2.1. Analysis and quantification of compounds in drug-like property assays

Generally, high-throughput assays like the ones for drug-like abilities, as they are performed at NIBR, use a high-performance liquid chromatography-tandem mass spectrometry (LC-MS/MS) approach for compound quantification and further assay evaluation. For quantification, an internal standard for data standardisation and comparison is used, after auto-tuning the MS/MS unit to the compound by optimising the compound ionisation polarity, MS/MS transition, cone voltage and collision energy. To assist in finding the optimal conditions and to verify their suitability for analysis, all compounds were assessed for their retention time, preference for positive ionisation using either APCI or ESI and for the major signal in MS (in accordance with isotope pattern), depending on ionisation, protonation or ion formation with e.g. sodium ions. The reversed phase HPLC runs (CH₃CN / 0.1% AcOH 5:95 to 100:0 in 9 min, hold for 2 min, 100:0 to 5:95 in 9 min, flow rate 1 mL/min) were thereby performed using a C18 column (150 x 4.6 mm, particle size 5 μm) after injection of 10 μL DMSO-solution (25 μM) at a column temperature of 30 °C. For LC-MS runs 20 μL of a 100 μM DMSO-solution were used and they were performed in the same manner. Retention times were defined from major absorbance at 254 nm. All compounds had thereby retention times between 6.1 and 11.4 min and a major mass signal was found as [M⁺] or [M+H⁺] using at least one of the ionisation techniques. However, some of the compounds had low signals and/or a high background in the mass spectrum, probably due to fragmentation, ligand exchange reactions or poor ionisation. The full overview of the conditions and results of the measurements can be found in the digital supplementary information of the work.

In the hands of Novartis, the complexes **60**, **80b**, **200** and **201b** could be analysed using a triple quadrupole mass spectrometer, while the other compounds caused some problems because of low

Results and discussion

sensitivity or the observation of signals with an unknown mass. For some of the compounds (e.g. **199**, **56**, **73**) a direct injection into the mass unit caused a loss of the CO ligand ($[M-28]$), and an CO-CH₃CN exchange ($[M+13]$) in the flow with CH₃CN and 0.1% FA_{aq} when using LC conditions was observed, indicating instability of the compounds under the given conditions. The mass differences indicate an additional oxidation of the compounds in the set-up, either at the metal-centre or some part of the ligands, which might have been caused by the oxidative environment of ion source in positive mode. These ligand loss and exchange reactions were further verified using HRMS in the mass department of the Philipps-Universität Marburg. During these experiments, very low signal intensities, probably caused by ion suppression, were observed, explaining the low signals in all previous experiments. A sample chromatogram with HRMS of the original complex (**199**) and the CO-CH₃CN exchange is shown in Fig. 37. As Fig. 37 clearly indicates, in addition to ligand exchange (A) or loss reactions, additional signals (e.g. C) appear which further complicate the assessment of drug like properties using LC-MS. Similar problems occurred with **202** and **203**.

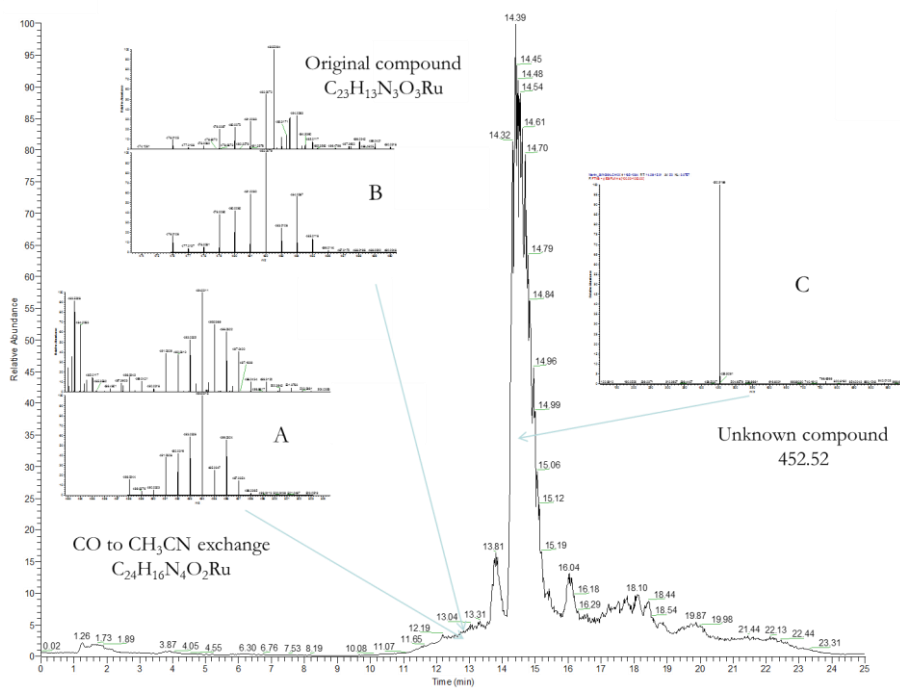


Fig. 37: Example LC-MS chromatogram of **199** showing an CO to CH₃CN ligand exchange in exact mass spectra. Additionally, a high background of a compound not containing Ru, as indicated by a missing isotopic pattern, can be found.

In summary, due to the described instabilities and analysis issues, only the complexes **80b**, **60**, **200** and **201b** were further investigated for their solubility, permeability and rat liver microsome stability using LC-MS/MS.

3.2.2. *In vitro* solubility, metabolic stability and permeability determination

3.2.2.1. Thermodynamic solubility assessment

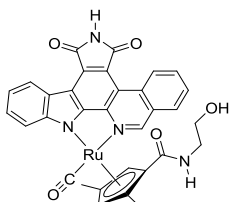
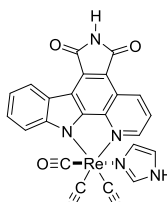
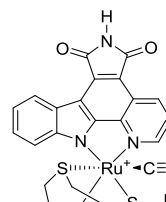
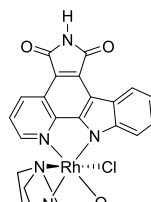
Solubility and dissolution rate of drug substances are critical for absorption, especially in the gastrointestinal (GI) tract, subsequent bioavailability and delivery to cellular targets.^[222,225,235] Low aqueous solubility can lead to precipitation in bioassay medium, leading to low or inconsistent bioactivity responses for *in vitro* bioassays,^[219] as it has previously been observed for compounds in this thesis e.g. **80a**. Therefore, solubility is important for proper interpretation of *in vitro* profiling results, as well as PK and PD data. It is most often determined as conventional thermodynamic solubility, starting with a solid material and using the “saturation shake-flask”-method, which is considered the gold-standard by industry and the FDA, as a result of its accuracy and reliability over a reasonable large solubility range.^[225] Thermodynamic solubility assays in general start with a solid material (either crystalline or obtained by evaporation of a solvent), taking packing information of the compound into account. Quantification of solubility and determination of purity and stability is monitored either by liquid chromatography coupled with ultraviolet spectroscopy (LC-UV) or mass spectrometry (LC-MS).^[225] The shake flask method has been further miniaturised towards a high-throughput method, saving time, cost and sample material to make it more feasible for early drug discovery.^[236,237]

Apart from simple aqueous buffers, solubility is nowadays often determined in biologically relevant media like fasted and fed state simulated intestinal fluids (FaSSIF and FESSIF), which provide a better prediction of the *in vivo* oral absorption behaviour.^[238] These buffers contain different concentrations of bile salts and phospholipids like lecithin, which are able to form negatively charged bile micelles (lecithin is zwitter ionic and tauchloric acid is fully deprotonated at physiological pH), as they are present in the intestinal fluid, and which are able to emulsify molecules. Thereby these buffers simulate the physiological conditions in the proximal small intestine.^[239] Even with poor thermodynamic solubility in standard buffers, an addition of bile salts can enhance solubility up to a level which is often sufficient for an adequate bioavailability.^[238] A study with 4148 organic compounds showed increased solubility in 82% of compounds in the updated FaSSIF-V2 (version 2) compared to a standard phosphate buffer,^[239] which shows the power of this kind of buffers.

Using the miniaturised shake-flask method, solubility of the complexes was determined at NIBR Cambridge, MA, USA using solid material obtained by evaporation of the solvent from a DMSO-stock solution. The solubility was tested at pH 6.8 in aqueous chloride free potassium phosphate buffer (KP_i) and FaSSIF-V2 and results were quantified using LC-MS/MS (Table 2).

Results and discussion

Table 2: High throughput thermodynamic solubility data for the first set of complexes tested. KP_i is an aqueous chloride free phosphate buffer, FaSSIF is fasted state simulated intestinal fluid. *All values < 5 μM are below their respective detection limit.

High throughput thermo- dynamic solubility				
	80b	60	200	201b
KP_i	< 5 μM*	< 5 μM*	< 5 μM*	< 5 μM*
FaSSIF-V2	< 5 μM*	17 μM	< 5 μM*	23 μM

As can be taken from Table 2 the solubility in potassium phosphate buffer at physiological pH (pH 6.8) is very low with values below the detection limit of 5 μM. The solubility for **60** and **201b** is thereby clearly enhanced when using FaSSIF-V2 buffer. In general ionisation, lipophilicity and crystal packing seem to play essential roles in controlling solubility in FaSSIF compared to that in aqueous buffer, and while lipophilicity driven solubility limitations in aqueous solution are improved in FaSSIF buffer, solubility limitations which are related to crystal lattice energy are not overcome by the FaSSIF ingredients.^[239] This suggests, that the solubility limitations we experienced here might be based on the hydrophobic character of the type of coordination compounds and not too much on the crystal lattice energy, at least in the crystal form used in the experiment. However a high crystal lattice energy induced by a low ratio of sp³ to sp and sp² carbons, gives the molecules increased π-π-stacking opportunities, and contained hydrogen bond donors and acceptors may additionally stabilise the crystal packing, indicating the possibility of a low solubility of our KIs based on crystal lattice energy.^[238]

Another probable explanation is, that electrostatic interactions might play a part in the solubility of these compounds in FaSSIF buffer. While the solubility of acids is generally not enhanced in FaSSIF buffer at physiological pH, probably because of the electrostatic repulsion of the deprotonated compounds and the FaSSIF micelles, the solubility of positively charged bases may undergo favourable electrostatic interactions with the micelles. These electronical repulsions, as observed for deprotonated acids, might explain why the solubility of **200** is not enhanced in FaSSIF buffer in comparison to KP_i buffer. Basic nitrogens from the ligand systems of **60** and **201b** however, should not contribute in an improved solubility of the compounds, since the basicity is lost due to the coordination to the positively charged Re/Rh centre.

3.2.2.2. Determination of metabolic stability in microsomes

Metabolism and subsequent *in vivo* clearance of drugs involve a multitude of enzymes and tissues including the hepatic, renal and biliary systems and is considered the most difficult ADMET parameter to predict.^[222] Metabolism thereby refers to the biotransformation process which converts drugs into e.g. more polar metabolites to facilitate biliary and renal clearance,^[222] where clearance describes the process of drug elimination from the body or from a single organ without identifying the individual processes involved and may be defined as the volume of fluid cleared of drug from the body per unit of time (e.g. mL/min).^[240]

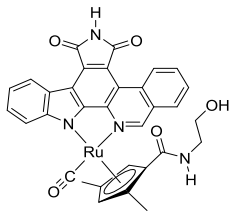
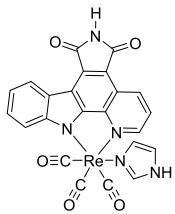
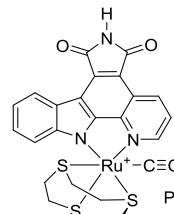
In general, when designing new drugs, metabolic rates of the compounds should be kept minimal to achieve low first pass metabolism and a half-life ($t_{1/2}$) that is suitable for once daily dosing.^[241] A metabolically labile drug might never reach adequate systemic exposure. The primary destination of orally administered compounds, and thereby the site of metabolism of most drugs, is the liver.^[225] Therefore hepatic clearance is one of the most important pharmacokinetic parameters influencing the clinical success of a molecule. It is fundamental to two of the key parameters that influence the *in vivo* exposure and thereby daily dose and dosage frequency: bioavailability (F) and the elimination half-life ($t_{1/2}$).^[241,242] To be able to determine metabolic rates and the risk that hepatic metabolic clearance may pose to pharmacokinetics and systemic exposure in early drug discovery, different high-throughput *in vitro* metabolic screens have been developed, including the usage of recombinant cytochrome P450s (CYPs), liver fractions (microsomes, S9 and cytosol), isolated hepatocytes and liver slices as source of metabolising enzymes.^[232,241] The use of these enzymatic sources reduces the requirement of animals (commercial and ethical advantages) and even makes it possible to evaluate metabolic rates in higher species like human.^[232] Metabolic stability assessment using liver microsomes generally has been widely accepted to predict metabolic clearance.^[243–245] The low cost and minimal interlot variability of microsomes make this model additionally amenable to high-throughput investigations.^[246] Mainly the contribution of cytochrome P450s (CYPs), which are highly enriched in the liver microsomal fraction along with UDP glucuronosyltransferases (UGTs), is monitored in liver microsomes, as this family of enzymes is known to dominate the metabolic clearance of ~75% of drugs. However, this model system has limitations in that extrahepatic and non-metabolic clearance routes are not represented.^[225,246]

Most often metabolic clearance is predicted by probing the disappearance of a compound in an incubation with microsomes and co-factors, and reporting the half-life and scaled clearance values,^[243–245] as it is also done in this study (please refer to the experimental part for complete mathematical procedure). The intrinsic clearance (Cl_{int}) is thereby the intrinsic ability of hepatic enzymes to metabolise a compound, and is expressed, as previously mentioned, as volume per

Results and discussion

time, extended by the amount of protein present in the incubation ($\mu\text{L}/\text{min}/\text{mg}$ of microsomal protein).^[241] It might be calculated either from the slope of the plotted results curve or by extrapolation of the substrate disappearance curve.^[241] In this compound depletion approach substrate concentrations have to be considerably below the MICHAELIS-MENTEN constant K_M (the substrate concentration at which the reaction rate is half-maximum) to stay in the linear part of kinetics. A concentration of 1 μM is thereby believed to be low enough to retain linear kinetics and minimise assay solubility challenges without compromising the detection limit for analysis. In addition to that, it is assumed that only one metabolite is formed.^[241] The *in vitro* Cl_{int} can further be scaled to the *in vivo* hepatic clearance (Cl_h) via different appropriate liver models like the “well-stirred” or the “parallel-tube” model, incorporating physiologically based scaling factors relating to the complete intact liver.^[241,246] The well stirred model thereby is the simplest and most widely used model.^[241] It accounts for portal blood flow (Q_h) and considers both microsomal and plasma (or blood) protein binding of the test compounds, if available, since only free, unbound drug may undergo ADME-processes.^[241,244,246] This clearance prediction however has its limitation due to necessary assumptions and caveats. These include, that metabolic clearance in the liver by oxidative metabolism is the major mechanism of clearance, that the rates of metabolism and enzyme activities *in vitro* are truly reflective of those that exist *in vivo*, and that there is no significant product inhibition or enzyme deactivation based mechanism.^[244] Finally using the obtained hepatic clearance, a theoretical hepatic extraction ratio ER_h , which accounts for the relative elimination efficiency of the liver (theoretical *in vivo* clearance), can be calculated, taking the portal blood flow into account again. The results for intrinsic clearance (Cl_{int}) and the hepatic extraction ratio (ER_h) calculated from rat liver microsome (RLM) stability are summarised in Table 3.

Table 3: Rat liver microsome stability data for the first set of complexes tested by NIBR. Cl_{int} is the intrinsic clearance, ER_h the hepatic extraction ratio.

Rat liver microsome- stability				
	80b	60	200	201b
Cl_{int}	42 $\mu\text{l}/\text{min}/\text{mg}$	51 $\mu\text{l}/\text{min}/\text{mg}$	100 $\mu\text{l}/\text{min}/\text{mg}$	29 $\mu\text{l}/\text{min}/\text{mg}$
ER_h	58%	62%	77%	48%

Drug-like properties of metal-based kinase inhibitors

Taken from Table 3 the intrinsic clearances of the compounds lie in a range of 29-100 $\mu\text{L}/\text{min}/\text{mg}$ which correlates to a low to medium clearance (> 150 high, 50-150 medium, < 50 low) under Novartis guidelines, with **201b** being the most metabolically stable compound in the series and **200** the most labile. Taken from these values, the metabolic stability against CYP-enzymes of the compounds should not pose a limiting factor for the bioavailability.

These values however take not into account, whether the metabolic clearance might be low due to a possible inhibition of the CYPs responsible for the evaluated form of metabolism. This kind of inhibition might also cause a pharmacokinetic drug-drug-interaction, where a second administered drug might be metabolised more slowly due to inhibition of the CYP enzymes.^[225] Therefore, **80b**, **60** and **200** have been tested towards their inhibition properties against three of the most abundant CYP isoforms 3A4, 2D6 and 2C9.^[225]

Table 4: Reversible CYP inhibition data (IC_{50} values) obtained by NIBR for the first set of complexes tested.

Reversible CYP Inhibition IC_{50}			
80b	60	200	
3A4	$< 0.5 \mu\text{M}$	-	-
2D6	$16.8 \mu\text{M}$	$> 20 \mu\text{M}$	$> 20 \mu\text{M}$
2C9	$< 0.5 \mu\text{M}$	$6.4 \mu\text{M}$	$> 20 \mu\text{M}$

Generally compounds with an IC_{50} below 1 μM for at least one CYP isoform are considered a possible risk towards CYP inhibition and therefore are likely to be linked to a potential for drug-drug interactions.^[225] In the series tested here (Table 4), only **80b** falls into this category, inhibiting not one, but two isoforms at IC_{50} of below 0.5 μM . This means that on the one hand, the metabolic stability is probably lower than expected, and that the compound, especially together with its very low solubility and very low permeability (see below), is definitively no potential drug-candidate. The comparison of the inhibition of these three compounds shows however, that either indolocarbazole-based inhibitors are more susceptible to inhibit CYP enzymes than pyridocarbazoles, or that the full structure interacts with the enzyme, allowing very different inhibition profiles dependant on the further ligands of the metal, as it has been shown for kinase inhibition.

3.2.2.3. Membrane and cell permeability assessment

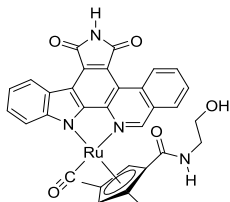
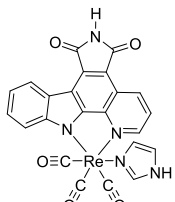
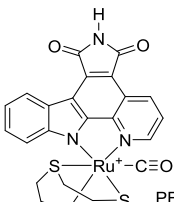
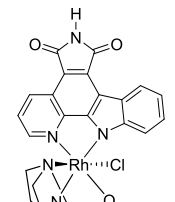
Permeability is another important property which generally is evaluated early during drug discovery, because a drug has to pass several membrane barriers to reach its target, including possibly the gastrointestinal tract (GI-tract), blood capillary walls, hepatocyte membranes, glomeruli, restrictive organ barriers, and the target cell membrane.^[232] Permeability assays use chemical or biochemical barriers to mimic the physicochemical properties of phospholipid bilayers.^[247] The simplest and fastest model thereby is the parallel artificial membrane permeability assay (PAMPA),^[247–249] which is preferably used as pre-screening tool for a permeability ranking.^[250] By using an artificial membrane without junctions, transporters, metabolism or real phospholipid membranes, it can however only be used to estimate permeability for compounds with transcellular diffusion mechanism which inherit a MW < 600 Da^[250] (based on classic organic compounds). A high-throughput variant of this assay uses a 9-10 µm hexadecane liquid layer as membrane, which is immobilised between two aqueous compartments.^[247] The enormous advantage of this robust assay is the possibility to measure a pH permeability profile (e.g. pH 4-8),^[225,247] which is a critical information to predict gastrointestinal absorption of ionisable drugs and very difficult to obtain from cell culture experiments.^[247] In addition to that, alkane water coefficients can be obtained from the assay.^[247] The compounds in this study (**80b**, **60**, **200**, **201b**) were also tested for their PAMPA permeability, but resulted in values well below the detection limit, showing that permeability, especially transcellular diffusion, is really low.

In general, different membranes can have different permeabilities for a compound. These differences are caused by differences in the membrane lipid mixture (passive diffusion), membrane transporter expression (active transport), or tightness of junctions between cells (paracellular transport).^[232] Permeability models which are closer to real physiological conditions, including transporters and cell junctions, involve *in vitro* cell monolayer assays, with the human colon adenocarcinoma cell line Caco-2 probably being the most widely used.^[251] Caco-2 assays are generally considered the model of choice since they are robust, reliable and the cells show morphological as well as functional similarities to human intestinal enterocytes, including tight junctions and brush border enzymes.^[252,253] Cellular models, in contrast to artificial membrane assays, include para- and transcellular permeability routes as well as various transport processes. Caco-2 cells for example express a variety of transporter systems normally found in small intestinal enterocytes, including efflux proteins from the ATP-binding cassette (ABC) family such as P-glycoprotein 1 (Pgp, also called multidrug resistance protein 1 MDR1) and members of the solute carrier (SLC) family, such as ion transporters (organic anion-transporting polypeptide (OATP) and organic cation transport proteins (OCT)).^[254] Therefore this cell-line serves as transepithelial

Drug-like properties of metal-based kinase inhibitors

permeability model in cell-monolayers and may be used to predict human oral absorption.^[252,253] In addition to that, the model, when used as bidirectional assay, may be used for studies of transport mechanisms in the gastrointestinal membrane, including transporter interplay and the degree of their impact compared to passive transport.^[252,253] Permeability of the four complexes of question was evaluated by NIBR using the Caco-2 cell model, as monolayers in a bidirectional assay. The results for the apparent permeability of the apical (A) to basolateral side (B) and *vice versa*, which connects the amount of complex transported during the incubation time with the surface area and the different sizes of the A and B chamber, as well as the calculated fraction absorbed (FA) are summarised in Table 5.

Table 5: Caco-2 permeability data for the first set of complexes tested. P_{app} is the apparent permeability, calc. FA the calculated fraction absorbed. The values for **201b** were not confirmed in a repeat experiment and are therefore indicated in grey.

Caco2-permeability				
	80b	60	200	201b
P_{app} A-B	0.04 x10 ⁻⁶ cm/s	0 x10 ⁻⁶ cm/s	0.23 x10 ⁻⁶ cm/s	0.64 x10 ⁻⁶ cm/s
P_{app} B-A	0.51 x10 ⁻⁶ cm/s	0.51 x10 ⁻⁶ cm/s	0.69 x10 ⁻⁶ cm/s	0.99 x10 ⁻⁶ cm/s
calc. FA	1%	0%	9%	24%
Mechanism	efflux	efflux	efflux	passive

As the numbers in Table 5 show, the permeability in Caco-2 is low to very low for all compounds with theoretical *in vivo* fractions absorbed (FA, derived from an empirical BOLTZMAN equation) ranging from 0% to 24%. The ratio of the apparent permeabilities from A (apical) to B (basolateral) and vice versa give a first idea about possible mechanisms which are involved in the transport of the drug. For **80b**, **60** and **200** this is probably efflux, since the B to A values are much larger than the A-B values, indicating some kind of additional transport from B to A. For **201b** these values are much closer to each other, indicating a passive permeability, which is obviously a much more appealing result. These results were however not confirmed in repeat experiments as presented later.

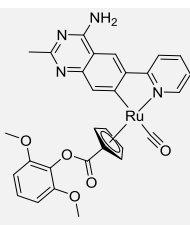
In summary, based on all *in vitro* results we can see that both solubility and permeability of our compound class is low, while metabolic stability seems to be fine.

3.2.2.4. Drug-like properties of further complexes

3.2.2.4.1. Metal-based MTH1 inhibitor

After obtaining the initial results of the four pyridocarbazole-based kinase inhibitors, we were curious if the trend on low solubility and permeability, as well as good metabolic stability, holds true for other inert metal-based inhibitors using different pharmacophore ligands. Especially a highly potent inhibitor for the human repair enzyme 7,8-dihydro-8-oxoguanosine triphosphatase (MTH1), which was currently developed in the group,^[137] came to mind as a good example compound and was therefore subjected to the same assays. The results are listed in Table 6.

Table 6: Basic *in vitro* ADME properties of a ruthenium-based MTH1-inhibitor.

	HT-Solubility	RLM stability	PAMPA permeability	Caco-2 permeability
 40	KPi 16 µM	Cl _{int} 364 µl/min/mg	logP _e <-6.2	P _{app} A-B 0.5 x 10 ⁻⁶ cm/s
	FaSSIF 73 µM	ER _b 92.5%		P _{app} B-A 10.4 x 10 ⁻⁶ cm/s calc. FA 19%

If we compare the obtained values towards the ones collected for the kinase inhibitors, we can see certain trends, but also differences. As for solubility, **40** has a much larger solubility in comparison to the pyridocarbazole-based inhibitors, both in KPi and FaSSIF with a factor of 3 and above. This indicates that the pyridocarbazole moiety is indeed the limiting factor, probably due to π-π-stacking of the large aromatic system, as well as probable intramolecular H-bonding of the maleimide part. The permeability in Caco-2 cells on the other hand is still very low from A-B but much higher than B-A, showing that **40** is definitively an efflux compound. The recovery of the compound in the assay however was not very good, showing a stability problem which also might lead to distorted results, i.e. the solubility might be higher as well as the permeability. PAMPA results however show a very low effective membrane permeability in the assay setting. Very high values have been obtained for intrinsic clearance and hepatic extraction ratio, correlating to a half-life time of about 3.8 min in the assay setting. Overall these results show us that the *in vitro* properties such as solubility, permeability and metabolic stability towards CYPs might indeed be manipulated by the structure surrounding the metal-centre. The compound shown here is, due to its very low microsome stability and probable stability issues, no candidate to further study for its potential as drug.

3.2.2.4.2. Drug-like properties investigations on stereoisomers of 201b

As **201b** seemed to be the most attractive compound so far and belongs to a family of 4 different stereoisomers (Fig. 38), of which the three other isomers show much better kinase inhibitory properties concerning affinity and selectivity,^[233] the other three isomers were resynthesised and tested in the same assay setting to compare their drug-like properties and to find a lead structure for further improvement of those properties. The two Λ -(R)-complexes **201a** and **201b** are thereby diastereomers, both derived from D-proline, with the Δ -(S)-complexes **204a** and **204b** being the enantiomeric counterparts, being again diastereomers to each other, derived from L-proline.

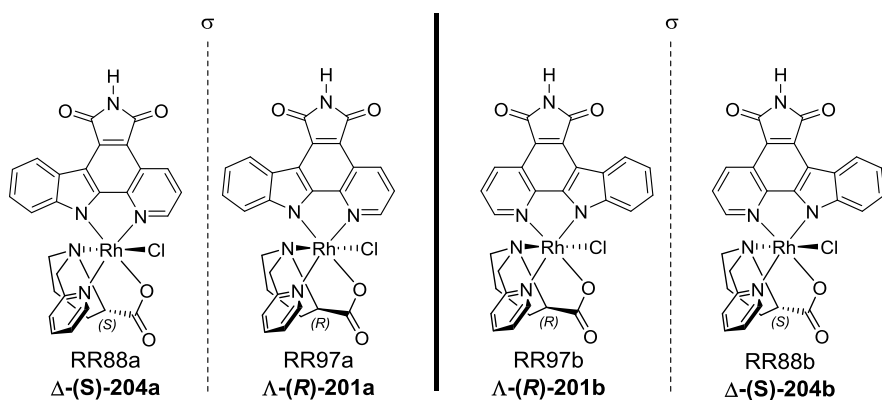


Fig. 38: Correlation between the three stereoisomers of **201b**. RR88a (**204a**) and RR97a (**201a**) are enantiomers to each other, as are RR88b (**204b**) and RR97b (**201b**). RR88a is additionally the diastereomer of RR97a, which holds true for the b isomers as well.

It is well known, that physicochemical and biochemical properties of individual stereoisomers can differ significantly from each other, making the results appealing on many levels. In a chiral environment, as it is provided in any biological system, stereoisomers might experience selective absorption, protein binding, transport, enzyme interactions and metabolism, receptor interactions, and DNA binding. Thus, each stereoisomer or isomeric mixture can have different pharmacokinetic, pharmacodynamic, therapeutic, and adverse effect profiles.^[255] The results obtained for all three complexes, in comparison to **201b**, are summarised in Table 7.

Results and discussion

Table 7: Basic *in vitro* ADME properties of **201a**, **201b**, **204a** and **204b**. *All values < 5 μM are below their respective detection limit.

	204a	204b	201a	201b
HT-solubility				
KP _i	6 μM	<5 μM^*	16 μM	< 5 μM^*
FaSSIF	19 μM	8 μM	29 μM	23 μM
RLM- stability				
Cl _{int}				
ER _b	28 $\mu\text{l}/\text{min}/\text{mg}$ 47%	24 $\mu\text{l}/\text{min}/\text{mg}$ 44%	12 $\mu\text{l}/\text{min}/\text{mg}$ 29%	29 $\mu\text{l}/\text{min}/\text{mg}$ 48%
Caco2-				
permeability				
P _{app} A-B	0.12 $\times 10^{-6}$ cm/s	0.18 $\times 10^{-6}$ cm/s	0.11 $\times 10^{-6}$ cm/s	0.64 $\times 10^{-6}$ cm/s
P _{app} B-A	1.46 $\times 10^{-6}$ cm/s	1.04 $\times 10^{-6}$ cm/s	6.8 $\times 10^{-6}$ cm/s	0.99 $\times 10^{-6}$ cm/s
calc. FA	5%	7%	4%	24%
Mechanism	efflux	efflux	efflux	passive
MDCK-MDR1				
P _{app} A-B				
P _{app} B-A	0.83 $\times 10^{-6}$ cm/s	2.17 $\times 10^{-6}$ cm/s	-	0.77 $\times 10^{-6}$ cm/s
Efflux ratio	1.33 $\times 10^{-6}$ cm/s	1.49 $\times 10^{-6}$ cm/s	-	1.30 $\times 10^{-6}$ cm/s
MDR1 efflux	1.6	0.7	-	1.7
	little to none	little to none	-	little to none

As the results in Table 7 indicate, all four isomers have quite similar properties, with exception of the passive permeability of RR97b (**201b**). One should keep in mind however, that these are single run experiments, which means that at least a factor two deviation is considered normal, and that outliers are possible. In detail, thermodynamic solubility of all four isomers is still poor, but improved in FaSSIF buffer. The rat liver microsome stability is again good, with **201a** maybe being more stable compared to the other isomers. The reversible inhibition towards the CYP isoforms 3A4, 2D6 and 2C9 of **204a** and **204b** was tested as well, showing values well over 20 μM , and thereby being not of consequence. Furthermore, the irreversible inhibition of CYP3A4 was evaluated, since time-dependant inhibition (TDI) is the cause of several failures in late-stage clinical candidates and is suspected to play a role in liver toxicities often observed in preclinical species.^[256] Values of $k_{\text{obs}} = 0.004 \text{ min}^{-1}$ (**204a**), 0.012 min^{-1} (**204b**) and 0.014 min^{-1} (**201a**) were obtained for the

Drug-like properties of metal-based kinase inhibitors

apparent inactivation rate constant. With a positive/negative bin of $k_{obs} = 0.02 \text{ min}^{-1}$ used as lower limit for positive compounds, all compounds are clearly ranked negative for relevant TDI.^[256]

The permeability in Caco-2 cells is low for all four compounds with **201b** showing the best calculated fraction absorbed and passive diffusion as possible mechanism compared to efflux for the other four isomers. Since the experiments of **201b** were run at another time point as for the other three isomers, they were repeated to exclude a possible outlier. The result indeed showed, that the values are outliers as the B-A value obtained was close to the original ($0.86 \times 10^{-6} \text{ cm/s}$) while the exact value from A-B could not be obtained because it was below the detection limit (< 0.03% transported).

To verify these results and to evaluate the possible efflux mechanism further, the isomers were tested in another permeability assay using an MDR1 overexpressing cell line. Understanding interactions with efflux transporters is thereby important,^[257] since efflux mechanisms play a major role in protecting the body from harmful substances and can severely limit the oral absorption of compounds.^[258] Efflux substrates can be identified in assay settings using the efflux ratio (ER), which is defined as the ratio of apparent permeability from the basolateral to the apical side to the permeability from the apical to the basolateral side.^[257,259,260] For the assay the dog kidney epithelial cell-line MDCK (Madin-Darby canine kidney) model was used, which is like Caco-2 cells frequently used for permeability evaluation of attractive compounds. These cells have a shorter cultivation period in comparison to Caco-2 cells, due to the fact that they differentiate much quicker (within 3-7 days), but transporter expression levels might differ from human intestines.^[261] These cells are however ideal for transfection,^[261] which has been used to create and establish a MDR1 overexpressing cell line in the late 1990s.^[262] The value of this cell line as a model of the human intestinal mucosa has been confirmed, even if there are possible differences in kinetics and affinities compared to the Caco-2 cell line.^[263] It was shown however that similar P_{app} -values were obtained compared for those from Caco-2 assays for potential anti-malarial compounds with low and medium permeability, while a higher variability was found for compounds with high permeability and compounds that were MDR1 substrates.^[264]

The results of the MDCK-MDR1 assay are also summarised in Table 7, whereby the values for the b isomers are the average of two independent experiments. The analytics for **201a** could not be obtained, due to issues in MS/MS quantification although the assay was run twice for the compound. In general, the A to B values are higher in the assay setting compared to the Caco-2 assay, but the compounds still show very poor permeability. **201b**, as expected, shows results which are much more in line with the other compounds. With efflux ratios below 2, all tested compounds show no to little efflux in the assay, indicating that MDR1 is not involved in a possible efflux. This

Results and discussion

means that either there are other efflux transporters involved, or that the original assumption that efflux plays a role is just not true and arises from the very low values in the assay which leads to higher deviations in the ER. In addition to that, results indicate, that either the high MW of the compounds or, to some extent solubility issues, might be responsible for the low permeability of the compounds, especially since recovery in the experiments was good and therefore no to little membrane retention was seen.

From the results obtained it was very feasible to use one of the isomers for further exploration as a lead structure. As previously mentioned the different isomers show very different kinase inhibitory properties,^[233] as discovered in a kinome scan using a panel of 456 kinases, and verified by IC₅₀ determination of potential hits from these screens by RAJATHEES RAJARATNAM. **204a** is thereby a potent Flt3 (IC₅₀ = 137 nM, 10 μM ATP) inhibitor, **204b** an AURKA (IC₅₀ = 121 nM, 10 μM ATP) inhibitor and **201a** a Pim1 (IC₅₀ = 15 nM, 10 μM ATP) inhibitor, while RR97b shows no significant inhibitory properties. All values thereby reflect the mean of two independent experiments.^[233] Since **201a** showed the best values concerning solubility and rat liver microsome stability, and since there is a lot of experience concerning the kinase Pim1 in the working group, including co-crystal structures of similar complexes bound to Pim1, the compound was chosen as the lead structure to try to improve its drug-like properties while conserving its inhibitory properties towards Pim1. To further test its suitability, the stability and toxicity of **201a** was evaluated and compared to the inactive compound **201b**.

3.2.2.4.3. Stability of 201a, 201b, 204a and 204b against light, solvents and physiological conditions

Stability of metal complexes is always an issue that should be addressed. Especially ligand exchange reactions and racemisation are major concerns when metal-based compounds are evaluated towards their suitability in biological systems. It is well known the e.g. pyridocarbazole-based RuCpCO complexes may racemise in solution both in the dark and under influence of light.^[265,266] To address this issue, a study has been performed to test the stability of this type of rhodium complexes against light, ligand exchange reactions and racemisation in presence of light at room temperature in DMSO and CH₃CN. For the investigation, a few milligrams of **204b**, based on the availability of the compound, were dissolved to DMSO-*d*₆ and a few microliters of that solution were further diluted into CH₃CN. Both samples were kept at room temperature in direct proximity to a window, to allow irradiation by both daylight and artificial light. Samples from the NMR tube were taken and diluted into CH₃CN at time points 0 h, 24 h, 4 d, 7 d, 14 d, 14 d and 24 d and kept at -20 °C until evaluation. At the same time points ¹H-NMR spectra were measured to ensure the integrity of the complex. The NMR spectra are summarised in Fig. 39, showing no transformation of the compound, which indicates no ligand exchange or racemisation to the respective diastereomer.

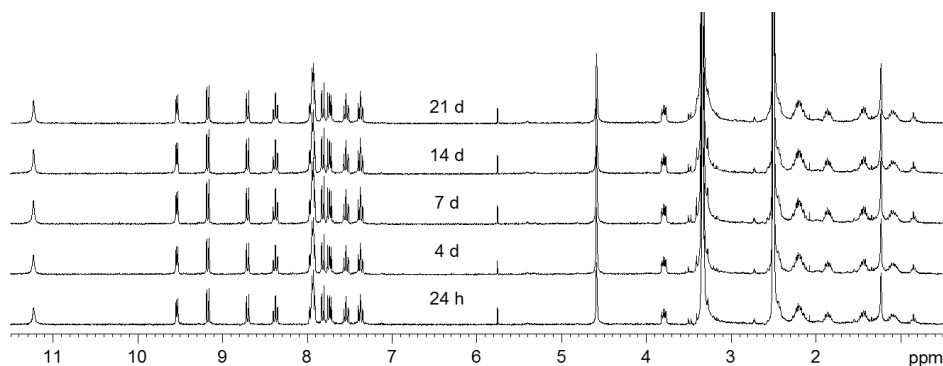


Fig. 39: ¹H-NMR spectra of **204b** in DMSO-*d*₆ after 24 h, 4 d, 7 d, 14 d and 21 d, during which the compound was exposed to natural and artificial light at room temperature. No change in the aromatic or aliphatic region can be observed whatsoever, which also holds true in comparison to the freshly synthesised compound.

As concluded from the NMR spectra, a racemisation to the diastereomer is not occurring, while a racemisation to the enantiomer can generally not be observed in NMR, due to the identical chemical shifts of enantiomers. This type of racemisation is generally very improbable for the complex, since it would include the racemisation of the stereocentre in the proline ligand, for which the ligand must probably first be at least partly released from the metal centre. For analysis of racemisation, the best conditions for separating all four possible isomers on HPLC, namely **204a**,

Results and discussion

204b, **201a** and **201b**, using a chiral column, were evaluated. The afore mentioned samples in CH₃CN were injected and checked for any probable racemisation of **204b** to **201b** (Fig. 40), according to a change in retention time under the given separation conditions.

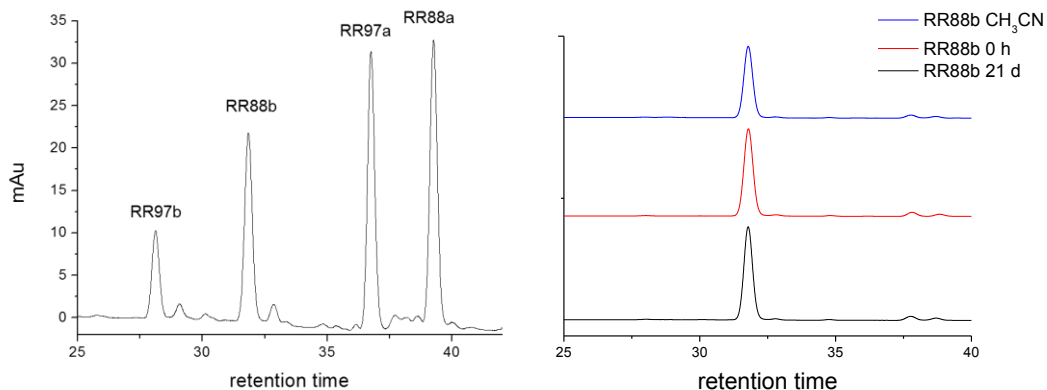


Fig. 40: Left: chromatogram of an isomeric mixture of the **201a**, **201b**, **204a** and **204b**, obtained by RP-HPLC using a CHIRALPAK® IC column. The isomers were assigned based on single runs with the respective compound. Right: Chromatograms of RR88b (**204b**) in CH₃CN, which was exposed to light and room temperature and of the 0 h and 21 d sample taken from the DMSO solution. There is no racemisation observable.

As Fig. 40 shows, no change in the chromatograms was observed in the 21 d in CH₃CN sample nor the sample taken from the DMSO solution after 21 days in comparison to the 0 h sample. This means that no racemisation to any other stereoisomer occurs under the given condition and that the complex generally does not react with the solvents, since a ligand exchange normally also leads to a change in retention time.

In addition to the stability towards light, DMSO and CH₃CN, the behaviour of the complexes under physiological conditions was of great interest. After administration, during their passage through the blood and eventually into the cells, drug molecules encounter biological substances that can modify their composition through ligand exchange reactions. Thereby serum proteins are often their first binding partners.^[267] To investigate the stability of RR97a and RR97b towards physiological conditions, they were incubated as an 5 mM solution in DMSO-*d*₆ /H₂O 9:1 with the addition of an equimolar amount of β-mercaptoproethanol. The thiol is thought to imitate nucleophilic thiol-groups of cysteine side chains, as they are present in biological systems. After 48 h, the solution was additionally incubated at 37 °C in an atmosphere containing 5% CO₂ to imitate the conditions used in cell and precision cut liver slice experiments. Fig. 41 and Fig. 42 show the aromatic and aliphatic regions of the respective ¹H-NMR spectra at the defined time points of measurement.

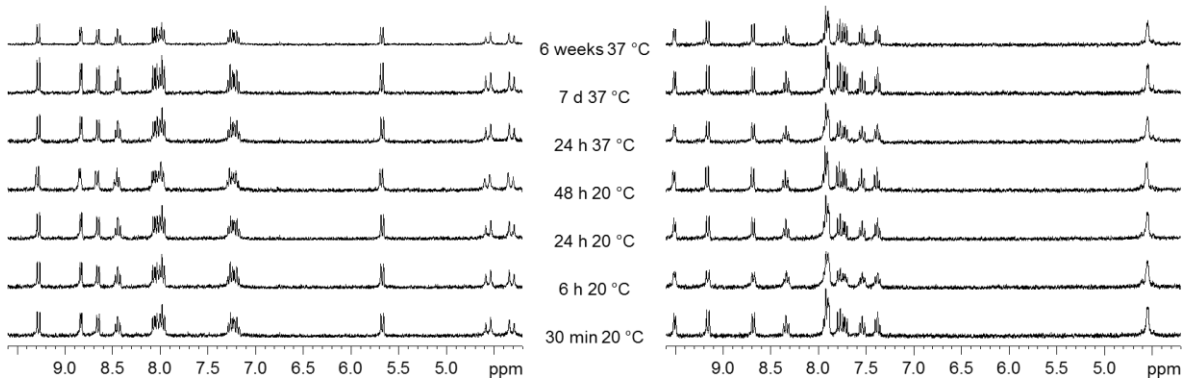


Fig. 41: Aromatic regions of ^1H -NMR spectra of RR97a (**201a** left) and RR97b (**201b** right) at defined points after addition of β -mercaptoproethanol. No changes are observable within 6 weeks at 37°C .

As Fig. 41 shows, there are no changes in the aromatic region of the two complexes at any point in the experiment, indicating no reaction with neither the solvent, nor the thiol. This includes both a ligand exchange reaction as well as an addition to the maleimide nitrogen or a ring open of the maleimide, since these reactions should shift the signals to some extent. In Fig. 42 no changes in the aliphatic signals of the complexes can be observed, leading to the same conclusion. However, the signal belonging to β -mercaptoproethanol slowly decreases, while two new signals form, as indicated in Fig. 43.

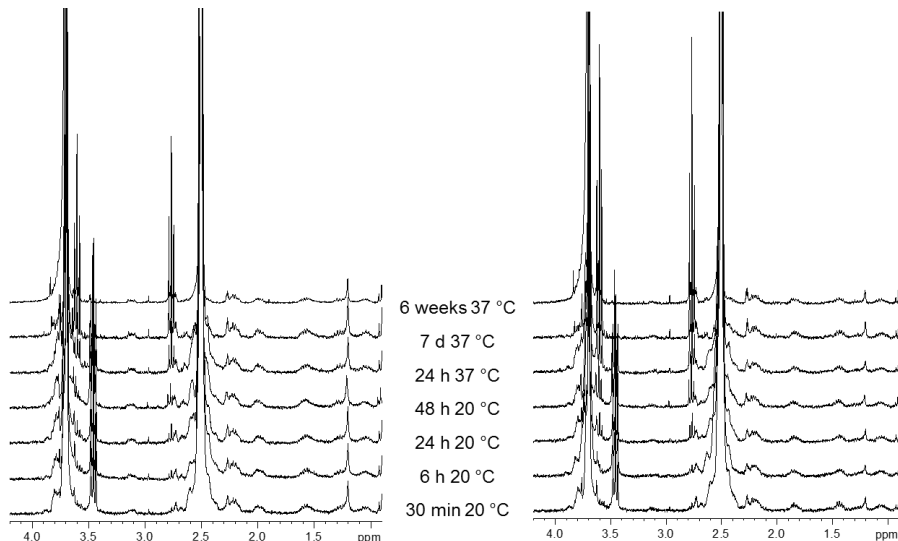


Fig. 42: Aliphatic region of ^1H -NMR spectra of RR97a and RR97b at defined points after addition of β -mercaptoproethanol. No changes in signals belonging to the complexes are observable within 6 weeks at 37°C . Signals at 2.50 ppm belong to the restprotons of the solvent DMSO, signals at ~ 3.7 to water.

The β -mercaptoproethanol can both be depleted by hydrolysis with water or by reaction with DMSO to a 2,2-dimethyl-1,2 λ^4 ,3-oxadithiolane, which is promoted by increased temperature. Fig. 43 shows

Results and discussion

that within the six weeks in which spectra were recorded, the signal belonging to β -mercaptoethanol (blue) fully reacts to another species with almost full conversion after 7 days at 37 °C. In the same ratio as the signal fades, two new signals form, which might belong to the described oxadithiolane.

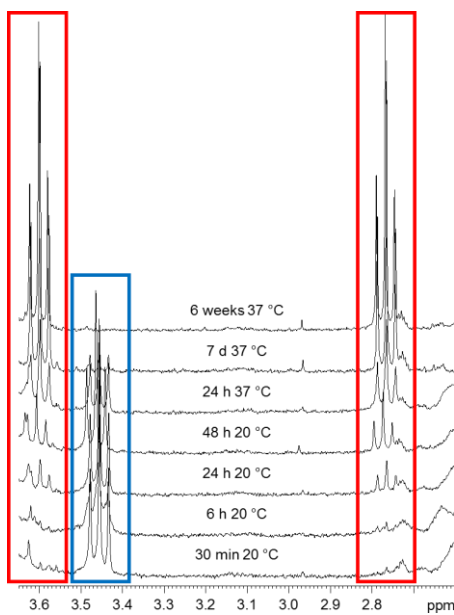


Fig. 43: Section of the ^1H -NMR spectra recorded for RR97b, showing the disappearance of the signal belonging to β -mercaptoproethanol and simultaneous formation of two new signal sets, probably belonging to an oxadithiolane formed by the reaction of the β -mercaptoproethanol with DMSO.

Overall these experiments show, that the complexes seem to be fully stable towards thiols, heating at 37 °C, racemisation and hydrolysis at the given conditions. It should be noted however, that when using larger amounts of β -mercaptoproethanol (1M; complex/thiol ratio of 1:10000) in aqueous buffer, the formation of a compound with an increased retention time can be observed for both RR97a and RR97b via HPLC. The new compound has not been further investigated but might be a result of either ligand exchange reaction or reaction of the thiol with the maleimide. This result shows that the stability of the complex might indeed be limited if high thiol concentrations are present, however thiols in e.g. blood are normally found in a micromolar scale rather than a molar.^[268]

3.2.3. Toxicity evaluation of 201a, 201b, 204a and 204b

3.2.3.1. *In vitro* cytotoxicity in cancer cells

All four complexes were tested for their toxicity in a concentration dependant HeLa human cervical cancer cell line after incubation of the compound for 24 h using the MTT standard method I. The isomer RR97b (**201b**) thereby always serves as a reference where the cytotoxicity is not related to kinase inhibition properties. The results are given in Fig. 44.

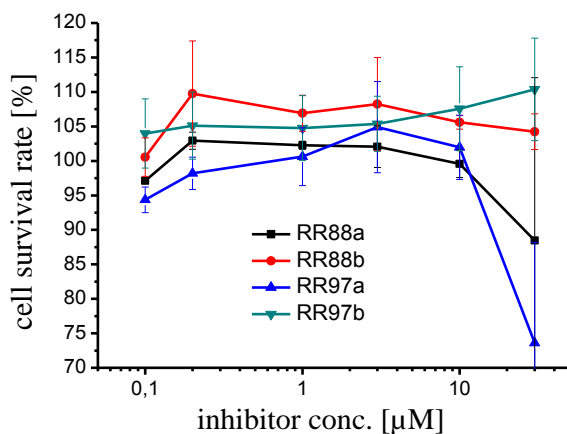


Fig. 44: Cell viability assay using the MTT method. All four compounds do not affect the cell survival up to a concentration of 10 μM at 24 h incubation time. The a isomers seem to be more cytotoxic at a concentration of 30 μM in comparison to the b isomers.

As the results in Fig. 44 show, all compounds show no significant cytotoxicity up to a concentration of 10 μM under the assay conditions given. For a concentration of 30 μM , the a isomers seem to show a small toxicity, while the b isomers seem to be less toxic. However, in the 30 μM wells the deviation is very high and allows not much of a definite conclusion. Therefore, RR97a and RR97b were further tested in human lung carcinoma A549 cells and human ovarian carcinoma A2780 cells using standard method II, including an incubation time of 72 h and a higher concentration range. The results of these experiments, which were conducted in Angela Casinis laboratory at the Rijksuniversiteit Groningen, are shown in Fig. 45.

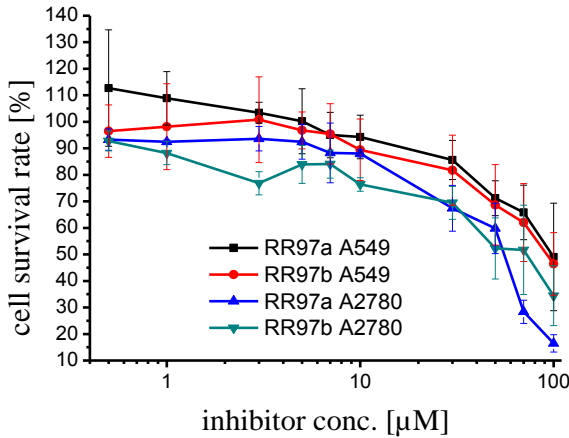


Fig. 45: Concentration dependant cell viability assay in human cancer cell lines A549 and A2780 using the MTT method. The two isomers do not affect the cell survival up to a concentration of 10 μM at 24 h incubation time. Both isomers show a similar trend in cytotoxicity in A549 cells with concentrations above 10 μM , which goes down to approximately 50% cell survival at 100 μM . In the A2780 cells the a isomers again seem to be more cytotoxic at a concentration of above 10 μM compared to the b isomers going down to around 16% for the a isomer at 100 μM and 34% for the b isomer.

Fig. 45 clearly shows a similar trend for the two isomers up to 30 μM in comparison to the HeLa experiments with 24 h incubation time. In A549 cells both isomers show a similar trend in antiproliferative properties with concentrations above 10 μM , which goes down to approximately 50% cell survival rate at 100 μM . In A2780 cells the a isomers again seem to be more cytotoxic at concentrations of above 10 μM compared to the b isomers going down to around 16% for the a isomer at 100 μM , and 34% for the b isomer. Overall the toxicity is comparably low for all compounds in all cell lines tested. However, at high concentrations with long incubation times some precipitate occurred, maybe falsifying the data insofar that the compound might be more toxic than it seems in the experiment. The results not only show low toxicity, but also that these cancer types are probably not treatable by the used inhibitors. Based on the Human Protein Atlas^[269] Pim1 expression in HeLa cells is moderate and for A549 cells low, indicating no obvious relation between the shown low cytotoxicity and Pim1 inhibition. As indicated in the introductory section, Pim1 inhibition however might rather lead to disease control than tumour killing. The possibility of combination treatment and whether RR97a enhances the effect of other cancer drugs was not explored further, since it was not the primary goal of this thesis.

3.2.3.2. *Ex vivo* hepatotoxicity of 201a and 201b in precision cut liver slices

As shown in the previous section, toxicity of is low in different cancer cell lines. In addition to the *in vitro* results, the toxicity towards healthy cells or rather tissue is an important property concerning a possible use of the compound as drug. An attractive model is thereby the use of precision cut liver slices (PCLS), in which hepatotoxicity can be evaluated. Hepatotoxicity is thereby one of the major reasons for termination and for limitations by labelling medicines.^[270]

Precision cut tissue are viable explants of the tissue cultured *ex vivo* with all cell types in their natural environment, providing toxicity results which are expected to be more relevant than those obtained in cell cultures. Using this technology, all cells remain in their natural environment with maintenance of the original cell-cell and cell-matrix contacts, which is absent in classical 2D cell cultures *in vitro*.^[271–276] Notably, the technique is an FDA-approved model for drug toxicity and metabolism studies, and it has previously been used for the assessment of toxicity of metal-based compounds like cisplatin (kidney),^[277] experimental gold compounds (liver, kidney, and colon),^[278] and amino-ferrocene-containing prodrugs (liver).^[279] The tissue in the experiment is sliced with a reproducible and well defined thickness, which is small enough to allow sufficient oxygen and nutrient supply to the inner cell layers, ensuring the viability of all cells. Slicing thereby allows a very efficient use of the organ tissue,^[280] since numerous compounds and conditions can be tested at the same time with only one organ. Precision cut tissue slices of the liver are frequently used to assess hepatotoxicity in healthy tissue.^[271–273] This is an enormous advantage compared for testing toxicity in single cell cultures, because drug-induced hepatotoxicity often is a multi-cellular process involving not only hepatocytes but also other cell types such as Kupffer and stellate cells.^[281]

Based on previously discussed criteria, RR97a (**201a**) and RR97b (**201b**) were selected for hepatotoxicity investigations at the Rijksuniversiteit Groningen according to established procedures using rat precision cut liver slices (PCLS). Again, RR97b as ineffective kinase inhibitor serves as control compound, since any toxicity should be induced by other mechanisms than kinase inhibition. For the hepatotoxicity evaluation, PCLS were prepared and pre-incubated for 1 h before exposing to the rhodium containing complexes as described in the experimental section. The preincubation thereby is necessary to allow the tissue to recover from the cold ischemia and the slicing procedure. The treatment with RR97a and RR97b was performed at three single concentrations of the compounds (1 µM, 10 µM and 50 µM) with a final DMSO concentration of less than 0.5% and slices were incubated for 24 h. Afterwards PCLS were collected and their viability was determined measuring their ATP content using a bioluminescence assay and normalising it to their protein content, obtained by the LAWRY method, and thereby to the size of the tissue slice.

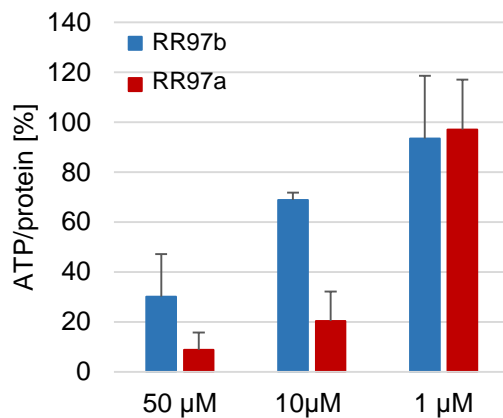


Fig. 46: Viability of precision cut liver slices (PCLS) after 24 h incubation with the two diastereomeric complexes RR97a and RR97b after 1 h of preincubation.

Fig. 46 reports the viability of the PCLS upon treatment with different compound concentrations. Based on the obtained results, both compounds are not toxic for the tissue at a concentration of 1 μM. At 10 μM concentration, some effects on tissue viability can be observed with respect to controls, with RR97a being markedly more toxic than RR97b (20% and 69% residual viability, respectively). The hepatotoxicity increases with the highest tested compound concentration (50 μM), RR97a leading to the most pronounced effect (9% residual viability compared to 30% for RR97b). Here again at high concentrations some precipitate occurred, maybe falsifying the data insofar that the compound might be more toxic than it seems in the experiment.

Notably, the inactive isomer RR97b presents reduced hepatotoxicity with respect to cisplatin in the same rat liver model. In fact, at 10 μM the anticancer Pt complex has been observed to induce a reduction of tissue viability up to 50% (unpublished data from Prof. Angela Casinis laboratory). In general anticancer agents are expected to show toxicity at therapeutically active doses, since the therapeutic effect and toxicities normally rely on the same mechanisms,^[189] so some overall toxicity of the more active KI is not surprising. As a general trend with KIs, the severity of organ toxicity seems to be associated with increased kinase promiscuity,^[22] which also aligns with the fact that RR97b does not inhibit kinases well, and RR97a targets more than one kinase.^[233]

Whether this toxicity is actually caused by inhibition of different kinases, or other tissue targets, is unclear. However the kinase Pim1, one of the preferred target kinases of RR97a, is known to be highly expressed in the fetal human liver but not in adult tissue,^[40] indicating that inhibition of Pim1 may not be the reason. To sum up, the different diastereomers seem to not only possess different KI properties, but also different toxicity effects, which seem not to be related to the Pim1 inhibition properties of RR97a, at least in the liver tissue, and may therefore arise from different physicochemical properties or off-target effects.

3.2.3.2.1. Metal uptake of PCLS after treatment with RR97a and RR97b

To investigate whether the amount of compound, respectively Rh, might influence the toxicity of the complexes RR97a and RR97b towards PCLS, the metal uptake after the incubation time was studied for the same concentration range. Therefore, PCLS were treated as described for the hepatotoxicity study until the end of the 24 h incubation time. The slices were then washed in Krebs medium and individually frozen at -80 °C and kept at this temperature until digestion with HNO₃ as described in the experimental section. The content of Rh was measured via ICP-MS in the mass department of the Philipps-Universität Marburg (inductively coupled plasma mass spectrometry) and determined using an external Rh calibration curve (Fig. 47). Due to the previously shown high stability of the compounds in assay medium, the values are expected to reflect the true values for the complex.

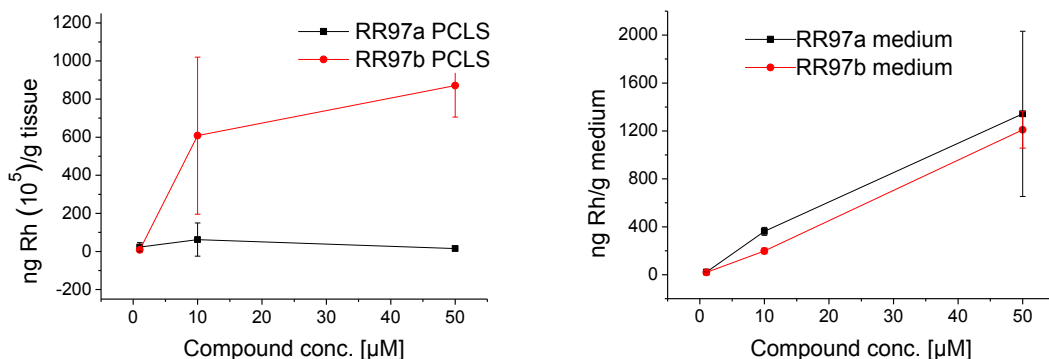


Fig. 47: Rh content of PCLS (left) and medium (right) after 24 h treatment. It seems that RR97b has a better uptake by the tissue compared to RR97a.

Taken from Fig. 47 it seems that RR97b is taken up to a higher degree compared to RR97a. However, based on the high deviation these results are rather an estimation than a real value, as the samples were weighted in after thawing in its wet states, and not always all tissue was transferred. Additionally, similar amounts of Rh is found in the medium for both samples. Both compounds precipitated to a certain degree from the solution at high concentrations, so that the amount of compound in the medium might not be truly reflective. The trend of a higher uptake of RR97b is thereby a disagreement to the higher hepatotoxicity and cytotoxicity obtained in the previous assays.

3.2.3.2.2. Morphology of PCLS after treatment

During the treatment of PCCLC with RR97a and RR97b some of the compound precipitated in wells with high concentrations, as previously described. In addition to that the colour of slices changed from its natural brownish colour^[280] to an intense pinkish red, indicating the confirmed uptake of the compound (see 3.2.3.2.1), as shown in Fig. 48.

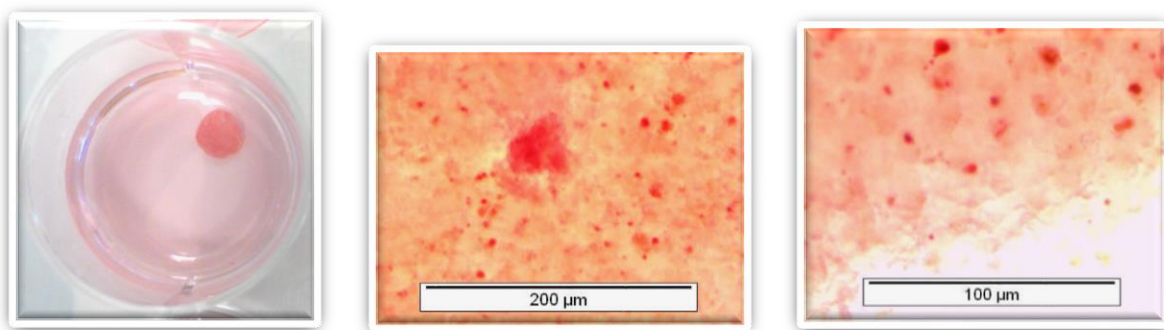


Fig. 48: Left: PCLS after 24 h incubation with 10 μ M RR97a. The intense pink colour reveals the uptake of the deep red complex. Middle and right: Light microscope pictures of the freshly incubated slices showing deep red spots, which might be accumulations of RR97a.

Since the colour seemed to be distributed unevenly in the slices, the question arose whether the compound accumulates on the surface of the slice, in structural features like blood capillaries or inside the cells. Therefore, the tissue was first examined in its wet state using a standard light microscope (Fig. 48). The samples indeed showed deep red spots, which were not to be seen in untreated samples and which were distributed unevenly. To further verify whether the compound accumulates on the surface or penetrates the tissue, morphology studies with tissue cross-sections were conducted. Therefore, the slices were treated according to the hepatotoxicity experiment until the 24 h incubation with the compound. The slices were then fixed in 4% w/v formalin, dehydrated using a graded EtOH series and paraffin embedded. Cross sections of 4 μ m thickness of the paraffin block were prepared and stained using haematoxylin and eosin. Haematoxylin thereby stains the nucleus (chromatin) blue and eosin stains the cytoplasm pink. The cover slips were scanned using an Aperio image capture device (LEICA BIOSYSTEMS). The treated sample and the 24 h reference control are show in Fig. 49.

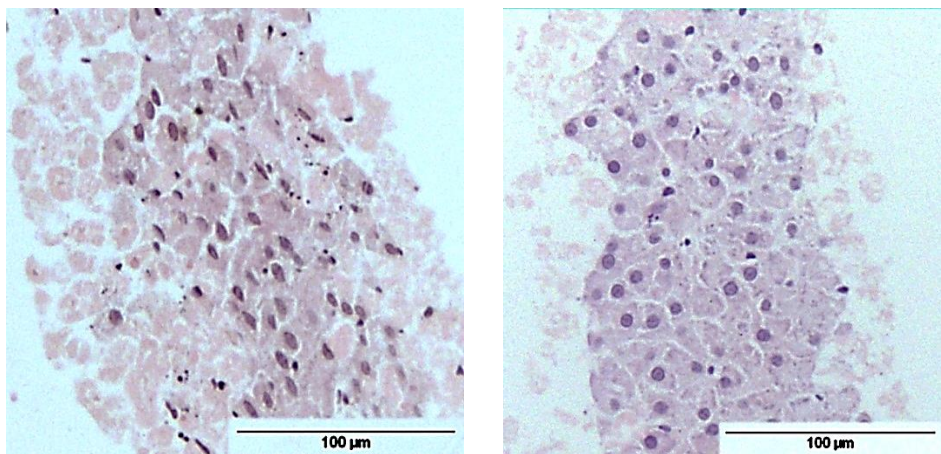


Fig. 49: Comparison of morphology of dried and stained PCLS. Left: After treatment with RR97a for 24 h. Right: 24 h control. The cell nuclei were stained blue using haematoxylin, the cytoplasm was stained pink with eosin. No signs of compound accumulation can be seen.

As can be seen from Fig. 49 the position of accumulation could not be verified using this method. One possible explanation is, that accumulations were dissolved in one of the solutions used in the dehydration, embedding or staining process. This would indicate, that the accumulations were located extracellular, so that the solvent could reach and dissolve them. Keeping the results from np829 (**80b**) in mind, the previously observed toxicity for RR7a might be related to accumulations. However, an effect like the crystallisation in cells, as it has been detected for **80b**, was not seen in any experiment with RR97a, pointing to another reason for the observed hepatotoxicity and minor cytotoxicity in cancer cells.

3.2.4. *In vivo* studies of RR97a and RR97b

3.2.4.1. *In vivo* pharmacokinetic-studies of RR97b in C57BL/6 mice

RR97b (201b), as previously mentioned, was the most attractive compound in regards to *in vitro* ADME properties from the first series of compounds. Therefore, a single low dose pharmacokinetic study of the compound was executed at NIBR Cambridge, USA in C57BL/6 mice. The compound was administered via three different routes of administration, namely intravenous (IV, 1 mg/kg, n = 2), oral (PO, 3 mg/kg, n = 3) and intraperitoneal (IP, 3 mg/kg, n = 3) administration. Blood samples were collected at determined time points and the processed plasma analysed to quantify the compound via LC-MS/MS. The pharmacokinetic profiles obtained are shown in Fig. 50. All animals remained normal throughout the study which indicates that acute toxicity is not an issue with the exposures observed and within the time frame of the experiment.

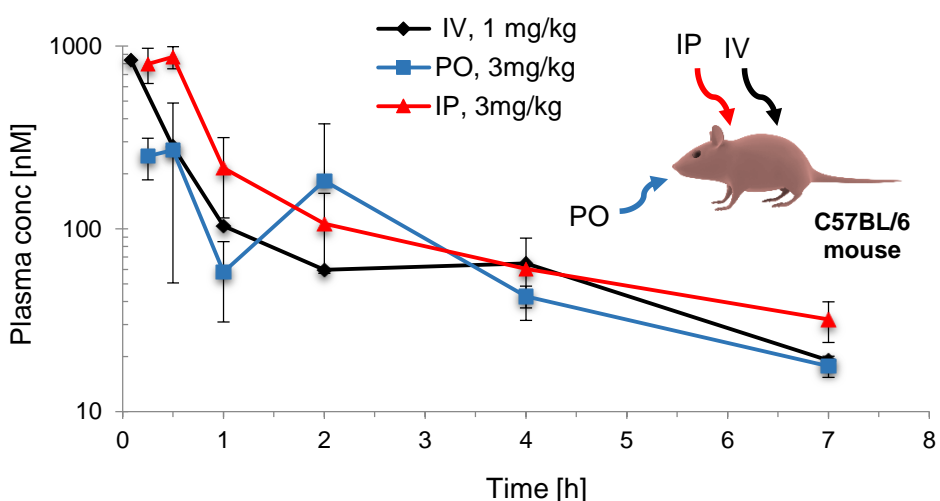


Fig. 50: Plasma concentration of compound RR97b after intravenous (IV), oral (PO) and intraperitoneal (IP) administration. Samples were taken at the determined time points and the processed plasma was analysed via LC-MS/MS to quantify the compound concentration.

Fig. 50 shows the PK profile for all three dosage routes. For IV dosing, the drug concentration-time profile shows a curve in which there is an initial rapid drop in drug concentration and a subsequently slower decline. This effect can be described by the two-compartment model, which resolves the body into a central and a peripheral compartment and which was used to calculate the values discussed below (please refer to the experimental section for calculations). Although these compartments have no direct physiological or anatomical meaning, it is assumed that the central compartment comprises tissues that are highly perfused such as heart, lungs, kidneys, liver and brain, while the peripheral compartment on the other hand comprises less well perfused tissues

such as muscle, fat and skin. A two-compartment model assumes that, following drug administration into the central compartment, the drug distributes between that compartment and the peripheral compartment, without reaching instantaneous equilibrium.^[282] Therefore, the rapid drug decline in the beginning can be attributed to elimination from the central compartment and distribution into the peripheral compartment. After a while, a distribution equilibrium is achieved between the central and peripheral compartments, and elimination of the drug is assumed to occur from the central compartment leading to a smaller slope in the PK curve. All rate processes are generally described by first-order reactions in the model.^[282] For PO and IP administration the beginning of the plot shows initially a rise in concentration, before it is distributed between the tissues and probably excreted in a similar fashion to the IV injection. This increase in the beginning is related to a relatively slow absorption of the compound before it reaches the vascular department. From the results obtained and profiles shown in Fig. 50 the following conclusions can be drawn: The IV clearance is moderate ($ER = 37\%$), relative to the respective hepatic blood flow. This value seems to align with the theoretical ER_b of 48% obtained in the rat liver microsome stability experiment. The volume of distribution at steady state V_{ss} , which is a theoretical value representing the ratio of the total amount of drug in the body to the drug blood/plasma concentration, is also moderate (5.1 L/kg) with respect to total body volume (~ 0.7 L/kg), indicating a diffusion outside the vascular department. The half-life time ($t_{1/2}$) of the compound in plasma is 2.9 h.

When comparing to other metal-based compounds like NAMI-A and KP1019, which are Ru-based compounds tested in clinical trials for their anti-cancer abilities, or the approved drug cisplatin we get the following picture: In Swiss CD1 mice NAMI-A is rapidly cleared from blood after IV injection, with 3.5-4.7% of the administered dose (15-50 mg/kg) remaining 5 min pd.^[283] In CBA mice, after administering 200 mg/kg IV, an initial $t_{1/2}$ from plasma of 1.4 min was calculated using a bi-compartment model. These values demonstrate a much quicker clearance from the blood compared to **201b**. The elimination half-life for NAMI-A was quite long, determined as 12 h,^[284] probably because the majority of the drug was protein-bound (albumin and transferrin) and accumulates in white blood cells.^[285] KP1019 is also highly bound to plasma proteins like albumin and to a lesser extent transferrin. The V_{ss} in human patients was therefore determined to be small (similarly to NAMI-A)^[286], while the terminal half-life is also quite long.^[286,287] RR97b in comparison has a moderate V_{ss} and seems therefore to be less plasma protein bound. Cisplatin, which was administered to dogs at 1 mg/kg, also showed a low $t_{1/2}$ of considerably less than 1 h, with plasma levels being cleared by 90% during the first 4 h of treatment.^[288] The half-life in plasma is here again smaller compared to RR97b, but for cisplatin again the final phase of clearance is protracted and the terminal elimination is not even completed 12 days pd.^[288]

Results and discussion

As Fig. 50 shows, RR97b reaches systemic circulation after PO and IP dosing. It has a low (27% PO) to moderate (47% IP) bioavailability, that is the fraction of dose that reaches systemic circulation, with PO-dosing showing much more variability among the three animals. Oral administration is the most preferable dosage route for drugs in general, but oral absorption includes a tandem process of dissolution and intestinal membrane permeation. A low solubility, a low dissolution rate and low permeability can thereby all result in incomplete and variable oral absorption.^[289] Thus, the high variability in the PO profile of RR97b is in accordance with the low solubility and very low permeability. However, it is not uncommon for KI to show high intra- and interpatient variability in c_{max} and plasma drug exposure e.g. in phase I clinical trials in cancer patients,^[226] and the bioavailability still does not seem incompatible with PO or IP delivery, if coupled with a reasonable potency against a given target, which is of course not given for RR97b, but might be applicable for one of its isomers.

Especially a possible PO delivery might be a great advantage over other metallodrugs, which often show a very limited solubility in oral formulations and are therefore usually given intravenously or subcutaneously. These routes of administration however, not only guarantee a smoother PK profile, but also allow to avoid the way through varies pH levels and conditions in the stomach and intestines, which might pose a threat to the structure of the complex, and allows to administer smaller amounts of metal ions avoiding possible toxic side effects.^[267,290]

3.2.4.2. *In vivo* pharmacokinetic-studies of RR97a in Sprague Dawley rats

As RR97a (**201a**) is a far more potent kinase inhibitor in comparison to RR97b (**201b**), and targets the potential cancer target Pim1, the pharmacokinetic properties of this inhibitor were of great interest, since it also showed adequate *in vitro* ADME properties. Therefore, a single low dose pharmacokinetic study of the compound was executed by NIBR in Basel, Switzerland in Sprague Dawley rats. The compound was administered via bolus injection intravenously (IV, 3 mg/kg), blood samples were collected and the processed plasma analysed to quantify the compound via LC-MS/MS in Basel and ICP-MS in the central mass department of the Philipps-Universität Marburg. The pharmacokinetic profiles obtained (expressed as ng Rh/g of plasma) are shown in Fig. 51. All animals remained normal throughout the study which indicates that acute toxicity is not an issue exposures observed and within the time frame of the experiment.

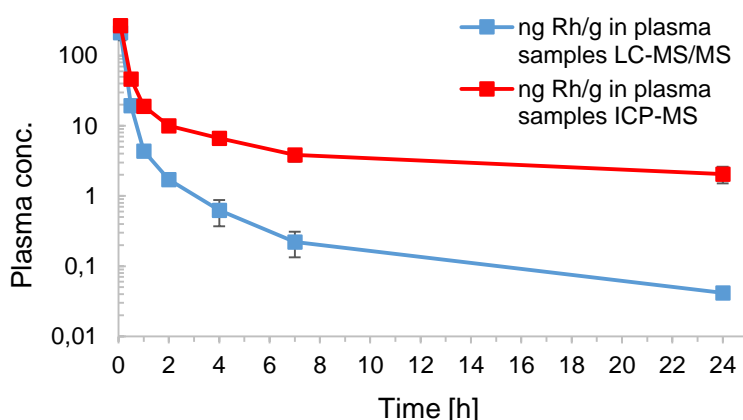


Fig. 51: Plasma concentration of **201a** after intravenous administration (3 mg/kg) in Sprague Dawley rats. Samples were taken at the determined time points and the processed plasma was analysed via LC-MS/MS or ICP-MS (using an internal In stand) to quantify the compound concentration. The complex concentration of LC-MS/MS results [nM] were recalculated to express the Rh-concentration ng Rh/g plasma.

Fig. 51 shows the PK profiles related to ng Rh/mg plasma for both analysis forms. As for IV dosing of **201b** in C57BL/6 mice, the drug concentration-time profile shows a curve in which there is an initial rapid drop in the drug concentration and a subsequently slower decline. This effect can again be described by the two-compartment model.

It is obvious, that for LC-MS/MS the decline in compound concentration is much quicker and stronger compared to the results obtained by ICP-MS. One reason might be that ICP-MS is more sensitive than LC-MS/MS yielding in higher values for lower concentrations. Also, the higher results for ICP-MS might indicate, that metabolites form, which are not detected by LC-MS/MS,

Results and discussion

because only the parent compound is monitored, but are detected in ICP-MS as long as they contain Rh. Another reason seems to be an interference of other metal species (endogenous and exogenous metal ions and polyatomic groups),^[291] containing e.g. monoatomic (e.g. Ru103 or Pd103) or polyatomic isobars (e.g. metal oxides), in ICP-MS measurement, even though an internal In standard was used to minimise interference (isobars of In may interfere as well). These compounds might have been contaminating the samples during sample preparation, e.g. during acidic digestion in plastic tubes, or already been contained in the administered complex. The smaller the Rh amount contained in the sample the more interference is expected, yielding in wrongly elevated Rh levels in the samples measured. Therefore, all further discussed PK parameters were calculated based on the LC-MS/MS plasma profile of **201a**.

From the results obtained and profile shown the following conclusions can be drawn. The IV clearance is high ($ER = 97\%$), relative to the respective hepatic blood flow (100 mL/min/kg).^[292] This value seems to not align with the theoretical ER_b of 27% obtained in the rat liver microsome stability experiment. The volume of distribution at steady state V_{ss} is moderate (4.0 L/kg) with respect to total body volume (~0.7 L/kg), again indicating a diffusion outside the vascular department. The medium residence time (MRT) in plasma is 0.7 h indicating a shorter residence in the blood in comparison to RR97b ($t_{1/2} = 2.9$ h, MRT = 1.6 h) as also indicated in Fig. 52.

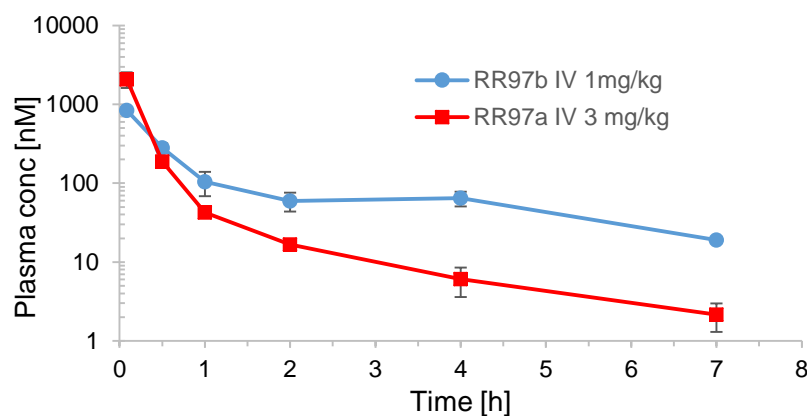


Fig. 52: Plasma concentration of compounds RR97a and RR97b after IV administration in Sprague Dawley rats (RR97a, 3 mg/kg) or C57BL/6 mice (**201b**, 1 mg/kg) over 7 h. Samples were taken at the determined time points and the processed plasma was analysed via LC-MS/MS to quantify the compound concentration. The concentration of **201a** in rats declines much faster in comparison to the concentration of **201b** in mice.

3.2.4.3. Metabolisation of RR97a *in vitro* and *in vivo*

To study possible metabolism formation, as both RR97a and RR97b are cleared from the blood in an unknown way, an *in vitro* hepatocyte assay with RR97a was performed by NIBR in Basel. Additionally, a possible *in vivo* metabolite formation from samples obtained from the rats which were administered 3mg/kg RR97a IV was investigated.

The compound was first tested *in vitro* in rat, dog and human hepatocytes and samples were analysed by LC-MS/MS. After two hours of incubation time, no oxidative metabolites were detected and the recovery rate was 100% for all species. This result aligns with the good stability results obtained in rat liver microsomes. However, based on the low permeability of the compound, there is the possibility that the compound only entered the hepatocytes to a small extend and thereby was not metabolised.

To qualitatively test a possible metabolic degradation or excretion in rats, 7 h post dose (pd) tissue samples (liver, kidney and lung) as well as urine were analysed for their RR97a content by LC-MS/MS, giving results for the respective parent compound. High levels of RR97a were thereby found in liver and lung, while lower concentrations were found in urine. These results are consistent with the determined V_{ss} of 4.0 L/kg from the PK studies, showing that the compound indeed diffuses outside the vascular department. All samples analysed 24 h pd contained significantly decreased levels of RR97a. These results indicate that the renal system is not the main route of elimination during that period of time and that metabolite formation is possible based on the drop in concentration in samples 24 h pd.

3.2.4.4. Excretion of RR97a *in vivo*

The excretion of **201a** was also investigated in more depth by means of ICP-MS/MS to study the total Rh-content, which also includes possible metabolites in the obtained results. Generally, first pass metabolites should be more water soluble in comparison to the parent complex and therefore expected in plasma, urine or faeces. While LC-MS/MS investigations found low levels of RR97a in urine for both 7 h and 24 h pd, ICP-MS analysis showed slightly elevated levels of Rh in urine and significantly higher levels in faeces compared to plasma, however as single determination (Fig. 53). Plasma and urine where thereby measured as liquids and faeces as dry weight but recalculated to the wet weight content. As some samples had a rhodium content above the maximum measurable amount, giving values above the highest concentration in the calibration curve, even higher levels are expected for urine 7 h and faeces 24 h.

After 7 h little Rh containing compound remains in the blood, as indicated previously in the PK studies, but is excreted via both urine and faeces, with a strong focus on biliary excretion. After 24 h additional Rh is excreted mainly as faeces, further reducing the plasma levels to 2 ng Rh/g plasma sample. Based on the results outside the calibration curve and a contaminated 24 h urine sample, these results have however only a limited information value.

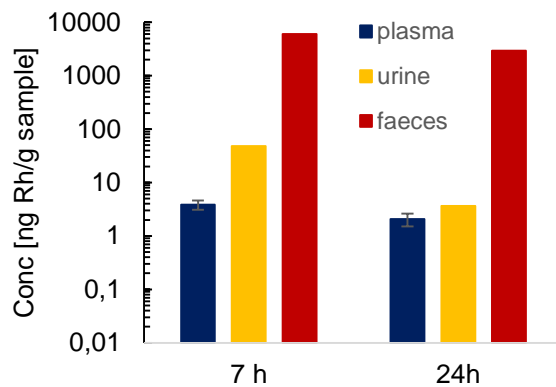


Fig. 53: Comparison of plasma, urine and faeces levels of **201a** obtained by ICP-MS analysis. Please be aware that the 24 h urine sample was contaminated and does not necessarily reflect the total Rh-amount. Additionally, the measured values for urine 7 h and faeces 24 h were above the highest value in the calibration curve. A higher total Rh content than shown is expected for both samples.

3.2.4.5. Tissue distribution of rhodium after 7 h and 24 h post IV injection of RR97a

During assessment of **201a** as a potential cancer drug it is important to understand the tissue distribution of the compound, as it has to reach its target but also be excreted at some point. This holds especially true for any metal species, which might otherwise accumulate in the body. During the metabolism studies, high concentrations of the complex were found in lung and liver, but little was found in kidney 7h pd by means of LC-MS/MS. These tissues account for highly perfused organs. We were therefore also interested in the concentration in other highly perfused tissues like brain (blood-brain barrier), heart and spleen, as well as less well perfused tissue like muscle. Tissue samples of the rats 7 h or 24 h pd were prepared as indicated in the experimental section and analysed for their total Rh content by ICP-MS using an internal Y standard. The results are given in Fig. 54.

Drug-like properties of metal-based kinase inhibitors

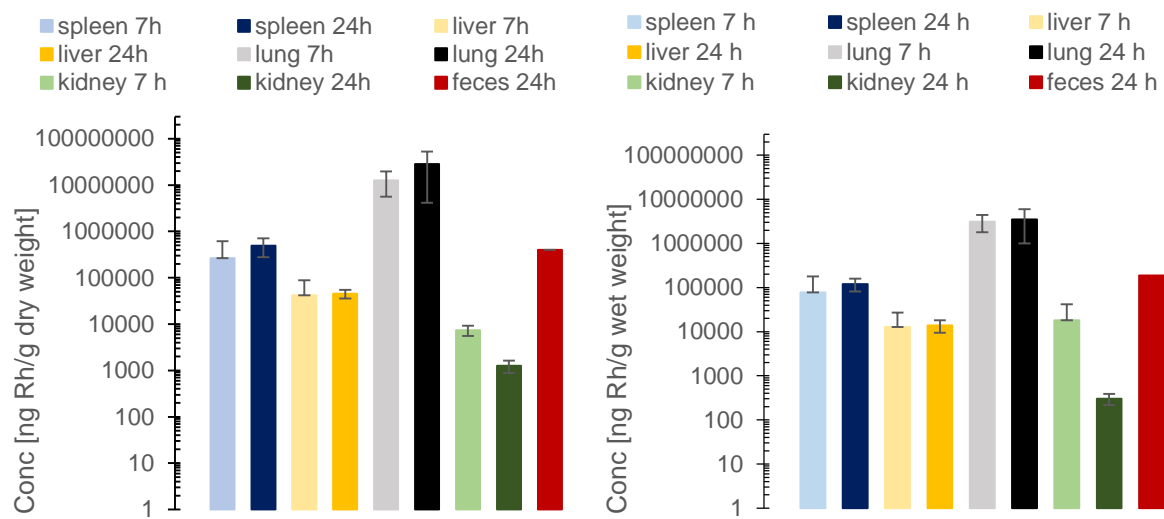


Fig. 54: ICP-MS results (ng Rh/g sample dry or wet weight) for tissue distribution studies. The content for dry weight (left) follows the order lung 24 h > lung 7 h > spleen 24 h > faeces 24 h > spleen 7 h > liver 24 h > liver 7 h > kidney 7 h > kidney 24 h using Y as internal standard. Taking the wet weight into account (right) the following descending order was obtained: lung 24 h > lung 7 h > faeces 24 h > spleen 24 h > spleen 7 h > kidney 7 h > liver 24 h > liver 7 h > kidney 24 h. All other samples had results below their respective detection limit.

Taken from Fig. 54 the highest concentrations of RR97a by far can be found in lung for both time points in accordance with the initial LC-MS/MS results. The second highest concentrations are found in spleen (7 and 24 h pd) and faeces (24 h pd). The concentration in faeces is even higher compared to the initial results as the sample was further diluted, based on being above the calibration curve in the first experiment. This again shows a strong indication of the biliary excretion of Rh. The faeces sample 7 h pd showed values below the respective detection limit, indicating a much lower Rh content at that time point as also determined in the initial experiment. A rather high Rh-concentration is also found in liver and kidney at both time points, while only amounts below the respective detection limit were found in muscle, heart and brain, indicating no penetration of the blood-brain barrier. Altogether most compound was found in lungs with similar content for both 7 and 24 h time points. In the lungs some form of metabolism might take place, but it is generally appreciated that the majority of exogenous compounds in the lung are rather bound more or less reversibly to some component of the lung tissue than being metabolised.^[293] If and how the compound is bound and/or metabolised in the lungs was not further investigated in this study.

Compared to the previously mentioned Ru-based NAMI-A differences in organ distribution are much more significant. NAMI-A was found by means of AAS mainly in kidney after single IV treatment of 200 mg/kg, indicating a selective clearance by the kidney,^[284] or in lung > kidney > liver after administration of 15, 35 or 50 mg/kg/day for 5 consecutive days to Swiss CD1 mice,

Results and discussion

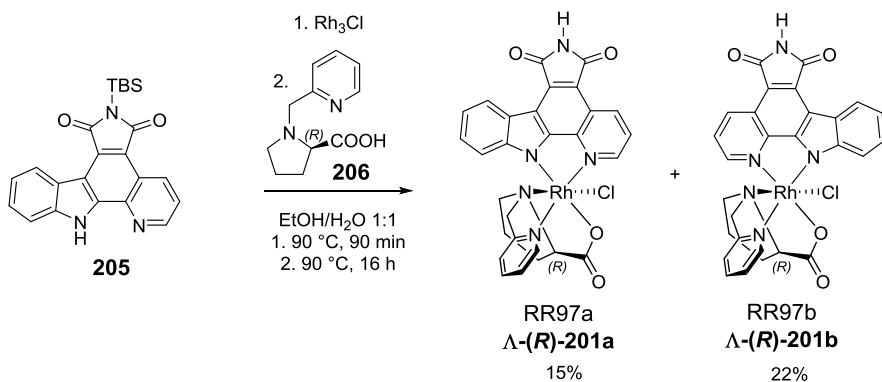
where the organs were removed 24 h after the last IV dose.^[283] In these studies also no penetration of the blood-brain-barrier was concluded for NAMI-A.^[283,284]

Cisplatin also shows highest levels of platinum in kidney after administration of 1 mg/kg in dogs, while initial concentrations generally were found in organs of excretion like gonads, spleen and adrenals and stayed elevated in kidney, liver, ovary and uterus for some days. The high values in kidney are thought to correspond to high urinary levels of platinum which appear immediately after administration. These high levels in kidney were found to persist 12 days or longer, irrespectively of much lower doses found in urine after that time, indicating a binding to the tissue. However while plasma levels after administration fall very quickly, as discussed previously, 60-70% of the applied dose could be recovered in urine.^[288] In the case of RR97a also high levels of Rh were found in urine after 7 h, but much less in kidneys and both not corresponding to high percentages of the initial dose given.

To sum up Rh is at least partially excreted via the biliary system and probably to a much lesser extent the renal system. After the 24 h observation time still very high amounts of Rh are found in the lung, indicating binding or side specific metabolism in this organ. As LC-MS determination showed decreased levels compared to the 7 h time point, metabolism in the lung might be a possibility but further studies are needed to verify these results and to identify possible metabolites. In addition to that, an experiment with a longer time-frame might be necessary to study how long the compound or other Rh-containing species stay in the lung. A long residence in the lung might lead to accumulations of Rh during long-term treatment, which might lead to adverse side-effects. Therefore, more in depth studies are indicated.

3.3. Upscaling possibilities of RR97a and derivatives

For the afore mentioned in depth studies, larger amounts of the complexes were required. Therefore, upscaling studies were performed during the course of this thesis to evaluate a possible improvement of the reported yields and also be able to achieve higher quantities per reaction. The final reaction steps, as well as reported yields are given in Scheme 7. The reported yields are based on a scale of 44.0 µmol (17.7 mg) pyridocarbazole (**205**).^[233] The reaction towards the pyridocarbazole-rhodium precursor was performed in a 1:1 mixture of ethanol/water since the substitution of the chlorido ligand in the first reaction step is favoured in aqueous solutions.^[294] This precursor was then further reacted in a one-pot synthesis to the final complexes **201a** and **201b** (or analogous to **204a** and **204b**) using the proline derived ligand **206**. It is generally known that this type of coordination chemistry is overall sluggish, indicated by the typical low to moderate yields for the ligand exchange reactions.^[295]



Scheme 7: Reported reaction scheme and yields for the synthesis of RR97a (**201a**) and RR97b (**201b**), using 44.0 µmol of pyridocarbazole (**205**). The pyridocarbazole was first reacted with Rh₃Cl in a 1:1 mixture of EtOH/H₂O to form the according complex precursor which is further reacted in a one-pot synthesis with the proline ligand **206** to the final complexes.^[233]

3.3.1. Upscaling of the amount of starting material

The first choice for upscaling was obviously a simple scale-up of the starting materials under the given reaction conditions. This was carried out using 250 µmol pyridocarbazole (100 mg) together with an adjusted reaction time of 24 h in the second reaction step to drive the reaction to completion. The extended reaction time was thereby validated using a scale of 125 µmol pyridocarbazole, which led to a yield of 20% of **201a**, in comparison to the reported 15% using a period of 16 h. The yield of the enhanced reaction scale (250 µmol of **205**) however dropped to <10% (~16-24 mg depending on the purity as determined from ¹H-NMR spectra). In addition, an increased amount of coloured by-products was observed by TLC analysis and a large amount of unreacted pyridocarbazole (at least partially deprotected) could be isolated after column

chromatography. High amounts of pyridocarbazole were however also isolated in smaller scales. Due to the raised number of by-products and a general smearing of both diastereoisomers, as well as the by-products, on silica during purification, the compound could only be obtained in a pure fashion after multiple flash columns using a gradient of CH₂Cl₂/MeOH (1:0 to 200:1 to 10:1). Hence, this approach was rejected due to the extensive purification procedure and the decreased yield.

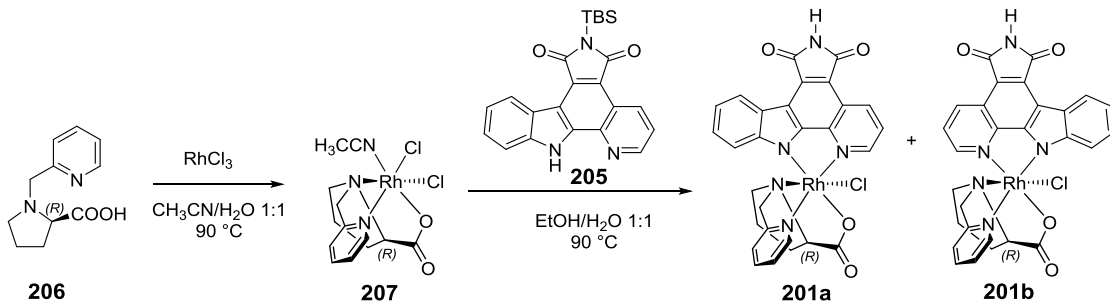
Since the yield for the half-scale was obviously larger compared to higher or smaller scales, four separate reactions of 125 µmol pyridocarbazole each were performed separately and two reactions each were pooled for purification. Flash chromatography separation of the diastereoisomers were performed over 40 g silica using the slow gradient of CH₂Cl₂/MeOH described above. The different diastereomers were further repeatedly purified over 1.5-3.0 g of silica. An exact yield for these reactions however could not be obtained, since part of the compound got lost during purification. The total yield of all reactions described in this chapter combined was 12% for **201a**. Altogether this second approach of splitting the reactions and pooling them for work-up meant again a huge amount of work for purification. Though a smaller extent of by-products was qualitatively determined on TLC, compared to the first approach using a larger scale. Therefore, the second option was not further pursued and other solutions for the upscaling problem were investigated, as described in the following chapter.

3.3.2. Optimisation of reaction conditions

Since the yields in the complex reactions were generally very low, which is most probably based on the sluggish chemistry,^[295] a study for improved reaction conditions was performed. The low yields in the original reaction are presumably based on a fast deprotection of the pyridocarbazole, deactivating it towards coordination. Moreover, this may also cause the formation of numerous by-products in the reaction, as indicated earlier by TLC analysis.

Based on this experience, another approach towards the synthesis of RR97a and RR97b as well as its derivatives was required. Conveniently, STEFAN MOLLIN showed in his PhD thesis^[296] that upon reacting structurally distantly related kinase inhibiting ligands (e.g. phenylquinoline derived ligand) first with RhCl₃ and afterwards with *N*-methyl-*N*-(pyridine-2-ylmethyl)glycine as tridentate ligand, the *cis*-isomer (carboxylate of the ligand is coordinated *cis* to the phenylquinoline nitrogen) was formed to a greater extent than the *trans*-isomer (~2:1). Reacting the glycine ligand first with RhCl₃ and then adding a benzyl-protected pyridocarbazole, a ratio of *cis* to *trans* isomers (carboxylate of the ligand is coordinated *cis* or *trans* to the indole nitrogen) of 1:3 was obtained. Based on these

results, a similar approach was pursued for the given system to obtain RR97a and RR97b (Scheme 8).



Scheme 8: Proposed reaction sequence for improvement of the *cis/trans* ratio of the formed complexes **201a** and **201b**.

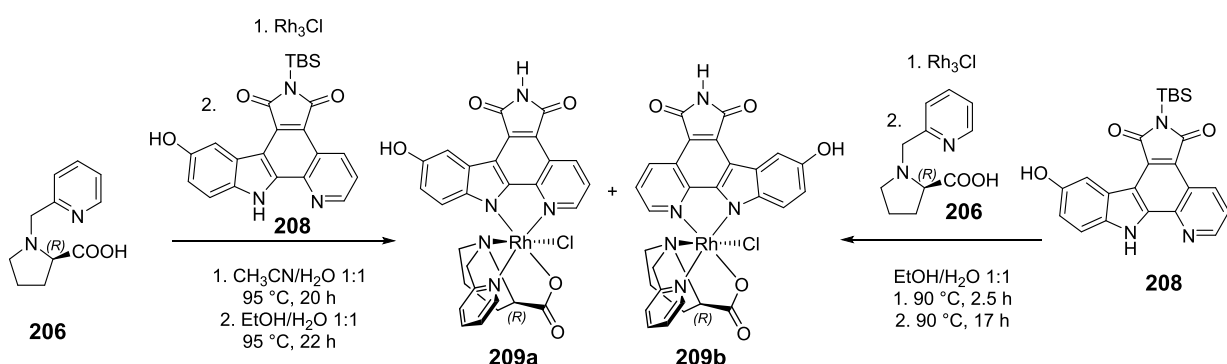
To test the hypothesis of positively influencing the ratio of **201a** (*trans*-isomer) to **201b** (*cis*-isomer) obtained in the reaction, the proline ligand **206** (38.0 µmol, 1.00 eq) was reacted in a small-scale with RhCl₃ (38.0 µmol, 1.00 eq) in a 1:1 mixture of CH₃CN/H₂O (3.8 mL) for 16 h at 90 °C, as indicated for the glycine ligand in STEFAN's thesis. A complex precursor is thereby expected to be formed in a way where the rhodium centre of RhCl₃ coordinates three acetonitrile ligands before one chlorido and two acetonitrile ligands were exchanged by the carboxylate of **206** to form **207** (Scheme 8). ¹H NMR analysis of the complex precursor **207** after flash chromatography (CH₂Cl₂/MeOH) however showed at least two sets of signals in the aromatic region. These might be based on either monodentate ligand exchange in the complex **207**, two proline ligands coordinated to one rhodium centre, or unreacted ligand in the spectrum. Without further purification, the precursor mixture was reacted in CH₃CN/H₂O 1:1 at 90 °C for 16 h with the TBS-protected pyridocarbazole. Hereby, no reaction was observed by TLC analysis. Therefore, the solvent was removed and replaced with EtOH/H₂O 1:1 and the reaction mixture was heated to 90 °C for 72 h. TLC analysis indeed showed the formation of the two expected diastereomers with the *trans* signal giving a more intense colouring, indicating that the reaction conditions shift the *cis/trans* ratio. It was attempted to drive the reaction to completion by adding pyridocarbazole at different time points (~0.5 eq directly after precursor synthesis, another 0.5 eq 3 h after the start, and extra 0.1 eq at time point 5 h and 0.1 eq after 15 h). However, a completion of the reaction could not be achieved.

Based on these positive results, a screening for the optimal solvent for the second reaction step was performed. Especially the high amounts of unreacted pyridocarbazole were of great concern. Therefore, 50 µmol of each the ligand and RhCl₃ were reacted under stirring in 50 mL CH₃CN/H₂O 1:1 at 90 °C for 16 h. Afterwards, the solvent was removed and either 5 mL EtOH,

Results and discussion

DMF or EtOH/H₂O 1:1 were added together with 1.0 eq of pyridocarbazole **205**. All solvents are polar and therefore able to coordinate and stabilise possible charged intermediates. The reactions were stirred at 90 °C for 65 h and the results were analysed qualitatively via TLC analysis. While the reaction with pure EtOH contained large amounts of unreacted pyridocarbazole, some complex and various by-products, the reaction using DMF showed hardly any reaction to the desired complexes as well as hardly any unreacted pyridocarbazole left (probably based on cleavage of the TBS-protecting group and subsequent abolishment of the reactivity of the pyridocarbazole). Both reaction conditions showed much lower product formation compared to the original solvent mixture, which might be associated to the missing water as aqueous solutions are known to promote the substitution of a chlorido-ligand^[294] as mentioned earlier. Another possibility for the low yields is a faster deprotection of the pyridocarbazole in the changed solvent system. Therefore, for both reactions the solvent was removed, replaced by EtOH/H₂O 1:1 and stirred for 24 h at 95 °C. TLC analysis after that reaction time showed a small improvement of the original EtOH reaction and no improvement of the DMF reaction, indicating indeed the loss of the TBS-protection group of the pyridocarbazole. Therefore, the precursor approach was generally dismissed for the unsubstituted pyridocarbazole.

In parallel to the studies using unmodified pyridocarbazole, a comparison study of the original one pot synthesis reaction conditions and the precursor approach was done by BENEDIKT HEINRICH using an indole-5-ol modified pyridocarbazole (**208**). This investigation was supposed to help understanding the influence of the electronic properties of the ligand.^[297]



Scheme 9: Different synthetic approaches towards the synthesis of **209a** and **209b**. On the left-hand side, the reaction conditions of the one pot synthesis are shown. On the right-hand side the conditions of the precursor approach.

Upscaling possibilities of RR97a and derivatives

Starting with very small reaction scales, both reaction pathways (Scheme 9) were confirmed to result into the desired complexes **209a** and **209b** as shown qualitatively by TLC analysis. The complex formation using the precursor approach was subsequently tested in both solvent systems, CH₃CN/H₂O 1:1 and EtOH/H₂O 1:1, for the second reaction step and evaluated qualitatively via TLC. Minimal reaction was thereby detected in the original solvent (CH₃CN/H₂O), even with a temperature increase up to 105 °C. The use of EtOH/H₂O resulted in the formation of a spot for the a isomer **209a** that has been much more intense compared to the one of the b isomer **209b**.

When scaling-up the precursor approach (152 µmol pyridocbazole), ¹H-NMR analysis of the two isomers after purification via silica flash chromatography using CH₂Cl₂/MeOH (1:0 to 100:1 to 10:1) showed an extensive number of by-products, probably unreacted precursor and/or unreacted ligands. These by-products were not easily removable by flash chromatography over silica since the complexes and by-products have similar retention factors (Rfs) in the given solvents and tend to smear on silica. An isolated spot from the 5-hydroxy pyridocbazole reaction, which was suggested to belong to the precursor **207**, was analysed by ¹H-NMR spectroscopy in DMSO-*d*₆, where it showed all signals of the ligand but the expected CH₃CN signal. A high-resolution mass spectrum however showed the exact mass of LRhCl(DMSO) (with L representing the deprotonated proline derived ligand **206**), so that the CH₃CN ligand might have been exchanged in the NMR tube due to its reactivity and excess DMSO present. The missing chlorido ligand in the exact mass was probably lost during ionisation. These results indicate a formation of metal precursor as suggested. Interestingly, a similar species as the precursor was also found when scaling-up the one-pot approach, indicating a lower reactivity of the pyridocbazole-ligand and therefore leftover RhCl₃ which might react with the later added proline ligand. However, this side product was present to a much smaller extent in comparison to the by-products detected in the precursor approach, which is probably based on the changed solvent system. Also, the a isomer **209a**, which is the isomer of interest, could be obtained in a pure fashion, while only the b isomer **209b** was inseparable from this side product, which was not the case for the precursor approach. Still **209a** was formed to a much smaller extent, compared to the precursor approach, deeming both reaction pathways as not very suitable to form larger amounts of **209a**.

To sum up, the precursor approach indeed leads to the formation of a higher ratio of a (*trans*) to b (*cis*) isomer, however with the draw-back that also more and partly inseparable by-products were formed. Therefore, this variant seems not to offer a suitable possibility to enhance the reaction yield, for scale-up or save time in work-up. All in all, no approach helped to scale the reactions or yield up to a significant extent.

3.4. Solubility and permeability optimisation

Based on the *in vitro* and *in vivo* data, the critical parameters for bioavailability of pyridocarbazole derived metal-based kinase inhibitors are solubility and permeability. Since **201a** is a potent Pim1 inhibitor and shows adequate *in vitro* and *in vivo* properties, it was considered as an attractive lead structure. It was therefore selected as a starting point for improvement of solubility and permeability by chemical modification of its structure.

In general, solubility is affected by physicochemical properties which are based on underlying structural properties. These include size (MW, shape), pK_a, crystal lattice energy and lipophilicity, which itself is based on VAN DER WAALS forces, polarity, number of H-bond acceptors and donors, as well as ionic interactions. General strategies to enhance solubility include e.g. the addition of an ionisable or polar group, H-bond acceptors or donors, or the reduction of logP or MW. Additional strategies might include the addition of an out-of-plane substitution to reduce the crystal packing, or to form a prodrug with higher solubility.^[232] Permeability on the other hand, as the rate of drug passage through a biological membrane barrier, is also influenced by various physicochemical parameters like ionisability and lipophilicity, especially with a focus on polarity and hydrogen bond donors and acceptors. While solubility limitations in a compound might be overcome by a solubility enhancing formulation, the only way to enhance permeability is structural modification. General strategies to enhance permeability include the replacement of ionisable groups by non-ionisable groups, the isosteric replacement of polar groups, the reduction of hydrogen bonding and polarity, the addition of lipophilicity e.g. by addition of nonpolar side chains, the reduction of size, and a probable prodrug approach.^[232]

When considering these classical options to improve solubility and permeability, it is obvious that most approaches disagree with each other as indicated in Table 8, and it seems almost impossible to improve one property without adversely affecting the other. On the other hand, approaches like the reduction in size or MW, the addition of an out-of-plane substituent and the addition of a nonpolar side chain, as well as the prodrug approach might complement each other.

Solubility and permeability optimisation

Table 8: General approaches to improve permeability and solubility. Approaches which are mutually exclusive when trying to improve both properties in one molecule are marked with a cross. Modifications which might complement each other are marked with a check mark.

Permeability		Solubility
• convert ionisable group to non-ionisable group	✗	• add ionisable group (e.g. salts)
• add lipophilicity	✗	• reduce logP (lipophilicity)
• reduce polarity	✗	• add polar groups
• reduce H-bonding	✗	• add H-bonding
• reduce size	✓	• reduce MW
• add nonpolar side chain	✓	• Out-of-plane substitution to reduce crystal packing
• prodrug approach	✓	• prodrug approach

When considering the proper strategy, first the prodrug approach was dismissed, since the evaluation of drug-like properties, as well as activity of a prodrug, is very complicated depending on the prodrug strategy. It was decided that this approach was out of the frame of this work.

A reduction of size and/or molecular weight sounded very promising in the beginning. However with a decrease in size of the largest ligand, the pyridocarbazole, most probably the kinase affinity would have gotten lost or at least decreased as SEBASTIAN BLANCK could show in his PhD-thesis when using quinolinemaleimides,^[298] pyridynaphthalimides^[299] and pyridylphtalimide^[158] as pharmacophore-ligands.^[300] All three ligand classes have been used to develop attractive KIs against e.g. MLCK,^[299] PKC δ ^[298] and PAK1,^[158] which however were not as potent as pyridocarbazole derived inhibitors. The best example might be the work of STEFAN MOLLIN who used a phenylquinoline ligand to synthesise structural analogues of **201a**, using the exact same tridentate proline derived ligands and RhCl₃. A kinome screen of an intentionally created racemic mixture of the main isomers, showed very low kinase affinity,^[296] while only **201b** showed very low affinity, whereas the other three complexes **201a**, **204a** and **204b** were very potent.^[233]

The second largest ligand is (pyridine-2-ylmethyl)-D-proline (**206**), which can hardly be reduced in size, since its structure is required both for coordination purposes and to decrease the number of possible isomers. Therefore, a significant reduction in size was not considered as a realistic option, especially in the context that more than 30% of approved SMKIs have a MW above 500, showing that the MW is not the sole limiting factor for drug-like properties.^[26] The best option to improve both solubility and permeability therefore seemed to be the addition of an out-of-plane substituent. However, since it was unclear how the compound binds in the Pim1 kinase active pocket, some *in silico* investigations were performed, to specify which position might be suitable for this approach.

3.4.1. Structural optimisation – *in silico* studies

For our compound of interest RR97a (**201a**), no co-crystal structure with a protein kinase was available at the point of lead optimisation studies. Therefore, very simple docking experiments were necessary, to evaluate positions which might be suitable for structural optimisation. It is well accepted, that the pyridocarbazole ligand always binds in a similar fashion due to the binding interactions explained in the introduction part. Since there are diverse kinase co-crystal structures of other pyridocarbazole-based compounds available, the easiest solution was to just pair-fit the pyridocarbazole moiety of **201a** to the available co-crystal structure to obtain a first impression of the orientation of the complex. In addition to a missing co-crystal structure, there was no simple crystal structure of RR97a available. Therefore, the complex was generated and optimised via MM3 geometry using the program CAChe WorkSystem Pro 7.5.0.85 (FUJITSU LIMITED). Given that the crystal structure of the diastereomer RR97b was obtained previously by RAJATHEES RAJARATNAM, the structure of RR97b (**201b**) was optimised in the same way as the one for RR97a to test the accuracy of the structure optimisation. The result is shown in Fig. 55 and gives an impression of how far the calculation of RR97a deviates from reality.

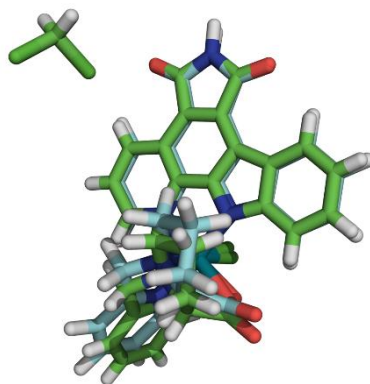


Fig. 55: Comparison of the crystal structure of RR97b (green) and the structure obtained by MM3 geometry optimisation (cyan). Obviously, the calculation shows deviations to the true structure, but the results are still rather close to the true values.

The structure obtained (Fig. 55) is obviously not absolutely correct, but was considered satisfactory for the planned binding investigation, since the overall accuracy was not expected to be very high, but also not required for the purpose of finding possible side pockets or solvent exposed residues. The calculated structure of **201a** was subsequently superimposed using the *pair-fitting* operation for the maleimide group of the pyridocarbazole ligand in PyMOL 1.5.0.4, to two existing co-crystal structures of Pim1 containing pyridocarbazole-based RuCpCO-complexes DW2 ((*S*)-**53**) and HB1 ((*R*)-**199**) (pdb 2BZI (DW2), 2BZH (HB1))^[48]. It is well established for this type of complexes, that the relatively small monodentate ligand always points in the direction of the glycine rich loop

(c.f. pdb files 2OI4, 2IWI, 3CST, 2JLD, 3FXZ, 3PUP, 2YAK amongst others) of the kinase, simplifying this approach by dictating the orientation. The results of the pair fittings are shown in Fig. 56 and Fig. 57.

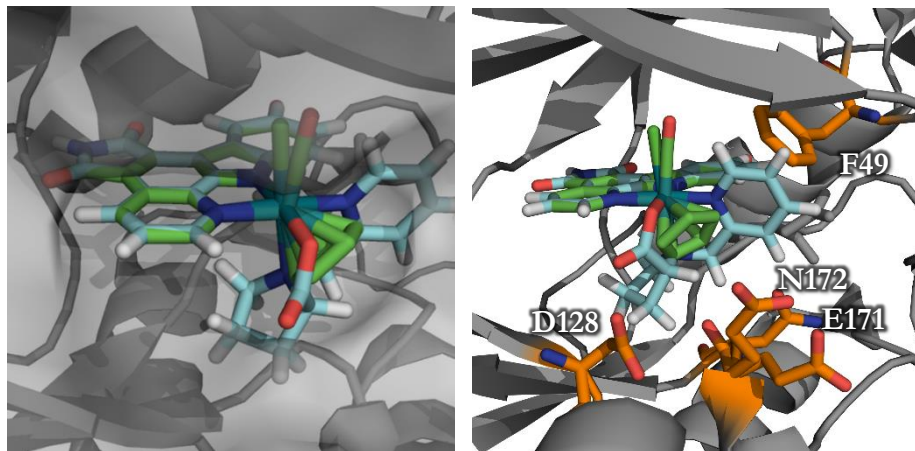


Fig. 56: Modelled **201a** (cyan) superimposed to the compound DW2 (green) in the Pim1 enzymes active pocket (pdb 2BZI). On the right-hand side, all amino acids which seem to prevent a binding of RR97a are shown, namely F49, D128, E171 and N172. Kinase active pockets are very dynamic structures, therefore these residues might take different orientations while **201a** binds to the pocket.

From Fig. 56 it is obvious that RR97a cannot fit into the enzymes active pocket in the conformation given, using the surface representation of PyMol (CONNOLLY surface). However, active pockets of kinases are very dynamic due to the flexibility of the hinge region. The model shows that there are only a few residues present, which conflict with the complex (F49, D128, E171 and N172) and all are flexible through rotation around single bonds. The orientation of **201a** thereby does not need to correlate exactly with DW2. The comparison to the superimposition to HB1 (Fig. 57) shows indeed the F49 residue as only conflict. From this figure, it is also obvious, that the space around the proline is very limited, while both the pyridines, belonging to the (pyridine-2-ylmethyl)-D-proline and the pyridocarbazole are at least partially solvent exposed, leaving a good starting point for the addition of out-of-plane substituents. Since the 4-pyridine position of the proline-based ligand **206** seemed to be much more solvent exposed and possesses no threat towards a sterical hindrance in complex formation, this position was selected for the out-of-plane modification. Notably, a pair fitting of **201b** to the same co-crystal structures did not explain the preference of binding of **201a** in comparison to **201b**.^[233]

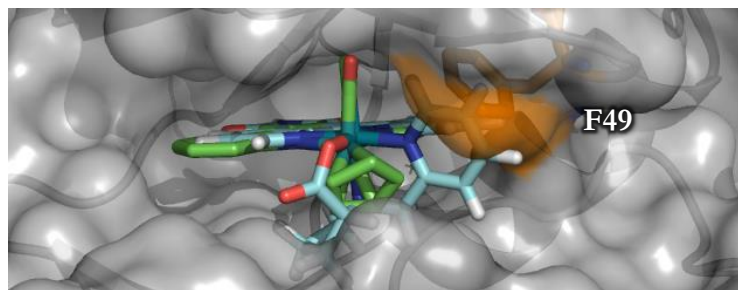


Fig. 57: Modelled RR97a superimposed to the compound HB1 in the Pim1 enzymes active pocket (pdb 2BZH). Here again a clash of the compound with F49 (orange) was identified.

To also get a first impression on which kind of substituents might help keeping or even improving the affinity towards Pim1, we were committed in investigating the surface charge of the protein, to find positions for possible attractive interactions.

For that matter the PyMol Plugin APBS^[301,302] (Adaptive Poisson-Boltzmann Solver) was used, after the pdb-file was converted to a pqr-file using the pdb2pqr server (Version 1.8)^[303,304] via a PARSE-forcefield (parameters for solvation energy) method,^[305,306] which prepares structures for further calculations by reconstructing missing atoms, adding hydrogens, assigning atomic charges and radii from specified force fields, and generating pqr files. Pqr files are generally pdb files where the occupancy and B-factor columns have been replaced by per-atom charge and radius. The Poisson-Boltzmann equation is used as a basis for a popular continuum model used to describe electrostatic interactions between solutes in salty, aqueous media. For the conversion (pdb2pqr) the complex had to be removed, because coordination compounds which contain e.g. ruthenium or rhodium are not supported by the forcefield methods. After the conversion, the color-coded electrostatic surface potential was calculated and presented as negative and positive potentials on the isosurfaces, providing information about the atomic surface charges and the shape of the protein (Fig. 58). The solvent-accessible surface (obtained by addition of 1.4 Å to every atomic radius before calculation of the area)^[307] tends to reveal more global features of the surface potential but limits the size of the active pocket. Therefore, no further conclusions towards the ligand binding and suitable available space could be drawn from that model. As second point of reference, the potential on the solvent accessible surface was chosen, which visualises both geometric information from the molecular surface and electrostatic potential information from the solvent-accessible surface simultaneously (Fig. 58). All potentials are displayed at pH 7.0 with default protonation states for all residues. As default thereby only charged residues (Arg, Lys, Glu, Asp) are taken into account, and the charges are located at the corresponding (non-H) atom positions. Overall the active site is negatively charged, as can be seen in Fig. 58, with the exception of an amine in the hinge region.

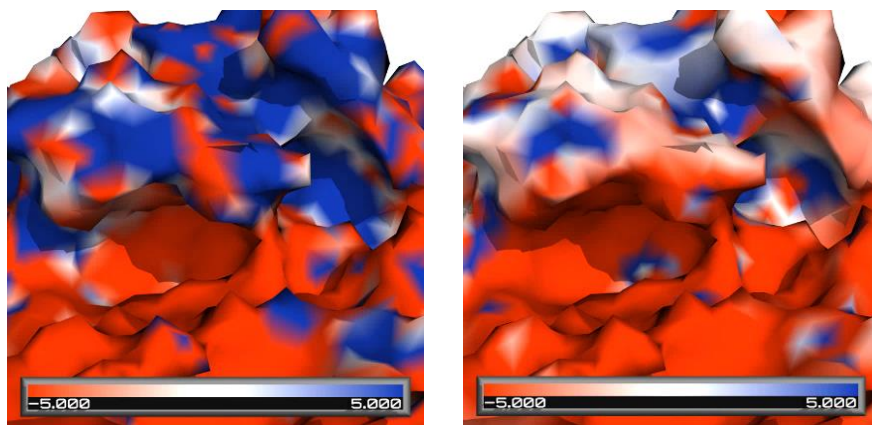


Fig. 58: Molecular surface potential (left) and surface potential on the solvent accessible surface (right) of Pim1 [$K_b/T/ec$ at pH 7.0] calculated using the PyMol plugin APBS, based on the pdb 2BZI, which was converted to a pqr using a PARSE-forcefield after removal of the binding complex. White colour indicates a neutral surface potential, blue a positive surface potential as it is induced by amines, and red a negative potential as it is found e.g. with carbonyl groups.

The potentials obtained were further aligned with the unmodified pdb-file, to reobtain the position of the complex. Afterwards, the optimised structure of RR97a was pair-fitted, to get an impression of potential positions where specific interactions might be obtained. To test the space available at the previously discussed 4-pyridine position, a 4-hexyl pyridine derivative of RR97a was calculated and pair-fitted (Fig. 59).

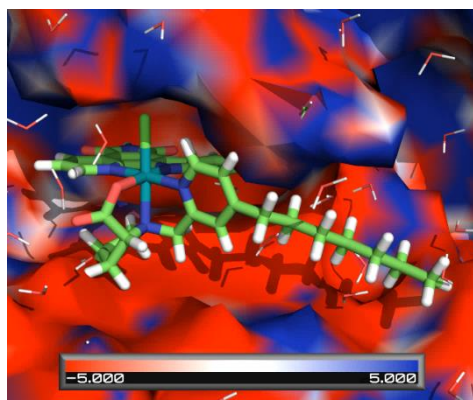


Fig. 59: A modelled 4-hexyl-pyridine derivative of RR97a bound to Pim1, which is represented as molecular surface potential. From the results a side chain that long should find sufficient space to not impair the binding of the complex.

The model presented in Fig. 59 indicates that there is indeed some space available in the Pim1 active pocket, to add substituents to the 4-position of the pyridine. The space however is obviously limited, so that mainly long but lean residues might be introduced. Overall the surface potential in the region is mainly negative (red), with some positive (blue) regions, giving the possibility of introducing different types of potentially charged residues to find the perfect fit, which might improve the affinity but additional positive interactions. Further considerations on which functional groups might be suitable, can be found in the following chapter.

3.4.2. Derivatisation of the proline derived ligand 206 – theoretical considerations

As indicated in the previous section (3.4.1), the largest space available to attach larger substituents seems to be in the *para*-pyridine position of the proline based ligand. Therefore, this position is the ideal starting point to add an out-of-plane residue, which is supposed to enhance solubility while not interfering with the binding to active site and decreasing the potency of the inhibitor. The molecular planarity of the pyridocarbazole ligands with their high degree of π - π -interactions are thought to strongly contribute to the low solubility of the complexes by increasing crystal packing. Using an out-of-plane residue might at least partially counteract these interactions. By disturbing molecular planarity and symmetry, generally the efficiency of crystal packing should be decreased^[12] and thereby the solubility probably enhanced.^[308] This kind of solubility enhancement could also avoid potential acute toxicological effects due to crystallisation *in vivo*,^[12] as seen *in vitro* for np829 (**80b**) and which might have been indicated as well for **201a** in PCLS studies.

As previously mentioned, SMKI tend to be quite large and hydrophobic during development stages, as increased hydrophobic interactions are a result of an increase in potency towards a given target but might also lead to lowered solubility.^[12] To improve their drug-like properties, especially their solubility, a common strategy for SMKI is the addition of water exposed solubilising side chains or appendages located outside of the binding pocket upon binding since the presence of strongly hydrophilic or ionisable groups in other positions will often interfere with ligand-protein binding.^[12] A solubilising appendage can be a basic, acidic, or a neutral group tethered to the drug via a linker.^[309] Typical structures include linkers which inherit piperidines (e.g. vandetanib (**13**)), piperazines (e.g. dasatinib (**5**), bosutinib (**18**) and nintedanib (**24**)) or morpholines (e.g. gefitinib (**2**) see bound to EGFR in pdb 2ITY^[310]), but the concept is also applied with other long solvent exposed chains as in erlotinib (**3**), sunitinib (**6**), lapatinib (**8**), axitinib (**19**) and afatinib (**21**).^[19]

Since Pim1 is rather negatively charged in its active site, as shown in the *in silico* section, especially appendages which inherit amine groups were thought to enhance the solubility and probably simultaneously the affinity of the derivative to the kinase. This assumption is based on the fact that amine groups form strong H-bonds with water and might form positively charged species, if the conjugated acid is formed at a pH corresponding to the according pKa, which might interact with negatively charged side chains of the kinase. Generally this pKa will determine the expected increase in solubility,^[309] it is however not easily determined for metal-complexes since most tools used to easily calculate pKa are not capable to include the shift obtained by electron withdrawal when coordinating to a metal. The amount of polar atoms like nitrogen to be added has to be carefully considered not to negatively influence membrane permeability^[309] as for neutral substances the main contributor to membrane permeability are molecular size and H-bond

capability.^[311] Therefore, to test a possible improvement in solubility by adding a pure aliphatic side chain for out-of-plane substitution, according derivatives were planned as well.

Based on this information as well as the synthetic access according to literature, the following complexes (only Λ -(R)-a isomer shown) were planned to be synthesised and tested for their drug-like properties (Fig. 60).

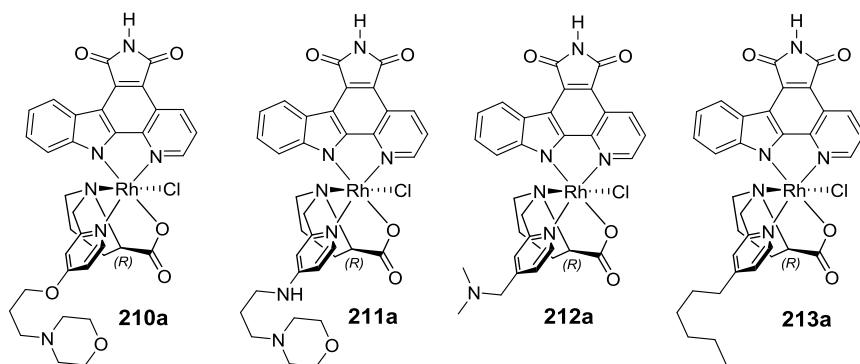


Fig. 60: Selected complexes to explore the possibility of solubilising side-chains outside of the Pim1 active site. Morpholines as in **210a** and **211a** are generally known to enhance solubility by their H-bond capability and the linker ensures an out-of-plane behaviour. The α -atom in the pyridine 4-position (N or O) is varied to explore possible interactions in the kinase active site. Complex **212a** thereby inherits a tertiary N in the β -position, which is supposed to be protonated under physiological conditions. The final complex **213a** is an example for a complex with a pure aliphatic side chain. It should represent the solubility enhancement with pure out-of-plane behaviour while enhancing the permeability at the same time.

As shown in Fig. 60, a small collection of different complexes was planned. In the first two complexes **210a** and **211a**, a morpholine residue is attached by a linker to the 4-pyridine position. Morpholines are generally known to enhance solubility by their H-bond capability and the linker ensures an out-of-plane behaviour, where the α -atom (O or secondary N) might be used to add favourable interactions in or close to the active site. In complex **212a**, the tertiary nitrogen is shifted to the β -position, to test favourable interaction in this position. The nitrogen is expected to be at least partially protonated at physiological pH since its pKa in the uncoordinated ligand was calculated to be ~ 8 .^[312] If unprotonated, the amine will not affect permeability, otherwise it should affect solubility in a positive way. The final complex **213a** inherits a pure aliphatic side chain, which should prove the hypothesis for solubility enhancement by out-of-plane substitution, while improving permeability as well.

3.4.2.1. *In silico* investigation of possible solubility and permeability improvement

To measure an improvement in solubility and permeability, mostly the partition coefficient in octanol and water ($\log P$) is used,^[313] which is often hard to measure because of the low solubility of most compounds in alkane/water.^[247] This is also true for metal-based kinase inhibitors. To assess the theoretical considerations for improvement of solubility and/or permeability of RR97a by structural modification, *in silico* calculations were performed using the software STARDROP (Version 5.5 Build 223) at NIBR.

Table 9: Calculated physicochemical properties for selected complexes which are based on considerations for improvement of the solubility and/or permeability of RR97a.

Complex	logS [μM]	logS (pH 7.4) [μM]	logP	logD
201a (RR97a)	2.8	5.6	0.8	2.0
210a	3.0	5.8	1.3	2.4
211a	3.1	5.8	1.1	2.3
212a	3.2	5.9	1.3	2.1
213a	2.2	5.2	3.0	2.6

In the program, the logarithm of the intrinsic aqueous solubility S is calculated using a continuous model predicting aqueous solubility of a neutral undissociated compound based upon *in vitro* data. The indication pH 7.4 stands for the apparent solubility at the given pH for charged and neutral species. The logP (octanol/water coefficient) is as the logS calculated based on a continuous model obtained from *in vitro* data, and the logD equals the logP at pH 7.4 for all species present.

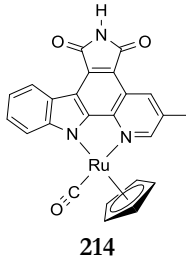
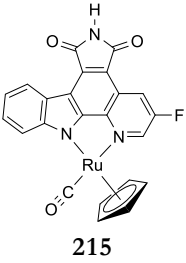
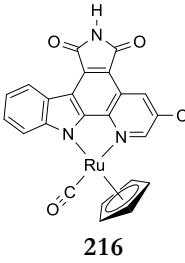
Based on the obtained data (Table 9), the initial complex **201a** has an intrinsic solubility of 631 μM, which is very high compared to the measured results of 16 μM in KP_i and 29 μM in FaSSIF. All newly designed compounds, except for the alkyl derivative **213a**, have however higher calculated solubilities, as expected. The same holds true for the solubility at pH 7.4, which is calculated to be even higher, indicating the presence of charged species. The calculated logP of 0.8 indicates that the neutral form of **201a** is a 6.3 times more soluble in octanol compared to water, while the partition coefficient shows that all available species are 100 time more soluble in octanol. All derivatives have therefore a higher lipophilicity in comparison to **201a**, represented in higher logPs and logDs. The logD value is thereby always higher compared to logD except for **213a**, in which charged species seem to have a much lower lipophilicity.

These data again show the low suitability of *in silico* models for metal-based drugs, but gives us still a first impression for the right trend, as anticipated for the planned derivatives.

3.4.3. Modifications of the pyridocarbazole ligand – theoretical considerations

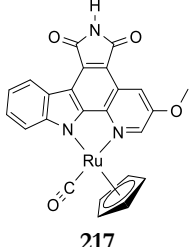
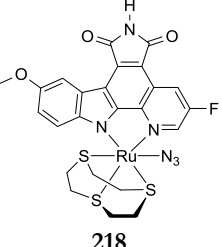
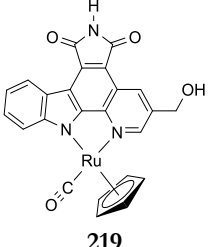
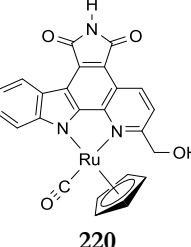
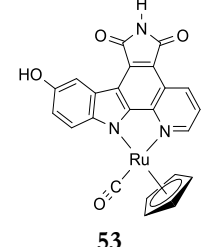
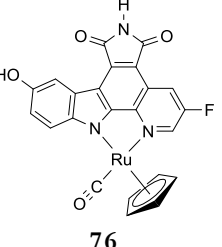
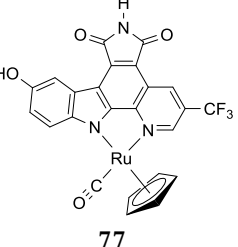
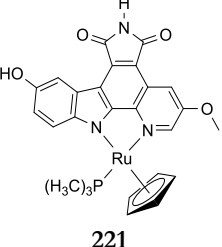
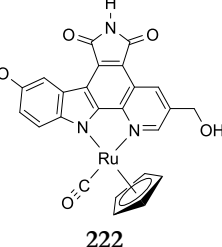
For modifying the drug-like abilities of the complexes, while maintaining or even improving Pim1 affinity, all previous work described in PhD theses and publications concerning Pim1-inhibition by pyridocarbazole-based metal-complexes were screened for possible modifications of the pyridocarbazole ligand. The results, including the inhibition properties towards Pim1, either as IC₅₀ value or as rest activity of the enzyme after treatment with a certain concentration of the inhibitor compared to the associated unmodified complex, are summarised in Table 10. The list is ordered by increased polarity as expected from the added functional groups. Side chains of other ligands e.g. cyclopentadiene, which increase Pim1 affinity, were not considered since they are expected to have a quite different orientation compared to the 4-pyridine position in the proline derived ligand, as can be seen e.g. in pdb file 2BZJ.^[314]

Table 10: Pyridocarbazole-based Pim1 inhibitors which show improved kinase affinity compared to the associated complexes with unmodified pyridocarbazoles. Values for inhibition of both the complex and the associated unmodified complex are given. Structures are sorted according to expected increased polarity of the pyridocarbazole ligand.

Complex			
Pim1 rest activity after treatment (c) or IC ₅₀	IC ₅₀ < 0.3 nM (10 μM ATP) ^[315]	26% (10 nM (100 μM ATP) ^[202])	35% (10 nM (100 μM ATP) ^[202])
unmodified pyridocarbazole	IC ₅₀ = 4 nM (100 μM ATP) ^[204]	52% (10 nM (100 μM ATP) ^[202])	52% (10 nM (100 μM ATP) ^[202])

Results and discussion

Table 10 (continued): Pyridocarbazole-based Pim1 inhibitors which show improved kinase affinity compared to the associated complexes with unmodified pyridocarbazoles. Values for inhibition of both the complex and the associated unmodified complex are given. Structures are sorted according to expected increased polarity of the pyridocarbazole ligand.

Complex			
Pim1 restactivity after treatment (c) or IC ₅₀	28% (10 nM) (100 μM ATP) ^[202]	IC ₅₀ = 44 nM (100 μM ATP) ^[316]	IC ₅₀ = 0.6 nM (100 μM ATP) ^[204]
unmodified pyridocarbazole	52% (10 nM) (100 μM ATP) ^[202]	IC ₅₀ = 58 nM (100 μM ATP) ^[316]	IC ₅₀ = 4 nM (100 μM ATP) ^[204]
Complex			
Pim1 restactivity after treatment (c) or IC ₅₀	8% (10 nM) (100 μM ATP) ^[202]	IC ₅₀ = 0.4 nM (100 μM ATP) ^[204]	8% (10 nM) (100 μM ATP) ^[202]
unmodified pyridocarbazole	52% (10 nM) (100 μM ATP) ^[202]	IC ₅₀ = 4 nM (100 μM ATP) ^[204]	52% (10 nM) (100 μM ATP) ^[202]
Complex			
Pim1 restactivity after treatment (c) or IC ₅₀	8% (10 nM) (100 μM ATP) ^[202]	IC ₅₀ = 4 nM (100 μM ATP) ^[315]	5% (10 nM) (100 μM ATP) ^[202]
unmodified pyridocarbazole	52% (10 nM) (100 μM ATP) ^[202]	IC ₅₀ = 20 nM (100 μM ATP) ^[315]	52% (10 nM) (100 μM ATP) ^[202]

Taken from the affinity list, six pyridocarbazoles were selected to be reacted to the corresponding rhodium complexes (**223-228**). These ligands cover a wide range of different functional groups and three positions of modification. The most polar ligands were avoided to reduce any further decline in permeability. In detail, the 3-methylpyridine derivative (see **214**) was considered the most unpolar ligand, probably not impairing the permeability any further. The 3-fluoro derivative (see **215**) adds a small polarity, while the 3-methoxy one (see **217**) adds some more polarity and a sole hydrogen acceptor. The 5-hydroxy indole derivative (see **53**) adds both hydrogen donor and acceptor functionality. The 6-methanol pyridine derivative (see **220**) should have similar polarity to the 5-hydroxy indole modification but covers yet another position of derivatisation. This position might be interesting towards diastereomeric ratios due to possible steric hindrance while coordinating the second ligand. The final ligand (see **76**) combines properties of the second and fourth, being the most polar of all.

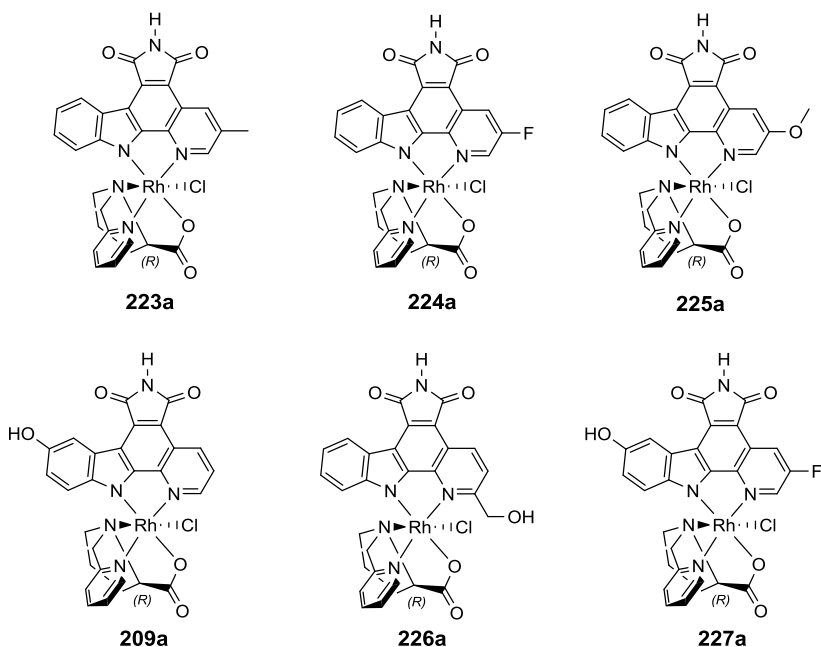


Fig. 61: Selected proposed complexes for improved solubility and affinity, while not impairing permeability to a great extent. The structures were handpicked for a broad range of polarity and structural diversity.

Both complexes **224a** and **227a**, using the pyridocarbazoles taken from the complexes **215** and **76**, were not synthesised successfully neither in a one pot synthesis nor in the precursor approach. Probably the electronical properties of the pyridocarbazoles are so much impaired by the fluoro residue that complex formation or “stable” coordination with it is no longer possible or much slower compared to the TBS deprotection.

3.4.3.1. *In silico* investigation of possible solubility and permeability improvements

In addition to the selection via expected affinity improvement, solubility as well as partition and distribution coefficients were calculated as described previously using STARDROP for selected complexes.

Table 11: Calculated physicochemical properties for selected complexes which are based on the pyridocarbazole modifications described above.

Complex	logS [μM]	logS (pH 7.4)	logP	logD
201a (RR97a)	2.8	5.6	0.8	2.0
223a	2.7	5.5	1.2	2.1
225a	2.8	5.9	0.7	2.2
226a	2.8	5.8	0.4	1.8
227a*	2.9	5.8	0.5	1.9

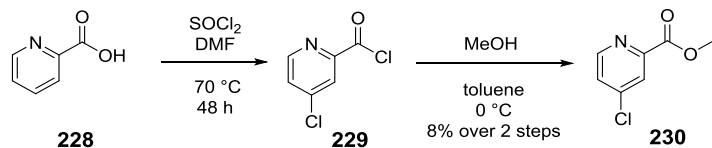
* Calculated for -CH₃OH residue in 3- not 2-position, which should result in similar properties.

Generally, the calculations show solubility values in the same range as compared to the results of **201a**. LogP and logD values are similar as well, with a maximum of factor 2 difference in logP and for **226a**. Based on these results, all proposed complexes seemed still attractive and were taken on to a synthetic realisation.

3.4.4. Synthetic realisation of structural modifications of 201a and 201b

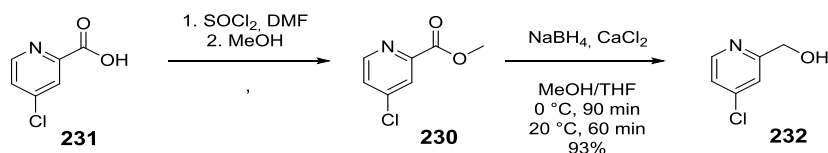
3.4.4.1. Modifications of (pyridine-2-ylmethyl)-D-proline in the 4-pyridine position

The probably most obvious and synthetically easiest way to modify the pyridine at the 4-position is the addition of a suitable leaving group for aromatic nucleophilic substitution in that position. In literature, mainly nitro^[317] and chloro^[317] groups were found for substitution reactions with nucleophiles like alcoholates, amines or thiols.^[317] The chloride group thereby seems to be more versatile concerning nucleophiles, and methyl 4-chloropicolinate (**230**) appeared to be a good starting point to prepare the desired ligands. According to literature,^[317] it is easily prepared from picolinic acid (**228**) by dual chlorination with thionyl chloride using DMF as catalyst. However, after following the procedure with about one third of the original reaction scale, a methyl 4-chloropicolinate (**229**)/methyl picolinate ratio of 1:4 (based on ¹H-NMR spectrum) was obtained. **229** could be isolated by taking the mixture up in a small portion of acetone, adding a layer of hexane and incubating at 4 °C for about a week, during which the product crystallises in the hexane layer. The crystals were filtered off with an overall yield of 8%.



Scheme 10: Synthesis methyl 4-chloropicolinate according to a literature procedure^[317] using thionyl chloride and methanol.

Since commercially available 4-chloropicolinic acid **231** is inexpensive, it was decided to perform the esterification according to another source of literature^[318] which yielded in 87% of the desired methyl 4-chloropicolinate **230**, starting with 4-chloropicolinic acid. Methyl 4-chloropicolinate was further reduced in very good yields using sodium borohydride according to a literature procedure^[317] to yield the hydroxy group (**232**, Scheme 11) required for a subsequent FINKELSTEIN reaction.

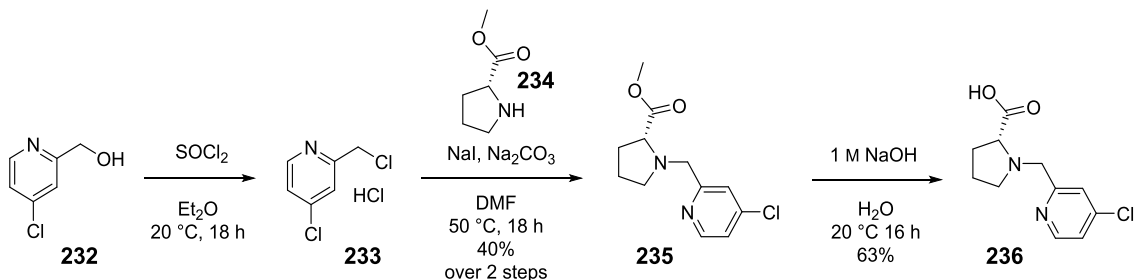


Scheme 11: Synthesis of (4-chloropyridine-2-yl) methanol starting from 4-chloropicolinate. The starting material was esterified using thionyl chloride and MeOH^[318] and further reduced using sodium borohydride^[317] according to literature procedures.

3.4.4.1.1. Synthesis of ((4-chloropyridine-2-yl)methyl)-D-proline

Since the 4-chloro modified pyridine-2-yl methanol was now available, the 4-chloro modified derivative of the original proline derived ligand **206** was synthesised in addition to the planned ligands and complexes to investigate whether a change in polarity and/or possible formation of halogen-bridges might influence binding to the kinase active site, as well as solubility and permeability. Interestingly, chloride groups are hydrophobic and therefore associated with a reduction in solubility, but in a significant number of examples in small molecules, the addition of a F, Cl, CF₃ or even CH₃ group leads to an improvement in solubility.^[309] So the chance to improve either solubility or permeability by adding a chloride group seemed quite promising.

The synthesis was partially performed by JOHANNA PLAG during her internship,^[310] according to a modified procedure of the original ligand, as reported by STEFAN MOLLIN.^[298] The hydroxy group of (4-chloropyridine-2-yl) methanol (**232**) was first chlorinated using thionyl chloride and the resulting HCl salt **233** was directly further converted with D-proline methyl ester (**234**) in a FINKELSTEIN reaction (Scheme 12). The obtained methyl ((4-chloropyridine-2-yl)methyl)-D-proline (40% yield over 2 steps) was further reacted by a simple basic ester hydrolysis using sodium hydroxide to obtain the desired ligand **236** in 63% yield.



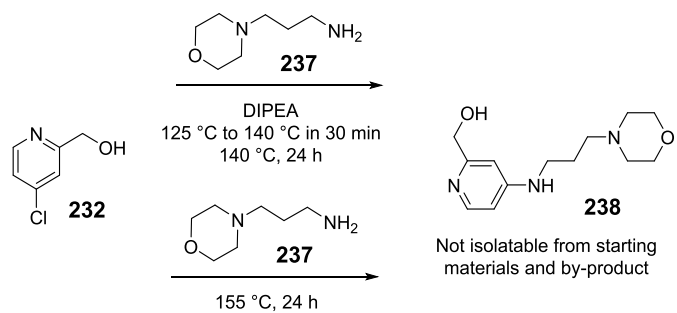
Scheme 12: Synthesis of ((4-chloropyridine-2-yl)methyl)-D-proline after a modified literature procedure.^[298] First the alcohol was chlorinated using thionyl chloride and further converted using a FINKELSTEIN reaction. The final ligand was obtained by basic ester cleavage.

3.4.4.1.2. Synthesis of ((4-(3-morpholinopropoxy)pyridine-2-yl)methyl)-D-proline and ((4-((3-morpholinopropyl)amino)pyridine-2-yl)- D-proline

3.4.4.1.2.1. Synthesis of (4-((3-morpholinopropyl)amino)pyridine-2-yl)methanol

For ligands containing solubilising morpholine-based out-of-plane appendages, nucleophilic reactions were planned using **232**, for both introducing an hydroxy group or amine in the 4-pyridine position. To introduce a structurally complex *N*-nucleophile, different reaction conditions can be found in literature, including the use of *N,N*-diisopropylethylamine (DIPEA, HÜNING's base) as base in toluene^[320] or a simple neat reaction e.g. with pyrrolidine as nucleophile.^[317]

Both conditions were used to introduce *N*-(3-aminopropyl)-morpholine to the (4-chloropyridine-2-yl) methanol in *para*-position (Scheme 13). In the first reaction, the resulting product could not be isolated from the HÜNING's base, its salts or other impurities using flash column chromatography or different extraction methods. Any further reaction towards the final ligand yielded in no product. For the second reaction conditions, JOHANNA PLAG was able to show during her internship^[319] that the desired (4-((3-morpholinopropyl)amino)pyridine-2-yl)methanol (**238**) was formed under neat reaction conditions as proven via HRMS and ¹H-NMR. However, it was found to be inseparable from the starting material **237** by silica flash column chromatography with a CH₂Cl₂/MeOH gradient or reversed phase HPLC (C18 CH₃CN/H₂O 1:1, 0.5% TFA).



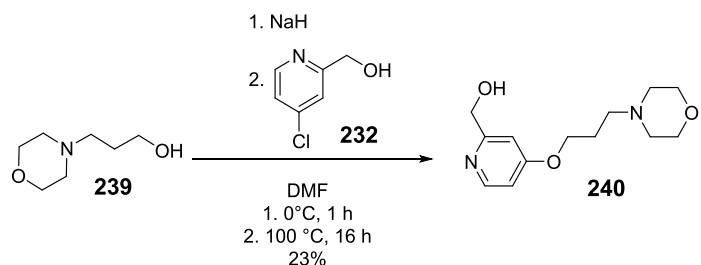
Scheme 13: Reaction conditions, based on a modified literature methods^[317,320] to synthesise (4-((3-morpholinopropyl)amino)pyridine-2-yl)methanol.

Using the same reaction conditions, JOHANNA tried to isolate **238** by distilling the starting material **237** of (boiling point of 224 °C according to the supplier's information). However, even under fine vacuum **238** would decompose (at around 180 °C) before the starting material starts to evaporate. The logical consequence seemed to consume all leftover **237** to get a pure product. However, even when reacting **232/237** in a 3:1 mixture, the morpholine was not fully converted. Therefore, the introduction of various protecting groups was pursued, to influence the retention factors of both

starting materials, to enhance chromatographical work-up. These included a TBS group for the hydroxy group of **238** (using TBSCl, imidazole, I₂), an acetyl group to both the primary and secondary amine in all species (using Ac₂O and 18-crown-6 for selectivity over the alcohol), a Boc group to the secondary amine (using Boc₂O and 4-DMAP) or a Cbz group to protect the primary amine (using CbzCl and NaH). All reactions were monitored by TLC analysis for conversion and a change of the R_f values of the starting materials and products. For both, the TBS and acetyl protection groups no change in R_f values was observed in the most polar combination CH₂Cl₂/MeOH 10:1, so that these groups were excluded. With the Boc group, a single protection of the starting material and a double protection of the product was achieved, accomplishing a change in R_f values. However, separation on silica using silica flash chromatography with a CH₂Cl₂/MeOH gradient was not possible. The same holds true for the Cbz protection group, where both starting material and product were protected. Since all these affords did not succeed in obtaining **238** in a pure fashion, the product and therefore ligand and final complex **211** were not further pursued.

3.4.4.1.2.2. Synthesis of (4-(3-morpholinopropoxy)pyridine-2-yl)methanol

Similar effort as for (4-((3-morpholinopropyl)amino)pyridine-2-yl)methanol was invested into the synthesis of (4-(3-morpholinopropoxy)pyridine-2-yl)methanol by JOHANNA,^[319] successfully.

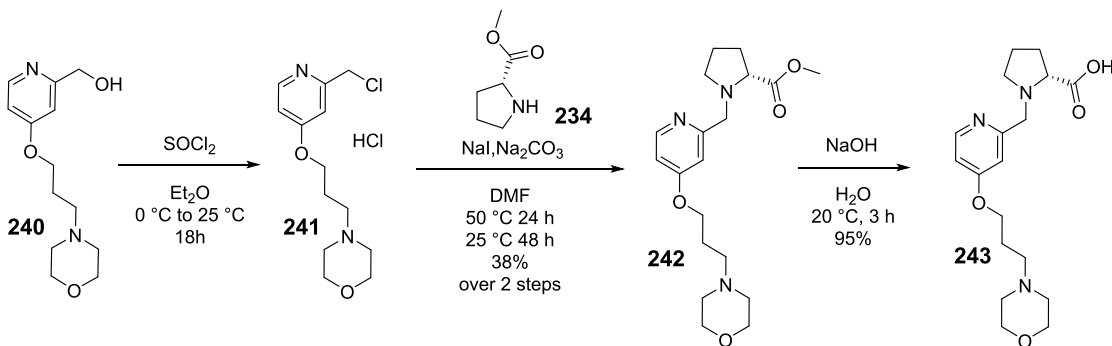


Scheme 14: Reaction conditions derived from modified literature methods^[321] to synthesise (4-((3-morpholinopropyl)amino)pyridine-2-yl)methanol.

The best procedure was modified from a literature known nucleophilic aromatic substitution^[321] using NaH to first prepare sodium 3-morpholinopropan-1-olate before adding **232** at low temperatures (0 °C). After reacting further at 100 °C for 16 h, **240** was isolated by doubly silica flash chromatography (5 g/3 g silica, CH₂Cl₂ to CH₂Cl₂/MeOH 10:1) with a yield of 23%.

3.4.4.1.3. Synthesis of ((4-(3-morpholinopropoxy)pyridine-2-yl)methyl)-D-proline

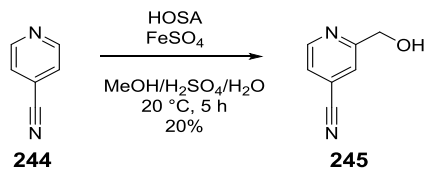
The final ligand ((4-(3-morpholinopropoxy)pyridine-2-yl)methyl)-D-proline (**243**) was prepared analogous to the previously described ligand by chlorination of the hydroxy group, a subsequent FINKELSTEIN reaction with D-proline methyl ester (**234**, 38% over both steps) and basic ester hydrolysis (95%) using aqueous sodium hydroxide (Scheme 15).



Scheme 15: Synthesis of ((4-(3-morpholinopropoxy)pyridine-2-yl)methyl)-D-proline after a modified literature procedure.^[298] First the hydroxy group was chlorinated using thionyl chloride and further converted with methyl-D-proline using a FINKELSTEIN reaction. The final ligand was obtained by basic ester cleavage.

3.4.4.1.4. Synthesis of ((4-((dimethylamino)methyl)pyridine-2-yl)methyl)-D-proline

The synthesis of the dimethylamino-ligand was performed by HENRIK LÖW and JOHANNA PLAG during their internships in the group.^[319,322] They both started with a radical hydroxymethylation of 4-cyanopyridine (**244**) to 2-hydroxymethyl-4-cyanopyridine (**245**) according to a reported procedure (Scheme 16).^[323] Mechanistically, this is a radical substitution where a nucleophilic hydroxymethyl radical is added to the heterocycle.^[323,324] The lower yield (20%) in comparison to the literature (28%) can be explained by aged starting materials. However, the yield was still much better in comparison to a radical hydroxymethylation using ammonium persulfate and methanol in aqueous sulphuric acid (6% as determined by HENRIK LÖW).^[325]

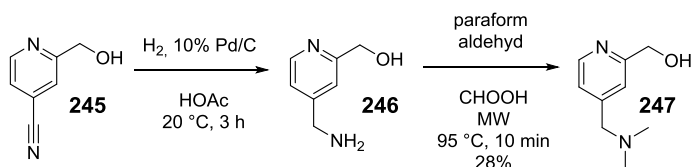


Scheme 16: Radical hydroxymethylation of 4-cyanopyridine using HOSA and Fe(II) in H₂SO₄ as catalyst.

The cyanopyridine **245** was further reduced using hydrogen and Pd on carbon (10%) in acetic acid (Scheme 17).^[326] Based on contained acetic acid in the raw ¹H-NMR spectrum with an unknown

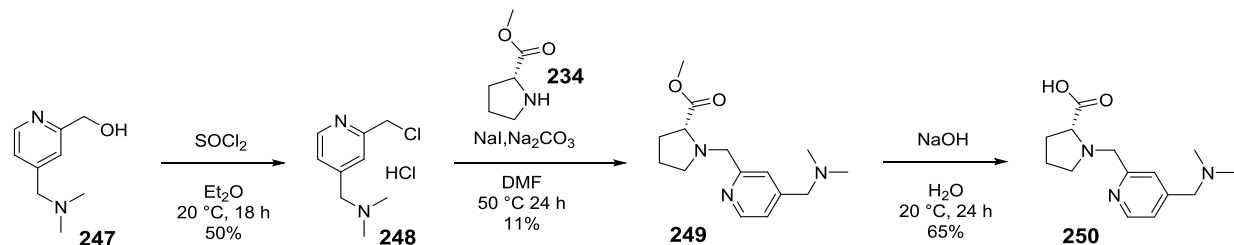
Results and discussion

stoichiometry to the product (probably due to salt formation), the (aminomethyl)pyridine **246** was directly used for the next step without further purification. *N*-alkylation using paraformaldehyde in formic acid in a microwave mediated reaction, according to a modified literature procedure,^[327] resulted in 28% of **247** as a yellow oil. Cleaner reaction paths, like reduction of **245** with lithium aluminium hydride in THF,^[325] did not lead to any yield in the reaction, based on the need for aqueous work-up and a high solubility of **246** in water, from which the product cannot be extracted or isolated.



Scheme 17: Synthesis of 2-hydroxymethyl-4-((dimethylamino)methyl)pyridine from 2-hydroxymethyl-4-cyanopyridine by reduction using H_2 and 10% Pd/C and subsequent *N*-alkylation using paraformaldehyde in a microwave (MW) mediated synthesis.

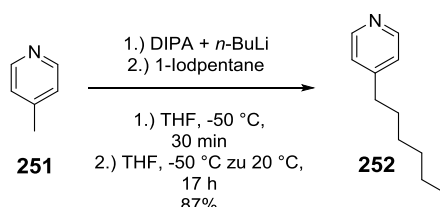
The final ligand ((4-((dimethylamino)methyl)pyridine-2-yl)methyl)-D-proline (**250**) was prepared analogously to the previously described ligands by chlorination of the hydroxy group (50%), a subsequent FINKELSTEIN reaction with D-proline methylester (**234**, 11%) and basic ester hydrolysis (65%) using aqueous sodium hydroxide (Scheme 18).



Scheme 18: Synthesis of ((4-((dimethylamino)methyl)pyridine-2-yl)methyl)-D-proline after a modified literature procedure.^[298] First the hydroxy group was chlorinated using thionyl chloride and further converted using a FINKELSTEIN reaction. The final ligand was obtained by basic ester cleavage.

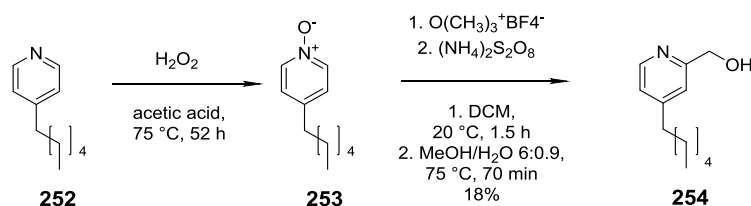
3.4.4.1.5. Synthesis of methyl ((4-hexylpyridine-2-yl) methyl)-D-proline

To explore the possibilities of a pure aliphatic side chain, a modified ligand was synthesised by MATTHIAS TRIPP during his bachelor thesis.^[328] Originally starting from 4-picoline (**251**), he was able to synthesis and 4-hexylpyridine (87%, Scheme 19) according to a modified literature synthesis using lithium diisopropylamine to deprotonate 4-picoline and the according iodoalkane in a S_N2 reaction.^[329]



Scheme 19: Synthesis of 4-hexylpyridine using a literature derived S_N2 reaction^[329] was performed by MATTHIAS TRIPP during his bachelor thesis.^[328]

The 4-alkylpyridine **252** was further converted to the *N*-oxide using hydrogen peroxide according to literature procedures (Scheme 20).^[330] A subsequent 2-hydroxymethylation was conducted using trimethyloxonium tetrafluoroborate and ammonium persulfate in methanol.^[331] Mechanistically, it is thought that (CH₃)₃OB⁺F⁻ methylates the oxygen of the *N*-oxide, while the persulfate is homolytically cleaved in the heat resulting in a radical which reacts with the solvent and forms a methanol radical. These methanol radicals might then react with the pyridines and are directed into ortho position, based on the electron donating methoxy group. The radical from the resulting compound is finally passed on to another methanol molecule in the solvent, after cleavage of the *N*-methanol group or by directly cleaving a methanol radical from the pyridine nitrogen. The hydroxymethylated product, in which the pyridine nitrogen is no longer oxidised, is thereby less reactive compared to the starting material, making a follow up reaction improbable.^[331]

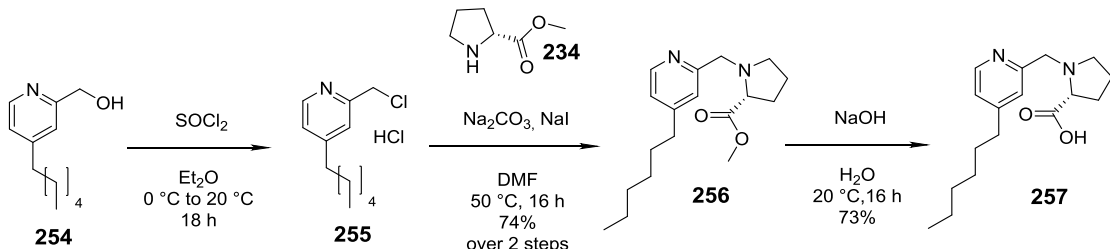


Scheme 20: *N*-oxidation using hydrogen peroxide^[330] and subsequent 2-hydroxymethylation of 4-hexylpyridine according to a literature described radical reaction mechanism^[331] was performed by MATTHIAS TRIPP.^[328]

This reaction however resulted (4-hexylpyridine-2-yl)-methanol (**254**) only in a low yield of 18% over both steps (Scheme 20).

Results and discussion

The final ligand, methyl ((4-hexylpyridine-2-yl)methyl)-D-proline (**257**), was prepared according to a modified literature procedure (Scheme 21).^[332] Analogous to the previously described ligands, first the hydroxy group was chlorinated (50%), followed by a FINKELESTEIN reaction with D-proline methylester (74%) and basic ester hydrolysis (73%) using aqueous sodium hydroxide to get to the final ligand (Scheme 21) in 11% yield over six steps.^[328]



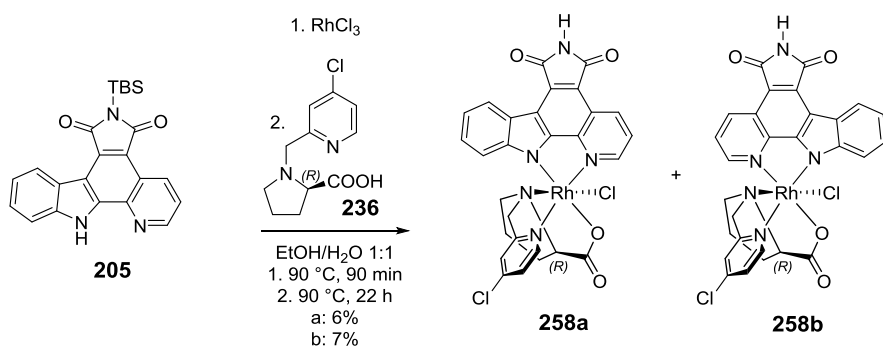
Scheme 21: Synthesis of methyl ((4-hexylpyridine-2-yl)methyl)-D-proline after a modified literature procedure.^[332] First the hydroxy group was chlorinated using thionyl chloride and further converted using a FINKELESTEIN reaction. The final ligand was obtained by basic ester cleavage.

The final ligand however contained some ethanol, which could not be removed by extensive drying, the yield is hence based on the ethanol free ligand according to $^1\text{H-NMR}$.^[328] As the following complex reactions were conducted in a mixture of $\text{EtOH}/\text{H}_2\text{O}$ 1:1, this posed however no problem.

3.4.4.2. Complex synthesis with modified (pyridine-2-ylmethyl)-D-proline ligands

3.4.4.2.1. Synthesis of the 4-chloro pyridine modified complexes

The 4-chloro modified complexes **258a** and **258b** were obtained using the standard reaction procedure reported by RAJATHEES RAJARATNAM (Scheme 22).^[233] One equivalent of the TBS-protected pyridocarbazole (**105**) was reacted with one equivalent of RhCl₃ in EtOH/H₂O 1:1 for 90 min at 90 °C before the 4-chloro modified ligand **236** was added and the mixture further reacted for 16 h at 90 °C to yield the final complexes in 6% (a isomer) and 7% (b isomer) yield after separation and purification using silica flash chromatography.

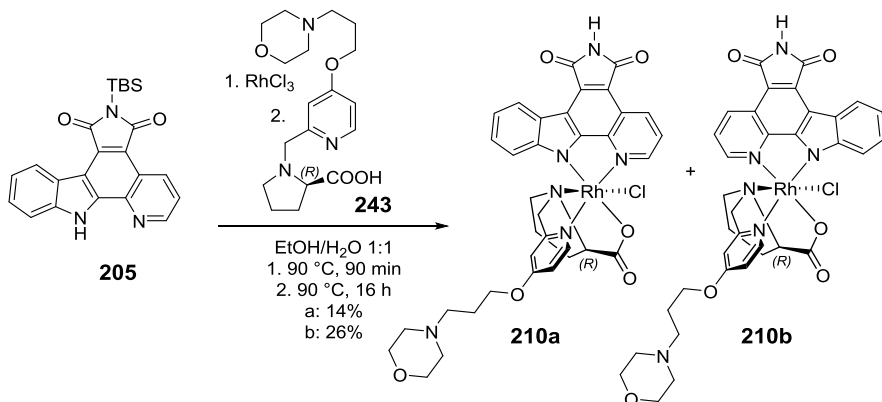


Scheme 22: Reaction conditions of the synthesis of the 4-chloro derivatives of RR97a and RR97b.

Both complexes however have not been isolated in a pure fashion using the reaction conditions and standard purification procedures (double flash chromatography for each isomer) given, with impurities in both the aliphatic and aromatic regions of the ¹H-NMR spectra. Since the main products were the complexes, both were carried to the drug-like abilities and kinase inhibition assays anyway, to get a first impression of their properties since all drug-like abilities assays were “normalised” to a pure sample as described in the experimental section.

3.4.4.2.2. Synthesis of 4-(3-morpholinopropan-1-ol) pyridine derivatised complexes

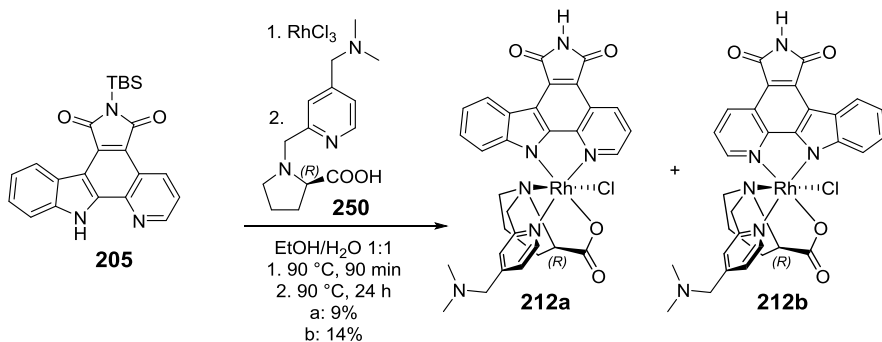
The 4-(3-morpholinopropan-1-ol) modified complex were obtained using the standard reaction procedure (Scheme 23).^[233] Briefly, one equivalent of TBS-protected pyridocarbazole (**105**) was reacted with one equivalent of RhCl₃ in EtOH/H₂O 1:1 for 90 min at 90 °C before the modified ligand **243** was added and the mixture further reacted for 16 h at 90 °C. The diastereomers were separated and purified using silica flash chromatography obtaining 14% (a, *cis*-isomer) and 26% (b, *trans*-isomer) as deep red solids.



Scheme 23: Reaction conditions of the synthesis of the 4-(3-morpholinopropan-1-ol) pyridine derivatives of RR97a and RR97b.

3.4.4.2.3. Synthesis of the 4-((dimethylamino)methyl) pyridine derivatised complexes

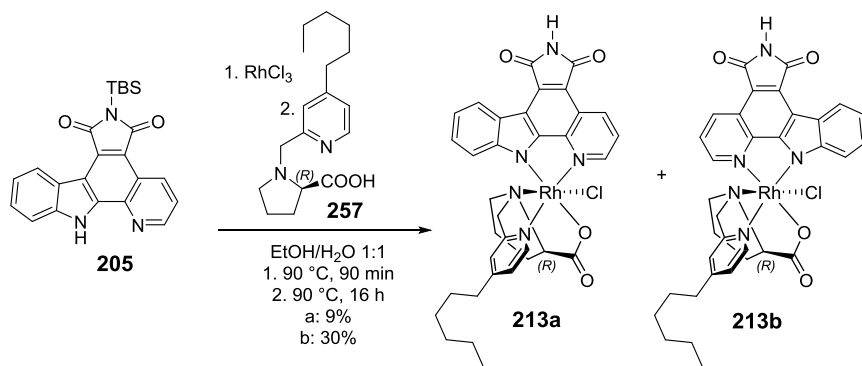
The 4-((dimethylamino)methyl) pyridine derivatives of the complexes were obtained using the standard reaction procedure reported.^[233] One equivalent of the TBS-protected pyridocarbazole (**105**) was reacted with one equivalent of RhCl₃ in EtOH/H₂O 1:1 for 90 min at 90 °C before the modified ligand **250** was added and the mixture further reacted for 24 h at 90 °C to yield the final complexes in 9% (**212a**) and 14% (**212b**) yield (Scheme 24) after separation and purification using silica flash chromatography.



Scheme 24: Reaction conditions of the synthesis of the 4-((dimethylamino)methyl) pyridine derivatives of RR97a and RR97b.

3.4.4.2.4. Synthesis of the 4-hexyl pyridine derivatised complexes

The 4-hexyl pyridine derivatives of the complexes were obtained using the standard reaction procedure reported (Scheme 25).^[233] Briefly, 1.0 eq of TBS-protected pyridocarbazole (**105**) was reacted with 1.0 eq of RhCl₃ in EtOH/H₂O 1:1 for 90 min at 90 °C under stirring before 1.1 equivalents of the modified ligand **257** were added in the one-pot synthesis and the mixture further reacted for 24 h at 90 °C. The diastereomers were separated and purified using silica flash chromatography, obtaining 9% (a, *trans*-isomer) and 30% (b, *cis*-isomer).

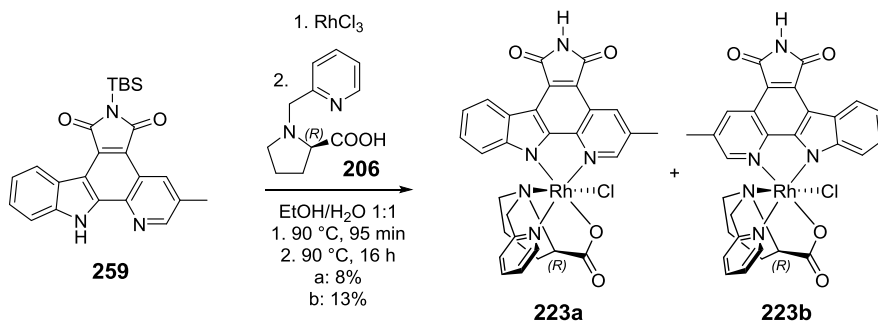


Scheme 25: Reaction conditions of the synthesis of the 4-hexyl pyridine derivatives of RR97a and RR97b.

3.4.4.3. Complex synthesis with modified pyridocarbazole ligands

3.4.4.3.1. Synthesis of 5-methylpyridine derivatised complexes

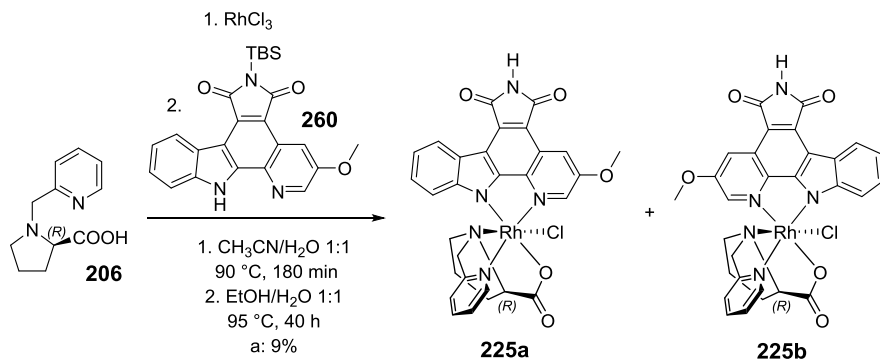
Pyridocarbazole **259** was synthesised by HENRIK LÖW during his internship in the group according to a modified procedure by STEFAN MOLLIN.^[296,322] Taking the pyridocarbazole, **223a** and **223b** were synthesised using slight variations of the previously described one-pot synthesis (Scheme 26).^[233] Briefly, one equivalent of **259** and RhCl₃ each were reacted under stirring for 90 min at 95 °C in 1:1 EtOH/H₂O. Ligand **206** was added and the reaction mixture further stirred for 16 h at 90 °C. The diastereomers were separated and purified using silica flash chromatography obtaining 8% of **223a** and 13% of **223b** in a slightly impure form.



Scheme 26: Reaction conditions of the synthesis of the 5-methylpyridine derivatives of RR97a and RR97b.

3.4.4.3.2. Synthesis of 5-methoxypyridine derivatised complex

Pyridocarbazole **260** was prepared by KATJA KRÄLING. When reacting the pyridocarbazole in the classical one-pot synthesis, many side-products were formed and a separation via flash chromatography was not possible for **225a**. Even separation on preparative TLC did not yield pure complex, due to at least 10 different smearing species. Therefore, the complex **225a** was synthesised using the precursor approach described earlier (Scheme 27). Briefly, one equivalent of **206** and RhCl_3 each were stirred in 1:1 $\text{CH}_3\text{CN}/\text{H}_2\text{O}$ for 3 h at 90 °C. The solvent was removed and the crude precursor was further reacted with **260** in 1:1 $\text{EtOH}/\text{H}_2\text{O}$ for 40 h at 95 °C under stirring. After purification using silica flash chromatography 9% of **225a** were obtained. **225b** was obtained as a 3:1 mixture with the precursor or a similar species in < 5% yield. **225b** could however obtained in a clean fashion from the previously mentioned one-pot reaction in a yield of 18% as described in the experimental section.



Scheme 27: Reaction conditions of the synthesis of the 5-methoxypyridine derivatives of RR97a and RR97b.

The complex was additionally successfully crystallised and the first crystal structure for an Λ -(*R*)-*a* isomer could be obtained. Single crystals suitable for X-ray analysis were obtained by slow evaporation of CH_2Cl_2 from a DMSO / CH_2Cl_2 solution. The intensity data of the single crystals were collected at 100 K using a Bruker D8 Quest system. The data were corrected for absorption effects using multi-scanned reflections.^[214] The structure was solved using direct methods (SHELXS-97)^[215] and refined using full matrix least squares procedure (SHELXL-2013). Hydrogen atoms were included at calculated positions. All measurement and structure determination was performed by KLAUS HARMS from the central crystal structure analysis department at the Philipps-Universität Marburg.

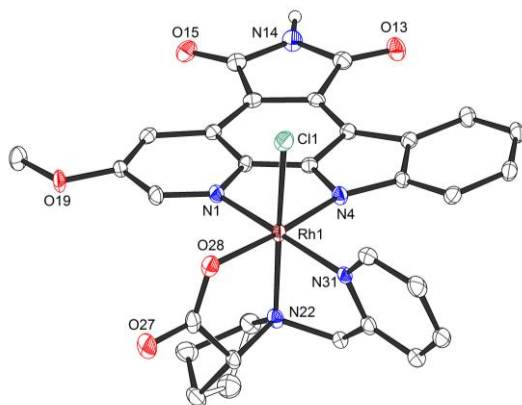
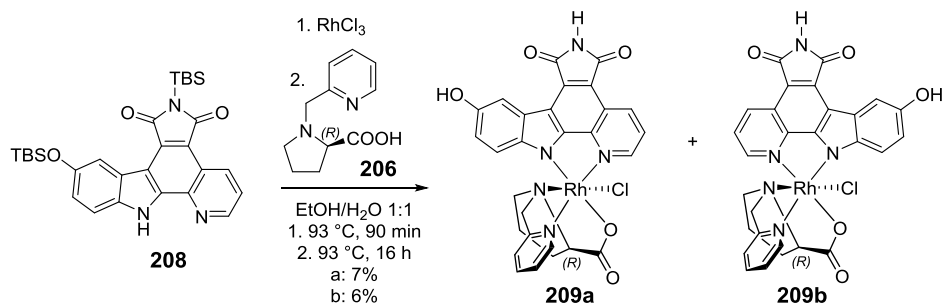


Fig. 62: Crystal structure of Λ -(R)-225a revealing the metal-centred chirality. ORTEP drawing with 50% probability thermal ellipsoids. Solvent is omitted for clarity.

3.4.4.3.3. Synthesis of indole-5-ol derivatised complex

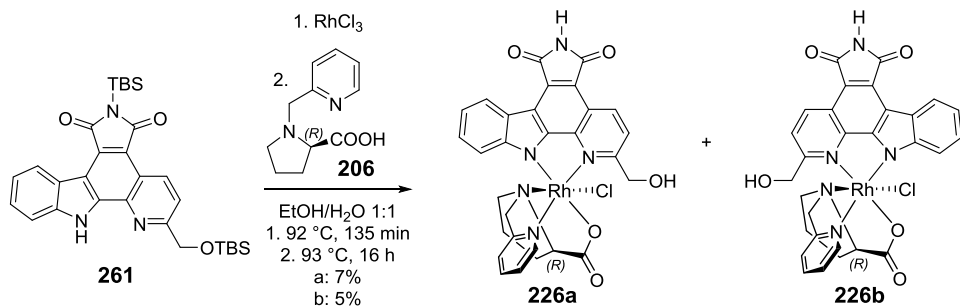
Pyridocarbazole **208** was synthesised by BENEDIKT HEINRICH during his internship in the group according to a modified procedure by DOUG WILLIAMS.^[265,297] Taking the pyridocarbazole, **226a** and **226b** were synthesised using slight variations of the previously described one-pot synthesis (Scheme 26).^[233] Briefly, one equivalent of **208** and RhCl_3 each were reacted under stirring for 90 min at 93 °C in 1:1 EtOH/H₂O. Ligand **206** was added and the mixture further stirred for 16 h at 93 °C. The diastereomers were separated, combined with some complex obtained using the precursor approach and purified using silica flash chromatography obtaining 7% (based on the amount of starting material for both reactions) of **226a** in a pure fashion and 6% of **226b** with roughly 30% impurity from the precursor approach.



Scheme 28: Reaction conditions of the synthesis of the indole-5-ol derivatives of RR97a and RR97b.

3.4.4.3.4. Synthesis of pyridine-6-yl methanol derivatised complex

Pyridocarbazole **261** was synthesised by BENEDIKT HEINRICH during his internship in the group according to a modified procedure by NICHOLAS PAGANO.^[202,297] Taking the pyridocarbazole **261**, **226a** and **226b** were synthesised using slight variations of the previously described one-pot synthesis reported by RAJATHEES RAJARATNAM (Scheme 29).^[233] Briefly, one equivalent of **261** and RhCl₃ each were reacted under stirring for 135 min at 92 °C in 1:1 EtOH/H₂O. Ligand **206** was added and the reaction mixture further stirred for 16 h at 93 °C. The diastereomers were separated and purified using silica flash chromatography obtaining 7% of **226a** and 5% of **226b** in a slightly impure form. The diastereomeric ratio thereby indeed shows that a sterical hindrance leads to a lower yield of the b isomer, as expected. In the a isomer, the smaller chloride ligand seems favourable for that position.



Scheme 29: Reaction conditions of the synthesis of the pyridine-6-yl methanol derivatives of RR97a and RR97b.

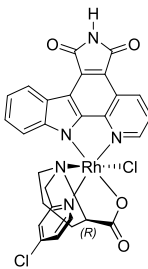
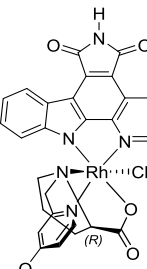
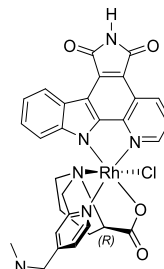
3.4.5. Drug-like properties of (4-pyridine-2-ylmethyl)-D-proline derivatives

The drug-like properties of all derivatives were tested at NIBR using the afore mentioned assay conditions for solubility and rat liver microsome stability to compare the data to the original complexes RR97a and RR97b. To determine the permeability a MDCK cell line was used instead of the Caco-2 cell line, based on the easier model.

3.4.5.1. Drug-like properties of *trans*-isomers (a isomers)

The determined *in vitro* drug-like abilities of all newly synthesised *trans*-isomers, based on pyridocarbazole modifications, are summarised in Table 12.

Table 12: Drug-like properties of (4-pyridine-2-ylmethyl)-D-proline derivatives of RR97a.

				
HT-solubility				
KP _i (pH 6.8)	17 µM	86 µM	6 µM	43 µM
KP _i (pH 4.0)	23 µM	713 µM	10 µM	381 µM
FaSSIF	45 µM	70 µM	10 µM	38 µM
RLM- stability				
Cl _{int}				
ER _b	<25 µl/min/mg <50%	125 µl/min/mg 79%	138 µl/min/mg 82%	<25 µl/min/mg <50%
MDCK- permeability				
P _{app} A-B	0.77 x10 ⁻⁶ cm/s	-	-	-
calc. FA	<40%	-	-	-

The solubility of **258a** and **213a** is not improved c.f. the original compound **201**. For both the 4-(3-morpholinopropan-1-ol) as the (dimethylamino)methyl derivative the solubility is highly elevated at pH 4, indicating a protonation of the tertiary amine. Sadly, at physiologically pH the amines seem not to be protonated, as it was assumed for the dimethylamine derivative. The

solubility of **210a** is the most elevated in the series both in FaSSIF and KP_i and the most soluble derivative in KP_i at pH 6.8 while it is worse than the later discussed **209a** in FaSSIF. For both tertiary amine containing compounds no improvement of solubility in FaSSIF buffer compared to KP_i was observable. The microsome stability is good for **258a** and **212a**, while it is medium for the other two compounds, probably related to the easier access of the CYP enzymes to the elevated side chains. Permeability of all compounds is really low with amounts which were not even quantifiable by LC-MS/MS for all compounds except **258a**.

3.4.5.2. Drug-like properties of *cis*-isomers (**b** isomers)

The determined *in vitro* drug-like abilities of all newly synthesised *cis*-isomers, based on pyridocarbazole modifications, are summarised in Table 13.

Table 13: Drug-like properties of (4-pyridine-2-ylmethyl)-D-proline derivatives of **201b**.

	258b	210b	213b	212b
HT-solubility				
KP _i (pH 6.8)	4 µM	65 µM	<4 µM	42 µM
KP _i (pH 4.0)	10 µM	149 µM	<4 µM	140 µM
FaSSIF	7 µM	8 µM	<4 µM	23 µM
RLM- stability				
Cl _{int}				
ER _b	<25 µl/min/mg <50%	<25 µl/min/mg <50%	82 µl/min/mg 73%	<25 µl/min/mg <50%
MDCK- permeability				
P _{app} A-B	1.17 x10 ⁻⁶ cm/s	0.75 x10 ⁻⁶ cm/s	<1.5 x10 ⁻⁶ cm/s	0.59 x10 ⁻⁶ cm/s
calc. FA	<40%	<40%	<40%	<40%

The *cis*-derivatives show the same trend in solubility as the *trans*-derivatives with the same modifications, except that the FaSSIF solubility of **210b** and **212b** are more obviously below that

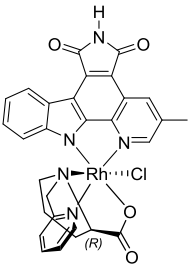
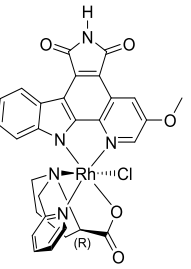
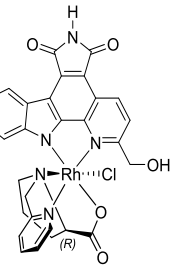
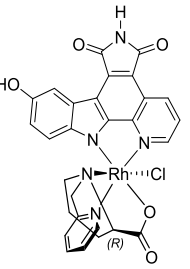
of their KP_i solubility. Microsome stability is good for **210b**, **212b** and **258b**, and medium for **213b**, which is in accordance with expectations as it is predicted, that the hexyl side chain is easily oxidised by CYP enzymes. The permeability is again very low, showing that no derivatisation at all which was tested in this study helped to raise permeability.

3.4.6. Drug-like properties of pyridocarbazole derivatives

3.4.6.1. Drug-like properties of *trans*-isomers (a isomers)

The determined *in vitro* drug-like abilities of all newly synthesised *trans*-isomers, based on pyridocarbazole modifications, are summarised in Table 14.

Table 14: Drug-like properties of pyridocarbazole derivatives of RR97a.

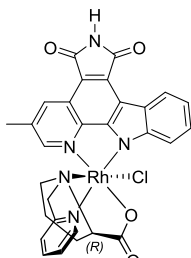
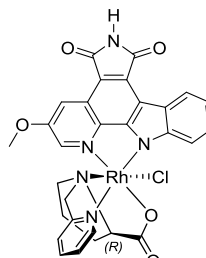
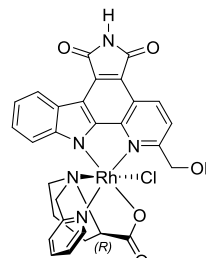
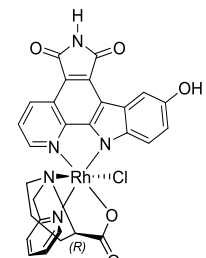
				
HT-solubility				
KP _i (pH 6.8)	15 µM	< 4 µM	9 µM	72 µM
KP _i (pH 4.0)	23 µM	6 µM	15 µM	167 µM
FaSSIF	27 µM	<4 µM	24 µM	164 µM
RLM- stability				
Cl _{int}				
ER _b	159 µl/min/mg 84%	<25 µl/min/mg <50%	<25 µl/min/mg <50%	114 µl/min/mg 79%
MDCK- permeability				
P _{app} A-B	<1.5 x10 ⁻⁶ cm/s	1.07 x10 ⁻⁶ cm/s	1.28 x10 ⁻⁶ cm/s	1.32 x10 ⁻⁶ cm/s
calc. FA	<40%	<40%	<40%	<40%

According to Table 14 the solubility is not significantly improved for **223a** and **226a** but clearly improved with factor >6 both in KP_i and FaSSIF for **209a**. However, this improvement comes with decreased metabolic stability. Stability values for **225a** and **226a** are very good, while **223a** possesses a high risk of having exposure problems due to high metabolic conversion. All compounds still have very low permeability. Overall metabolic stability and solubility seem to be tuneable by modifying the pyridocarbazole, while the permeability stays low.

3.4.6.2. Drug-like properties of *cis*-isomers (**b** isomers)

The determined *in vitro* drug-like abilities of all newly synthesised *cis*-isomers, based on pyridocarbazole modifications, are summarised in Table 15.

Table 15: Drug-like properties of pyridocarbazole derivatives of RR97b.

				
HT-solubility				
KP _i (pH 6.8)	36 μM	9 μM	24 μM	7 μM
KP _i (pH 4.0)	62 μM	32 μM	59 μM	132 μM
FaSSIF	19 μM	8 μM	44 μM	155 μM
RLM-stability				
Cl _{int}	35 μl/min/mg	30 μl/min/mg	183 μl/min/mg	<25 μl/min/mg
ER _b	54%	50%	86%	<50%
MDCK-permeability				
P _{app} A-B	1.11 x10 ⁻⁶ cm/s	1.31 x10 ⁻⁶ cm/s	-	1.25 x10 ⁻⁶ cm/s
calc. FA	<40%	<40%	-	<40%

For solubility, the same trends as for the *trans*-isomers is valid with a less obvious result in KP_i buffer (pH 6.8) for **209b**. Metabolic stability shows a high metabolic risk for **226b** and low risks for the other compounds. This result is especially appealing as **226a** shows a very high metabolic stability and **209a** a medium stability. This indicates that the stereoinformation of the complexes might be important for binding to the CYP enzyme and making a transformation somewhere at the complex possible only in a certain orientation. Since **209b** and **226b** incorporate hydroxy groups at the opposite sides of the pyridocarbazole, and these are probably the enzymatically labile groups as indicated earlier,^[122] this information might help to prevent the design of metabolically labile compounds for certain isomers. For permeability, all compounds display very low permeability in MDCK cells with **226b** showing such a low amount that quantification was not even possible.

3.4.7. Kinase inhibition properties of derivatives

To further verify and test whether the addition of functional groups to both, the pyridocarbazole or the *para*-position of the pyridine belonging to the proline derived ligand, changes the inhibitory properties towards Pim1, all *trans*-isomers were tested in a two concentration setting towards Pim1 using the commercially available ATP-GloTM assay. The kit was previously tested towards its suitability using the compounds RR97a (**201a**) and RR97b (**201b**), as well as an ADP/ATP calibration curve, and showed decent results, with up to 4-fold deviation in IC₅₀ from results obtained by radioactive assays. The Pim1 activity is low in the assay conditions used and would need further optimisation for more accurate tests and further experiments. The assay conditions were required due to concentration limits of the buffer ingredients by the assay provider. Activity of Pim1 in the assay seemed to have even worsened probably due to long storage times of the enzyme (Pim1 can e.g. undergo autophosphorylation)^[17] and assay kit. Therefore, about three times the amount of protein was used in the assay compared to the original IC₅₀ determination.

In the assay setting derivatives were tested at 50 nM and 1 µM for their Pim1 inhibition, since the previous IC₅₀ for RR97a in this assay was determined to be 50-60 nM. Three controls were introduced in quadruplicate, in which ingredients were replaced by the according buffer or solvent, including control 1 (without inhibitor) which represents 100% activity, control 2 (without inhibitor and without enzyme) which was used for background correction and control 3 (using the inactive isomer of the 4-hexylpyridine derivative without enzyme) to test possible self-luminescence of the complex. The obtained results are shown in Fig. 63.

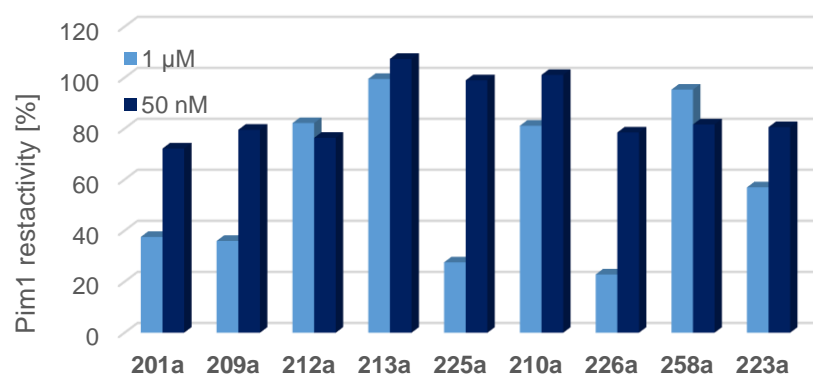


Fig. 63: Inhibition of Pim1 expressed as enzyme restactivity after treatment with the synthesised derivatives of RR97a (**201a**).

Results and discussion

Taken from the results obtained, there was little inhibition of Pim1 by all complexes, including **121a**, at 50 nM. This result might be a consequence of the high amount of Pim1 used, so that the effective concentration of the inhibitor compared to Pim1 was lower in this assay in comparison to the previously performed one. However, in the inhibition at 1 μ M an obvious trend can be observed, with control **213b** showing similar values to the background, indicating little to no interference of the compound with the assay. While all derivatives containing a modified pyridocarbazole showed obvious inhibition with **226a** being the most effective and **223a** the worst inhibitor, all derivatives containing derivatisation at the pyridine show little to no inhibition. Since the assay was only performed once, this result represents just a trend and no absolute numbers. However, it seems that derivatisation at the given pyridine position might lead to a decline in inhibition properties. A further determination of IC₅₀ values towards Pim1 is required to verify these results and show how much the inhibition properties are impaired. A co-crystal structure of **201a** or one of the derivatives might help to find better substituents and maybe positions to modify the complex further.

3.5. Gold-based HDAC inhibitors as potential anticancer drugs

As a side project in this thesis, the HDAC inhibitory properties of the gold(III) compound $[\text{Au}_2(\mu\text{-O})_2(6,6'\text{-}(\text{CH}_3)_2\text{bpy}_2](\text{PF}_6)_2$ (**262** Fig. 64) was investigated, since HDACs are another attractive cancer target as described in the introduction. All experiments in this chapter were conducted in Angela Casinis laboratory at the Rijksuniversiteit Groningen.

The compound **262** belongs to a class of μ -oxo-bridged dinuclear gold(III) compounds with different bipyridine derived ligands, which were developed and reported as antiproliferative compounds over the last decade.^[333,334] Complex **262** has previously been suggested to have a “DNA-independent” mechanism, different from that of platinum drugs, with promising antiproliferative properties and a high score of selectivity.^[334] A compare analysis of the antiproliferative properties of this compound against 36 human cell lines to approximately 110 reference compounds with a known mechanism of action revealed that it might be a HDI,^[334] since it showed striking similarities to various HDIs, i.e. $Q = 0.72$ for both the benzamide acetyldinaline and the cyclic peptide apicidin and a Q -value of 0.61 for suberic bishydroxamate on the IC_{70} level. The Q -values are thereby SPEARMAN correlation coefficients. High correlations (> 0.6) between the sensitivity patterns of two compounds indicate a similar mechanism of action.^[334,335]

3.5.1. Toxicity evaluation

3.5.1.1. *In vitro* cytotoxicity in cancer cell lines

To verify the compounds antiproliferative behaviour, first **262**, as well as other compounds including the structural analogues including $[\text{Au}_2(\mu\text{-O})_2(\text{N}^{\text{+}}\text{N}^-)_2](2\text{PF}_6)_2$ with $\text{N}^{\text{+}}\text{N}^-$ =bipyridine (bpy) (**263**), 6-methyl-2,2'-bipyridine (bpy^{Me}) (**264**) and 6-ethyl-2,2'-bipyridine (bpy^{Et}) (**265**) and other gold(III)-complexes like $[\text{Au}(\text{bnpy})](\text{Cl})_2$ ($\text{bnpy} = 2\text{-benzylpyridine}$) (**266**) and $[\text{Au}(\text{bpy}^{\text{dmb}})(\text{OH})](\text{PF}_6)$ ($\text{bpy}^{\text{dmb}} = 6\text{-}(1,1\text{-dimethylbenzyl})\text{-}2,2'\text{-bipyridine}$) (**267**), were tested in the human lung carcinoma cell line A549, which has been used previously to investigate the cytotoxicity of metal-containing HDAC-inhibitors,^[172,183] using the MTT standard method II.

Results and discussion

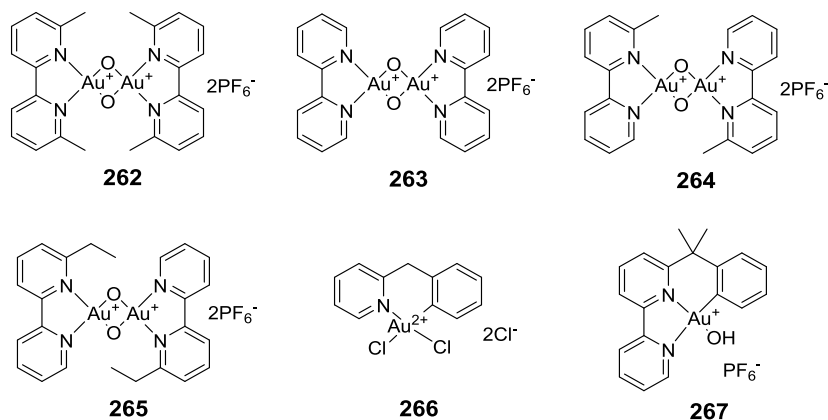


Fig. 64: Structures of gold-complexes studied for their antiproliferative properties. Some were further investigated towards their HDAC inhibition properties.

Indeed, compound **262** showed superior antiproliferative behaviour ($IC_{50} = 1.2 \pm 0.2 \mu\text{M}$) compared to the other five compounds after treatment for 72 h (Table 16). Further comparison of its cytotoxicity to its most related structural analogue (**264**) in A2780 human ovarian carcinoma and the p53+/+ human colorectal carcinoma cell line HCT116++ yielded similarly good results (Table 16).

Table 16: Overview of the antiproliferative properties for compounds **262-267** obtained via the MIT method after treatment for 72 h in the human lung carcinoma cell line A549, the human ovarian carcinoma cell line A2780 and the p53+/+ human colorectal carcinoma cell line HCT116++. As can be seen compound **262** is superior compared for all other compounds tested and in all cell lines tested.

Compound	A549 [μM]	A2780 [μM]	HCT116++ [μM]
262	$1.2 \pm 0.2^*$	$0.8 \pm 0.1^\#$	$1.3^\#$
263	$> 50^\#$	-	-
264	$22.8 \pm 1.0^*$	$6.4 \pm 0.2^*$	$44.3 \pm 1.7^\#$
265	$10.7 \pm 1.8^\#$	-	-
266	$9.5 \pm 1.8^\#$	-	-
267	$> 50^\#$	-	-

* 8000 cells/well; # 10000 cells per well

Interestingly, **262** has been reported to show antiproliferative activity comparable to cisplatin ($IC_{50} \sim 2 \mu\text{M}$) in A2780 cells, with being five times more active in the cisplatin resistant analogue, and an order of magnitude more effective in comparison to similar compounds.^[333,336] The much higher potency of **262** compared to compounds **263-267** was confirmed, with **262** being even 2.5 times more effective in A2780 cells in comparison to the previous study.

The type of gold-compounds used in this study are thought to be prodrugs with their biological activities based on gold coordination to biomolecules, or on redox reactions and consequent oxidative damage.^[336] It is well established, that these compounds are generally stable against dissociation in aqueous solution, but are reduced and activated by ascorbic acid, glutathione, human serum albumin (hSA) and cytochrome c (cyt c).^[333,337] It has been suggested that by reduction, the dinuclear gold(III) compounds break down and release their bipyridyl ligands and possibly naked gold(I) ions. These ions form adducts with proteins, as it has been shown by ICP measurements and by the ESI-MS features of gold(III)-treated cyt c.^[333] This type of interaction seems also to hold true for bigger target proteins.^[338] While the compounds generally bind to proteins, a similar reaction with calf-thymus DNA has only been shown for compound **262** as confirmed by spectroscopic and analytical determinations including inductively coupled plasma optical emission spectroscopy (ICP-OES), where more than 80% of total gold from **262** was found associated with DNA. **263** on the other hand did not bind to DNA.^[333] Compound **262** generally deviates most from similar derivatives, not only concerning antiproliferative behaviour, but also in terms of structural features, thermal stability, and redox properties,^[337] related to a small but significant modification in the Au₂O₂ core and higher oxidising character.^[334,337] Reduction by hSA and cyt c of **262** for example is about five times faster than reduction of **263**.^[333] In the previously mentioned 36 cell line study **262**, the compound with the highest redox potential, was also ranked top on the basis of tumour selectivity and antitumor potency^[334]

3.5.1.2. *Ex vivo* hepatotoxicity of **262**

In addition to the antiproliferative behaviour, a toxicity study of **262** towards healthy tissue was pursued. The previously described precision cut liver slices (PCLS) model was used to study the hepatotoxicological properties of **262**. For the hepatotoxicity evaluation according to established procedures, PCLS were prepared and pre-incubated for 1 h before exposing to **262** as described in the experimental section. The treatment was performed at three single concentrations of the compounds (1 µM, 10 µM and 50 µM) with a final DMSO concentration of less than 0.5% and slices were incubated for 24 h. Afterwards PCLS were collected and their viability was determined measuring their ATP content and normalising it to their protein content.

Fig. 65 reports the viability of the PCLS upon treatment with different compounds' concentrations. According to the obtained results, compound **262** shows low to no hepatotoxicity in the concentration range of 1–10 µM. At 50 µM concentration, some effects on tissue viability can be observed with respect to controls, however **262** presents reduced hepatotoxicity with respect to cisplatin as also previously discussed for RR97b (**201b**). These results indicate a more tissue specific

Results and discussion

activity of compound **262**, which seems to be limited to cancer cells. One hypothesis for this observation is, that the behaviour might be related to the hypoxic environment of cancer cells, which might facilitate the reductive activation of the compound.

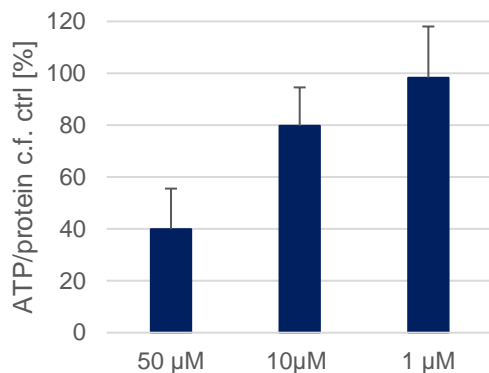


Fig. 65: Viability of precision cut liver slices (PCLS) following 24 h incubation with compound **262** after 1 h of preincubation.

A previous proteomic study with A2780 human ovarian carcinoma cells showed, that the protein expression after treatment of **262** for 24 h showed limited changes with only 11 out of 1300 monitored protein types altered. This implies that cell damage, at least in the early phases of treatment, is quite selective and limited. Some of the altered proteins were found to be mainly involved in the redox metabolism and stress response, suggesting that cell damage probably is a consequence of severe oxidative stress. This theory is also proved by the fact that two proteins that are biomarkers of apoptosis were found to be greatly perturbed. The mode of action hereby relates directly to that of auranofin. This result again strongly suggests that reduction of **262** to a gold(I) species takes place within the biological milieu.^[339]

3.5.2. HDAC inhibitory properties

To determine the grade of HDAC inhibition of **262**, firstly its potential, as well as that of compounds **263–267** and $[\text{Au}(\text{phen})(\text{Cl})_2](\text{Cl})$ (**268**) for comparison, was tested at single concentrations of 5, 10 and 50 μM in A549 nuclear cell extract with a commercially available fluorometric assay kit (MOLECUTOOLS *FluoroFire HDAC Activity Assay Kit*). The kit and its reliability towards metal-based compounds was previously tested with HDIs designed by FLORIAN RITTERBUSCH^[340] and showed good correlations with previously obtained data.

Briefly, A549 nuclear extract was obtained by a method described in literature.^[172] Its protein content was determined via LAWRY-assay and 5 μg nuclear protein was used per well in the assay. Each condition was tested in duplicate. The results of the assay, with the compounds being preincubated with the nuclear extract for 1 h, were compared to the values of untreated nuclear extract and a rest activity was calculated respectively. As negative control for the assay, TSA was used. In the assay setting, by using nuclear cell extract a reductive environment including biomolecules like the previously mentioned glutathione and cytochrome c is present, making an activation of the gold-compounds possible.

The results illustrated in Fig. 66 indicate that **262** is indeed the best HDAC inhibitor with rest activities of $51.8 \pm 1.9\%$ for 5 μM , $31.5 \pm 5.0\%$ for 10 μM and $4.1 \pm 0.6\%$ for 50 μM . Especially at the highest concentration **268** falls into the same range with a rest activity of $-7.5 \pm 4.4\mu\text{M}$. The next best inhibitors from these preliminary results are **266** and **267** with $17.2 \pm 4.1\%$ and $18.0 \pm 1.7\%$ rest activity at 50 μM respectively as well as rest activities below 50% at 10 μM . These results suggest, that inhibition of HDACs by gold complexes is indeed structure dependant and not based on the pure presence of gold-ions.

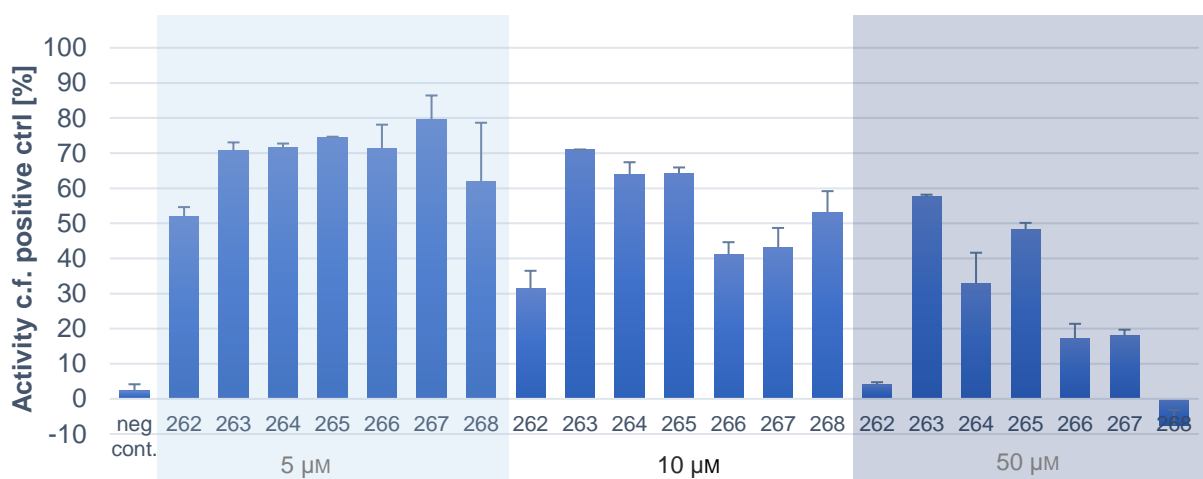


Fig. 66: Screening results for the HDAC restactivity in A549 nuclear extract after 1 h of incubation with compounds **262–268** at 5, 10 and 50 μM obtained by using the *FluoroFire HDAC Activity Assay Kit*.

Results and discussion

After having these preliminary results, the IC₅₀ values of **262** compared to its structural analogue **264** and the other potentially attractive compounds **266** and **267** were determined under the same assay conditions. Table 17 summarises these results, showing, that the best two inhibitors **262** and **267** inhibit the HDAC activity in A549 nuclear extract in the low micromolar region.

Table 17: Determined IC₅₀ values after preincubating A549 nuclear extract with ten different concentrations of the compound for one hour before measuring the HDAC activity. Each value reflects the results of two independent experiments (logistics dose response fitting, areas are given for values where the concentration limits were insufficient).

Compound	HDAC IC ₅₀
262	1.2 ± 3.2 μM
264	~12.8–27.0 μM
266	~5–30 μM
267	3.9 ± 1.3 μM
TSA	7.5 ± 11.7 nM

Here again **262** stands out as the best HDAC inhibitor in the series, closely followed by **267**, and at least an order of magnitude better than **264** and **266**. In general, these gold-based compounds inhibit HDACs in a low micromolar region and are therefore less potent compared to e.g. TSA, which inhibits in the nanomolar region. With the results for TSA the assay setting was evaluated under the given conditions. TSA has been shown to inhibit HDAC1–4 with 2 ± 0; 3 ± 0, 4 ± 1 and 6 ± 2 nM and HDAC6–9 with 3 ± 1, 5 ± 2, 456 ± 59 and 6 ± 5 nM respectively,^[76] showing that we are well within the range of inhibition expected for this inhibitor in our experiments.

To further assess whether the antiproliferative behaviour and HDAC inhibitory activity are related to each other, the HDAC activity of A549 and A2780 nuclear extract of cells, which have been treated with defined concentrations of **262** or **264** was tested. It is thought that gold-ions might replace the zinc-ion in the active site forming “gold-fingers”, and therefore serve as a kind of irreversible inhibitor, similar to Cys₄ zinc-finger domains for which such a mechanism has been elucidated recently.^[341] For the assay, A549 or A2780 cells were cultured in 6-well plates and treated according the MTT-test conditions, with the exception, that after 72 h of incubation with the compound, cells were harvested and nuclear extracts obtained, which were further used in the HDAC activity assay after normalising to the protein content.

The experimental results however were somewhat inconclusive, since the HDAC activity, although the protein content of the nuclear extracts is normalised, varies strongly with the cell number and from experiment to experiment, so that in a first experiment with A549 cells, it was observed that the lower the cell number was, the higher the HDAC activity seemed to be. In a second experiment

the 10 µM samples (low cell number due to high cytotoxicity) showed lower HDAC activity compared to the control. Samples containing 5 µM of **262** showed intermediate HDAC activity compared to the control and a control using half the number of cells during seeding, and samples using 5 µM of the control **264** showed the highest HDAC activity. In A2780 cells (single experiment), the control with a smaller number of cells showed lower HDAC activity compared to the control, as well as all treated samples. Overall, we were not able to show any significant inhibition of HDAC activity in A549 cells, on the contrary, it seems that HDAC activity might even be upregulated. A similar effect has been described for *cis*-[Pt(NH₃)₂(malSAHA)] (**63**) in CH1 cells, when the level of histone 3 and 4 acetylation was determined via western blot analysis, which was considerably decreased for the Pt-compound, indicating an increase in HDAC-activity. A somewhat smaller increase could also be observed for cisplatin and *cis*-[Pt(NH₃)₂(mal)]. The same trend has been further observed in a colorimetric HDAC activity assay using CH1 nuclear extract of cells treated for 24 h with isotoxic concentrations of the compounds.^[172]

The reason for such results might be the cell cycle and cell density dependency of HDAC expression, which has been shown for instance for the catalytically most active class I HDACs in different cancer cell lines.^[342] Using two different cell numbers in the controls of the experiment, we could already indicate that the cell density might play an important role in this kind of assay setting. Cells with a lower density might be more involved in cell division and thereby occupy different percentages in the cell cycle distribution. Another possibility might be a potential delocalisation of HDACs from the nucleus to the cytoplasm. Since solely nuclear extracts were examined and compared such a shift cannot be ruled out. Even if the catalytically most active class I HDACs are solely localised in the nucleus, it is unclear how much influence other isoforms have in the obtained results. Since the histone acetylation grade only focusses on HDAC activity in the cell nucleus, it was decided to compare the expression level of a single HDAC isoform in a whole cell sample after treatment for 72 h via western blot analysis. Therefore HDAC4 was chosen, since it has been previously shown to be upregulated after treatment with some platinum drugs, as well as being involved in platinum chemotherapy resistance.^[343] For direct western blot analysis, the cells were treated as previously described and lysed them in radioimmunoprecipitation assay (RIPA) buffer, before resolving the proteins using SDS-PAGE with 30 µg of total protein per sample and blotting to a polyvinylidene fluoride membrane electrophoretically. The membranes were treated with the primary monoclonal HDAC4 antibody. After washing, the membrane was further incubated with relevant gate-keeper monoclonal antibodies (β-actin and GADPH) as loading controls, and with a secondary peroxidase antibody accordingly. The protein bands were developed with an enhanced chemoluminescence detection kit and quantified using the GeneSnap program. Results are shown in Fig. 67.

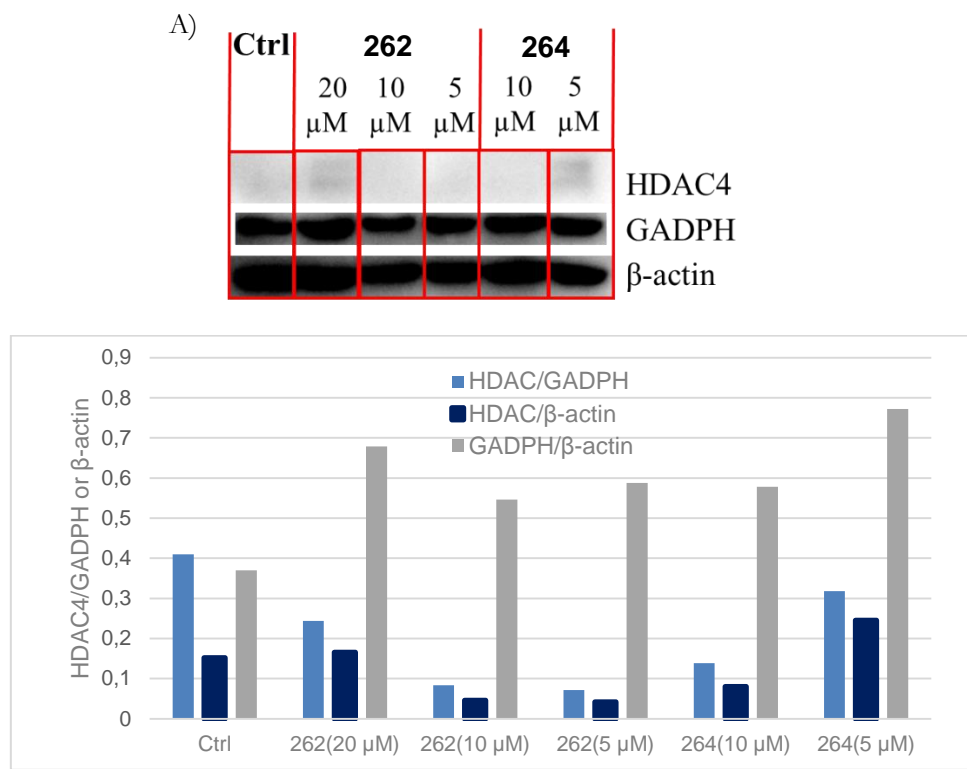


Fig. 67: Western blot analysis of HDAC4 activity in A549 cell extracts treated with **262** and **264** for 72 h previous to harvesting. A) HDAC4 expression level of the control and in response to compound treatment with different concentrations. B) Normalisation of HDAC4 expression levels to GADPH and β -actin, which were used as loading controls.

As can be taken from Fig. 67, HDAC4 with a size of 119 kDa, is expressed in all samples to various extends. The intensity integration was done over both bands, which are indicated in the manufacturer's protocol. However, the signals were very faint probably due to not optimal experimental conditions. The expression patterns for the housekeeping proteins GADPH and β -actin varied as well, with a higher level of GADPH than β -actin in treated cells c.f. the control cells. Therefore, the results from HDAC4 (pixel intensities) were normalised to both housekeeping genes individually. The results show various HDAC4 expression patterns, with lower HDAC4 contents the lower the concentration of **262** and the higher the concentration of **264** if correlated to both GADPH and β -actin. In general, HDAC4 expression is indeed downregulated for most treated samples compared to the control in contrast to the results previously obtained by comparing the overall HDAC activity in nuclear cell extracts, where the general HDAC activity seemed to be upregulated. The experiments were discontinued due to time reasons, so that a verification of the results remains to be done.

4. Summary and outlook

4.1. Summary and outlook metal-based kinase inhibitors

Kinases are a large family of transferase enzymes, of which at least 538 different members are present in the human body.^[11] By catalysing the transfer of the γ -phosphate group of ATP onto a specific side chain of their substrate, they mediate most cellular signal transductions in the body, thereby regulating various critical cellular activities. These include proliferation, survival, apoptosis, metabolism, transcription, differentiation, and a wide array of other cellular processes.^[9,10] It is no surprise that the kinome has been extensively investigated as a family of potential drug targets^[12] and the development of kinase inhibitors has therefore become an essential part of biological and medical research. Small molecule kinase inhibitors have been studied to treat various human diseases including cardiovascular diseases,^[23] autoimmune disorders such as rheumatoid arthritis,^[24] neurodegenerative conditions like Alzheimer's disease, diabetes or liver disorders.^[25] Originally based on unselective natural product inhibitors like staurosporine (**51**), research has led to almost 30 FDA approved inhibitors by the middle of 2016.^[26] Most of them were developed to treat oncological conditions, which are still a major focus of kinase inhibitor research today.

Over the last decade the MEGGERS group has established highly potent and selective kinase inhibitors using inert metal centres as unique structural templates, thus mimicking and enhancing the globular shape of the non-selective inhibitor staurosporine (**51**).^[120]

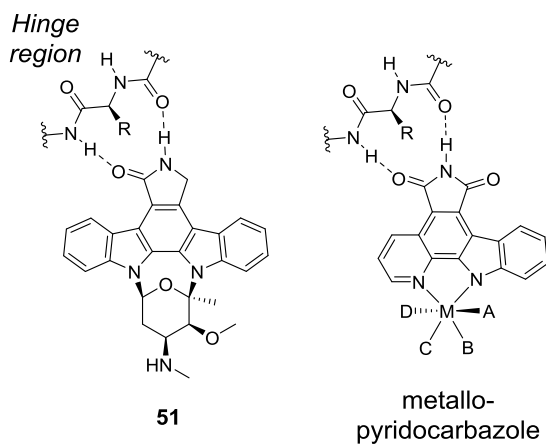


Fig. 68: The natural product staurosporine (**51**) served as structural template for the development of various inert metal based kinase inhibitors. The indolo[2,3-*a*]carbazole of **51** is thereby displaced by pyrido[2,3-*a*]carbazole which serves as a bidentate ligand for easy metal-coordination, and both groups occupy the hydrophobic adenine-binding cleft, mimicking the hydrogen-bonding pattern of the adenine base in ATP.^[48,109,119,120]

The use of this type of inert metal complexes as kinase inhibitors has repeatedly been demonstrated *in vitro*.^[151,162,166] In addition, some selected complexes have also been proven to successfully inhibit

kinases *in vivo* in species of the chordate phylum.^[121,149,171] This includes the *in vivo* inhibition of GSK-3 in the development of *xenopus laevis*^[149] and *danio rerio* embryos^[121] by two different Ru-complexes (**S-53** and **R-61**, see introduction for structures and more details), as well as the Flt4 inhibition related antiangiogenic properties in a xenotransplanted proangiogenic human cancer cell experiment in living zebrafish by an Ir-complex (**62**).^[171] Based on these properties, and many more different kinase targets of the compound group, these inhibitors might be regarded as potential anti-cancer drugs. In addition to that, various ATPase inhibitors have been developed in the group, using the same concept. Further studies towards their suitability as potential therapeutic drugs concerning their ADME properties were however not conducted previous to this thesis.

To address this issue, in a first approach it was attempted to find a suitable lead structure for ADME investigations by a classical empiric screening for cytotoxicity against cancer cells. This approach was chosen due to the fact that all complexes possess known kinase and ATPase inhibitory properties, thereby combining this classical approach with the appreciation of their activity as molecularly targeting agents. For that matter, a compound library with all available inhibitors was created, and all complexes (441 compounds), some only synthesised during the thesis, were tested in a single dose experiments in HT-29 human colorectal adenocarcinoma cells for their effect on cell viability via the MTT method. An exception were 33 compounds which were previously tested by ANJA LUDEWIG in HeLa human cervical cancer cells and deemed unsuitable. The most interesting compound from that screening (np829 (**80b**) Fig. 69), based on highest cytotoxicity, was additionally tested in different cancer cell lines in concentration dependent cytotoxicity assays resulting in LD₅₀ values of 0.4 to 2.9 µM after 24 h incubation time.

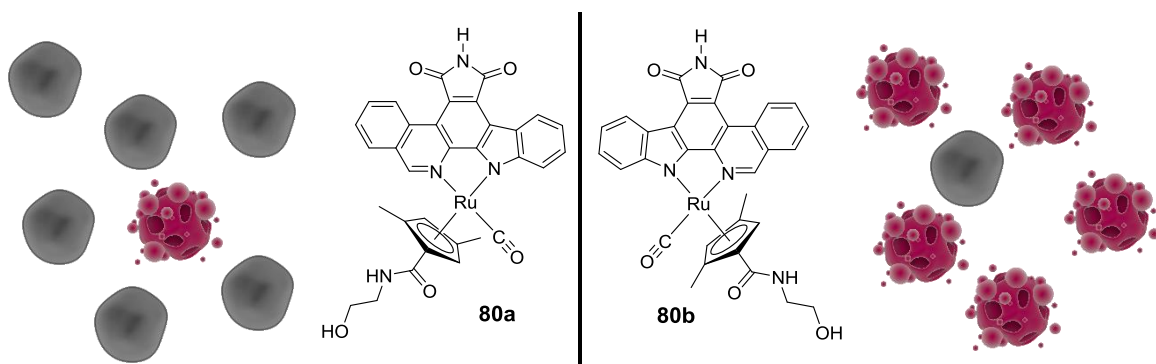


Fig. 69: The most interesting hit found in the classical cytotoxic approach is **80b**, which induced the highest amount of cell death as indicated by apoptotic cells. It is a mixture of enantiomers, as is its diastereomeric counterpart **80a**, which is much less cytotoxic as indicated by healthy cells. Absolute configuration was determined by a single crystal X-ray structure of **80a**.

Its diastereomer (**80a**) showed cytotoxicity to a much lesser extent, indicating that the geometrical structure of **80b** is important for its cytotoxicity and therefore its mode of action is probably based

Summary and outlook metal-based kinase inhibitors

on kinase inhibition. To verify the exclusiveness of its structure, another 44 compounds with side chain modifications were tested, but np829 still remained as the most cytotoxic complex in HT-29 cells. However, the compound, as well as some of its derivatives, showed toxicity, which might not solely be explainable by kinase inhibition, as it seems to crystallise inside or on the surface of cells. Therefore, the approach was terminated in favour of another way to identify a suitable lead structure.

As a second approach a focus was set on the drug-like abilities of this kind of kinase inhibitors, to move forward towards an application in cancer treatment. Therefore, selected compounds were tested for basic *in vitro* drug-like properties like solubility, permeability and metabolic stability towards CYP enzymes in rat liver microsomes in collaboration with the Novartis Institutes for BioMedical research (NIBR). Other interesting inhibitors were excluded from the study due to problems in MS quantification.

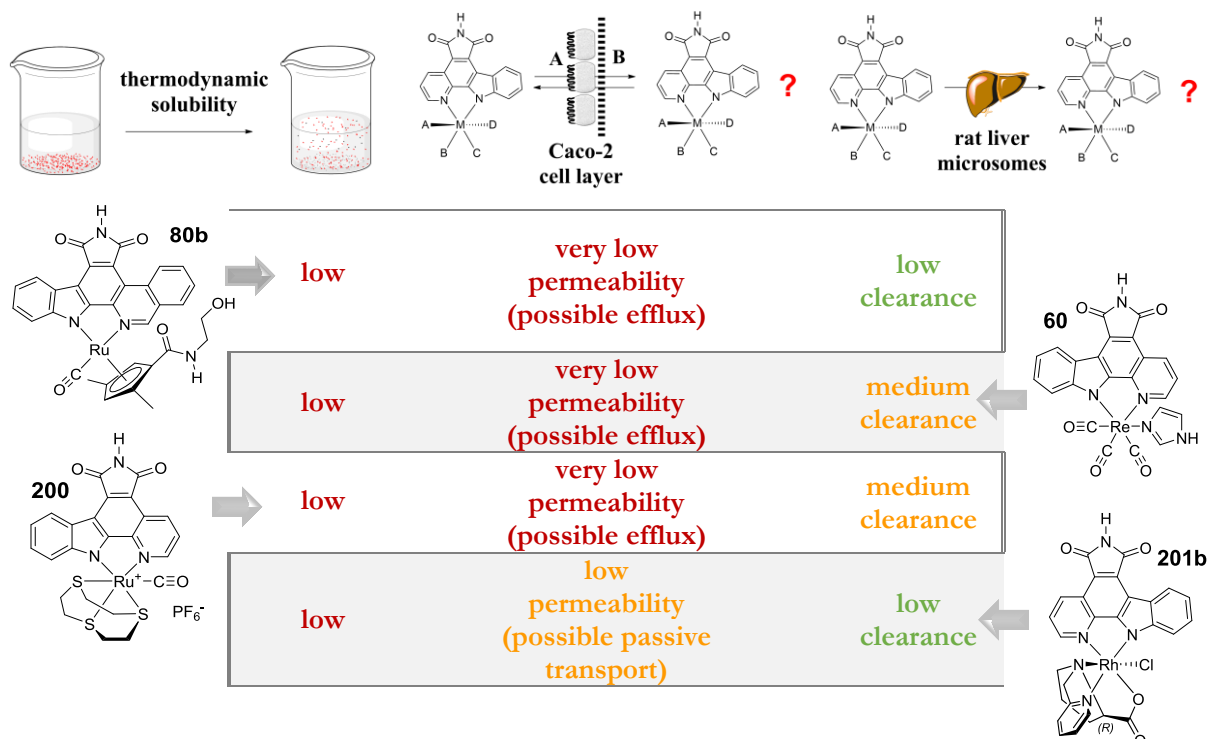


Fig. 70: Summary of simple ADME properties (thermodynamic solubility, cell membrane permeability and metabolic stability) as determined by *in vitro* assays at NIBR. **201b** has the best properties in the series tested and was therefore investigated further.

After identifying an enantiopure rhodium complex (**201b**) with adequate properties concerning *in vitro* rat liver microsome stability, permeability and solubility, some properties of its three remaining stereoisomeric counterparts were tested and yielded in comparable results. However, permeability was lower than expected from the initial results for all four compounds. One diastereoisomer of the identified complex is a potent Pim1 inhibitor ($IC_{50} = 15 \text{ nM}$), as determined by RAJATHEES RAJARATNAM, while **201b** is a very unpotent kinase inhibitor.^[233] Since Pim1 is one of the major

targets covered by the research in the MEGGERS group during the development of their promising kinase inhibitors, it seemed as a good starting point to improve the compounds properties while maintaining its kinase inhibitory properties as discussed below. The inhibitor **201a** and some of its isomers were at the same time investigated for their overall ADME properties. Starting with a stability study against solvents (e.g. CH₃CN, DMSO), no change in ¹H-NMR spectra and HPLC traces was observed after 3 weeks for **204b**. When exposing to an equimolar amount of thiols at 37 °C, again no change could be observed within 6 weeks in the ¹H-NMR spectra of **201a** and **201b**, indicating a strong stability of the tested complexes.

Both diastereomers showed low cytotoxicity in three different cancer cell lines within 24 or 72 h as determined by the MIT method, with **201a** demonstrating a more pronounced effect compared to **201b**. This effect might be related to the expected problems in cancer treatment with Pim1 as single target and might correlate to a low expression of Pim1 in these cell lines. Another explanation is the previously discussed possible compensation mechanisms by the other Pim family members. Based on a KINOMEscan^[23] Pim1 and Pim3 are inhibited by **201a** to a similar extent (1.8% rest activity), but Pim2 is inhibited much less (50% rest activity) and might therefore compensate for the inhibition of the other two isoforms. The toxicity in an *ex vivo* rat PCLS experiment was quite low for **201b**, but again showing a markedly higher degree for **201a**, indicating an overall toxicity of the complex, which is however not surprising for a functional kinase inhibitor. One has to consider that other kinases like HIPK2 and HIPK3 (3.3 and 2.4% rest activity respectively) and PRKG2 (2.4% rest activity) are probably strongly inhibited as well, as determined in the KINOMEscan. Therefore, the observed toxicity might be based on the inhibition of other kinases. Still other causes that might be responsible cannot be excluded without further studies. When measuring the uptake of the complexes in PCLS, **201b** shows a higher metal content in the liver tissue compared to **201a** as determined by ICP-MS measurements. In morphology PCLS samples, no changes compared to a control tissue were observed, even if strong localisations of the compound were prepared in freshly incubated samples.

In parallel to these basic *in vitro* and *ex vivo* studies, first *in vivo* pharmacokinetic studies in mice were conducted with **201b** and gave encouraging results. The compound was dosed by three different routes of administration (IV, PO, IP) and plasma samples were obtained at determined time points. From the IV results over 7 h, a moderate clearance and volume of distribution at steady state were observed, indicating adequate stability and a diffusion outside the vascular department. The half-life time in plasma was determined to be 2.9 h. Based on PO and IP results, a systemic circulation after administration by these routes was concluded possible, with low (PO) to moderate (IP) bioavailability. These results show, that our complexes might even be dosed by different routes of administration than IV, which is a major advantage over other drugs, especially metal-based ones.

Summary and outlook metal-based kinase inhibitors

As **201a** is the more interesting stereoisomer, additional PK studies were performed in rats. The IV results obtained are in a similar range compared to **201b** in mice, however **201a** is eliminated somewhat more quickly from plasma. As the fate of the metal is an important aspect in this compound class, according investigations were pursued using ICP-MS to determine the total metal content of different organs and bodily fluids after IV injection. Since **201a** shows high stability in various solvents, liver microsomes, hepatocytes and against thiols, the total metal content was assumed to reflect true values of the complex concentration. These studies show that **201a** is partially excreted via the biliary and probably the renal system, but that high amounts are present in the lungs within the 24 h time frame of the experiment. It can be speculated that the complex or metabolites are tissue-bound. Further studies are needed to determine if this effect is reversed after some time and whether the bound rhodium belongs to the parent complex or possible metabolites.

All obtained results show a certain suitability of the complex **201a** as a lead structure for a potential anti-cancer drug. However, reported yields and batch sizes are low.^[233] Therefore, the upscaling possibilities of **201a**, as well as a possible optimisation of reaction conditions were investigated, but did not deliver the expected improvements. Both simple upscaling and access of a different reaction path, as well as screening for optimised reaction conditions were without success.

Finally, **201a** was used as a lead structure for the development of structurally modified complexes with regard to improved properties concerning ADME, while maintaining its original kinase activity. Based on *in silico* considerations, the para pyridine position of (pyridine-2-ylmethyl)-D-proline was identified as potentially solvent exposed, with additional space for large solubility and/or permeability-enhancing appendages. These studies were conducted using a simplified model of *pair-fitting* the originally selected compound **201a** into an existing co-crystal structure of a pyridocarbazole based inhibitor in the active site of Pim1. After careful consideration, including attention to the surface charges of Pim1's active site, different potential side chains to enhance solubility, while at least maintaining permeability, were proposed. Some of the proposed side chains were successfully introduced in **201a** yielding in the selected complexes given in Fig. 71.

The synthesised complexes include solubility-enhancing side chains like a pure aliphatic side chain in **213a** or a linker-connected morpholine in **210a**. While morpholine itself is generally referred to as solubility enhancing based on its H-bond capacity, the linker ensures an additional out of plane behaviour, loosening up the crystal packing of the complex. The pure aliphatic hexyl side chain in **213a** is supposed to enhance the permeability by its lipophilic character and meanwhile enhancing the solubility by out of plane behaviour. Dimethylamine substituents as in **212a** are thought to be at least partially protonated under physiological conditions, thereby enhancing the solubility of the

complex as well as the affinity to Pim1 by interacting with its generally negatively charged surface in and around the active site. Finally, **258a** was synthesised to evaluate the influence of possible halogen-bridges, as well as the influence of a change in polarity and hydrophobicity in the ligand.

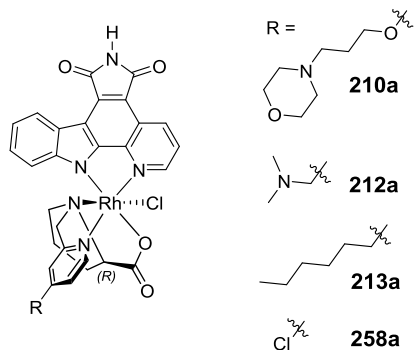


Fig. 71: Successfully synthesised derivatives of **201a** which were supposed to improve the drug-like properties of the original compound by modification of the (pyridine-2-ylmethyl)-D-proline ligand.

The solubility was enhanced for **210a** (86 µM) and **212a** (43 µM) in phosphate buffer, especially at a low pH of 4, indicating indeed a positive effect of protonation of the tertiary amines, although only at low pH. This enhancement in solubility was however not further improved in FaSSIF. Permeability of all compounds was not enhanced by the modifications, still resulting in very low permeabilities, most often below the respective detection limit. Additionally, the rat liver microsome stability was tested and showed good results for **258a** and **212a**, while the other two compounds showed only medium stability, probably related to the easier access of the CYP enzymes to the elevated side chains. All compounds are therefore no real improvement to **201a**.

Additionally, taking the affinity for Pim1 into consideration, modifications of the pyridocarbazole ligand were pursued. These modifications were based on previously designed pyridocarbazole-based Pim1 inhibitors, which showed enhanced Pim1 affinity in comparison to their unmodified counterparts, and which might be able to enhance solubility and/or permeability, while not negatively impairing the other property too much. Therefore, a selection of complexes was prepared (see Fig. 72).

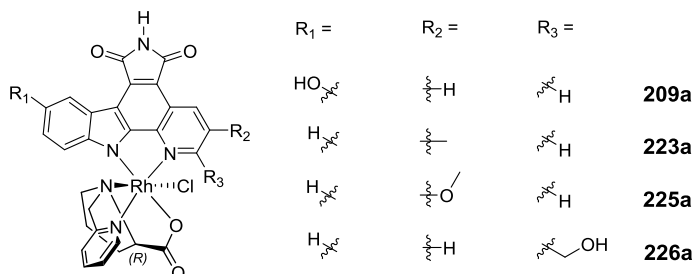


Fig. 72: Successfully synthesised derivatives of **201a**, which were supposed to improve the drug-like properties of the original compound by modification of the pyridocarbazole ligand.

After subjecting the compounds to the drug-like abilities assays as the previous series, especially **209a** stood out with an enhanced solubility of 72 µM in phosphate buffer at pH 7, while both solubilities in FaSSIF and in phosphate buffer at pH 4 were raised to >160 µM. All other complexes showed no enhanced solubility and again all complexes had low permeability. Both **209a** and **223a** had a medium to high risk concerning metabolic stability, while the other two compounds are quite stable in microsomes. Again none of the compounds is a real improvement concerning drug-like abilities compared to **201a**, because while improving one property, another is negatively affected. The results of both series of compounds synthesised however show a certain margin in influencing the properties of the complex, so that only the best combination has to be found in future investigations.

For testing the structure activity relationship of the newly designed complexes towards inhibition of Pim1, a quantitative inhibitory assay was conducted for all *trans*-isomers. Based on the obtained results **209a**, **225a** and **226a** are similarly good inhibitors compared to **201a**, but all derivatives with modifications in the (pyridine-2-ylmethyl)-D-proline showed little to no inhibition, indicating that the initial *in silico* considerations and assumed space opportunity actually was a misconception. Therefore, the strategy for modifying the complex **201a** has to be reconsidered and optimally based on an actual co-crystal structure.

In summary, different approaches for the discovery of a potential lead complex have been conducted. A screening for cytotoxic compounds thereby led to a dead end. Using an *in vitro* investigation of ADME properties, an interesting complex was pointed out and its properties were further improved by structural optimisation. The kinase inhibitory properties might thereby be retained. A combination of the different modifications might lead to a structure with sufficient properties to be tested in further preclinical settings. Additionally, studies concerning PK parameters *in vivo* yielded promising results. The fate of the metal was partially determined, but needs more investigations in the future to study possible tissue binding and metabolism. Overall many insights into ADMET parameters of inert metal based compounds were obtained, which is a solid basis for further investigations in the future.

4.2. Summary and outlook gold-based HDIs

In a side project, the anticancer and histone deacetylase (HDAC) inhibitory properties of a well-established dinuclear gold(III)-complex **262** (Fig. 73) in comparison to structural analogues as well as distinct gold complexes were evaluated. HDACs are another potential target to treat cancer, as covered in more detail in the introductory section.

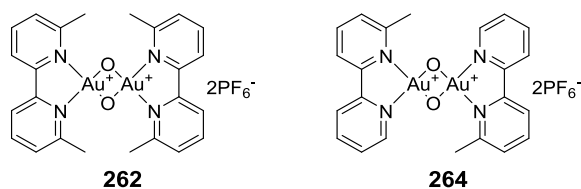


Fig. 73: Structures of two of the gold-complexes studied for their antiproliferative and HDAC inhibition properties.

It was demonstrated that the compound **262**, which was previously described as antiproliferatively active compound and possible HDAC inhibitor, indeed is the most cytotoxic compound against cancer cells in the series tested. Additionally, it was the best HDAC inhibitor with a single digit micromolar activity in A549 nuclear extract. While **262** is quite toxic against cancer cells, it showed little toxicity against rat liver tissue, indicating a very good selectivity. These results confirm previously suggested evidence for **262**'s HDAC inhibitory properties, which was based on a comparative analysis of the cytotoxicity against 36 different cancer cell lines.^[334] A correlation of the interconnection of that HDAC inhibitory activity with the antiproliferative behaviour of **262** however failed, as the HDAC activity in A549 lung cancer cells nuclear extract is rather elevated than lowered after the treatment of the cells for 72 h. Such a phenomenon has been previously described for particular platinum compounds.^[172] Since controls with a lower cell number also showed higher HDAC activity, effects like cell cycle distribution and elevated cell-cell contacts might play a role in these results, leaving the need for other tools to elucidate the HDAC inhibitory properties in living cells, which excludes such factors. Western Blot results for HDAC4 indicated that this single HDAC isoform was inhibited in A549 cells after 72 h of treatment with both **262** and to a smaller extent its less toxic derivative **264**. Further tools and studies to understand the assay conditions to a greater extent might be needed, before follow-up experiments can fully elucidate the underlying HDAC inhibitory mechanism of **262**.

5. Experimental part

5.1. General methods

Reactions were carried out under an atmosphere of nitrogen unless otherwise specified. Water and oxygen sensitive reactions were carried out in dried glassware using SCHLENK techniques. For oxygen but not moisture sensitive reactions the solvent was purged with N₂ for 5-20 min. Solvents used for reactions were distilled under an N₂ atmosphere from calcium hydride (CH₃CN, CH₂Cl₂, CHCl₃), sodium/benzophenone (THF), or sodium (benzene) using standard techniques,^[344] or directly used in HPLC quality. If not stated otherwise, commercially available reagents were used without further purification. Commercial thionyl chloride was distilled and stored under N₂ on dried mole sieve (4 Å) at 4 °C under exclusion of light.

Microwave reactions were performed with a mono-mode Discover LabMate (CEM GmbH). Photolysis reactions were performed in a photoreactor using a medium pressure Hg lamp (150 W or 700 W).

5.1.1. Chromatography methods

Flash column chromatography was performed on freshly packed silica gel 60 (particle size 0.040-0.063 mm, MERCK KGAA) or neutral Al₂O₃ (BROCKMANN activity I, particle size 0.05-0.15 mm, FLUKA) columns at room temperature under positive pressure (0.5-2 bar) as described in the experimental section. All solvents used for flash chromatography were distilled before usage.

Thin layer chromatography for reaction control, chromatography control, or semi preparative separation was performed on aluminium TLC plates with silica 60 F₂₅₄ coating (MERCK KGAA or MACHERY NAGEL) or neutral Al₂O₃ F₂₅₄ coating (MERCK KGAA or MACHERY NAGEL). Eluted compounds were visualised by their intrinsic colour, self-fluorescence ($\lambda = 254$ nm or 366 nm) or fluorescence quenching ($\lambda = 254$ nm or 366 nm). In all other cases, TLC sheets were immersed in a KMnO₄ dip and stained by subsequent heating treatment (~200 °C).

Analytical and semi-preparative HPLC chromatography was performed on an Agilent 1200 Series HPLC System using different columns and flow rates as indicated in the according discussion or experimental sections. UV absorption was detected at 254 nm. Preparative HPLC was performed on a PLC 2020 Personal Purification System (Gilson) as described in the according discussion or experimental section. UV absorption was detected at $\lambda = 254$ nm if not stated otherwise.

5.1.2. Analytical methods

5.1.2.1. Nuclear magnetic resonance spectroscopy

NMR spectra were recorded using deuterated NMR-solvents on a *Bruker DPX-250* (^1H -NMR resonance: 250.1 MHz, ^{13}C -NMR resonance: 62.9 MHz), a *Bruker Avance 300* (^1H -NMR resonance: 300.1 MHz, ^{13}C -NMR resonance: 75.5 MHz) as automated systems, and on a *Bruker DRX 400* (^1H -NMR resonance: 400.0 MHz, ^{13}C -NMR resonance: 100.6 MHz), a *Bruker DRX 500* (^1H -NMR resonance: 500.2 MHz, ^{13}C -NMR resonance: 125.8 MHz), or a *Bruker Avance 500* (^1H -NMR resonance: 500.2 MHz, ^{13}C -NMR resonance: 125.8 MHz) spectrometer by the staff of the NMR department of the Philipps-Universität Marburg. Chemical shifts of compounds and solvents are indicated in relation to tetramethylsilane in ppm on a δ -scale.^[345] The spectra were calibrated using the rest proton signal of the solvents as indicated in Table 18.

Table 18: Rest proton signals of deuterated NMR-solvents used for calibration of NMR-spectra.

CDCl_3	$^1\text{H}: \delta = 7.26 \text{ ppm}$	$^{13}\text{C}: \delta = 77.16 \text{ ppm}$
DMSO- δ_6	$^1\text{H}: \delta = 2.50 \text{ ppm}$	$^{13}\text{C}: \delta = 39.52 \text{ ppm}$
CD_3CN	$^1\text{H}: \delta = 1.94 \text{ ppm}$	$^{13}\text{C}: \delta = 1.32 \text{ ppm}, 118.26 \text{ ppm}$
$(\text{CD}_3)_2\text{CO}$	$^1\text{H}: \delta = 2.05 \text{ ppm}$	$^{13}\text{C}: \delta = 29.84 \text{ ppm}, 206.26 \text{ ppm}$
CD_3OD	$^1\text{H}: \delta = 3.31 \text{ ppm}$	$^{13}\text{C}: \delta = 49.00 \text{ ppm}$

Spectra were analysed using BRUKER Topspin 3.0. Coupling constants nJ , over n bonds, are given in Hertz (Hz). Multiplicities are given as found in the spectra and are not necessarily in accordance to the theoretically expected multiplicities. They are given as s (singlet), d (doublet), t (triplet), q (quartet), quin. (quintet) or combinations thereof. Broad signals are indicated by br. Signals with insufficient resolution or overlayed signals are given as m (multiplet). Signals were allocated by coupling constants and in more difficult cases using 2D spectra (COSY, HSQC, HMBC).

5.1.2.2. Infrared spectroscopy

Infrared spectra were recorded from neat compounds using a Bruker Alpha-P FTIR spectrometer and ATR (attenuated total reflection) sampling technique. The spectra were analysed using BRUKER Opus 6.5. The locations of absorption bands are given in wavenumbers $\tilde{\nu}$ in cm^{-1} . The relative intensity and characteristics of the bands are given as s (strong), m (medium), w (weak), and if necessary additionally specified as br (broad) or v (very).

5.1.2.3. Mass spectrometry

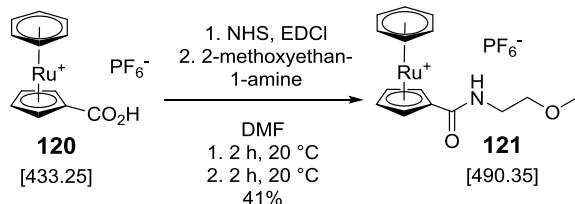
High-resolution mass spectra were obtained on a THERMO FINNIGAN LTQ FT instrument using ESI or APCI ionisation by the staff of the MS department of the Philipps-Universität Marburg. The ionic masses m/z are given in u for the most abundant isotopes. It was ensured that the observed isotopic patterns were in accordance with the expected isotopic patterns.

Reaction controls and investigations of best ionisation techniques were performed on an LC-MS (AGILENT 1200 series, 6120 quadrupole system) as indicated in the according discussion or experimental section.

5.2. Compound preparation for toxicity approach

5.2.1. Synthesis of structural derivatives of np829 (80b) and np830 (80a)

5.2.1.1. Synthesis of (η^6 -benzene)(η^5 -N-(2-methoxyethyl)cyclopentadienyl carboxamide) ruthenium hexafluorophosphate

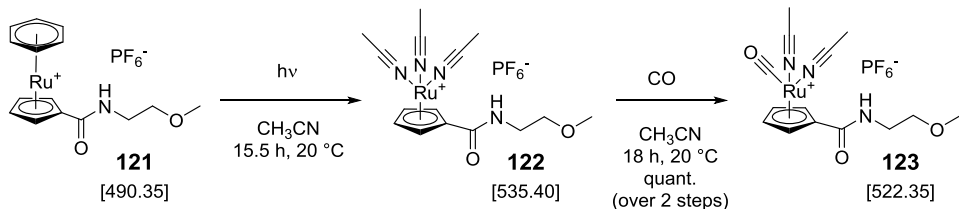


The sandwich complex **120**^[49] (250 mg, 0.58 mmol, 1.00 eq) was dissolved in 10.5 mL DMF and degassed for 10 min. 88 mg NHS (0.77 mmol, 1.33 eq) and 147 mg EDCl (0.77 mmol, 1.33 eq) were added and the solution stirred for 20 h at 20 °C. Afterwards, 60.5 µL 2-methoxyethan-1-amine ($\rho = 0.86$, 0.70 mmol, 1.2 eq) in 0.75 mL DMF were added and stirred for another 2 h at 20 °C. The solvent was removed under reduced pressure and azeotroped with CH₃CN. The complex was purified via flash chromatography (27 g silica, CH₃CN/H₂O/KNO_{aq.} sat. 50:3:1). After removal of the solvent, the residue was taken up in 20 mL H₂O and some drops of NH₄PF₆ aq. sat. were added and the aqueous layer was extracted with CH₂Cl₂ (3 x 20 mL). The combined organic layers were washed with H₂O (2x 10 mL) and dried over Na₂SO₄. After removal of the solvent under reduced pressure, 116 mg of the complex **121** (0.23 mmol, 41%) was obtained.

¹H-NMR (300.1 MHz, CD₃CN): $\delta = 6.84$ (s, 1H, NH), 6.11 (s, 6H, H_{benzene}), 5.77 (t, 2H, $^3J = 1.9$ Hz, H_{Cp}), 5.40 (t, 2H, $^3J = 1.9$ Hz, H_{Cp}), 3.50-3.46 (m, 2H), 3.44-3.39 (m, 2H), 3.35 (s, 3H, OCH₃) ppm.

¹³C-NMR (75.5 MHz, CD₃CN): $\delta = 163.6$, 118.3, 88.3 (6C), 82.6 (2C), 80.6 (2C), 71.2, 58.7, 40.0 ppm.

5.2.1.2. Synthesis of η^5 -N-(2-methoxyethyl)cyclopentadienyl carboxamide precursor **123**



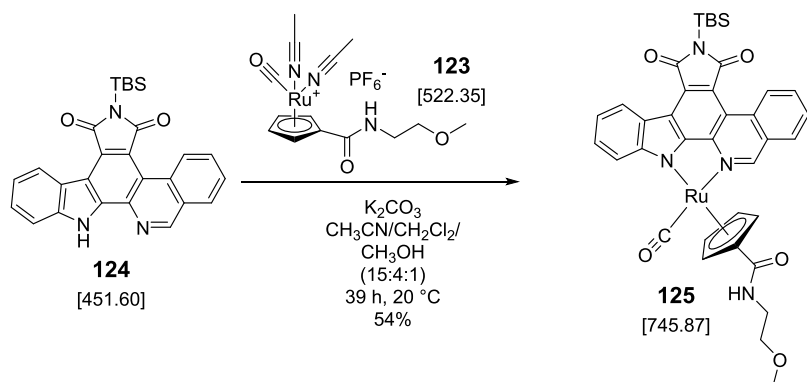
The sandwich complex **121** (116 mg, 0.23 mmol, 1.00 eq) was dissolved in 600 mL CH₃CN and irradiated with a medium pressure Hg lamp (750 W) for 15.5 h with a stream of N₂ flowing through the solution throughout the photolysis. The solvent was removed *in vacuo* and the tris-acetonitrile

complex **122** was redissolved in 20 mL CH₃CN. The resulting solution was purged with CO (g) for 5 min and stirred under CO atmosphere for 18 h at 20 °C. After removal of the solvent under reduced pressure, 124 mg of the complex **123** (0.24 mmol, quant.) was obtained as a brown oil.

¹H-NMR (300.1 MHz, CD₃CN): δ = 6.84 (s, 1H, NH), 5.75 (t, 2H, ³J = 2.1 Hz, H_{Cp}), 5.13 (t, 2H, ³J = 2.1 Hz, H_{Cp}), 3.47-3.86 (m, 4H), 3.31 (s, 3H, OCH₃) ppm.

¹³C-NMR (75.5 MHz, CD₃CN): δ = 163.5, 118.3, 86.7 (2C), 81.1 (2C), 71.4, 58.8, 40.2 ppm.

5.2.1.3. Synthesis of TBS-protected η^5 -N-(2-methoxyethyl)cyclopentadienyl carboxamide complex **125**



A mixture of 45 mg TBS-protected isoquinolinocarbazole **124** (101 μ mol, 0.90 eq), 58 mg of the Ru-precursor **123** (112 μ mol, 1.00 eq), and 16 mg K_2CO_3 (112 μ mol, 1.00 eq) were dissolved in 5 mL CH₃CN/CH₂Cl₂/CH₃OH (15:4:1) and degassed with N₂ for 10 min. The reaction was stirred for 16 h and additional 0.5 mL CH₂Cl₂ were added before it was further stirred for 5.5 h. Another 0.3 mL CH₂Cl₂, 0.25 mL MeOH, and 2 mL CH₃CN were added before the reaction was stirred further for 17.5 h. Since some side product appeared, the reaction was terminated and the solvent was removed *in vacuo*. The complex was diluted in CH₃CN to remove some of the less soluble unreacted ligand and the solvent was again removed under reduced pressure. The complex was purified via flash column chromatography (silica, CH₂Cl₂ to CH₂Cl₂/MeOH 10:1). After removal of the solvent *in vacuo* a pure fraction of 20 mg and an impure fraction of 21 mg of the complex **125** as racemic mixture (54.9 μ mol, 54%) was obtained as a deep red solid.

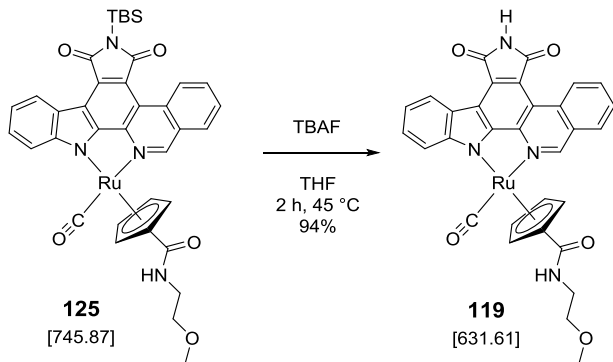
¹H-NMR (300.1 MHz, CD₃CN): δ = 10.48 (d, ³J = 8.6 Hz, 1H), 9.63 (s, 1H), 8.90 (d, ³J = 7.8 Hz, 1H), 8.16 (d, ³J = 8.0 Hz, 1H), 8.01 (ddd, ³J = 8.3 Hz, ³J = 7.2 Hz, ⁴J = 1.3 Hz, 1H), 7.86-7.81 (m, ³J = 7.5 Hz, 1H), 7.62-7.55 (m, 2H), 7.35 (ddd, ³J = 7.9 Hz, ³J = 6.0 Hz, ⁴J = 1.8 Hz, 1H), 6.50 (t, ³J = 5.66 Hz, 1H), 6.03-6.03 (m, 1H, H_{Cp}), 5.92-5.92 (m, 1H, H_{Cp}), 5.36-5.34 (m, 2H, H_{Cp}), 3.00 (q, J = 6.0 Hz, 2 H), 2.88 (s, 3H, CH₃), 2.72-2.68 (m, 2H), 1.04 (s, 9H, TBS), 0.60 (s, 6H, TBS) ppm.

¹³C-NMR (62.9 MHz, CD₃CN): δ = 201.4, 176.1, 175.6, 164.4, 161.8, 156.7, 154.6, 141.0, 134.2, 133.5, 133.0, 130.2, 130.0, 129.4, 129.0, 127.7, 126.0, 124.7, 121.3, 120.2, 117.4, 117.2, 116.1, 90.0, 88.9, 86.1, 80.3, 78.9, 71.0, 58.5, 39.5, 26.9, 19.8, -3.4 ppm.

ATR-IR (neat): $\tilde{\nu}$ = 3088 (vw), 3060 (vw), 2928 (w), 2888 (vw), 2856 (vw), 2055 (vw), 1954 (s), 1737 (w), 1679 (m), 1636 (w), 1575 (w), 1533 (m), 1466 (w), 1436 (w), 1368 (w), 1328 (w), 1293 (s), 1226 (m), 1153 (vw), 1118 (w), 1080 (w), 1023 (vw), 969 (vw), 917 (vw), 821 (m), 732 (s), 693 (w), 657 (w), 583 (vw), 554 (vw), 515 (vw), 475 (vw), 438 (vw), 411 (vw) cm⁻¹.

HR-MS (ESI): C₃₇H₃₆N₄O₅RuSiNa (M+Na)⁺ calcd.: 769.1401, found: 769.1396.

5.2.1.4. Synthesis of η^5 -N-(2-methoxyethyl)cyclopentadienyl carboxamide complex 119



The TBS-protected complex **125** (20 mg, 26.8 μmol, 1.00 eq) was dissolved in 2.5 mL THF, and cooled to 0 °C. 134 μL of a 1 M solution of TBAF in THF (134 μmol, 5.00 eq) was added and the solution was heated to 45 °C for 2 h. Afterwards, the solution was cooled to 0 °C, and 7.7 μL acetic acid were added. After warming to 20 °C, the solvent was removed under reduced pressure and the complex was purified via flash column chromatography (5 g silica, CH₂Cl₂ to CH₂Cl₂/MeOH 40:1). After removal of the solvent *in vacuo*, 16 mg of the racemic complex **119** (25.3 μmol, 94%) were obtained as a deep red solid.

¹H-NMR (300.1 MHz, DMSO-*d*₆): δ = 11.35 (s, 1H, NH), 10.54 (d, ³J = 8.5 Hz, 1H), 9.88 (s, 1H), 8.85 (d, ³J = 7.9 Hz, 1H), 8.35 (d, ³J = 7.4 Hz, 1H), 8.19-8.13 (m, ⁴J = 1.4 Hz, 1H), 8.02-7.97 (m, ⁴J = 0.8 Hz, 1H), 7.64-7.57 (m, ⁴J = 1.2 Hz, 2H), 7.17 (ddd, ³J = 7.8 Hz, ³J = 6.4 Hz, ⁴J = 1.8 Hz, 1H), 6.28-6.27 (m, ³J = 1.3 Hz, 1H, H_{Cp}), 6.21-6.21 (m, ³J = 1.3 Hz, 1H, Cp), 5.62-5.59 (m, 2H, H_{Cp}), 3.09-3.02 (m, 2 H), 2.89 (s, 3H, CH₃), 2.81-2.71 (m, 2H) ppm.

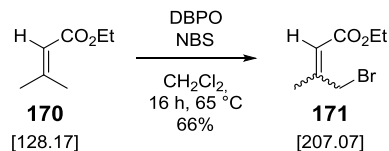
¹³C-NMR (125.8 MHz, DMSO-*d*₆): δ = 200.8, 171.0, 170.0, 163.1, 160.8, 155.1, 153.3, 139.1, 132.9, 131.4, 131.3, 129.4, 128.9, 128.6, 127.6, 126.8, 124.7, 123.1, 120.0, 119.1, 116.3, 115.3, 114.1, 89.2, 87.9, 85.0, 79.9, 79.5, 70.0, 57.6, 38.4 ppm.

ATR-IR (neat): $\tilde{\nu}$ = 3073 (vw), 2931 (vw), 2845 (vw), 2765 (vw), 1946 (s), 1740 (w), 1692 (m), 1667 (m), 1623 (vw), 1578 (w), 1550 (m), 1487 (vw), 1463 (vw), 1438 (vw), 1378 (w), 1327 (m), 1293 (m), 1224 (m), 1155 (vw), 1108 (vw), 1082 (m), 1017 (w), 969 (vw), 923 (vw), 848 (w), 815 (vw), 754 (m), 694 (w), 645 (m), 595 (vw), 556 (w), 527 (w), 501 (vw), 488 (vw), 464 (w), 433 (vw) cm^{-1} .

HR-MS (ESI): $\text{C}_{31}\text{H}_{22}\text{N}_4\text{O}_5\text{RuNa}$ ($\text{M}+\text{Na}$)⁺ calcd.: 655.0534, found: 655.0523.

5.2.2. Preparation of 80b

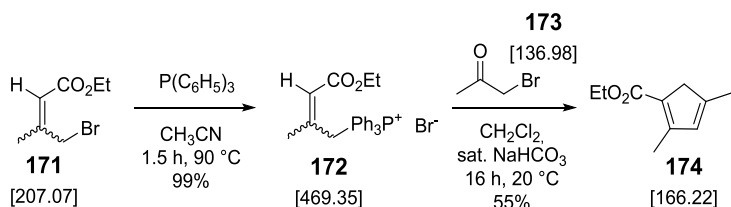
5.2.2.1. Synthesis of *E/Z*-ethyl 4-bromo-3-methylbut-2-enoate



The synthesis was modified from a well-established literature protocol,^[205–207] to avoid the use of CCl_4 . To a solution of 5.42 mL ethyl-3-methylbut-2-enoate (39.0 mmol, 1.00 eq) in 40 mL CH_2Cl_2 , which was degassed for 15 min with N_2 , was added a mixture of 6.85 g *N*-bromosuccinimide (38.5 mmol, 0.99 eq) and 85 mg dibenzoyl peroxide (0.35 mmol, 0.01 eq) portionwise. The suspension was heated to 65°C (oil bath temperature) for 16 h. After cooling the yellow suspension to 20°C , the precipitated succinimide was filtered off and the reaction mixture was concentrated under reduced pressure. The starting material **170** (55 °C, 30 mbar) was removed from the *E/Z*-ethyl 4-bromo-3-methylbut-2-enoate (**171**) (103 °C, 30 mbar/67 °C, 4.6 mbar) by fractional distillation and **171** was obtained as colourless liquid in good yields 66% (5.29 g, 25.5 mmol) by distillation. Analytical data was in accordance to reported data.^[346–349]

¹H-NMR (300.1 MHz, CDCl_3): δ = 5.95-5.95 (m, 1H, *E* CHCO), 5.77 (d, J = 1.4 Hz, 1H, *Z* CHCO), 4.55 (s, 2H, *Z* CH_2Br), 4.21-4.13 (m, 4H, *E/Z* CH_3CH_2), 3.94 (d, J = 0.6 Hz, 2H, *E* CH_2Br), 2.27 (d, J = 1.3 Hz, 3H, *E* CH_3C_6), 2.04 (d, J = 1.4 Hz, 3H, *Z* CH_3C_6), 1.28 (dt, J = 7.1 Hz, J = 0.4 Hz, 6H, *E/Z* CH_3CH_2) ppm.

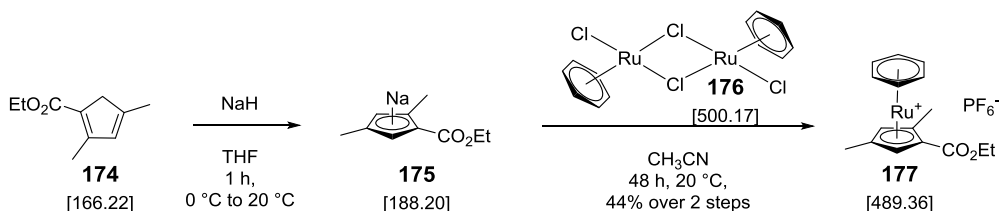
5.2.2.2. Synthesis of ethyl-2,4-dimethylcyclopenta-1,2-diencarboxylate



E/Z-ethyl 4-bromo-3-methylbut-2-enoate (**171**) was treated according to a modified literature procedure.^[208] 4.27 g of the enoate (20.6 mmol, 1.00 eq) was dissolved in 65 mL CH₃CN and 5.41 g triphenylphosphine (20.6 mmol, 1.00 eq) was added and stirred until a clear solution remained. This solution was heated to 95 °C for 90 min, then cooled to 20 °C and the solvent was slowly removed under reduced pressure to yield (*E/Z*)-(4-ethoxy-2-methyl-4-oxobut-2-en-1-yl) triphenylphosphoniumbromide quantitatively (9.61 g, 20.5 mmol, 99%). The phosphonium salt **172** was converted to the cyclopentadiene without characterisation according to a modified literature procedure.^[209,210] The phosphoniumbromide **172** (9.61 g, 20.5 mmol, 1.00 eq) was dissolved in 170 mL CH₂Cl₂ and 205 mL of a saturated NaHCO₃ _{aq.} solution was added and the biphasic system was stirred vigorously. A solution of 1.91 mL 95% chloroacetone (22.5 mmol, $\rho = 1.15$, 1.10 eq) in 35 mL of CH₂Cl₂ was added, the mixture was degassed with N₂ for 20 min, and stirred vigorously for 16 h at 20 °C. The layers were separated and the aqueous layer was extracted two times with 100 mL CH₂Cl₂. The combined organic layers were washed with 200 mL of H₂O, dried over MgSO₄, filtered and concentrated *in vacuo*. The product was pre-purified via rapid short column flash chromatography (silica, hexane/Et₂O 1:1, loading with CH₂Cl₂) and further purified via flash chromatography (dry load, silica, hexane/EtOAc 10:1 → 6:1). The pure fractions were concentrated under reduced pressure to obtain 1.84 g (11.6 mmol, 55%) of the cyclopentadiene **174** as a light yellow oil. Analysis was in accordance with the reported literature data.^[210]

¹H-NMR (300.1 MHz, CDCl₃): δ = 6.05 (s, 1H, CH_{CP}), 4.19 (q, $J = 7.1$ Hz, 2H, CH₃CH₂), 3.21 (d, $J = 2.3$ Hz, 2H, CH₂CP), 2.30 (t, $J = 2.3$ Hz, 3H, CH₃CP), 2.07 (s, 3H, CH₃CP), 1.30 (t, $J = 7.1$ Hz, CH₃CH₂) ppm.

5.2.2.3. Synthesis of (η^6 -benzene)(η^5 -ethyl 2,4-dimethylcyclopentadienylcarboxylate) ruthenium hexafluorophosphate



A modified literature procedure was used in order to avoid the use of Ti_2SO_4 .^[203] A solution of 1.00 g of ethyl-2,4-dimethylcyclopenta-1,3-dienecarboxylate **174** (6.00 mmol, 1.00 eq) in 6 mL THF was added dropwise to a suspension of 276 mg sodium hydride (mineral oil dispersion, 6.90 mmol, 1.15 eq) in 3 mL THF at 0 °C. The suspension was stirred for 60 min at room temperature and added to a N_2 -purged suspension of 1.50 g $[\text{Ru}(\text{benzene})_2\text{Cl}_2]$ **176**^[211] (3.00 mmol, 0.50 eq) in 160 mL CH_3CN under N_2 atmosphere. The reaction mixture was stirred for 48 h at room temperature and then filtered over celite. The solvent was removed *in vacuo* and the residue was redissolved in water. Excess NH_4PF_6 was added and the product was extracted with CH_2Cl_2 . The organic layer was dried over MgSO_4 , filtered, and the solvent removed under reduced pressure. The residue was subjected to flash chromatography with aluminium oxide as stationary phase and acetone as eluting solvent. The combined product eluents were dried *in vacuo* to result in 1.28 g (2.62 mmol, 44%) of the sandwich complex **177** as a light brown solid.

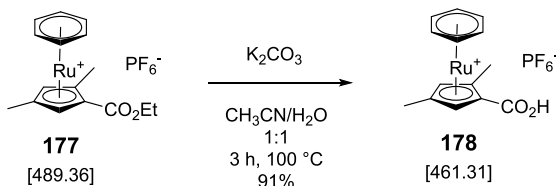
$^1\text{H-NMR}$ (300.1 MHz, $(\text{CD}_3)_2\text{CO}$): $\delta = 6.33$ (s, 6H), 5.88 (d, $^4J = 1.4$ Hz, 1H), 5.73 (d, $^4J = 1.1$ Hz, 1H), 4.35-4.25 (m, 2H), 2.30 (s, 3H), 2.08 (s, 3H), 1.34 (t, $^3J = 7.1$ Hz, 3H) ppm.

$^{13}\text{C-NMR}$ (75.5 MHz, $(\text{CD}_3)_2\text{CO}$): $\delta = 166.4$ (C_q), 101.1 (C_q), 100.4 (C_q), 89.0, 86.8, 84.4 (C_q), 82.7, 62.3, 14.4, 13.6, 13.5 ppm.

ATR-IR (neat): $\tilde{\nu} = 3110$ (vw), 3094 (vw), 2987 (vw), 2924 (vw), 2854 (vw), 1703 (m), 1480 (vw), 1461 (w), 1440 (w), 1414 (w), 1391 (w), 1373 (vw), 1307 (w), 1234 (m), 1181 (w), 1120 (vw), 1079 (w), 1048 (vw), 1015 (w), 977 (vw), 950 (vw), 921 (vw), 904 (vw), 878 (vw), 829 (vs), 781 (m), 742 (vw), 704 (w), 624 (vw), 611 (vw), 583 (vw), 555 (s), 446 (w), 419 (w), 390 (m) cm^{-1} .

HR-MS (ESI $^+$): $\text{C}_{16}\text{H}_{19}\text{O}_2\text{Ru}$ (M^+) calcd.: 345.0428, found: 345.0418.

5.2.2.4. Synthesis of (η^6 -benzene)(η^5 -2,4-dimethylcyclopentadienylcarboxylic acid) ruthenium hexafluorophosphate



The deprotection was performed according to a similar literature procedure using a non-methylated cyclopentadiene.^[49] A solution of 1.90 g of the sandwich complex **177** (3.88 mmol, 1.00 eq) in CH₃CN (61 mL) was prepared and a solution of 3.22 g K₂CO₃ (23.3 mmol, 6.01 eq) in 61 mL H₂O was added. The reaction mixture was stirred at 100 °C for 3 h and then cooled to 0 °C. The solution was acidified to pH 1-2 with 6 N HCl_{aq.} and excess solid NH₄PF₆ was added. The CH₃CN was removed under reduced pressure and the aqueous solution was left at 4 °C over night. The resulting precipitate was filtered, washed with H₂O and diethyl ether, and dried *in vacuo* to give 1.62 g of the carboxylic acid **178** (3.51 mmol, 91%) as a light brown solid.

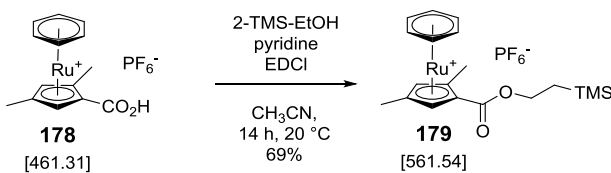
¹H-NMR (300.1 MHz, CD₃CN): δ = 9.82 (br s, 1H), 6.06 (s, 6H), 5.69 (d, ⁴J = 1.5 Hz, 1H), 5.49 (d, ⁴J = 1.4 Hz, 1H), 2.20 (s, 3H), 1.97 (s, 3H) ppm.

¹³C-NMR (75.5 MHz, CD₃CN): δ = 167.3 (C_q), 101.4 (C_q), 100.4 (C_q), 88.9, 86.8, 84.0 (C_q), 83.0, 13.8, 13.7 ppm.

ATR-IR (neat) $\tilde{\nu}$ = 3095 (vw), 2611 (vw), 1707 (m), 1443 (w), 1385 (vw), 1306 (vw), 1265 (w), 1074 (vw), 1040 (vw), 924 (vw), 825 (vs), 744 (m), 616 (vw), 553 (m), 480 (m) cm⁻¹.

HR-MS (ESI⁺): C₁₄H₁₅O₂Ru (M)⁺ calcd.: 317.0114, found: 317.0109.

5.2.2.5. Synthesis of (η^6 -benzene)(η^5 -2-(trimethylsilyl)ethyl-2,4-dimethylcyclopenta-dienylcarboxylat) ruthenium hexafluorophosphate



The ester coupling was performed according to a similar literature procedure using a non-methylated cyclopentadiene.^[49] A solution of 800 mg of the carboxylic acid **178** (1.73 mmol, 1.00 eq) in 7.8 mL CH₃CN was purged with N₂ before 497 μL 2-(trimethylsilyl)ethanol (3.47 mmol, 2.00 eq), 283 μL pyridine (3.47 mmol, 2.00 eq) and 352 mg *N*-(3-dimethylaminopropyl)-*N'*-

Compound preparation for toxicity approach

ethylcarbodiimide hydrochloride (2.27 mmol, 1.31 eq) were added. The reaction mixture was left to stir over night at room temperature. The mixture was diluted with 80 mL CH_2Cl_2 , washed with saturated $\text{NH}_4\text{Cl}_{\text{aq}}$ solution and brine (each 20 mL) dried over Na_2SO_4 and filtered. The solvent was removed *in vacuo* and the crude material was subjected to silica gel chromatography ($\text{CH}_3\text{CN}/\text{H}_2\text{O}/\text{KNO}_3$ $_{\text{aq sat}}$ 50:3:1 to 50:6:2). The combined product eluents were dried under reduced pressure and the remaining residue was dissolved in 50 mL H_2O . Excess NH_4PF_6 was added and the product extracted with CH_2Cl_2 (250 mL). The organic layer was washed with 40 mL H_2O , dried over Na_2SO_4 , filtered, and removed *in vacuo* to result in 669 mg (1.19 mmol, 69%) of the ethyl-TMS-ester **179** as brown solid.

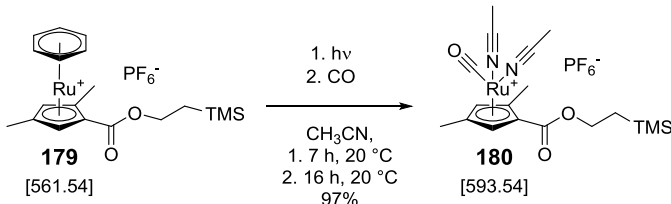
$^1\text{H-NMR}$ (300.1 MHz, CD_3CN): δ = 6.05 (s, 6H), 5.68 (d, 4J = 1.5 Hz, 1H), 5.48 (d, 4J = 1.4 Hz, 1H), 4.35-4.28 (m, 2H), 2.21 (s, 3H), 1.97 (s, 3H), 1.13-1.07 (m, 2H), 0.08 (s, 9H, TMS) ppm.

$^{13}\text{C-NMR}$ (75.5 MHz, CD_3CN): δ = 166.7 (C_q), 101.2 (C_q), 100.4 (C_q), 88.8, 86.7, 84.7 (C_q), 82.6, 65.0, 18.0, 13.8, 13.7, -1.5 (3C) ppm.

ATR-IR (neat) $\tilde{\nu}$ = 3096 (vw), 2952 (vw), 2928 (vw), 1725 (m) 1492 (vw), 1442 (w), 1417 (w), 1386 (w), 1301 (vw), 1251 (w), 1224 (s), 1174 (w), 1062 (m), 1041 (w), 943 (vw), 929 (vw), 825 (vs), 781 (w), 761 (w), 717 (w), 695 (w), 627 (w), 613 (vw), 556 (s), 464 (w), 414 (w), 396 (w) cm^{-1} .

HR-MS (ESI $^+$): $\text{C}_{19}\text{H}_{27}\text{O}_2\text{RuSi} (\text{M})^+$ calcd.: 417.0823, found: 417.0839.

5.2.2.6. Synthesis of η^5 -2-(trimethylsilyl)ethyl-2,4-dimethylcyclopentadienyl carboxylate ruthenium hexafluorophosphate



A clear solution of 669 mg of the TMS-ester **179** (1.19 mmol, 1.00 eq) in 800 mL CH_3CN was irradiated with a medium pressure Hg lamp (750 W) for 5.5 h with a stream of N_2 flowing through the solution throughout the photolysis. The solvent was removed *in vacuo* and the tris-acetonitrile complex was redissolved in 80.5 mL CH_3CN . The resulting solution was purged with CO (g) for 10 min and stirred under CO atmosphere for 16 h at room temperature. After removal of the solvent under reduced pressure, 691 mg of the desired product **180** (1.16 mmol, 97%) was obtained as a brown solid.

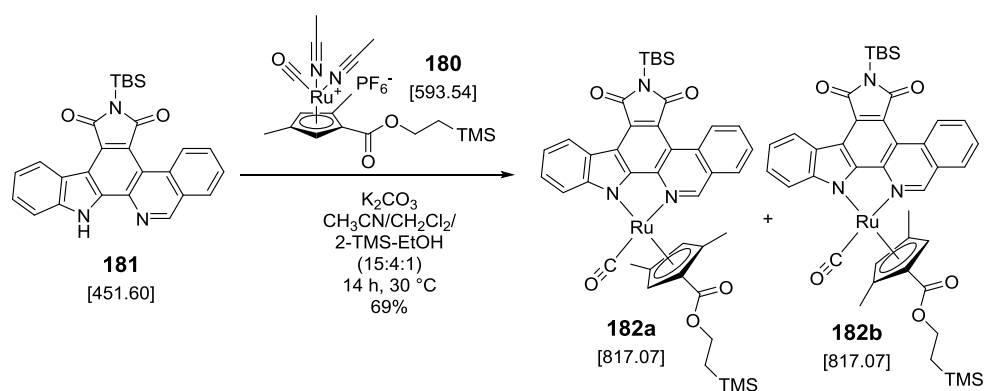
¹H-NMR (300.1 MHz, CD₃CN): δ = 5.36 (d, ⁴J = 1.7 Hz, 1H), 5.00 (d, ⁴J = 1.7 Hz, 1H), 4.31-4.25 (m, 2H), 2.39 (s, 3H), 2.39 (s, 3H), 2.06 (s, 3H), 1.81 (s, 3H), 1.08-1.02 (m, 2H), 0.06 (m, 9H) ppm.

¹³C-NMR (75.5 MHz, CD₃CN): δ = 198.8 (*C_q*), 167.0 (*C_q*), 129.2 (*C_q*), 114.5 (*C_q*), 102. (*C_q*), 82.4, 80.9, 75.2 (*C_q*), 64.8, 18.1, 13.3, 12.9, 4.4, 1.5 (*3C*) ppm.

ATR-IR (neat) $\tilde{\nu}$ = 2954 (vw), 2924 (vw), 2854 (vw), 1994 (m), 1712 (m), 1491 (vw), 1415 (w), 1377 (vw), 1298 (vw), 1248 (w), 1223 (m), 1177 (w), 1067 (w), 1037 (w), 945 (vw), 827 (vs), 775 (w), 740 (w), 697 (w), 611 (vw), 556 (s), 508 (w), 456 (w), 422 (vw), 389 (vw).

HR-MS (ESI⁺): C₁₈H₂₇N₂O₃RuSi (M)⁺ calcd.: 449.0834, found: 449.0831.

5.2.2.7. Synthesis of η^5 -2-(trimethylsilyl)ethyl-2,4-dimethylcyclopentadienyl carboxylate diastereomeric complexes **182a** and **182b**



A suspension of 452 mg TBS-protected isoquinolinocarbazole **181**^[148] (1.00 mmol, 1.00 eq), 669 mg precursor **180** (1.12 mmol, 1.12 eq), and 152 mg K₂CO₃ (1.10 mmol, 1.10 eq) in a 15:4:1 mixture of CH₃CN/CH₂Cl₂/2-TMS-EtOH (35 mL, 9.3 mL, 2.3 mL) was stirred at 30 °C over night. The solvent was removed *in vacuo* and the crude material was subjected to silica gel chromatography with toluene as eluent. The combined product eluents were dried resulting in 565 mg of the diastereomeric mixture **182a** and **182b** (0.69 mmol, 69%) as a dark red solid. Before HPLC separation, the material was dissolved in 3.5 mL CH₂Cl₂ and filtered through a syringe filter (PVDF, 0.2 μm). The diastereomers were separated via semipreparative HPLC using a 100-5 NUCLEODUR® silica column (10 x 250 mm, MACHEREY-NAGEL, 30 °C, 93:7 hexane/ethyl acetate, flow rate = 6.0 mLmin⁻¹). For each run 50 μL of the prepared CH₂Cl₂ solution was injected which resulted in a clean separation of the two diastereomers.

182a:

¹H-NMR (300.1 MHz, CDCl₃): δ = 10.58 (dd, ³J = 8.5 Hz, ⁴J = 0.5 Hz, 1H), 9.47 (s, 1H), 9.10 (d, ³J = 7.8 Hz, 1H), 8.14-8.05 (m, 2H), 7.84 (ddd, ³J = 7.9 Hz, ³J = 7.0 Hz, ⁴J = 0.9 Hz, 1H), 7.62-7.52 (m, 2H), 7.38 (ddd, ³J = 7.9 Hz, ³J = 6.7 Hz, ⁴J = 1.4 Hz, 1H), 5.48 (d, ⁴J = 1.6 Hz, 1H), 4.92 (d, ⁴J = 1.6 Hz, 1H), 3.78 (ddd, ²J = 12.2 Hz, ³J = 10.9 Hz, ³J = 5.6 Hz, 1H), 3.61 (ddd, ²J = 12.2 Hz, ³J = 10.9 Hz, ³J = 5.6 Hz, 1H), 2.14 (s, 3H, Cp-CH₃), 1.91 (s, 3H, Cp-CH₃), 1.09 (s, 9H, TBS), 0.67 (s, 6H, TBS), 0.21-0.00 (m, 2H), -0.25 (s, 9H, TMS) ppm.

¹³C-NMR (125.8 MHz, CDCl₃): δ = 200.6 (C_q), 175.4 (C_q), 174.8 (C_q), 165.9 (C_q), 159.6, 156.0 (C_q), 152.4 (C_q), 140.0 (C_q), 133.6 (C_q), 133.0, 132.8 (C_q), 130.3, 128.5, 128.2, 128.2 (C_q), 126.6, 126.2, 124.5 (C_q), 120.4 (C_q), 119.6, 117.3 (C_q), 116.2 (C_q), 116.1 (C_q), 114.9, 100.0 (C_q), 82.6 (C_q), 79.5, 73.5, 63.0, 26.8, 19.4 (C_q), 17.2, 14.4, 13.9, -1.7, -3.4 ppm.

ATR-IR (neat) $\tilde{\nu}$ = 3121 (vw), 3089 (vw), 3062 (vw), 2952 (w), 2892 (w), 2856 (w), 1952 (vs), 1737 (w), 1683 (vs), 1619 (w), 1577 (w), 1533 (w), 1465 (w), 1433 (w), 1370 (w), 1327 (m), 1293 (vs), 1254 (w), 1221 (s), 1172 (w), 1069 (m), 1034 (w), 938 (w), 827 (vs), 756 (s), 690 (w), 659 (w), 612 (vw), 581 (vw), 550 (vw), 502 (vw), 438 (vw), 407 (vw) cm⁻¹.

HR-MS (ESI⁺): C₄₁H₄₅N₃O₅RuSi₂Na (M+Na⁺) calcd.: 840.1844, found: 840.1838.

182b:

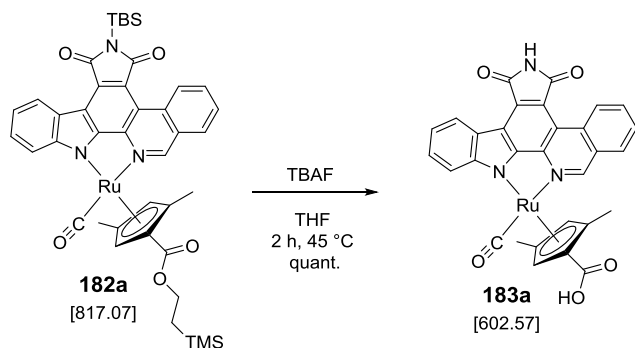
¹H-NMR (300.1 MHz, CDCl₃): δ = 10.58 (d, ³J = 8.5 Hz, 1H), 9.36 (s, 1H), 9.09 (d, ³J = 7.9 Hz, 1H), 8.12-8.03 (m, 2H), 7.82 (ddd, ³J = 8.0 Hz, ³J = 7.0 Hz, ⁴J = 0.9 Hz, 1H), 7.65-7.58 (m, 2H), 7.38 (ddd, ³J = 8.0 Hz, ³J = 5.9 Hz, ⁴J = 2.1 Hz, 1H), 5.72 (d, ⁴J = 1.4 Hz, 1H), 5.11 (d, ⁴J = 1.7 Hz, 1H), 4.24-4.05 (m, 2H), 2.30 (s, 3H), 1.69 (s, 3H), 1.09 (s, 9H, TBS), 0.77-0.69 (m, 2H), 0.67 (s, 6H, TBS), 0.02 (s, 9H, TMS) ppm.

¹³C-NMR (125.8 MHz, CDCl₃): δ = 200.1 (C_q), 175.4 (C_q), 174.7 (C_q), 168.2 (C_q), 158.1, 155.6 (C_q), 152.7 (C_q), 140.2 (C_q), 133.6 (C_q), 133.0 (C_q), 133.0, 130.3, 128.4, 128.2 (C_q), 128.0, 126.8, 126.2, 124.5 (C_q), 120.7 (C_q), 119.6, 117.1 (C_q), 116.4 (C_q), 114.7, 107.5 (C_q), 104.7 (C_q), 90.4, 75.9 (C_q), 73.7, 63.3, 26.8, 19.4 (C_q), 17.4, 14.3, 13.2, -1.4, -3.4 ppm.

ATR-IR (neat) $\tilde{\nu}$ = 3120 (vw), 3091 (vw), 3061 (vw), 2950 (w), 2892 (w), 2855 (w), 1954 (vs), 1738 (w), 1682 (vs), 1619 (w), 1577 (w), 1533 (w), 1466 (w), 1431 (w), 1368 (w), 1327 (m), 1293 (vs), 1255 (w), 1220 (s), 1069 (m), 1034 (w), 935 (w), 826 (s), 755 (s), 690 (w), 658 (w), 612 (vw), 581 (vw) cm⁻¹.

HR-MS (ESI⁺): C₄₁H₄₅N₃O₅RuSi₂Na (M+Na)⁺ calcd.: 840.1844, found: 840.1831.

5.2.2.8. Synthesis of η^5 -2,4-dimethylcyclopentadienylcarboxylic acid complex 183a



To a solution of the bisprotected complex **182a** (140 mg, 171 μmol , 1.00 eq) in 14 mL THF was added 685 μL tetrabutylammoniumfluoride (1 M in THF, 685 μmol , 4.00 eq) and the reaction mixture was heated to 45 $^\circ\text{C}$ for 2 h under nitrogen atmosphere. After cooling to 0 $^\circ\text{C}$, 7 mL saturated $\text{NH}_4\text{Cl}_{\text{aq}}$ solution was added. The complex was extracted with EtOAc (2x 20 mL) and washed with 15 mL HCl_{aq} (1 M), 20 mL water, and 15 mL brine. The organic layer was dried using MgSO_4 , filtered, and the solvent *in vacuo*. The crude material was subjected to silica gel chromatography (dry load, CH_2Cl_2 to $\text{CH}_2\text{Cl}_2/\text{MeOH}$ 50:1 to 10:1). The combined product eluents were dried to provide carboxylic acid **183a** (107 mg, quant.) as a red-purple solid. Small aliphatic impurities were carried over to the next step.

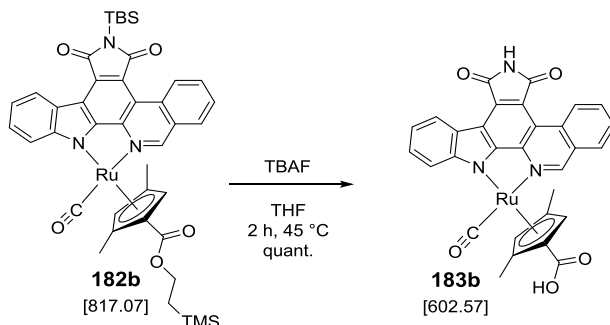
$^1\text{H-NMR}$ (300.1 MHz, $\text{DMSO}-d_6$): $\delta = 12.35$ (br s, 1H), 11.35 (s, 1H), 10.55 (d, $^3J = 8.5$ Hz, 1H), 10.06 (s, 1H), 8.88 (d, $^3J = 7.8$ Hz, 1H), 8.43 (d, $^3J = 7.6$ Hz, 1H), 8.16 (ddd, $^3J = 8.8$ Hz, $^3J = 7.2$ Hz, $^4J = 1.0$ Hz, 1H), 8.02-7.97 (m, 1H), 7.68 (d, $^3J = 8.2$ Hz, 1H), 7.60-7.54 (m, 1H), 7.36-7.31 (m, 1H), 5.87 (d, $^4J = 1.0$ Hz, 1H), 5.44 (d, $^4J = 1.2$ Hz, 1H), 2.01 (s, 3H), 1.92 (s, 3H) ppm.

$^{13}\text{C-NMR}$ (100.6 MHz, $\text{DMSO}-d_6$): $\delta = 201.8$ (C_q), 170.9 (C_q), 170.0 (C_q), 166.8 (C_q), 161.3, 154.9 (C_q), 151.9 (C_q), 138.8 (C_q), 132.9, 131.5 (C_q), 131.3 (C_q), 129.4, 128.9, 128.6, 128.0 (C_q), 126.6, 125.0, 123.4 (C_q), 119.8 (C_q), 119.1, 116.3 (C_q), 115.3, 114.7 (C_q), 114.3 (C_q), 101.4 (C_q), 82.7, 82.0 (C_q), 72.3, 13.6, 13.3 ppm.

ATR-IR (neat) $\tilde{\nu} = 2922$ (w), 2853 (vw), 2736 (vw), 1940 (s), 1740 (w), 1692 (s), 1618 (vw), 1577 (m), 1533 (w), 1483 (w), 1459 (w), 1433 (w), 1377 (w), 1328 (w), 1294 (w), 1223 (m), 1164 (vw), 1124 (vw), 1019 (m), 996 (m), 863 (vw), 818 (w), 752 (s), 691 (m), 639 (m), 582 (vw), 549 (w), 512 (w), 494 (w), 461 (m), 440 (w) cm^{-1} .

HR-MS (ESI $^+$): $\text{C}_{30}\text{H}_{19}\text{N}_3\text{O}_5\text{RuNa}$ ($M+\text{Na}$) $^+$ calcd.: 626.0269, found: 626.0260.

5.2.2.9. Synthesis of η^5 -2,4-dimethylcyclopentadienylcarboxylic acid complex **183b**



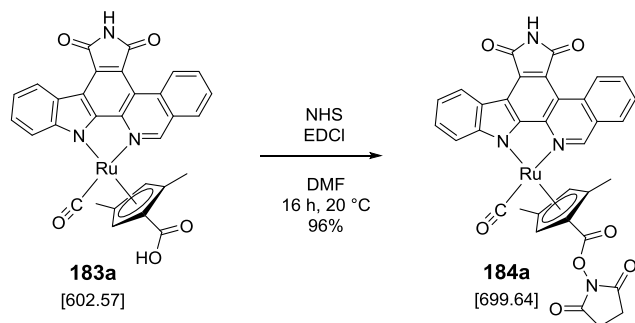
To a solution of 181 mg of the TMS-ester **182b** (222 μ mol, 1.00 eq) in 18.1 mL THF was added 886 μ L of tetrabutylammoniumfluoride in THF (1 M, 886 μ mol, 4.00 eq). The reaction mixture was stirred for 2 h at 45 °C under nitrogen atmosphere and was then cooled to 0 °C. The reaction was quenched by dropwise addition of 9 mL saturated NH₄Cl_{aq} solution. The product was extracted with EtOAc (2 x 20 mL) and the combined organic layers were washed with 1 M HCl and brine (each 20 mL), dried over Na₂SO₄, filtered, and evaporated. The solvent was removed under reduced pressure and the crude product was subjected to silica gel chromatography (CH₂Cl₂ to CH₂Cl₂/MeOH 40:1 to 5:1). Insoluble residues were washed from the column with acetone and subjected to a second silica gel chromatography. The combined product eluents were dried to provide carboxylic acid **183b** (157 mg, quant.) as a red-purple solid. Small aliphatic impurities were carried over to the next step.

¹H-NMR (300.1 MHz, DMSO-*d*₆): δ = 11.35 (s, 1H, NH), 10.52 (d, ³*J* = 8.6 Hz, 1H), 9.82 (s, 1H), 8.88 (d, ³*J* = 7.8 Hz, 1H), 8.38 (d, ³*J* = 7.7 Hz, 1H), 8.14-8.09 (m, 1H), 7.94-7.89 (m, 1H), 7.79 (d, ³*J* = 8.2 Hz, 1H), 7.63-7.58 (m, 1H), 7.37-7.32 (m, 1H), 5.87 (s, 1H, *H*_{Cp}), 5.49 (d, *J* = 1.5 Hz, 1H, *H*_{Cp}), 2.23 (s, 3H, Cp-CH₃), 1.65 (s, 3H, Cp-CH₃) ppm.

¹³C-NMR (100.6 MHz, DMSO-*d*₆): δ = 201.6 (*C*_q), 171.0 (*C*_q), 170.0 (*C*_q), **169.3 (C_q)**, **158.9**, 154.7 (*C*_q), 152.2 (*C*_q), 139.2 (*C*_q), 132.8, 131.5 (*C*_q), 131.4 (*C*_q), 129.2, 128.9, 128.5, 127.5 (*C*_q), 126.7, 124.9, 123.4 (*C*_q), 120.0 (*C*_q), 119.1, 116.3 (*C*_q), 115.3, 114.2 (*C*_q), **108.2 (C_q)**, **104.8 (C_q)**, **89.7**, 77.9 (*C*_q), **74.1**, 13.5, 12.6 ppm. Signals belonging to the Cp-system appear as tiny broad signals in the spectrum and are indicated as bold characters.

ATR-IR (neat) $\tilde{\nu}$ = 3091 (vw), 3048 (vw), 2957 (vw), 2870 (vw), 1972 (s), 1939 (m), 1740 (w), 1684 (s), 1621 (vw), 1579 (m), 1536 (vw), 1460 (w), 1436 (m), 1376 (w), 1345 (w), 1327 (m), 1298 (w), 1261 (w), 1225 (m), 1157 (vw), 1125 (vw), 1069 (w), 1019 (w), 972 (vw) 911 (vw), 867 (w), 742 (m), 691 (w), 638 (m), 612 (vw), 580 (vw), 546 (w), 506 (w), 463 (m), 436 (w) 395 (vw) cm⁻¹.

HR-MS (ESI⁺): C₃₀H₁₉N₃O₅RuNa (M+Na)⁺ calcd.: 626.0265, found: 626.0256.

5.2.2.10. Synthesis of NHS-ester complex **184a**

A solution of the carboxylic acid **183a** (85 mg, 141 μmol , 1.00 eq) in 5 mL DMF was purged with nitrogen and cooled to 0 °C. *N*-hydroxysuccinimide (24 mg, 212 μmol , 1.50 eq) and 1-ethyl-3-(3-dimethylaminopropyl)carbodiimide (41 mg, 212 μmol , 1.50 eq) were added and the mixture was stirred at room temperature overnight. The solution was cooled to 0 °C, diluted with 10 mL CH_2Cl_2 , and 6 mL saturated $\text{NH}_4\text{Cl}_{\text{aq}}$ solution were added dropwise. The organic layers were separated and the aqueous layer was extracted with CH_2Cl_2 (15 mL). The combined organic layers were washed with water (2 x 15 mL) and brine (15 mL), dried over Na_2SO_4 , filtered, and concentrated *in vacuo*. The crude material was purified via silica gel chromatography (CH_2Cl_2 to $\text{CH}_2\text{Cl}_2/\text{MeOH}$ 200:1 to 100:1). The combined product eluents were dried to provide the active ester **184a** (95 mg, 136 μmol , 96%) as a dark red solid. Small aliphatic impurities were carried over to the next step.

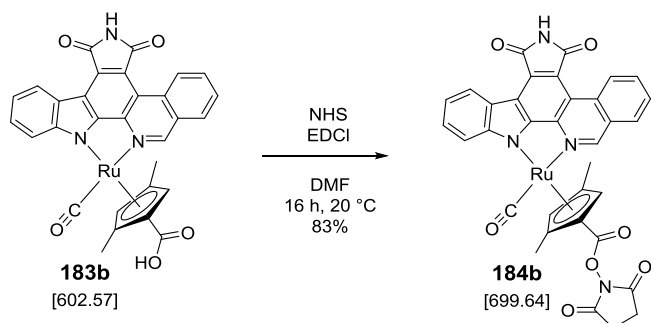
$^1\text{H-NMR}$ (300.1 MHz, $\text{DMSO}-d_6$): $\delta = 11.35$ (s, 1H), 10.55 (d, $^3J = 8.6$ Hz, 1H), 10.08 (s, 1H), 8.87 (d, $^3J = 7.2$ Hz, 1H), 8.36 (dd, $^3J = 8.2$ Hz, $^4J = 0.9$ Hz, 1H), 8.14 (ddd, $^3J = 8.5$ Hz, $^3J = 7.1$ Hz, $^4J = 1.4$ Hz, 1H), 7.99-7.94 (m, 2H), 7.66 (d, $^3J = 8.2$ Hz, 1H), 7.56 (ddd, $^3J = 8.0$ Hz, $^3J = 7.0$ Hz, $^4J = 1.1$ Hz, 1H), 7.33 (ddd, $^3J = 7.8$ Hz, $^3J = 7.1$ Hz, $^4J = 0.8$ Hz, 1H), 6.26 (d, $^4J = 1.2$ Hz, 1H), 5.66 (d, $^4J = 1.3$ Hz, 1H), 2.16 (s, 3H), 2.07 (s, 3H) ppm. The signals of the succinimide CH_2 groups are located under the DMSO signal.

$^{13}\text{C-NMR}$ (100.6 MHz, $\text{DMSO}-d_6$): $\delta = 200.8$ (C_q), 171.1 (2 C_q), 170.0 (2 C_q), 161.6 (C_q), 161.5, 155.2 (C_q), 151.5 (C_q), 139.1 (C_q), 132.8, 131.7 (C_q), 131.3 (C_q), 129.3, 128.9, 128.4, 128.3 (C_q), 126.6, 125.0, 123.5 (C_q), 120.5 (C_q), 119.1, 116.5 (C_q), 116.2, 115.2 (C_q), 114.7 (C_q), 100.7 (C_q), 83.6, 75.4 (C_q), 73.8, 25.1 (2C), 14.0, 13.4 ppm.

ATR-IR (neat) $\tilde{\nu} = 3051$ (vw), 2961 (vw), 2923 (vw), 2854 (vw), 1956 (s), 1735 (s), 1697 (s), 1660 (s), 1578 (m), 1533 (w), 1484 (w), 1459 (w), 1433 (w), 1404 (w), 1378 (w), 1330 (w), 1328 (w), 1295 (w), 1263 (w), 1224 (w), 1197 (m), 1158 (w), 1093 (w), 1062 (s), 1017 (m), 964 (w), 935 (w), 865 (vw), 804 (w), 747 (s), 689 (w), 639 (w), 608 (w), 549 (vw), 515 (vw), 462 (w), 438 (w), 393 (w) cm^{-1} .

HR-MS (ESI $^+$): $\text{C}_{34}\text{H}_{22}\text{N}_4\text{O}_7\text{RuH}$ ($M+\text{H}$) $^+$ calcd. 701.0614, found 701.0610.

5.2.2.11. Synthesis of NHS-ester complex **184b**



A solution of the carboxylic acid **183b** (52 mg, 86.3 μmol , 1.00 eq) in 5 mL DMF was purged with nitrogen and cooled to 0 °C. *N*-hydroxysuccinimide (15 mg, 129 μmol , 1.50 eq) and 1-ethyl-3-(3-dimethylaminopropyl)carbodiimide (25 mg, 129 μmol , 1.50 eq) were added and the mixture was stirred at room temperature overnight. The solution was cooled to 0 °C, diluted with 5 mL CH_2Cl_2 , 5 mL saturated NH_4Cl solution were added dropwise and further diluted with 5 mL H_2O . The organic layers were separated and the aqueous layer was extracted with CH_2Cl_2 (3 x 5 mL). The combined organic layers were washed with water (2 x 20 mL), dried over Na_2SO_4 , filtered, and concentrated *in vacuo*. The crude material was purified via silica gel chromatography (eluent hex/EtOAc 10:1 to 1:1). The combined product eluents were dried to provide the active ester **184b** (50 mg, 83%) as a dark red solid. Small aliphatic impurities were carried over to the next step.

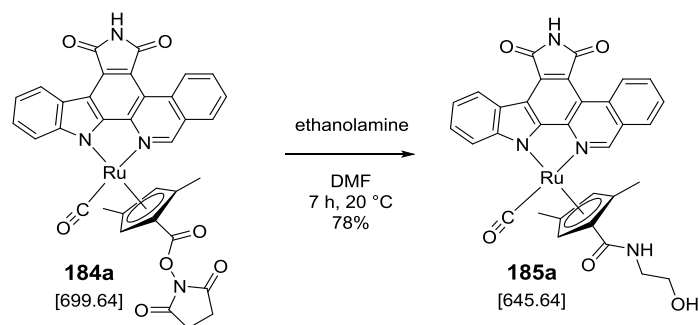
$^1\text{H-NMR}$ (300.1 MHz, $\text{DMSO}-d_6$): $\delta = 11.40$ (s, 1H), 10.56 (d, ${}^3J = 8.6$ Hz), 9.96 (s, 1H), 8.89 (d, ${}^3J = 7.6$ Hz, 1H), 8.44 (dd, ${}^3J = 8.3$ Hz, ${}^4J = 0.9$ Hz, 1H), 8.18 (ddd, ${}^3J = 8.6$ Hz, ${}^3J = 7.1$ Hz, ${}^4J = 1.4$ Hz, 1H), 8.00 (ddd, ${}^3J = 8.0$ Hz, ${}^3J = 7.0$ Hz, ${}^4J = 0.8$ Hz, 1H), 7.83 (d, ${}^3J = 8.3$ Hz, 1H), 7.63 (ddd, ${}^3J = 8.2$ Hz, ${}^3J = 7.1$ Hz, ${}^4J = 1.2$ Hz, 1H), 7.37 (ddd, ${}^3J = 7.8$ Hz, ${}^3J = 7.1$ Hz, ${}^4J = 0.7$ Hz, 1H), 6.19 (d, ${}^4J = 1.0$ Hz, 1H), 6.00 (d, ${}^4J = 1.6$ Hz, 1H), 2.98 (br s, 4H), 2.40 (s, 3H), 1.46 (s, 3H) ppm.

$^{13}\text{C-NMR}$ (100.6 MHz, $\text{DMSO}-d_6$): $\delta = 200.0$ ($2C_q$), 170.9 ($2C_q$), 169.9 ($2C_q$), 164.5 (C_q), 159.4, 154.6 (C_q), 151.8 (C_q), 139.0 (C_q), 133.2, 131.6 ($2C_q$), 129.3, 128.9, 128.7, 127.8 (C_q), 127.0, 125.0, 123.5 (C_q), 120.4 (C_q), 119.3, 116.3 (C_q), 114.9, 114.7 (C_q), 109.6 (C_q), 106.5 (C_q), 94.7, 75.1 (C_q), 66.9, 25.6 (2C), 14.0, 11.9 ppm.

ATR-IR (neat) $\tilde{\nu} = 3441$ (w), 3110 (vw), 304 (vw), 2925 (vw), 1934 (s), 1734 (vs), 1621 (w), 1580 (w), 1534 (w), 1483 (w), 1462 (w), 1433 (w), 1405 (w), 1373 (w), 1329 (w), 1296 (w), 1204 (m), 1158 (w), 1064 (m), 1013 (w), 968 (w), 936 (w), 875 (vw), 814 (vw), 743 (s), 691 (w), 642 (m), 609 (w), 556 (w), 496 (m), 461 (m), 432 (vw), 395 (vw) cm^{-1} .

HR-MS (ESI $^+$): $\text{C}_{34}\text{H}_{22}\text{N}_4\text{O}_7\text{RuH}$ ($M+\text{H}$) $^+$ calcd.: 701.0614, found: 701.0610.

5.2.2.12. Synthesis of np830 (80a)



A solution of the active ester **184a** (46 mg, 65.7 μmol , 1.00 eq) and ethanolamine (235 μL , 240 μmol , 3.65 eq) in 5 mL DMF was purged with nitrogen for 10 min and stirred at room temperature for 7 h. The reaction mixture was diluted with CH_2Cl_2 and washed with water (2 \times 10 mL) and brine (5 mL). The aqueous layer was extracted with CH_2Cl_2 and the combined organic layers were dried over MgSO_4 and filtered. The solvent was removed *in vacuo* after addition of 300 mg silica gel and the crude material was purified via silica gel chromatography using CH_2Cl_2 and $\text{CH}_2\text{Cl}_2/\text{MeOH}$ (100:1 to 50:1). The combined product eluents were concentrated, extensively washed with water and subjected a second time to silica gel chromatography to provide the desired complex **185a** (33 mg, 51.1 μmol , 78%) as a red-purple solid.

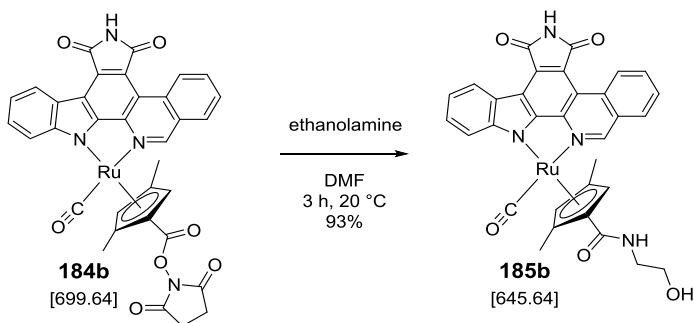
$^1\text{H-NMR}$ (300.1 MHz, $\text{DMSO}-d_6$): $\delta = 11.33$ (s, 1H), 10.54 (d, ${}^3J = 8.6$ Hz, 1H), 9.97 (s, 1H), 8.87 (d, ${}^3J = 7.8$ Hz, 1H), 8.37 (dd, ${}^3J = 8.1$ Hz, ${}^4J = 1.0$ Hz, 1H), 8.15 (ddd, ${}^3J = 8.6$, ${}^3J = 7.1$, ${}^4J = 1.5$ Hz 1H), 8.01-7.96 (m, 2H), 7.62 (d, ${}^3J = 8.0$ Hz, 1H), 7.57 (ddd, ${}^3J = 6.8$ Hz, ${}^3J = 8.2$ Hz, ${}^4J = 1.2$ Hz, 1H), 7.33 (ddd, ${}^3J = 6.8$ Hz, ${}^3J = 7.9$ Hz, ${}^4J = 1.2$ Hz, 1H), 5.89 (d, ${}^4J = 1.2$, 1H), 5.36 (d, ${}^4J = 1.3$ Hz, 1H), 4.47 (t, ${}^3J = 4.4$ Hz, 1H), 3.04-2.69 (m, 4H), 1.94 (s, 3H), 1.93 (s, 3H) ppm.

$^{13}\text{C-NMR}$ (125.8 MHz, $\text{DMSO}-d_6$): $\delta = 202.0$ (C_q), 171.0 (C_q), 170.0 (C_q), 164.1 (C_q), 160.6, 155.0 (C_q), 152.2 (C_q), 138.8 (C_q), 132.8, 131.5 (C_q), 131.2 (C_q), 129.1, 128.9, 128.6, 127.9 (C_q), 126.5, 124.9, 123.4 (C_q), 119.8 (C_q), 119.0, 116.3 (C_q), 115.3, 114.1 (C_q), 112.9 (C_q), 102.5 (C_q), 86.6, 78.7 (C_q), 72.1, 59.2, 41.4, 13.3, 13.2 ppm.

ATR-IR (neat) $\tilde{\nu} = 3303$ (vw), 3183 (vw), 3074 (vw), 2919 (vw), 2852 (vw), 1927 (s), 1745 (w), 1697 (m), 1631 (m), 1577 (w), 1537 (m), 1464 (w), 1434 (w), 1378 (w), 1335 (m), 1296 (m), 1261 (w), 1224 (m), 1168 (vw), 1110 (vw), 1071 (w), 1016 (w), 939 (vw), 866 (vw), 807 (w), 758 (s), 719 (m), 690 (m), 639 (m), 507 (w), 559 (w), 513 (w), 463 (m), 435 (w) cm^{-1} .

HR-MS (ESI $^+$): $\text{C}_{32}\text{H}_{24}\text{N}_4\text{O}_5\text{RuNa}$ ($M+\text{H}$) $^+$ calcd.: 669.0691, found.: 669.0669.

5.2.2.13. Synthesis of np829 (80b)



A solution of the active ester **184b** (50 mg, 71.5 μ mol, 1.00 eq) and ethanolamine (210 μ L, 214 μ mol, 3.00 eq) in 5 mL DMF was purged with nitrogen for 10 min and stirred at room temperature for 3 h. The reaction mixture was diluted with CH_2Cl_2 and washed with water (2 x 15 mL) and brine (15 mL). The aqueous layer was extracted with CH_2Cl_2 and the combined organic layers were dried over MgSO_4 , filtered, and the residue was washed extensively with CH_2Cl_2 and traces of acetone. The solvents were removed *in vacuo* after addition of 200 mg silica gel and the crude material was purified via silica gel chromatography using CH_2Cl_2 and $\text{CH}_2\text{Cl}_2/\text{MeOH}$ (100:1 to 50:1). The combined product eluents were dried to provide the desired complex **185b** (43 mg, 66.6 μ mol, 93%) as a red-purple solid.

$^1\text{H-NMR}$ (300.1 MHz, $\text{DMSO}-d_6$): $\delta = 11.35$ (s, 1H), 10.56 (d, $^3J = 8.7$ Hz, 1H), 9.66 (s, 1H), 8.87 (d, $^3J = 7.5$ Hz, 1H), 8.40 (d, $^3J = 7.2$ Hz, 1H), 8.16 (ddd, $^3J = 7.0$ Hz, $^3J = 8.6$ Hz, $^4J = 1.4$, 1H), 8.02-7.95 (m, 2H), 7.78 (d, $^3J = 8.2$ Hz, 1H), 7.60 (ddd, $^3J = 7.1$ Hz, $^3J = 8.2$ Hz, $^4J = 1.2$ Hz, 1H), 7.36-7.31 (m, 1H), 5.96 (d, $^4J = 1.4$ Hz, 1H), 5.42 (d, $^4J = 1.5$ Hz, 1H), 4.69 (t, $^3J = 5.5$ Hz, 1H), 3.33-3.23 (m, 2H), 3.22-3.11 (m, 2H), 2.21 (s, 3H), 1.63 (s, 3H) ppm.

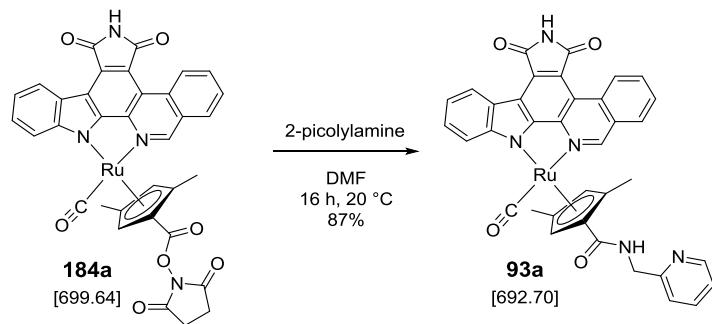
$^{13}\text{C-NMR}$ (100.6 MHz, $\text{DMSO}-d_6$): $\delta = 201.6$ (C_g), 171.0 (C_g), 170.0 (C_g), 165.4 (C_g), 159.1, 154.7 (C_g), 152.0 (C_g), 139.1 (C_g), 132.8, 131.5 (C_g), 131.4 (C_g), 129.4, 128.9, 128.6, 127.6 (C_g), 126.6, 124.9, 123.4 (C_g), 120.0 (C_g), 119.1, 116.3 (C_g), 115.3, 114.1 (C_g), 107.6 (C_g), 106.4 (C_g), 84.9, 81.9 (C_g), 72.4, 59.4, 41.7, 13.4, 12.8 ppm.

ATR-IR (neat) $\tilde{\nu} = 3456$ (vw), 3361 (vw), 3173 (vw), 3085 (vw), 2929 (vw), 1943 (s), 1742 (m), 1688 (m), 1628 (w), 1577 (w), 1527 (m), 1481 (vw), 1459 (w), 1434 (w), 1378 (w), 1330 (w), 1293 (m), 1268 (w), 1224 (m), 1162 (vw), 1123 (vw), 1063 (w), 1020 (w), 905 (vw), 864 (vw), 847 (vw), 811 (vw), 743 (s), 691 (w), 642 (w), 579 (vw), 555 (w), 498 (w), 462 (w), 433 (vw).

HR-MS (ESI $^+$): $\text{C}_{32}\text{H}_{24}\text{N}_4\text{O}_5\text{RuH}$ ($\text{M}+\text{H}$) $^+$ calcd.: 647.0872, found: 647.0866.

5.2.3. Synthesis of structural derivatives of 80a and 80b

5.2.3.1. Synthesis of picolylamine derivative (93a)



A solution of the active ester **184a** (10 mg, 14.3 µmol) and 2-picolyamine (4.6 µL, 44.6 µmol) in 1 mL DMF was purged with nitrogen for 10 min and stirred at room temperature for 16 h. The reaction mixture was diluted with CH₂Cl₂ and washed with H₂O (2x10 mL) and brine (5 mL). The solvent was removed *in vacuo* and the crude material was purified via silica gel chromatography using CH₂Cl₂ and CH₂Cl₂/MeOH (100:1 to 40:1). The combined product eluents were concentrated to provide the desired complex **93a** (8.6 mg, 12.4 µmol, 87%) as a red-purple solid.

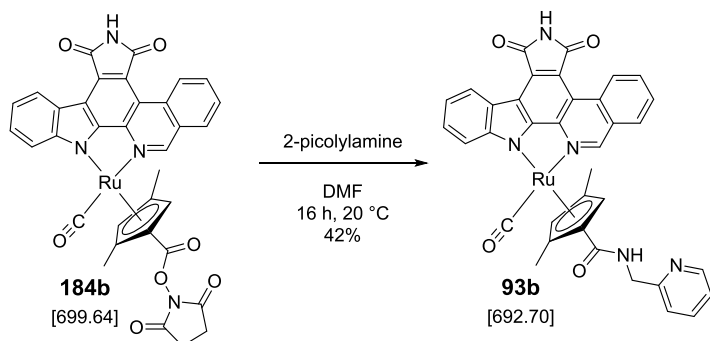
¹H-NMR (300.1 MHz, DMSO-*d*₆): δ = 11.35 (s, 1H), 10.54 (d, ³J = 7.6 Hz, 1H), 10.0 (s, 1H), 8.88 (d, ³J = 7.5 Hz, 1H), 8.56 (t, ³J = 5.9 Hz, 1H), 8.29 (dd, ³J = 8.1 Hz, ⁴J = 0.8 Hz, 1H), 8.22 (dq, ³J = 4.8 Hz, ⁴J = 0.9 Hz, 1H), 8.14 (ddd, ³J = 7.0 Hz, ³J = 8.5 Hz, ⁴J = 1.4 Hz, 1H), 7.95 (ddd, ³J = 7.1 Hz, ³J = 7.9 Hz, ⁴J = 0.9 Hz, 1H), 7.66 (d, ³J = 8.2 Hz, 1H), 7.56 (ddd, ³J = 7.0 Hz, ³J = 8.1 Hz, ⁴J = 1.1 Hz, 1H), 7.33 (ddd, ³J = 7.9 Hz, ³J = 7.0 Hz, ⁴J = 0.9 Hz, 1H), 7.13 (td, ³J = 7.6 Hz, ⁴J = 1.8 Hz, 1H), 7.16 (ddd, ³J = 7.4 Hz, ³J = 4.8 Hz, ⁴J = 1.1 Hz, 1H), 6.49 (d, ³J = 8.1 Hz, 1H), 6.01 (d, ⁴J = 1.2 Hz, 1H), 5.39 (d, ⁴J = 1.2 Hz, 1H), 4.04 (t, ³J = 6.1 Hz, 2H), 2.02 (s, 3H), 1.96 (s, 3H) ppm.

¹³C-NMR (100.6 MHz, DMSO-*d*₆): δ = 201.9 (*C*_q), 171.0 (*C*_q), 170.0 (*C*_q), 164.3 (*C*_q), 160.8, 157.9, 155.0 (*C*_q), 152.0 (*C*_q), 148.4, 138.9 (*C*_q), 136.0, 132.8, 131.5 (*C*_q), 131.3 (*C*_q), 129.2, 128.9, 128.5, 127.8 (*C*_q), 126.6, 124.9, 123.4 (*C*_q), 121.7, 120.1, 119.8 (*C*_q), 119.0, 116.3 (*C*_q), 115.3, 114.3 (*C*_q), 114.2 (*C*_q), 101.4, 86.5, 78.5, 72.0, 44.2, 13.6, 13.5 ppm.

HR-MS (ESI⁺): C₃₆H₂₅N₅O₄RuH (M+H)⁺ calcd.: 694.1033, found: 694.1020.

ATR-IR (neat): $\tilde{\nu}$ = 3059 (vw), 2923 (vw), 2851 (vw), 2724 (vw), 1942 (s), 1745 (w), 1695 (m), 1643 (w), 1578 (w), 1534 (w), 1479 (vw), 1461 (w), 1435 (w), 1377 (w), 1340 (w) 1325 (w), 1295 (w), 1271 (w), 1226 (m), 1167 (vw), 1149 (vw), 1078 (m), 1128 (vw), 1074 (vw), 1048 (vw), 1021 (m), 1006 (w), 971 (w), 945 (vw), 865 (vw), 748 (s), 690 (w), 645 (w), 634 (w), 610 (vw), 552 (w), 514 (vw), 500 (w), 463 (m) cm⁻¹.

5.2.3.2. Synthesis of picolylamine derivative (**93b**)



A solution of 10 mg of the active ester **184b** (14.3 μmol) and 4.6 μL 2-picolyamine (44.6 μmol) in 1 mL DMF was purged with nitrogen for 10 min and stirred at room temperature for 16 h. The reaction mixture was diluted with CH_2Cl_2 and washed with H_2O (2 x 10 mL) and brine (5 mL). The solvent was removed *in vacuo* and the crude material was purified via flash chromatography (3 g silica, CH_2Cl_2 to $\text{CH}_2\text{Cl}_2/\text{MeOH}$ 100:1 to 10:1). The combined product eluents were concentrated to provide the desired complex **93b** (4.2 mg, 6.1 μmol , 42%) as a red-purple solid.

$^1\text{H-NMR}$ (300.1 MHz, $\text{DMSO}-d_6$): $\delta = 11.36$ (s, 1H), 10.54 (d, $^3J = 8.6$ Hz, 1H), 9.73 (s, 1H), 8.89 (d, $^3J = 7.5$ Hz, 1H), 8.57 (t, $^3J = 5.8$ Hz, 1H), 8.39 (ddd, $^3J = 4.7$ Hz, $^4J = 1.7$ Hz, $^4J = 0.8$ Hz, 1H), 8.28 (dd, $^3J = 8.4$ Hz, $^4J = 0.9$ Hz, 1H), 8.15 (ddd, $^3J = 7.1$ Hz, $^3J = 8.5$ Hz, $^4J = 1.4$ Hz, 1H), 7.96 (ddd, $^3J = 7.0$ Hz, $^3J = 7.9$ Hz, $^4J = 0.9$ Hz, 1H), 7.78 (d, $^3J = 8.2$ Hz, 1H), 7.59 (ddd, $^3J = 7.1$ Hz, $^3J = 8.2$ Hz, $^4J = 1.1$ Hz, 1H), 7.41 (td, $^3J = 7.7$ Hz, $^4J = 1.8$ Hz, 1H), 7.34 (ddd, $^3J = 7.1$ Hz, $^3J = 7.9$ Hz, $^4J = 0.7$ Hz, 1H), 7.16 (ddd, $^3J = 7.5$ Hz, $^3J = 4.8$ Hz, $^4J = 0.9$ Hz, 1H), 6.67 (d, $^3J = 7.8$ Hz, 1H), 6.13 (d, $^4J = 1.2$ Hz, 1H), 5.38 (d, $^4J = 1.3$ Hz, 1H), 4.32 (t, $^3J = 5.0$ Hz, 2H), 2.18 (s, 3H), 1.78 (s, 3H) ppm.

$^{13}\text{C-NMR}$ (100.6 MHz, $\text{DMSO}-d_6$): $\delta = 201.6$ (C_q), 171.0 (C_q), 170.0 (C_q), 165.4 (C_q), 159.2, 158.3, 154.8 (C_q), 152.3 (C_q), 148.6, 139.2 (C_q), 136.4, 132.9, 131.5 (C_q), 131.4 (C_q), 129.3, 128.9, 128.6, 127.7 (C_q), 126.8, 124.9, 123.4 (C_q), 121.9, 120.4, 119.9 (C_q), 119.1, 116.3 (C_q), 115.3, 114.2 (C_q), 109.4 (C_q), 103.5, 83.5, 82.5, 73.7, 44.3, 13.1, 13.0 ppm.

HR-MS (ESI $^+$): $\text{C}_{36}\text{H}_{25}\text{N}_5\text{O}_4\text{RuH}$ ($M+\text{H}$) $^+$ calcd.: 694.1033, found: 694.1020.

ATR-IR (neat): $\tilde{\nu} = 3345$ (vw), 2962 (vw), 2923 (vw), 2733 (vw), 1949 (s), 1746 (w), 1687 (m), 1651 (w), 1579 (w), 1525 (m), 1479 (vw), 1461 (w), 1438 (w), 1378 (w), 1342 (w) 1325 (w), 1309 (w), 1294 (w), 1258 (m), 1227 (m), 1149 (vw), 1078 (m), 1017 (s), 865 (vw), 795 (s), 747 (s), 711 (vw), 691 (w), 642 (w), 579 (vw), 555 (w), 500 (w), 463 (m), 432 (vw) cm^{-1} .

5.2.3.3. Libraries of derivatives of np829 (80b)

For the synthesis of the amide libraries 100 μM stock solutions of the according primary amine in DMF were prepared. In the case of availability as HCl salts, they were dissolved in 4:1 DMF/0.5 M LiOH_{aq}. A mixture of 14.0 μL DMF, 10.0 μL NHS-ester solution (32.8 μM in DMF, final c = 8.2 μM) and 16.0 μL of the 100 μM amine stock solution (100 μM , final c = 40 mM) was prepared in a 96-well polypropylene plate, mixed, heat-sealed and left to react overnight. After TLC analysis, the reactions were terminated by addition of 40 μL of 16.4 μM acetic acid in DMSO and stored at -78 °C. All assays with the compound were executed without further purification.

5.3. Compound preparation for the drug-like abilities approach

5.3.1. General working procedures for complex synthesis

5.3.1.1. Standard working procedure I

The appropriate TBS-protected pyridocbazole ligand was suspended in a 1:1 mixture of EtOH/H₂O (~5 mM) and purged with nitrogen for 10-15 min before an equimolar amount of RhCl₃·3 H₂O was added, the flask was sealed, and the suspension heated to 90-95 °C for at least 90 min. The flask was cooled to 20 °C and the tridentate ligand (1.10 eq) was added before the solution or suspension reacted for at least another 16 h. After cooling to 20 °C, the solvent was removed under reduced pressure, the dry residue was redissolved in CH₂Cl₂ and MeOH and adsorbed on silica. The diastereomers were separated by silica flash chromatography with CH₂Cl₂ to CH₂Cl₂/MeOH 100:1 to 10:1 as eluent. The separated isomers were further purified 1-3 times via flash chromatography over 1-3 g silica using the same eluents and a dry load.

5.3.1.2. Standard working procedure II

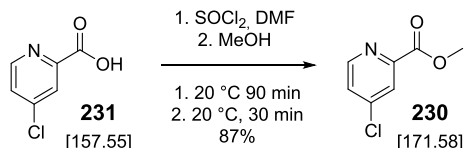
The tridentate ligand was dissolved in a 1:1 mixture of CH₃CN/H₂O (~5.6 mM) and degassed for 10-15 min before an equimolar amount of RhCl₃·3 H₂O was added, the flask sealed, and the suspension heated to 90-95 °C for at least 3 h. After cooling to 20 °C, the solvent was removed under reduced pressure, the TBS-protected pyridocbazole ligand was added (1.10 eq), the residue taken up in a 1:1 mixture of EtOH/H₂O (~0.18 mL/μmol), and the suspension heated for at least 40 h at 95 °C. After cooling, the solvent was removed under reduced pressure, the dry residue redissolved in CH₂Cl₂ and MeOH, and adsorbed on silica. The diastereomers were separated by silica flash chromatography with CH₂Cl₂ to CH₂Cl₂/MeOH 100:1 to 10:1 as eluent with very slow increase of MeOH content until the first diastereomer was eluted from the column. The separated isomers were further purified 1-3 times via flash chromatography over 1-3 g silica using the same eluents and a dry load.

5.4. Compound preparation drug-like abilities approach

5.4.1. Modification of the (pyridine-2-ylmethyl)-D-proline in the 4-pyridine position

5.4.1.1. 4-chloropyridine modification

5.4.1.1.1. Synthesis of methyl 4-chloropicolinate



The procedure was modified from a literature known esterification.^[318] Thionyl chloride (1.11 mL, $\rho = 1.64 \text{ g/cm}^3$, 15.2 mmol, 1.20 eq) was added dropwise to a solution of 2.00 g 4-chloropicolinic acid (12.7 mmol, 1.00 eq) in 54 mL CH₂Cl₂. The solution was cooled to 0 °C and 220 µL of DMF were added dropwise. The solution was allowed to come to 20 °C and was stirred for 90 min before the solvent was removed *in vacuo*. The residue was taken up in 22 mL MeOH and the resulting solution was stirred for 30 min at 20 °C. The solvent was removed under reduced pressure, the residue taken up in 20 mL of aqueous 5% NaHCO₃ solution, and extracted three times with 10 mL EtOAc. The combined organic layers were washed with brine (3 x 5 mL) and dried over MgSO₄. After removal of the solvent under reduced pressure 1.89 g (11.0 mmol, 87%) of the ester **230** was obtained as slightly off-white crystals.

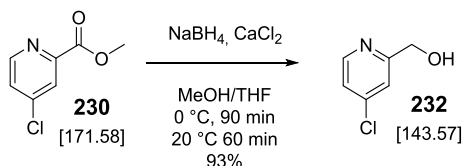
¹H-NMR (300.1 MHz, CDCl₃): $\delta = 8.63$ (dd, $^3J = 5.2$ Hz, $^4J = 1.9$ Hz, 1H, H₆), 8.12 (dd, $^4J = 2.0$ Hz, $^5J = 0.5$ Hz, 1H, H₃), 7.48 (dd, $^3J = 5.2$ Hz, $^4J = 2.1$ Hz, 1H, H₅), 4.00 (s, 3H, OCH₃) ppm.

¹³C-NMR (75.5 MHz, CDCl₃): $\delta = 164.8$ (CO), 150.7 (C₆), 149.4 (C₂), 145.6 (C₄), 127.3 (C₅), 125.8 (C₃), 53.3 (CH₃) ppm.

ATR-IR (neat): $\tilde{\nu} = 2959$ (vw), 1800 (vw), 1714 (s), 1640 (vw), 1574 (m), 1556 (m), 1489 (vw), 1439 (m), 1392 (m), 1297 (m), 1263 (m), 1239 (m), 1190 (w), 1145 (w), 1088 (w), 1046 (vw), 993 (m), 965 (w), 900 (m), 846 (m), 782 (m), 747 (m), 703 (w), 686 (w), 619 (vw), 523 (m), 425 (vw) cm⁻¹.

HR-MS (ESI): C₇H₆ClNO₂Na (M+Na)⁺ calcd.: 193.9979, found: 193.9978.

5.4.1.1.2. Synthesis of (4-chloropyridine-2-yl)methanol



The procedure was taken from literature.^[317] Anhydrous CaCl_2 (3.07 g, 27.6 mmol, 4.04 eq) and 1.15 g methyl 4-chloropicolinate (6.84 mmol, 1.00 eq) were suspended in a mixture of 6.6 mL MeOH and 3.9 mL THF and cooled down to 0 °C. NaBH_4 (518 mg, 13.7 mmol, 2.00 eq) was added portionwise and the resulting suspension was stirred for 2 h at 0 °C and 60 min at 20 °C. The reaction was quenched by addition of 11 mL H_2O and stirred for 2 h at 20 °C. The mixture was extracted with EtOAc (3 x 35 mL) and CH_2Cl_2 (35 mL), and the combined organic layers were dried over Na_2SO_4 . After removal of the solvent *in vacuo* 916 mg of the alcohol **232** (6.38 mmol, 93%) was obtained as a white solid.

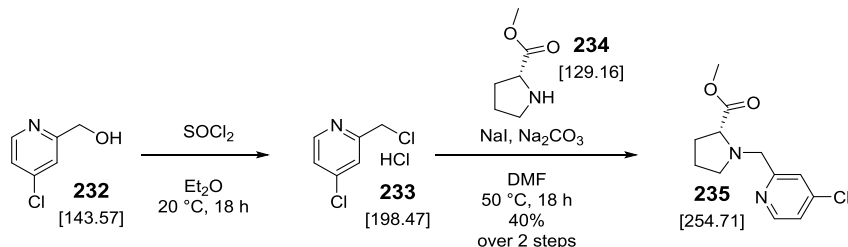
$^1\text{H-NMR}$ (300.1 MHz, CDCl_3): $\delta = 8.46$ (d, $^3J = 5.4$ Hz, 1H, H_6), 7.35 (s, 1H, H_3), 7.21 (dd, $^3J = 5.3$ Hz, $^4J = 1.8$ Hz 1H, H_5), 4.77 (s, 2H, $\text{CH}_2\text{-OH}$), 3.49 (br s, 1H, OH) ppm.

$^{13}\text{C-NMR}$ (75.5 MHz, CDCl_3): $\delta = 161.1$ (C_2), 149.2 (C_4), 123.1 ($C_{3/5}$), 121.2 ($C_{3/5}$), 64.0 (CH_2) ppm.

ATR-IR (neat): $\tilde{\nu} = 3172$ (br m), 3072 (vw), 2902 (vw), 2846 (vw), 2667 (vw), 1581 (s), 1557 (s), 1470 (w), 1453 (w), 1399 (m), 1390 (m), 1361 (vw), 1264 (vw), 1221 (m), 1108 (m), 1094 (m), 1057 (s), 1000 (m), 878 (m), 832 (m), 823 (s), 759 (vw), 722 (vw), 705 (s), 603 (m), 539 (vw), 433 (m), 416 (vw), 397 (vw) cm^{-1} .

HR-MS (ESI): $\text{C}_6\text{H}_6\text{ClNOH} (\text{M}+\text{H})^+$ calcd.: 144.0211, found: 144.0209.

5.4.1.1.3. Synthesis of methyl ((4-chloropyridine-2-yl)methyl)-D-proline



(4-chloropyridine-2-yl)methanol (**232**) was chlorinated by dissolving 100 mg (697 µmol, 1.00 eq) in 700 µL Et₂O, cooling to 0 °C and adding 101 µL (166 mg, ρ = 1.64 g/cm³, 1.39 mmol, 2.00 eq) SOCl₂ dropwise, during which a white precipitate formed. The suspension was allowed to warm to room temperature and was further stirred at 20 °C for 18 h. Solvent and excess SOCl₂ were removed under reduced pressure. 163 mg anhydrous Na₂CO₃ (1.53 mmol, 2.20 eq) and 5 mg NaI (30.7 µmol, 4.4 mol%), and 1.6 mL DMF were added. A solution of 138 mg D-proline methylester (836 µmol, 1.2 eq) in 1.6 mL DMF was added to the first suspension at 50 °C. The resulting suspension was stirred for 18 h at 50 °C and subsequently diluted with 3 mL H₂O. The solution was extracted with CH₂Cl₂ (3 x 10 mL) and the organic layer dried over Na₂SO₄. The solution was concentrated under reduced pressure and the crude product purified by flash column chromatography (25 g silica gel, CH₂Cl₂ to CH₂Cl₂/MeOH 50:1 to 10:1). After removal of the solvent *in vacuo*, the compound was further purified via reversed phase preparative HPLC (C₁₈ HTec-column (5 µm, 250x16 mm, MACHERY-NAGEL), H₂O to CH₃CN over 20 min, flow rate 10 mL/min). After removal of the solvent under reduced pressure, 70 mg (275 µmol, 40%) of **235** was obtained as colourless oil over two steps.

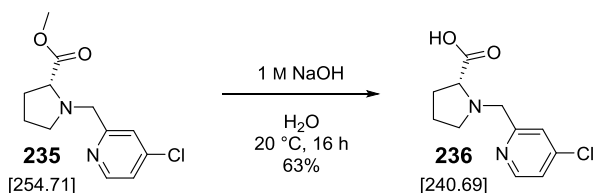
¹H-NMR (300.1 MHz, CDCl₃): δ = 8.41 (d, ³J = 5.4 Hz, 1H, H₆), 7.54 (d, ⁴J = 2.0 Hz, 1H, H₃), 7.18 (dd, ³J = 5.4 Hz, ⁴J = 2.0 Hz, 1H, H₅), 4.07 (d, ²J = 14.0 Hz, 1H, _{pro}CH₂pyr), 3.81 (d, ²J = 14.0 Hz, 1H, _{pro}CH₂pyr), 3.69 (s, 3H, CH₃), 3.48 (dd, ³J = 8.8 Hz, ³J = 5.7 Hz, 1H, H₂), 3.16-3.10 (m, 1H, H_{5a}), 2.62-2.54 (m, 1H, H_{5b}), 2.26-2.19 (m, 1H, H_{3a}), 2.08-1.79 (m, 3H, H_{3b}, H₄) ppm.

¹³C-NMR (75.5 MHz, CDCl₃): δ = 174.2 (COO), 150.0 (C₆), 144.9 (C₄), 123.8 (C_{3/5}), 122.8 (C_{3/5}), 65.5 (_{pro}CH₂pyr), 59.7 (C₂), 53.7 (CH₃), 52.0 (C₅), 29.4 (C_{3'}), 23.4 (C_{4'}) ppm. One signal (C₂) either overlaps with the C₆ signal or is not obvious due to little concentration and insufficient measurement time of the sample.

ATR-IR (neat): $\tilde{\nu}$ = 3049 (w), 2950 (vw), 2877 (vw), 2812 (vw), 1732 (m), 1574 (s), 1554 (m), 1463 (vw), 1434 (w), 1389 (w), 1360 (w), 1274 (vw), 1198 (m), 1171 (m), 1133 (w), 1092 (w), 1038 (vw), 993 (vw), 931 (vw), 889 (w), 825 (w), 765 (vw), 706 (m), 604 (vw), 537 (vw), 439 (w), 400 (vw), 392 (vw), 383 (vw) cm⁻¹.

HR-MS (ESI⁺): C₁₂H₁₅ClN₂O₂H (M+H)⁺ calcd.: 255.0895, found: 255.0903.

5.4.1.1.4. Synthesis of ((4-chloropyridine-2-yl)methyl)-D-proline



Ligand **236** was obtained by saponification. Therefore, methyl ((4-chloropyridine-2-yl)methyl)-D-proline was dissolved in 830 μL 1 M NaOH_{aq}, which was previously purged with N₂ for 10 min. The solution was stirred at 20 °C for 16 h, before the mixture was diluted with 3 mL H₂O and CH₂Cl₂ each. The aqueous layer was separated and set to pH 7 by addition of 1 M HCl_{aq} and the solution further stirred for 30 min at 20 °C. Afterwards the aqueous layer was washed with 10 mL CH₂Cl₂ and the solvent removed under reduced pressure. The residue was dissolved in 5 mL EtOH and treated by sonication for 15 min. The insoluble salts were removed by filtration. After removing the solvent under reduced pressure 41.8 mg (174 μmol, 63%) of the proline **236** was obtained as colourless oil.

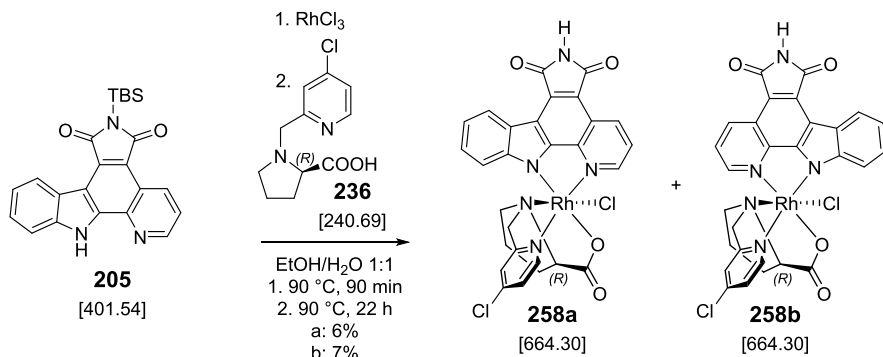
¹H-NMR (300.1 MHz, CD₃OD): δ = 8.59 (d, ³J = 5.4 Hz, 1H, H₆), 7.67 (d, ⁴J = 1.7 Hz, 1H, H₃), 7.53 (dd, ³J = 5.4 Hz, ⁴J = 1.8 Hz, 1H, H₅), 4.80 (d, ²J = 14.3 Hz, 1H, _{pro}CH₂_{pyr}), 4.63 (d, ²J = 14.2 Hz, 1H, _{pro}CH₂_{pyr}), 4.62 (dd, ³J = 9.2 Hz, ³J = 7.0 Hz, 1H, H₂), 3.86-3.78 (m, 1H, H_{5a}), 3.47-3.38 (m, 1H, H_{5b}), 2.71-2.57 (m, 1H, H_{3a}), 2.30-2.18 (m, 2H, H_{3b}, H_{4a}), 2.13-2.06 (m, 1H, H_{4a}) ppm.

¹³C-NMR (75.5 MHz, CD₃OD): δ = 170.9 (COO), 153.7 (C₂), 151.8 (C₆), 146.6 (C₄), 125.7 (C_{3/5}), 125.7 (C_{3/5}), 68.4 (C₂), 59.6 (_{pro}CH₂_{pyr}), 57.0 (C₅), 29.3 (C₃), 23.7 (C₄) ppm.

ATR-IR (neat): $\tilde{\nu}$ = 3366 (br w), 2962 (w), 2815 (w), 2513 (br w), 2340 (br w), 1726 (m), 1695 (vw), 1616 (vw), 1579 (s), 1558 (m), 1403 (s), 1299 (vw), 1228 (s), 1104 (w), 1062 (vw), 996 (vw), 932 (vw), 878 (w), 836 (m), 710 (m), 662 (vw), 575 (vw), 526 (vw), 433 (vw), 394 (w) cm⁻¹.

HR-MS (ESI⁺): C₁₁H₁₃ClN₂O₂H (M+H)⁺ calcd.: 241.0738, found: 241.0742.

5.4.1.1.5. Synthesis of the 4-chloro-pyridine modified complexes 258a and 258b



The 4-chloro pyridine derivatives of the complexes **201a** and **201b** were prepared according to standard procedure I using 52.6 mg TBS-protected pyridocarbazole (131 μmol , 1.00 eq) and 34.4 mg $\text{RhCl}_3 \cdot 3\text{H}_2\text{O}$ (131 μmol , 1.00 eq) in 25.0 mL $\text{H}_2\text{O}/\text{EtOH}$ 1:1 for 90 min at 90 °C, before adding 34.8 mg of the proline ligand **236** (145 μmol , 1.10 eq) and reacting for another 22 h. After removal of the solvent *in vacuo* the complexes were adsorbed on silica (~ 0.5 g) and the diastereomers were separated according to the standard procedure on 5 g silica. The isomers were combined with the according isomers obtained from a smaller scale of 25 μmol and every isomer was further purified twice (2 g and 1.5 g silica) via flash column chromatography. **258a** (5.8 mg, 8.73 μmol , 6%) and **258b** (6.8 mg, 10.2 μmol , 7%) were obtained as deeply red solids.

258a:

$^1\text{H-NMR}$ (500.1 MHz, $\text{DMSO}-d_6$): $\delta = 11.26$ (br s, NH), 9.61 (d, $^3J = 6.3$ Hz, 1H, H_6'), 9.29 (dd, $^3J = 8.4$ Hz, $^4J = 1.1$ Hz, 1H, H_3''), 8.84 (d, $^3J = 5.2$ Hz, 1H, H_7''), 8.70-8.68 (m, 1H, H_4''), 8.22 (dd, $^3J = 5.0$ Hz, $^4J = 1.4$ Hz, 1H, H_5), 8.19 (d, $^4J = 2.2$ Hz, H_2), 8.08 (dd, $^3J = 8.4$ Hz, $^3J = 5.2$ Hz, 1H, H_2''), 7.30-7.28 (m, 2H, H_6'', H_5''), 5.88-5.86 (m, 1H, H_7'), 4.55 (d, $^4J = 15.9$ Hz, 1H, $_{pro}\text{CH}_{2pyr}$), 4.33 (d, $^4J = 15.9$ Hz, 1H, $_{pro}\text{CH}_{2pyr}$), 3.88 (dd, $^3J = 9.6$ Hz, $^3J = 4.2$ Hz, 1H, H_2'), 2.21-2.16 (m, 2H, H_{5b}' , H_{3a}'), 2.02-1.97 (m, 1H, H_{3b}'), 1.58-1.53 (m, 1H, H_{4a}'), 1.06-1.01 (m, 1H, H_{4b}') ppm. The missing H_{5a}' signal overlaps with the DMSO signal as confirmed by $^1\text{H}-^{13}\text{C}$ -HSQC-spectroscopy.

ATR-IR (neat): $\tilde{\nu} = 2923$ (w), 2853 (vw), 1751 (w), 1703 (s), 1651 (m), 1624 (m), 1602 (m), 1556 (w), 1522 (w), 1496 (w), 1472 (w), 1418 (m), 1403 (vw), 1342 (s), 1293 (m), 1263 (w), 1229 (s), 1150 (m), 1133 (vw), 1107 (vw), 1082 (vw), 1022 (m), 1008 (m), 936 (vw), 902 (vw), 880 (w), 819 (m), 796 (w), 743 (m), 724 (vw), 710 (w), 688 (vw), 639 (m), 593 (vw), 575 (vw), 521 (vw), 495 (m), 482 (w), 441 (w), 407 (vw), 387 (m) cm^{-1} .

HR-MS (APCI $^+$): $\text{C}_{28}\text{H}_{20}\text{Cl}_2\text{N}_5\text{O}_4\text{RhH}$ ($\text{M}+\text{H}$) $^+$ calcd.: 664.0020, found: 664.0019.

258b:

¹H-NMR (500.2 MHz, DMSO-*d*₆): δ = 11.24 (br s, NH), 9.46 (d, ³J = 6.3 Hz, 1H, *H*₆), 9.18 (dd, ³J = 8.4 Hz, ⁴J = 0.9 Hz, 1H, *H*_{3'}), 8.70 (d, ³J = 7.9 Hz, 1H, *H*_{4'}), 8.13 (dd, ³J = 6.2 Hz, ⁴J = 2.3 Hz, 1H, *H*_{5'}), 8.11-8.19 (m, 2H, *H*_{1'}, *H*_{3'}) 7.82 (d, ³J = 8.3 Hz, 1H, *H*_{7'}), 7.74 (dd, ³J = 8.4 Hz, ³J = 5.2 Hz, 1H, *H*_{2'}), 7.54 (ddd, ³J = 8.3 Hz, ³J = 7.1 Hz, ⁴J = 1.3 Hz, 1H, *H*_{6'}), 7.37 (ddd, ³J = 7.9 Hz, ³J = 7.1 Hz, ⁴J = 0.9 Hz, 1H, *H*_{5'}), 4.58 (d, ²J = 16.4 Hz, 1H, _{pyr}CH₂N_{pro}), 4.51 (d, ⁴J = 16.4 Hz, 1H, _{pyr}CH₂N_{pro}), 3.86 (dd, ³J = 9.4 Hz, ³J = 4.6 Hz, 1H, *H*_{2'}), 2.48-2.45 (m, 1H, *H*_{5a'}), 2.22-2.12 (m, 2H, *H*_{5b'}, *H*_{3a'}), 1.89-1.83 (m, 1H, *H*_{3b'}), 1.46-1.39 (m, 1H, *H*_{4a'}), 1.10-1.03 (m, 1H, *H*_{4b'}) ppm.

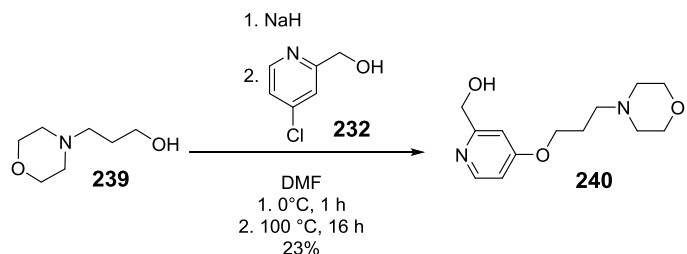
¹³C-NMR (125.8 MHz, DMSO-*d*₆): δ = 182.3 (COO), 170.7 (CO), 170.3 (CO), 161.6 (*C*_q), 152.5 (*C*₆), 152.2 (*C*_q), 150.9 (*C*_{1'}), 149.8 (*C*_q), 147.3 (*C*_q), 142.3 (*C*_q), 134.9 (*C*_{3'}), 131.2 (*C*_q), 126.6 (*C*_{6'}), 126.5 (*C*₅), 124.5 (*C*₃), 124.3 (*C*_{4'}, *C*_{2'}), 123.1 (*C*_q), 121.1 (*C*_q), 119.7 (*C*_{5'}), 115.0 (*C*_{7'}), 114.9 (*C*_q), 114.1 (*C*_q), 73.6 (*C*₂), 69.0 (_{pyr}CH₂N_{pro}), 61.5 (*C*₅), 30.3 (*C*₃), 23.9 (*C*₄) ppm.

ATR-IR (neat): $\tilde{\nu}$ = 3230 (vw), 3059 (vw), 2958 (vw), 2921 (w), 2853 (vw), 1754 (w), 1710 (m), 1624 (s), 1523 (vw), 1499 (w), 1470 (vw), 1422 (w), 1342 (s), 1302 (w), 1265 (w), 1230 (m), 1132 (vw), 1102 (w), 1018 (m), 933 (vw), 876 (w), 854 (vw), 797 (m), 751 (m), 713 (w), 686 (vw), 640 (m), 579 (vw), 523 (vw), 492 (m), 441 (m), 397 (m) cm⁻¹.

HR-MS (APCI⁺): C₂₈H₂₀Cl₂N₅O₄RhH (M+H)⁺ calcd.: 664.0020, found: 664.0021.

5.4.1.2. 4-(3-(pyridine-4-yloxy)propyl)morpholine modification

5.4.1.2.1. Synthesis of (4-(3-morpholinopropoxy)pyridine-2-yl)methanol



The synthesis was modified from a literature procedure.^[321] Sodium 3-morpholinopropan-1-olate was prepared by adding 85 mg of sodium hydride dispersion in mineral oil (2.13 mmol, 3.05 eq) to a solution of 289 µL 3-morpholinopropan-1-ol (2.09 mmol, $\rho = 1.05$, 3.00 eq) in DMF (600 µL) at 0 °C. The suspension was stirred for 60 min at 0 °C. A solution of 100 mg (4-chloropyridine-2-yl)methanol (697 µmol, 1.00 eq) in DMF (360 µL) was added dropwise at 0 °C. While warming to 20 °C the suspension turned dark green. The reaction mixture was heated to 100 °C for 16 h, during which time the colour changed to red and later brown. After cooling the reaction mixture to 20 °C the solvent was removed *in vacuo*, the residue was taken up in Et₂O and sonicated for 5 min before it was filtered. The solvent of the filtrate was removed *in vacuo* and the residue was subjected to flash chromatography twice (5 g/3 g silica, CH₂Cl₂ to CH₂Cl₂/MeOH 10:1, loading with CH₂Cl₂ plus a few drops of MeOH). The combined product eluents were dried to provide **240** (40 mg, 159 µmol, 23%) as a yellow oil.

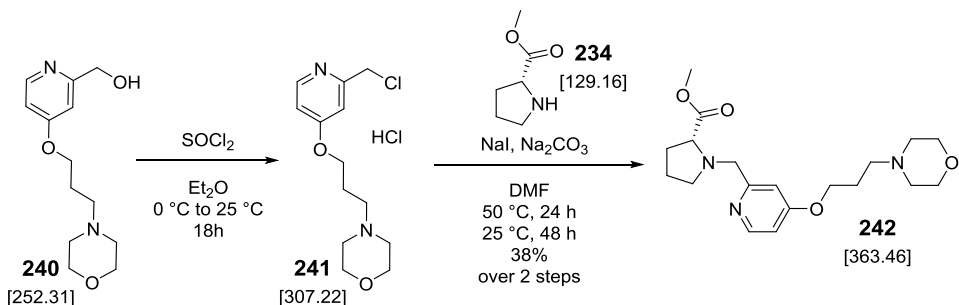
¹H-NMR (300.2 MHz, (CD₃)₂CO): $\delta = 8.28$ (d, $^3J = 5.7$ Hz, 1H, H_6), 7.04 (d, $^4J = 2.3$ Hz, 1H, H_3), 6.78 (d, $^3J = 5.70$ Hz, $^4J = 2.6$ Hz, 1H, H_5), 4.63 (s, 2H, CH₂OH), 4.16 (t, $^3J = 6.4$ Hz, 2H, H_8), 3.99 (br s, 1H, OH), 3.64-3.58 (m, 4H, H_{13} , H_{15}), 2.49 (t, $^3J = 7.0$ Hz, 2H, H_{10}), 2.45-2.36 (m, 4H, H_{12} , H_{16}), 1.97 (quin., $^3J = 6.7$ Hz, 2 H, H_9) ppm.

¹³C-NMR (75.5 MHz, (CD₃)₂CO): $\delta = 166.8$ (C_4), 164.3 (C_2), 150.8 (C_6), 109.7 (C_3), 107.0 (C_5), 67.5 (C_{13} , C_{15}), 66.9 (C_8), 65.3 (_{pro}CH₂pyr), 55.9 (C_{10}), 54.7 (C_{12} , C_{16}), 26.9 (C_9) ppm.

ATR-IR (neat): $\tilde{\nu} = 3239$ (vw), 2953 (w), 2854 (w), 2691 (w), 1597 (s), 1567 (m), 1448 (m), 1393 (w), 1359 (w), 1303 (s), 1271 (m), 1208 (vw), 1165 (w), 1142 (w), 1114 (vs), 1031 (s), 1002 (m), 917 (vw), 899 (vw), 861 (m), 827 (w), 747 (w), 631 (vw), 612 (vw), 562 (vw), 529 (vw), 505 (vw), 490 (vw), 446 (w), 394 (w) cm⁻¹.

HR-MS (ESI⁺): C₁₃H₂₀N₂O₃H (M+H)⁺ calcd.: 253.1547, found: 253.1545.

5.4.1.2.2. Synthesis of methyl ((4-(3-morpholinopropoxy)pyridine-2-yl)methyl)-D-proline



To a solution of (4-(3-morpholinopropoxy)pyridine-2-yl)methanol (40 mg, 159 µmol, 1.00 eq) in 300 µL Et₂O at 0 °C was added SOCl₂ (17.3 µL, $\rho = 1.64$, 238, 1.50 eq) dropwise during which a white precipitation formed. The solution was brought to 25 °C and another 300 µL Et₂O and 8 µL SOCl₂ (111 µmol, 0.70 eq) were added due to evaporation of the Et₂O in the N₂ stream. The reaction mixture was stirred at 25 °C for 16 h and the solvent and excess SOCl₂ were removed *in vacuo* to yield the chloride salt **241** as white solid, which was then subjected to an nucleophilic substitution using a modification of an reported method.^[332] The obtained crude product was dissolved in 0.4 mL DMF and Na₂CO₃ (37.0 mg, 348.7 µmol, 2.20 eq) and NaI (~1 mg, 7.0 µmol, 4 mol%) were added and the flask protected against light and heated to 50 °C. Methyl D-proline (24.6 mg, 190.2 µmol, 1.2 eq) was dissolved in 0.4 mL DMF and the solution added to the suspension. The reaction was stirred for 24 h at 50 °C and for 48 h at 25 °C before the solvent was removed under reduced pressure. The residue was taken up in CH₂Cl₂, MeOH and acetone to remove insoluble side products and the solvent was decanted and collected each time. The solvent of the collected fractions was removed *in vacuo* and the crude product was subjected to flash chromatography twice (5 g silica each, CH₂Cl₂ to CH₂Cl₂/MeOH 10:1, loading with CH₂Cl₂ plus a few drops of MeOH). The combined product eluents were dried to provide **242** (22 mg, 38%) as a yellow oil.

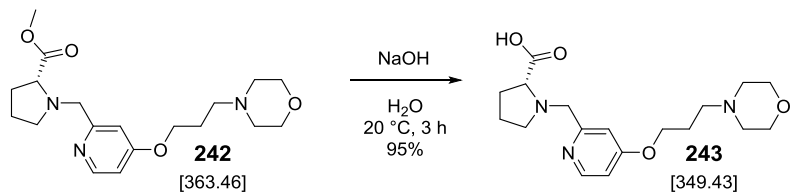
¹H-NMR (300.2 MHz, CD₃OD): δ = 8.23 (d, ³J = 5.9 Hz, 1H, H₆), 7.14 (d, ⁴J = 2.4 Hz, 1H, H₃), 6.86 (d, ³J = 5.9 Hz, ⁴J = 2.5 Hz, 1H, H₅), 4.16 (t, ³J = 6.2 Hz, 2H, H₈), 3.94 (d, ²J = 13.8 Hz, 1H, _{pro}CH₂pyr), 3.75-3.68 (m, 5H, H₁₃, H₁₅, _{pro}CH₂pyr), 3.63 (s, 1H CH₃), 3.38 (dd, ³J = 9.0 Hz, ³J = 5.6 Hz, H₂) 3.08-3.02 (m, 1H, H_{5a}), 2.58-2.47 (m, 7 H, H₁₀, H₁₂, H₁₆, H_{5b}), 2.21-2.15 (m, 1H, H_{3a}), 2.07-1.98 (m, 2H, H_{4a}, H_{3b}), 1.95-1.80 (m, 3H, H_{4b}, H₉) ppm.

¹³C-NMR (75.5 MHz, CD₃OD): δ = 176.1 (CO), 167.8 (C₄), 161.6 (C₂), 150.5 (C₆), 110.9 (C₃), 110.8 (C₅), 67.7 (C₁₃, C₁₅), 67.4 (C_{2'}), 66.5 (C₈), 60.8 (C_{5'}), 56.4 (C₁₀), 54.8 (C₁₂, C₁₆), 54.7 (_{pro}CH₂pyr), 52.2 (OCH₃), 30.3 (C_{3'}), 26.9 (C₉), 24.2 (C_{4'}) ppm.

ATR-IR (neat): $\tilde{\nu}$ = 2951 (w), 2851 (vw), 2811 (w), 2689 (w), 1733 (m), 1644 (vw), 1594 (s), 1565 (m), 1459 (w), 1435 (m), 1360 (w), 1301 (m), 1198 (w), 1169 (m), 1142 (w), 1116 (s), 1069 (vw), 1035 (w), 1002 (vw), 918 (vw), 895 (vw), 862 (w), 828 (vw), 752 (vw), 684 (vw), 634 (vw), 611 (vw), 451 (w), 416 (vw), 396 (vw), 385 (vw) cm^{-1} .

HR-MS (ESI $^+$): $\text{C}_{19}\text{H}_{29}\text{N}_3\text{O}_4\text{H}$ ($\text{M}+\text{H}^+$)⁺ calcd.: 364.2231, found: 364.2230.

5.4.1.2.3. Synthesis of ((4-(3-morpholinopropoxy)pyridine-2-yl)methyl)-D-proline



A solution of 22 mg (60.5 μmol , 1.00 eq) methyl ((4-(3-morpholinopropoxy)pyridine-2-yl)methyl)-D-proline (**242**) in 1 M NaOH_{aq} (182 μmol , 3.00 eq) was stirred for 3 h at 20 °C. The solution was diluted with 400 μL H_2O and washed with 180 μL CH_2Cl_2 . The pH was adjusted to 7 using 1 M aqueous HCl. The solution was further stirred for 30 min and finally washed again with 180 μL CH_2Cl_2 . The solvent was removed *in vacuo* and the remaining residue was suspended in 3 mL EtOH and insoluble salts were filtered off. The solvent was removed *in vacuo* to yield in 20 mg (57.2 μmol , 95%) of the ligand **243** as a colourless film.

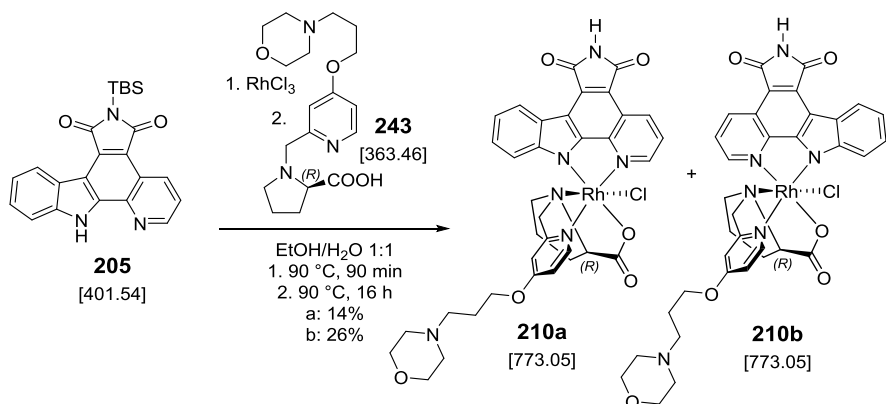
¹H-NMR (300.2 MHz, CD_3OD): δ = 8.42 (d, 3J = 5.8 Hz, 1H, H_6), 7.14 (d, 4J = 2.3 Hz, 1H, H_3), 6.98 (d, 3J = 5.9 Hz, 4J = 2.4 Hz, 1H, H_5), 4.52 (d, 2J = 13.8 Hz, 1H, $_{\text{pro}}\text{CH}_2\text{pyr}$), 4.39 (d, 2J = 13.8 Hz, 1H, $_{\text{pro}}\text{CH}_2\text{pyr}$), 4.20 (t, 3J = 6.1 Hz, 2H, H_8), 4.04 (dd, 3J = 9.0 Hz, 3J = 5.8 Hz, 1H, H_2), 3.76 (t, 3J = 4.7 Hz, 4 H, H_{13}, H_{15}), 3.72-3.67 (m, 1H, H_{5a}), 3.27-3.17 (m, 1H, H_{5b}), 2.75-2.69 (m, 6 H, H_{10}, H_{12}, H_{16}), 2.53-2.40 (m, 1H, $H_{3/4}$), 2.22-1.96 (m, 5H, H_9, H_3, H_4) ppm.

¹³C-NMR (75.5 MHz, CD_3OD): δ = 173.5 (CO), 167.6 (C_4), 154.0 (C_2), 152.0 (C_6), 112.0 (C_3), 111.9 (C_5), 70.6 (C_2), 67.5 (C_8), 67.1 (C_{13}, C_{15}), 59.9 (C_5), 56.2 ($_{\text{pro}}\text{CH}_2\text{pyr}/ C_{10}$), 56.1 ($_{\text{pro}}\text{CH}_2\text{pyr}/ C_{10}$), 54.4 (C_{12}, C_{16}), 30.1 (C_3), 26.3 (C_9), 24.5 (C_4) ppm.

ATR-IR (neat): $\tilde{\nu}$ = 3387 (m), 2957 (w), 2868 (vw), 2821 (vw), 1599 (s), 1567 (m), 1486 (vw), 1448 (w), 1392 (m), 1361 (w), 1308 (m), 1208 (vw), 1183 (vw), 1142 (vw), 1112 (m), 1067 (w), 1043 (w), 997 (w), 974 (vw), 919 (vw), 897 (vw), 861 (w), 775 (vw), 739 (vw), 634 (vw), 563 (vw), 477 (vw), 416 (vw) cm^{-1} .

HR-MS (ESI $^+$): $\text{C}_{18}\text{H}_{27}\text{N}_3\text{O}_4\text{H}$ ($\text{M}+\text{H}^+$)⁺ calcd.: 350.2074, found: 350.2071.

5.4.1.2.4. Synthesis of 3-morpholinopropan-1-ol derivatised complexes **210a** and **210b**



The complexes **210a** and **210b** were prepared according to standard procedure I using 20.9 mg TBS-protected pyridocarbazole (52.0 µmol, 1.00 eq) and 13.7 mg RhCl₃·3H₂O (52.0 µmol, 1.00 eq) in 10.5 mL H₂O/EtOH 1:1 for 90 min at 90 °C before adding this suspension to 20 mg of the proline-ligand **243** (57.2 µmol, 1.10 eq) and reacting for another 16 h. After removal of the solvent under reduced pressure, the compound was adsorbed on silica (~500 mg) and the diastereomers were separated according to the standard procedure using 3 g silica. Isomer **a** and **b** were both further purified twice over 1 g silica gel each, yielding in 5.8 mg of **210a** (7.50 µmol, 14%) and 10.3 mg **210b** (13.3 µmol, 26%) as deep red solids.

210a:

¹H-NMR (500.1 MHz, DMSO- δ): δ = 11.23 (br s, 1H, NH), 9.37 (d, 3J = 6.7 Hz, 1H, H_6), 9.28 (dd, 3J = 8.5 Hz, 4J = 1.1 Hz, 1H, $H_{3''}$), 8.85 (d, 3J = 4.8 Hz, 1H, $H_{1''}$), 8.70-8.68 (m, 1H, $H_{4''}$), 8.07 (dd, 3J = 8.4 Hz, 3J = 5.2 Hz, 1H, $H_{2''}$), 7.61 (dd, 3J = 6.8 Hz, 4J = 2.8 Hz, 1H, H_5), 7.56 (d, 4J = 2.8 Hz, 1H, H_3), 7.29-7.27 (m, 2H, $H_{5''}$, H_6''), 5.96- 5.95 (m, 1H, $H_{7''}$), 4.44-4.39 (m, 3H, _{pro}CH₂pyr, H_8), 4.24 (d, 3J = 15.3 Hz, 1H, _{pro}CH₂pyr), 3.74 (dd, 3J = 9.7 Hz, 3J = 4.4 Hz, 1H, H_2), 3.61 (t, J = 4.5 Hz, 4 H, H_{13} , H_{15}), 2.48-2.46 (m, 1H, $H_{5'a}$), 2.41 (br s, 4 H, H_{12} , H_{16}), 2.28-2.16 (m, 2H, $H_{5'b}$, $H_{3'd}$), 2.07-1.97 (m, 3H, $H_{3'b}$, H_9), 1.59-1.52 (m, 1H, $H_{4'b}$), 1.06-1.03 (m, 1H, $H_{4'a}$) ppm. The missing H_{10} proton signal overlaps with the DMSO signal as confirmed by COSY and HSQC-NMR-spectroscopy.

¹³C-NMR (125.8 MHz, DMSO- δ): δ = 182.0 (COO), 170.6 (CO), 170.2 (CO), 167.7 (C_q), 161.8 (C_q), 153.0 (C_6), 152.7 (C_q), 148.9 (C_q), 148.7 ($C_{1''}$), 142.1 (C_q), 135.1 ($C_{3''}$), 131.2 (C_q), 126.7 ($C_{6''}$), 124.7 ($C_{4''}$), 123.8 ($C_{2''}$), 123.4 (C_q), 121.3 (C_q), 119.6 ($C_{5''}$), 115.1 (C_q), 114.5 (C_q), 112.8 (C_5), 112.1 ($C_{7''}$), 110.1 (C_3), 72.8 (C_2), 69.9 (_{pro}CH₂pyr), 67.9 (C_8), 66.2 (C_{13} , C_{15}), 61.2 (C_5), 54.5 (C_{10}), 53.4 (C_{12} , C_{16}), 30.4 (C_3), 25.3 (C_9), 24.3 (C_4) ppm.

Experimental part

ATR-IR (neat): $\tilde{\nu}$ = 3056 (vw), 2924 (w), 2852 (vw), 2187 (vw), 2120 (vw), 1753 (w), 1704 (m), 1651 (m), 1617 (s), 1523 (vw), 1492 (w), 1461 (w), 1419 (w), 1338 (s), 1262 (m), 1226 (m), 1180 (w), 1113 (m), 1019 (m), 929 (vw), 890 (vw), 856 (w), 825 (w), 795 (w), 747 (m), 708 (vw), 637 (w), 493 (w), 438 (vw) cm^{-1} .

HR-MS (ESI): $\text{C}_{35}\text{H}_{34}\text{ClN}_6\text{O}_6\text{RhH}$ ($\text{M}+\text{H}$)⁺ calcd.: 773.1356, found: 773.1364.

210b:

¹H-NMR (500.1 MHz, DMSO- δ_6): δ = 11.20 (br s, 1H, NH), 9.25 (d, 3J = 6.7 Hz, 1H, H_6), 9.17 (dd, 3J = 8.4 Hz, 4J = 1.0 Hz, 1H, $H_{3''}$), 8.70 (d, 3J = 8.0 Hz, 1H, $H_{4''}$), 8.01 (d, 3J = 5.4 Hz, 1H, $H_{1''}$), 7.82 (d, 3J = 8.3 Hz, 1H, H_7), 7.75 (dd, 3J = 8.4 Hz, 3J = 5.2 Hz, 1H, $H_{2''}$), 7.54-7.52 (m, 2H, H, H_5 , H_6''), 7.48 (d, 4J = 2.7 Hz, 1H, H_3), 7.37 (ddd, 3J = 8.0 Hz, 3J = 7.0 Hz, 4J = 1.0 Hz, 1H, $H_{5''}$), 4.48 (d, 3J = 15.9 Hz, 1H, _{pro}CH₂pyr), 4.41 (d, 3J = 16.0 Hz, 1H, _{pro}CH₂pyr), 4.33 (td, 3J = 6.4 Hz, 4J = 1.1 Hz, 2H, H_8), 3.74 (dd, 3J = 9.5 Hz, 3J = 4.8 Hz, 1H, H_2), 3.60 (t, 3J = 9.1 Hz, 4 H, H_{13} , H_{15}), 2.51-2.46 (m, 3H, H_{5a} , H_{10}), 2.40 (br s, 4 H, H_{12} , H_{16}), 2.21-2.15 (m, 2H, H_{5b} , H_{3a}), 2.03-1.98 (m, 2H, H_9), 1.90-1.85 (m, 1H, H_{3b}), 1.44-1.40 (m, 1H, H_{4b}), 1.14-1.04 (m, 1H, H_{4a}) ppm. The H_{10} proton signal partially overlaps with the DMSO signal as confirmed by COSY and HSQC-NMR-spectroscopy.

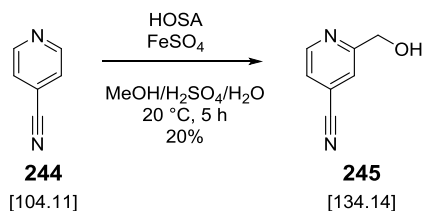
¹³C-NMR (125.8 MHz, DMSO- δ_6): δ = 182.3 (COO), 170.6 (CO), 170.3 (CO), 167.4 (C_g), 161.0 (C_g), 152.3 (C_6), 152.2 (C_g), 150.4 ($C_{1''}$), 149.9 (C_g), 142.4 (C_g), 134.7 ($C_{3''}$), 131.2 (C_g), 126.5 (C_6''), 124.2 (C_4 , $C_{2''}$), 123.0 (C_g), 121.1 (C_g), 119.6 (C_5), 114.9 (C_7 , C_g), 113.9 (C_g), 112.5 (C_5), 110.4 (C_3), 73.4 (C_2), 69.2 (_{pro}CH₂pyr), 67.7 (C_8), 66.2 (C_{13} , C_{15}), 61.4 (C_5), 54.5 (C_{10}), 53.3 (C_{12} , C_{16}), 30.3 (C_3), 25.3 (C_9), 23.8 (C_4) ppm.

ATR-IR (neat): $\tilde{\nu}$ = 2921 (w), 2853 (vw), 1751 (vw), 1705 (m), 1648 (m), 1617 (m), 1524 (vw), 1493 (w), 1454 (w), 1419 (w), 1339 (s), 1301 (m), 1264 (m), 1230 (m), 1175 (vw), 1112 (w), 1020 (m), 894 (vw), 855 (w), 824 (w), 796 (w), 753 (m), 708 (vw), 636 (w), 532 (vw), 492 (w), 439 (vw) cm^{-1} .

HR-MS (ESI): $\text{C}_{35}\text{H}_{34}\text{ClN}_6\text{O}_6\text{RhH}$ ($\text{M}+\text{H}$)⁺ calcd.: 773.1356, found: 773.1369.

5.4.1.3. ((4-((dimethylamino)methyl)pyridine-2-yl)methyl) modification

5.4.1.3.1. Synthesis of 2-hydroxymethyl-4-cyanopyridine



The hydroxymethylation of 4-cyanopyridine was performed according to a reported procedure.^[323] 1.04 g of **244** (10 mmol, 1.00 eq) was dissolved in 10 mL MeOH, 5 mL H₂O, and 0.5 mL conc. H₂SO₄ and the solution degassed for 10 min. Afterwards, 91 mg FeSO₄ (0.30 mmol, 0.03 eq) was added, the solution treated for 20 min with sonication and finally 1.13 g hydroxylamine-O-sulfonic acid (10.0 mmol, 1.00 eq) was added. The mixture was stirred for 5 h at 20 °C. Afterwards, 1.8 g Na₂CO₃ (17.0 mmol, 1.70 eq) and 10 mL water were added to quench the reaction. The suspension was filtered, the solvent was removed under reduced pressure from the filtrate and the residue was taken up in H₂O and EtOAc. The layers were separated and the aqueous layer was extracted (5 x 25 mL) with EtOAc. The combined organic layers were dried over MgSO₄ and the solvent was removed *in vacuo*. The residue was adsorbed on 0.5 g silica gel and purified via flash column chromatography (20 g silica gel, CH₂Cl₂/acetone 10:1 to 4:1). The solvent was removed under reduced pressure to obtain 278 mg 2-hydroxymethyl-4-cyanopyridine (2.07 mmol, 20%) as a colourless solid.

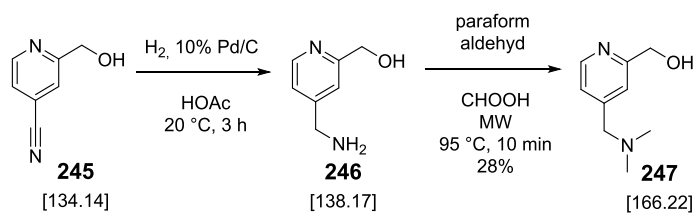
¹H-NMR (300.1 MHz, CDCl₃): δ = 8.71 (dd, ³J = 5.0 Hz, ⁴J = 0.5 Hz, 1H, H₆), 7.61 (d, ⁴J = 0.6 Hz, 1H, H₃), 7.43 (dt, ³J = 5.0 Hz, ³J = 0.7 Hz, 1H, H₅), 4.82 (s, 2H, H₇), 3.53 (br s, 1H, OH) ppm.

¹³C-NMR (75.5 MHz, CDCl₃): δ = 161.7 (C₂), 149.8 (C₆), 123.9 (C_{3/5}), 122.4 (C_{3/5}), 121.2 (C₇), 116.5 (C₄), 64.3 (CH₂OH) ppm.

ATR-IR (neat): $\tilde{\nu}$ = 3235 (br w), 2954 (vw), 2914 (vw), 2845 (vw), 1727 (s), 1603 (w), 1561 (w), 1432 (m), 1393 (m), 1363 (m), 1301 (s), 1208 (s), 1104 (m), 1056 (s), 979 (m), 895 (w), 852 (w), 798 (vw), 759 (m), 680 (m), 609 (m), 475 (vw), 434 (m) cm⁻¹.

HR-MS (ESI⁺): C₇H₆N₂OH (M+H)⁺ calcd.: 135.0553, found: 135.0552.

5.4.1.3.2. Synthesis of 2-hydroxymethyl-4-(dimethylamino)pyridine



Nitrile **245** was reduced according to a modified reported procedure using Pd/C.^[326] 270 mg of the starting material (2.01 mmol, 1.00 eq) was dissolved in 24 mL HOAc and the solution was degassed for 15 min. To that solution 80 mg Pd/C (10%, 0.75 mmol, 0.40 eq) was added and an additional 5 min degassed. The reaction was placed under an atmosphere of hydrogen gas (balloon) and stirred for 3 h at 20 °C under an H₂ atmosphere. The resulting suspension was filtered over celite and washed with warm HOAc. The solvent was removed under reduced pressure and the product **246** subjected to a reported dimethylation procedure^[327] without characterisation. 2-hydroxymethyl-4-(aminomethyl)pyridine was dissolved in 400 mg formic acid (8.68 mmol, 4.32 eq) and 220 mg paraformaldehyde (5.43 mmol, 2.70 eq) were added. The mixture was reacted for 10 min in a microwave (95 °C, 30 W), before H₂O was added. The solution was washed with Et₂O, and the pH was adjusted to 12 with aqueous KOH. The aqueous solution was extracted with Et₂O (4 x 50 mL) and the combined organic layers were dried over Na₂SO₄. The solvent was removed *in vacuo* and **247** was obtained as a yellow oil (95 mg, 0.57 mmol, 28%) over two steps.

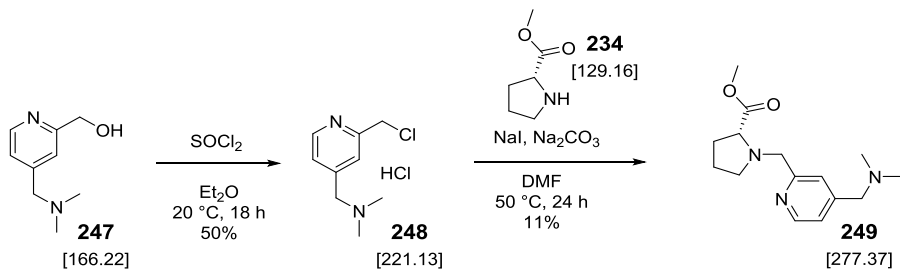
¹H-NMR (300.1 MHz, CDCl₃): δ = 8.44 (d, ³J = 5.1 Hz, 1H, H_δ), 7.26 (d, ⁴J = 0.5 Hz, 1H, H_β), 7.14 (d, ³J = 4.9 Hz 1H, H_γ), 4.72 (s, 2H, CH₂OH), 4.02 (br s, 1H, OH), 4.41 (s, 2H, H_η), 2.22 (s, 6H, N(CH₃)₂) ppm.

¹³C-NMR (75.5 MHz, CDCl₃): δ = 159.8 (C₂), 149.0 (C₄), 148.6 (C₆), 122.7 (C_{3/5}), 120.7 (C_{3/5}), 64.3 (CH₂OH), 64.2 (C₇), 45.6 (N(CH₃)₂) ppm.

ATR-IR (neat): $\tilde{\nu}$ = 3235 (br m), 2943 (vw), 2862 (vw), 2823 (w), 2777 (w), 1665 (vw), 1607 (s), 1562 (w), 1456 (m), 1411 (m), 1362 (w), 1265 (w), 1172 (w), 1149 (w), 1106 (vw), 1037 (s), 996 (w), 900 (vw), 858 (m), 821 (m), 775 (vw), 601 (m), 533 (w), 432 (w) cm⁻¹.

HR-MS (ESI⁺): C₉H₁₄N₂OH (M+H)⁺ calcd.: 167.1179, found: 167.1176.

5.4.1.3.3. Synthesis of methyl((4-((dimethylamino)methyl)pyridine-2-yl)methyl)-D-proline



2-hydroxymethyl-4-(dimethylamino)pyridine (78 mg, 0.47 mmol, 1.00 eq) was dissolved in 3 mL Et_2O . The solution was cooled to 0°C and thionyl chloride (0.05 mL, $\rho = 1.64$, 0.69 mmol, 1.47 eq) was added. The reaction was stirred at room temperature for 18 h. The solvent was removed and 2×7 mL cold Et_2O was added to coevaporate remaining thionyl chloride. After removal of the solvent under reduced pressure 2-chlormethyl-4-(dimethylamino)pyridine (**248**) was obtained as a pale rose solid (52.3 mg, 0.24 mmol, 50%), which was directly taken on to the next step without characterisation. Hence Na_2CO_3 (27.0 mg, 0.25 mmol, 1.10 eq), NaI (1.50 mg, 0.01 mmol, 4.4 mol%), and 1.5 mL DMF were added, the mixture degassed for 10 minutes and heated to 50°C . Methyl D-proline (78.0 mg, 0.47 mmol, 1.97 eq) was added. The reaction was stirred for 24 h at 50°C . 4 mL water were added and the solvent was removed under reduced pressure. The brown solid was taken up in 5 mL EtOH and the precipitating salts were removed by filtration. The solvent was removed under reduced pressure and the product was combined with other batches (0.62 mmol + 0.68 mmol). The combined batches were purified by flash column chromatography (silica gel, $\text{CH}_2\text{Cl}_2/\text{MeOH}$ 100:1 → 10:1) to obtain **249** as a brown solid (56 mg, 0.20 mmol, 11%).

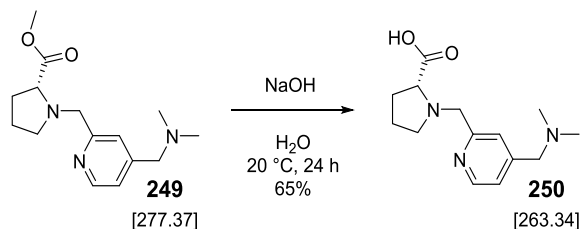
$^1\text{H-NMR}$ (300.1 MHz, CDCl_3): $\delta = 8.49$ (d, $^3J = 4.9$ Hz, 1H, H_6), 7.39 (s, 1H, H_3), 7.21 (d, $^3J = 4.6$ Hz 1H, H_5), 4.02 (d, $^2J = 13.4$ Hz, 1H, $_{\text{pyr}}\text{CH}_2\text{N}_{\text{pro}}$), 3.77 (d, $^2J = 13.4$ Hz, 1H, $_{\text{pyr}}\text{CH}_2\text{N}_{\text{pro}}$), 3.66 (s, 3H, COOCH_3), 3.49 (s, 2H, H_7), 3.41 (dd, $^3J = 8.8$ Hz, $^3J = 5.8$ Hz, 1H, H_2), 3.13-3.06 (m, 1H, H_{5a}), 2.57-2.49 (m, 1H, H_{5b}), 2.30 (s, 6H, $\text{N}(\text{CH}_3)_2$), 2.21-2.13 (m, 1H, H_{3a}), 2.04-1.75 (m, 3H, H_{3b} , H_4) ppm.

$^{13}\text{C-NMR}$ (75.5 MHz, CDCl_3): $\delta = 174.6$ (COO), 159.1 (C_2), 149.3 (C_6), 147.3 (C_4), 123.8 ($C_{3/5}$), 122.6 ($C_{3/5}$), 65.5 (C_2), 62.9 ($_{\text{pm}}\text{CH}_2\text{pyr}$), 60.4 (C_7), 53.7 (C_5), 51.8 (OCH_3), 45.2 ($\text{N}(\text{CH}_3)_2$), 29.5 (C_3), 23.3 (C_4) ppm.

ATR-IR (neat): $\tilde{\nu} = 2947$ (w), 2817 (w), 2775 (w), 1737 (s), 1604 (w), 1561 (vw), 1447 (w), 1361 (w), 1267 (w), 1169 (s), 1092 (vw), 1036 (m), 996 (vw), 910 (vw), 857 (w), 818 (w), 728 (vw), 607 (vw), 528 (vw), 436 (w) cm^{-1} .

HR-MS (APCI $^+$): $\text{C}_{15}\text{H}_{23}\text{N}_3\text{O}_2\text{H}$ ($\text{M}+\text{H}$) $^+$ calcd.: 278.1863, found: 278.1864.

5.4.1.3.4. Synthesis of ((4-((dimethylamino)methyl)pyridine-2-yl)methyl)-D-proline



An aqueous 1 M NaOH solution was purged with N₂ for 10 min and 705 µL were added to 65.2 mg methyl prolineate **249** (0.235 mmol, 1.00 eq). The solution was stirred for 24 h at 20 °C before 3 mL H₂O and 3 mL CH₂Cl₂ were added and the layers separated. The aqueous layer was washed with 10 mL CH₂Cl₂ and neutralised with 1 M HCl_{aq} until pH = 7 was reached. The solution was stirred for 30 min and washed with another 10 mL CH₂Cl₂. The solvent was removed under reduced pressure and the yellow residue was dissolved in 5 mL EtOH and treated by sonication for 15 min. The white precipitate was removed by filtration and the filtrate was concentrated under reduced pressure to yield the ligand **250** as a yellow oil (35.8 mg, 0.15 mmol, 65%).

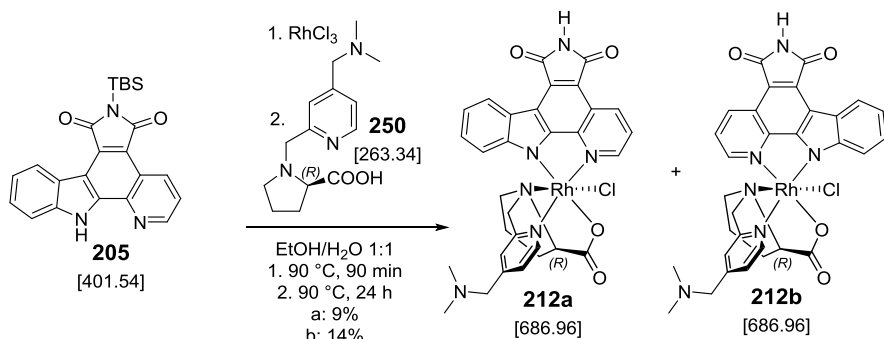
¹H-NMR (300.1 MHz, CD₃OD): δ = 8.68 (d, ³J = 5.0 Hz, 1H, H₆), 7.65 (s, 1H, H₃), 7.52 (d, ³J = 5.0 Hz, ⁴J = 1.3 Hz 1H, H₅), 4.64 (d, ²J = 13.9 Hz, 1H, _{pyr}CH₂N_{pro}), 4.54 (d, ²J = 13.9 Hz, 1H, _{pyr}CH₂N_{pro}), 4.10 (dd, ³J = 9.0 Hz, ³J = 5.8 Hz, H₂), 4.07 (s, 2H, H₇), 3.82-3.74 (m, 1H, H_{5a}), 3.29-3.23 (m, 1H, H_{5b}), 2.65 (s, 6H, N(CH₃)₂), 2.53-2.42 (m, 1H, H_{3a}), 2.24-2.08 (m, 2H, H_{3b}, H_{4a}), 2.05-1.95 (m, 1H, H_{4b}) ppm.

¹³C-NMR (75.5 MHz, CD₃OD): δ = 173.3 (COO), 153.3 (C₂), 151.5 (C₆), 145.4 (C₄), 126.5 (C_{3/5}), 126.4 (C_{3/5}), 70.6 (C₂), 61.6 (_{pyr}CH₂_{pyr}), 59.9 (C₇), 56.4 (C₅), 44.4 (N(CH₃)₂), 30.1 (C₃), 24.5 (C₄) ppm.

ATR-IR (neat): $\tilde{\nu}$ = 3319 (br m), 2942 (w), 2831 (w), 1450 (vw), 1114 (vw), 1021 (s), 625 (br m) cm⁻¹.

HR-MS (ESI⁺): C₁₄H₂₁N₃O₂H (M+H)⁺ calcd.: 264.1707, found: 264.1707.

5.4.1.3.5. Synthesis of the 4-((dimethylamino)methyl) pyridine complexes **212a** and **212b**



The 4-((dimethylamino)methyl) pyridine derivatives of the complexes **201a** and **201b** were prepared according to standard procedure I using 49.6 mg TBS-protected pyridocarbazole (124 μmol, 1.00 eq) and 32.4 mg RhCl₃·3H₂O (124 μmol, 1.00 eq) in 25.0 mL H₂O/EtOH 1:1. The mixture was reacted for 90 min at 90 °C before adding the solution to 35.8 mg of the modified proline-ligand **250** (136 μmol, 1.10 eq) and reaction for another 24 h. After removal of the solvent under reduced pressure, the complex was adsorbed on silica gel (~0.5 g) and the diastereomers were separated according to the standard procedure by flash chromatography (6 g silica). The b isomer eluted very late after washing heavily with CH₂Cl₂/MeOH 5:1, acetone and iPrOH, probably due to basic interactions with the positively charged silica. Each isomer was further subjected to twofold purification by flash chromatography (**212b** 2 x 1.2 g, **212a** 1.5 g and 1.2 g silica) via flash column chromatography. **212a** yielded in 7.8 mg (11.4 μmol, 9%), **212b** in 11.7 mg (17.0 μmol, 14%) as deep red solids.

212a:

¹H-NMR (500.1 MHz, DMSO-*d*₆): δ = 11.26 (br s, NH), 9.57 (d, ³J = 6.0 Hz, 1H, *H*₆), 9.29 (dd, ³J = 8.4 Hz, ⁴J = 1.1 Hz, 1H, *H*_{3''}), 8.86 (d, ³J = 5.1 Hz, 1H, *H*_{1''}), 8.68 (d, ³J = 7.8 Hz, 1H, *H*_{4''}), 8.08 (dd, ³J = 8.4 Hz, ³J = 5.2 Hz, 1H, *H*_{2''}), 7.95 (dd, ³J = 6.0 Hz, ⁴J = 1.4 Hz, 1H, *H*₅), 7.91 (s, 1H, *H*₃), 7.26 (ddd, ³J = 7.9 Hz, ³J = 7.1 Hz, ⁴J = 0.9 Hz, 1H, *H*_{5''}), 7.26 (ddd, ³J = 8.3 Hz, ³J = 7.1 Hz, ⁴J = 1.2 Hz, 1H, *H*_{6''}), 5.66 (d, ³J = 8.4 Hz, 1H, *H*_{7''}), 4.58 (d, ⁴J = 16.5 Hz, 1H, *pro*CH₂_{pyr}), 4.29 (d, ⁴J = 15.7 Hz, 1H, *pro*CH₂_{pyr}), 3.82 (dd, ³J = 9.6 Hz, ³J = 4.2 Hz, 1H, *H*₂), 3.78 (s, 2H, *H*₇), 2.47-2.45 (m, 2H, *H*_{5a}), 2.33 (s, 6 H, N(CH₃)₂), 2.22-2.17 (m, 2H, *H*_{5b}, *H*_{3a}), 2.04-1.98 (m, 1H, *H*_{3b}), 1.60-1.55 (m, 1H, *H*_{4a}), 1.10-1.07 (m, 1H, *H*_{4b}) ppm.

¹³C-NMR (125.8 MHz, DMSO-*d*₆): δ = 182.1 (COO), 170.7 (CO), 170.3 (CO), 161.0 (*C*_{arom}), 154.2 (*C*_{arom}), 152.7 (*C*₆), 152.1 (*C*_{3/q}), 148.9 (*C*_q), 148.8 (*C*_{1'}), 142.1 (*C*_q), 135.2 (*C*_{3''}), 131.3 (*C*_q), 126.5 (*C*_{6''}), 125.8 (*C*_{arom}), 124.8 (*C*_{4''}), 124.0 (*C*_{2''}), 123.5 (*C*_q), 122.7 (*C*_{arom}), 121.4 (*C*_q), 119.6 (*C*_{5''}), 115.1 (*C*_q), 114.6

Experimental part

(C_q), 111.8 (C_{7''}), 72.9 (C₂), 69.9 (_{pro}CH₂_{pyr}), 61.6 (C₇), 61.3 (C₅), 45.2 (N(CH₃)₂), 30.4 (C₃), 24.4 (C₄) ppm.

ATR-IR (neat): $\tilde{\nu}$ = 2920 (m), 2852 (w), 1751 (w), 1703 (s), 1646 (m), 1626 (m), 1581 (w), 1521 (vw), 1494 (vw), 1464 (vw), 1415 (w), 1339 (s), 1262 (m), 1226 (m), 1172 (vw), 1127 (vw), 1087 (vw), 1018 (s), 932 (vw), 858 (vw), 823 (w), 796 (m), 747 (m), 705 (w), 636 (m), 581 (vw), 520 (vw), 491 (s), 439 (m), 412 (vw) cm⁻¹.

HR-MS (APCI⁺): C₃₁H₂₈ClN₆O₄RhH (M+H)⁺ calcd.: 687.0988, found: 687.0989.

212b:

¹H-NMR (500.2 MHz, DMSO-*d*₆): δ = 11.23 (br s, NH), 9.43 (d, ³J = 5.9 Hz, 1H, H₆), 9.17 (dd, ³J = 8.4 Hz, ⁴J = 0.9 Hz, 1H, H_{3''}), 8.71 (d, ³J = 8.0 Hz, 1H, H_{4''}), 7.95 (d, ³J = 5.2 Hz, 1H, H_{1''}), 7.95 (d, ³J = 5.2 Hz, 1H, H₅), 7.84 (s, 1H, H₃), 7.81 (d, ³J = 8.2 Hz, 1H, H_{7''}), 7.74 (dd, ³J = 8.4 Hz, ³J = 5.3 Hz, 1H, H_{2''}), 7.53 (ddd, ³J = 8.3 Hz, ³J = 7.1 Hz, ⁴J = 1.3 Hz, 1H, H_{6''}), 7.37 (ddd, ³J = 7.9 Hz, ³J = 7.1 Hz, ⁴J = 0.9 Hz, 1H, H_{5''}), 4.55 (s, 2H, _{pyr}CH₂N_{pro}), 3.79 (dd, ³J = 9.5 Hz, ³J = 4.8 Hz, 1H, H₂), 3.72 (s, 2H, H₇), 2.48-2.42 (m, 1H, H_{5a}), 2.23-2.12 (m, 2H, H_{5b}, H_{3a}), 1.91-1.83 (m, 1H, H_{3b}), 1.47-1.40 (m, 1H, H_{4a}), 1.11-1.05 (m, 1H, H_{4b}) ppm.

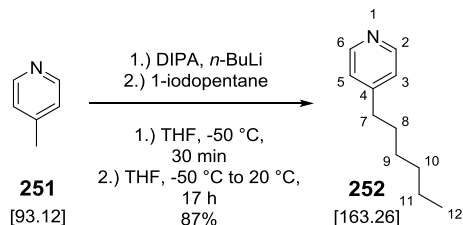
¹³C-NMR (125.8 MHz, DMSO-*d*₆): δ = 182.4 (COO), 170.7 (CO), 170.4 (CO), 159.9 (C_q), 152.3 (C_q), 151.2 (C_q, C₆), 150.5 (C_{1''}), 149.9 (C_q), 142.4 (C_q), 134.8 (C_{3''}), 131.2 (C_q), 126.6 (C_{6''}), 125.5 (C₅), 124.3 (C₄), 124.3 (C_{2''}), 123.1 (C_q), 123.0 (C₃), 121.1 (C_q), 119.7 (C_{5''}), 115.0 (C_{7''}), 114.9 (C_q), 114.0 (C_q), 73.5 (C₂), 69.3 (_{pyr}CH₂N_{pro}), 61.6 (C₇), 61.5 (C₅), 45.4 (N(CH₃)₂), 30.3 (C₃), 23.9 (C₄) ppm.

ATR-IR (neat): $\tilde{\nu}$ = 2921 (m), 2852 (w), 1752 (w), 1706 (s), 1649 (m), 1524 (vw), 1497 (vw), 1467 (vw), 1420 (m), 1342 (s), 1300 (w), 1268 (w), 1229 (m), 1178 (vw), 1130 (vw), 1020 (m), 944 (vw), 864 (vw), 825 (w), 795 (w), 748 (m), 709 (w), 638 (m), 575 (vw), 520 (m), 493 (w) cm⁻¹.

HR-MS (APCI⁺): C₃₁H₂₈ClN₆O₄RhH (M+H)⁺ calcd.: 687.0988, found: 687.0989.

5.4.1.4. 4-hexylpyridine modification

5.4.1.4.1. Synthesis of 4-hexylpyridine



4-hexylpyridine (**251**) was prepared according to a modified literature procedure.^[329] To a solution of 4.6 mL diisopropylamine (32.7 mmol, 1.02 eq) in 200 mL THF at 0 °C were slowly added 13.3 mL of an *n*-BuLi solution (2.5 M in hexane, 33.2 mmol, 1.03 eq). The yellow reaction mixture was stirred for 30 min at 0 °C before it was cooled to –50 °C and 3.00 g 4-methylpyridine (32.2 mmol, 1.00 eq) was added slowly. The resulting red solution was stirred at –50 °C for 30 min. Subsequently a solution of 4.2 mL 1-iodopentane (32.2 mmol, 1.00 eq) was added dropwise at -50 °C and the resulting mixture stirred for 60 min at –50 °C before it was allowed to warm-up to 20 °C under stirring for 17 h. The reaction was quenched by addition of 200 mL saturated aqueous NH₄Cl solution and the layers were separated. The aqueous layer was further extracted with Et₂O (3 x 30 mL) and the combined organic layers were washed with 150 mL H₂O and 150 mL brine, dried over MgSO₄ and reduced *in vacuo*. The crude product was purified using flash column chromatography with neutral aluminium oxide as stationary phase using hexane/Et₂O 9:1. After solvent removal *in vacuo* the desired product **252** (4.57 g, 28.0 mmol, 87%) was obtained as an off-white liquid.

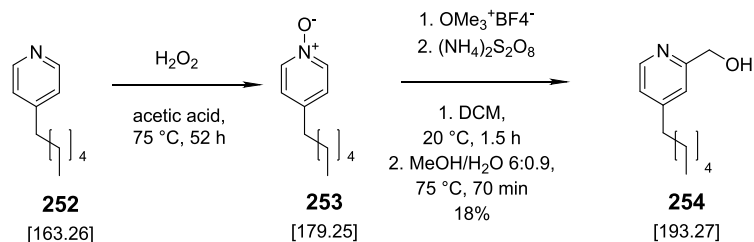
¹H-NMR (300.1 MHz, CDCl₃): δ = 8.46 (dd, ³J = 4.6 Hz, ⁵J = 1.5 Hz, 2H, H₂, H₆), 7.08 (dd, ³J = 4.6 Hz, ⁵J = 1.6 Hz, 2H, H₃, H₅), 2.57 (t, ³J = 7.7 Hz, 2H, H₇), 1.65-1.55 (m, 2H, H₈), 1.35-1.24 (m, 6H, H₉, H₁₀, H₁₁), 0.89-0.84 (m, 3H, H₁₂) ppm.

¹³C-NMR (75.7 MHz, CDCl₃): δ = 151.9 (C₄), 149.7 (2C, C₂, C₆), 124.0 (2C, C₃, C₅), 35.3 (C₇), 31.7 (C₁₀), 30.3 (C₈), 28.9 (C₉), 22.6 (C₁₁), 14.1 (C₁₂) ppm.

ATR-IR (neat): $\tilde{\nu}$ = 3066 (w), 3026 (w), 2926 (vs), 2858 (s), 2019 (w), 1932 (w), 1846 (w), 1650 (w), 1600 (vs), 1558 (m), 1459 (s), 1415 (s), 1374 (w), 1264 (w), 1218 (w), 1174 (w), 1111 (w), 1070 (w), 993 (m), 801 (vs), 726 (m), 673 (w), 585 (s), 506 (s), 421 (w) cm⁻¹.

HR-MS (ESI⁺): C₁₁H₁₇NH (M+H)⁺ calcd.: 164.1434; found: 164.1433.

5.4.1.4.2. Synthesis of (4-hexylpyridine-2yl)-methanol



(4-hexylpyridine-2yl)-methanol (**254**) was prepared according to modified literature procedures.^[330,331] 4-hexylpyridine (4.57 g, 28.0 mmol, 1.00 eq) was dissolved in 20 mL acetic acid and aqueous hydrogen peroxide (30%, 27.3 mmol, 0.98 eq) was added. The resulting yellow solution was heated to 75 °C for 4 h. After cooling to 20 °C, an additional 3.3 mL of H₂O₂ aq. (29.1 mmol, 1.04 eq) were added and the solution stirred at 75 °C for 48 h. After cooling to 20 °C, the solvent was removed under reduced pressure and the resulting oil was taken up in 110 mL CH₂Cl₂. To this solution 4.18 g Me₃OB₄ (28.0 mmol, 1.00 eq) was added and the resulting solution stirred for 90 min at 20 °C, before the solvent was removed under reduced pressure. The remaining residue was taken up in 60 mL of boiling MeOH and 6 mL of a solution of 1.92 g ammonium persulfate (8.40 mmol, 0.30 eq) in 9 mL H₂O was added. The reaction was heated to 75 °C for 30 min, before the remaining persulfate solution was added and the solution stirred at 75 °C for another 40 min. After cooling to 20 °C, the solvent was removed *in vacuo* and the residue was taken up in 85 mL brine, 85 mL H₂O and 60 mL of a 3 M HCl_{aq} solution and stirred for 60 min at 20 °C. The pH of the solution was adjusted to pH 9 with aqueous NH₃ solution and extracted with CHCl₃ (1 x 100 mL, 3 x 30 mL). The combined organic layers were dried over MgSO₄ and the solvent was removed *in vacuo*. The crude product was subjected to flash column chromatography (170 g silica, CH₂Cl₂/MeOH 50:1 to 10:1) and the product fractions were dried under reduced pressure to obtain 971 mg (5.02 mmol, 18%) of the methanol derivative **254** as a brown oil over 2 steps.

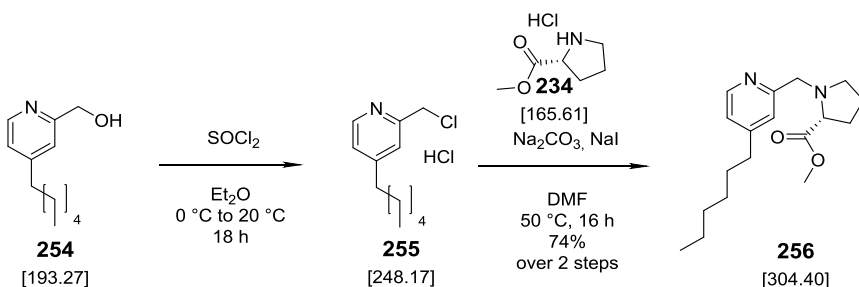
¹H-NMR (300.1 MHz, CDCl₃): δ = 8.42 (d, ³J = 5.2 Hz, 1H, H₆), 7.11 (s, 1H, H₃), 7.06 (dd, ³J = 5.1 Hz, ⁵J = 1.6 Hz, H₅), 4.75 (s, 2H, CH₂OH), 4.23 (s, 1H, OH), 2.62 (t, ³J = 7.7 Hz, 2H, H₇), 1.67-1.57 (m, 2H, H₈), 1.35-1.26 (m, 6H, H₉, H₁₀, H₁₁), 0.89-0.84 (m, 3H, H₁₂) ppm.

¹³C-NMR (75.7 MHz, CDCl₃): δ = 158.9 (C₉), 153.3 (C₉), 148.0 (C₆), 122.9 (C₃), 120.8 (C₅), 64.1 (CH₂OH), 35.5 (C₇), 31.7 (C₁₀), 30.4 (C₈), 29.0 (C₉), 22.7 (C₁₁), 14.2 (C₁₂) ppm.

ATR-IR (neat): $\tilde{\nu}$ = 3224 (br, w), 3055 (w), 3013 (w), 2925 (vs), 2857 (s), 1925 (w), 1650 (w), 1606 (vs), 1560 (m), 1457 (s), 1415 (s), 1367 (m), 1261 (w), 1222 (w), 1159 (w), 1112 (m), 1058 (vs), 1001 (s), 896 (w), 832 (s), 769 (w), 728 (m), 598 (m), 543 (m), 440 (s) cm⁻¹.

HR-MS (ESI⁺): C₁₂H₁₉NOH (M+H)⁺ calcd.: 194.1539; found: 194.1537.

5.4.1.4.3. Synthesis of methyl ((4-hexylpyridine-2-yl)methyl)-D-proline



Methyl ((4-hexylpyridine-2-yl)methyl)-D-proline was prepared according to a modified literature procedure.^[332] A solution of 486 mg (4-hexylpyridine-2-yl)-methanol (2.51 mmol, 1.00 eq) in 2.5 mL Et₂O was cooled to 0 °C and 0.30 mL SOCl₂ ($\rho = 1.64\text{g/cm}^3$, 3.77 mmol, 1.50 eq) were added dropwise. The reaction was stirred for 16 h at 20 °C before the solvent and excess SOCl₂ were removed under reduced pressure. The resultant brown solid **255** was dissolved in 6 mL DMF, 587 mg powdered NaCO₃ (5.54 mmol, 2.20 eq) and 19 mg NaI (0.13 mmol, 0.04 eq) were added and the suspension was heated to 50 °C under exclusion from light. To the suspension a solution of 502 mg D-proline methylester hydrochloride (3.03 mmol, 1.20 eq) in 6 mL DMF was added dropwise and the resulting suspension was stirred at 50 °C for 16 h. After cooling to 20 °C, 30 mL H₂O were added. The aqueous layer was extracted with CH₂Cl₂ (3 x 20 mL), the combined organic layers were dried over MgSO₄, and the solvent removed *in vacuo*. The crude residue was purified using flash column chromatography (silica 66 g, CH₂Cl₂/MeOH 50:1 to 10:1). After removal of the solvent *in vacuo* 565 mg (1.86 mmol, 74%) of the proline **256** were isolated as a yellow oil.

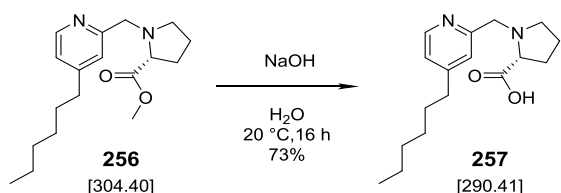
¹H-NMR (300.1 MHz, CDCl₃): $\delta = 8.39$ (dd, ³J = 5.1 Hz, ⁵J = 0.4 Hz, 1H, H₆), 7.29 (s, 1H, H₃), 7.00 (dd, ³J = 5.1 Hz, ⁴J = 1.8 Hz, 1H, H₅), 4.04 (d, ²J = 13.4 Hz, 1H, _{pyr}CH₂N_{pro}), 3.79 (d, ²J = 13.4 Hz, 1H, _{pyr}CH₂N_{pro}), 3.66 (s, 3H, COOCH₃), 3.43 (dd, ³J = 8.8 Hz, ⁵J = 5.9 Hz, 1H, H₂), 3.14-3.17 (m, 1H, H_{5'}), 2.62-2.51 (m, 3H, H₇, H_{5''}), 2.24-2.10 (m, 1H, H_{3'}), 2.04-1.75 (m, 3H, H_{4'}, H_{3''}), 1.66-1.56 (m, 2H, H₈), 1.34-1.24 (m, 6H, H₉, H₁₀, H₁₁), 0.87 (t, 3H, ³J = 6.9 Hz, H₁₂) ppm.

¹³C-NMR (75.7 MHz, CDCl₃): $\delta = 174.4$ (COOCH₃), 158.1 (C_q), 153.1 (C_q), 148.5 (C₆), 123.9 (C₃), 122.6 (C₅), 65.5 (C₂), 60.1 (_{pyr}CH₂N_{Pro}), 53.7 (C_{5'}), 51.9 (OCH₃), 35.5 (C₇), 31.7 (C₁₀), 30.4 (C₈), 29.4 (C_{3'}), 29.1 (C₉), 23.3 (C_{4'}), 22.7 (C₁₁), 14.2 (C₁₂) ppm.

ATR-IR (neat): $\tilde{\nu} = 2928$ (s), 2857 (m), 1739 (vs), 1679 (vs), 1603 (s), 1558 (m), 1441 (m), 1412 (m), 1379 (m), 1266 (m), 1195 (vs), 1170 (vs), 1089 (s), 1040 (w), 997 (m), 902 (w), 835 (m), 767 (w), 725 (w), 659 (w), 598 (w), 539 (w), 443 (m) cm⁻¹.

HR-MS (ESI⁺): C₁₈H₂₈N₂O₂H (M+H)⁺ calcd.: 305.2224; found: 305.2220.

5.4.1.4.4. Synthesis of ((4-hexylpyridine-2-yl)methyl)-D-proline



256 (565 mg, 1.86 mmol, 1.00 eq) was dissolved in 5.6 mL aqueous NaOH (1 M, 3.00 eq) and the resulting solution was stirred for 16 h at 20 °C. Then, the solution was diluted by addition of 10 mL H₂O and the solution washed with 10 mL CH₂Cl₂, which resulted in the precipitation of a white solid, which was removed by filtration. The aqueous layer was neutralised by addition of 1 M HCl_{aq} and further stirred for 30 min at 20 °C. The solution was washed again with 10 mL CH₂Cl₂ and the resulting precipitate was removed. The solvent of the aqueous layer was removed under reduced pressure, and the resulting residue was taken up in 20 mL EtOH with the help of sonication for 15 min. The precipitate was filtered off, washed with some EtOH, and the filtrate concentrated *in vacuo* to yield in 498 mg of a brownish resin, which contained residual EtOH (factor 1.65:1) resulting in a yield of 73% (1.36 mmol) of the desired ligand **257** in its ethanol free form.

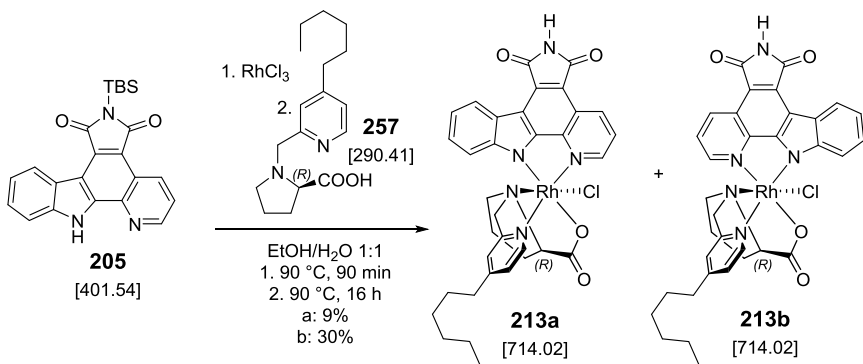
¹H-NMR (500.2 MHz, CDCl₃): δ = 8.42 (d, ³J = 5.1 Hz, 1H, H₆), 7.06 (s, 1H, H₃), 7.00 (d, ³J = 5.0 Hz, 1H, H₅), 4.77 (br s, 1H, COOH), 4.21 (d, ²J = 12.4 Hz, 1H, _{pyr}CH₂N_{pro}), 3.79 (br s, 1H, _{pyr}CH₂N_{pro}), 3.56 (br s, 1H, H₂), 3.32-3.29 (m, 1H, H_{5'a}), 2.66-2.60 (m, 1H, H_{5'b}), 2.53 (t, ³J = 7.9 Hz, 2H, H₇) 2.25-2.17 (m, 1H, H_{3'a}), 2.15-2.08 (m, 1H, H_{3'b}), 1.93-1.84 (m, 1H, H_{4'a}), 1.82-1.79 (m, 1H, H_{4'b}), 1.59-1.53 (m, 2H, H₈), 1.31-1.23 (m, 6H, H₉, H₁₀, H₁₁), 0.85 (t, 3H, ³J = 6.9 Hz, H₁₂) ppm.

¹³C-NMR (75.7 MHz, CDCl₃): δ = 175.8 (COOH), 155.5 (C₂), 153.3 (C₄), 149.5 (C₆), 123.7 (C₃), 123.3 (C₅), 68.5 (C_{2'}), 59.6 (_{pyr}CH₂N_{Pro}), 53.9 (C_{5'}), 35.3 (C₇), 31.6 (C₁₀), 30.3 (C₈), 29.7 (C_{3'}), 29.0 (C₉), 23.7 (C_{4'}), 22.6 (C₁₁), 14.1 (C₁₂) ppm.

ATR-IR (neat): $\tilde{\nu}$ = 3380 (br, w), 3053 (w), 2927 (s), 2861 (m), 1703 (w), 1602 (vs), 1452 (m), 1400 (s), 1307 (m), 1210 (w), 1175 (w), 1091 (m), 1049 (s), 998 (w), 919 (w), 885 (w), 840 (w), 775 (w), 717 (w), 690 (w), 599 (w), 437 (m) cm⁻¹.

HR-MS (ESI⁺): C₁₇H₂₆N₂O₂H (M+H)⁺ calcd.: 291.2067; found: 291.2064.

5.4.1.4.5. Synthesis of the hexyl derivatised complexes **213a** and **213b**



The 4-hexyl-pyridine derivatives of the complexes **201a** and **201b** were prepared according to standard procedure I using 50 mg TBS-protected pyridocarbazole (125 μmol, 1.00 eq) and 33 mg RhCl₃·3H₂O (125 μmol, 1.00 eq) in 25.0 mL H₂O/EtOH 1:1. The reaction mixture was reacted for 90 min at 90 °C before addition of 40 mg of the proline-ligand **257** (137 μmol, 1.10 eq) and reacting for another 16 h. After removal of the solvent under reduced pressure, the compound was adsorbed on silica (~1.00 g) and the diastereomers were separated by flash chromatography (12 g silica gel).¹ **213b** (*cis*-isomer) was further purified twice over 2 g silica each yielding in 16.1 mg of the complex as a deep red solid. The extensive purification of mixed fractions yielded in additional 11.0 mg giving a total yield of 27.1 mg (38.0 μmol, 30%). **213a** (*trans*-isomer) was further purified twice over 4 g silica using CH₂Cl₂/MeOH and 2 g using CH₂Cl₂/CH₃CN (2:1 to 1:1) yielding in 8.1 mg (11.3 μmol, 9%) of the complex as a deep red solid.

¹Please be aware that both isomers have the same R_f on TLC in CH₂Cl₂/MeOH 10:1. They will be separated if you run the TLC twice or use a mixture of CH₂Cl₂/CH₃CN 2:1 or 1:1

213b:

¹H-NMR (500.1 MHz, DMSO-*d*₆): δ = 11.24 (br s, NH), 9.50 (d, ³J = 6.0 Hz, 1H, H₆), 9.29 (dd, ³J = 8.4 Hz, ⁴J = 1.0 Hz, 1H, H_{3''}), 8.84 (d, ³J = 5.2 Hz, 1H, H_{1''}), 8.68 (d, ³J = 7.9 Hz, 1H, H_{4''}), 8.07 (dd, ³J = 8.2 Hz, ³J = 5.2 Hz, 1H, H_{2''}), 7.89 (dd, ³J = 5.0 Hz, ⁴J = 1.4 Hz, 1H, H₅), 7.84 (s, 1H, H₃), 7.26 (t, ³J = 7.2 Hz, 1H, H_{6''}), 7.16 (ddd, ³J = 8.3 Hz, ³J = 7.2 Hz, ⁴J = 1.2 Hz, 1H, H_{5''}), 5.69 (d, ³J = 8.3 Hz, 1H, H_{7''}), 4.52 (d, ⁴J = 15.6 Hz, 1H, *pro*CH₂_{pyr}), 4.28 (d, ⁴J = 15.7 Hz, 1H, *pro*CH₂_{pyr}), 3.79 (dd, ³J = 9.6 Hz, ³J = 4.2 Hz, 1H, H₂), 2.98-2.90 (m, 2H, H₇), 2.47-2.45 (m, 1H, H_{5a}), 2.24-2.16 (m, 2H, H_{5b}, H_{3a}), 2.03-1.97 (m, 1H, H_{3b}), 1.83-1.75 (m, 2H, H₈), 1.60-1.55 (m, 1H, H_{4a}), 1.42-1.36 (m, 4H, H₉, H₁₀), 1.27-1.26 (m, 2H, H₁₁), 1.10-1.02 (m, 1H, H_{4b}), 0.92 (t, 3H, H₁₂) ppm.

¹³C-NMR (125.8 MHz, DMSO-*d*₆): δ = 73.0 (C₂), 69.9 (CH₂N_{pro}), 61.3 (C₅), 34.4 (C₇), 31.0 (C₁₀), 30.4 (C₃), 29.4 (C₈), 28.1 (C₉), 24.3 (C₄), 22.0 (C₁₁), 14.0 (C₁₂) ppm. Not all carbon atoms could be found due to low signal to noise ratio (solubility issue).

Experimental part

ATR-IR (neat): $\tilde{\nu} = 2922$ (m), 2851 (m), 1754 (w), 1705 (s), 1665 (s), 1621 (m), 1582 (vw), 1559 (vw), 1522 (w), 1492 (w), 1465 (vw), 1414 (w), 1400 (w), 1378 (vw), 1340 (s), 1294 (m), 1259 (m), 1228 (s), 1177 (vw), 1129 (w), 1079 (vw), 1066 (vw), 1045 (vw), 1011 (m), 973 (vw), 953 (vw), 936 (vw), 874 (vw), 829 (m), 803 (m), 747 (s), 725 (vw), 709 (m), 639 (m), 496 (m), 440 (m), 388 (m) cm^{-1} .

HR-MS (ESI $^+$): $\text{C}_{34}\text{H}_{34}\text{ClN}_5\text{O}_4\text{Rh} (\text{M}+\text{H})^+$ calcd.: 714.1349, found: 714.1350.

213a:

$^1\text{H-NMR}$ (500.2 MHz, DMSO- d_6): $\delta = 11.20$ (br s, NH), 9.37 (d, ${}^3J = 6.0$ Hz, 1H, H_6), 9.17 (dd, ${}^3J = 8.4$ Hz, ${}^4J = 1.0$ Hz, 1H, $H_{3''}$), 8.71 (dt, ${}^3J = 8.0$ Hz, ${}^4J = 0.9$ Hz, 1H, $H_{4''}$), 7.92 (d, ${}^3J = 5.3$ Hz, 1H, $H_{1''}$), 7.83-7.80 (m, 2H, $H_{7''}$, H_5), 7.76 (d, ${}^4J = 1.8$ Hz, 1H, H_3), 7.74 (dd, ${}^3J = 8.4$ Hz, ${}^3J = 5.3$ Hz, 1H, $H_{2''}$), 7.54 (ddd, ${}^3J = 8.3$ Hz, ${}^3J = 7.1$ Hz, ${}^4J = 1.2$ Hz, 1H, H_6), 7.37 (ddd, ${}^3J = 8.0$ Hz, ${}^3J = 7.0$ Hz, ${}^4J = 1.0$ Hz, 1H, $H_{5''}$), 4.55 (d, ${}^2J = 16.0$ Hz, 1H, ${}_{\text{pyr}}\text{CH}_2\text{N}_{\text{pro}}$), 4.49 (d, ${}^4J = 16.1$ Hz, 1H, ${}_{\text{pyr}}\text{CH}_2\text{N}_{\text{pro}}$), 3.76 (dd, ${}^3J = 9.4$ Hz, ${}^3J = 4.9$ Hz, 1H, H_2), 2.88-2.85 (m, 2H, H_7), 2.48-2.43 (m, 1H, H_{5a}), 2.23-2.13 (m, 2H, H_{5b} , H_{3a}), 1.88-1.83 (m, 1H, H_{3b}), 1.77-1.71 (m, 2H, H_8), 1.45-1.39 (m, 3H, H_{4a} , H_9), 1.36-1.33 (m, 4H, H_{10} , H_{11}), 1.09-1.04 (m, 1H, H_{4b}), 0.92-0.89 (m, 3H, H_{12}) ppm.

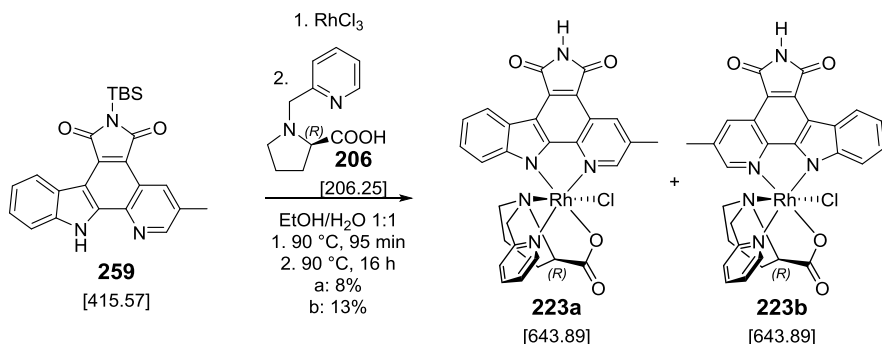
$^{13}\text{C-NMR}$ (125.8 MHz, DMSO- d_6): $\delta = 182.3$ (COO), 170.6 (CO), 170.3 (CO), 159.6 (C_q), 156.8 (C_q), 152.2 (C_q), 150.9 (C_6), 150.3 ($C_{1''}$), 149.9 (C_q), 142.4 (C_q), 134.8 ($C_{3''}$), 131.2 (C_q), 126.5 ($C_{6''}$), 126.0 (C_5), 124.3 ($C_{4''}$), 124.2 ($C_{2''}$), 123.5 (C_3), 123.1 (C_q), 121.1 (C_q), 119.6 ($C_{5''}$), 114.9 ($C_{7''}$), 114.9 (C_q), 113.9 (C_q), 73.5 (C_2), 69.2 (${}_{\text{pyr}}\text{CH}_2\text{N}_{\text{pro}}$), 61.4 ($C_{5'}$), 35.0 (C_7), 31.0 (C_{10}), 30.3 ($C_{3'}$), 29.3 (C_8), 28.4 (C_9), 23.8 ($C_{4'}$), 22.0 (C_{11}), 13.9 (C_{12}) ppm.

ATR-IR (neat): $\tilde{\nu} = 3108$ (w), 2923 (m), 2853 (m), 2719 (w), 1750 (w), 1710 (m), 1648 (m), 1520 (w), 1493 (w), 1449 (w), 1415 (m), 1340 (s), 1296 (m), 1267 (w), 1230 (m), 1174 (vw), 1134 (w), 1084 (vw), 1018 (m), 934 (w), 853 (w), 823 (w), 797 (w), 754 (m), 706 (w), 635 (m), 571 (vw), 521 (vw), 493 (m), 442 (w), 416 (w) cm^{-1} .

HR-MS (ESI $^+$): $\text{C}_{34}\text{H}_{33}\text{ClN}_5\text{O}_4\text{RhNa} (\text{M}+\text{Na})^+$ calcd.: 736.1179, found: 736.1179.

5.4.2. Modification of the pyridocarbazole ligand

5.4.2.1. Synthesis of 5-methylpyridine derivatised complexes 223a and 223b



The methyl-derivatives **223a** and **223b** were prepared according to standard procedure I using 50 mg (120 µmol, 1.00 eq) of TBS-protected methyl-pyridocarbazole (**259**) and 32 mg (120 µmol, 1.00 eq) RhCl₃·3 H₂O in 24 mL H₂O/EtOH 1:1, which were reacted for 90 min at 95 °C. After cooling to 20 °C, 27.3 mg of proline ligand **206** (133 µmol, 1.10 eq) was added and further reacted for 16 h at 90 °C. This batch was combined with a small scale reaction (24.0 µmol) for purification. The diastereoisomers were separated by flash chromatography (8 g silica gel) using the standard procedure and each isomer was further purified twice (2 g and 1.5 g of silica) yielding in **223a** (7.1 mg, 11.0 µmol, 8%) and **223b** (11.9 mg, 18.5 µmol, 13%) as orange-red solids. However, after repetitive purification both diastereomers still contained some traces of impurities.

223a:

¹H-NMR (300.1 MHz, DMSO-*d*₆): δ = 11.23 (s, NH), 9.67 (d, ³J = 5.7 Hz, 1H, *H*₆), 9.09 (dd, ⁴J = 1.5 Hz, ⁴J = 1.1 Hz, 1H, *H*_{3'}), 8.66 (m, ³J = 7.5 Hz, 2H, *H*_{1'}, *H*_{4'}), 8.47 (td, ³J = 7.8 Hz, ⁴J = 1.5 Hz, 1H, *H*₄), 8.03 (ddd, ³J = 7.3 Hz, ³J = 6.4 Hz, ⁴J = 0.9 Hz, 1H, *H*₅), 7.98 (d, ³J = 7.7 Hz, 1H, *H*₃), 7.25 (ddd, ³J = 8.0 Hz, ³J = 7.0 Hz, ⁴J = 0.9 Hz, 1H, *H*_{5'}), 7.17 (ddd, ³J = 8.3 Hz, ³J = 7.1 Hz, ⁴J = 1.3 Hz, 1H, *H*_{6'}), 5.65 (d, ³J = 8.3 Hz, 1H, *H*_{7'}), 4.60 (d, ⁴J = 15.7 Hz, 1H, *pro*CH₂_{pyr}), 4.33 (d, ⁴J = 15.5 Hz, 1H, *pro*CH₂_{pyr}), 3.79 (dd, ³J = 9.6 Hz, ³J = 4.5 Hz, 1H, *H*₂), 2.76 (s, 3H, CH₃), 2.24-2.20 (m, 2H, *H*_{5'b}, *H*_{3'a}), 2.05-2.02 (m, 1H, *H*_{3'b}), 1.61-1.57 (m, 1H, *H*_{4'a}), 1.16-1.07 (m, 1H, *H*_{4'b}) ppm. The missing H_{5'a} signal overlaps with the DMSO signal.

¹³C-NMR (125.8 MHz, DMSO-*d*₆): δ = 182.1 (COO), 170.7 (CO), 170.3 (CO), 161.2 (C_q), 153.0 (C_q), 152.6 (C₆), 149.2 (C_{1'}), 148.8 (C_q), 141.2 (C₄), 140.5 (C_q), 134.3 (C_{3'}), 134.1 (C_q), 131.4 (C_q), 126.5 (C_{6'}), 126.3 (C₅), 124.7 (C_{4'}), 123.6 (C_q), 123.5 (C₃), 121.3 (C_q), 119.6 (C_{5'}), 114.6 (C_q), 114.0 (C_q), 111.7 (C₇), 73.0 (C₂), 70.0 (*pro*CH₂_{pyr}), 61.3 (C₅), 30.5 (C₃), 24.4 (C₄), 19.3 (CH₃) ppm.

Experimental part

ATR-IR (neat): $\tilde{\nu}$ = 3051 (vw), 2922 (w), 2854 (w), 1749 (w), 1711 (m), 1649 (m), 1486 (w), 1419 (w), 1341 (m), 1295 (m), 1231 (w), 1149 (w), 1017 (w), 933 (vw), 896 (vw), 857 (vw), 820 (w), 747 (m), 639 (w), 514 (w), 483 (w), 450 (vw), 401 (vw) cm^{-1} .

HR-MS (ESI $^+$): $\text{C}_{29}\text{H}_{23}\text{ClN}_5\text{O}_4\text{RhH}$ ($\text{M}+\text{H}$) $^+$ calcd.: 644.0566, found: 644.0561.

223b:

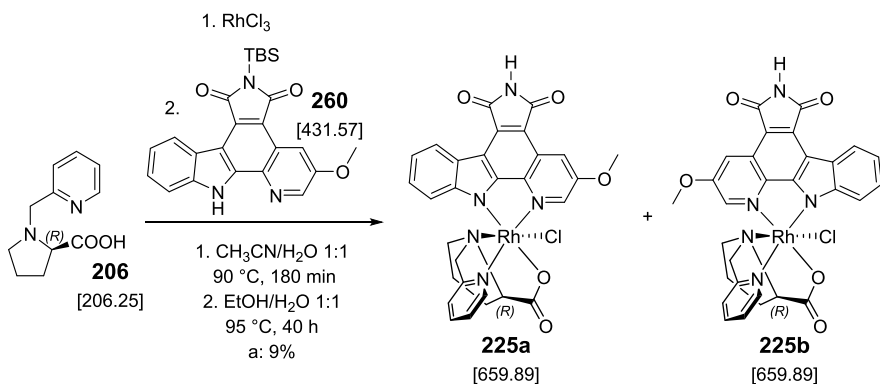
$^1\text{H-NMR}$ (500.1 MHz, DMSO- d_6): δ = 11.18 (s, NH), 9.53 (d, 3J = 5.7 Hz, 1H, H_6), 8.97 (dd, 4J = 1.4 Hz, 4J = 1.0 Hz, 1H, $H_{3''}$), 8.68 (d, 3J = 7.8 Hz, 1H, $H_{4''}$), 8.37 (td, 3J = 7.8 Hz, 4J = 1.5 Hz, 1H, H_4), 7.96-7.91 (m, 3J = 6.3 Hz, 3J = 8.1 Hz, 2H, H_5 , H_3), 7.79 (d, 3J = 8.3 Hz, 2H, $H_{7''}$, H_1''), 7.52 (ddd, 3J = 8.3 Hz, 3J = 7.1 Hz, 4J = 1.3 Hz, 1H, $H_{6''}$), 7.17 (ddd, 3J = 8.0 Hz, 3J = 7.1 Hz, 4J = 0.9 Hz, 1H, $H_{5''}$), 4.67 (d, 4J = 15.1 Hz, 1H, $_{\text{pro}}\text{CH}_{2\text{pyr}}$), 4.55 (d, 4J = 16.0 Hz, 1H, $_{\text{pro}}\text{CH}_{2\text{pyr}}$), 3.77 (dd, 3J = 9.5 Hz, 3J = 4.9 Hz, 1H, H_2), 2.47-2.43 (m, 1H, $H_{5'a}$), 2.24-2.14 (m, 2H, $H_{5'b}$, $H_{3'a}$), 1.87-1.82 (m, 1H, $H_{3'b}$), 1.47-1.41 (m, 1H, $H_{4'a}$), 1.11-1.04 (m, 1H, $H_{4'b}$) ppm. The missing signal belonging to the -CH₃ group overlaps with the DMSO signal as confirmed by ^1H - ^1H -COSY-NMR spectroscopy.

$^{13}\text{C-NMR}$ (125.8 MHz, DMSO- d_6): δ = 182.4 (COO), 170.7 (CO), 170.4 (CO), 160.2 (C_q), 152.5 (C_q), 151.7 (C_6), 151.2 ($C_{1''}$), 149.8 (C_q), 140.7 (C_4), 134.6 (C_q), 133.9 ($C_{3''}$), 131.2 (C_q), 126.4 ($C_{6''}$), 126.1 (C_5), 124.1 ($C_{4''}$), 123.9 (C_3), 123.1 (C_q), 121.0 (C_q), 119.6 ($C_{6''}$), 114.8 ($C_{7''}$), 114.4 (C_q), 113.3 (C_q), 73.5 ($C_{2''}$), 69.5 ($_{\text{pro}}\text{CH}_{2\text{pyr}}$), 61.5 (C_5), 30.4 (C_3), 23.8 (C_4), 19.0 (CH₃) ppm.

ATR-IR (neat): $\tilde{\nu}$ = 3052 (vw), 2922 (w), 2856 (vw), 1750 (w), 1708 (m), 1643 (s), 1573 (vw), 1493 (vw), 1418 (w), 1339 (s), 1296 (m), 1268 (w), 1231 (m), 1153 (vw), 1112 (vw), 1017 (m), 933 (vw), 891 (vw), 858 (vw), 822 (w), 751 (s), 712 (w), 635 (w), 569 (vw), 506 (w), 484 (vw), 452 (w), 432 (vw), 421 (vw), 410 (vw), 401 (w) cm^{-1} .

HR-MS (ESI $^+$): $\text{C}_{29}\text{H}_{23}\text{ClN}_5\text{O}_4\text{RhNa}$ ($\text{M}+\text{Na}$) $^+$ calcd.: 666.0386, found: 666.0381.

5.4.2.2. Synthesis of 5-methoxypyridine derivatised complexes 225a and 225b



225a was prepared according to standard procedure II by heating a solution of 21 mg of proline-ligand **206** (99.6 µmol, 1.00 eq) and 26 mg RhCl₃·3H₂O (99.6 µmol, 1.00 eq) in 18.0 mL H₂O/CH₃CN 1:1 for 3 h at 90 °C. After cooling to 20 °C, the solvent was removed under reduced pressure, 47 mg TBS-protected methoxy pyridocbazole **260** (110 µmol, 1.10 eq) and 18 mL H₂O/EtOH 1:1 were added and further reacted for 40 h at 95 °C. After solvent removal, the compound was adsorbed on silica, and the diastereomers were separated using flash chromatography according to the standard procedure on 15 g silica. The diastereomer a was further purified over 1.5 g silica respectively yielding in 5.6 mg (8.49 µmol, 9%) of **225a** as a deep red solid. **225b** was obtained with a trace of the corresponding precursor (3:1 mixture, ~3 mg).

225a:

¹H-NMR (300.1 MHz, DMSO-*d*₆): δ = 11.25 (s, NH), 9.66 (d, ³*J* = 5.7 Hz, 1H, *H*₆), 8.64-8.62 (m, 2H, *H*_{3'}, *H*_{4'}), 8.47 (td, ³*J* = 7.8 Hz, ⁴*J* = 1.4 Hz, 1H, *H*₅), 8.40 (dd, ⁴*J* = 2.4 Hz, ⁴*J* = 0.7 Hz, 1H, *H*_{7'}), 8.04-7.99 (m, 1H, *H*₄), 7.98 (d, ³*J* = 7.9 Hz, 1H, *H*₃), 7.24 (m, ⁴*J* = 0.9 Hz, 1H, *H*_{6'}), 7.17 (ddd, ³*J* = 8.3 Hz, ³*J* = 6.9 Hz, ⁴*J* = 1.4 Hz, 1H, *H*_{5'}), 5.63 (d, ³*J* = 7.9 Hz, 1H, *H*₇), 4.61 (d, ⁴*J* = 15.5 Hz, 1H, *p*ro_{CH}₂pyr), 4.32 (d, ⁴*J* = 15.6 Hz, 1H, *p*ro_{CH}₂pyr), 4.14 (s, 3H, OCH₃), 3.82 (dd, ³*J* = 9.4 Hz, ³*J* = 4.7 Hz, 1H, *H*_{2'}), 2.58-2.53 (m, 1H, *H*_{5'}), 2.29-2.16 (m, 2H, *H*₅, *H*₃), 2.06-1.98 (m, 1H, *H*₃), 1.67-1.60 (m, 1H, *H*_{4'a}), 1.18-1.09 (m, 1H, *H*_{4'b}) ppm.

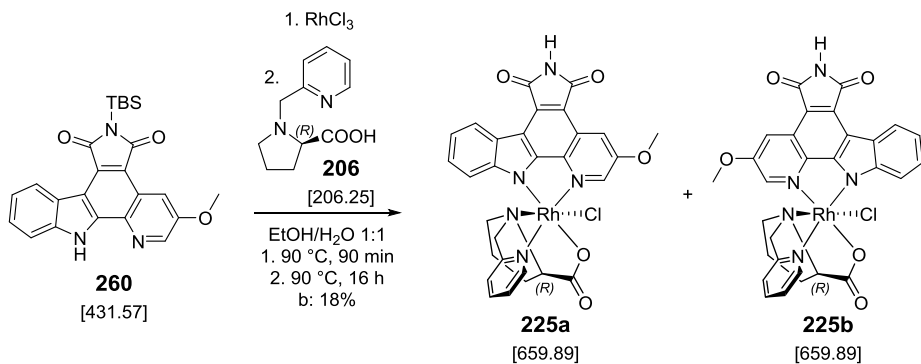
¹³C-NMR (125.8 MHz, DMSO-*d*₆): δ = 182.0 (COO), 170.8 (CO), 170.2 (CO), 161.2 (*C*_q), 155.0 (*C*_q), 153.5 (*C*_q), 152.6 (*C*₆), 148.9 (*C*_{1'}), 141.2 (*C*₅), 140.7 (*C*_q), 136.9 (*C*_{3'}), 131.5 (*C*_q), 126.4 (*C*_{5'}), 126.3 (*C*₄), 124.6 (*C*_{4'}), 123.6 (2C, *C*_q + *C*₃), 122.1 (*C*_q), 119.5 (*C*_{6'}), 114.0 (*C*_q), 113.4 (*C*_q), 113.3 (*C*_q), 111.5 (*C*_{7'}), 72.8 (*C*_{2'}), 69.9 (*p*ro_{CH}₂pyr), 61.1 (*C*₅), 56.7 (OCH₃), 30.1 (*C*₃), 24.4 (*C*₄) ppm.

ATR-IR (neat): $\tilde{\nu}$ = 2917 (w), 2850 (w), 1752 (w), 1703 (m), 1661 (m), 1607 (w), 1568 (w), 1518 (vw), 1491 (vw), 1474 (vw), 1459 (vw), 1450 (vw), 1407 (w), 1347 (m), 1299 (w), 1259 (m), 1223 (m), 1162 (vw), 1114 (vw), 1070 (vw), 1058 (vw), 1010 (m), 972 (vw), 933 (vw), 881 (vw), 855 (vw),

Experimental part

826 (w), 790 (vw), 743 (m), 713 (w), 682 (vw), 660 (vw), 639 (w), 569 (vw), 521 (w), 471 (w), 451 (vw), 438 (w), 428 (vw), 400 (m), 383 (w) cm^{-1} .

HR-MS (ESI $^+$): $\text{C}_{29}\text{H}_{23}\text{ClN}_5\text{O}_5\text{RhNa}$ ($\text{M}+\text{Na}$) $^+$ calcd.: 682.0335, found: 682.0351.



225b was prepared according to standard procedure I using 36 mg TBS-protected methoxy pyridocarbazole **260** (83.4 μmol , 1.00 eq) and 22 mg $\text{RhCl}_3 \cdot 3\text{H}_2\text{O}$ (83.4 μmol , 1.00 eq) in 16.6 mL H₂O/EtOH 1:1 for 90 min at 90 °C before adding the resulting suspension to 19 mg of proline-ligand **206** (91.8 μmol , 1.10 eq) in 0.5 mL EtOH and reacting the mixture for 40 h. After removal of the solvent under reduced pressure, the compound was adsorbed on silica gel (~500 mg) and the diastereomers were separated according to the standard procedure. Isomer b was further purified twice (1.5 g silica gel each) yielding **225b** (9.8 mg, 15.0 μmol , 18%) as a deep red solid. **225a** could not be obtained purely with this procedure, even when using preparative TLC and additional flash column chromatography for purification.

225b:

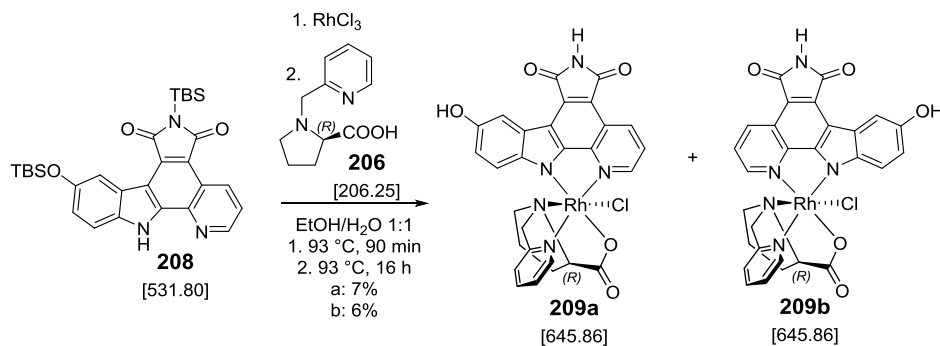
¹H-NMR (300.1 MHz, DMSO-*d*₆): δ = 11.19 (s, NH), 9.52 (d, ³*J* = 5.3 Hz, 1H, *H*₆), 8.66 (d, ³*J* = 7.7 Hz, 1H, *H*_{4'}), 8.53 (s, 1H, *H*_{3'}), 8.36 (t, ³*J* = 7.7 Hz, 1H, *H*₄), 7.96-7.90 (m, 2H, *H*₅, *H*₃), 7.76 (d, ³*J* = 7.9 Hz, 1H, *H*_{7'}), 7.53-7.48 (m, 2H, *H*_{1'}, *H*_{6'}), 7.34 (t, ³*J* = 7.3 Hz, *H*_{5'}), 4.74 (d, ²*J* = 15.6 Hz, 1H, *pro*CH₂_{pyr}), 4.56 (d, ²*J* = 16.3 Hz, 1H, *pro*CH₂_{pyr}), 3.99 (s, 3H, OCH₃), 3.79 (dd, ³*J* = 8.8 Hz, ³*J* = 4.2 Hz 1H, *H*₂), 2.29-2.22 (m, 2H, *H*_{5b'}, *H*_{3a'}), 2.22-2.12 (m, 1H, *H*_{3b'}), 1.89-1.83 (m, 1H, *H*_{3b'}), 1.48-1.44 (m, 1H, *H*_{4a'}), 1.14-1.00 (m, 1H, *H*_{4b'}) ppm. The missing *H*_{5a'}-proton overlaps with the DMSO-signal.

¹³C-NMR (75.5 MHz, DMSO-*d*₆): δ = 182.4 (COO), 170.8 (CO), 170.2 (CO), 160.3 (*C*_q), 155.1 (*C*_q), 153.0 (*C*_q), 151.6 (*C*₆), 149.8 (*C*_{1'}), 143.1 (*C*₅), 140.7 (*C*_q), 137.2 (*C*_{3'}), 131.3 (*C*_q), 126.3 (*C*_{5'}), 126.1 (*C*₄), 124.1 (*C*_{4'}), 123.9 (*C*₃), 123.1 (*C*_q), 121.7 (*C*_q), 119.5 (*C*_{6'}), 114.6 (*C*_{7'}), 113.9 (*C*_q), 112.8 (*C*_q), 112.6 (*C*_q), 73.5 (*C*₂), 69.4 (*pro*CH₂_{pyr}), 61.6 (*C*_{5'}), 56.3 (OCH₃), 30.4 (*C*₃), 23.9 (*C*₄) ppm.

ATR-IR (neat): $\tilde{\nu}$ = 2922 (w), 1748 (w), 1704 (m), 1649 (m), 1570 (m), 1495 (w), 1449 (vw), 1413 (w), 1345 (s), 1299 (w), 1262 (m), 1222 (s), 1110 (vw), 1016 (s), 940 (vw), 876 (vw), 824 (vw), 750 (m), 708 (w), 663 (vw), 635 (m), 568 (vw), 519 (vw), 469 (w), 441 (w), 405 (w) cm^{-1} .

HR-MS (ESI): $\text{C}_{29}\text{H}_{23}\text{ClN}_5\text{O}_5\text{RhNa}$ ($\text{M}+\text{Na}$)⁺ calcd.: 682.0335, found: 682.0342.

5.4.2.3. Synthesis of indole-5-ol derivatised complexes 226a and 226b



The complexes were prepared according to standard procedure I using 60 mg doubly TBS-protected 5-TBS-1*H*-indole derivatised pyridocarbazole **208** (113 μmol , 1.00 eq), 30 mg RhCl₃·3H₂O (113 μmol , 1.00 eq) and 23 mL EtOH/H₂O, which was reacted for 90 min at 93 °C, before 26 mg proline ligand **206** (124 μmol , 1.10 eq) was added and further reacted for 16 h at 93 °C. The diastereoisomers were separated by flash chromatography (18 g silica gel). The isomers a and b were further purified individually by flash chromatography (1.0 g silica gel each). Isomer a was further purified over 1.5 g silica and pooled with previously heavily purified complex from two scales using a total of 37.6 μmol RhCl₃·3H₂O via the standard approach I and one scale with 38.0 μmol using standard procedure II, yielding in 8.5 mg of **209a** (13.2 μmol , 7%) as deep reddish purple solid. Isomer b was combined with complex obtained from the same scales as isomer a and was further purified over 1.0 g silica to yield **209b** (7.6 mg, 11.8 μmol , 6%) with roughly 30% (¹H-NMR) non pyridocarbazole containing impurity as a deep red-purple solid.

226a:

¹H-NMR (500.1 MHz, DMSO-*d*₆): δ = 11.16 (s, NH), 9.66 (d, ³*J = 5.7 Hz, 1H, *H*₆), 9.24 (s, 1H, OH), 9.23 (dd, ³*J = 8.5 Hz, ⁴*J = 1.1 Hz, 1H, *H*_{3'}), 8.79 (d, ³*J = 5.1 Hz, 1H, *H*_{1'}), 8.46 (td, ³*J = 7.8 Hz, ⁴*J = 1.5 Hz, 1H, *H*₄), 8.12 (d, ⁴*J = 2.5 Hz, 1H, *H*_{4'}), 8.03-8.00 (m, 2H, *H*₅, *H*_{2'}), 7.97 (d, ³*J = 7.8 Hz, 1H, *H*₃) 6.72 (dd, ³*J = 8.8 Hz, ³*J = 2.5 Hz, 1H, *H*_{6'}), 5.52 (d, ³*J = 8.8 Hz, 1H, *H*_{7'}), 4.58 (d, ⁴*J = 15.7 Hz, 1H, *pro*CH₂*pyr*), 4.31 (d, ⁴*J = 15.6 Hz, 1H, *pro*CH₂*pyr*), 3.79 (dd, ³*J = 9.6 Hz,**************

Experimental part

$^3J = 4.2$ Hz, 1H, H_2), 2.48-2.45 (m, 1H, H_{5a}), 2.25-2.17 (m, 2H, H_{5b} , H_{3a}), 2.02-1.97 (m, 1H, H_{3b}), 1.61-1.54 (m, 1H, H_{4a}), 1.08-1.00 (m, 1H, H_{4b}) ppm.

$^{13}\text{C-NMR}$ (125.8 MHz, DMSO- d_6): $\delta = 182.1$ (COO), 170.6 (CO), 170.3 (CO), 161.1 (C_q), 152.6 (C_q), 152.5 (C_q), 151.6 (C_6), 148.2 (C_1'), 142.8 (C_q), 142.4 (C_q), 141.1 (C_4), 135.0 (C_3'), 131.5 (C_q), 126.2 (C_5), 124.1 (C_2'), 123.5 (C_q), 123.5 (C_3), 121.4 (C_q), 116.8 (C_6'), 114.8 (C_q), 113.2 (C_7'), 112.2 (C_q), 109.1 (C_4'), 72.9 (C_2), 70.0 ($_{pro}\text{CH}_2\text{pyr}$), 61.2 (C_5'), 30.5 (C_3'), 24.3 (C_4) ppm.

ATR-IR (neat): $\tilde{\nu} = 3112$ (vw), 3056 (vw), 2991 (vw), 2954 (vw), 2922 (w), 2855 (vw), 2729 (w), 1750 (w), 1705 (s), 1652 (s), 1608 (m), 1563 (w), 1523 (vw), 1493 (vw), 1466 (w), 1415 (w), 1337 (s), 1299 (vw), 1238 (vw), 1212 (w), 1123 (w), 1017 (s), 895 (vw), 859 (w), 827 (w), 779 (m), 694 (s), 637 (w), 580 (vw), 529 (vw), 497 (m), 443 (vw) cm^{-1} .

HR-MS (APCI $^+$): $\text{C}_{28}\text{H}_{21}\text{ClN}_5\text{O}_5\text{RhH}$ ($\text{M}+\text{H}$) $^+$ calcd.: 646.0359, found: 646.0360.

226b:

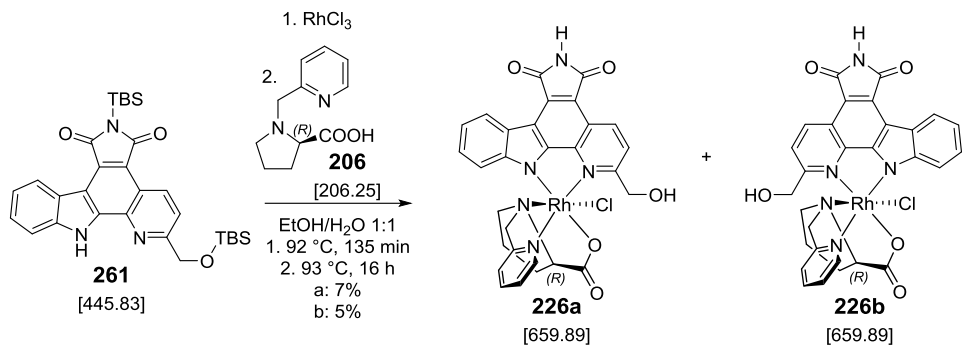
$^1\text{H-NMR}$ (500.2 MHz, DMSO- d_6): $\delta = 11.17$ (s, NH), 9.52 (d, $^3J = 5.6$ Hz, 1H, H_6), 9.32 (s, 1H, OH), 9.10 (dd, $^3J = 8.3$ Hz, $^4J = 0.9$ Hz, 1H, $H_{3'}$), 8.37 (td, $^3J = 7.8$ Hz, $^4J = 1.5$ Hz, 1H, H_4), 8.12 (d, $^4J = 2.5$ Hz, 1H, $H_{4'}$), 8.03-8.00 (m, 2H, H_5 , H_3), 7.86 (d, $^3J = 5.2$ Hz, 1H, $H_{1'}$), 7.68 (dd, $^3J = 8.4$ Hz, $^3J = 5.3$ Hz, 1H, $H_{2'}$), 7.61 (d, $^3J = 8.8$ Hz, 1H, H_7), 7.06 (dd, $^3J = 8.8$ Hz, $^3J = 2.5$ Hz, 1H, H_6'), 4.56 (s, 1H, $_{pro}\text{CH}_2\text{pyr}$), 3.78 (dd, $^3J = 9.5$ Hz, $^3J = 4.8$ Hz, 1H, H_2), 2.45-2.41 (m, 1H, H_{5a}), 2.20-2.15 (m, 2H, H_{5b} , H_{3a}), 1.87-1.82 (m, 1H, H_{3b}), 1.49-1.41 (m, 1H, H_{4a}), 1.11-1.07 (m, 1H, H_{4b}) ppm.

$^{13}\text{C-NMR}$ (125.8 MHz, DMSO- d_6): $\delta = 182.4$ (COO), 170.7 (CO), 170.4 (CO), 160.2 (C_q), 152.1 (C_q), 151.7 (C_q), 151.6 (C_6), 149.8 (C_1'), 143.8 (C_q), 142.7 (C_q), 140.7 (C_4), 134.6 (C_3'), 131.5 (C_q), 126.1 (C_5), 123.9 (C_3 , C_2'), 123.8 (C_q), 121.1 (C_q), 117.0 (C_6'), 115.4 (C_7'), 114.7 (C_q), 112.6 (C_q), 108.5 (C_4'), 73.5 (C_2), 69.4 ($_{pro}\text{CH}_2\text{pyr}$), 61.4 (C_5'), 30.4 (C_3'), 23.8 (C_4) ppm.

ATR-IR (neat): $\tilde{\nu} = 2923$ (m), 2854 (w), 2727 (vw), 1747 (vw), 1707 (m), 1634 (m), 1501 (vw), 1422 (w), 1337 (s), 1241 (w), 1214 (w), 1181 (vw), 1129 (w), 1016 (s), 951 (w), 863 (vw), 823 (w), 767 (m), 696 (m), 635 (w), 576 (vw), 525 (vw), 496 (m), 442 (vw), 398 (w) cm^{-1} .

HR-MS (APCI $^+$): $\text{C}_{28}\text{H}_{21}\text{ClN}_5\text{O}_5\text{RhH}$ ($\text{M}+\text{H}$) $^+$ calcd.: 646.0359, found: 646.0374.

5.4.2.4. Synthesis of pyridine-6-yl methanol derivatised complexes 209a and 209b



The complexes were prepared according to the standard procedure I using 73 mg doubly TBS-protected methanol-pyridocarbazole **261** (133.7 μmol , 1.00 eq), 35 mg $\text{RhCl}_3 \cdot 3\text{H}_2\text{O}$ (133.7 μmol , 1.00 eq), and 27 mL EtOH/ H_2O , which was reacted for 135 min at 92 $^\circ\text{C}$, before 30 mg proline ligand **206** (147.1 μmol , 1.10 eq) was added and further reacted for 16 h at 93 $^\circ\text{C}$. The diastereoisomers were separated via flash chromatography (18 g silica gel). The isomers a and b were further purified twice over 2 g for a/1.5 g for b and 1.0 g silica each respectively, yielding in 5.7 mg **226a** (8.6 μmol , 7%) and 4.5 mg **226b** (6.8 μmol , 5%) as deep red solids.

209a:

$^1\text{H-NMR}$ (300.1 MHz, $\text{DMSO}-d_6$): $\delta = 11.21$ (s, NH), 9.66 (dt, $^3J = 5.8$ Hz, $^4J = 0.6$ Hz, 1H, H_6), 9.34 (d, $^3J = 8.7$ Hz, 1H, $H_{3''}$), 8.71 (ddd, $^3J = 7.9$ Hz, $^4J = 1.2$ Hz, $^4J = 0.7$ Hz, 1H, $H_{4''}$), 8.48 (td, $^3J = 7.8$ Hz, $^4J = 1.5$ Hz, 1H, H_4), 8.23 (d, $^3J = 8.7$ Hz, 1H, $H_{2''}$), 8.05 (t, $^3J = 6.5$ Hz, 1H, H_5), 7.94 (d, $^3J = 7.8$ Hz, 1H, H_3), 7.24 (ddd, $^3J = 7.8$ Hz, $^3J = 7.2$ Hz, $^2J = 0.9$ Hz, 1H, $H_{5''}$), 7.14 (ddd, $^3J = 8.4$ Hz, $^3J = 7.1$ Hz, $^4J = 1.3$ Hz, 1H, H_6'), 6.07 (t, $^3J = 5.4$ Hz, 1H, OH), 5.42 (d, $^3J = 8.4$ Hz, 1H, H_7), 5.36 (dd, $^2J = 17.8$ Hz, $^3J = 4.4$ Hz, 1H, CH_2OH), 4.88 (dd, $^2J = 17.9$ Hz, $^3J = 5.4$ Hz, 1H, CH_2OH), 4.48 (d, $^4J = 15.5$ Hz, 1H, $_{pro}\text{CH}_{2\text{pyr}}$), 4.16 (d, $^4J = 15.6$ Hz, 1H, $_{pro}\text{CH}_{2\text{pyr}}$), 3.74 (dd, $^3J = 10.1$ Hz, $^3J = 5.1$ Hz, 1H, H_2), 2.45-2.40 (m, 1H, H_{5b}), 2.31-2.26 (m, 1H, H_{5b}') 2.24-2.18 (m, 1H, H_{3a}), 1.98-1.92 (m, 1H, H_{3b}), 1.59-1.55 (m, 1H, H_{4a}), 1.05-0.99 (m, 1H, H_{4b}) ppm. The missing H_{5a}' signal overlaps with the DMSO signal.

$^{13}\text{C-NMR}$ (500.2 MHz, $\text{DMSO}-d_6$): $\delta = 182.1$ (COO), 170.8 (CO), 170.3 (CO), 168.9 (C_{arom}), 161.2 (C_{arom}), 152.7 (C_{arom}), 152.3 (C_{arom}), 148.1 (C_{arom}), 141.7 (C_{arom}), 141.5 (C_{arom}), 135.6 (C_{arom}), 130.2 (C_{arom}), 126.6 (C_{arom}), 126.5 (C_{arom}), 124.8 (C_{arom}), 123.6 (C_{arom}), 123.5 (C_{arom}), 121.7 (C_{arom}), 120.4 (C_{arom}), 119.5 ($C_{5/6''}$), 115.3 (C_q), 114.9 (C_q), 111.4 ($C_{7''}$), 73.3 (C_2), 69.9 ($_{pro}\text{CH}_{2\text{pyr}}$), 62.2 (CH_2OH), 61.3 (C_5), 30.9 (C_3), 24.1 (C_4) ppm.

ATR-IR (neat): $\tilde{\nu} = 3214$ (br, w), 2921 (m), 2852 (w), 1752 (w), 1701 (m), 1615 (m), 1534 (vw), 1496 (w), 1447 (vw), 1419 (w), 1341 (s), 1295 (w), 1230 (m), 1188 (vw), 1164 (vw), 1115 (vw), 1078

Experimental part

(w), 1013 (m), 934 (vw), 901 (vw), 834 (w), 739 (m), 671 (vw), 636 (w), 581 (vw), 494 (vw), 452 (w), 398 (w) cm^{-1} .

HR-MS (APCI $^+$): $\text{C}_{29}\text{H}_{23}\text{ClN}_5\text{O}_5\text{RhH}$ ($\text{M}+\text{H}^+$) calcd.: 660.0516, found: 660.0517.

209b:

$^1\text{H-NMR}$ (300.1 MHz, DMSO- d_6): $\delta = 11.17$ (s, NH), 9.63 (d, $^3J = 5.4$ Hz, 1H, H_6), 9.25 (d, $^3J = 8.6$ Hz, 1H, H_3), 8.73 (d, $^3J = 8.0$ Hz, 1H, H_4), 8.37 (td, $^3J = 7.8$ Hz, $^4J = 1.5$ Hz, 1H, H_4), 8.01 (m, $^3J = 7.3$ Hz, $^3J = 5.9$ Hz, $^4J = 1.4$ Hz 1H, H_5), 8.00 (d, $^3J = 8.7$ Hz, 1H, H_2), 7.88 (d, $^3J = 7.7$ Hz, 1H, H_3), 7.87 (d, $^3J = 8.4$ Hz, 1H, H_7), 7.50 (ddd, $^3J = 8.4$ Hz, $^3J = 7.0$ Hz, $^4J = 1.3$ Hz, 1H, H_6), 7.35 (ddd, $^3J = 8.0$ Hz, $^3J = 7.1$ Hz, $^4J = 0.9$ Hz, 1H, H_5), 5.81 (t, $^3J = 5.4$ Hz, 1 H, OH), 4.69 (d, $^4J = 15.8$ Hz, 1H, $_{\text{pro}}\text{CH}_2\text{pyr}$), 4.52 (d, $^4J = 15.9$ Hz, 1H, $_{\text{pro}}\text{CH}_2\text{pyr}$), 4.28 (dd, $^2J = 15.7$ Hz, $^3J = 4.4$ Hz, 1H, CH_2OH), 3.77 (dd, $^2J = 15.7$ Hz, $^3J = 5.9$ Hz, 1H, CH_2OH), 3.66 (dd, $^3J = 9.3$ Hz, $^3J = 6.9$ Hz, 1H, H_2), 2.45-2.40 (m, 1H, H_{5a}), 2.13-2.06 (m, 1H, H_{5b}), 2.02-1.96 (m, 1H, H_{3a}), 1.56-1.47 (m, 1H, H_{3b}), 1.41-1.35 (m, 1H, H_{4a}), 0.72-0.65 (m, 1H, H_{4b}) ppm.

$^{13}\text{C-NMR}$ (125.8 MHz, DMSO- d_6): $\delta = 182.7$ (COO), 170.8 (CO), 170.4 (CO), 167.5 (C_{arom}), 160.5 (C_{arom}), 151.9 (C_{arom}), 151.7 (C_{arom}), 149.5 (C_{arom}), 142.3 (C_{arom}), 140.9 (C_{arom}), 135.4 (C_{arom}), 130.3 (C_{arom}), 126.6 (C_{arom}), 126.5 (C_{arom}), 124.2 (C_{arom}), 123.8 (C_{arom}), 123.1 (C_{arom}), 121.9 (C_{arom}), 120.4 (C_{arom}), 119.6 ($C_{5/6}$), 115.2 (C_7), 114.9 (C_q), 114.4 (C_q), 73.5 (C_2), 70.9 ($\text{CH}_2\text{N}_{\text{Pro}}$), 61.6 (C_5), 60.8 (CH_2OH), 30.4 (C_3), 23.3 (C_4) ppm.

ATR-IR (neat): $\tilde{\nu} = 3224$ (br, w), 2920 (m), 2852 (w), 1750 (w), 1707 (m), 1649 (m), 1615 (m), 1534 (vw), 1498 (vw), 1447 (vw), 1418 (w), 1341 (s), 1294 (w), 1261 (vw), 1233 (w), 1187 (vw), 1150 (vw), 1081 (w), 1006 (m), 936 (vw), 901 (vw), 827 (vw), 744 (m), 671 (vw), 632 (w), 583 (vw), 519 (vw), 489 (vw), 451 (w), 403 (w) cm^{-1} .

HR-MS (APCI $^+$): $\text{C}_{29}\text{H}_{23}\text{ClN}_5\text{O}_5\text{RhH}$ ($\text{M}+\text{H}$) calcd.: 660.0516, found: 660.0516.

5.5. Preparation of single crystals for X-ray analysis

5.5.1. Preparation of single crystals of **80a**

Single crystals of np830 (**80a**) were obtained upon slow diffusion of dichloromethane at 22 °C from a 10 mM DMSO solution which was diluted with dichloromethane in a ratio of about 1:10. The intensity data were collected at 100 K using a Bruker D8 Quest system. The data were corrected for absorption effects using multi-scanned reflections.^[214] The structure was solved using direct methods (SHELXS-97)^[215] and refined using full matrix least squares procedure (SHELXL-2013). Hydrogen atoms were included at calculated positions. All data collection and processing was done by KLAUS HARMS from the central x-ray department of the chemistry department of the Philipps-Universität Marburg.

5.5.2. Preparation of single crystals of **225a**

Single crystals of the 5-methoxy derivatised complex **225a** were obtained upon slow diffusion of dichloromethane at 4 °C from a DMSO solution of undefined concentration, which was diluted with dichloromethane in a ratio of about 1:10. The intensity data were collected at 100 K using a Bruker D8 Quest system. The data were corrected for absorption effects using multi-scanned reflections.^[350] The structure was solved using direct methods (SHELXS-97)^[215] and refined using full matrix least squares procedure (SHELXL-2013). Hydrogen atoms were included at calculated positions. All data collection and processing was done by KLAUS HARMS from the central x-ray department of the chemistry department of the Philipps-Universität Marburg.

5.6. Cell experiments**5.6.1. Cell cultures**

Cell lines utilised in standard method I were HeLa human cervical cancer cells, HT-29 human colorectal adenocarcinoma cells, WM1366 human primary malignant melanoma cells and WM983B human metastatic malignant melanoma cells. HeLa cells were cultured in DULBECCO's Modified Eagle's Medium (DMEM) containing 10% fetal bovine serum (FBS), 2 mM L-glutamine, 100 units/mL penicillin and 100 µg/mL streptomycin. For cell documentation experiments DMEM without the pH-indicator phenolred was used. HT-29 cells were cultured in Roswell Park Memorial Institute medium (RPMI) 1640 with the same supplements as above, plus an additional 50 mg gentamycin per 560 mL medium. WM1366 and WM983B were cultured in tumour (tu) 2% containing 80% molecular cellular and developmental biology (MCDB) 153 medium, 20% LEIBOVITZ's L-15 medium, 2% FBS and 1.68 mM calcium chloride. Cells were maintained in 75 cm² flasks with 25 mL medium in a 5% CO₂-humidified atmosphere at 37 °C. Passage took place every 2-3 days. All cell culture ingredients were purchased from SIGMA-ALDRICH.

For maintenance or plating, old cell culture medium was discarded, the cells were washed with 6 mL PBS (phosphate buffered saline) and 4 mL trypsin solution was added. The cells were incubated at 37 °C and 5% CO₂ atmosphere until detached (3-6 min). The suspension was diluted with 4 mL of fresh medium and the cells centrifuged for 5 min at 1000 rpm and 20 °C. The supernatant was discarded and the cells resuspended in 3-6 mL of fresh medium, depending on the cell pellet size. For plating (see according experimental sections), cells were diluted 1:10 in medium, counted using a haemocytometer and diluted accordingly to the cell number needed.

Cell lines utilised for standard method II were A549 human lung carcinoma cells, SK-OV-3 human ovarian adenocarcinoma cells, A2780 human ovarian carcinoma and HCT-116 (p53 +/+) human colorectal carcinoma cells. A549, SK-OV-3 and HCT-116 (p53 +/+) cells were cultured in DMEM GlutaMAX™ containing 10% FBS, 4 units/mL penicillin and 4 µg/mL streptomycin. A2780 cells were cultured in RPMI with the same supplements as above. Cells were maintained in 75 cm² or 25 cm² flasks in a 5% CO₂-humidified atmosphere at 37 °C. Passage took place every 3-4 days using enzyme free solution. All cell culture ingredients were purchased from GIBCO.

In detail, cells were cultured in 75 cm² flasks with 12 mL or in 25 cm² flasks with 6 mL medium. For maintenance or plating, the old cell culture medium was discarded, the cells were washed with 10 mL (5 mL) DPBS (Dulbecco's phosphate buffered saline) respectively and 3 mL (1 mL) enzyme free solution was added. The cells were incubated at 37 °C and 5% CO₂ atmosphere until detached (5-15 min). The suspension was diluted with 8 mL (2mL) of fresh medium and the cells centrifuged for 5 min at 1000 rpm and 20 °C. The supernatant was discarded and the cells resuspended in

2-3 mL of fresh medium. For plating cells were diluted 1:10 in medium, then 1:1 in a 4% tryphan blue solution (SIGMA ALDRICH), counted using a haemocytometer and diluted accordingly to the cell number needed.

5.6.2. Determination of cell viability

The toxicity effect of the synthesised compounds was determined using the 3-(4,5-dimethylthiazol-2-yl)-2,5-diphenyltetrazolium bromide (MTT) cell viability assay method. Using standard method I, cells were cultured in 96-well plates with a density of 90 cells/ μ L (100 μ L/well) for HeLa and WM1366 cells, 200 cells/ μ L for HT-29 and WM983B cells and incubated in a 5% CO₂-humidified atmosphere at 37 °C for 24 h. For library testing the cell medium was diluted 1:1 with medium containing 2 μ M amide and 2% DMSO, for concentration dependant assays with increasing concentrations of the synthesised compounds and 2% DMSO in quadruplicate. Cells were left to grow 24 h before the medium was replaced by MTT (SIGMA-ALDRICH for HeLa and HT-29, BIOMOL for WM1366 and WM983B) solution (5 mg/mL in PBS further diluted in culture medium (1:11)). The cells were incubated for another 3 h under normal culture conditions. Afterwards 155 μ L of the solution was discarded and 90 μ L of DMSO was added. The plates were incubated for 10 min at 37 °C and 150 rpm for complete dissolving of the formed formazan salts. The formazan was then quantified by measuring the absorbance at 535 nm with a *Spectramax M5* microplate reader (MOLECULAR DEVICES). The cell viability was calculated as percentage of surviving cells compared to untreated control cells using 1% DMSO in the cell medium. Data show the mean of at least two independent experiments for concentration dependant assays and one experiment for library screening.

Using standard method II cells were cultured in 96-well plates (COSTAR) with a density of 8000 or 10000 cells/well in 200 μ L medium and incubated in a 5% CO₂-humidified atmosphere at 37 °C for 24 h. The medium was then replaced by medium containing the testing substance, with increasing concentrations and DMSO of up to 1%, in quadruplicate. Cells were left to grow 72 h before the medium was replaced by MTT (SIGMA-ALDRICH) solution (500 μ g/mL in DPBS). The cells were incubated for another 3-4 h under normal culture conditions. Afterwards the solution was removed by aspiration and 200 μ L DMSO was added. The plates were incubated for 20 min at 20 °C and 600 rpm for complete dissolution of the formed formazan salts. The formazan was then quantified by measuring the absorbance at 550 nm with a Thermomax microplate reader (MOLECULAR DEVICES). The cell viability was calculated as percentage of surviving cells compared to untreated control cells. Data show the mean of at least two independent experiments for concentration dependant assays with little toxicity and at least three independent experiments for IC₅₀ determination.

5.6.3. Scanning electron microscopy**5.6.3.1. Chemical fixation**

For chemical fixation HeLa cells were grown on small cover glasses, incubated for 16 h after addition of 10 µM of the compound and afterwards chemically fixed.^[216] Each cover glass was washed with 1 mL PBS after aspiration of the medium, and fixed for 1 h with 2.5% glutaraldehyde in 0.1 M cacodylic acid (CAC, pH 7.4). It was then washed three times for 5 min with each 1 mL 0.1 M CAC and fixed with 1 mL aqueous 1% osmium tetroxide/ 8% potassium ferrocyanide (pH 7.4). After washing once with 1 mL 0.1 M CAC and twice with *dd*H₂O, the samples were dehydrated once with 95% EtOH for 1 min and three times with 100% EtOH for 5 min followed by dehydration with 1:1 EtOH/HDMS (15 min) and 100% HDMS (two times 15 min each). The supernatant was discarded and excess liquid was removed with a filter paper. The samples were dried over night at room temperature and measured with a cold-field emission scanning electron microscope *JEOL JSM-7500* by Michael Hellwig at the centre for material sciences at the Philipps-Universität University Marburg.

5.6.3.2. Freeze drying of cells

For freeze dried samples HeLa cells were grown on small cover glasses, incubated for 16 h after addition of 30 µM, 15 µM and 7.5 µM of the compound and afterwards washed and freeze dried. The wells were washed with PBS (1.5 mL) and *dd*H₂O after aspiration of the medium, and the entire plate was frozen in liquid nitrogen before lyophilisation over night. Due to a defect with the lyophiliser, the plates were kept at ~ 30 °C during that time. The samples were measured with a cold-field emission scanning electron microscope *JEOL JSM-7500* by Michael Hellwig at the centre for material sciences at the Philipps-Universität Marburg.

5.7. Enzyme inhibition assays

5.7.1. Pim1 inhibition assay

Inhibition of Pim1 was determined using the commercially available ATP-GloTM assay (PROMEGA). The kit was previously tested towards its suitability using the compounds RR97a (**201a**) and RR97b (**201b**), as well as an ADP/ATP calibration curve, and showed decent results, with up to 4-fold deviation in IC₅₀ from results obtained by radioactive assays as performed by RAJATHEES RAJARATNAM. The exact assay conditions were chosen due to concentration limits of the buffer ingredients by the assay provider. The Pim1 activity is low in the assay conditions used and would need further optimisation for more accurate tests and further experiments.

In the assay setting derivatives were tested at 50 nM and 1 μM for their Pim1 inhibition, since the previous IC₅₀ for **201a** in this assay was determined as 50-60 nM. Therefore, a 10 mM DMSO stock solution was diluted 1:1000 (10 μM) and further 1:20 (500 nM) in DMSO, since the inhibitor is further diluted 1:10 in the assay. A solution of a 1:1 mixture of the substrate P70S6 (500 μM in 5x P1) and ultrapure ATP (100 μM in ddH₂O) was prepared. Pim1 solution (10 μL, 1.0 ng) was diluted in 160 μL PA and kept at 4 °C until the experiment. Please be aware that about one third of the amount of Pim1 should be sufficient in the assay setting. The high amount was chosen due to very low activity of the Pim1 batches available and thereby falsifies the obtained results to a certain degree. Each kinase reaction was prepared according to the following list (Table 19) in duplicate.

Table 19: Composition of P1, PA and kinase reaction mixture in Pim1 ATP-GloTM assay.

5 x P1 (pH 7.0)		PA (pH 7.5)		kinase reaction mixture	
Mops/NaOH	40 mM	Tris/HCl	40 mM	ddH ₂ O	1.5 μL
MgOAc	50 mM	MgCl ₂	20 mM	inhibitor (10 mM)	0.75 μL
		BSA	0.1 mg/mL	Pim1 in PA	3.75 μL
				ATP/P70S6 1:1	1.5 μL

Three controls were introduced in quadruplicate, in which the ingredient was replaced by the according buffer or solvent, including control 1 (without inhibitor) which represents 100% activity, control 2 (without inhibitor and without enzyme) which was used for background correction and control 3 (using the inactive isomer of the hexyl derivative without enzyme) to test possible self-luminescence of the complexes.

Experimental part

The kinase reactions were prepared in 200 µL PCR- tubes, spun down, and incubated for 40 min at 20 °C and 200 rpm. Afterwards 5 µL of each mixture was transferred to a white flat bottom 384-well plate (GREINER BIO-ONE) and 5 µL ADP-Glo reagent (equilibrated to room temperature) was added. The mixture was incubated for another 40 min at 20 °C and 10 µL kinase detection reagent (equilibrated to room temperature) was added to each well. The plate was further incubated for 30 min at 20 °C in the dark. Afterwards the luminescence was measured using *Spectramax M5* microplate reader (MOLECULAR DEVICES, integration time 1500 ms). The obtained values were averaged and background corrected using control 2, and compared to control 1, which represents 100% Pim1 activity in the assay setting. Results were thereby calculated as percent activity compared to the untreated enzyme sample, using the formula (test sample RLU – control2 RLU) / (control1 RLU – control2 RLU) x 100 with RLU = relative luminescence units. Values given are a percentage of rest-activity of the enzyme after inhibitor treatment at an ATP concentration of 10 µM.

5.7.2. HDAC inhibition assay

5.7.2.1. Preparation of A549 nuclear extracts

Nuclear extracts for HDAC-activity assays were prepared according to a modified protocol from literature.^[172] A549 cells were grown in a 75 cm² cell culture flask for 3-4 days in 12 mL medium. After aspiration of the medium, the flask was washed with 5 mL DPBS, 3 mL enzyme free solution was added and the flask incubated for 10 min at 37 °C and 5% CO₂. After detachment of the cells, 5 mL ice-cold DPBS was added and the cells centrifuged 5 min at 4 °C (1000g). The supernatant was discarded, the cells resuspended in 1 mL cold DPBS and centrifuged 5 min at 4 °C. The pellets were resuspended in five times the packed cell volume (~250 µL) of ice-cold lysis buffer (Table 20), incubated for 10 min on ice and centrifuged for 4 min at 4 °C (1000g). Be aware that DTT and PMSF should be added to the lysis buffer right before usage, since the final buffer is not stable and should only be used during the same day.

Table 20: Composition of used lysis and nuclear extraction buffers. DTT and PMSF have to be added right before use.

lysis buffer/washing buffer*	nuclear extraction buffer
Tris/HCl (pH 8.0)	20 mM
KCl	420 mM
EDTA	0.7 mM
DTT	0.25 mM
PMSF (0.25 mM in iPrOH)	25% (v/v)

Igepal CA-630	0.05% (v/v)
---------------	-------------

* washing buffer equals lysis buffer
without DTT and PMSF

The pellets were resuspended with 80 µL of washing buffer (Table 20) and centrifuged for 4 min at 4 °C and 1000g. The resulting nuclei were resuspended in 80 µL nuclear extraction buffer (Table 20) and incubated for 30 min on ice before they were ultracentrifuged for 15 min at 4 °C and 15000g. The protein content was determined via LAWRY assay and compared to BSA according to the supplier's protocol (DCTTM Protein Assay, BIO-RAD). The total protein content was in the range of 5-10 µg/µL and the nuclear extracts were stored at -80 °C until further use after quick freezing in liquid nitrogen.

Nuclear extracts of treated cells were obtained in a similar fashion. Cells were grown in 6-well plates (COSTAR) in 5.94 mL medium (50 cells/µL) for 24 h, compounds were added at defined concentrations and after another 72 h incubation time, the cells were harvested. Each well was washed with 1 mL DPBS and 380 µL of enzyme free solution was added. The cells were incubated at 37 °C and 5% CO₂ for 10 min and 1 mL ice-cold DPBS was added after detachment of the cells. The suspension was transferred to 1.5 mL tubes and centrifuged for 10 min at 4 °C (1000g). The supernatant was discarded, the cells resuspended in 150 µL cold DPBS, the content of two wells each was combined and the suspension was spun down for 5 min at 4 °C. The remaining pellets were resuspended in 65 µL of cold lysis buffer, incubated for 10 min on ice and centrifuged for 4 min at 4 °C (1000g). The pellets were resuspended in 20 µL washing buffer and centrifuged for 4 min at 4 °C (1000g). The resulting nuclei were resuspended in 20 µL nuclear extraction buffer and incubated for 30 min on ice before they were ultracentrifuged for 15 min at 4 °C (15000g). The protein content was determined via LAWRY assay and compared to BSA according to the supplier's protocol (DCTTM Protein Assay, BIO-RAD).

5.7.2.2. HDAC activity assay

To determine the HDAC inhibition rate of gold-compounds, the commercially available fluorometric FluoroFire HDAC Activity Assay (MOLECUTOOLS) was used. HDAC activity was measured according to the supplier's protocol in a 96-well plate format. Briefly, 10 mM or 1 mM DMSO-stock solutions of the compounds were diluted in assay buffer to 10x the final assay concentration. Nuclear protein extract derived from A549 cells was diluted in the supplied assay buffer to a final concentration of 0.125 µg/µL. To 40 µL of the nuclear extract dilution in a black 96-well plate (COSTAR) was added either 10 µL assay buffer (positive control), 10 µL of a 30 µM trichostatin A solution (negative control) or 10 µL of test compound in duplicate. For the blank

Experimental part

50 µL pure assay buffer was used. The plate was incubated for 60 min at 20 °C and afterwards 50 µL of freshly prepared HDAC Emerald Substrate working solution (0.2 µL of HDAC Emerald Substrate, and 1.0 µL of signal enhancer in 50 µL of assay buffer) was added per well. The plate was incubated at 20 °C for 60 min and the fluorescence (Ex/Em = 490/525 nm) was monitored with a Spectramax GeminiXPS microplate reader (MOLECULAR DEVICES). All wells were background corrected and compared to the positive control which represents 100% HDAC activity. Results were thereby calculated as % activity compared to the untreated enzyme, using the formula (test sample RFU - blankRFU) / (untreated controlRFU - blankRFU) x 100.

For the HDAC-activity of nuclear extracts obtained from pretreated cells, the extract was diluted to 0.1 µg/µL protein in assay buffer and 50 µL each were incubated for 20 min at 20 °C. To each well 50 µL freshly prepared substrate working solution was added and the plate incubated for 60 min at 20 °C before monitoring the fluorescence.

5.7.2.3. Quantification of HDAC 4 expression in treated cells

5.7.2.3.1. Cell treatment and protein extracts for Western Blot

For HDAC4 quantification via western blot, A549 cells were grown and treated in 6-well plates as described for nuclear extracts of treated cells. Cells were harvested, after discarding the medium, using 250 µL RIPA buffer per well by incubating for 10 min on ice and scraping the cells of two wells each into a 1.5 mL tube. The protein content was determined via LAWRY assay and compared to BSA according to the supplier's protocol (DCTTM protein assay, BIO-RAD). Extracts were stored at -80 °C until further use.

Table 21: Composition of radioimmunoprecipitation assay (RIPA) buffer.

RIPA buffer	
Tris/HCl (pH 7.5)	50 mM
NaCl	150 mM
sodiumdeoxycholate	1.0%
sodium dodecyl sulphate	0.1%
Igepal CA-630	1%
one miniROCHE protease inhibitor cocktail tablet/10 mL	

5.7.2.3.2. SDS-PAGE and Western Blot

For separating the proteins of the whole cell sample by their molecular weight the SDS-PAGE technique was used. Therefore, a 1.5 mm thick 10% SDS gel was prepared according to Table 22. Briefly the separation gel was added to the caster, a layer of *i*PrOH was added and the gel left to harden for 60 min. The alcohol layer was discarded, the top layer washed with water and the stacking fluid added, followed by the addition of a comb. The gel was left to harden for 45 min and stored in moist environment and 4 °C over night. The SDS-PAGE was performed as previously described in literature.^[351]

Table 22: Composition of 1.5 mm 10% SDS-gel.

	Separating gel (2x)	Stacking gel (2x)
<i>ddH₂O</i>	7.26 mL	6.30 mL
1.5 M Tris/HCl (pH 8.8)	3.75 mL	2.50 mL
10% (v/w) SDS	150 µL	100 µL
Acrylamide/bis	3.75 mL	1.00 mL
10% APS	75.0 µL	50 µL
TEMED	22.5 µL	15 µL

The protein samples (40 µg total protein as derived from the LAWRY assay) were further diluted with the appropriate amount of 4x loading buffer, the samples were sonicated at 50% amplitude for 5 s (SONICS VIBRACELL™), heated to 95 °C for 5 min, spun down for 30 s and an amount which contained 15 µg of protein was loaded to the gel. A Precision Plus Protein All Blue Standard ladder (BIO-RAD) was added to two remaining pockets. Gels were run for ~ 40 min at 150 V in SDS running buffer (24.8 mM Tris, 0.2 M glycine, 3.5 mM SDS).

For Western-Blot, the separated protein bands were transferred onto an activated PVDF membrane by semi-dry blotting (25 mM Tris, 192 mM glycine, 5% methanol) for 90 min at 100 V. The membranes were dried and stored at -20 °C until further use. All further steps were performed by ANDREIA DE ALMEIDA at the Rijksuniversiteit Groningen. For antibody incubation, the membranes were reactivated with methanol and, to avoid unspecific binding, further washed with blocking buffer (5% w/v non-fat milk in TBST (Tris buffered saline + 0.2% Tween 20)) for 1 h. Afterwards the buffer was discarded, the HDAC4 monoclonal antibody (ABNOVA) in blocking buffer (1:500) was added and the membrane incubated at 4 °C over night under motion. The membrane was then washed with TBST for 30 min and further incubated with the monoclonal house-keeping gene antibodies (anti-β-actin (SIGMA-ALDRICH) and anti-GADPH (SIGMA-

ALDRICH)) diluted 1:10000 in blocking buffer accordingly. Afterwards the membrane was further incubated with a secondary polyclonal rabbit anti-mouse peroxidase-labelled antibody (Dako), that was diluted 1:2000 in blocking buffer, for 2 h at room temperature under motion. The membrane was washed again with first TBST and secondly with TBS over night at 4 °C. The membrane was treated with chemoluminescent reagents (ECL detection reagent Perkin-Elmer) and the chemoluminescence of the immune complexes was detected using the GeneSnap program (SYNGENE) with an exposure time of 5 ms.

5.8. Assays for drug-like abilities determination

5.8.1. Stability studies

5.8.1.1. Ligand exchange and racemisation studies of 204b

RR88b (**204b**) was tested for its ligand exchange and racemisation properties at standard laboratory conditions (20 °C, daylight and electric lighting) for 24 days. The sample was therefore dissolved in DMSO-*d*₆, ¹H-NMR spectra were recorded at time points 0 h, 24 h, 4 d, 7 d, 14 d and 24 d and compared for ligand exchange reaction by superimposition of the spectra. The NMR-tube was stored directly next to the laboratory window to ensure exposure to light. At each time point, a small sample was extracted from the NMR tube and diluted into CH₃CN. These samples were frozen at -20 °C until analysis, except for an additional 0 h sample, which was stored next to the NMR tube at room temperature to ensure exposure to light. Possible ligand exchange and racemisation reactions were examined using reversed phase analytical HPLC (Chiralpak ® IC column 250mm x 4.6 mm), with a program previously tested to be able to separate all 4 isomers of the series (flow rate 0.5 mL, 0.1%TFA_{aq.}/CH₃CN 80:20 to 50:50 in 30 min, 50:50 for 10 min, 50:50 to 80:20 over 20 min, column temperature 40 °C). The CH₃CN samples were injected and the HPLC spectra obtained were compared for elution time and the appearance of new signals.

5.8.1.2. Stability of 201a and 201b at physiological conditions

The stability of RR97a and RR97b at physiological conditions was tested as 5 mM solutions of the compound in a 9:1 mixture of DMSO-*d*₆/D₂O in the presence of 5 mM β-mercaptopropanoic acid. The solution was kept in an NMR-tube at 37 °C under an atmosphere of 5% CO₂ during the time of study, except during NMR-measurement. ¹H-NMR spectra were recorded at time points 30 min, 6 h, 24 h, 48 h, 4 d, 7 d and 6 weeks. The spectra were compared by superimposition.

5.8.2. Equilibrium solubility assay (miniaturised shake-flask method)

The thermodynamic solubility of the metal-based compounds has been determined by an upgraded version of a method previously described in literature^[237] by staff of NIBR Cambridge, MA, USA. Briefly the solvent of 20 µL of a 10 mM DMSO-stock solution in a 96-well microtiter plate (CORNING 3363) was removed under reduced pressure and high-rotor speed centrifugation (GENEVAC HT4X) for 1.6 h at 30 °C. Afterwards, 200 µL of the appropriate buffer was added (nominal concentration of 1 mM), the plate heat-sealed and shacked overnight at 800-900 rpm on an orbital shaker at room temperature to reach an equilibrium between solid and saturated solution. Buffers used were chloride free potassium phosphate buffer (KPi, 67 mM KH₂PO₄, pH 6.8) and fasted state simulated intestinal fluid version 2 (FaSSIF-V2^[352], 3 mM sodium taurocholate, 0.2 mM lecithin, 19.12 mM maleic acid and 68.62 mM NaCl at pH 6.8). The plate was then ultracentrifuged for 18 min at 3600 rpm (HETTICH high speed robotic centrifuge) for phase separation. Afterwards, 5µL of the supernatant were transferred to a new plate and backfilled with 1:1 CH₃CN/H₂O to 1 mL. For LC-MS/MS quantification the internal standard glyburide (final concentration 1 µM) was added previous to the analysis. The concentration of samples was quantified via LC-MS/MS using the software QuickQuan (intensity data of all fragments related to the MW of the test compound). The ratio of peak area of the compounds to the internal standard was calculated to standardise the data for comparisons. For best results, the LC-MS/MS unit was auto-tuned to give maximum results for the compounds previously to assay analysis. For compounds with trouble in MS/MS quantification LC/UV detection was used and the area under the curve compared to a standard curve as described previously.^[237]

5.8.3. Metabolic stability in rat liver microsomes (*in vitro* half-life approach)

The CYP-mediated metabolic stability of the complexes was determined via an *in vitro* half-life assay using rat liver microsomes, related to literature reported assays^[353] by staff of NIBR Cambridge, MA, USA. Briefly a 10 mM stock solution of the compound in DMSO was diluted 1:1000 with 0.6% CH₃CN_{aq.} (v/v), of which 35 µL were added to 140 µL microsomal protein suspension (1 mg/mL) in 50 mM KPi (pH 7.4). This mixture was preincubated for 15 min on a thermoshaker at 37 °C. One aliquot (25 µL) was used as time zero (t = 0) sample. Therefore, it was quenched with 50 µL of CH₃CN containing 2 µM alprenolol as internal MS standard, and 25 µL of cofactor solution (50 mM KPi supplemented with 2mM NADPH and 4 mM MgCl₂) was added to simulate the complete reaction mixture. Another aliquot (25 µL) was mixed with an equal amount of 50 mM KPi containing MgCl₂ but no cofactor, and further treated as the main sampled. This

Experimental part

negative control was used to assess CYP-unrelated stability issues (e.g. chemical instability and CYP-independent metabolism). The main reaction, used to determine the metabolism after 5, 15 and 30 min, was started by addition of 125 µL of cofactor solution to the remaining 125 µL complex/enzyme mixture. The mixture was further incubated at 37 °C and vertical shaking. Incubation mixtures contained a final concentration of 50 mM potassium phosphate buffer (pH 7.4), 2.0 mM MgCl₂, 1.0 mM NADPH, 0.5 mg/mL liver microsomes, 1.0 µM test compound, 0.06% CH₃CN (v/v) and 0.01% DMSO (v/v). At the specific reaction time points, aliquots of 50 µL were removed and the reaction was terminated by addition of 50 µL CH₃CN containing 2 µM alprenolol. All samples were stored at 4 °C until completion of the assay and then centrifuged at 3400 x g and 4 °C for 10 min to pellet precipitated protein. The parent compound in the supernatant was analysed via a high-performance liquid chromatography-tandem mass spectrometry system (LC-MS/MS) consisting of a Thermo TSQ mass spectrometer and a H-ESI ion source. Samples were separated on a WATERS XTerra C18 column (2.1x20 mm, 3.5 µm) using a fast mobile phase gradient at 0.8 mL/min (A 0.1% formic acid in H₂O, B 0.1% formic acid in CH₃CN; 2% B in 0.5 min to 98%, hold for 0.25 min, in 0.27 min back to 2% and hold for 1.21 min) and quantified using the software QuickQuan (intensity data of all fragments related to the MW of the test compound). The ratio of peak area of the compounds to the internal standard was calculated to standardise the data for comparisons. For best results the LC-MS/MS unit was auto-tuned to give maximum results for the compounds previously to assay analysis.

The concentration of the reaction time points (0, 5, 15 and 30 min) tested in singlet were plotted versus the natural logarithm of percent test compound remaining relative to 0 minutes (based on relative peak area ratio). The slope of this clearance plot, which equals the microsomal elimination rate (k_{mic}), was determined and used to calculate the *in vitro* half-life ($t_{1/2}$). Data points representing < 10% remaining test compound were generally excluded from the definition of the clearance plot slope, to focus on linear reaction kinetics. The relationship between the *in vitro* half-life and the kinetic constants is derived by the integrated MICHAELIS-MENTEN equation at one time point ($t_{1/2}$),^[245] which is simplified to eq. 1 since the initial complex concentration is supposed to be much lower than K_m .

$$t_{1/2} = \frac{1}{-k_{mic}} \cdot (0.693 + \frac{0.5[C]_{t=0}}{K_m}) \text{ for } [C]_{t=0} \ll K_m \text{ is valid } t_{1/2} = \frac{\ln 2}{-k_{mic}} \quad \text{eq. 1}$$

Equation 1: k_{mic} is the *in vitro* elimination rate constant ($-k_{mic} = V_{max}/K_m$), $[C]_{t=0}$ is the initial concentration of complex and K_m is the MICHAELIS-MENTEN constant.

Assays for drug-like abilities determination

Using the *in vitro* half-life ($t_{1/2}$), the intrinsic clearance CL_{int} ($\mu\text{L}/\text{min}/\text{mg}$ microsomal protein) can be calculated. This value standardises the observed $t_{1/2}$ for the used *in vitro* reaction conditions, adding the incubation volume (V) and the microsomal protein content (M).

$$CL_{int} = \frac{0.693}{t_{1/2}} \cdot \frac{V}{M} = \frac{1386}{t_{1/2}} \quad \text{eq. 2}$$

Equation 2: V is the incubation volume (μL) and M the microsomal protein content (mg).

This data can further be used for IVIVC (*in vitro-in vivo* correlation) giving a theoretical hepatic extraction ratio (ER_h) for the test compounds *in vivo*. Therefore the experimental results are scaled to normalise for the whole liver microsomal content ($CL_{int,s}$) using two scaling factors accounting for milligrams microsomal protein per gram liver ($SF_1 = 45^{[354-357]}$) and gram liver per kilogram animal ($SF_2 = 40^{[357,358]}$). Since the whole liver intrinsic clearance is expressed in $\text{mL}/\text{min}/\text{kg}$ this gives:

$$CL_{int,s} = (CL_{int} \cdot \frac{\text{mL}}{1000\mu\text{L}}) \cdot SF_1 \cdot SF_2 = 1.8 CL_{int} \quad \text{eq. 3}$$

Equation 3: SF_1 is the scaling factor accounting mg microsomal protein per g liver, SF_2 for g liver per kg animal.

This value can further be used to calculate the hepatic clearance (CL_h [$\text{mL}/\text{min}/\text{kg}$]) via the “well-stirred model”, assuming that CYP metabolism limits clearance rates. The f_{ub}/f_{um} (fractions unbound in blood or plasma (ub) and microsomes (um)) term captures ratio of compound binding to blood/plasma and microsomes, and therefore captures whether the drug is available for extraction in metabolic tissue. Often these terms are set to be equal.^[244] The portal blood flow (Q_h [$\text{mL}/\text{min}/\text{kg}$]) is another empirical scaling factor required for eq. 4 and equals 100^[292] for rats.

$$CL_h = \frac{Q_h \frac{f_{ub}}{f_{um}} CL_{int,s}}{Q_h + \frac{f_{ub}}{f_{um}} CL_{int,s}} = \frac{Q_h \frac{f_{ub}}{f_{um}} CL_{int,s}}{Q_h + \frac{f_{ub}}{f_{um}} CL_{int,s}} = \frac{180 \frac{f_{ub}}{f_{um}} CL_{int}}{100 + 1.8 \frac{f_{ub}}{f_{um}} CL_{int}} \quad \text{eq. 4}$$

Equation 4: Q_h is the portal blood flow, f_{ub} is the fraction unbound in blood or plasma, f_{um} the fraction unbound in microsomes and are set equal for simplicity and due to missing values for most complexes

The theoretical hepatic extraction ratio (ER_h) for the test compound during *in vivo* clearance equals the ratio of CL_h to the portal blood flow (Q_h):^[243]

$$ER_h = \frac{CL_h}{Q_h} = \frac{CL_h}{100} = \frac{1.8 \frac{f_{ub}}{f_{um}} CL_{int}}{1 + 0.018 \frac{f_{ub}}{f_{um}} CL_{int}}$$
 eq. 5

Equation 5: Calculation of the theoretical hepatic extraction ratio using the previously calculated values.

The values obtained were used to identify potential exposure-limiting metabolic clearance using the Novartis guidance summarised in the following table.

Table 23: Guidance for interpretation of $t_{1/2}$ values and the assessment of a potential metabolic risk.

$t_{1/2}$ (min)	CL_{int} (mL/min/mg)	estimated ER_h	potential metabolic risk
<10	>150	>0.7	high
10-30	50-150	0.5-0.7	medium
>30	<50	<0.5	low

5.8.4. Metabolic stability in hepatocytes

The metabolic stability towards hepatocytes was tested cross-species in rat, dog and human hepatocytes by NIBR staff in Basel. Before use, the cells, which were stored under liquid nitrogen, were thawed in a 37 °C water bath for up to 2 min and then transferred to a tube of 40 mL of pre-warmed (37 °C) medium (WME supplemented with 10% FBS). The cell-suspension was centrifuged for 1 min at 50 x g, the supernatant was discarded and the cell-pellet resuspended by gentle agitation in a small volume (2-5 mL) of medium. Cell viability was tested by mixing one aliquot (50 µL) of cell suspension with one aliquot (50 µL) of trypan blue and living cells were counted. The cell suspension was further diluted to obtain a suspension with a final concentration of 1·10⁶ cells/mL. Of that suspension, 1 mL per well was transferred to a 12-well plate and RR97a (201a) was added as 2 mM stock solution in DMSO to a final concentration of 10 µM. The cells were incubated at 37 °C and 50 rpm under an atmosphere of 75% O₂, 5% CO₂ and 20% N₂, and 98% humidity in a HERAcell 240i incubator (THERMO FISCHER SCIENTIFIC). At time points 0 h and 2 h, 200 µL of incubation sample each was collected and added to one volume of cold CH₃CN. The internal MS standard was added (8 µL, final concentration 5 µM) and the mixture frozen at -80 °C until analysis. After thawing, the samples were centrifuged (5 min at 10000g) and 100 µL of supernatant was diluted with 400 µL water and filtered (0.45 µm) if necessary to remove precipitate. LC separation was performed using a binary syringe pump at a flow rate of 4.5 µL/min,

a 150 mm x 0.3 mm capillary HPLC column containing C18 material at 40 °C. The column effluent is directly injected into the ion source of a linear ion trap-Orbitrap hybrid mass spectrometer (THERMO FISCHER SCIENTIFIC) using positive ion electrospray ionisation.

5.8.5. Permeability assessment via hexadecane membrane (HDM)-PAMPA

The permeability in this assay was assessed by staff of NIBR Cambridge using a 9-10 µm thick hexadecane layer and 100 mM KCl buffers containing 5% DMSO at different pH values (4.0, 6.8, 8.0). The layer was prepared freshly previously to the experiment by addition of 5 µL of a 15% hexadecane/hexane solution to a 96-well polycarbonate filterplate (0.4 µm PCTE membrane) followed by 15 min incubation at room temperature, during which the hexane evaporates. The final hexadecane volume in each well is thereby 0.75 µL and represents a minimal membrane volume to reduce membrane retention in the experiment. To each filterwell 300 µL buffer and 4.5 µL of three 300 µM sample solution (final concentration 5 µM) in DMSO was added in triplicate and the insert assembled with a teflon acceptor plate which also contained 300 µL buffer/well. The plate was then incubated at 150 rpm for 4 h and the membrane integrity was tested at the end of the incubation time (electrical resistance must be above 25 kΩ). The well with the highest resistivity was chosen and 37.5 µL taken of, mixed with a second sample and 75 µL of internal standard solution. Quantification of the sample was performed via a high-performance liquid chromatography-tandem mass spectrometry system (LC-MS/MS) using propranolol as control substance. The apparent permeability, which is identical to the effective membrane permeability P_a , was calculated per the following equation:

$$P_a = - \frac{V_D}{V_D + V_R} \cdot \frac{V_R}{A \cdot \Delta t} \cdot \ln(1-r) \quad \text{eq. 6}$$

Equation 6: V_R is the volume of the acceptor compartment (0.3 cm^3), V_D of donor compartment (0.3 cm^3), A is the accessible filter area (total area 0.24 cm^2 , multiplied by a porosity of 20%), Δt is the incubation time (240 min) and r is peak area of compound in the acceptor compartment divided by the theoretical equilibrium peak area ($c_D(0)$ replaced by independent equilibrium concentration).

PAMPA mimics pure transcellular permeability. Paracellular contribution can be added mathematically^[359] via a hydrodynamic model.^[360-362] Since the calculation was not possible for coordination compounds using the available resources, the paracellular contribution was not determined. Therefore, also logPAMPA, which contains para- and transcellular components, was not determined which is necessary to obtain a calculated fraction absorbed and to rank the compounds according to high, medium or low permeability.

5.8.6. Permeability assessment in Caco-2 cells

The cell permeability of the complexes was assessed by staff of NIBR Cambridge using a well evaluated human epithelial colorectal adenocarcinoma cell-line (Caco-2 cells) based assay.^[257] The cells (11.840 cells/well in 75 µL) were seeded on PET filters in a 96-well format (BD BIOSCIENCE) and cultured (37 °C, 5% CO₂, > 95% RH; medium change every 2-3 days) for 21 days during which optimally differentiated properties developed. Medium used in this assay is DMEM containing 10% FBS, MEM non-essential amino acid solution, MEM sodium, penicillin and streptomycin solution. The complexes were used as 2 mM DMSO stock solution, of which 7 µL was diluted to a 10 µM solution in transport buffer (Hank's Balanced Salt Solution (HBSS) pH 7.4 supplemented with 10 mM HEPES). The Caco-2 cells were rinsed three times with transport buffer (75 µL in the apical and 250 µL in the basolateral chambers) and the electronic resistance across the monolayer was measured via TEER (trans epithelial electric resistance) with an EVOM ohmmeter. Wells with a TEER < 200 Ω·cm² were excluded from the assay. The complex dilution was added either to the apical (A: 75 µL) or basolateral (B: 250 µL) side of the cells and the other side filled accordingly with transport buffer. Samples for t = 0 were taken from the compound plate before the assay plate was incubated for 120 min at 37 °C and 40 rpm. At the end of the incubation time, samples were taken from the donor (10 µL) and acceptor (40 µL) chamber. To the donor samples 30 µL transport buffer was added and all samples were further diluted with 50 µL CH₃CN containing 0.01% formic acid and 0.36 µM alprenolol (MS standard) to precipitate potential protein content. The samples were centrifuged for 10 min at 4 °C and 3500 rpm and the supernatant quantified using a high-performance liquid chromatography-tandem mass spectrometry system (LC-MS/MS). MS/MS conditions for compounds were previously optimised using the software QuanOptimize, which will optimize the compound ionisation polarity, MSMS transition, cone voltage and collision energy. The apparent permeability P_{app} [cm/s] can further be calculated from the MS-results (sample peak area ratios normalised to internal MS standard) using eq. 7, which expresses the interconnection of P_{app} with the amount of complex transported during the incubation time, the surface area and the different sizes of the A and B chamber:^[253]

$$P_{app} = \frac{C_t^R \cdot V^R}{\Delta t} \cdot \frac{1}{C_0^D \cdot A} \quad \text{eq. 7}$$

Equation 7: C_t^R is the compound concentration in the receiver chamber after the incubation period (µM), V^R is the volume of the solution in the receiver chamber after the incubation period (mL), Δt is the incubation time (120 min); C₀^D is the compound concentration in the donor chamber measured at t = 0 (C₀^D ~10 µM) and A is the surface area of the transport membrane (0.0804 cm²).

Originating with the apparent permeability from the apical to the basolateral side and *vice versa*, an efflux ratio can be calculated giving a first indication in the transport mechanisms involved. An $ER = P_{app}(B-A)/P_{app}(A-B)$ ratio of ≥ 3 indicates efflux, ≥ 2 but < 3 might be reflux, values below that indicate passive or even active transport of the compound through the membrane.

Taken the $P_{app}(A-B)$ -values, a theoretical *in vivo* intestinal absorption (fraction absorbed FA) can be calculated using an empirically derived sigmoidal Boltzman function (eq. 8), which was based on data comparing the *in vivo* FA and the $P_{app}(A-B)$ -values of a test set of 93 compounds.^[257] The compounds were then classified according to Table 24.

$$\%FA = \frac{[min + (max-min)]}{[1 + (\exp(\frac{V_{50}-X}{slope}))]} \quad \text{eq. 8}$$

Equation 8: $X = \log P_{app}(A-B)$; min = 1; max = 100, slope = 0.39 and $V_{50} = -5.74$ with slope and V_{50} being empirical constants, which assumes being in linear range of kinetics.^[257]

Table 24: Guidance for interpretation of %FA and $P_{app}(A-B)$ - values and the assessment of a potential permeability risk.

$P_{app}(A-B)$ [cm/sec]	estimated %FA	permeability
$\geq 5 \times 10^{-6}$	$\geq 75\%$	high
$\geq 1 \times 10^{-6}$ but $< 5 \times 10^{-6}$	≥ 35 but $< 75\%$	medium
$< 1 \times 10^{-6}$	$< 35\%$	low

5.8.7. Permeability assessment in MDCK cells

The permeability in MDCK-LE cells was determined by staff of NIBR Cambridge, using an evaluated dog kidney epithelial cell-line (MDCK (Madin-Darby canine kidney) cells). The cells (37.500 cells/well in 75 µL) were seeded on PET filters in a 96-well format (CORNING) and cultured (37 °C, 5% CO₂, > 95% RH) for 3-4 days during which optimally differentiated properties developed. Medium used in this assay was DMEM containing 10% FBS, 2 mM L-Glu and 1% penicillin-streptomycin. The complexes were used as 10 mM DMSO stock solution, of which 600 nL were diluted to a bestatin containing 10 µM solution in transport buffer (Hank's Balanced Salt Solution (HBSS) pH 7.4 supplemented with 10 mM HEPES, 0.02% BSA). The cells and basolateral chambers were rinsed three times with transport buffer without BSA. The complex dilution was added to the apical (A: 75 µL) side of the cells and the basolateral side (B: 250 µL) was filled accordingly with transport buffer. Samples for t = 0 were taken from the test solution plate

Experimental part

before the assay plate was incubated for 120 min at 37 °C and 40 rpm. At the end of the incubation time, samples were taken from the donor (10 µL) and acceptor (50 µL) chamber. To the donor samples 50 µL HBSS was added and all samples were further diluted with 50 µL internal MS standard solution (glibenclamide in H₂O/CH₃CN) to precipitate potential protein content. The samples were centrifuged for 10 min at 4 °C and 4000 rpm and the supernatant quantified using a high-performance liquid chromatography-tandem mass spectrometry system (LC-MS/MS). The apparent permeability was calculated as described for Caco-2.

5.8.8. Determination of MDR1 impact on efflux

The impact of the efflux transporter MDR1 on cell permeability of the complexes was assessed by staff of NIBR Cambridge, MA, USA, using an evaluated dog kidney epithelial cell-line (MDCK cells), which overexpress MDR1.^[262-264] The cells (37.500 cells/well in 75 µL medium) were seeded on PET filters in a 96-well format (CORNING) and cultured (37 °C, 5% CO₂, > 95% RH) for 3-4 days during which optimally differentiated properties developed. Medium used in this assay was DMEM containing 10% FBS, 2 mM L-Glu and 1% penicillin-streptomycin. The complexes were used as 10 mM DMSO stock solution, of which 600 nL were diluted to a bestatin containing 10 µM solution in transport buffer (Hank's Balanced Salt Solution (HBSS) pH 7.4 supplemented with 10 mM HEPES 0.02% BSA). The cells and basolateral chambers were rinsed three times with transport buffer without BSA. The complex dilution was added either to the apical (A: 75 µL) or basolateral (B: 235 µL) side of the cells and the other side filled accordingly with transport buffer. Samples for t = 0 were taken from the test solution plate before the assay plate was incubated for 120 min at 37 °C and 40 rpm. At the end of the incubation time, samples were taken from the donor (10 µL) and acceptor (50 µL) chamber. To the donor samples 50 µL HBSS was added and all samples were further diluted with 50 µL internal MS standard solution (glibenclamide in H₂O/CH₃CN) to precipitate potential protein content. The samples were centrifuged for 10 min at 4 °C and 4000 rpm and the supernatant quantified using a high-performance liquid chromatography-tandem mass spectrometry system (LC-MS/MS). The apparent permeability and efflux ratios were calculated as described for Caco-2. An ER > 3 thereby indicates efflux, ER = 2-3 indicates possible efflux.

5.8.9. Determination of *ex vivo* hepatotoxicity in PCLS

Precision cut liver slice (PCLS) experiments were performed in Angela Casinis laboratory at the Rijksuniversiteit Groningen, the Netherlands. PCLS were prepared from liver tissue obtained from male Wistar rats (HsdCpb:WU, HARLAN LABORATORIES) weighing 300-350 g. The rats were housed on a 12 h light/dark cycle in a temperature- and humidity-controlled room with food (Harlan chow no 2018, HARLAN LABORATORIES) and tap water *ad libitum*. The animals were allowed to acclimatise for at least seven days before experimentation. The experimental protocols were approved by the Animal Ethical Committee of the University of Groningen and were performed according to strict governmental and international guidelines. The organ was excised under 5% isoflurane / 95% O₂ anaesthesia and placed into ice-cold University of Wisconsin (UW, DU-PONT) organ preservation solution until directly following preparation of PCLS as previously described.^[280] Caretaking of the animals and harvesting of tissue was performed by the technical staff at the Rijksuniversiteit Groningen. The viability of rat PCLS after 24 h incubation with the compounds and the 0 h, 1 h and 24+1 h control was determined via the ATP content of the PCLS which was measured according to a method described in literature.^[280] Briefly, liver tissue cores were prepared by drilling out cores of the fresh tissue, which are stored in UW until slicing. Therefore, the tissue was transferred to a petri dish with a silicone insert and was held loosely down by hand while rapidly drilling symmetrical cylindrical cores at a drill speed setting of 2. The tissue must be held covered by UW at all times during that procedure. The tissue was transferred back to ice-cold UW solution using a spatula and further kept in ice-cold UW until slicing.

For slicing a KRUMDIEK slicer was assembled following the supplier's protocol using a fresh razor blade and the system was cooled down by circulating 4 °C cold KHB (KHB1 (Table 25) at 4 °C mixed with 500 mL 10 x KHB (filtered through a 0.45 µm filter) upfilled to 5 L with *dd*H₂O at 4 °C, oxygenated (gas dispersion tube with fritted disc) with 95% O₂ / 5% CO₂ on ice for 30 min, pH adjusted to 7.42 with 5 N NaOH_{aq.}).

Table 25: Composition of 10 x KHB and KHB1.

10 x KHB		KHB1	
CaCl ₂ ·2H ₂ O	36.7 g	NaHCO ₃	10.5 g
KCl	37.3 g	D-glucose·H ₂ O	24.75 g
NaCl	690 g	HEPES	11.9 g
MgSO ₄ ·7H ₂ O	27.1 g	<i>dd</i> H ₂ O	backfill to 2 L
KH ₂ PO ₄	16.3 g		
<i>dd</i> H ₂ O	backfill to 10 L		

Experimental part

One liver core is further transferred to the cylindrical core holder of the slicer using a spatula and the plunge holder is inserted before the core holder is transferred to the slicer. Slices were prepared at a speed of 30-40 and the thickness was adjusted to a value where the gently dried tissue, using blotting paper to remove adherent water, would weight ~ 5 mg. After finishing slicing one core, the slices were removed from the slicer into a beaker and healthy looking slices (equal thickness, uniform colour, smooth edges, no obvious damage) were directly transferred to ice-cold UW using a spatula where they were stored until the immediate following use. This step was repeated until sufficient healthy slices for the experiment were obtained. Each slice was then placed in one well of a 12-well plate containing 1.3 mL of preoxygenated and prewarmed (conditions see below) Williams medium E (WME, containing L-glutamine, INVITROGEN) with supplements (1.375 g D-glucose and 500 µL gentamicin (50 mg/mL) per 500 mL WME), after washing them with the prepared preheated WME. The slices were incubated for 1 h at 37 °C under an atmosphere of 95% O₂ / 5% CO₂ and 500 rpm in a shaker with moisture saturated atmosphere. Afterwards the slices were transferred to new plates containing fresh prewarmed and -oxygenated medium, and compound in DMSO as 10 mM or 1 mM DMSO stock solution was added to the according final incubation concentration and mixed in by mild shaking. The plates were thereby stored on heating mats and the working steps were performed as fast as possible. The plates were further incubated for 24 h at the described conditions.

After the designated incubation time, the slices were collected individually in 1 mL 70% ethanol containing 2 mM EDTA (pH 10.9), quick-frozen in liquid nitrogen and stored at -80 °C. The samples were thawed on ice, homogenised for 45 s using a Mini-BeadBeater (BIOSPEC PRODUCTS) and centrifuged for 5 min at 13000 rpm and 4 °C. The supernatant was separated from the pellet and diluted with Tris/HCl (0.1 M) containing 2 mM EDTA (pH 7.8). The ATP content of this dilution was measured in a black 96-well microplate format using the ATP Bioluminescence Assay Kit CLS II (ROCHE DIAGNOSTICS GMBH) and a LumiCount microplate luminometer BL10001 (PACKARD). The ATP content was further calculated by comparing the results to a standard calibration curve. The remaining pellet was dried at room temperature for at least 72 h, dissolved in 200 µL NaOH (5 M) and incubated at 37 °C in a shaking water bath for 30 min. The solution was diluted with 800 µL H₂O (final NaOH concentration 1 M) and homogenised again for 40 s with a Mini-BeadBeater. The protein content was then determined using the Bio-Rad DC Protein Assay (BIO-RAD) in a 96-well microplate assay format compared for a bovine serum albumin (BSA) calibration curve. The ATP content of the slice was then normalised to the protein content (pmol ATP/µg protein) and expressed as the relative value to the 24 h control tissue. Obtained values are the mean of at least two independent experiments.

5.8.10. Determination of metal uptake of PCLS after treatment with 201a and 201b

For the determination of metal uptake in PCLS, slices were prepared and treated according to the protocol for determination of *ex vivo* hepatotoxicity as described above. After 24 h incubation with medium containing the test substance, the tissue slices were removed from the medium and washed with fresh KREBS medium. They were individually placed in 1.5 mL Eppendorf tubes, quick frozen in liquid nitrogen and stored at -20 °C until further use. In addition to that, medium samples both from pure medium as well as the used medium with compound were taken to measure their rhodium content to ensure a proper concentration during the experiment.

All further steps were performed by JAN BAMBERGER from the central mass department of the chemistry department of the Philipps-Universität Marburg. The samples were thawed, either slices or medium transferred to 50 mL Falcon tubes, and the organic material was digested at 60 °C using conc. HNO₃, where 2 mL of the acid were added gradually to ensure slow oxidation. In case there was still tissue visible, additional acid was added and further oxidised at 60 °C. The resulting solution was diluted with water to a final concentration of 5% HNO₃.

For ICP-MS measurement these samples were sucked into the system (Element II™ ICP-MS (THERMO FISHER SCIENTIFIC)) using a peristaltic pump at a flow rate of 0.05 mL/scan and the rhodium content in ng Rh per g sample was calculated from the obtained results by the supplier's software against a Rh concentration curve.

5.8.11. Preparation of PCLS for morphology studies

PCLS for morphology studies were prepared and treated with compound according to the hepatotoxicity study protocol until the end of the final incubation time. The treated samples were compared to untreated 0 h and 24 h control. After the incubation time, three slices each were transferred in 500 µL 4% w/v formalin (0 h control at time point 0 respectively) in a 24-well plate, sealed with a plastic paraffin film and incubated at 4 °C for 24 h. They were then transferred to an according well containing 70% EtOH_{aq} and incubated at 4 °C for at least 24 h. The sections were transferred to special dehydration casks and dehydrated using a graded ethanol series, eosin stained and paraffinized in the pathology department of the university medical centre Groningen. Afterwards the slices were bedded in paraffin and dried at 20 °C over night. The paraffin blocks were cut into 4 µm thick stripes, which were incubated in a 50 °C water bath to remove cracks and tension from cutting, before they were transferred to a glass slide. The water from the cover slips was removed using a soft tissue, the slips were dried for 15-30 min on a 60 °C heating plate and further at 37 °C in an oven over night. For deparaffination the slides were incubated two times 5 min each in fresh ultraclear solution (isoparaffin based clearing reagent) and two times 1 min

Experimental part

each in 100% EtOH. They were rehydrated for 1 min in 50% EtOH_{aq.} and stained with haematoxylin-solution for 10 min before they were rinsed with tap-water for 1 min. Haematoxylin thereby stains the chromatin in the nucleus purple-blue. The slides were incubated in 50% acidic EtOH_{aq.} (500 mL 50% EtOH_{aq.} + 1.25 mL HCl_{aq.}), in 70% EtOH and in 80% basic EtOH_{aq.} (500 mL 80% EtOH + 7.5 mL 25% NH₃aq.) for 1 min each. Afterwards they were incubated for 2 min in eosin solution to dye the cytoplasm pink, before they were two times incubated in 100% EtOH for 1 min and two times in ultraclear for 1 min. The slides were dried at room temperature until all drops were evaporated. Afterwards some DPX mounting medium was added to the slides and a coverslip was added. The slides were left to dry at room temperature for a couple of hours and further stored at room temperature until further examination.

5.9. *In vivo* studies

5.9.1. *In vivo* pharmacokinetics of 201b in mice

In vivo pharmacokinetic studies of RR97b (**201b**) were performed by NIBR staff in Cambridge using male C57BL/6 mice weighting 28-31 g (HARLAN LABORATORIES). The mice were singly housed on a 12 h light/dark cycle in a temperature- and humidity-controlled room (18-22 °C, humidity 50 ± 20%) with tap water *ad libitum* before and during the experiment. Food (PICOLAB Rodent Diet 20) was provided unless otherwise specified. All animal related procedures were conducted under a Novartis IACUC (Institutional Animal Care and Use Committee) approved protocol in compliance with Animal Welfare Act regulations and the Guide for the Care and Use of Laboratory Animals. The compound, formulated as solution in 5% NMP, 20% PEG300, 10% solutol backfilled with PBS at pH 7.4 - 7.7, was administered to the mice intravenously via tail vein (1 mg/kg, 5 mL/kg, n = 2), intraperitoneally (3 mg/kg, 5 mL/kg, n = 3) or orally via gavage (3 mg/kg, 10 mL/kg, n = 3). The animals were placed on wire grate cage bottoms until the end of the experiment. Serial blood samples (50 µL, EDTA as anti-coagulant) were taken via tail vein for early time points and by cardiac puncture at the last time point, at scheduled times over 7 h after dosing. The plasma was separated by centrifugation at 3000 rpm. The concentration of the compound was determined by LC-MS/MS. Relevant estimated pharmacokinetic parameters for plasma such as clearance, volume of distribution and half-life were derived by non-compartmental analysis using the program Watson (Version 7.4.2., THERMO FISHER SCIENTIFIC, INC.).

Therefore, for the intravenous dose, the concentration of unchanged compound at time zero was calculated based on a log-linear regression of the first two data points to back-extrapolate C₍₀₎. The area under the concentration-time curve from time zero to the last measurable concentration

(AUC_{last}) for all administration routes was calculated using the linear trapezoidal rule. Based on the AUC_{last} , the area under the plasma concentration-time curve from time zero extrapolated to infinite time (AUC_{inf}) was calculated using eq. 9, where λ_z is the terminal elimination rate constant of the unchanged compound, which was obtained from the slope of the log linear fit from at least the last three data points.

$$AUC_{inf} = AUC_{last} + \frac{c_{last}}{\lambda_z} \quad \text{eq. 9}$$

Equation 9: AUC_{inf} = area under the plasma concentration-time curve from time zero extrapolated to infinite time; AUC_{last} = area under the plasma concentration-time curve from time zero until the last measurable concentration; c_{last} = last quantifiable concentration, λ_z = terminal elimination rate constant.

Based on λ_z the half-life ($t_{1/2}$) was further calculated for IV administration. The total body clearance from the plasma (CL) and the apparent volume of distribution at steady state (V_{ss}) were also calculated from the intravenous data. Clearance thereby relates to the IV dose per AUC_{inf} as shown in eq. 10.

$$CL = \frac{Dose_{IV}}{AUC_{inf}} \quad \text{eq. 10}$$

Equation 10: CL = total body clearance from plasma, which is calculated from the ratio of the dose administers IV to AUC_{inf} .

The apparent volume of distribution at steady state was obtained using the IV dose, the AUC_{inf} and the area under the first moment concentration-time curve from time zero to infinity ($AUMC_{inf}$) according to eq. 11.

$$V_{ss} = \frac{Dose_{IV} \cdot AUMC_{inf}}{(AUC_{inf})^2} \quad \text{eq. 11}$$

Equation 11: V_{ss} = apparent volume of distribution at steady state; $AUMC_{inf}$ = area under the first moment concentration-time curve from time zero to infinity.

The bioavailability for PO and IP dosing was estimated according to eq. 12 (AUC_{last} if %extrapolation is >20%) for PO administration, using either PO or IP data for AUC_{inf} and Dose.

$$\%F = \frac{AUC_{inf\ PO}}{AUC_{inf\ IV}} \cdot \frac{Dose_{IV}}{Dose_{PO}} \quad \text{eq. 12}$$

Equation 12: Determination of bioavailability %F based on the calculated values $AUC_{inf\ PO/IV}$ and the dose given.

5.9.2. *In vivo* pharmacokinetics of **201a** in rats

In vivo pharmacokinetics of RR97a (**201a**) was determined using pre-cannulated male Sprague Dawley rats (Hsd: SD HARLAN LABORATORIES) weighing 310-355 g by NIBR staff in Basel. The rats were singly housed on a 12 h light/dark cycle in a temperature- and humidity-controlled room (21 °C, humidity 60%) with food and tap water *ad libitum* before and during the experiment. The animals were allowed to acclimatise for at least seven days before experimentation. All *in vivo* research was reviewed and approved by the Novartis Institute of Biomedical Research Institutional Animal Care and Use Committee (IACUC) in accordance with all local, state, and federal regulations. The compound formulated as solution in 30% NMP, 60% PEG200 and 10% solutol HS15 was administered intravenously (3 mg/kg, 6 mg/mL) over 8:45 – 8:52 h into the jugular vein via the catheter implanted. Serial blood samples of (EDTA as anti-coagulant) were taken at scheduled time points post dose (~150 µL blood samples at 0.08 h, 0.5, 1, 2, 4, 7, 24 h n = 3; ~600 µL blood samples at 1 h, 4 h, 7 h n = 2) via the catheter implanted after gentle manipulation and restraining of the rat. Plasma samples of ~70 µL or 300 µL accordingly were prepared by centrifugation (6800 x g, 10 min, 4 °C) from the blood samples. The concentration of RR97a was determined by LC-MS/MS, in a way that aliquots of the sample solutions, as well as calibration samples, were spiked with an internal standard and separated on a C18 HPLC column (150 mm x 0.3mm) with a mobile phase gradient at a flow rate of 4.5 µL/min and a column temperature of 40 °C. The column effluent is directly introduced into the ion source of a quadrupole-orbitrap hybrid mass spectrometer (THERMO FISCHER SCIENTIFIC) operating with positive electrospray ionisation.

Relevant estimated pharmacokinetic parameters for plasma such as clearance, volume of distribution and half-life were derived by noncompartmental analysis as described before. The Rh-content of the samples was determined using ICP-MS as described below. For comparison of the two measurement methods, the obtained results from LC-MS/MS were converted from mean nM (ng/L) to ng/mL complex (by dividing through 1000 and multiplying with the exact mass of the complex (629.03)) and converting from ng/mL complex to ng Rh/mL (multiplying with the exact mass of the complex and dividing through the exact mass of the most abundant Rh isotope). The results obtained from ICP-MS in ng/g were divided by the literature value of the density of blood plasma (1.025 kg/m³)^[363] to derive ng Rh/mL. Generally, based on the metabolism data in hepatocytes and *in vivo*, the Rh content is thought to reflect the true content of **201a**.

5.9.3. Metabolic stability of 201a *in vivo*

For the identification of the metabolic stability *in vivo*, samples of liver, kidney, lung and urine (see 5.9.4) 7 h pd were prepared for LC-MS/MS analysis as described under 5.8.4. Tissue samples were prepared by treatment of 300 µL homogenised tissue with 300 µL cold CH₃CN and incubation at 0 °C for 20 min. The procedure was repeated twice and then the mixture was centrifuged for 5 min at 10000g. From the supernatant 1 mL was removed and concentrated using a cyclone high speed evaporator (PROLAB). The residue was reconstituted with 250 µL H₂O/CH₃CN 9:1 and filtered (0.45 µm) if necessary, to remove precipitate. The urine sample was therefore prepared by dilution in 9:1 H₂O/CH₃CN and filtration (0.45 µm) to remove precipitate if necessary.

5.9.4. *In vivo* distribution of 201a in rats

For determination of *in vivo* distribution of RR97a the same rats as for pharmacokinetic observation were used. The rats were therefore deeply anaesthetised with isoflurane inhalation 7 h or 24 h pd. The organs of interest (spleen, muscle, liver, kidney, lung, heart and brain) were dissected out and the animals were euthanised by exsanguination. Blood contaminations on the tissue samples were gently removed with a paper tissue. The samples were bisected, frozen and kept -20 °C until further use.

An additional Sprague Dawley rat (Crl: CD (SD) Charles River Laboratories) was dosed accordingly and kept in a metabolic cage with free access to food and water for the experimental time span to collect urine and faeces quantitatively over 24 h pd. These samples were divided in 0-7 h and 7-24 h, frozen and kept at -20 °C until further use in metabolism analysis, drug concentration analysis via LC-MS/MS and total Rh-content analysis via ICP-MS. All samples were further prepared for analysis as described below.

5.9.4.1. Sample preparation for ICP-MS quantification

The organs and faeces samples were thawed at 20 °C, bisected and transferred to balanced out 50 mL conical plastic tubes (SARSTEDT). The wet weight of the samples was determined and they were dried in a drying oven at 90 °C for 28-48 h until they reached constant weight. Afterwards the dry weight was determined and the samples stored at -20 °C until further use. After thawing, the organic material was digested with conc. HNO₃ at 60 °C (2-8 mL until all organic material was digested), where the acid was added gradually to ensure a slow oxidation. The resulting solution was further diluted with water to a final concentration of 5% HNO₃. In some samples an Y

Experimental part

standard was added before backfilling to the final HNO₃ concentration as indicated in the discussion part. Where applicable, results were normalised to the internal Y standard.

Plasma samples were weighed into 50 mL conical tubes as liquid and digested with 2 mL conc. HNO₃. Samples were backfilled to 40 mL with H₂O and 100 ppt indium standard was added. Samples were measured as described below and results were normalised to the internal In concentration.

5.9.4.2. ICP-MS based determination of Rh content

The samples were measured on an Element II™ ICP-MS system (THERMO FISHER SCIENTIFIC), in a way that they were sucked into the system with a peristaltic pump, using e.g. a flow of 0.05 mL/scan. With high viscosities that volume might be reduced which leads to variations in results in comparison to the standards in the calibration curve, which do not contain any organic material and therefore have a lower viscosity. The system has an upper measurement range of 5000ppt (5 µg/L), all values above that value might not be accurate results. For that reason, some samples were diluted down with a factor of up to 1:1000 gravimetrically, which might lead to further deviations. The upper measurement range was especially problematic in the initial measurement of urine and faeces, since some samples contained a content above the calibration curve and are therefore expected to have higher results than obtained in the experiment. For urine no repeat experiments were possible, due to no more sample available.

To get more accurate results in some measurements the internal standard Indium was used. However, the measurement interferes with isobars containing Sn and Pd so that quite high deviations were still in place for samples with a low Rh content which were not diluted down. Therefore, later Yttrium was added as internal standard for the latest experiments. If and where internal standards are used for the samples is indicated in the according results and discussion or experimental section. The Rh content was determined against a measured calibration curve and normalised (if applicable) to the standard by the supplier's program Element (THERMO FISHER SCIENTIFIC).

6. Appendix

6.1. List of abbreviations

6.1.1. Amino Acids

A	Ala	alanine
C	Cys	cysteine
D	Asp	aspartic acid
E	Glu	glutamic acid
F	Phe	phenylalanine
G	Gly	glycine
H	His	histidine
I	Ile	isoleucine
K	Lys	lysine
L	Leu	leucine
M	Met	methionine
N	Asn	asparagine
P	Pro	proline
Q	Gln	glutamine
R	Arg	arginine
S	Ser	serine
T	Thr	threonine
V	Val	valine
W	Trp	tryptophane
Y	Tyr	tyrosine

6.1.2. Nucleobases

A	adenine
C	cytosine
G	guanine
T	thymine
U	uracil

6.1.3. General abbreviations

(CD ₃) ₂ CO	deuterated acetone
(g)	gaseous
(NH ₄) ₂ S ₂ O ₈	ammonium persulfate
¹³ C-NMR	nuclear magnetic resonance for carbon atoms (¹³ C isotope)
¹ H-NMR	nuclear magnetic resonance for protons (¹ H isotope)
2D	two dimensional
2-TMS-EtOH	2-(trimethylsilyl)ethanol
4EPB2	initiation factor 4E binding protein B2
A	apical
A	accessible filter area (PAMPA)
A	surface area of transport membrane (cell permeability)
A2780	human ovarian carcinoma cell line
A549	human lung carcinoma cell line
ABC	ATP-binding cassette
abs.	absolute/absolutised
AcOH	acetic acid
ADME(T)	absorption distribution metabolism excretion (toxicity)
ADP	adenosine diphosphate
AGC	protein kinases A, G and C-like
AIBN	azobis(isobutyronitrile)
Akt	protein kinase B
ALK	anaplastic lymphoma kinase
AML	acute myeloid leukemia
APBS	adaptive Poisson-Boltzmann solver
APCI +/-	atmospheric pressure chemical ionisation positive/negative mode
APS	ammonium persulfate
aq.	aqueous
ASK1	apoptosis signal-regulating kinase 1
ATP	adenosine triphosphate
ATR	attenuated total reflection
AUC	area under the curve
AUC _{inf}	area under the plasma concentration-time curve from time zero extrapolated to infinite time
AUC _{last}	area under the plasma concentration-time curve from time zero until the last measurable concentration
B	basolateral
BAD	Bcl-2-associated death promoter
BC	before Christ

List of abbreviations

Bcl 2	B-cell lymphoma 2
BCR-Abl	breakpoint cluster region-abelson murine leukemia viral oncogene homolog
bnpy	2-benzylpyridine
Boc	<i>tert</i> -butyloxycarbonyl
bpy	bipyridine
bpy ^{dmh}	1,1-dimethylbenzyl)-2,2'-bipyridine
bpy ^{Me/Et}	6-methyl/ethyl-2,2'-bipyridine
br	broad
B-Raf/BRAF	rapidly accelerated fibrosarcoma homolog B
BSA	bovine serum albumin
BTK	bruton's tyrosine kinase
c/conc.	concentration
C ₀ ^D	compound concentration in the donor chamber measured at t = 0
CAC	cacodylic acid
Caco-2	human colon adenocarcinoma cell line
calcd.	calculated
CAMK	Ca ²⁺ /calmodulin-dependent protein kinase
cAMP	cyclic adenosine monophosphate
CBX3	chromobox protein homolog 3
Cbz	carboxybenzyl
CD ₃ CN	deuterated acetonitrile
CD ₃ OD	deuterated methanol
Cdc25c/A	cell division cycle 25c/A
CDCl ₃	deuterated chloroform
CDK	cyclin-dependent kinase
CDK	chemistry development kit
CH1	human ovarian carcinoma cell line
CK1	casein kinase 1
c _{last}	last quantifiable concentration
CLDI	crystal-like drug inclusions
Cl _h	hepatic clearance
Cl _{int}	intrinsic clearance
Cl _{int,s}	intrinsic clearance scaled to entire liver
cMET	cellular-mesenchymal to epithelial transition factor
CMGC	cyclin-dependant, mitogen-activated, glycogen synthase, and DDK-like kinases
CNS	central nervous system
COSY	correlation spectroscopy

Cp	cyclopentadiene
C _q	quaternary carbon atom
Crl: CD (SD)	sprague dawley rat strain
C-TAK1	Cdc25C-associated kinase 1
CTCL	cutaneous T-cell lymphoma
C _t ^R	compound concentration in the receiver chamber after the incubation period
CYP	cytochrome P450
cyt c	cytochrome c
d	doublet
D ₂ O	deuterated water
DAPK1	death-associated protein kinase 1
DBPO	dibenzoyl peroxide
DCM	dichloromethane
DFG	amino acid sequence aspartic acid-phenylalanine-glutamine
dfppy	2-(2,4-difluorophenyl)pyridine
DIP	4,7-diphenyl-1,10-phenanthroline
DIPA	diisopropylamine
DIPEA	N,N-diisopropylethylamine
DMAP	4-dimethylaminopyridine
DMEM	Dulbecco´s modified eagle´s medium
DMF	N,N-dimethylformamide
DMSO	dimethylsulfoxide
DMSO- δ_6	deuterated dimethylsulfoxide
DNA	deoxyribonucleic acid
DPBS	DULBECCO´s phosphate buffered saline
DTT	dithiothreitol
DW	DOUG WILLIAMS
DYRK	dual specificity tyrosine-phosphorylation-regulated kinase
e.g.	exempli gratia
E/Z	entgegen (opposite)/zusammen (together) configuration of double bonds
EDCl	N-(3-dimethylaminopropyl)-N'-ethylcarbodiimide hydrochloride
EDTA	ethylenediaminetetraacetic acid
EGFR	epidermal growth factor receptor
elF4E	eukaryotic translation initiation factor 4E
Em	emission
eq	equivalent
eq-	equation
ER	efflux ratio (permeability)
ER	extraction ratio (metabolic stability)

List of abbreviations

ErbB2	avian erythroblastosis oncogene B (equals HER2)
ER _h	hepatic extraction ratio
ESI+/-	electron spray ionisation positive/negative mode
Et ₂ O	diethyl ether
EtOAc	ethyl acetate
EtOH	ethanol
Ex	excitation
F	bioavailability
F ₂₅₄	fluorescence indicator for short wavelength light
FA	fraction absorbed
FabF	β ketoacyl acyl carrier protein synthase II
FaSSIF	fasted state simulated intestinal fluid
FBS	fetal bovine serum
FDA	US food and drug administration
FeSSIF	fed state simulated intestinal fluids
Fig.	figure
FL	FENG LI
FLT	fms like tyrosine kinase
FTIR	fourier transform infrared spectroscopy
f _{ub}	fraction unbound in blood or plasma
f _{um}	fraction unbound in microsomes
g	gram
G-361	human malignant melanoma cell line
GADPH	glyceraldehyde 3-phosphate dehydrogenase
GFP	green fluorescent protein
GI	gastrointestinal
GSH	glutathione
GSK3	glycogen synthase kinase 3
GTP	guanosine triphosphate
h	hours
H3	histone 3
HAT	histone acetyltransferase
HB	HOWARD BREGMAN
H-bond	hydrogen bond
HBSS	Hank's balanced salt solution
hCA	human carbonic anhydrase II
HCT-116++	human colorectal carcinoma cell line p53 +/+
HDA	yeast histone deacetylase
HDAC	histone deacetylase

HDI	histone deacetylase inhibitor
HDMS	hexamethyldisilazane
HEL	human erythroleukemia
HEL92.1.7	human caucasian erythroleukaemia cell line
HeLa	HENRIETTA LACKS (cervical cancer) cell line
HEPES	4-(2-hydroxyethyl)-1-piperazineethanesulfonic acid
HER2	human epidermal growth factor receptor 2
hex	hexane
HIV	human immunodeficiency virus
HMBC	heteronuclear multiple bond correlation
HOAc	acetic acid
HOS	human caucasian osteosarcoma cell line
HOSA	hydroxylamine-O-sulfonic acid
HP1y	heterochromatin protein 1y
hpf	hours post fertilisation
HPLC	high pressure liquid chromatography
HR	high resolution
HRMS	high resolution mass spectrometry
hSA	human serum albumin
Hsd: SD	Sprague Dawley rat strain
HsdCpb:WU	wistar rat strain
HSP	heat shock protein
HSQC	heteronuclear single quantum coherence
HT	high throughput
HT-29	human colorectal adenocarcinoma cell line
Hz	Hertz
hv	luminous exposure
IACUC	institutional animal care and use committee
IC ₅₀	half maximum inhibition concentration
ICP-MS	inductively coupled plasma mass spectrometry
IL	interleukin
IP	intraperitoneal
IR	infrared spectroscopy
IV	intravenous
IVIVC	<i>in vitro-in vivo</i> correlation
J	coupling constant
JAHA	jay amin hydroxamic acid
JAK	janus kinase
K-562	myelogenous leukemia cell line
kD	kilo Dalton

List of abbreviations

KHB	KREBS-HENSELEIT buffer
KI	kinase inhibitor
K _i	inhibition constant
K _M	MICHAELIS-MENTEN constant
k _{mic}	microsomal elimination rate
k _{obs}	apparent inactivation rate constant
KP _i	potassium inorganic phosphate buffer
KW	KATHRIN WÄHLER
L	liter
L	ligand
LC-MS(/MS)	liquid chromatography (tandem) mass spectrometry
LD ₅₀	median lethal dose
LICCS	Excel-CDK system
logD	logarithm of distribution coefficient
logP	logarithm of partition coefficient
logS	logarithm of solubility
m	milli
m	meter
M	mega
m	multiplet (NMR)
m	medium (IR)
M	molar
M	metal
M	microsomal protein content
mAb	monoclonal antibody
mal-p-Bel	malonate derivate of belinostat
malSAHA	malonate derivative of SAHA
MAPK	mitogen-activated protein kinase
MCDB	molecular cellular and developmental biology
MCF7	human breast adenocarcinoma cell line
MDA-MB-231	human breast adenocarcinoma cell line
MDCK(-LE)	Madin-Darby canine kidney cell line (low efflux)
MDR1	multidrug resistance protein1 (see Pgp)
Me ₃ OBF ₄	trimethyloxonium tetrafluoroborate/ MEERWEIN salt
MEM	modified eagles medium
MeOH	methanol
MET	receptor tyrosine kinase
min	minutes
MLCK	myosin light-chain kinase
Mops	3-(N-morpholino)propanesulfonic acid

mRNA	messenger ribonucleic acid
MS	mass spectrometry
MS	Microsoft
MST-1	mammalian sterile 20-like kinase-1
MTH1	7,8-dihydro-8-oxoguanosine triphosphatase
mTOR	mammalian target of rapamycin
MTT	3-(4,5-dimethylthiazol-2-yl)-2,5-diphenyltetrazolium bromide
MW	molecular weight
MW	microwave
Myc	avian myelocytomatisis viral oncogene homolog
NAD ⁺ /NADH	nicotinamide adenine dinucleotide
NADPH	nicotinamide adenine dinucleotide phosphate
NAE	NEDD8-activating enzyme
NBS	N-bromosuccinimide
n-BuLi	n-buthyllithium
NEDD8	neural precursor cell expressed, developmentally down-regulated 8
NFATC1	nuclear factor of activated T-cells, cytoplasmic 1
NHS	N-hydroxysuccinimide
NIBR	Novartis institutes of biomedical research
ⁿ J	coupling constant over n bonds
NMP	N-methyl-2-pyrrolidone
NMR	nuclear magnetic resonance
np	NICHOLAS PAGANO
NRAS	neuroblastoma RAS viral oncogene homolog
NuMa	nuclear mitotic apparatus protein
OATP	organic anion-transporting polypeptide
OCT	organic cation transport proteins
OES	optical emission spectroscopy
ORTEP	oak ridge thermal-ellipsoid plot program
p21	protein 21, cyclin-dependent kinase inhibitor
p27	protein 27, cyclin-dependent kinase inhibitor
p56	protein 56, phosphoglycerate kinase
PA	buffer A
P _a	apparent permeability (equals P _c)
PAGE	polyacrylamide gel electrophoresis
PAK1	p21 (RAC1) activated kinase 1
PAMPA	parallel artificial membrane permeability assay
P _{app}	apparent permeability
PARSE	parameters for solvation energy
PBS	phosphate buffered saline

PCLS	precision-cut liver slices
PCR	polymerase chain reaction
PCT	patent cooperation treaty
PCTE	polycarbonate track etch
PD	pharmacodynamic
pd	post dose
Pd/C	palladium on charcoal
pdb	protein database
P _e	effective membrane permeability (equals P _a)
PEG	polyethylene glycol
PET	polyethylene terephthalate
Pgp	permeability glycoprotein 1 (see MDR1)
phen	1,10-phenanthroline
PI3K	phosphatidylinositol-4,5-bisphosphate 3-kinase
Pim	provirus integration site for Moloney murine leukemia virus
PK	pharmacokinetic
PKA	protein kinase A
pK _a	logarithm of acid dissociation constant
PKC	protein kinase C
P-loop	phosphate binding loop
PMSF	phenylmethylsulfonyl fluoride
PO	per oral
ppm	parts per million
ppy	phenylpyridine
pqr	protein (p) atomic partial charge (q) and radius (r)
PRAS40	proline-rich Akt substrate
PTCL	peripheral T-cell lymphoma
PVDF	polyvinylidene fluoride
py	pyridine
q	quartet
Q _h	portal blood flow in liver
quant.	quantitative
quin.	quintet
r	peak area
RAC1	Ras-related C3 botulinum toxin substrate 1
RAS	rat sarcoma (protein family of small GTPases)
RelA	v-rel avian reticuloendotheliosis viral oncogene homolog A
RET	rearranged during transfection
R _f	retention factor
RFU	relative fluorescence units

RGC	receptor guanylate cyclase related
RH	relative humidity
RIPA	radioimmunoprecipitation assay
RLM	rat liver microsome
RLU	relative luminescence units
ROS	reactive oxygen species
RPD3	reduced potassium dependency (yeast HDAC)
rpm	revolutions per minute
RPMI	Roswell Park Memorial Institute medium
RR	RAJATHEES RAJARATNAM
s	singlet (NMR)
s	strong (NMR)
S9	liver homogenate fraction
SAHA	suberanilohydroxamic acid
SAR	structure activity relationship
sat.	saturated
SDS	sodium dodecyl sulphate
SEK	SANDRA ELISABETH KLARA (DIECKMANN)
SEM	scanning electron microscopy
SF	scaling factor
Sirt	sirtuin
SK-OV-3	human ovarian adenocarcinoma cell line
SLC	solute carrier
SM	small molecule
SM	STEFAN MOLLIN
SMILES	simplified molecular input line entry specification
SMKI	small molecule kinase inhibitor
SOCS	suppressor of cytokine signalling
STAT	signal transducers and activators of transcription
STE	homologues of the yeast sterile kinases
t	triplet
$t_{1/2}$	elimination half-life
TBAF	tetrabutylammoniumfluoride
TBS	tert-butyldimethylsilyl
TBST	tris buffered saline containing Tween 20
TDI	time-dependant inhibition
TEER	trans epithelial electric resistance
TEMED	tetramethylethylenediamine
THF	tetrahydrofurane
thpy	3-(2-pyridinyl)-coumarin, 2-(2-thienyl)pyridine

TK	tyrosine kinases
TKI	tyrosine kinase inhibitor
TKL	Tyrosine kinase like
TLC	thin layer chromatography
TMS	trimethylsilyl
TNF- α	tumour necrosis factor- α
Tris	tris(hydroxymethyl)aminomethane
TrkA	neurotrophic tyrosine kinase receptor type 1
TSA	Trichostatin A
TSC2	tuberous sclerosis complex 2
UDP	uridine diphosphate
UGT	UDP glucuronosyltransferases
ULS	universal linker system
USA	United States of America
UV	ultraviolet
UW	university of wisconsin organ preservation solution
v	very
V	volt
V	incubation volume
V_D	volume of the donor compartment
VEGFR	vascular endothelial growth factor receptor
VPA	valproic acid
V_R	volume of the receiver compartment
V^R	volume of solution in the receiver chamber after the incubation period
V_{ss}	volume of distribution at steady state
W	watt
w	weak
w/v	weight per volume
WM1366	NRAS mutated (61L) human primary malignant melanoma cell line
WM983B	BRAF mutated (V600E) human metastatic malignant melanoma cell line with p53 wt
WME	WILLIAMS medium E
Wnt	wingless-related integration site
wt	wild type
WWI/II	world war 1/2
Δt	incubation time
λ	wavelength
λ_z	terminal elimination rate constant
ϱ	density
\tilde{v}	wavenumber

6.2. Bibliography

- [1] A. Sudhakar, *J. Cancer Sci. Ther.* **2009**, *1*, i–iv.
- [2] D. Galmarini, C. M. Galmarini, F. C. Galmarini, *Crit. Rev. Oncol. Hematol.* **2012**, *84*, 181–199.
- [3] W. H. J. Ward, in *Kinase Drug Discovery* (Eds.: R.A. Ward, F.W. Goldberg), RSC Publishing, Cambridge, **2012**, 96–125.
- [4] N. T. Ross, C. J. Wilson, *Front. Pharmacol.* **2014**, *5*, 1–6.
- [5] W. B. Morrison, *J. Vet. Intern. Med.* **2010**, *24*, 1249–1262.
- [6] V. T. DeVita, E. Chu, *Cancer Res.* **2008**, *68*, 8643–8653.
- [7] D. Drygin, M. Haddach, F. Pierre, D. M. Ryckman, *J. Med. Chem.* **2012**, *55*, 8199–8208.
- [8] G. Klebe, *Wirkstoffdesign*, Spektrum Akademischer Verlag, Heidelberg, **2009**.
- [9] L. N. Johnson, R. J. Lewis, *Chem. Rev.* **2001**, *101*, 2209–2242.
- [10] J. A. Adams, *Chem. Rev.* **2001**, *101*, 2271–2290.
- [11] A. F. Wilks, I. Lucet, in *Kinase Drug Discovery* (Eds.: R.A. Ward, F.W. Goldberg), RSC Publishing, Cambridge, **2012**, 262–285.
- [12] M. E. Swarbrick, in *Kinase Drug Discovery* (Eds.: R.A. Ward, F.W. Goldberg), RSC Publishing, Cambridge, **2012**, 79–95.
- [13] O. Fedorov, S. Müller, S. Knapp, *Nat. Chem. Biol.* **2010**, *6*, 166–169.
- [14] D. H. Drewry, P. Bamforth, K. Schneider, G. K. Smith, in *Kinase Drug Discovery* (Eds.: R.A. Ward, F.W. Goldberg), RSC Publishing, Cambridge, **2012**, 1–53.
- [15] J. Cheung, C. Ginter, M. Cassidy, M. C. Franklin, M. J. Rudolph, N. Robine, R. B. Darnell, W. A. Hendrickson, *Proc. Natl. Acad. Sci.* **2015**, *112*, 1374–1379.
- [16] Q. Wang, J. A. Zorn, J. Kuriyan, *Methods Enzymol.* **2014**, *548*, 23–67.
- [17] L. Brault, C. Gasser, F. Bracher, K. Huber, S. Knapp, J. Schwaller, *Haematologica* **2010**, *95*, 1004–1015.
- [18] T. Zhou, L. Commodore, W.-S. Huang, Y. Wang, T. K. Sawyer, W. C. Shakespeare, T. Clackson, X. Zhu, D. C. Dalgarno, *Chem. Biol. Drug Des.* **2010**, *75*, 18–28.
- [19] P. Wu, T. E. Nielsen, M. H. Clausen, *Trends Pharmacol. Sci.* **2015**, *36*, 422–439.

Bibliography

- [20] I. Simpson, R. A. Ward, in *Kinase Drug Discovery* (Eds.: R.A. Ward, F.W. Goldberg), RSC Publishing, Cambridge, **2012**, 54–78.
- [21] P. Cohen, *Nat. Rev. Drug Discov.* **2002**, *1*, 309–315.
- [22] A. J. Ratcliffe, in *Kinase Drug Discovery* (Eds.: R.A. Ward, F.W. Goldberg), RSC Publishing, Cambridge, **2012**, 218–243.
- [23] A. Cai, L. Li, Y. Zhou, *J. Hypertens.* **2016**, *34*, 3–10.
- [24] K. Yamaoka, *Curr. Opin. Chem. Biol.* **2016**, *32*, 29–33.
- [25] R. Yarza, S. Vela, M. Solas, M. J. Ramirez, *Front. Pharmacol.* **2015**, *6*, 321.
- [26] P. Wu, T. E. Nielsen, M. H. Clausen, *Drug Discov. Today* **2016**, *21*, 5–10.
- [27] J. A. Bikker, in *Kinase Drug Discovery* (Eds.: R.A. Ward, F.W. Goldberg), RSC Publishing, Cambridge, **2012**, 126–160.
- [28] R. Roskoski Jr., “USFDA approved protein kinase inhibitors,” can be found under <http://www.brimr.org/PKI/PKIs.htm>, **2016**.
- [29] M. Rask-Andersen, J. Zhang, D. Fabbro, H. B. Schiöth, *Trends Pharmacol. Sci.* **2014**, *35*, 604–620.
- [30] M. A. Fabian, W. H. Biggs, D. K. Treiber, C. E. Atteridge, M. D. Azimioara, M. G. Benedetti, T. A. Carter, P. Ciceri, P. T. Edeen, M. Floyd, J. M. Ford, M. Galvin, J. L. Gerlach, R. M. Grotzfeld, S. Herrgard, D. E. Insko, M. A. Insko, A. G. Lai, J.-M. Lélias, S. A. Mehta, Z. V. Milanov, A. M. Velasco, L. M. Wodicka, H. K Patel, P. P. Zarrinkar, D. J. Lockhart, *Nat. Biotechnol.* **2005**, *23*, 329–336.
- [31] S. J. Lee, B.-G. Han, J.-W. Cho, J.-S. Choi, J. Lee, H.-J. Song, J. S. Koh, B. Il Lee, *PLoS One* **2013**, *8*, e70358.
- [32] C. J. Saris, J. Domen, A. Berns, *EMBO J.* **1991**, *10*, 655–664.
- [33] H. Theo Cuypers, G. Selten, W. Quint, M. Zijlstra, E. R. Maandag, W. Boelens, P. van Wezenbeek, C. Melief, A. Berns, *Cell* **1984**, *37*, 141–150.
- [34] D. Wingett, R. Reeves, N. S. Magnuson, *Nucleic Acids Res.* **1992**, *20*, 3183–3189.
- [35] D. S. Hoover, D. G. Wingett, J. Zhang, R. Reeves, N. S. Magnuson, *Cell Growth Differ.* **1997**, *8*, 1371–1380.
- [36] N. S. Magnuson, Z. Wang, G. Ding, R. Reeves, *Future Oncol.* **2010**, *6*, 1461–1478.

- [37] N. A. Keane, M. Reidy, A. Natoni, M. S. Raab, M. O'Dwyer, *Blood Cancer J.* **2015**, *5*, e325.
- [38] K. Petersen Shay, *Mol. Cancer Res.* **2005**, *3*, 170–181.
- [39] Y. Tursynbay, J. Zhang, Z. Li, T. Tokay, Z. Zhumadilov, D. Wu, Y. Xie, *Biomed. Reports* **2016**, *4*, 140–146.
- [40] R. Amson, F. Sigaux, S. Przedborski, G. Flandrin, D. Givol, A. Telerman, *Proc. Natl. Acad. Sci.* **1989**, *86*, 8857–8861.
- [41] X. F. Hu, J. Li, S. Vandervalk, Z. Wang, N. S. Magnuson, P. X. Xing, *J. Clin. Invest.* **2009**, *119*, 362–375.
- [42] Y. Xie, S. Bayakhmetov, *Mol. Clin. Oncol.* **2016**, *4*, 13–17.
- [43] P. W. Laird, N. M. van der Lugt, A. Clarke, J. Domen, K. Linders, J. McWhir, A. Berns, M. Hooper, *Nucleic Acids Res.* **1993**, *21*, 4750–4755.
- [44] J. Li, X. F. Hu, B. E. Loveland, P. X. Xing, *Exp. Hematol.* **2009**, *37*, 1284–1294.
- [45] K. Saurabh, M. T. Scherzer, P. P. Shah, A. S. Mims, W. W. Lockwood, A. S. Kraft, L. J. Beverly, *Oncotarget* **2014**, *5*, 8503–8514.
- [46] J. Wang, J. Kim, M. Roh, O. E. Franco, S. W. Hayward, M. L. Wills, S. A. Abdulkadir, *Oncogene* **2010**, *29*, 2477–2487.
- [47] M. D. Jacobs, J. Black, O. Futer, L. Swenson, B. Hare, M. Fleming, K. Saxena, *J. Biol. Chem.* **2005**, *280*, 13728–13734.
- [48] J. É. Debreczeni, A. N. Bullock, G. E. Atilla, D. S. Williams, H. Bregman, S. Knapp, E. Meggers, *Angew. Chemie Int. Ed.* **2006**, *45*, 1580–1585.
- [49] H. Bregman, E. Meggers, *Org. Lett.* **2006**, *8*, 5465–5468.
- [50] A. N. Bullock, J. E. Debreczeni, O. Y. Fedorov, A. Nelson, B. D. Marsden, S. Knapp, *J. Med. Chem.* **2005**, *48*, 7604–7614.
- [51] V. Pogacic, A. N. Bullock, O. Fedorov, P. Filippakopoulos, C. Gasser, A. Biondi, S. Meyer-Monard, S. Knapp, J. Schwaller, *Cancer Res.* **2007**, *67*, 6916–6924.
- [52] I. W. Cheney, S. Yan, T. Appleby, H. Walker, T. Vo, N. Yao, R. Hamatake, Z. Hong, J. Z. Wu, *Bioorg. Med. Chem. Lett.* **2007**, *17*, 1679–1683.
- [53] S. Holder, M. Lilly, M. L. Brown, *Bioorg. Med. Chem.* **2007**, *15*, 6463–6473.

- [54] S. Holder, M. Zemskova, C. Zhang, M. Tabrizizad, R. Bremer, J. W. Neidigh, M. B. Lilly, *Mol. Cancer Ther.* **2007**, *6*, 163–72.
- [55] A. C. Pierce, M. Jacobs, C. Stuver-Moody, *J. Med. Chem.* **2008**, *51*, 1972–1975.
- [56] Y. Tong, K. D. Stewart, S. Thomas, M. Przytulinska, E. F. Johnson, V. Klinghofer, J. Leverson, O. McCall, N. B. Soni, Y. Luo, N. Lin, T. J. Sowin, V. L. Giranda, T. D. Penning, *Bioorg. Med. Chem. Lett.* **2008**, *18*, 5206–5208.
- [57] Z. Xia, C. Knaak, J. Ma, Z. M. Beharry, C. McInnes, W. Wang, A. S. Kraft, C. D. Smith, *J. Med. Chem.* **2009**, *52*, 74–86.
- [58] K. Qian, L. Wang, C. L. Cywin, B. T. Farmer, E. Hickey, C. Homon, S. Jakes, M. A. Kashem, G. Lee, S. Leonard, J. Li, R. Magboo, W. Mao, E. Pack, C. Peng, A. Prokopowicz, M. Welzel, J. Wolak, T. Morwick, *J. Med. Chem.* **2009**, *52*, 1814–1827.
- [59] Z.-F. Tao, L. A. Hasvold, J. D. Leverson, E. K. Han, R. Guan, E. F. Johnson, V. S. Stoll, K. D. Stewart, G. Stamper, N. Soni, J. J. Bouska, Y. Luo, T. J. Sowin, N.-H. Lin, V. S. Giranda, S. H. Rosenberg, T. D. Penning, *J. Med. Chem.* **2009**, *52*, 6621–6636.
- [60] X. Wang, S. Magnuson, R. Pastor, E. Fan, H. Hu, V. Tsui, W. Deng, J. Murray, M. Steffek, H. Wallweber, J. Moffat, J. Drummond, G. Chan, E. Harstad, A. J. Ebens, *Bioorg. Med. Chem. Lett.* **2013**, *23*, 3149–3153.
- [61] M. T. Burger, W. Han, J. Lan, G. Nishiguchi, C. Bellamacina, M. Lindval, G. Atallah, Y. Ding, M. Mathur, C. McBride, E. L. Beans, K. Muller, V. Tamez, Y. Zhang, K. Huh, P. Feucht, T. Zavorotinskaya, Y. Dai, J. Holash, J. Castillo, J. Langowski, Y. Wang, M. Y. Chen, P. D. Garcia, *ACS Med. Chem. Lett.* **2013**, *4*, 1193–1197.
- [62] J. Cortes, K. Tamura, D. J. DeAngelo, J. de Bono, D. Lorente, M. Minden, G. L. Uy, H. Kantarjian, K. Keating, K. McEachern, K. Vishwanathan, R. E. Godin, J. E. Pease, E. Dean, *Cancer Res.* **2016**, *76*, CT147-CT147.
- [63] H. Koblish, N. Shin, L. Hall, S. O'Connor, Q. Wang, K. Wang, L. Leffet, M. Covington, K. Burke, J. Boer, K. Bowman, K. Zhang, H. Feng, C.-B. Xue, Y.-L. Li, W. Yao, R. Huber, K. Vaddi, P. Scherle, *Cancer Res.* **2015**, *75*, 5416–5416.
- [64] N. Shin, M. Covington, R. Wynn, Y. Li, A. Margulis, Q. Wang, K. Wang, C. Marando, P. Feldman, L. Leffet, K. Gallagher, X. He, H. Chang, H. Zhang, H. Feng, Y.-L. Li, C.-B. Xue, W. Yao, T. Burn, K. Vaddi, S. Diamond-Fosbenner, S. Yeleswaram, G. Hollis, R. Newton, R. Huber, P. Scherle, H. Koblish, *Cancer Res.* **2015**, *75*, 5397–5397.

- [65] “ClinicalTrials.gov database,” can be found under <https://clinicaltrials.gov>, **2016**.
- [66] O. A. Botrugno, F. Santoro, S. Minucci, *Cancer Lett.* **2009**, *280*, 134–144.
- [67] A. V. Bieliauskas, M. K. H. Pflum, *Chem. Soc. Rev.* **2008**, *37*, 1402–1413.
- [68] A. J. M. de Ruijter, A. H. van Gennip, H. N. Caron, S. Kemp, A. B. P. van Kuilenburg, *Biochem. J.* **2003**, *370*, 737–749.
- [69] F. Thaler, C. Mercurio, *ChemMedChem* **2014**, *9*, 523–526.
- [70] K. J. Falkenberg, R. W. Johnstone, *Nat. Rev. Drug Discov.* **2014**, *13*, 673–691.
- [71] A. Abend, I. Kehat, *Pharmacol. Ther.* **2015**, *147*, 55–62.
- [72] C. Choudhary, C. Kumar, F. Gnad, M. L. Nielsen, M. Rehman, T. C. Walther, J. V Olsen, M. Mann, *Science* **2009**, *325*, 834–840.
- [73] S. Schäfer, M. Jung, *Arch. Pharm.* **2005**, *338*, 347–357.
- [74] I. V Gregoretti, Y.-M. Lee, H. V Goodson, *J. Mol. Biol.* **2004**, *338*, 17–31.
- [75] J. Zhang, Q. Zhong, *Cell. Mol. Life Sci.* **2014**, *71*, 3885–3901.
- [76] P. Bertrand, *Eur. J. Med. Chem.* **2010**, *45*, 2095–2116.
- [77] Y. Luo, W. Jian, D. Stavreva, X. Fu, G. Hager, J. Bungert, S. Huang, Y. Qiu, *J. Biol. Chem.* **2009**, *284*, 34901–34910.
- [78] J. J. Buggy, M. L. Sideris, P. Mak, D. D. Lorimer, B. McIntosh, J. M. Clark, *Biochem. J.* **2000**, *350*, 199–205.
- [79] E. Verdin, F. Dequiedt, H. G. Kasler, *Trends Genet.* **2003**, *19*, 286–293.
- [80] A. C. West, R. W. Johnstone, *J. Clin. Invest.* **2014**, *124*, 30–39.
- [81] W. Fischle, F. Dequiedt, M. J. Hendzel, M. G. Guenther, M. A. Lazar, W. Voelter, E. Verdin, *Mol. Cell* **2002**, *9*, 45–57.
- [82] M. Mottamal, S. Zheng, T. L. Huang, G. Wang, *Molecules* **2015**, *20*, 3898–3941.
- [83] A. Schuetz, J. Min, A. Allali-Hassani, M. Schapira, M. Shuen, P. Loppnau, R. Mazitschek, N. P. Kwiatkowski, T. A. Lewis, R. L. Maglathin, T. H. McLean, A. Bochkarev, A. N. Plotnikov, M. Vedadi, C. H. Arrowsmith, *J. Biol. Chem.* **2008**, *283*, 11355–11363.
- [84] A. J. Frew, R. W. Johnstone, J. E. Bolden, *Cancer Lett.* **2009**, *280*, 125–133.

Bibliography

- [85] M. Dickinson, R. W. Johnstone, H. M. Prince, *Invest. New Drugs* **2010**, *28*, 3–20.
- [86] S. Spange, T. Wagner, T. Heinzel, O. H. Krämer, *Int. J. Biochem. Cell Biol.* **2009**, *41*, 185–198.
- [87] D. J. P. Ellis, Z. K. Lawman, K. Bonham, *Biochem. Biophys. Res. Commun.* **2008**, *367*, 656–662.
- [88] F. Thaler, *Pharm. Pat. Anal.* **2012**, *1*, 75–90.
- [89] T. Watanabe, *Expert Opin. Investig. Drugs* **2010**, *19*, 1113–1127.
- [90] K. P. Garnock-Jones, *Drugs* **2015**, *75*, 695–704.
- [91] P. Gupta, R. C. Reid, A. Iyer, M. J. Sweet, D. P. Fairlie, *Curr. Top. Med. Chem.* **2012**, *12*, 1479–1499.
- [92] C. M. Salisbury, B. F. Cravatt, *Proc. Natl. Acad. Sci.* **2007**, *104*, 1171–1176.
- [93] P. Tessier, D. V Smil, A. Wahhab, S. Leit, J. Rahil, Z. Li, R. Déziel, J. M. Besterman, *Bioorg. Med. Chem. Lett.* **2009**, *19*, 5684–5688.
- [94] P. Bose, Y. Dai, S. Grant, *Pharmacol. Ther.* **2014**, *143*, 323–336.
- [95] H. V. K. Diyabalanage, M. L. Granda, J. M. Hooker, *Cancer Lett.* **2013**, *329*, 1–8.
- [96] K. T. Thurn, S. Thomas, A. Moore, P. N. Munster, *Future Oncol.* **2011**, *7*, 263–283.
- [97] M. Bots, R. W. Johnstone, *Clin. Cancer Res.* **2009**, *15*, 3970–3977.
- [98] S. Grant, Y. Dai, *Adv. Cancer Res.* **2012**, *116*, 199–237.
- [99] B. Groselj, N. L. Sharma, F. C. Hamdy, M. Kerr, A. E. Kiltie, *Br. J. Cancer* **2013**, *108*, 748–754.
- [100] G. P. Delcuve, D. H. Khan, J. R. Davie, *Expert Opin. Ther. Targets* **2013**, *17*, 29–41.
- [101] K. H. Thompson, C. Orvig, *Science* **2003**, *300*, 936–939.
- [102] M. Gielen, E. R. T. Tiekkink, *Metallotherapeutic Drugs and Metal-Based Diagnostic Agents*, John Wiley & Sons, Ltd, Chichester, UK, **2005**.
- [103] B. Desoize, *Anticancer Res.* **2004**, *24*, 1529–1544.
- [104] R. A. Alderden, M. D. Hall, T. W. Hambley, *J. Chem. Educ.* **2006**, *83*, 728–734.
- [105] I. Ott, R. Gust, *Arch. Pharm.* **2007**, *340*, 117–126.
- [106] H.-J. Zhong, K.-H. Leung, L.-J. Liu, L. Lu, D. S.-H. Chan, C.-H. Leung, D.-L. Ma, *ChemPlusChem* **2014**, *79*, 508–511.

- [107] P. Sharma, D. Perez, A. Cabrera, N. Rosas, J. L. Arias, *Acta Pharmacol. Sin.* **2008**, *29*, 881–890.
- [108] S. Page, *Educ. Chem.* **2012**, 26–29.
- [109] E. Meggers, G. Atilla-Gokcumen, H. Bregman, J. Maksimoska, S. Mulcahy, N. Pagano, D. Williams, *Synlett* **2007**, *2007*, 1177–1189.
- [110] E. Meggers, *Chem. Commun.* **2009**, 1001–1010.
- [111] E. A. Hillard, G. Jaouen, *Organometallics* **2011**, *30*, 20–27.
- [112] L. Salassa, *Eur. J. Inorg. Chem.* **2011**, *2011*, 4931–4947.
- [113] M. Patra, G. Gasser, *ChemBioChem* **2012**, *13*, 1232–1252.
- [114] N. L. Kilah, E. Meggers, *Aust. J. Chem.* **2012**, *65*, 1325–1332.
- [115] K. J. Kilpin, P. J. Dyson, *Chem. Sci.* **2013**, *4*, 1410–1419.
- [116] A. de Almeida, B. L. Oliveira, J. D. G. Correia, G. Soveral, A. Casini, *Coord. Chem. Rev.* **2013**, *257*, 2689–2704.
- [117] N. P. E. Barry, P. J. Sadler, *Chem. Commun.* **2013**, *49*, 5106–5131.
- [118] M. Dörr, E. Meggers, *Curr. Opin. Chem. Biol.* **2014**, *19*, 76–81.
- [119] L. Zhang, P. Carroll, E. Meggers, *Org. Lett.* **2004**, *6*, 521–523.
- [120] L. Feng, Y. Geisselbrecht, S. Blanck, A. Wilbuer, G. E. Atilla-Gokcumen, P. Filippakopoulos, K. Kräling, M. A. Celik, K. Harms, J. Maksimoska, R. Marmorstein, G. Frenking, S. Knapp, L.-O. Essen, E. Meggers, *J. Am. Chem. Soc.* **2011**, *133*, 5976–5986.
- [121] G. E. Atilla-Gokcumen, D. S. Williams, H. Bregman, N. Pagano, E. Meggers, *ChemBioChem* **2006**, *7*, 1443–1450.
- [122] N. Pagano, J. Maksimoska, H. Bregman, D. S. Williams, R. D. Webster, F. Xue, E. Meggers, *Org. Biomol. Chem.* **2007**, *5*, 1218–1227.
- [123] A. J. Salmon, M. L. Williams, A. Innocenti, D. Vullo, C. T. Supuran, S.-A. Poulsen, *Bioorg. Med. Chem. Lett.* **2007**, *17*, 5032–5035.
- [124] B. T. Loughrey, M. L. Williams, P. C. Healy, A. Innocenti, D. Vullo, C. T. Supuran, P. G. Parsons, S.-A. Poulsen, *J. Biol. Inorg. Chem.* **2009**, *14*, 935–945.
- [125] A. J. Salmon, M. L. Williams, Q. K. Wu, J. Morizzi, D. Gregg, S. A. Charman, D. Vullo, C.

- T. Supuran, S.-A. Poulsen, *J. Med. Chem.* **2012**, *55*, 5506–5517.
- [126] A. J. Salmon, M. L. Williams, A. Hofmann, S.-A. Poulsen, *Chem. Commun.* **2012**, *48*, 2328–2330.
- [127] J. Spencer, J. Amin, P. Coxhead, J. McGeehan, C. J. Richards, G. J. Tizzard, S. J. Coles, J. P. Bingham, J. A. Hartley, L. Feng, E. Meggers, M. Guille, *Organometallics* **2011**, *30*, 3177–3181.
- [128] O. Payen, S. Top, A. Vessières, E. Brulé, A. Lauzier, M.-A. Plumont, M. J. McGlinchey, H. Müller-Bunz, G. Jaouen, *J. Organomet. Chem.* **2011**, *696*, 1049–1056.
- [129] M. Patra, G. Gasser, M. Wenzel, K. Merz, J. E. Bandow, N. Metzler-Nolte, *Eur. J. Inorg. Chem.* **2011**, *2011*, 3295–3302.
- [130] M. Patra, G. Gasser, A. Pinto, K. Merz, I. Ott, J. E. Bandow, N. Metzler-Nolte, *ChemMedChem* **2009**, *4*, 1930–1938.
- [131] H. Bielig, J. Velder, A. Saiai, M. Menning, S. Meemboor, W. Kalka-Moll, M. Krönke, H.-G. Schmalz, T. A. Kufer, *ChemMedChem* **2010**, *5*, 2065–2071.
- [132] D. Can, B. Spingler, P. Schmutz, F. Mendes, P. Raposinho, C. Fernandes, F. Carta, A. Innocenti, I. Santos, C. T. Supuran, R. Alberto, *Angew. Chemie* **2012**, *124*, 3410–3413.
- [133] S. Sulieman, D. Can, J. Mertens, H. W. P. N'Dongo, Y. Liu, P. Schmutz, M. Bauwens, B. Spingler, R. Alberto, *Organometallics* **2012**, *31*, 6880–6886.
- [134] F. W. Monnard, T. Heinisch, E. S. Nogueira, T. Schirmer, T. R. Ward, *Chem. Commun.* **2011**, *47*, 8238–8240.
- [135] J. X. Ong, C. W. Yap, W. H. Ang, *Inorg. Chem.* **2012**, *51*, 12483–12492.
- [136] P. Paira, M. J. Chow, G. Venkatesan, V. K. Kosaraju, S. L. Cheong, K.-N. Klotz, W. H. Ang, G. Pastorin, *Chemistry* **2013**, *19*, 8321–8330.
- [137] M. Streib, K. Kräling, K. Richter, X. Xie, H. Steuber, E. Meggers, *Angew. Chemie Int. Ed.* **2014**, *53*, 305–309.
- [138] D.-L. Ma, D. S.-H. Chan, C.-H. Leung, *Acc. Chem. Res.* **2014**, *47*, 3614–3631.
- [139] E. S. Child, S. N. Georgiades, K. N. Rose, V. S. Stafford, C. B. K. Patel, J. H. G. Steinke, D. J. Mann, R. Vilar, *J. Chem. Biol.* **2011**, *4*, 159–165.
- [140] Y. Wei, D. C. Poon, R. Fei, A. S. M. Lam, S. C. F. Au-Yeung, K. K. W. To, *Sci. Rep.* **2016**, *6*, 25363.

- [141] L. Szűčová, Z. Trávníček, M. Zatloukal, I. Popa, *Bioorg. Med. Chem.* **2006**, *14*, 479–491.
- [142] S. Harmsen, M. E. M. Dolman, Z. Nemes, M. Lacombe, B. Szokol, J. Pato, G. Kéri, L. Orlfi, G. Storm, W. E. Hennink, R. J. Kok, *Bioconjug. Chem.* **2011**, *22*, 540–545.
- [143] R. Kok, K. Temming, M. Fretz, *Curr. Mol. Pharmacol.* **2008**, *1*, 1–12.
- [144] J. Spencer, J. Amin, S. K. Callear, G. J. Tizzard, S. J. Coles, P. Coxhead, M. Guille, *Met. Integr. biometal Sci.* **2011**, *3*, 600–608.
- [145] J. Amin, I. Chuckowree, G. J. Tizzard, S. J. Coles, M. Wang, J. P. Bingham, J. A. Hartley, J. Spencer, *Organometallics* **2013**, *32*, 509–513.
- [146] C.-H. Leung, H. Yang, V. P.-Y. Ma, D. S.-H. Chan, H.-J. Zhong, Y.-W. Li, W.-F. Fong, D.-L. Ma, *Med. Chem. Commun.* **2012**, *3*, 696–698.
- [147] H. Bregman, D. S. Williams, G. E. Atilla, P. J. Carroll, E. Meggers, *J. Am. Chem. Soc.* **2004**, *126*, 13594–13595.
- [148] H. Bregman, D. S. Williams, E. Meggers, *Synthesis* **2005**, 1521–1527.
- [149] D. S. Williams, G. E. Atilla, H. Bregman, A. Arzoumanian, P. S. Klein, E. Meggers, *Angew. Chemie Int. Ed.* **2005**, *44*, 1984–1987.
- [150] H. Bregman, P. J. Carroll, E. Meggers, *J. Am. Chem. Soc.* **2006**, *128*, 877–884.
- [151] K. S. M. Smalley, R. Contractor, N. K. Haass, A. N. Kulp, G. E. Atilla-Gokcumen, D. S. Williams, H. Bregman, K. T. Flaherty, M. S. Soengas, E. Meggers, M. Herlyn, *Cancer Res.* **2007**, *67*, 209–217.
- [152] J. Maksimoska, D. S. Williams, G. E. Atilla-Gokcumen, K. S. M. Smalley, P. J. Carroll, R. D. Webster, P. Filippakopoulos, S. Knapp, M. Herlyn, E. Meggers, *Chemistry* **2008**, *14*, 4816–4822.
- [153] J. Maksimoska, L. Feng, K. Harms, C. Yi, J. Kissil, R. Marmorstein, E. Meggers, *J. Am. Chem. Soc.* **2008**, *130*, 15764–15765.
- [154] G. E. Atilla-Gokcumen, N. Pagano, C. Streu, J. Maksimoska, P. Filippakopoulos, S. Knapp, E. Meggers, *ChemBioChem* **2008**, *9*, 2933–2936.
- [155] A. N. Bullock, S. Russo, A. Amos, N. Pagano, H. Bregman, J. É. Debreczeni, W. H. Lee, F. von Delft, E. Meggers, S. Knapp, *PLoS One* **2009**, *4*, e7112.
- [156] P. Xie, C. Streu, J. Qin, H. Bregman, N. Pagano, E. Meggers, R. Marmorstein, *Biochemistry*

Bibliography

- 2009, 48, 5187–5198.
- [157] G. E. Atilla-Gokcumen, L. Di Costanzo, E. Meggers, *J. Biol. Inorg. Chem.* **2011**, 16, 45–50.
- [158] S. Blanck, J. Maksimoska, J. Baumeister, K. Harms, R. Marmorstein, E. Meggers, *Angew. Chemie Int. Ed.* **2012**, 51, 5244–5246.
- [159] S. P. Mulcahy, P. J. Carroll, E. Meggers, *Tetrahedron Lett.* **2006**, 47, 8877–8880.
- [160] N. Pagano, E. Y. Wong, T. Breiding, H. Liu, A. Wilbuer, H. Bregman, Q. Shen, S. L. Diamond, E. Meggers, *J. Org. Chem.* **2009**, 74, 8997–9009.
- [161] C. Streu, L. Feng, P. J. Carroll, J. Maksimoska, R. Marmorstein, E. Meggers, *Inorganica Chim. Acta* **2011**, 377, 34–41.
- [162] E. Meggers, G. E. Atilla-Gokcumen, K. Gründler, C. Frias, A. Prokop, *Dalt. Trans.* **2009**, 10882–10888.
- [163] R. Anand, J. Maksimoska, N. Pagano, E. Y. Wong, P. a Gimotty, S. L. Diamond, E. Meggers, R. Marmorstein, *J. Med. Chem.* **2009**, 52, 1602–1611.
- [164] A. Wilbuer, D. H. Vlecken, D. J. Schmitz, K. Kräling, K. Harms, C. P. Bagowski, E. Meggers, *Angew. Chemie* **2010**, 122, 3928–3932.
- [165] A. Kastl, A. Wilbuer, A. L. Merkel, L. Feng, P. Di Fazio, M. Ocker, E. Meggers, *Chem. Commun.* **2012**, 48, 1863–1865.
- [166] J. K. John, K. H. T. Paraiso, V. W. Rebecca, L. P. Cantini, E. V Abel, N. Pagano, E. Meggers, R. Mathew, C. Krepler, V. Izumi, B. Fang, J. M. Koomen, J. L. Messina, M. Herlyn, K. S. M. Smalley, *J. Invest. Dermatol.* **2012**, 132, 2818–2827.
- [167] H. Chen, J. A. Parkinson, O. Novakova, J. Bella, F. Wang, A. Dawson, R. Gould, S. Parsons, V. Brabec, P. J. Sadler, *Proc. Natl. Acad. Sci.* **2003**, 100, 14623–14628.
- [168] S. Dieckmann, R. Riedel, K. Harms, E. Meggers, *Eur. J. Inorg. Chem.* **2012**, 2012, 813–821.
- [169] K. Wähler, A. Ludewig, P. Szabo, K. Harms, E. Meggers, *Eur. J. Inorg. Chem.* **2014**, 2014, 807–811.
- [170] D. S. Williams, P. J. Carroll, E. Meggers, *Inorg. Chem.* **2007**, 46, 2944–2946.
- [171] A. Wilbuer, D. H. Vlecken, D. J. Schmitz, K. Kräling, K. Harms, C. P. Bagowski, E. Meggers, *Angew. Chemie Int. Ed.* **2010**, 49, 3839–3842.
- [172] V. Brabec, D. M. Griffith, A. Kisova, H. Kostrhunova, L. Zerzankova, C. J. Marmion, J. 256

Kasparkova, *Mol. Pharm.* **2012**, *9*, 1990–1999.

- [173] J. P. Parker, H. Nimir, D. M. Griffith, B. Duff, A. J. Chubb, M. P. Brennan, M. P. Morgan, D. A. Egan, C. J. Marmion, *J. Inorg. Biochem.* **2013**, *124*, 70–77.
- [174] D. Griffith, M. P. Morgan, C. J. Marmion, *Chem. Commun.* **2009**, 6735–6737.
- [175] D. M. Griffith, B. Duff, K. Y. Suponitsky, K. Kavanagh, M. P. Morgan, D. Egan, C. J. Marmion, *J. Inorg. Biochem.* **2011**, *105*, 793–799.
- [176] J. Yang, X. Sun, W. Mao, M. Sui, J. Tang, Y. Shen, *Mol. Pharm.* **2012**, *9*, 2793–2800.
- [177] M. Alessio, I. Zanellato, I. Bonarrigo, E. Gabano, M. Ravera, D. Osella, *J. Inorg. Biochem.* **2013**, *129*, 52–57.
- [178] V. Novohradsky, L. Zerzankova, J. Stepankova, O. Vrana, R. Raveendran, D. Gibson, J. Kasparkova, V. Brabec, *Biochem. Pharmacol.* **2015**, *95*, 133–144.
- [179] J. Spencer, J. Amin, M. Wang, G. Packham, S. S. S. Alwi, G. J. Tizzard, S. J. Coles, R. M. Paranal, J. E. Bradner, T. D. Heightman, *ACS Med. Chem. Lett.* **2011**, *2*, 358–362.
- [180] J. Spencer, J. Amin, R. Boddiboyena, G. Packham, B. E. Cavell, S. S. Syed Alwi, R. M. Paranal, T. D. Heightman, M. Wang, B. Marsden, P. Coxhead, M. Guille, G. J. Tizzard, S. J. Coles, J. E. Bradner, *Med. Chem. Commun.* **2012**, *3*, 61–64.
- [181] R.-R. Ye, C.-P. Tan, Y.-N. Lin, L.-N. Ji, Z.-W. Mao, *Chem. Commun.* **2015**, *51*, 8353–8356.
- [182] R.-R. Ye, Z.-F. Ke, C.-P. Tan, L. He, L.-N. Ji, Z.-W. Mao, *Chemistry* **2013**, *19*, 10160–9.
- [183] R.-R. Ye, C.-P. Tan, L. He, M.-H. Chen, L.-N. Ji, Z.-W. Mao, *Chem. Commun.* **2014**, *50*, 10945–10948.
- [184] K. H.-M. Chow, R. W.-Y. Sun, J. B. B. Lam, C. K.-L. Li, A. Xu, D.-L. Ma, R. Abagyan, Y. Wang, C.-M. Che, *Cancer Res.* **2009**, *70*, 329–337.
- [185] C. M. Che, Y. Wang, R. W. Y. Sun, K. H.-M. Chow, *Hydroxy-Substituted gold(III) Porphyrin Complexes as Histone Deacetylase Inhibitors*, **2013**, US8563712 B2.
- [186] K. Bishayee, A. R. Khuda-Bukhsh, S.-O. Huh, *Mol. Cells* **2015**, *38*, 518–527.
- [187] P. Fonteh, D. Meyer, *BMC Infect. Dis.* **2014**, *14*, 680.
- [188] M. Suggitt, M. C. Bibby, *Clin. Cancer Res.* **2005**, *11*, 971–981.
- [189] A. S. Narang, D. S. Desai, *Pharmaceutical Perspectives of Cancer Therapeutics*, Springer US, New

York, NY, **2009**.

- [190] A. A. Nazarov, C. G. Hartinger, P. J. Dyson, *J. Organomet. Chem.* **2014**, *751*, 251–260.
- [191] N. Muhammad, Z. Guo, *Curr. Opin. Chem. Biol.* **2014**, *19C*, 144–153.
- [192] S. M. Schmitt, M. Frezza, Q. P. Dou, *Front. Biosci. (Schol. Ed.)* **2012**, *4*, 375–391.
- [193] A. Bergamo, C. Gaiddon, J. H. M. Schellens, J. H. Beijnen, G. Sava, *J. Inorg. Biochem.* **2012**, *106*, 90–99.
- [194] C. G. Hartinger, N. Metzler-Nolte, P. J. Dyson, *Organometallics* **2012**, *31*, 5677–5685.
- [195] A. L. Noffke, A. Habtemariam, A. M. Pizarro, P. J. Sadler, *Chem. Commun.* **2012**, *48*, 5219–5246.
- [196] W. H. Ang, A. Casini, G. Sava, P. J. Dyson, *J. Organomet. Chem.* **2011**, *696*, 989–998.
- [197] G. S. Smith, B. Therrien, *Dalton Trans.* **2011**, *40*, 10793–10800.
- [198] E. S. Antonarakis, A. Emadi, *Cancer Chemother. Pharmacol.* **2010**, *66*, 1–9.
- [199] K. R. Lawson, J. Lawson, *J. Cheminform.* **2012**, *4*, 1–7.
- [200] “ChemAxon Academic License,” can be found under <https://www.chemaxon.com/my-chemaxon/my-academic-license/>, **2016**.
- [201] T. Mosmann, *J. Immunol. Methods* **1983**, *65*, 55–63.
- [202] N. Pagano, Ruthenium Half-Sandwich Complexes as Protein Kinase Inhibitors, University of Pennsylvania, **2009**.
- [203] Y. Matsushima, N. Komatsuzaki, Y. Ajioka, M. Yamamoto, H. Kikuchi, Y. Takata, N. Dodo, K. Onitsuka, M. Uno, S. Takahashi, *Bull. Chem. Soc. Jpn.* **2001**, *74*, 527–537.
- [204] H. Bregman, The Synthesis and Evaluation of Protein Kinase Inhibitors, University of Pennsylvania, **2007**.
- [205] W. Herz, O. F. Izulenes, *J. Am. Chem. Soc.* **1956**, *78*, 1485–1494.
- [206] E. J. Corey, B. W. Erickson, *J. Org. Chem.* **1974**, *39*, 821–825.
- [207] S. Bittner, M. Gorodetsky, I. Har-Paz, Y. Mizrahi, A. E. Richmond, *Phytochemistry* **1977**, *16*, 1143–1151.
- [208] R. K. Howe, *J. Am. Chem. Soc.* **1971**, *93*, 3457–3462.

- [209] M. Hatanaka, Y. Himeda, I. Ueda, *J. Chem. Soc., Chem. Commun.* **1990**, 526–527.
- [210] M. Hatanaka, Y. Himeda, I. Ueda, *J. Chem. Soc. Perkin Trans. 1* **1993**, 2269–2274.
- [211] M. A. Bennett, A. K. Smith, *J. Chem. Soc. Dalton Trans.* **1974**, 233–241.
- [212] T. P. Gill, K. R. Mann, *Organometallics* **1982**, *1*, 485–488.
- [213] E. K. Martin, N. Pagano, M. E. Sherlock, K. Harms, E. Meggers, *Inorganica Chim. Acta* **2014**, *423*, 530–539.
- [214] *SADABS 2012/1 Bruker AXS Inc.*, Madison, Wisconsin, USA, **2012**.
- [215] G. M. Sheldrick, *Acta Crystallogr. A* **2008**, *64*, 112–122.
- [216] E. R. Fischer, B. T. Hansen, V. Nair, F. H. Hoyt, D. W. Dorward, *Curr. Protoc. Microbiol.* **2012**, Chapter 2, Unit 2B.2.
- [217] J. Baik, G. R. Rosania, *PLoS One* **2012**, *7*, e47494.
- [218] J. Baik, G. R. Rosania, *Mol. Pharm.* **2011**, *8*, 1742–1749.
- [219] E. H. Kerns, L. Di, in *Drug-like Properties Concepts Structure Design and Methods*, Elsevier Ltd, Oxford, **2008**, 6–16.
- [220] C. A. Lipinski, F. Lombardo, B. W. Dominy, P. J. Feeney, *Adv. Drug Deliv. Rev.* **1997**, *23*, 3–25.
- [221] C. A. Lipinski, *J. Pharmacol. Toxicol. Methods* **2000**, *44*, 235–249.
- [222] J. A. Arnott, S. L. Planey, *Expert Opin. Drug Discov.* **2012**, *7*, 863–875.
- [223] C. A. Lipinski, F. Lombardo, B. W. Dominy, P. J. Feeney, *Adv. Drug Deliv. Rev.* **2001**, *46*, 3–26.
- [224] S. P. Fricker, *Dalt. Trans.* **2007**, 4903–4917.
- [225] B. Faller, J. Wang, A. Zimmerlin, L. Bell, J. Hamon, S. Whitebread, K. Azzaoui, D. Bojanic, L. Urban, *Expert Opin. Drug Metab. Toxicol.* **2006**, *2*, 823–833.
- [226] C. García-Echeverría, in *Kinase Drug Discovery* (Eds.: R.A. Ward, F.W. Goldberg), RSC Publishing, Cambridge, **2012**, 286–302.
- [227] H. Sun, Z.-F. Chai, *Annu. Reports Sect. “A” Inorg. Chem.* **2010**, *106*, 20–38.
- [228] S. Mounicou, J. Szpunar, R. Lobinski, *Chem. Soc. Rev.* **2009**, *38*, 1119–1138.

Bibliography

- [229] M. P. Gleeson, *J. Med. Chem.* **2008**, *51*, 817–834.
- [230] F. Klein, Synthese von Ruthenium-(II)-Komplexen Und Validierung Ihrer in Vitro Anti-Krebs-Eigenschaften an Ausgewählten Krebszelllinien, Philipps-Universität Marburg, **2013**.
- [231] S. M. Weber, In Vitro Untersuchungen Zur Zellviabilität Ausgewählter Krebszelllinien Nach Behandlung Mit Dargestellten Ruthenium(II)-Komplexen Auf Basis Eines Pyridocarbazolliganden., Philipps-Universität Marburg, **2013**.
- [232] E. H. Kerns, L. Di, *Drug-like Properties: Concepts, Structure Design and Methods*, Elsevier, **2008**.
- [233] R. Rajaratnam, E. K. Martin, M. Dörr, K. Harms, A. Casini, E. Meggers, *Inorg. Chem.* **2015**, *54*, 8111–8120.
- [234] K. M. Wähler, Entwicklung Metallorganischer Verbindungen Für Die Verwendung in Der Krebstherapie, Philipps-Universität Marburg, **2014**.
- [235] J. Wang, L. Urban, *Drug Discov. World* **2004**, *5*, 73–86.
- [236] A. Glomme, J. März, J. B. Dressman, *J. Pharm. Sci.* **2005**, *94*, 1–16.
- [237] L. Zhou, L. Yang, S. Tilton, J. Wang, *J. Pharm. Sci.* **2007**, *96*, 3052–3071.
- [238] S. Nakashima, K. Yamamoto, Y. Arai, Y. Ikeda, *Chem. Pharm. Bull.* **2013**, *61*, 1228–1238.
- [239] G. Ottaviani, D. J. Gosling, C. Patissier, S. Rodde, L. Zhou, B. Faller, *Eur. J. Pharm. Sci.* **2010**, *41*, 452–457.
- [240] L. Shargel, S. Wu-Pong, A. B. C. Yu, *Applied Biopharmaceutics & Pharmacokinetics*, McGraw-Hill Education, **2000**.
- [241] W. Klopf, P. Worboys, *Comb. Chem. High Throughput Screen.* **2010**, *13*, 159–169.
- [242] A. K. Mandagere, T. N. Thompson, K.-K. Hwang, *J. Med. Chem.* **2002**, *45*, 304–311.
- [243] Y. Y. Lau, G. Krishna, N. P. Yumibe, D. E. Grotz, E. Sapidou, L. Norton, I. Chu, C. Chen, A. D. Soares, C.-C. Lin, *Pharm. Res.* **2002**, *19*, 1606–1610.
- [244] R. S. Obach, *Drug Metab. Dispos.* **1999**, *27*, 1350–1359.
- [245] R. S. Obach, J. G. Baxter, T. E. Liston, B. M. Silber, B. C. Jones, F. Macintyre, D. J. Rance, P. Wastall, *J. Pharmacol. Exp. Ther.* **1997**, *283*, 46–58.
- [246] L. C. Bell, J. Wang, *Expert Opin. Drug Metab. Toxicol.* **2012**, *8*, 1131–1155.
- [247] F. Wohnsland, B. Faller, *J. Med. Chem.* **2001**, *44*, 923–930.

- [248] A. Avdeef, *Expert Opin. Drug Metab. Toxicol.* **2005**, *1*, 325–342.
- [249] M. Kansy, F. Senner, K. Gubernator, *J. Med. Chem.* **1998**, *41*, 1007–1010.
- [250] E. H. Kerns, L. Di, S. Petusky, M. Farris, R. Ley, P. Jupp, *J. Pharm. Sci.* **2004**, *93*, 1440–1453.
- [251] P. Artursson, J. Karlsson, *Biochem. Biophys. Res. Commun.* **1991**, *175*, 880–885.
- [252] P. Artursson, S. Tavelin, in *Drug Bioavailability: Estimation of Solubility, Permeability, Absorption and Bioavailability* (Eds.: H. van de Waterbeemd, H. Lennernäs, P. Artursson), Wiley-VCH Verlag GmbH & Co. KGaA, Weinheim, FRG, **2003**, 72–89.
- [253] A.-L. Ungell, J. Karlsson, in *Drug Bioavailability: Estimation of Solubility, Permeability, Absorption and Bioavailability* (Eds.: H. van de Waterbeemd, H. Lennernäs, P. Artursson), Wiley-VCH Verlag GmbH & Co. KGaA, Weinheim, FRG, **2003**, 90–131.
- [254] G. Englund, F. Rorsman, A. Rönnblom, U. Karlbom, L. Lazorova, J. Gråsjö, A. Kindmark, P. Artursson, *Eur. J. Pharm. Sci.* **2006**, *29*, 269–277.
- [255] S. W. Smith, *Toxicol. Sci.* **2009**, *110*, 4–30.
- [256] A. Zimmerlin, M. Trunzer, B. Faller, *Drug Metab. Dispos.* **2011**, *39*, 1039–1046.
- [257] S. Skolnik, X. Lin, J. Wang, X.-H. Chen, T. He, B. Zhang, *J. Pharm. Sci.* **2010**, *99*, 3246–3265.
- [258] D. T. Manallack, R. J. Prankerd, E. Yuriev, T. I. Oprea, D. K. Chalmers, *Chem. Soc. Rev.* **2013**, *42*, 485–496.
- [259] P. V Balimane, K. Patel, A. Marino, S. Chong, *Eur. J. Pharm. Biopharm.* **2004**, *58*, 99–105.
- [260] J. W. Polli, S. A. Wring, J. E. Humphreys, L. Huang, J. B. Morgan, L. O. Webster, C. S. Serabjit-Singh, *J. Pharmacol. Exp. Ther.* **2001**, *299*, 620–628.
- [261] P. V Balimane, S. Chong, *Drug Discov. Today* **2005**, *10*, 335–343.
- [262] R. Evers, N. H. Cnubben, J. Wijnholds, L. van Deemter, P. J. van Bladeren, P. Borst, *FEBS Lett.* **1997**, *419*, 112–116.
- [263] F. Tang, K. Horie, R. T. Borchardt, *Pharm. Res.* **n.d.**, *19*, 765–772.
- [264] X. Jin, T.-L. Luong, N. Reese, H. Gaona, V. Collazo-Velez, C. Vuong, B. Potter, J. C. Sousa, R. Olmeda, Q. Li, L. Xie, J. Zhang, P. Zhang, G. Reichard, V. Melendez, S. R. Marcisin, B. S. Pybus, *J. Pharmacol. Toxicol. Methods* **2014**, *70*, 188–194.
- [265] D. Williams, From Ruthenium to Platinum: The Development of Organometallic

- Complexes as Enzyme Inhibitors, University of Pennsylvania, **2008**.
- [266] G. E. Atilla-Gökcümen, Design and Investigation of Bioactive Ruthenium-Based Protein Kinase Inhibitors, University of Pennsylvania, **2008**.
- [267] A. K. Bytzek, C. G. Hartinger, *Electrophoresis* **2012**, *33*, 622–634.
- [268] A. Andersson, A. Lindgren, M. Arnadottir, H. Prytz, B. Hultberg, *Clin. Chem.* **1999**, *45*, 1084–1087.
- [269] “The Human Protein Atlas,” can be found under <http://www.proteinatlas.org/>, **2016**.
- [270] W. M. Lee, *N. Engl. J. Med.* **2003**, *349*, 474–485.
- [271] A. R. Parrish, A. J. Gandolfi, K. Brendel, *Life Sci.* **1995**, *57*, 1887–1901.
- [272] P. Olinga, D. K. F. Meijer, M. J. H. Slooff, G. M. M. Groothuis, *Toxicol. Vitr.* **1997**, *12*, 77–100.
- [273] A. E. M. Vickers, R. L. Fisher, *Expert Opin. Drug Metab. Toxicol.* **2005**, *1*, 687–699.
- [274] P. Olinga, D. Schuppan, *J. Hepatol.* **2013**, *58*, 1252–1253.
- [275] R. L. Fisher, A. E. M. Vickers, *Xenobiotica* **2013**, *43*, 8–14.
- [276] A. Koch, S. Saran, D. D. H. Tran, S. Klebba-Färber, H. Thiesler, K. Sewald, S. Schindler, A. Braun, R. Klopfleisch, T. Tamura, *Cell Commun. Signal.* **2014**, *12*, 73.
- [277] A. E. M. Vickers, K. Rose, R. Fisher, M. Saulnier, P. Sahota, P. Bentley, *Toxicol. Pathol.* **2004**, *32*, 577–590.
- [278] B. Bertrand, L. Stefan, M. Pirrotta, D. Monchaud, E. Bodio, P. Richard, P. Le Gendre, E. Warmerdam, M. H. de Jager, G. M. M. Groothuis, M. Picquet, A. Casini, *Inorg. Chem.* **2014**, *53*, 2296–2303.
- [279] S. Daum, V. F. Chekhun, I. N. Todor, N. Y. Lukianova, Y. V Shvets, L. Sellner, K. Putzker, J. Lewis, T. Zenz, I. A. M. de Graaf, G. M. M. Groothuis, A. Casini, O. Zozulia, F. Hampel, A. Mokhir, *J. Med. Chem.* **2015**, *58*, 2015–2024.
- [280] I. A. M. de Graaf, P. Olinga, M. H. de Jager, M. T. Merema, R. de Kanter, E. G. van de Kerkhof, G. M. M. Groothuis, *Nat. Protoc.* **2010**, *5*, 1540–1551.
- [281] M. G. L. Elferink, P. Olinga, A. L. Draaisma, M. T. Merema, S. Bauerschmidt, J. Polman, W. G. Schoonen, G. M. M. Groothuis, *Toxicol. Appl. Pharmacol.* **2008**, *229*, 300–309.

- [282] S. Dhillon, K. Gill, in *Clinical Pharmacokinetics*, Pharmaceutical Press, RPS Publishing, London, **2006**, 1–43.
- [283] M. Cocchietto, G. Sava, *Pharmacol. Toxicol.* **2000**, *87*, 193–197.
- [284] M. Cocchietto, G. Salerno, E. Alessio, G. Mestroni, G. Sava, *Anticancer Res.* **2000**, *20*, 197–202.
- [285] J. M. Rademaker-Lakhai, D. Van Den Bongard, D. Pluim, J. H. Beijnen, J. H. M. Schellens, *Clin. Cancer Res.* **2004**, *10*, 3717–3727.
- [286] F. Lentz, A. Drescher, A. Lindauer, M. Henke, R. A. Hilger, C. G. Hartinger, M. E. Scheulen, C. Dittrich, B. K. Keppler, U. Jaehde, *Anticancer. Drugs* **2009**, *20*, 97–103.
- [287] M. M. Henke, H. Richly, A. Drescher, M. Grubert, D. Alex, D. Thyssen, U. Jaehde, M. E. Scheulen, R. A. Hilger, *Int. J. Clin. Pharmacol. Ther.* **2009**, *47*, 58–60.
- [288] C. L. Litterst, T. E. Gram, R. L. Dedrick, A. F. Leroy, A. M. Guarino, *Cancer Res.* **1976**, *36*, 2340–2344.
- [289] K. Sugano, A. Okazaki, S. Sugimoto, S. Tavornvipas, A. Omura, T. Mano, *Drug Metab. Pharmacokinet.* **2007**, *22*, 225–254.
- [290] K. D. Mjos, C. Orvig, *Chem. Rev.* **2014**, *114*, 4540–4563.
- [291] C. Tang, C. Li, C. Tang, W. Zhan, H. Zheng, X. Peng, *Anal. Methods* **2013**, *5*, 7117–7126.
- [292] G. Pollack, K. Brouwer, K. Demby, J. Jones, *Drug Metab. Dispos.* **1990**, *18*, 197–202.
- [293] Y. S. Bakhle, *Br. J. Anaesth.* **1990**, *65*, 79–93.
- [294] M. H. Zaghal, B. F. Ali, *Polyhedron* **1995**, *14*, 1011–1019.
- [295] S. Mollin, R. Riedel, K. Harms, E. Meggers, *J. Inorg. Biochem.* **2015**, *148*, 11–21.
- [296] S. Mollin, Oktaedrische Ruthenium(II)- Und Rhodium(III)-Komplexe Mit Mehrzähnigen Liganden Als Kinaseinhibitoren, Philipps-Universität Marburg, **2012**.
- [297] B. Heinrich, Synthese Verschieden Substituierter Pyridokarbazol-Rhodium(III)-Komplexe Als Mögliche Proteinkinaseinhibitoren, Philipps-Universität Marburg, **2014**.
- [298] S. Mollin, S. Blanck, K. Harms, E. Meggers, *Inorganica Chim. Acta* **2012**, *393*, 261–268.
- [299] S. Blanck, T. Cruchter, A. Vultur, R. Riedel, K. Harms, M. Herlyn, E. Meggers, *Organometallics* **2011**, *30*, 4598–4606.

Bibliography

- [300] S. Blanck, Neuartige Metallkomplexe Als Proteinkinaseinhibitoren, Philipps-Universität Marburg, **2012**.
- [301] N. A. Baker, D. Sept, S. Joseph, M. J. Holst, J. A. McCammon, *Proc. Natl. Acad. Sci. U. S. A.* **2001**, *98*, 10037–10041.
- [302] M. G. Lerner, H. A. Carlson, *APBS Plugin for Pymol*, University Of Michigan, Ann Arbor, **2006**.
- [303] T. J. Dolinsky, J. E. Nielsen, J. A. McCammon, N. A. Baker, *Nucleic Acids Res.* **2004**, *32*, W665-657.
- [304] T. J. Dolinsky, P. Czodrowski, H. Li, J. E. Nielsen, J. H. Jensen, G. Klebe, N. A. Baker, *Nucleic Acids Res.* **2007**, *35*, W522-525.
- [305] D. Sitkoff, K. A. Sharp, B. Honig, *J. Phys. Chem.* **1994**, *98*, 1978–1988.
- [306] C. L. Tang, E. Alexov, A. M. Pyle, B. Honig, *J. Mol. Biol.* **2007**, *366*, 1475–1496.
- [307] B. Lee, F. M. Richards, *J. Mol. Biol.* **1971**, *55*, 379–400.
- [308] M. Ishikawa, Y. Hashimoto, *J. Med. Chem.* **2011**, *54*, 1539–1554.
- [309] M. A. Walker, in *Tactics in Contemporary Drug Design* (Ed.: N.A. Meanwell), Springer Berlin Heidelberg, **2014**, 69–106.
- [310] C.-H. Yun, T. J. Boggon, Y. Li, M. S. Woo, H. Greulich, M. Meyerson, M. J. Eck, *Cancer Cell* **2007**, *11*, 217–227.
- [311] H. van de Waterbeemd, G. Camenisch, G. Folkers, J. R. Chretien, O. A. Raevsky, *J. Drug Target.* **1998**, *6*, 151–165.
- [312] “ACD pKa,” can be found under <https://ilab.acdlabs.com/iLab2/>, **2017**.
- [313] G. Caron, G. Steyaert, A. Pagliara, F. Reymond, P. Crivori, P. Gaillard, P.-A. Carrupt, A. Avdeef, J. Comer, K. J. Box, H. H. Girault, B. Testa, *Heb. Chim. Acta* **1999**, *82*, 1211–1222.
- [314] “RSCB protein data bank,” can be found under <http://www.rcsb.org/pdb/home/home.do>, **2016**.
- [315] C. N. Streu, Bioactive Organometallic Complexes: From Structure to Function, University of Pennsylvania, **2009**.
- [316] L. Feng, Octahedral Ruthenium Complexes as Protein Kinase Inhibitors, Philipps-Universität Marburg, **2010**.

- [317] P. Comba, M. Morgen, H. Wadeohl, *Inorg. Chem.* **2013**, *52*, 6481–6501.
- [318] D. Classen-Houben, A. Wolkerstorfer, O. Szolar, M. Smith, S. S. So, S. Cusack, T. Langer, B. Giethlen, C. Morice, C. Michaut-Simon, C. Zubietta, *Heteroaryl Hydroxamic Acid Derivatives and Their Use in the Treatment, Amelioration or Prevention of a Viral Disease*, **2013**, US2004/186114 A1.
- [319] J. Plag, New Ligand Design for Soluble Octahedral rhodium(III) Kinase Inhibitors, Philipps-Universität Marburg, **2015**.
- [320] K. Gee, S. Grecian, U. Singh, *Compounds and Methods for Conjugation of Biomolecules*, **2012**, WO 2012121973 A1.
- [321] W.-W. Li, X.-Y. Wang, R.-L. Zheng, H.-X. Yan, Z.-X. Cao, L. Zhong, Z.-R. Wang, P. Ji, L.-L. Yang, L.-J. Wang, Y. Xu, J.-J. Liu, J. Yang, C.-H. Zhang, S. Ma, S. Feng, Q.-Z. Sun, Y.-Q. Wei, S.-Y. Yang, *J. Med. Chem.* **2012**, *55*, 3852–3866.
- [322] H. Löw, Synthese Neuer Liganden Für Proteinkinase-Inhibitoren, Philipps-Universität Marburg, **2014**.
- [323] A. Citterio, A. Gentile, F. Minisci, M. Serravalle, S. Ventura, *Tetrahedron* **1985**, *41*, 617–620.
- [324] F. Minisci, R. Galli, M. Cecere, *Tetrahedron Lett.* **1965**, *6*, 4663–4667.
- [325] D. G. Cooper, G. S. Sach, *Pyrimidone Derivatives*, **1983**, US4385058 A.
- [326] J. F. J. Engbersen, A. Koudijs, M. H. A. Joosten, H. C. van der Plas, *J. Heterocycl. Chem.* **1986**, *23*, 989–990.
- [327] S. Torch, D. Barbry, *J. Chem. Res.* **2001**, *2001*, 292–293.
- [328] M. W. Tripp, Darstellung Neuartiger Liganden Zur Verbesserung Der Zellpermeabilität von Rhodium-Haltigen Kinase-Inhibitoren, Philipps-Universität Marburg, **2014**.
- [329] R. Hulst, I. Muizebelt, P. Oosting, C. van der Pol, A. Wagenaar, J. Šmisterová, E. Bulten, C. Driessens, D. Hoekstra, J. B. F. N. Engberts, *European J. Org. Chem.* **2004**, *2004*, 835–849.
- [330] G. Hunter, H. McNab, K. Withell, *Synthesis* **2010**, *2010*, 1707–1711.
- [331] R. B. Katz, J. Mistry, M. B. Mitchell, *Synth. Commun.* **1989**, *19*, 317–325.
- [332] G. Chelucci, M. Falorni, G. Giacomelli, *Tetrahedron: Asymmetry* **1990**, *1*, 843–849.
- [333] A. Casini, M. A. Cinelli, G. Minghetti, C. Gabbiani, M. Coronello, E. Mini, L. Messori, *J. Med. Chem.* **2006**, *49*, 5524–5531.

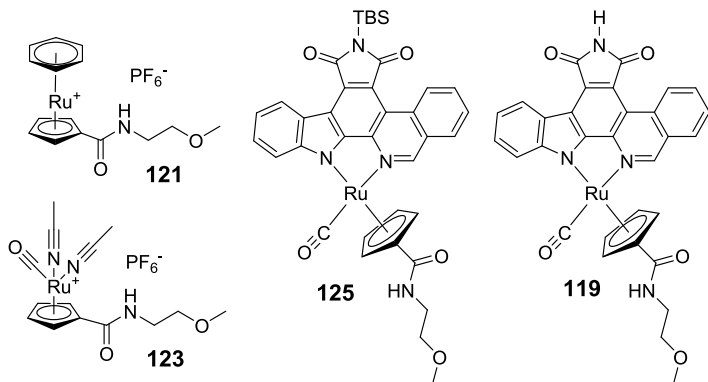
Bibliography

- [334] A. Casini, G. Kelter, C. Gabbiani, M. A. Cinelli, G. Minghetti, D. Fregoni, H.-H. Fiebig, L. Messori, *J. Biol. Inorg. Chem.* **2009**, *14*, 1139–1149.
- [335] X. Fang, L. Shao, H. Zhang, S. Wang, *J. Chem. Inf. Comput. Sci.* **2004**, *44*, 249–257.
- [336] C. Gabbiani, A. Guerri, M. A. Cinelli, L. Messori, *Open Crystallogr. J.* **2010**, *3*, 29–40.
- [337] C. Gabbiani, A. Casini, L. Messori, A. Guerri, M. A. Cinelli, G. Minghetti, M. Corsini, C. Rosani, P. Zanello, M. Arca, *Inorg. Chem.* **2008**, *47*, 2368–2379.
- [338] C. Gabbiani, M. A. Cinelli, L. Maiore, L. Massai, F. Scaletti, L. Messori, *Inorganica Chim. Acta* **2012**, *393*, 115–124.
- [339] F. Magherini, A. Modesti, L. Bini, M. Puglia, I. Landini, S. Nobili, E. Mini, M. A. Cinelli, C. Gabbiani, L. Messori, *J. Biol. Inorg. Chem.* **2010**, *15*, 573–582.
- [340] F. Ritterbusch, Entwicklung Metallorganischer Enzyminhibitoren Für Histondeacetylasen Und Carboanhydrasen, **2012**.
- [341] A. Jacques, C. Lebrun, A. Casini, I. Kieffer, O. Proux, J.-M. Latour, O. Sénèque, *Inorg. Chem.* **2015**, *54*, 4104–4113.
- [342] F. Dangond, M. Henriksson, G. Zardo, P. Caiafa, T. J. Ekström, S. G. Gray, *Int. J. Oncol.* **2001**, *19*, 773–777.
- [343] E. A. Stronach, A. Alfraidi, N. Rama, C. Datler, J. B. Studd, R. Agarwal, T. G. Guney, C. Gourley, B. T. Hennessy, G. B. Mills, A. Mai, R. Brown, R. Dina, H. Gabra, *Cancer Res.* **2011**, *71*, 4412–4422.
- [344] W. L. F. Armarego, C. L. L. Chai, *Purification of Laboratory Chemicals*, Butterworth-Heinemann, **2003**.
- [345] H. E. Gottlieb, V. Kotlyar, A. Nudelman, *J. Org. Chem.* **1997**, *62*, 7512–7515.
- [346] E. G. Mata, E. J. Thomas, *J. Chem. Soc. Perkin Trans. 1* **1995**, 785–799.
- [347] E. Röder, H. Wiedenfeld, M. Frisse, *Arch. Pharm.* **1980**, *313*, 803–806.
- [348] R. Riclea, J. S. Dickschat, *Chemistry* **2011**, *17*, 11930–11934.
- [349] G. E. Magoulas, S. E. Bariamis, C. M. Athanassopoulos, A. Haskopoulos, P. G. Dedes, M. G. Krokidis, N. K. Karamanos, D. Kletsas, D. Papaioannou, G. Maroulis, *Eur. J. Med. Chem.* **2011**, *46*, 721–737.
- [350] Bruker AXS Inc., *SAINt V8.34A*, **2013**.

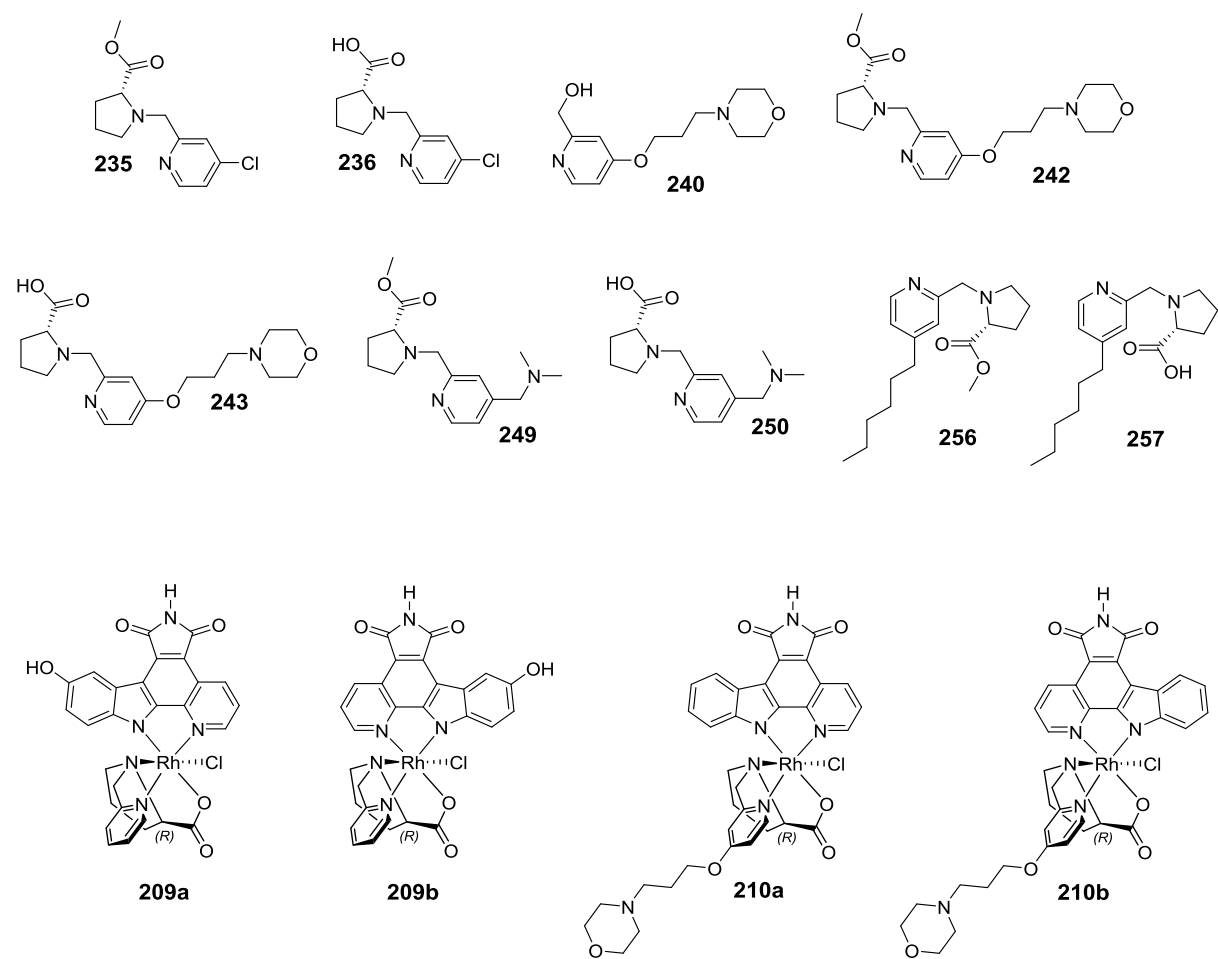
- [351] U. K. Laemmli, *Nature* **1970**, *227*, 680–685.
- [352] E. Jantratid, N. Janssen, C. Reppas, J. B. Dressman, *Pharm. Res.* **2008**, *25*, 1663–1676.
- [353] M. Trunzer, B. Faller, A. Zimmerlin, *J. Med. Chem.* **2009**, *52*, 329–335.
- [354] T. Iwatsubo, H. Suzuki, Y. Sugiyama, *J. Pharmacol. Exp. Ther.* **1997**, *283*, 462–469.
- [355] D. J. Carlile, N. Hakooz, M. K. Bayliss, J. B. Houston, *Br. J. Clin. Pharmacol.* **1999**, *47*, 625–635.
- [356] C. Bäärnhielm, H. Dahlbäck, I. Skånberg, *Acta Pharmacol. Toxicol. (Copenh.)* **2009**, *59*, 113–122.
- [357] J. Knaak, *Toxicol. Appl. Pharmacol.* **1993**, *120*, 106–113.
- [358] B. Davies, T. Morris, *Pharm. Res.* **1993**, *10*, 1093–1095.
- [359] A. Adson, T. J. Raub, P. S. Burton, C. L. Barsuhn, A. R. Hilgers, N. F. H. Ho, K. L. Audus, *J. Pharm. Sci.* **1994**, *83*, 1529–1536.
- [360] A. Adson, P. S. Burton, T. J. Raub, C. L. Barsuhn, K. L. Audus, N. F. H. Ho, *J. Pharm. Sci.* **1995**, *84*, 1197–1204.
- [361] K. Sugano, N. Takata, M. Machida, K. Saitoh, K. Terada, *Int. J. Pharm.* **2002**, *241*, 241–251.
- [362] K. Sugano, Y. Nabuchi, M. Machida, Y. Aso, *Int. J. Pharm.* **2003**, *257*, 245–251.
- [363] K. Benson, *MCAT Review*, **1999**.

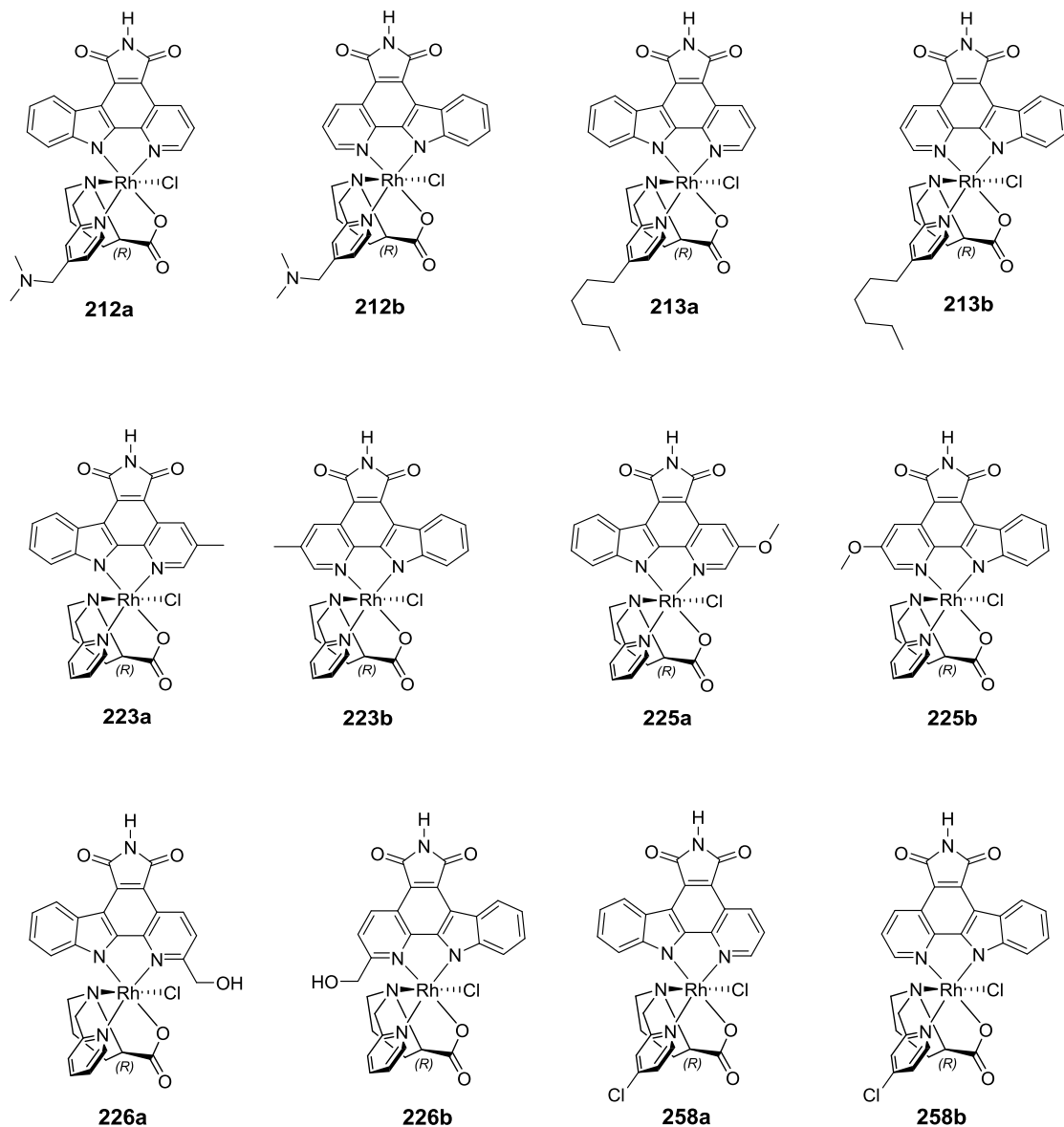
6.3. List of newly developed compounds

6.3.1. List of synthesised compounds from chapter 3.1



6.3.2. List of synthesised compounds from chapter 3.4





6.4. Crystal structure data

6.4.1. Crystallographic data of complex 80a

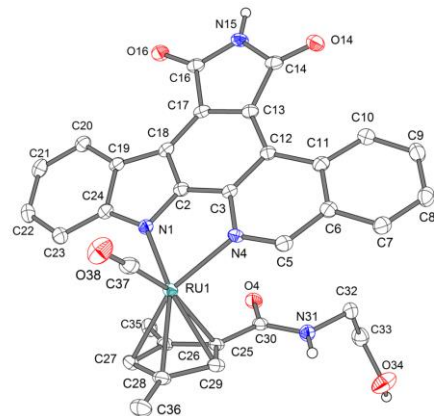


Table 26: Crystallographic data of complex np830 (80a).

formula	C₃₆H₃₆N₄O₇RuS₂
fw	801.88
a(Å)	14.3457(9)
b(Å)	14.4275(8)
c(Å)	16.6220(11)
α(°)	90
β(°)	92.679(2)
γ(°)	90
V(Å ³)	3436.5(4)
Z	4
space group	P 1 2 ₁ /c 1
dcalcd(Mg/m ³)	1.550
μ(mm ⁻¹)	0.634
Θ range(°)	2.003 to 27.205
no. of indep. reflections	7652
no. of parameters	466
wR2 (all data) ^b	0.0794
R1 (I > 2σ(I)) ^b	0.0327
CCDC no. ^c	968409

^aMoKα radiation ($\lambda = 0.71073 \text{ \AA}$). ^bR1 = $\sum |F_o| - |F_c| | / \sum |F_o|$; wR2 = $[w(F_o^2 - F_c^2)^2 / \sum w(F_o^2)^2]^{1/2}$.

^cCrystallographic data (excluding structure factors) have been deposited in the Cambridge Crystallographic Data Center.

6.4.2. Crystallographic data of complex 225a

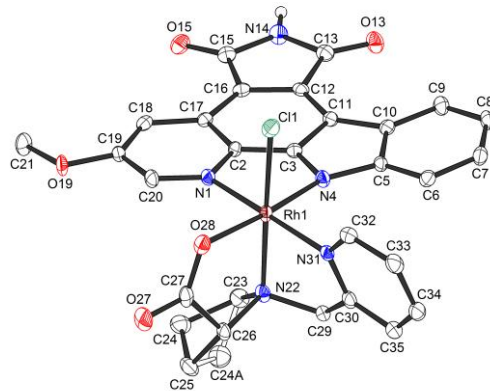


Table 27: Crystallographic data of 5-methoxypyridine derivatised RR97a

formula	$C_{31}H_{29}ClN_5O_6RhS$
fw	738.01
a(Å)	7.4160(3)
b(Å)	14.6172(7)
c(Å)	27.4671(11)
$\alpha(^{\circ})$	90
$\beta(^{\circ})$	90
$\gamma(^{\circ})$	90
$V(\text{\AA}^3)$	2977.5(2)
Z	4
space group	P 2 ₁ 2 ₁ 2 ₁
dcalcd(Mg/m ³)	1.646
$\mu(\text{mm}^{-1})$	0.788
Θ range($^{\circ}$)	2.625 to 27.526
no. of indep. reflections	6840
no. of parameters	414
wR2 (all data) ^b	0.0595
R1 ($I > 2\sigma(I)$) ^b	0.0325

^aMoK α radiation ($\lambda = 0.71073 \text{ \AA}$). ^b $R1 = \sum |F_o| - |F_c| / \sum |F_o|$; $wR2 = [w(F_o^2 - F_c^2)^2 / \sum w(F_o^2)]^{1/2}$.

NMR-spectra of selected compounds

6.5. NMR-spectra of selected compounds

6.5.1. ^1H - and ^{13}C -NMR-spectra of 119

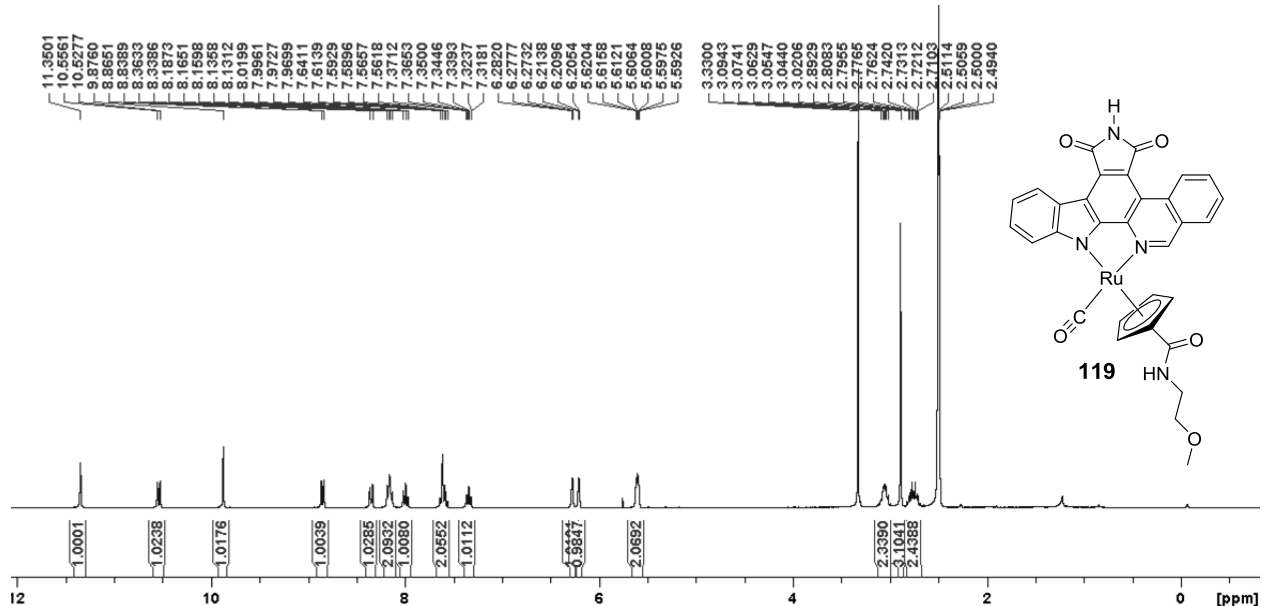


Fig. 74: ^1H -NMR-spectrum of 119.

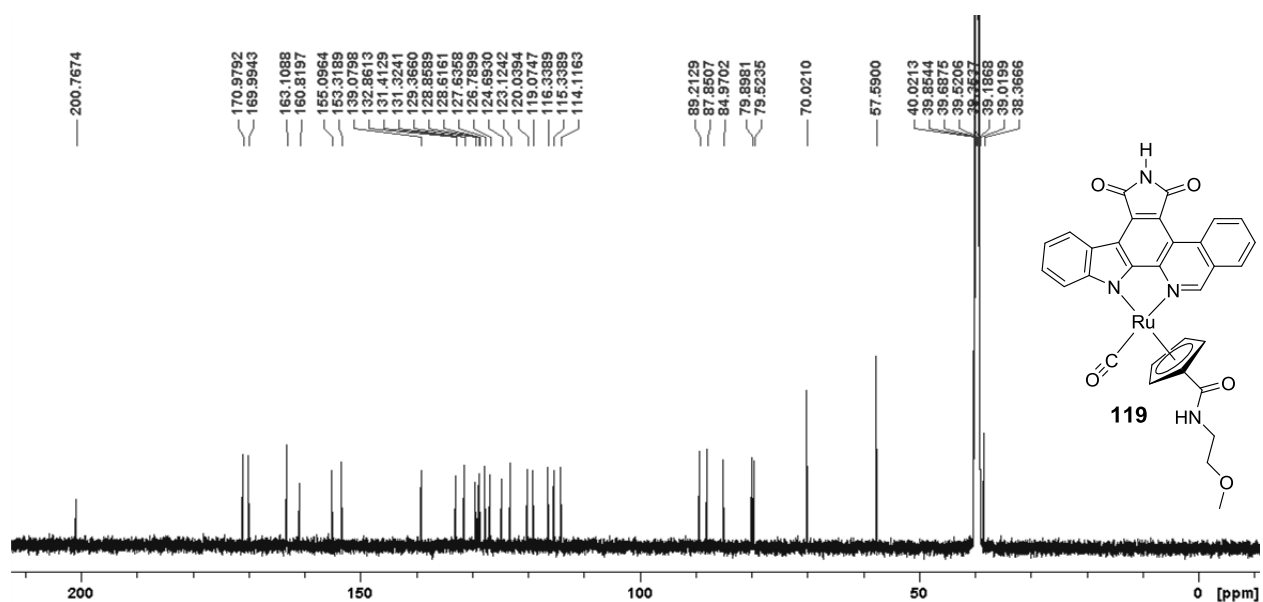
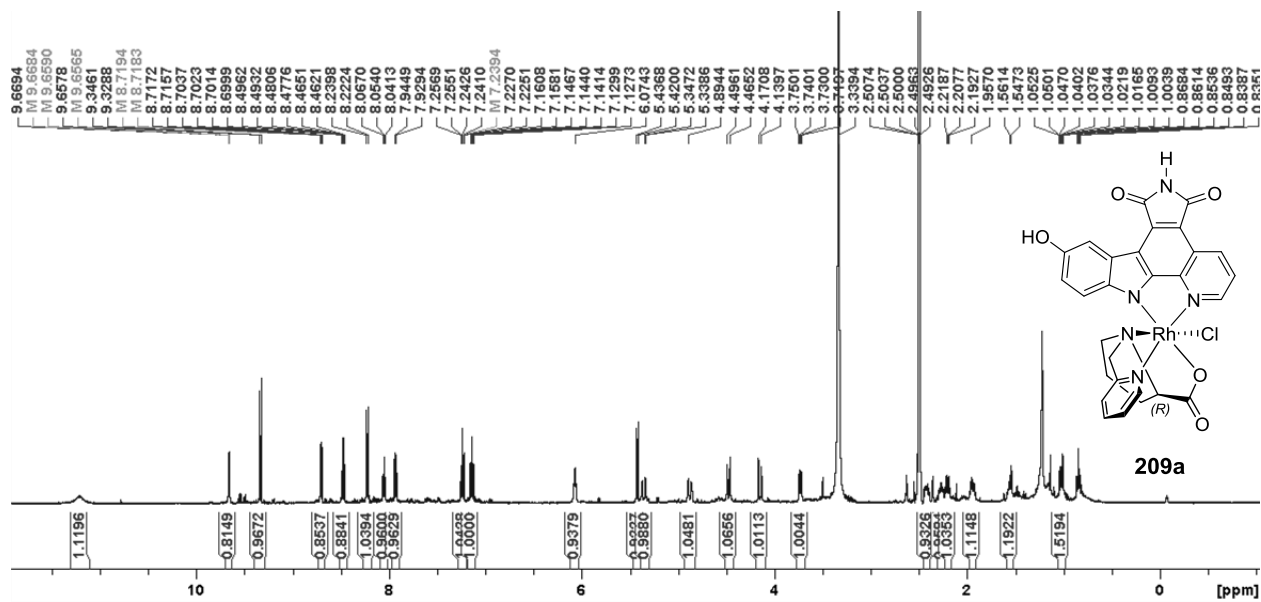
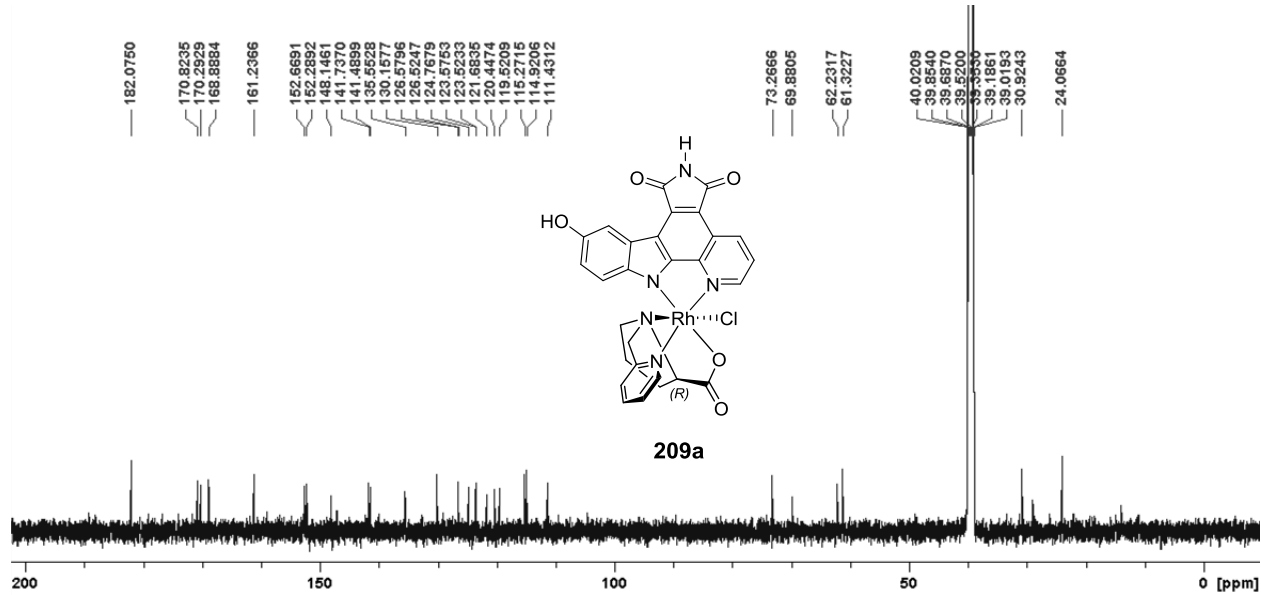


Fig. 75: ^{13}C -NMR-spectrum of 119.

6.5.2. ^1H - and ^{13}C -NMR-spectra of 209aFig. 76: ^1H -NMR-spectrum of 209a.Fig. 77: ^{13}C -NMR-spectrum of 209a.

NMR-spectra of selected compounds

6.5.3. ^1H - and ^{13}C -NMR-spectra of 209b

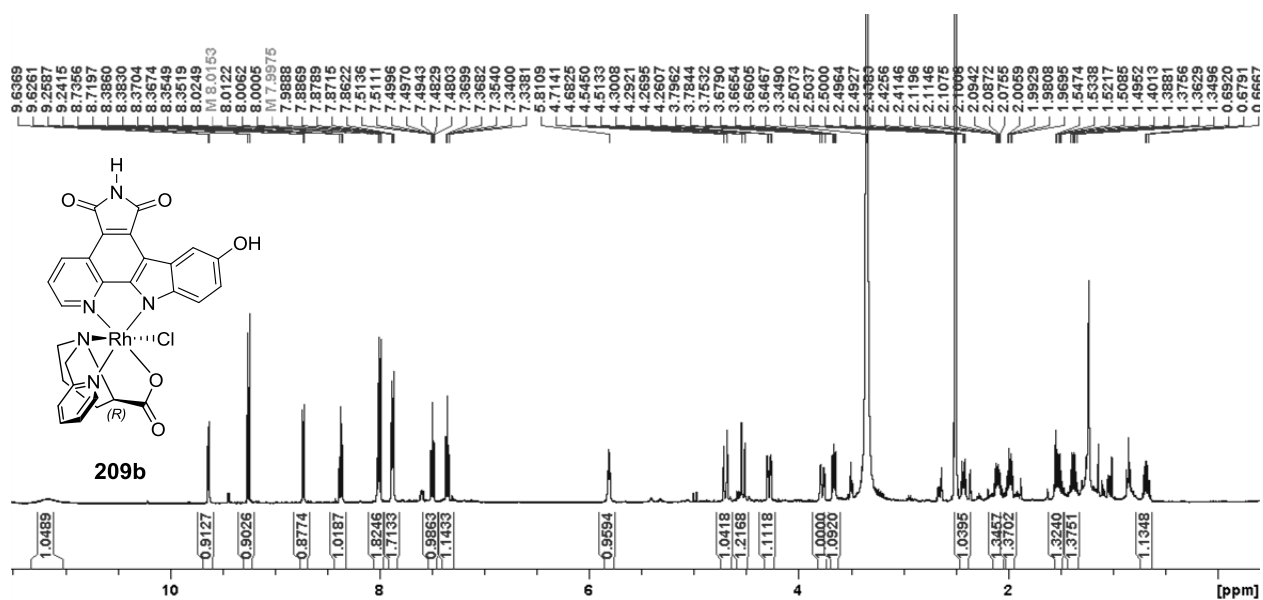


Fig. 78: ^1H -NMR-spectrum of 209b.

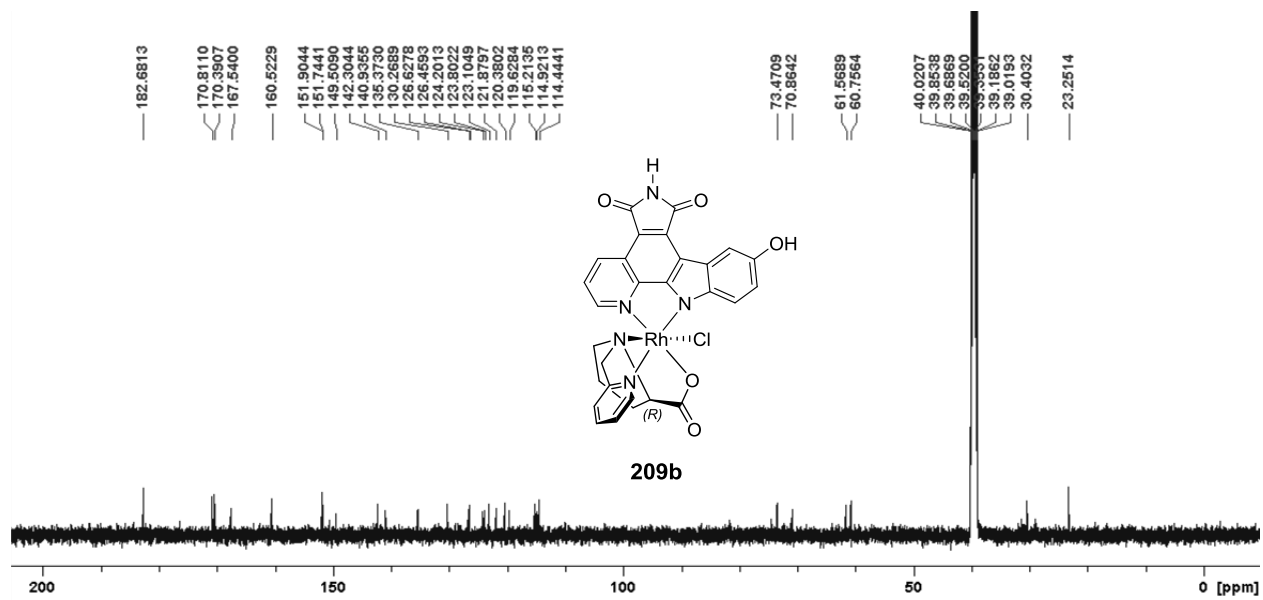


Fig. 79: ^{13}C -NMR-spectrum of 209b.

6.5.4. ^1H - and ^{13}C -NMR-spectra of 210a

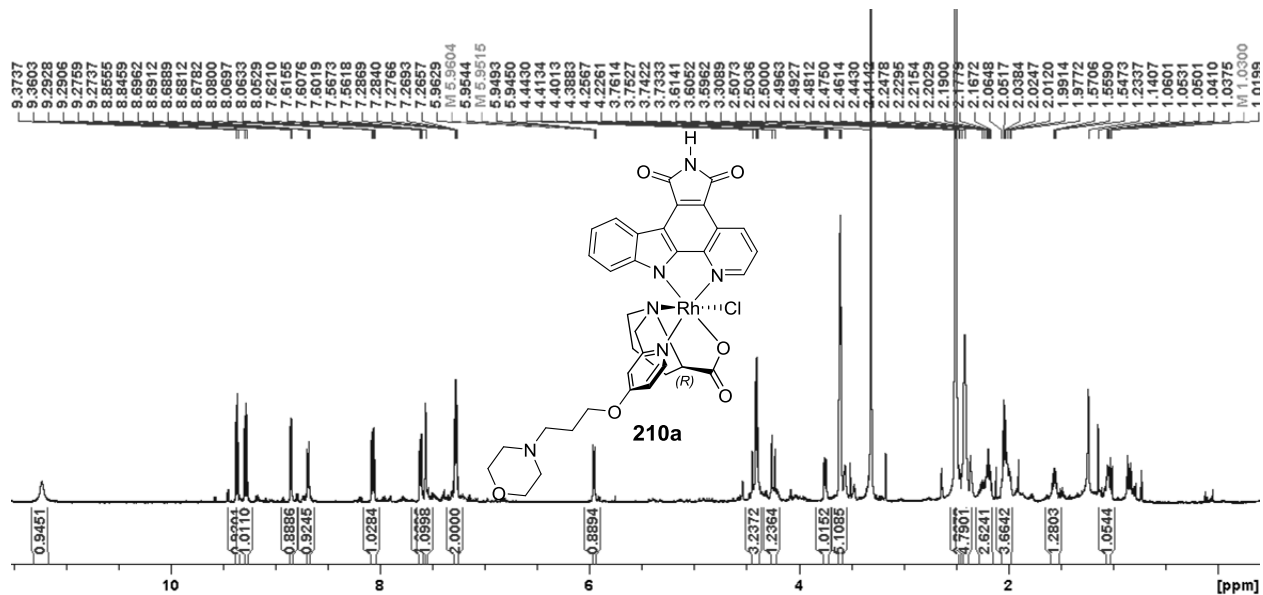


Fig. 80: ^1H -NMR-spectrum of 210a.

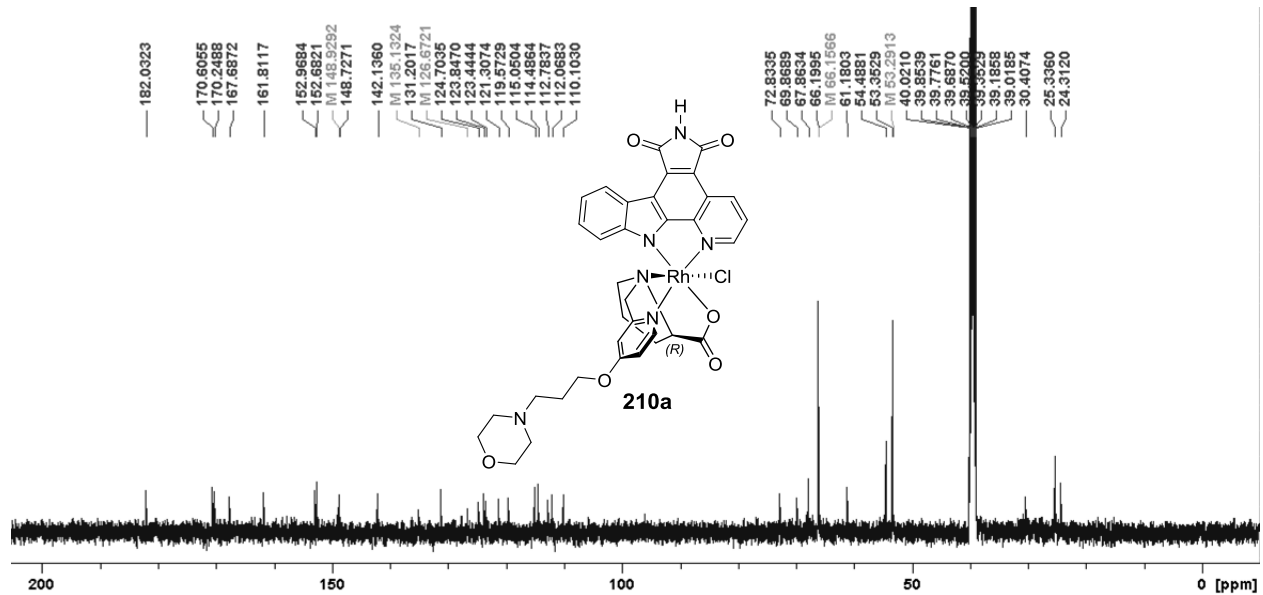


Fig. 81: ^{13}C -NMR-spectrum of 210a.

NMR-spectra of selected compounds

6.5.5. ^1H - and ^{13}C -NMR-spectra of 210b

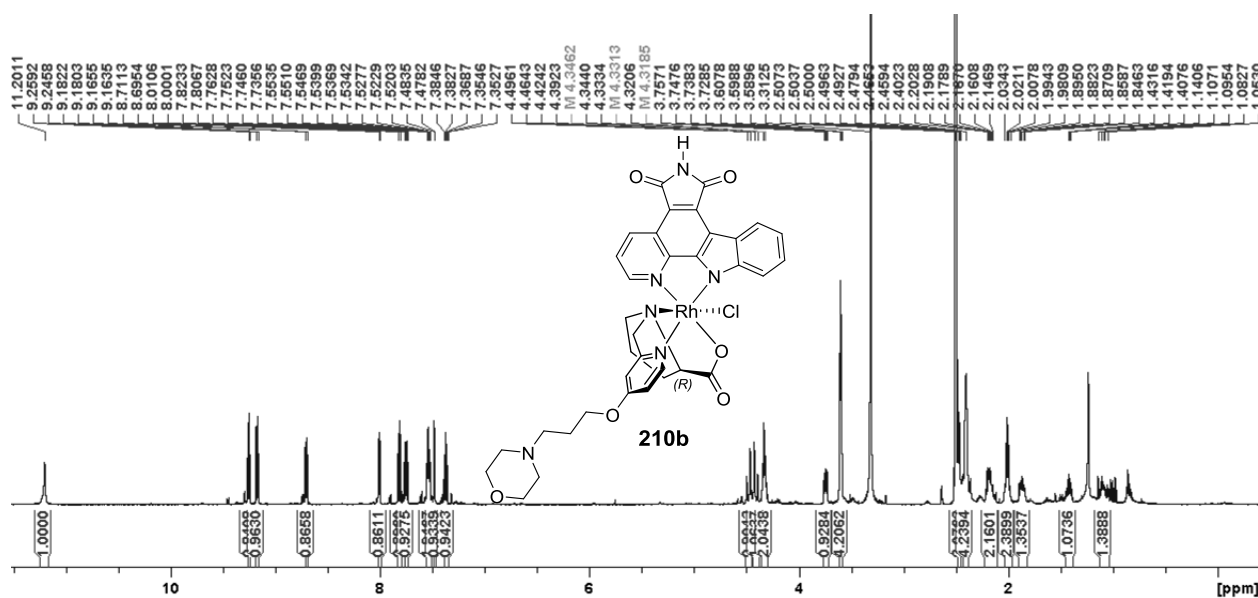


Fig. 82: ^1H -NMR-spectrum of **210b**.

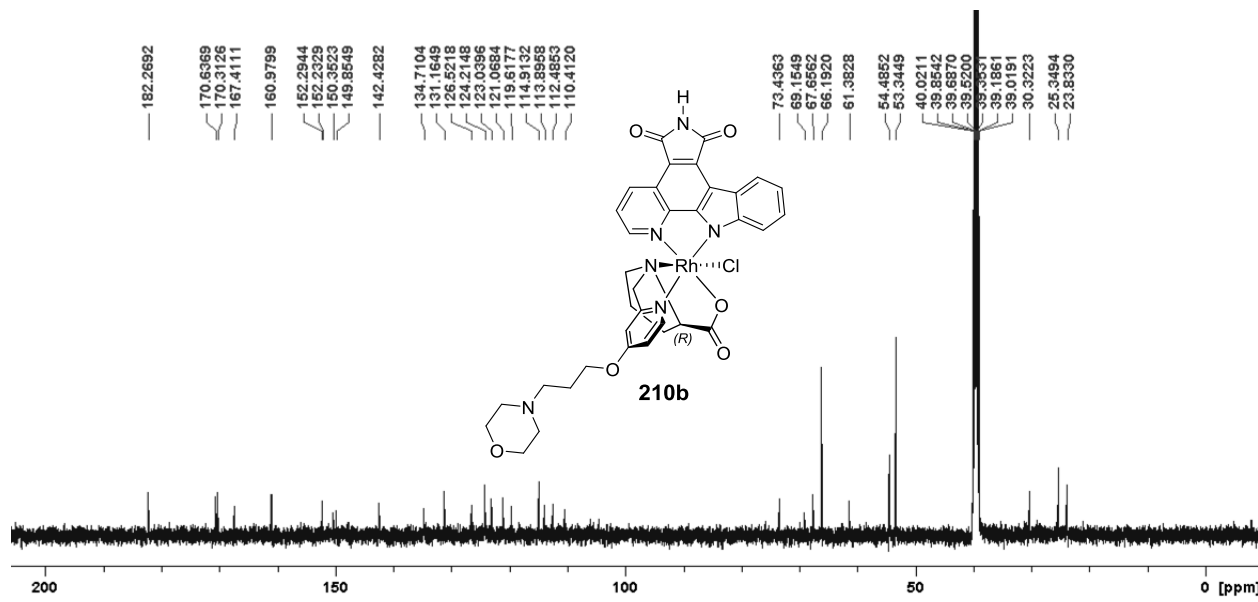
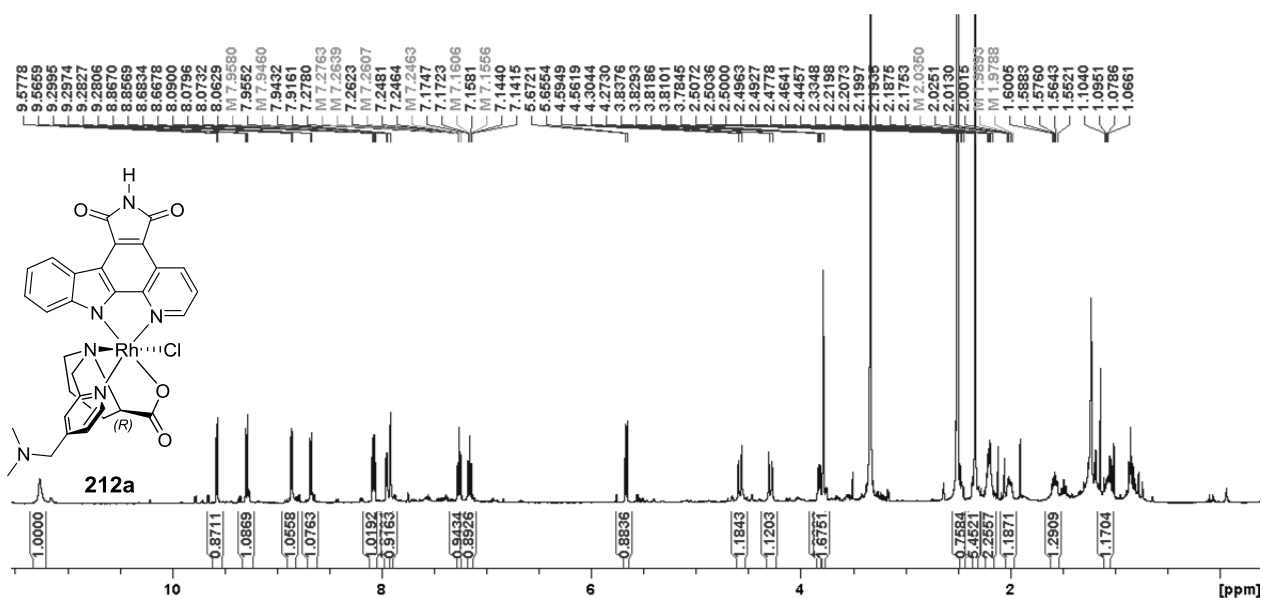
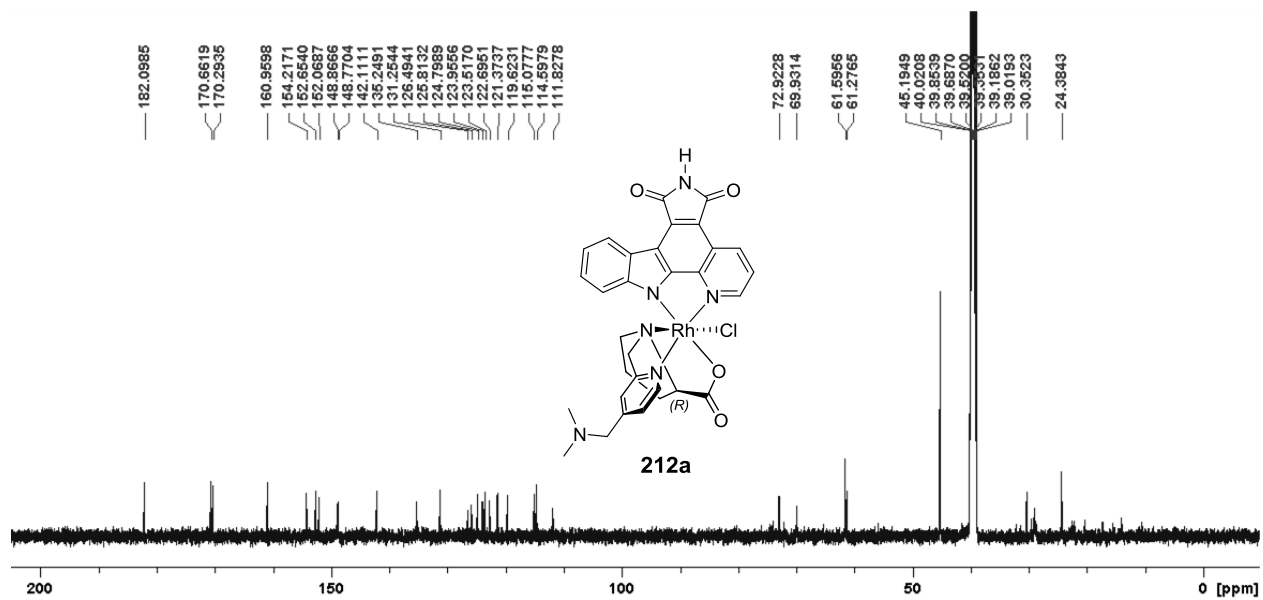


Fig. 83: ^{13}C -NMR-spectrum of **210b**.

6.5.6. ^1H - and ^{13}C -NMR-spectra of 212aFig. 84: ^1H -NMR-spectrum of 212a.Fig. 85: ^{13}C -NMR-spectrum of 212a.

6.5.7. ^1H - and ^{13}C -NMR-spectra of 212b

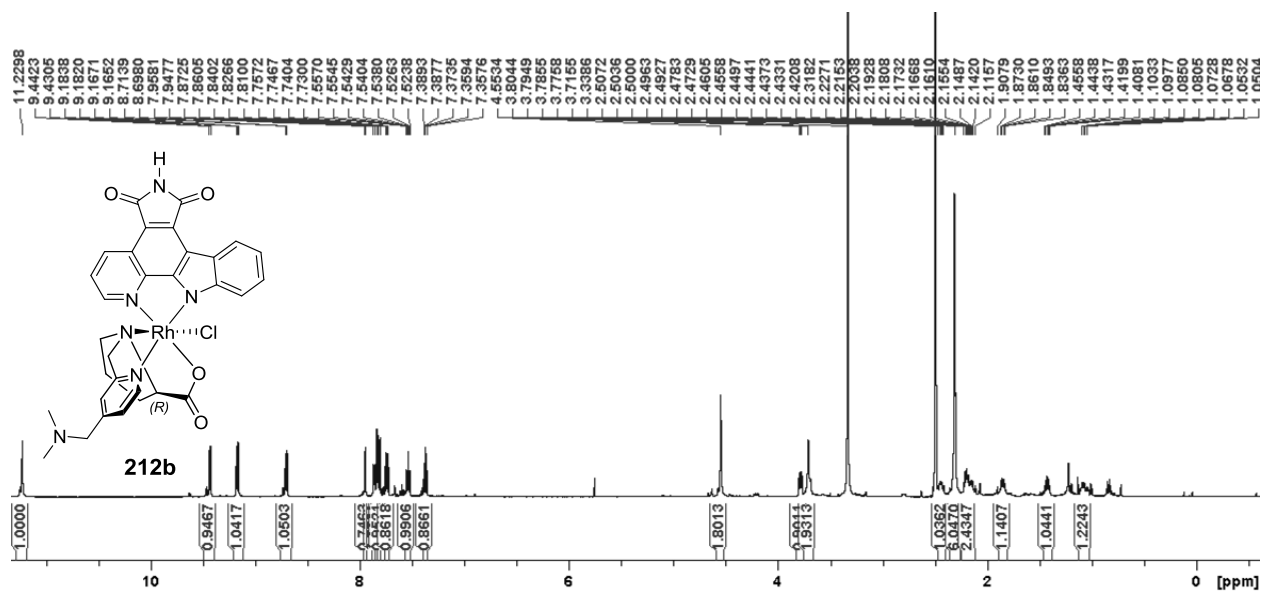


Fig. 86: ^1H -NMR-spectrum of 212b.

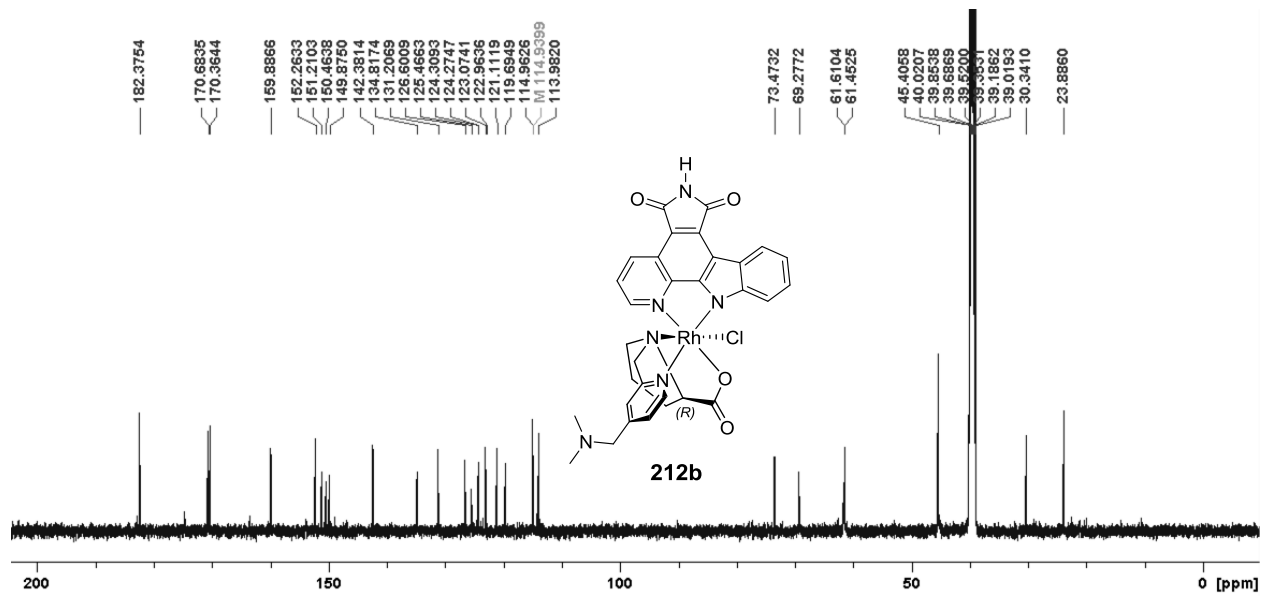


Fig. 87: ^{13}C -NMR-spectrum of 212b.

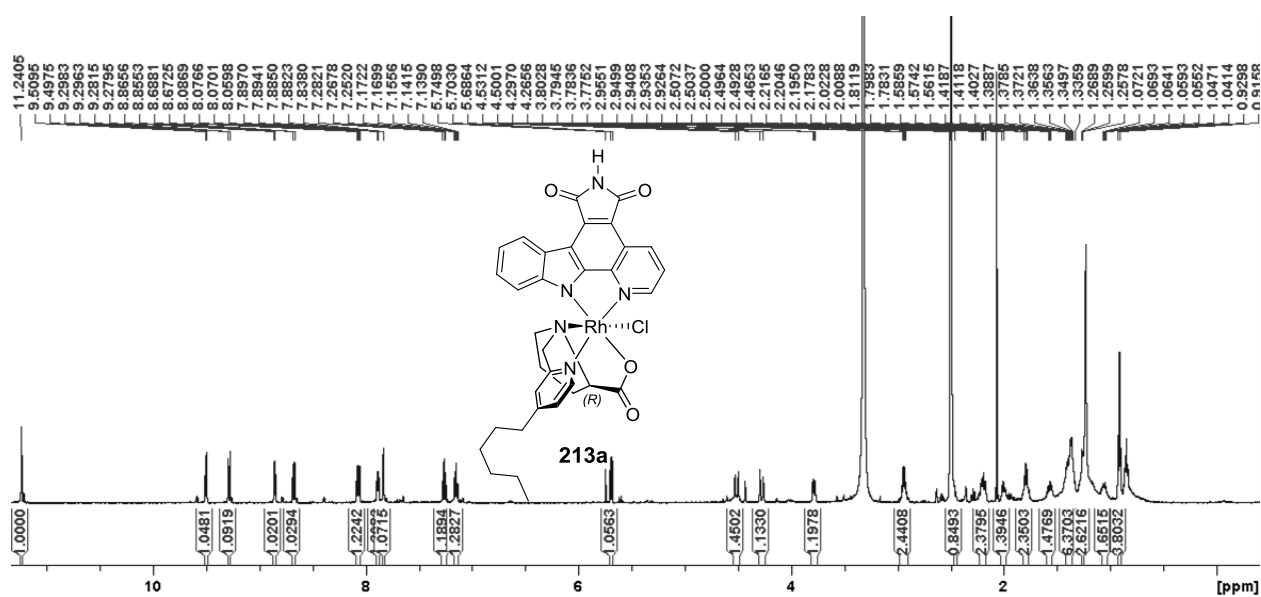
6.5.8. ^1H -NMR-spectrum of 213a

Fig. 88: ^1H -NMR-spectrum of 213a.

The ^{13}C -NMR spectrum of 213a was only measured partially due to low solubility and is therefore not shown.

NMR-spectra of selected compounds

6.5.9. ^1H - and ^{13}C -NMR-spectra of 213b

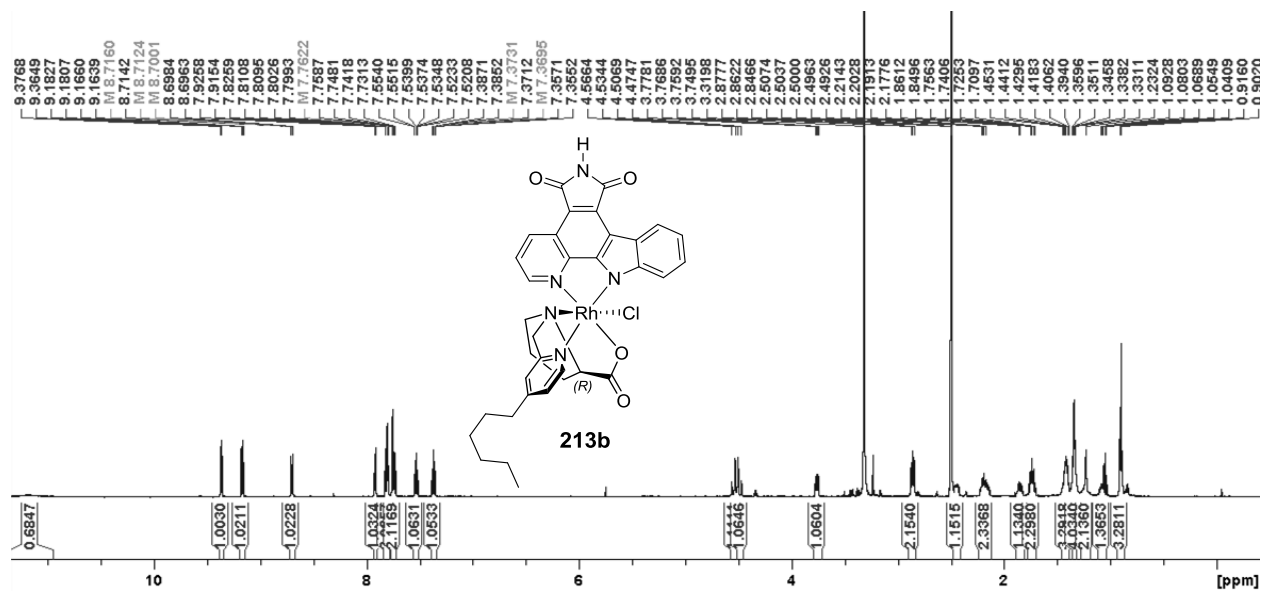


Fig. 89: ^1H -NMR-spectrum of 213b.

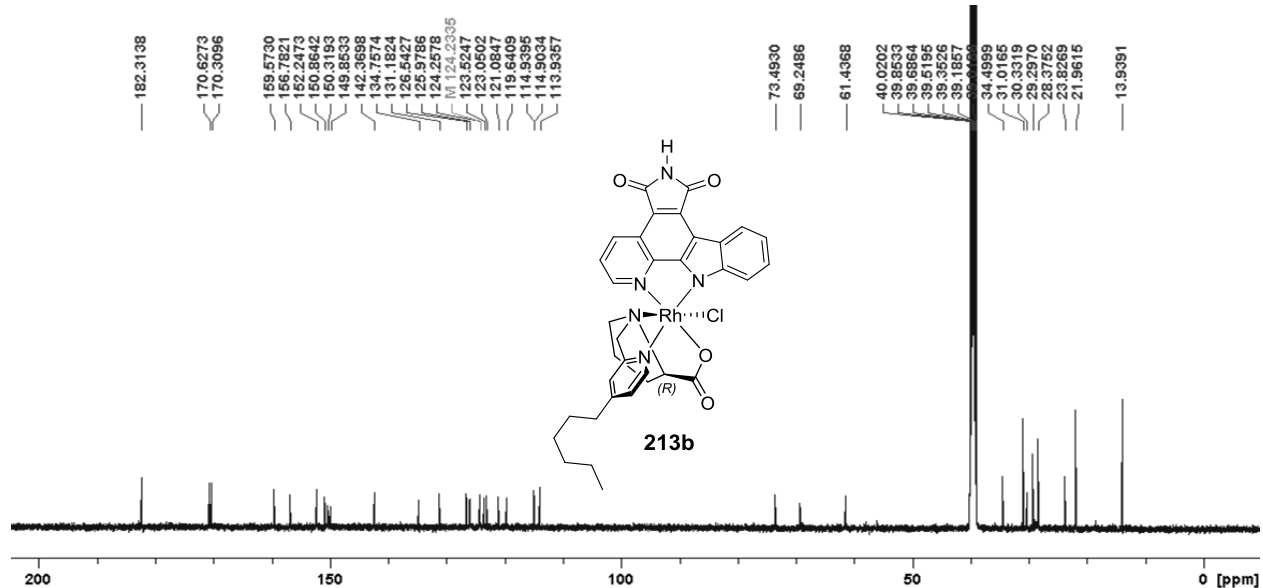
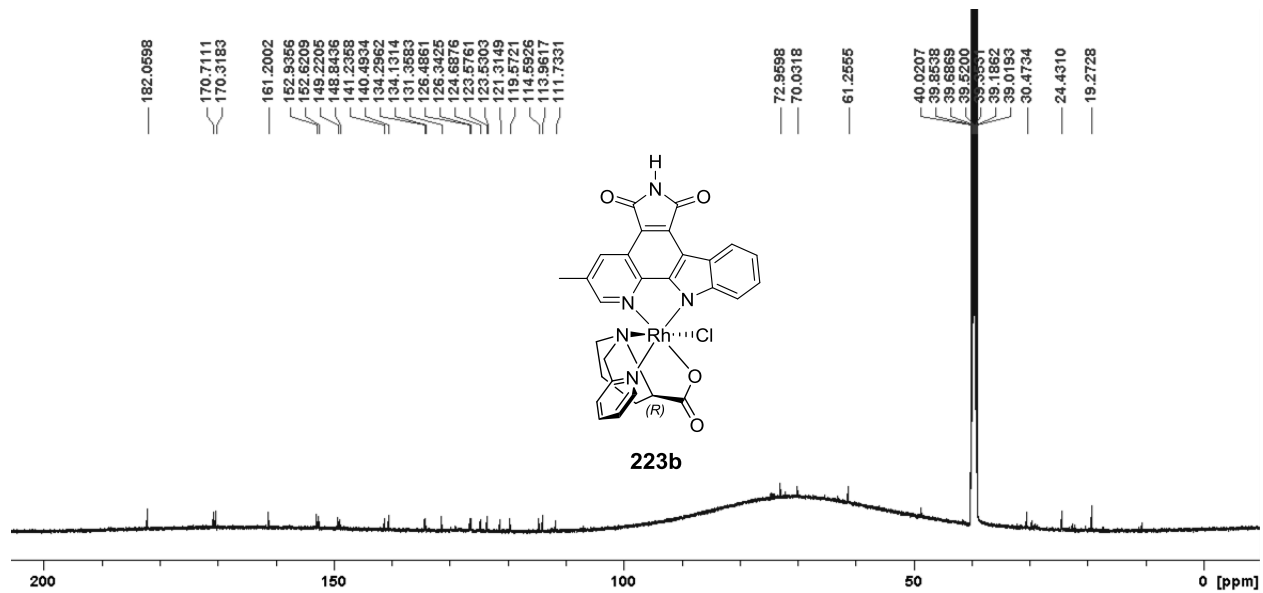
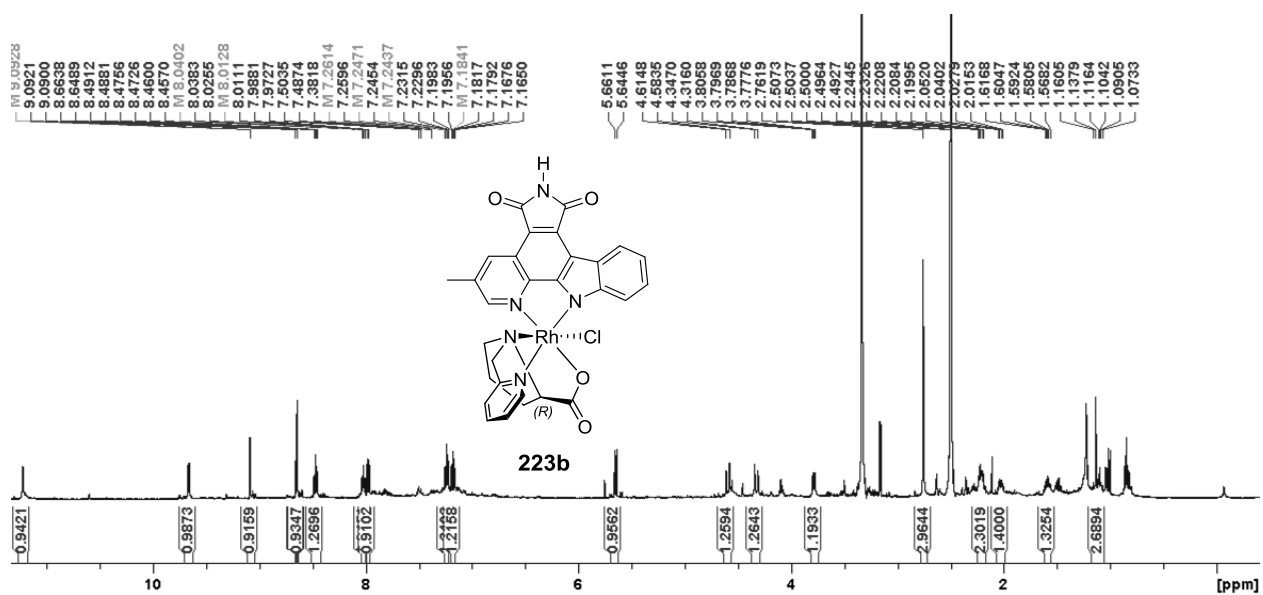


Fig. 90: ^{13}C -NMR-spectrum of 213b.

6.5.10. ^1H - and ^{13}C -NMR-spectra of 223aFig. 92: ^{13}C -NMR-spectrum of 223a.

NMR-spectra of selected compounds

6.5.11. ^1H - and ^{13}C -NMR-spectra of 223b

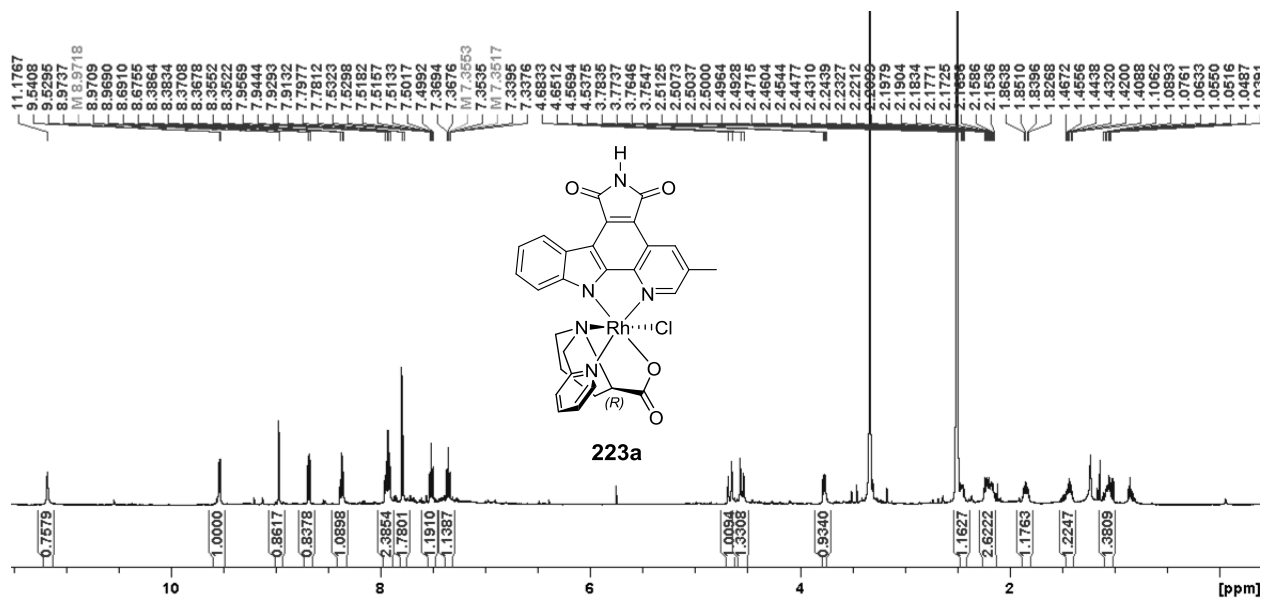


Fig. 93: ^1H -NMR-spectrum of 223b.

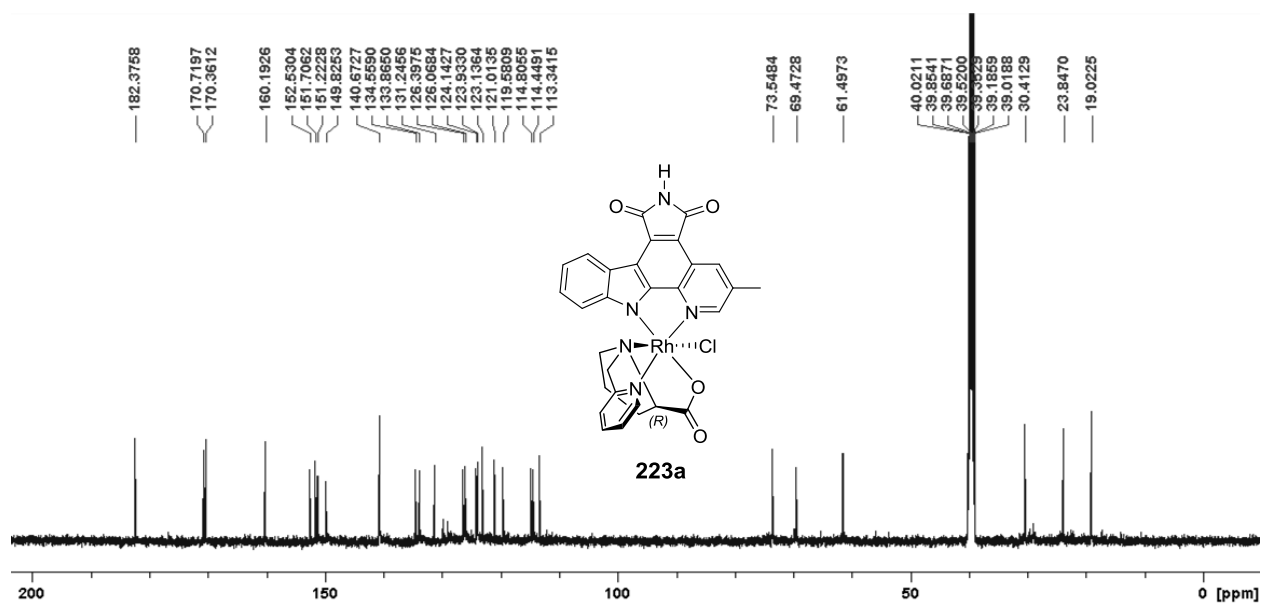
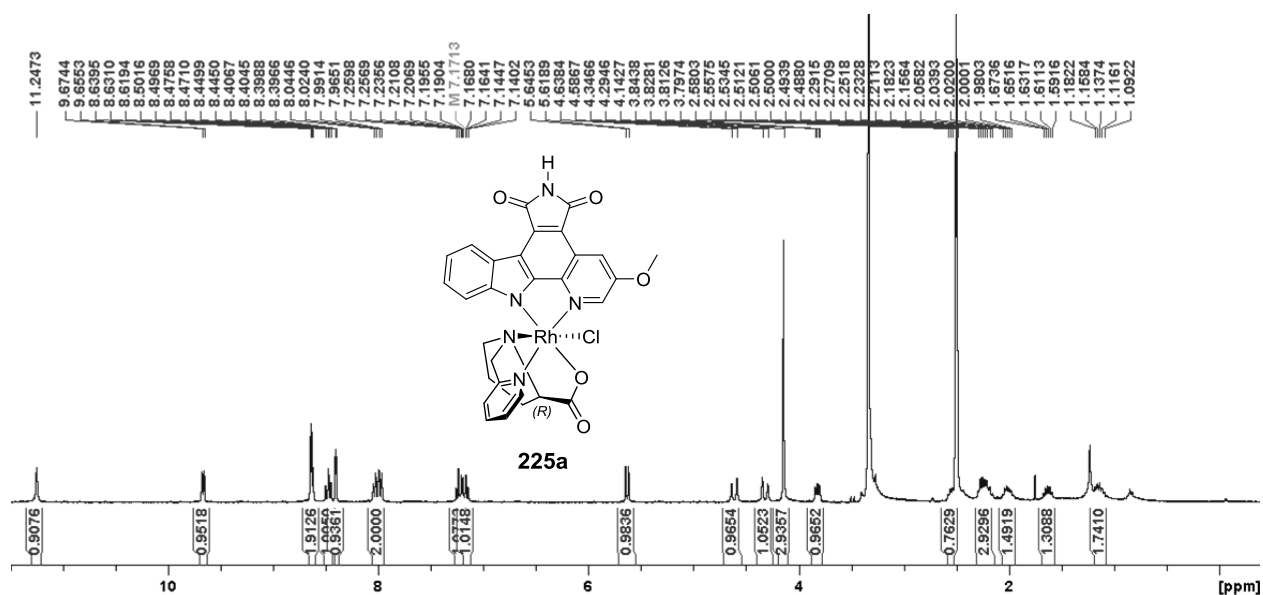
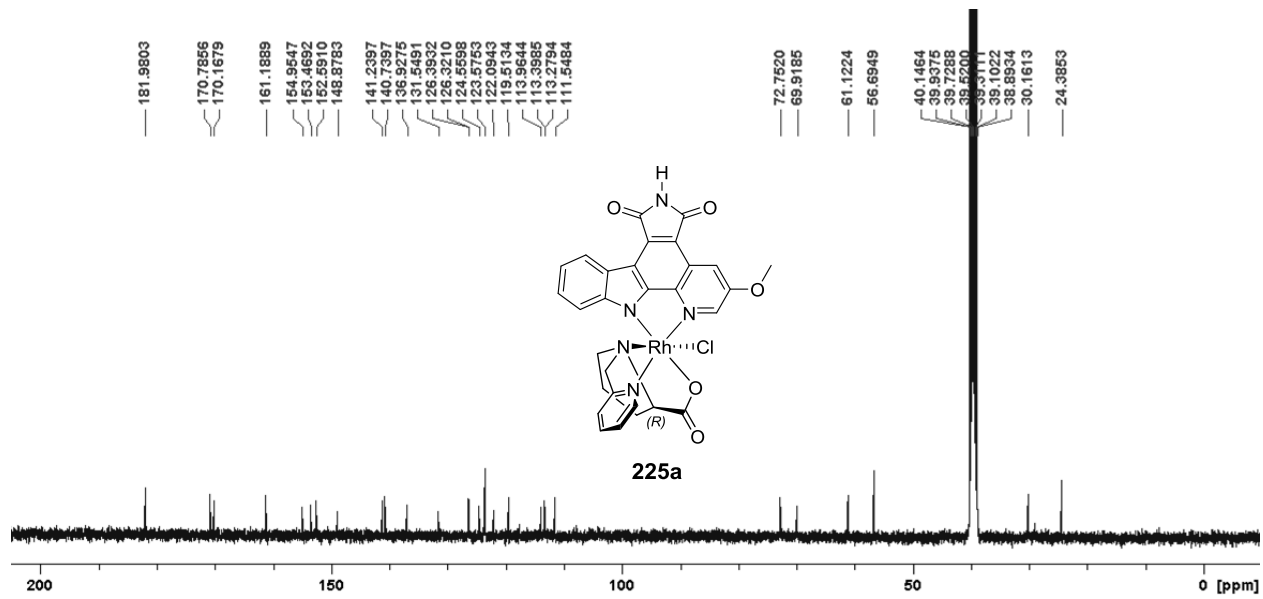


Fig. 94: ^{13}C -NMR-spectrum of 223b.

6.5.12. ^1H - and ^{13}C -NMR-spectra of 225aFig. 95: ^1H -NMR-spectrum of 225a.Fig. 96: ^{13}C -NMR-spectrum of 225a.

NMR-spectra of selected compounds

6.5.13. ^1H - and ^{13}C -NMR-spectra of 225b

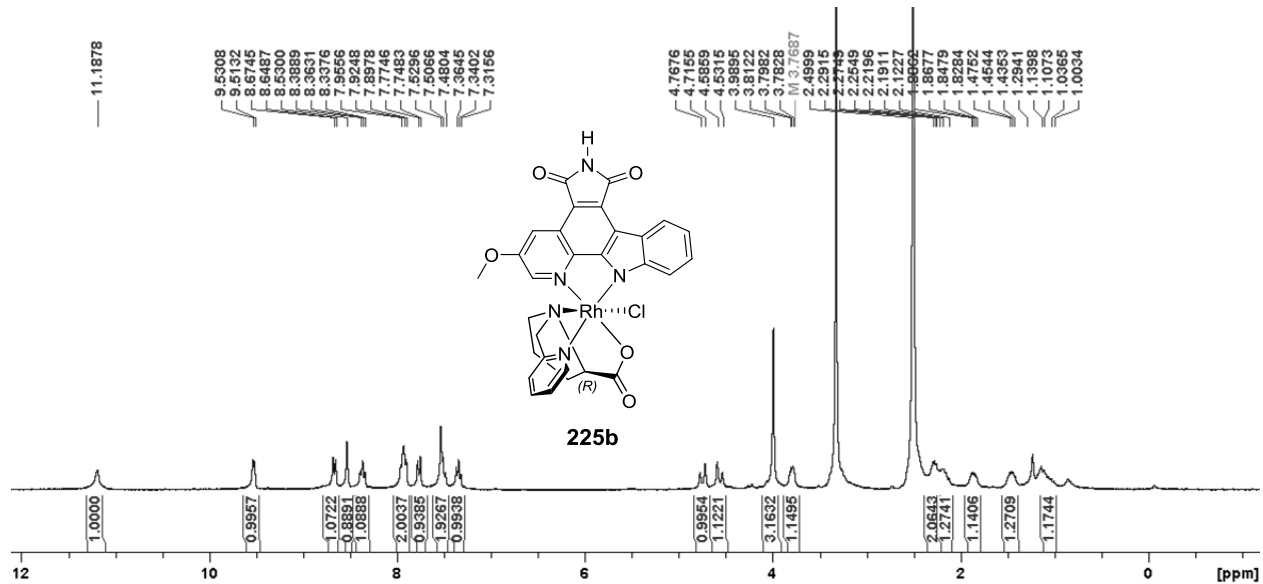


Fig. 97: ^1H -NMR-spectrum of 225b.

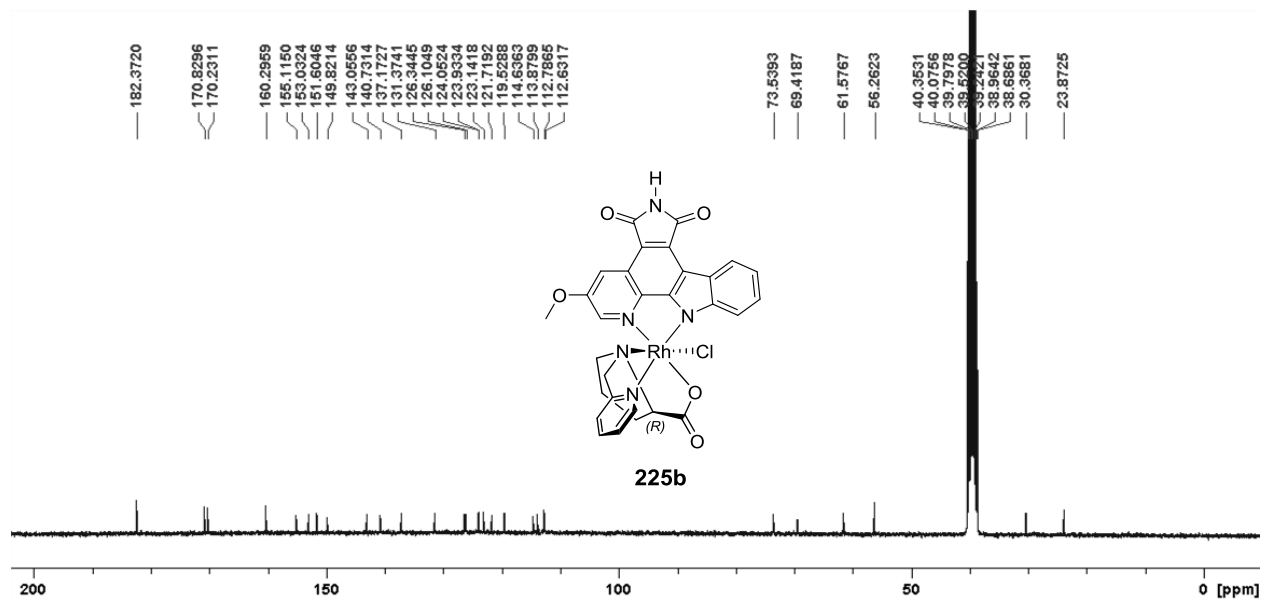
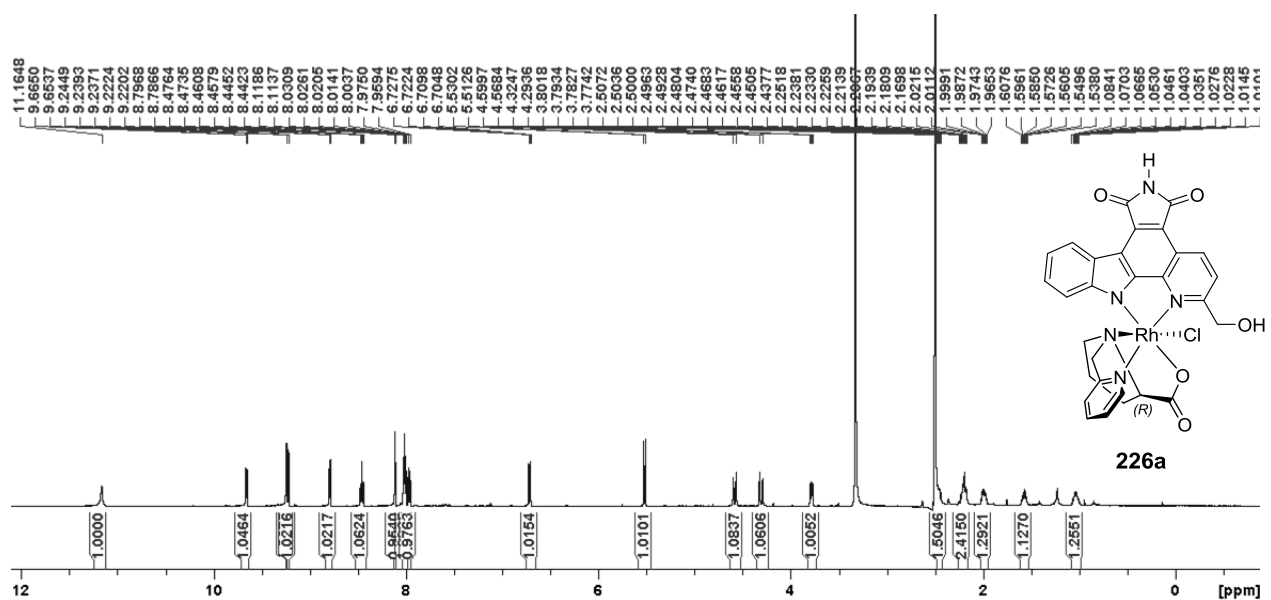
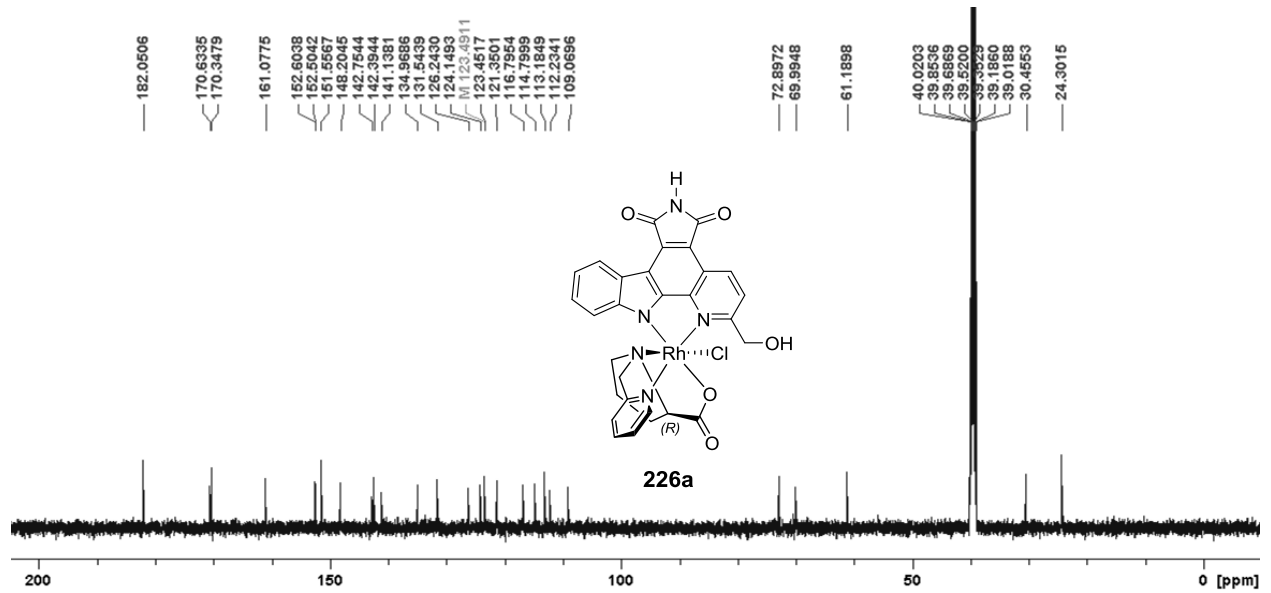


Fig. 98: ^{13}C -NMR-spectrum of 225b.

6.5.14. ^1H - and ^{13}C -NMR-spectra of 226aFig. 99: ^1H -NMR-spectrum of 226a.Fig. 100: ^{13}C -NMR-spectrum of 226a.

NMR-spectra of selected compounds

6.5.15. ^1H - and ^{13}C -NMR-spectra of 226b

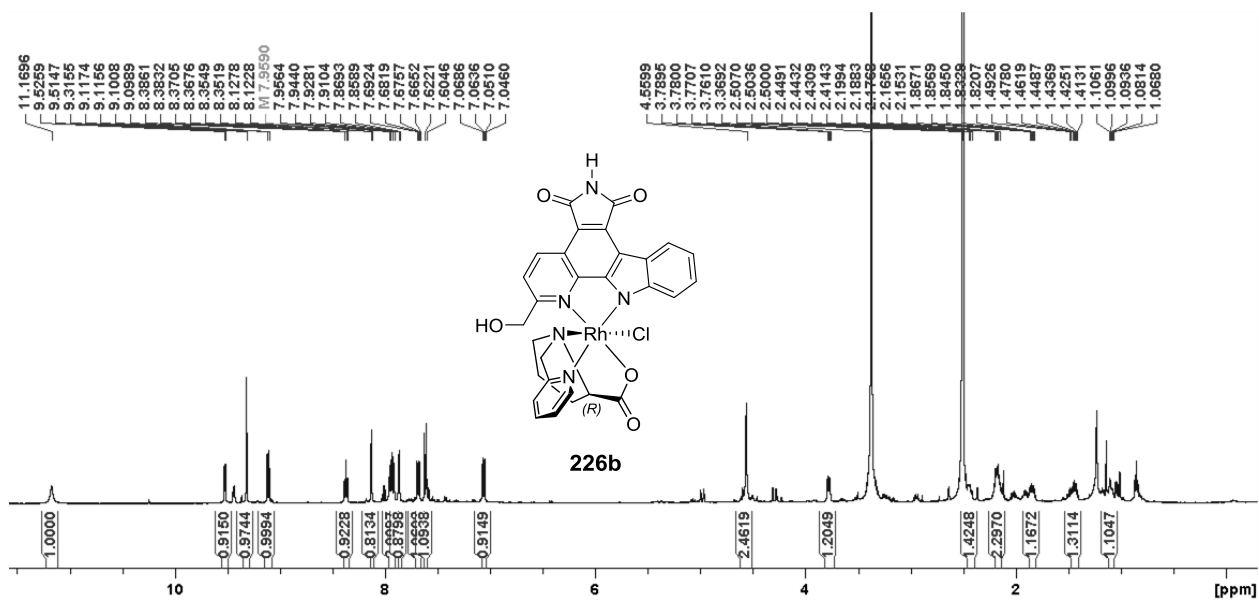


Fig. 101: ^1H -NMR-spectrum of **226b**.

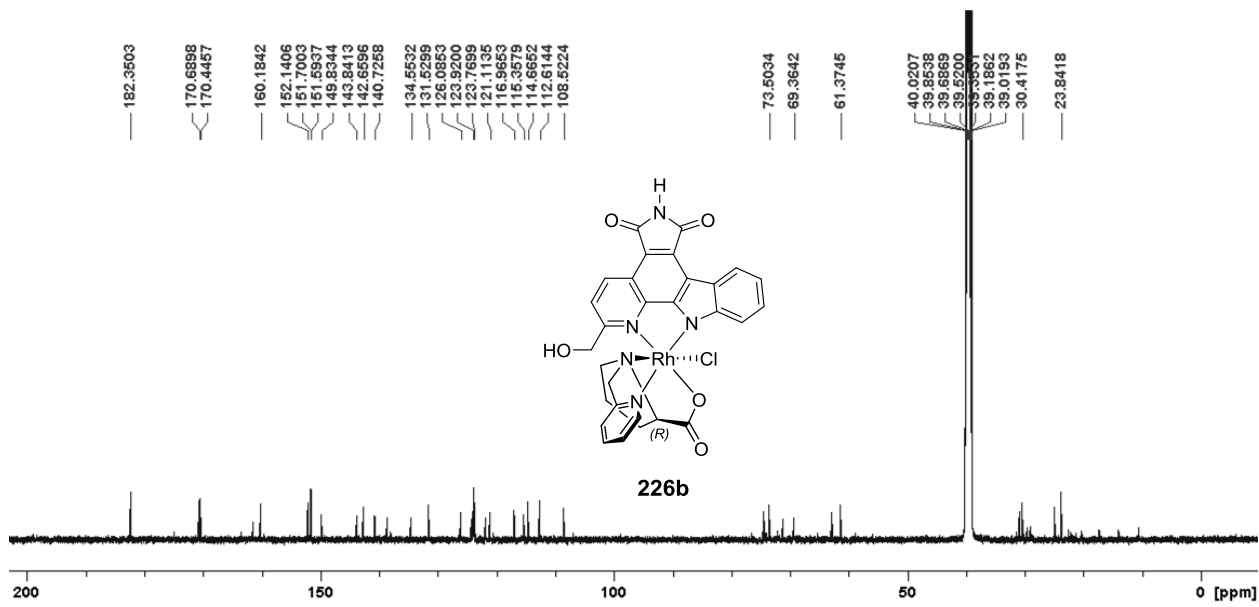
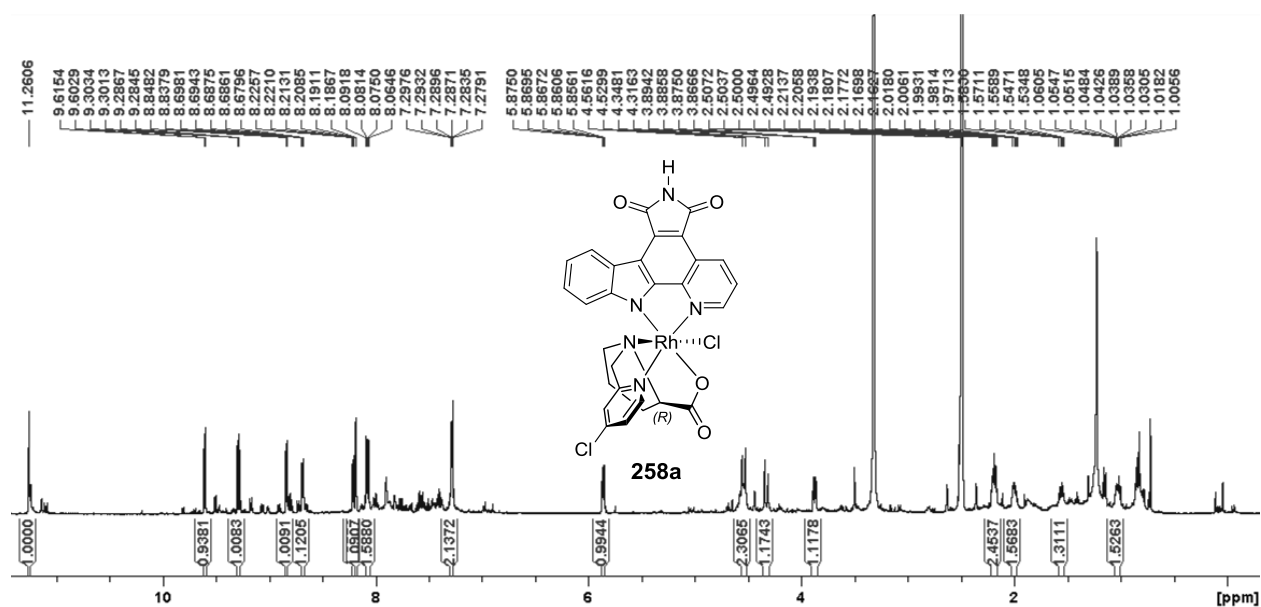


Fig. 102: ^{13}C -NMR-spectrum of **226a**.

6.5.16. ^1H -NMR-spectrum of 258aFig. 103: ^1H -NMR-spectrum of 258a.

The ^{13}C -NMR spectrum of **213a** was not measured due to a low amount of unclean compound available (c.f. ^1H -NMR spectrum).

NMR-spectra of selected compounds

6.5.17. ^1H - and ^{13}C -NMR-spectra of 258b

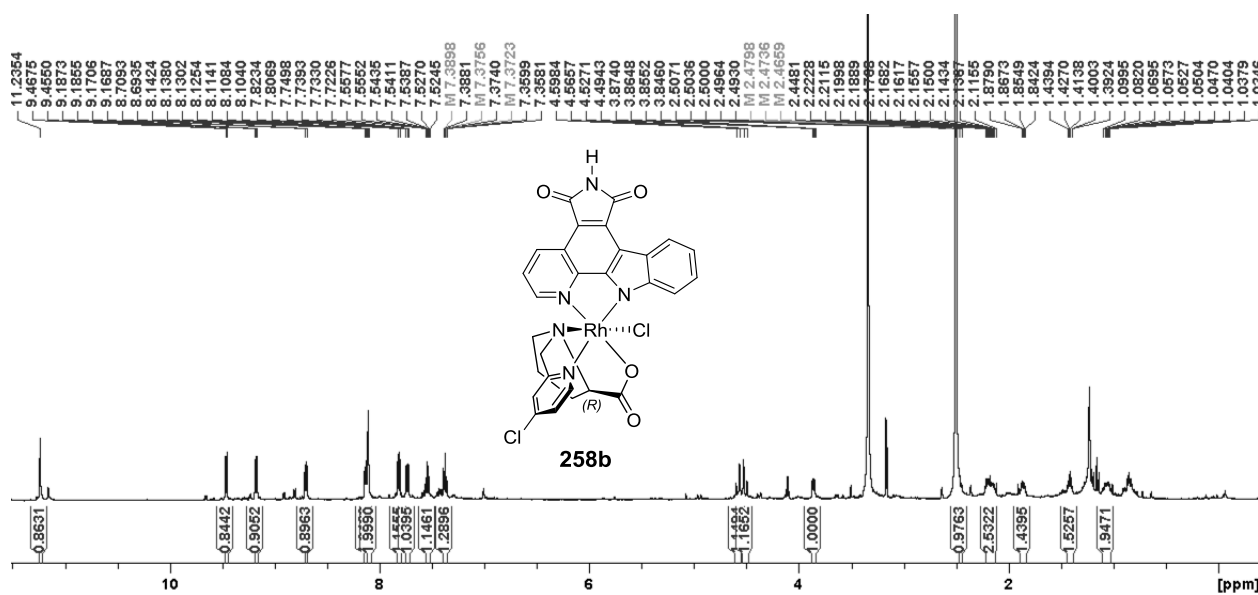


Fig. 104: ^1H -NMR-spectrum of **258b**.

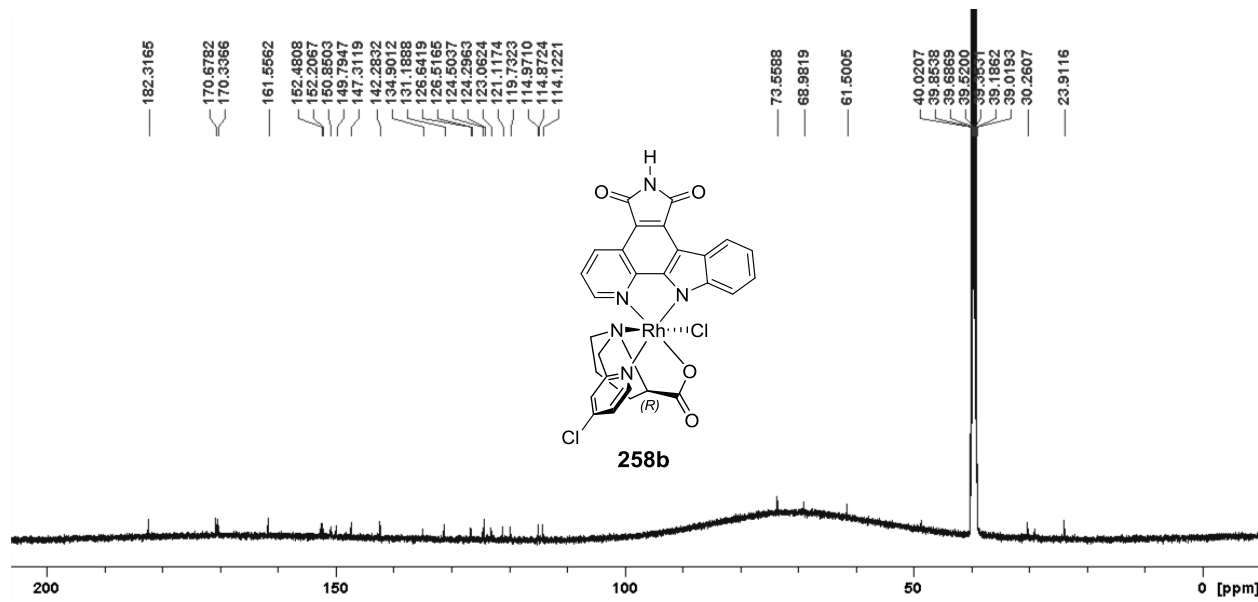


Fig. 105: ^{13}C -NMR-spectrum of **258b**.

6.6. Content of the electronic supporting information

- Compound library and further *in vitro* data (chapter 3.1)
- Summary of initial LC-MS measurements (chapter 3.2.1)
- Stability data (chapter 3.2.2.4.3)
- Toxicity data (chapter 3.2.3)
- *In vivo* data (chapter 3.2.4)
- *In silico* data (chapter 3.4.1)
- Pim1 inhibition data (chapter 3.4.7)
- Cytotoxicity and HDAC inhibitory data (chapter 3.5)
- PDF-files of spectra (1H, 13C, IR, HRMS if applicable; chapter 5)
- Complete crystallographic data (chapter 5.5)

Content of the electronic supporting information

7. Statement

Erklärung

gemäß § 10, Abs. 1 der Promotionsordnung der Mathematisch-Naturwissenschaftlichen Fachbereiche und des Medizinischen Fachbereichs für seine mathematisch-naturwissenschaftlichen Fächer der Philipps-Universität Marburg vom 15.07.2009:

Ich erkläre, dass eine Promotion noch an keiner anderen Hochschule als der Philipps- Universität Marburg, Fachbereich Chemie, versucht wurde. Ich versichere, dass ich meine vorgelegte Dissertation

Development of a New Generation of Metal-Based Anticancer Drugs

selbst und ohne fremde Hilfe verfasst, nicht andere als die in ihr angegebenen Quellen oder Hilfsmittel benutzt, alle vollständig oder sinngemäß übernommene Zitate als solche gekennzeichnet sowie die Dissertation in der vorliegenden oder ähnlichen Form noch bei keiner anderen in- oder ausländischen Hochschule anlässlich eines Promotionsgesuchs oder zu anderen Prüfungszwecken eingereicht habe.

Marburg, den 29.05.2017



Elisabeth Martin

Content of the electronic supporting information

8. Biographical Sketch